



LOMA LINDA UNIVERSITY

Loma Linda University
TheScholarsRepository@LLU: Digital
Archive of Research, Scholarship &
Creative Works

Loma Linda University Electronic Theses, Dissertations & Projects

6-2019

Characterization of Cross-Bed Depositional Processes in the Coconino Sandstone

Sarah A. Maithel

Follow this and additional works at: <https://scholarsrepository.llu.edu/etd>



Part of the [Earth Sciences Commons](#)

Recommended Citation

Maithel, Sarah A., "Characterization of Cross-Bed Depositional Processes in the Coconino Sandstone" (2019). *Loma Linda University Electronic Theses, Dissertations & Projects*. 1870.
<https://scholarsrepository.llu.edu/etd/1870>

This Dissertation is brought to you for free and open access by TheScholarsRepository@LLU: Digital Archive of Research, Scholarship & Creative Works. It has been accepted for inclusion in Loma Linda University Electronic Theses, Dissertations & Projects by an authorized administrator of TheScholarsRepository@LLU: Digital Archive of Research, Scholarship & Creative Works. For more information, please contact scholarsrepository@llu.edu.

LOMA LINDA UNIVERSITY
School of Medicine
in conjunction with the
Faculty of Graduate Studies

Characterization of Cross-Bed Depositional Processes in the Coconino Sandstone

by

Sarah A. Maithel

A Dissertation submitted in partial satisfaction of
the requirements for the degree
Doctor of Philosophy in Earth Science

June 2019

© 2019

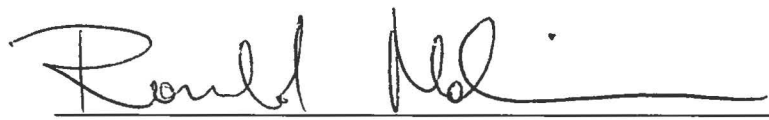
Sarah A. Maithel
All Rights Reserved

Each person whose signature appears below certifies that this dissertation in his/her opinion is adequate, in scope and quality, as a dissertation for the degree Doctor of Philosophy.

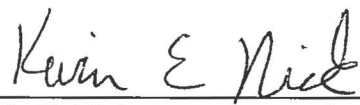

_____, Chairperson
Leonard R. Brand, Professor of Biology and Paleontology



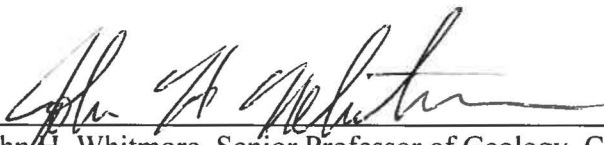
Raúl Esperante, Professor of Paleontology



Ronald Nalin, Adjunct Assistant Professor of Geology



Kevin E. Nick, Associate Professor of Geology



John H. Whitmore, Senior Professor of Geology, Cedarville University

ACKNOWLEDGEMENTS

I am so thankful for the professors, friends, and family who have supported me throughout this substantial research endeavor. Many technical challenges arose during my project, but it was in learning to deal with those challenges that I truly became a scientist. Your instruction and encouragement played a critical role in helping me overcome the obstacles to get to where I am today.

Thank you to my committee, who taught me what it really means to take ownership of and defend my research. I specifically want to recognize my advisor, Dr. Brand, who was always available to discuss ideas, and who supported my project from its earliest stages. Our many field work trips to Arizona and to the sand dunes serve as great memories that I will take from my PhD program. Laboratory methods became a much bigger part of my research than I initially anticipated, and equipment issues seemed to characterize large portions of my graduate experience. Dr. Nick spent considerable time helping me with the equipment and providing ideas for different ways to collect my data. It was because of his help that I was able to develop the once-impossible sandstone disaggregation methods which became so essential to my project. Finally, I am thankful to Dr. Whitmore, who introduced me to Coconino Sandstone research as an undergraduate, and whose encouragement and support has meant so much to me since the beginning of my geology education.

I also want to thank my family, including my parents and my sister Priya, who have supported me in moving far away from home to pursue my goals. It is from my family that I learned the work ethic and perseverance which have enabled me to overcome many obstacles and reach this milestone.

CONTENT

Approval Page.....	iii
Acknowledgements.....	iv
List of Figures.....	ix
List of Tables.....	xii
List of Abbreviations.....	xiv
Abstract.....	xvi
Chapter	
1. The Coconino Sandstone: An Eolian Deposit?.....	1
Stratigraphic Context.....	2
Composition.....	5
Texture.....	9
Sand-Filled Cracks.....	11
Trackways.....	14
Bedding-Plane Sedimentary Structures.....	16
Cross-Bedding.....	18
Problems and Solutions.....	24
Toward a Better Model.....	26
References.....	26
2. Dune Stratification Types: Fine-Scale Sedimentation Processes and their Deposits.....	34
Fluids, Processes, and Environments in Cross-Bedded Sandstone Research.....	34
Depositional Processes on Dunes.....	40
Dune Stratification Types.....	41
Grainfall.....	43
Grainflow.....	44
The Case of Continuous Avalanching.....	46
Ripple Lamination.....	48
Dune Shape and Stratification Type Distribution.....	48

Using Stratification Types to Interpret Cross-Bedded Sandstones.....	49
References.....	50
3. A Methodology for Disaggregation and Textural Analysis of Quartz- Cemented Sandstones	55
Abstract.....	55
Introduction.....	56
Methods.....	60
Disaggregation Methods	61
Lithified-Rock Analysis.....	64
Sources of Discrepancy between Results from each Method.....	66
Grain Fracturing during Disaggregation.....	67
Sample Loss	72
Removal of Aggregated Grains	72
Overgrowths Remaining on Grains	74
Comparison between Thin-Section and Laser-Particle-Analysis Methods.....	77
Mineralogical Constraints.....	79
Conclusions.....	81
Acknowledgements.....	82
References.....	82
4. Characterization of Cross-Bed Facies and Associated Depositional Processes in the Permian Coconino Sandstone (Arizona, USA)	89
Abstract.....	89
Introduction.....	90
Sedimentological Criteria for Distinguishing Dune Stratification Types.....	94
Methods.....	99
Field Methods	102
Petrographic Methods	106
Disaggregation and Grain-Size Analysis	106
Results.....	107
Sedimentary Structures	107
Textural Trends.....	111

Microfacies	118
Diagenetic Features.....	121
Discussion.....	128
Sedimentary Structures	129
Textural Trends.....	132
Microfacies	136
Large Pores	138
Dune Morphology and Controls on Stratification Type Distribution.....	141
Cross-Bed Depositional Processes: Undifferentiable Grainflow and Grainfall	143
Acknowledgements.....	145
References.....	146
5. Discussion and Future Work.....	155
Future Work	157
References.....	158
Appendices	
A. The Path to Sandstone Disaggregation: An Adventure in Methodology	161
Image Analysis.....	161
Petrographic Methods	162
Tracing Grain Outlines	165
Measuring Long Axes of Grains.....	165
Counting Grains $\geq 150 \mu\text{m}$	166
Magnetic Susceptibility	167
Disaggregation: A New Hope.....	168
Acknowledgements.....	168
References.....	168
B. Outcrop GPS Coordinates	170
C. Outcrop Photo Mosaics with Sample Locations	171
D. Cross-Bed Dip-Angle Data	175
E. Particle-Analyzer Data	177
Coconino Sandstone Data Summary Tables.....	178

Coconino Sandstone Sample Data	181
Poorly Disaggregated TM-1 Sample Data	278
Select Re-Disaggregated Samples for Comparison with Thin-Section Data	282
Algodones Dune Sand Sample Data for Sonication Test	287
F. Thin-Section Long-Axis Data	303
Long-Axis Data Summary Table	304
All Long-Axis Measurements from Each Sample	305
G. X-Ray-Diffraction Data	341
Coconino Sandstone Sample Data	342
Whole-Rock versus Disaggregated Sample Comparison Data	352
H. High-Resolution Scans of Thin Sections	366

FIGURES

Figure	Page
Chapter 1	
1. Geographic Distribution of the Coconino Sandstone	4
2. Scanning-Electron-Microscope Images of Mineral Components.....	7
3. Thin-Section Photographs of Mineralogy and Textures	10
4. Sand-Filled Cracks	13
5. “Sideways” Trackway.....	15
6. Bedding-Plane Sedimentary Structures	17
7. Cross-Bedding.....	20
8. Deformed Cross-Bedding	22
Chapter 2	
1. Diagram of the Relationship between Sedimentary Environments, Fluids, and Processes	35
2. Modern Eolian Dune in the Algodones Dune Field, Southern California	37
3. Flow and Grain Trajectories over a Dune Bedform.....	41
4. Composite Grainflow Beds in Horizontal Exposures	45
5. Grainflow Deposits on Eolian and Subaqueous Dunes	46
Chapter 3	
1. Map of Sample Locations and Relative Degrees of Cementation	60
2. Comparison of Thin-Section and Laser-Diffraction-Analysis Histograms	69
3. Comparison of Average Grain Sizes for Poorly versus Well-Disaggregated Samples	73
4. Images of Select Coconino Sandstone Samples Before and After Disaggregation	75
5. Disaggregated Sand in Thin Section.....	76

6. Boxplot Comparing Particle-Analyzer and Thin-Section Data	78
Chapter 4	
1. Comparison of Outcrop Weathering Patterns in the Navajo and Coconino Sandstones.....	93
2. Vertical Cross-Bed Sorting Trends, after Kleinhans (2004).....	99
3. Map of Study Areas and Specific Outcrop Locations	101
4. Explanation of Relative Vertical Sample-Position Method.....	103
5. Relationship between Bounding Surface Exposures and Underlying Cross-Beds	105
6. Cross-Bed Dip Angle Data	108
7. Diagram Comparing the Overall Average Dip with a Cross-Bed Profile	109
8. Photo Mosaics of Bounding Surfaces with Traced Bedding Planes.....	110
9. Photo Mosaics with Average Grain-Size and Dip-Angle Annotations	113
10. Graphs of Vertical Grain-Size Trends, in the Style of Kleinhans (2004).....	115
11. Graphs of Vertical Grain-Size Trends, in the Style of Loope et al. (2012)	117
12. High-Resolution Scans of Laminated Thin Sections	119
13. Distribution of Dip Angles and Select Textural Data in a Cross-Bed Set with Prevalent Lamination.....	120
14. Textures and Corresponding Dip Angles along a Single Cross-Bed.....	121
15. Stylolite Seams in Thin Section	122
16. Scanning-Electron-Microscope Images of Probable Detrital Illite Associated with a Stylolite Seam.....	123
17. Stylolite Seams in Hand Sample and Thin Section	124
18. Thin-Section Images of Large Pores in an Ash Fork Outcrop.....	125
19. Outcrop Distribution of Samples with Large Pores	126
20. Large Pores in Cross Section and on a Cut Epoxied Surface	126
21. Micro-Pitted Quartz Surfaces in Association with Large Pores	128

22. Comparison between Eolian Grainflow Morphology and the Cross-Bedding Observed in the Coconino Sandstone.....	131
23. Comparison of Cross-Bedding Geometries (as Exposed on Bounding Surfaces) in an Eolian Dune and the Coconino Sandstone.....	132
24. Dolomite Clasts along New Hance Trail, Grand Canyon.....	141
25. Comparison of Crescentic Dune and Coconino Sandstone Cross-Stratification.....	145

Appendix A

1. Backscattered-Electron and Cathodoluminescence Images of a Coconino Sandstone Sample	162
2. Photographic Techniques used for Petrographic Methods	164
3. Light Table Method for Counting Coarse Grains in Thin-Section Photos	167

TABLES

Table	Page
Chapter 1	
1. Estimated Mineral Weight Percentages (%) from X-Ray Diffraction.....	6
2. Problems and Solutions in Coconino Sandstone Research.....	25
Chapter 2	
1. Interpretive Scale of Common Cross-Bedded Sandstone Descriptors	38
2. Overview of the Three Primary Dune Sedimentation Processes and their Deposits.....	42
Chapter 3	
1. Workflow of our Sandstone-Disaggregation and Particle-Analysis Method	62
2. Samples Selected for Petrographic Analysis	65
3. Sources of Discrepancy between Petrographic and Disaggregated- Sediment Analyses.....	66
4. Correlation between Average Grain Sizes (ϕ) with and without the Fine Fraction (Finest 10%).....	68
5. Skewness of Thin-Section Data	70
6. Mean Grain Size (ϕ) after Time Sonicated for Four Loose-Sand Samples	71
7. Correlation between Average Grain Sizes (ϕ) from Thin-Section and Laser-Diffraction Particle Analysis	79
8. Relative Feldspar Percentages (%) from X-Ray-Diffraction Analysis of Whole-Rock and Disaggregated Samples.....	81
Chapter 4	
1. Summary of Select Criteria for Distinguishing Dune Stratification Types	98
2. Vertical Range Sampled within Each Cross-Bed Set	103
3. Summary of Textural Data for Each Outcrop.....	111

4. Changes in Texture with Respect to Relative Vertical Position in Cross-Bed Sets	114
5. Summary of Criteria Supporting an Undifferentiable Grainfall/Grainflow Model	144
Appendix A	
1. Outcrop Names and Location Information	163

ABBREVIATIONS

2D	Two-Dimensional
3D	Three-Dimensional
ALC	Alkali Creek Road, Wyoming
ASF	Ash Fork, Arizona
AZ	Arizona
CCSEM	Computer-Controlled Scanning Electron Microscopy
COW	Penrith, England
CPE	Chino Point East
D	Disaggregated
GPS	Global Positioning System
HCl	Hydrochloric Acid
HF	Hydrofluoric Acid
HMT	Hermit Trail, Grand Canyon South Rim, Arizona
HOL	Holbrook, Arizona
K-Feldspar	Potassium Feldspar
KIN	Kinver, England
NaHMP	Sodium Hexametaphosphate
Rd	Road
SEM	Scanning Electron Microscope
SEM-CL	Scanning Electron Microscope-Cathodoluminescence
TEN	Tensleep, Wyoming
TM	Trinity Mountain Quadrangle (Arizona)

ULM	Universal Liquid Module
USA	United States of America
XRD	X-Ray Diffraction
WR	Whole Rock

ABSTRACT OF THE DISSERTATION

Characterization of Cross-Bed Depositional Processes in the Coconino Sandstone

by

Sarah A. Maithel

Doctor of Philosophy, Graduate Program in Earth Science
Loma Linda University, June 2019
Dr. Leonard R. Brand, Chairperson

The Permian Coconino Sandstone of northern and central Arizona is widely recognized as a classic eolian dune deposit, with conspicuous large-scale cross-beds that are interpreted as preserved dune foresets. On modern bedforms, fine-scale processes – which include grainflow, grainfall, and ripple migration – transport and deposit sediment, and these may provide useful analogs for interpreting ancient deposits. Even though the Coconino Sandstone is well known, such fine-scale process models have not been adequately developed to explain its cross-bed deposition. Furthermore, observed discrepancies between the sandstone and some eolian criteria suggest that additional study is needed to explore and refine these process models.

To interpret cross-bed depositional processes, sedimentary textures and structures were described in multiple outcrops across northern Arizona. A methodology was developed to disaggregate the well-cemented sandstone, which is characteristic of most localities. These disaggregation methods are less tedious than petrographic approaches, and allow for expedited textural analysis of many samples.

Cross-beds were observed to be laterally extensive along strike, with most dip angles ranging from the mid-teens to mid-twenties. Some cross-bed sets are coarser at their bases, but others exhibit variable changes in grain size with no significant vertical

trends. While both massive and laminated textures occur, these do not show a preferred distribution within the studied cross-bed sets. Lamination – as observed in high-resolution scans of thin sections – appears to exhibit both normal and reverse grading, but these trends are difficult to define where laminae contacts are diffuse. Diagenetic features, which include stylolite seams and large pores, mimic primary structures and likely relate to both depositional and post-depositional processes. These features also show no preferred vertical distribution within their respective cross-beds.

Observed textures and sedimentary structures suggest that the cross-beds may consist of grainflow and grainfall deposits, but these are difficult to differentiate at outcrop and thin-section scales. Such a model explains massive textures and vertical coarsening in some outcrops, but also predicts that the beds may differ from those produced by modern grainflows (due to the inclusion of grainfall). This characterization of fine-scale processes will serve as a critical piece of the puzzle as researchers seek to understand the deposition of the Coconino Sandstone.

CHAPTER ONE

THE COCONINO SANDSTONE: AN EOLIAN DEPOSIT?

Famously recognized by its distinct, continuous exposure as the third layer down from the top of the Grand Canyon, the Permian Coconino Sandstone is widely known as a classic eolian dune deposit. While a few earlier authors had written about the formation (Dake, 1920; Darton, 1910; Noble, 1922), McKee (1934) was the first to develop its eolian depositional model based on various compositional, textural, and structural criteria. After McKee's paper (1934), several other publications described textures and sedimentary structures in the sandstone (Fisher, 1961; Johnson, 1962; McKee, 1945; Middleton et al., 2003; Reiche, 1938), but most references focused on trace fossils (Alf, 1968; Bartlett and Elliott, 2015; Braddy, 1995; Brady, 1939, 1947; Brand, 1979, 1996; Brand and Kramer, 1996; Brand and Tang, 1991; Citton et al., 2012; Erickson et al., 2011; Gilmore, 1926, 1927a, b, 1928; Hunt et al., 1995; Hunt and Santucci, 1998a, b, 2001; Santucci and Wall, 1995) or regional stratigraphic correlations (Baars, 1961, 1979; Blakey, 1979a, 1979b, 1980, 1990, 2003; Blakey and Knepp, 1989; Elston and DiPaolo, 1979). For many years, the sedimentology of the Coconino Sandstone had not been investigated or described in the literature, with the exception of a few theses that evaluated compositional, textural, stratigraphic, or trackway data (Elcock, 1993; Fisher, 1961; Lundy, 1973; Millhouse, 2009; Sumner, 1999). This lack of documentation on its sedimentology left the eolian interpretation largely undeveloped and unquestioned.

Stratigraphic Context

The Coconino Sandstone is a Permian (Leonardian) sedimentary unit that crops out on the Colorado Plateau across northern Arizona (figure 1). Most authors agree that the sandstone is of Permian age (Fisher, 1961; McKee, 1934; Noble, 1922; Stokes, 1961), but a couple of earlier papers (Dake, 1920; Darton, 1910) suggested that it is Pennsylvanian. An absence of body fossils makes dating and correlation difficult for the Coconino Sandstone, so Sorauf (1962) derived the unit's Leonardian age from its stratigraphic position between the Hermit and Toroweap Formations (which both contain adequate fossils for age determination).

The thickest sections are exposed near Pine, Arizona (1000 ft/305 m; McKee, 1934; Middleton et al., 2003), and the unit thins toward the north and west (McKee, 1974). Even though the sandstone does not currently extend across much of southern Arizona, it was probably removed by erosion; Twenter and Metzger (1963) specifically suggest that it was eroded from the Black Hills area in the central part of the state. Miller and McKee (1971) identified metamorphosed Coconino Sandstone in the Plomosa Mountains near Quartzsite, Arizona (west of Phoenix, near the California border), and Stone et al. (1983) described metamorphosed sections in several isolated ranges (southeastern California and southwestern Arizona), supporting a much greater depositional extent than what is currently preserved. Possible equivalents include the Glorieta Sandstone (Baars, 1961), Scherrer Formation (Blakey and Knepp, 1989; Dunbar et al., 1960), White Rim Sandstone, Black Creek Member of the DeChelly Sandstone (Blakey, 1980), and the Weber and Tensleep Sandstones (Middleton et al., 2003).

The lower contact of the Coconino Sandstone is sharp in most localities, but in some sections, the sandstone interfingers with the underlying Hermit Formation (Fisher,

1961). McKee (1934) and Sorauf (1962) noted a gradational contact between these formations in the eastern Grand Canyon region, and a more recent study by Whitmore and Peters (1999) similarly documented a gradational contact along the Tanner Trail on the South Rim. The Coconino Sandstone also locally interfingers with the overlying Toroweap Formation (Baars, 1961; Fisher, 1961; Stokes, 1961), and with the underlying Schnebly Hill Formation, which sits between the Coconino and Hermit Formations in the Sedona area (Blakey and Knepp, 1989). Where the Toroweap Formation is missing in some eastern exposures, the Coconino Sandstone is conformably overlain by the Kaibab Limestone (Middleton et al., 2003), and farther east, it is directly overlain by the Moenkopi Formation (Blakey, 1988).

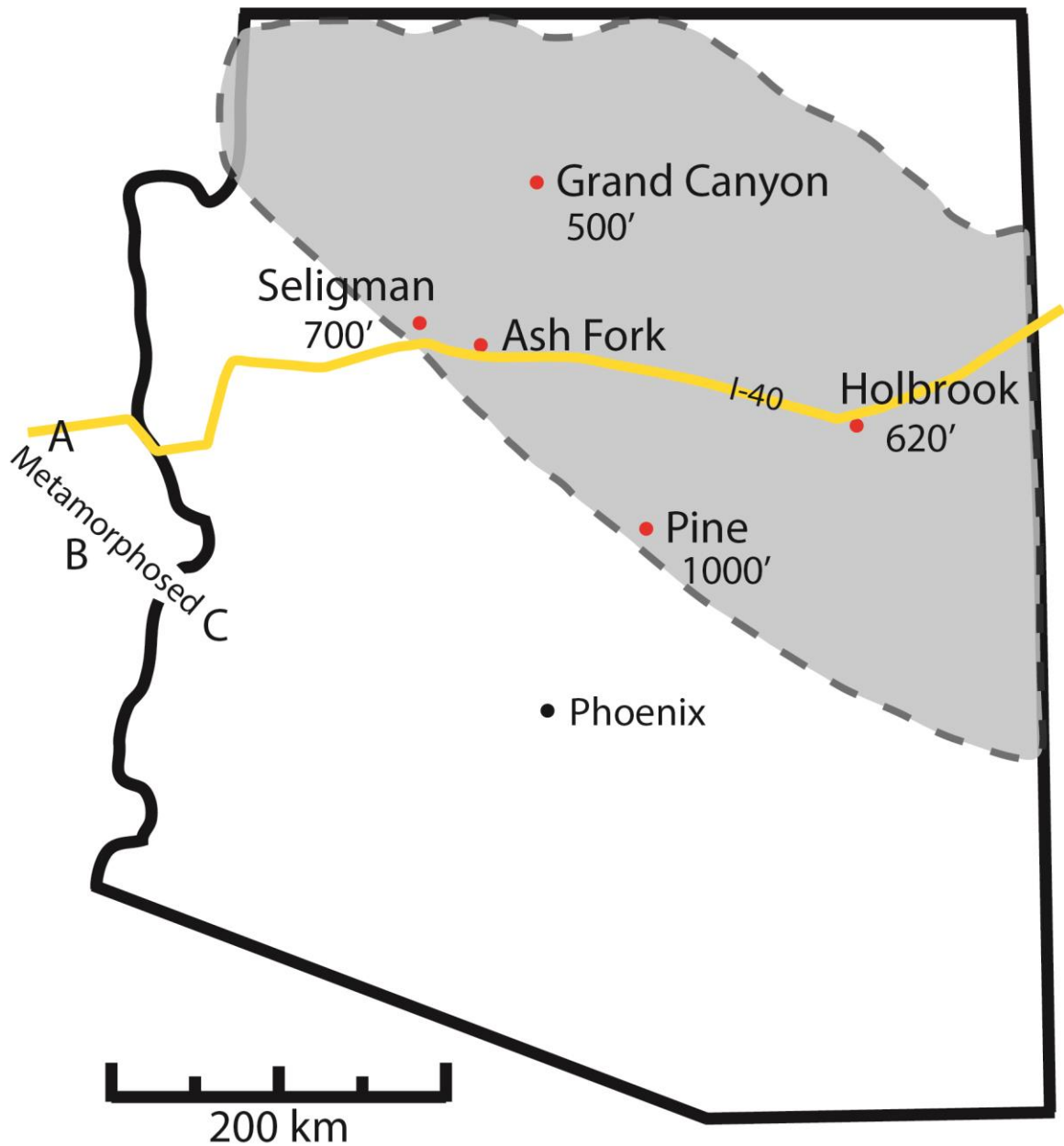


Figure 1: Map of Arizona showing the geographic distribution of the Coconino Sandstone and approximate thicknesses measured near several locations, as described in the published literature: Grand Canyon South Rim (500', Billingsley and Hampton, 2000); Seligman (700', McKee, 1934); Holbrook (620', McKee, 1934); and Pine (1000', McKee, 1934; Middleton et al., 2003). The grey region marks the approximate extent of the contiguous unit across northern Arizona (Blakey, 1988; Blakey and Knepp, 1989; McKee, 1934; Middleton et al., 2003; Richard et al., 2000). Discontinuous metamorphosed sections were described in some California and southwestern Arizona mountain ranges and interpreted as Coconino Sandstone by Stone et al. (1983): Little Piute Mountains (A), Arica Mountains (B), and Plomosa Mountains (C). Thicknesses on the map are given in feet to reflect the values from the publications. The sandstone was likely deposited south of the boundary marked on the map and eroded from many areas across southern Arizona (e.g., Twenter and Metzger, 1963).

Composition

The Coconino Sandstone may vary in composition between outcrops, but it consists mostly of quartz and K-feldspar, with smaller percentages of illite, kaolinite, heavy minerals, and calcite (from x-ray diffraction; table 1). Trace muscovite occurs in many thin sections, and while their bulk percentages remain small, authigenic illite and kaolinite are common (figure 2C-F). Framework grains are generally cemented by quartz overgrowths (figure 2A-B), but calcite and iron-carbonate cement have been observed in some samples.

Table 1: Estimated mineral weight percentages (%) from x-ray diffraction

Sample	ASF-5-8	ASF-5-24	ASF-22e-A	ASF-22e-J	HMT-4	HOL-E-A-4	HOL-E-B-1	HOL-E-B-10	TM-1-26	TM-3-8
Quartz	82	92	85	84	85	91	93	89	90	88
Feldspars	12	3	9	9	10	7	6	6	8	9
Muscovite/ Illite	2	3	3	5	1	trace	1	1	1	2
Kaolinite	0	trace	trace	trace	1	1	1	3	0	trace
Calcite	trace	trace	trace	trace	trace	trace	0	trace	0	0
Iron Carbonates	trace	trace	trace	trace	trace	trace	0	0	trace	trace
Heavy Minerals	4	1	2	2	2	1	1	1	1	1

Samples were collected from Ash Fork (ASF), Grand Canyon, Hermit Trail (HMT), Holbrook (HOL), and Seligman (TM) outcrops. Trace mineral components were estimated as < 0.5%. The calculated percentages exclude corundum, which was added to the samples during grinding. Feldspar phases include k-feldspars and anorthoclase, and heavy-mineral phases include tourmaline (schorl), zircon, and rutile. Iron-carbonate phases include ferroan dolomite, ankerite, and siderite.

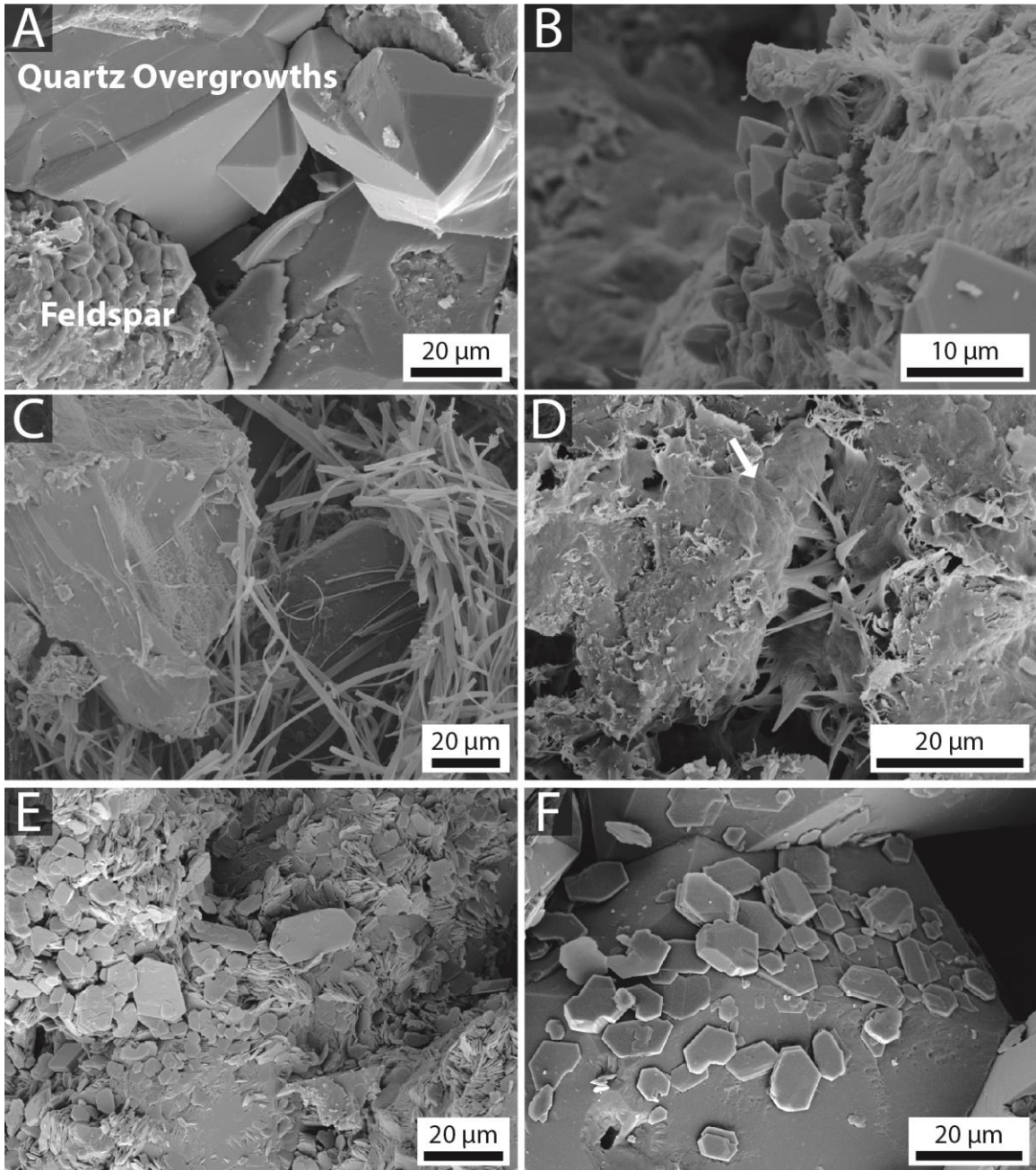


Figure 2: Scanning-electron-microscope images of Coconino Sandstone samples from various locations. In most outcrops, the predominantly quartz sandstone is cemented by quartz overgrowths. **A)** A weathered feldspar grain and adjacent quartz overgrowths in a sample from Chino Wash, near Seligman; **B)** Small, euhedral quartz crystals in an Ash Fork sample. Illite fibers are visible near the upper right corner of the photo. **C, D)** Fibrous illite in Ash Fork-area samples. In **D**, the arrow highlights an authigenic illite mat; such mats may grow on quartz-overgrowth surfaces and help to control porosity by limiting additional cementation (Welton, 1984). **E, F)** Kaolinite in a sample from Five Mile Wash, near Holbrook. Feldspar alteration may provide a source for some of the kaolinite in the Coconino Sandstone.

Earlier work generally agrees with these compositional trends. Point counts and thin-section estimates have revealed quartz (61-95%), chert (0-28%), K-feldspar (0-18%), and smaller amounts of kaolinite, plagioclase, mica, and other trace minerals (John Whitmore, pers. comm.). McKee (1934) described the Coconino Sandstone as consisting primarily of quartz sand, localized siliciclastic clay, carbonates, and iron oxide, with traces of heavy minerals and feldspar. Others have made similar observations, defining the composition as mostly quartz (Blakey and Knepp, 1989; McKee, 1974), with only minimal feldspar (Middleton et al., 2003) and chert (Sumner, 1999). Johnson (1962) recognized limonite and pyrite in addition to the quartz and feldspar, and Sumner (1999) noted four types of cement: quartz overgrowths, chalcedony, calcite, and iron oxide. Carbonates are not present in all outcrops; however, Fisher (1961) described limestone and dolomite beds with marine fossils in Parashant and Andrus Canyons where the Coconino Sandstone interfingers with the Toroweap Formation. Fisher (1961) proposed that the cement in his study area was mostly calcareous and only locally siliciclastic, which differs from the quartz cement characteristic of the majority of the formation (Middleton et al., 2003). A few others have also documented dolomite in the form of fossiliferous beds, clasts, ooids, and cement, mostly in select northern outcrops (Cheung et al., 2010; Cheung et al., 2009; Whitmore and Strom, 2009).

Dune sand may commonly contain feldspar grains ($H \approx 6$), but these are softer than quartz ($H \approx 7$) and should be rounded quickly by abrasion on eolian dunes (Marsland and Woodruff, 1937; Pye and Tsoar, 2009). Mica, which is even more fragile, should generally not be preserved. While Swezey (1998) suggested that the presence of orthoclase and mica does not preclude eolian deposition, Anderson et al. (2017)

demonstrated experimentally that micas are readily abraded during eolian transport. Where modern eolian dunes are located near an igneous source, however, these grains may persist in the dune sand (e.g., micas have been observed in sand from the Algodones Dunes, Southern California).

Primary dolomite formation remains poorly understood, but secondary (replacement) dolomite occurs in many rocks. Since primary dolomite is typically associated with marine and lacustrine environments, evidence for such dolomite precipitation may imply subaqueous deposition for the associated Coconino Sandstone facies, but more work should be done to explore possible depositional and diagenetic models for these beds.

Texture

While the Coconino Sandstone exhibits variation in composition and texture, its predominantly quartz and feldspar sand is generally well to moderately sorted, with poor sorting observed in some samples. Grain angularity ranges from rounded to angular (figure 3).

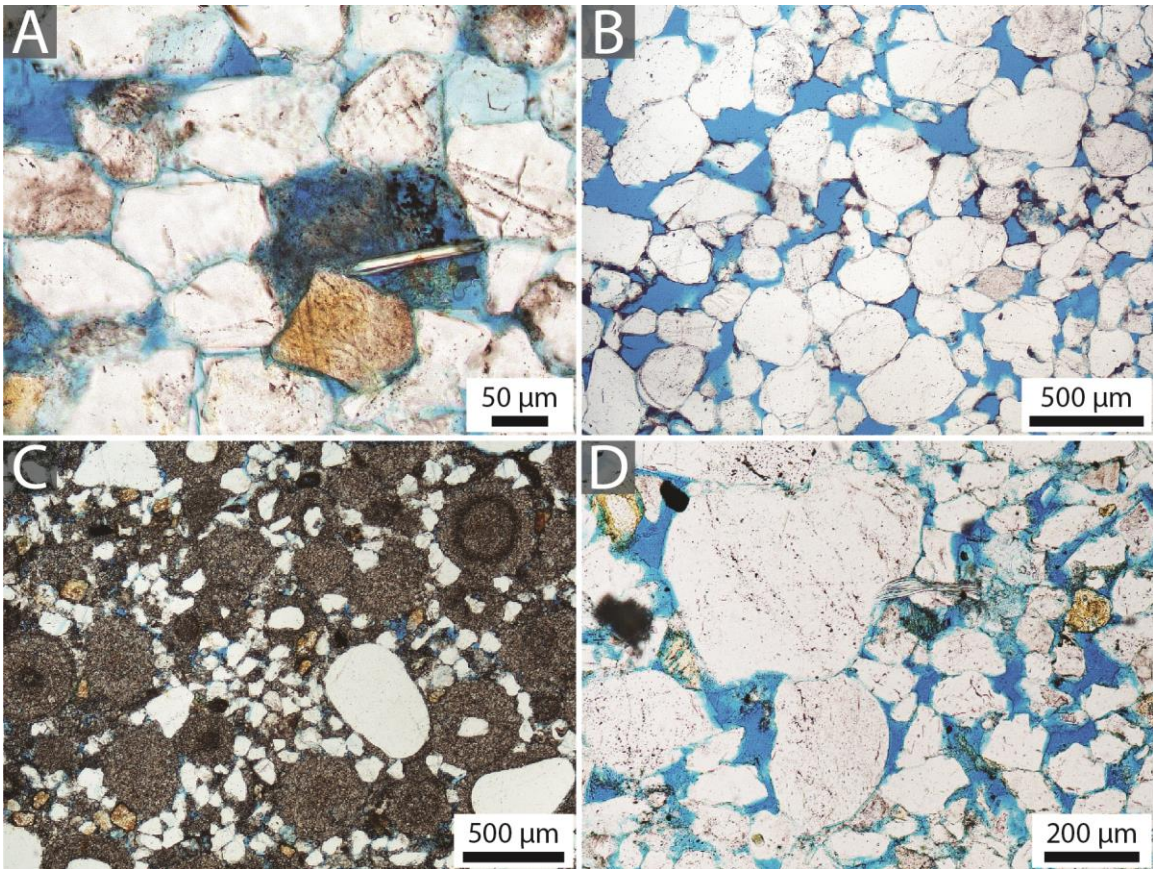


Figure 3: Coconino Sandstone in thin section under plane-polarized light (brightness, contrast, and levels adjusted with Adobe Photoshop). These photos illustrate examples of textural and compositional variation across the formation. Quartz grains are white in color and orthoclase grains have been stained yellow-orange. Pore space has been filled with blue epoxy. **A)** Muscovite grain with adjacent quartz and angular orthoclase. Sample collected from the Chino Point West section near Seligman. **B)** Nearly pure quartz Coconino Sandstone from the Pine Creek Trail section east of Sedona. **C)** Dolomite ooids, along with quartz and orthoclase, from the Andrus Point section on the Grand Canyon North Rim. The ooids are notably coarser than most of the adjacent sand, with the exception of a few large quartz grains. **D)** Poorly sorted quartz, along with orthoclase and muscovite, from the Jumpup Spring section on the Grand Canyon North Rim.

Previously published literature claimed that the sandstone was well sorted (Fisher, 1961; Johnson, 1962; McKee, 1934, 1945, 1974; Middleton et al., 2003; Reiche, 1938) and well rounded (Blakey and Knepp, 1989) or “rounded” (Middleton et al., 2003), though some have noted sub-rounded (Fisher, 1961; Johnson, 1962; Twenter and Metzger, 1963) to sub-angular (McKee, 1934) grains. Subsequent petrographic studies

(Maithel and Whitmore, 2010; Whitmore and Strom, 2009, 2010b) suggested that the sand was moderately sorted overall but ranged from well sorted to very poorly sorted (after Johnson, 1994), and that while some larger quartz grains were rounded, most were sub-rounded to sub-angular according to the roundness scale developed by Powers (1953). Orthoclase grains were also described as sub-angular.

Modern eolian dunes are typically composed of moderately to well-sorted, sand-size grains that range from rounded to somewhat angular (Pye and Tsoar, 2009). While well-rounded sand has historically been associated with eolian transport and deposition, studies of modern dunes have suggested that grains may range from rounded to rather angular, with large particles being better-rounded than the finer ones (Goudie and Watson, 1981; Khalaf and Gharib, 1985; Pye and Tsoar, 2009). Softer minerals should probably be rounder than adjacent quartz grains (Garzanti, 2017; Garzanti et al., 2015; Marsland and Woodruff, 1937; Pye and Tsoar, 2009). Very poor sorting, bimodal-size distributions, and variable grain composition and angularity may imply multiple and/or local sediment sources, or they might suggest that the transport process or fluid was unable to promote substantial sorting and rounding of the sediment. In either case, examples of poor sorting and sub-angular orthoclase grains in the Coconino Sandstone illustrate that the transport and depositional processes were probably more complex than the simpler eolian dune models proposed in the early literature.

Sand-Filled Cracks

In the Grand Canyon region, sand-filled cracks penetrate from the base of the Coconino Sandstone into the Hermit Formation (figure 4). These structures were previously interpreted as desiccation cracks (Abbott and Cook, 2004; McKee, 1934;

Sorauf, 1962; White, 1929). However, Whitmore and Strom (2010a) described banding, clast breccias, lateral sand bodies, preferred orientation, and zoned spatial distribution with respect to the Bright Angel Fault, and suggested that the sand-filled cracks were actually sand injectites produced by seismic activity and liquefaction.

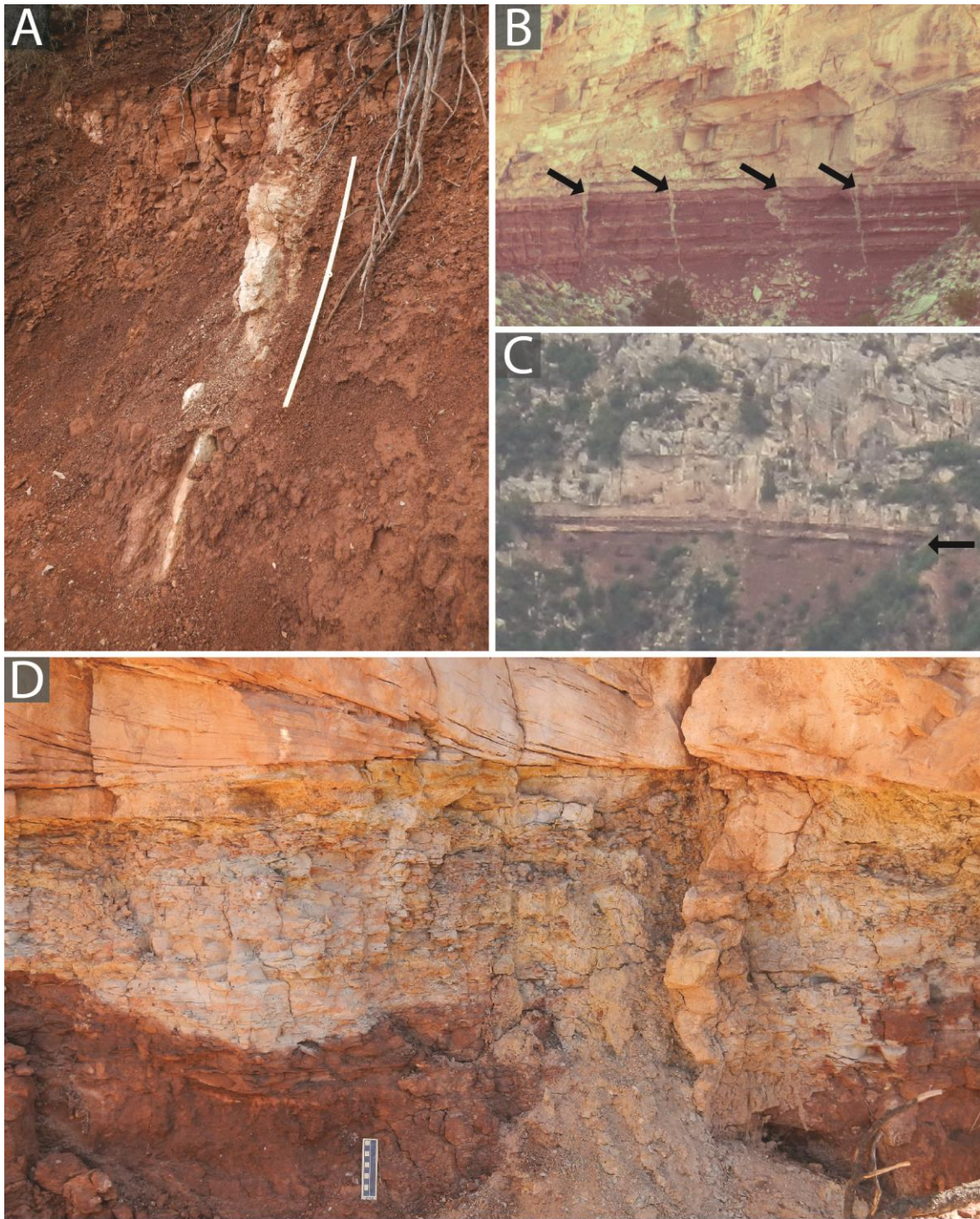


Figure 4: Sand-filled cracks extending from the base of the Coconino Sandstone into the underlying Hermit Formation. All photos were taken in Grand Canyon National Park. **A)** Sand-filled crack exposed along Grandview Trail, South Rim. Scale Bar = 1 m. **B)** Sand-filled cracks viewed from Hermit Trail, South Rim (image brightness, contrast, and levels adjusted in Adobe Photoshop). Photo was taken by John Whitmore. **C)** Sandstone bed in the Hermit Formation below the lower Coconino Sandstone contact, viewed from the North Rim. **D)** Weathered contact and sand-filled crack (right) exposed along Hermit Trail, South Rim. Scale Bar = 10 cm.

Trackways

Invertebrate and vertebrate trackways/traces have been observed on many bedding surfaces in the Coconino Sandstone (Alf, 1968; Bartlett and Elliott, 2015; Braddy, 1995; Brady, 1939, 1947; Brand, 1979; Citton et al., 2012; Erickson et al., 2011; Gilmore, 1926, 1927a, b, 1928; Hunt et al., 1995; Hunt and Santucci, 1998a, b, 2001; McKee, 1934; Millhouse, 2009; Santucci and Wall, 1995). Brand and Kramer (1996) studied underprints, or subsurface deformation beneath tracks, and found that the underprints can show more detail than the surface prints when formed in fine sand (versus mud). Many slabs containing trackways have been collected for display in various museums.

Within the eolian model, it is generally believed that these tracks were made in damp sand (McKee, 1934), or emplaced in dry sand and later preserved by moisture (McKee, 1947). In an experimental study, however, Brand (1979) described tracks produced on dry, damp, and wet sand, and suggested that the underwater tracks most closely resembled those observed in the Coconino Sandstone. A later experiment also proposed similarity between the sandstone tracks and those produced on sloping, submerged sand/mud and on damp sand (Brand, 1996). Furthermore, Brand and Tang (1991) noted “sideways” and “disappearing” trackways, and suggested that the organisms were displaced by currents flowing over the bedforms (figure 5). These studies may reveal evidence that the tracks were made underwater, and potentially with lateral currents flowing across the dune foresets. Lockley and Hunt (1995) argued that reptiles can produce lateral trackways with toes pointing upslope, noting observations of modern lizard trackways and providing a sketch (p. 42). They did not, however, give photographs or additional data to support this claim. In the comment and reply on Brand

and Tang (1991), the potential for sideways movement of the track makers was also suggested, but a clear alternate mechanism was not provided to explain how this movement could realistically occur. Moreover, both critiques of the proposed subaqueous model submitted that weird trackways should not be used to negate the sedimentological evidence for eolian deposition (Lockley et al., 1992). While unusual tracks alone might not be enough to suggest a new depositional model for the sandstone, they present an anomaly that prompts additional study of the other features.

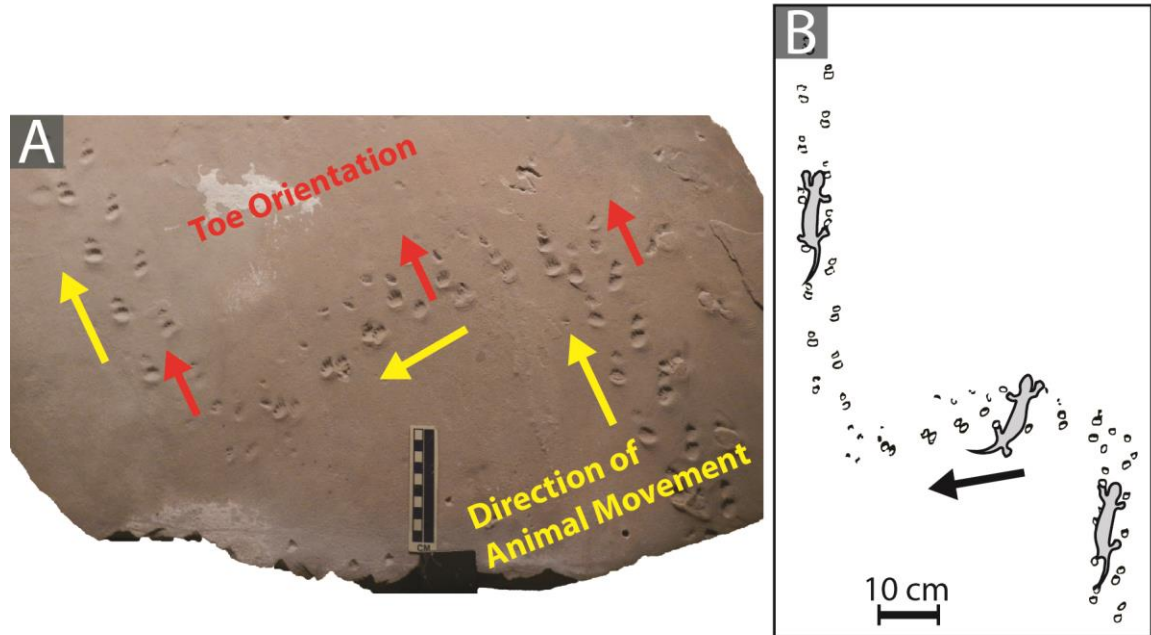


Figure 5: “Sideways” trackway on a Coconino Sandstone bedding plane. **A)** The trackway was collected in Chino Wash, near the town of Seligman, and it is currently on display at the Raymond Alf Museum in Claremont, California (where this photo was taken). In the middle section of the trackway, footprints are oriented roughly perpendicular to the apparent direction of animal movement. Scale bar = 10 cm. **B)** Diagram illustrating possible animal motion during track emplacement. Brand and Tang (1991) proposed that the “sideways” orientation implied organism displacement by currents. Drawing modified from Brand and Tang (1991), p. 1203, figure 4I.

Bedding-Plane Sedimentary Structures

Low-relief sedimentary structures, previously interpreted as “slump features,” “ripple marks,” and “rainprints” (McKee, 1945), have been documented on Coconino Sandstone bedding planes. Maithel et al. (2014), however, described elements that appear inconsistent with these interpretations, including “rainprints” in linear bands and “slump marks” on beds that dip notably below the angle of repose. These sedimentary structures are commonly associated with each other on bedding planes, and some have been observed alongside deformation features, so alternative process models should be considered (figure 6).

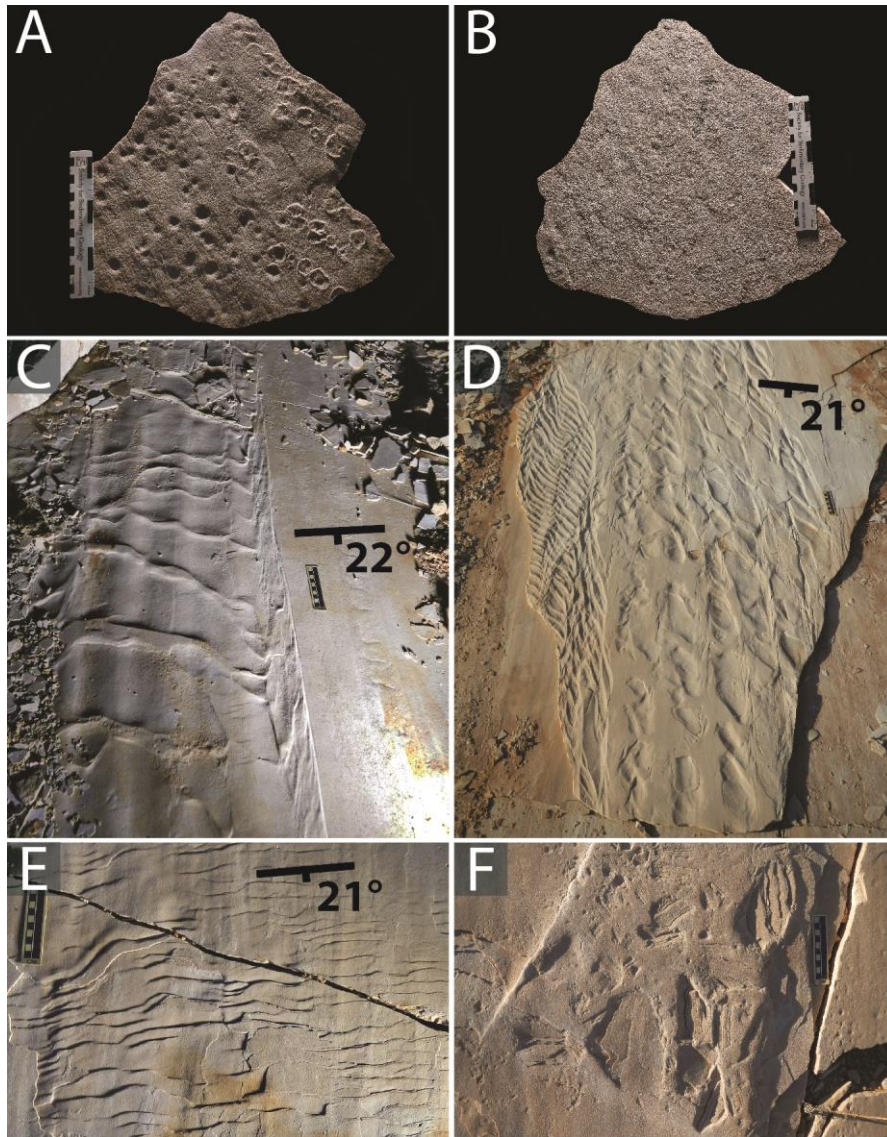


Figure 6: Bedding-plane sedimentary structures observed in outcrops near Ash Fork. The structures are generally shallow and some appear to be associated with deformed bedding. While McKee (1945) interpreted these as slump features, ripple marks, and rainprints, the problems with those models (discussed in text) as well as associated deformation may suggest that different processes produced the structures. Scale bar = 10 cm unless otherwise specified. **A)** Varying “rainprint” morphologies on a single slab. Scale bar = 15 cm. **B)** The underside of the same slab shown in figure 6A. This slab was only ~ 2-3 mm thick, so the absence of these structures on its underside illustrates that they are shallow. Scale bar = 15 cm. **C)** “Slump feature” with associated “ripple marks” oriented roughly parallel to the cross-bed dip. **D)** Extensive “slump-like” feature on a cross-bed dipping at only 21°; notably below the angle of repose for sand. **E)** “Slump feature” exhibiting the “step-like” morphology described by McKee (1945). **F)** Cross-bed that appears to contain clasts of displaced sandstone, which may suggest that at least some of the sediment was lithified before it was deformed. Similar deformation was observed in association with other “slump” structures, which may imply a relationship between depositional and post-depositional processes.

Cross-Bedding

Large-scale cross-beds, which have been interpreted as preserved eolian dune foresets, are some of the most prominent features of the Coconino Sandstone (figure 7). Beds form mostly wedge-planar (McKee, 1974) and planar-tabular (Blakey and Knepp, 1989; Middleton et al., 2003) set geometries, with cross-bed dips oriented generally toward the south (Reiche, 1938) with some variation to the southeast (Blakey and Knepp, 1989) and southwest (Sorauf, 1962). McKee (1945, 1974) suggested that the Coconino dunes were mostly transverse bedforms with localized barchans. However, even though McKee (1945) said that some along-strike bedding plane curvature may suggest barchan dunes, the relatively consistent dip direction probably implies a transverse morphology for most of the sandstone. Furthermore, Sorauf (1962) notes a, “uniform direction of dip in each unit” (p. 106-107) which may imply a straight-crested dune morphology. Johnson (1962) describes the cross-bedding as “barchan-type” but he does not elaborate on how he reached that conclusion.

A wide range of cross-bed dip angles have been published, but most describe the beds as relatively steeply dipping: from 15-30° (Baars, 1961; McKee, 1945; Noble, 1922), up to 34° (McKee, 1974), and as high as 40-60° (Hunt et al., 1995; Santucci and Wall, 1995). Despite the high angles in the literature, Emery et al. (2011) reported strike and dip measurements revealing an average cross-bed dip of 20.2° and range of 3-32°. Coconino Sandstone cross-beds commonly exhibit a tangential form (decreasing in angle near their bases), so this may explain some of the lowest values. Earlier cross-bed data published by Reiche (1938) similarly reveals an average dip of ~ 20°, which is also much lower than most of the literature suggests.

Cross-bed dip-angle measurements should account for the regional dip of the formation, especially where significant structural deformation occurs. A structural dip of $\sim 1.5^\circ$ to the east was measured along the top of the Coconino Sandstone near Seligman (Leonard Brand, pers. comm.). If the cross-beds dip generally toward the south (with some variation, as previously cited), this slight regional dip should probably have minimal impact on the bedding plane measurements, but might introduce some error. On a regional scale, the Coconino Sandstone does not exhibit notable structural dip in an east-west geologic cross section (Blakey, 1988), further suggesting that formation-scale dips should only minimally affect cross-bed dip angle measurements.

Bounding surfaces separate sets of cross-beds in the Coconino Sandstone. These surfaces have been described as laterally extensive (hundreds of meters), horizontal to low angle, and in some areas, associated with a thin bed of fine sand and silt (Middleton et al., 2003). Little has been published on the bounding surfaces in the Coconino Sandstone. In several localities, however, vertebrate trackways are prevalent on these surfaces, which place a constraint on the processes that produced them (Brand, 1996).

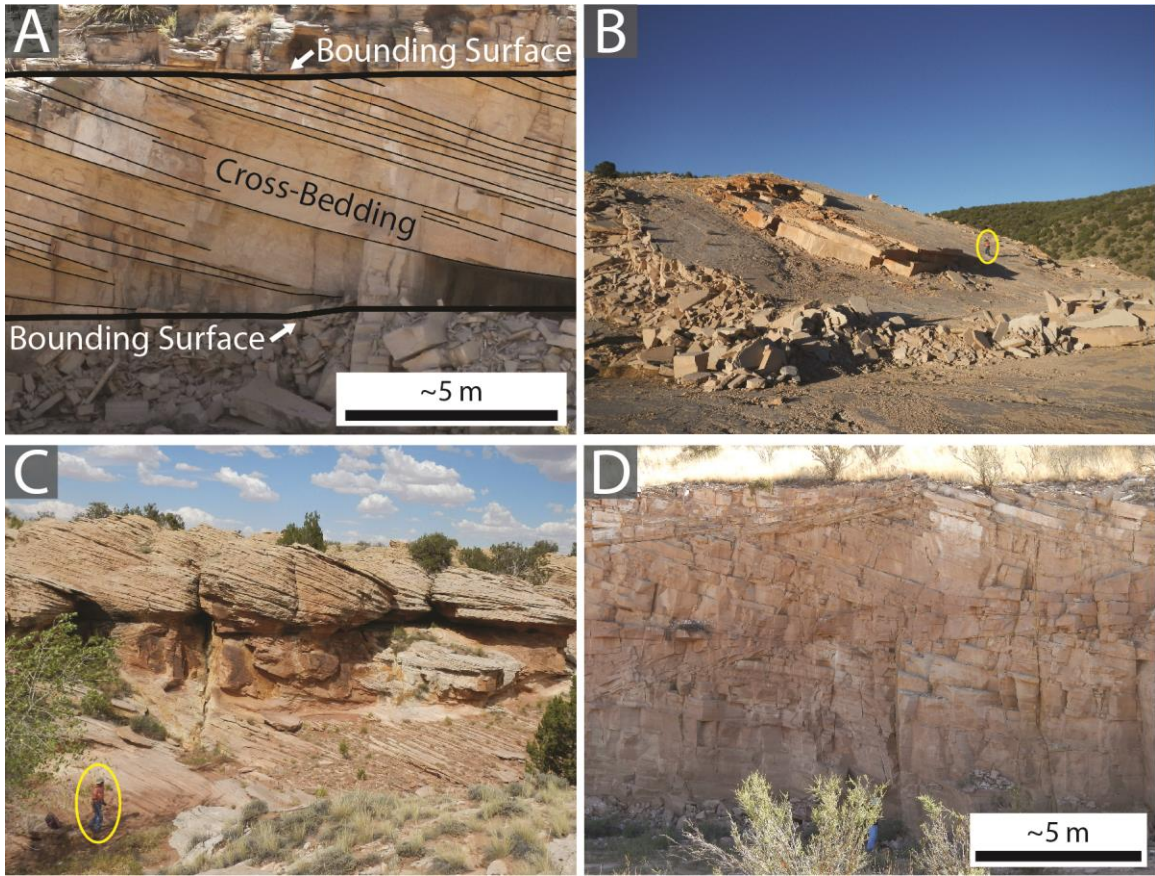


Figure 7: The Coconino Sandstone is characterized by large-scale cross-bedding that is exposed in the Grand Canyon as well as in cliffs, quarries, and washes across northern Arizona. **A)** A cross-bed set defined by upper and lower bounding surfaces at a retired quarry in Chino Wash, near the town of Seligman. Bounding surfaces and bedding planes have been traced on the image. **B)** Cross-bedding exposed in a retired quarry (Santa Cruz Quarry) near the town of Ash Fork. Person in photo (circled) is ~ 1.8 m tall. **C)** Cross-bedding exposed in Five Mile Wash, south of the town of Holbrook. Person in photo (circled) is ~ 1.6 m tall. **D)** Cross-beds exposed in a retired quarry near the town of Ash Fork.

Near the town of Sedona, some Coconino Sandstone cross-beds have been deformed or completely overturned to form parabolic recumbent folds (figure 8). McKee and Bigarella (1979) noted another example of contorted cross-bedding near Flagstaff, but it is unclear whether that folding resembles the Sedona-area deformation.

These recumbent folds often occur between horizontal beds or sets of undeformed cross-beds, and Whitmore et al. (2012) suggested that they may resemble the types I and

II deformation described by Allen and Banks (1972). Similar deformation has been observed in the Sharon Formation (northeast Ohio), which consists of sandstone and conglomerate (although folds were only found in the sandstone). The folding in the Sharon Formation has been interpreted as the result of flash floods in a fluvial environment (Wells et al., 1993). Furthermore, Allen and Banks (1972) suggested that such deformation must occur in “water-saturated” sand (p. 262). Whitmore et al. (2012) ascribed a similar syndepositional subaqueous interpretation to the deformed Coconino Sandstone cross-beds near Sedona.

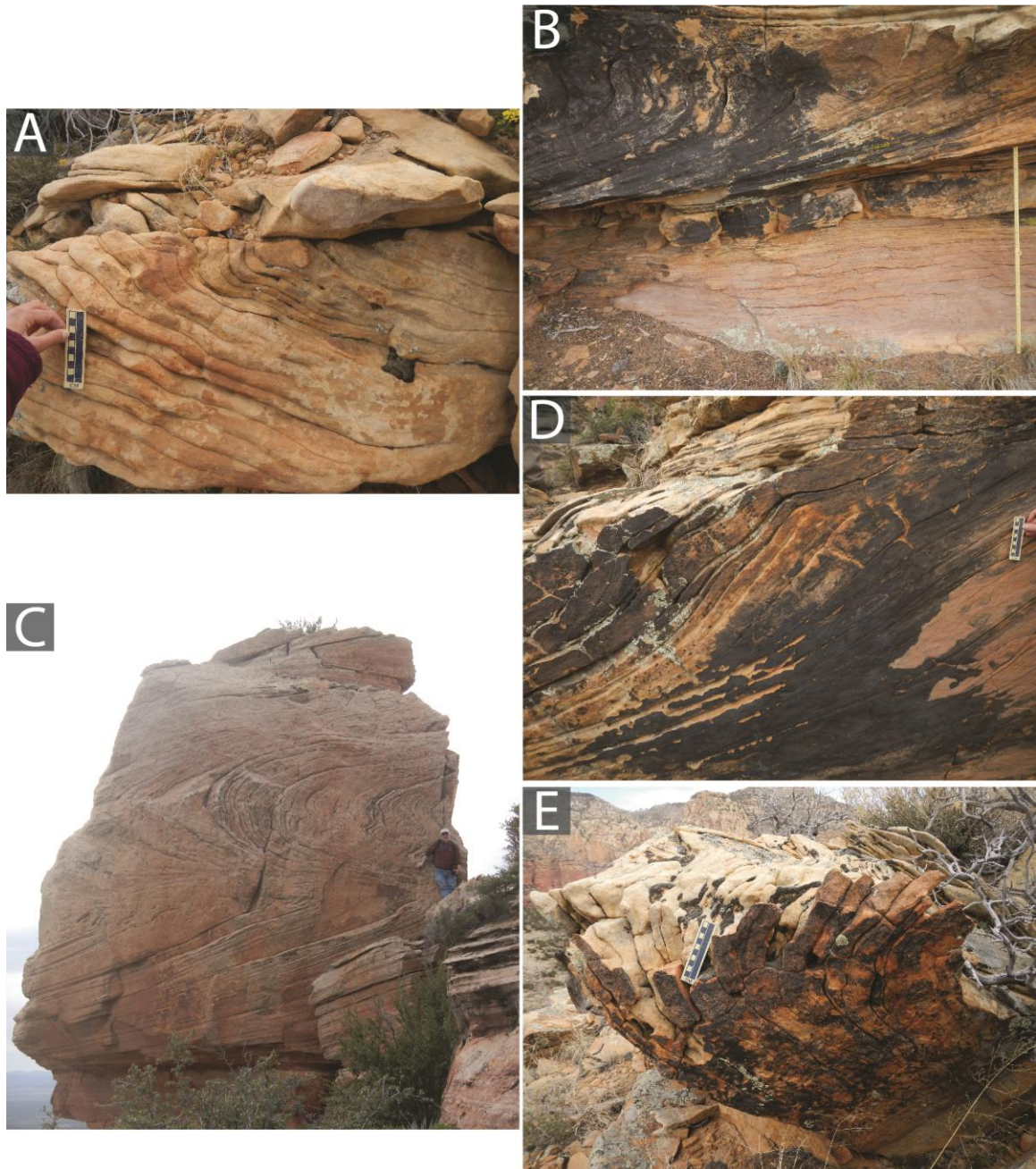


Figure 8: Deformed cross-bedding observed in Coconino Sandstone outcrops near Sedona, Arizona. Whitmore et al. (2012) suggested that the deformation styles may resemble the types I and II deformation described by Allen and Banks (1972). Fold lengths for figures 8B and C were provided by John Whitmore (pers. comm.). **A)** Partially overturned cross-beds exposed on Brins Ridge. Scale bar = 10 cm. **B)** Overturned cross-bedding and underlying low-angle or planar beds on Brins Ridge. This folded zone is almost 400 m long. Scale bar = 1 m. **C)** A recumbent fold at Lizard Head (at least 50 m long; the full extent of the deformation is not visible in the photo). Person in photo is ~ 1.7 m tall. **D, E)** Deformed cross-beds on Brins Ridge. Scale bar = 10 cm.

In cross-bedded sandstones, distinct massive and laminated beds are interpreted as the deposits of fine-scale processes that occur on dune foresets. The massive facies are thought to be grainflow, or avalanche, deposits (Collinson and Thompson, 1989) while the laminated beds are usually interpreted as ripple lamination (“translatent strata”) or grainfall (Kocurek and Dott, 1981). Blakey and Middleton (1983), when discussing the upper Schnebly Hill Formation and lower Coconino Sandstone, referred to climbing translatent strata and a “few beds” formed by grainflow and grainfall. They described the grainflow beds as being “cone shaped” and showed them interfingering with other stratification types near West Fork, north of Sedona (see p. 563, figure 11c of their paper). These facies associations do not resemble cross-beds observed in many other Coconino Sandstone outcrops, so it is possible that the bedding styles reflect unique processes associated with the Schnebly Hill-Coconino transition zone. Blakey and Knepp (1989) mentioned grainflow and grainfall deposits that tangentially approach the base of the cross-bed sets. The authors noted these as the “only facies” in the Coconino and Glorieta Sandstones (p. 329 of their paper). Finally, Middleton et al. (2003) suggested that the majority of the cross-bedding formed as wind ripple deposits, and they also mentioned “wedge-shaped” avalanches. These “avalanche” beds were described as 7.5 cm thick or less and tapering downslope, and they were more prevalent in the thicker cross-bed packages. The authors did not provide any photographs of the grainflow beds, but they did show lamination interpreted as wind ripple deposits. While these references have mentioned possible dune stratification types within the cross-bedding, more work must be done to characterize and interpret the fine-scale depositional processes in the Coconino Sandstone.

Problems and Solutions

When Brand and Tang (1991) suggested that vertebrate trackways in the Coconino Sandstone were formed under water, some argued that their hypothesis was, “at odds with all paleontological and sedimentological evidence” (Hunt et al., 1995, p. 214), and, “doubtful [based] on sedimentological characters” (Santucci and Wall, 1995, p. 92). This confidence in the eolian interpretation was derived from “sedimentological evidence” that had not been adequately tested or verified. Recent studies on Coconino Sandstone sedimentology (Cheung et al., 2010; Cheung et al., 2009; Emery et al., 2011; Maithel et al., 2013, 2014, 2015; Maithel and Whitmore, 2010; Whitmore et al., 2012; Whitmore et al., 2011; Whitmore and Strom, 2009, 2010a, b) have documented attributes that appear incompatible with eolian dune deposition and with previously published descriptions of the sandstone. However, while these recent studies have highlighted broad problems with the eolian model, most did not propose alternative processes to explain “anomalous” data at the cross-bed scale. In short, they have defined problems, but have not provided adequate solutions (table 2).

Table 2: Problems and solutions in Coconino Sandstone research

Proposed Eolian Criteria for the Coconino Sandstone	Observed in Coconino Sandstone (“Problem”)	Alternate Interpretation (“Solution”)
Sand-filled cracks, interpreted as desiccation cracks (Abbott and Cook, 2004; McKee, 1934; Sorauf, 1962; White, 1929)	Sand-filled cracks associated with lateral structures, banding, clast breccias, and orientation relative to the Bright Angel Fault in the Grand Canyon region (Whitmore and Strom, 2010a)	Seismically triggered injectites (Whitmore and Strom, 2010a)
Contorted bedding in a Flagstaff-area outcrop, with deformation ascribed to either dry or wet conditions (McKee and Bigarella, 1979)	Parabolic recumbent folds and other deformed cross-bedding near Sedona (types I and II, after Allen and Banks, 1972; Whitmore et al., 2012)	Syn depositional folding, possibly as a result of strong subaqueous currents and liquefaction (Whitmore et al., 2012)
Trackways; lack of body fossils (McKee, 1934)	Trackways that end abruptly; sideways trackways (Brand and Tang, 1991); footprint quality similar to modern examples in subaqueous (Brand, 1979) or wet (Brand, 1996) sand	Tracks not produced on subaerial bedforms; organisms possibly displaced by currents over subaqueous sand (Brand and Tang, 1991); specific nature of the currents yet to be interpreted
Well-sorted sand (McKee, 1934 and others; see text)	Moderately sorted sand; ranging from well to very poorly sorted (Maithel and Whitmore, 2010; Whitmore and Strom, 2010b)	Not eolian dune deposition; specific processes yet to be interpreted
Well-rounded sand (Blakey and Knepp, 1989)	Sub-rounded to sub-angular sand (after Powers, 1953); larger grains rounded; some sub-angular orthoclase grains (Maithel and Whitmore, 2010; Whitmore and Strom, 2009, 2010b)	Rounded quartz not a diagnostic characteristic of eolian dune sand; feldspars should probably be better-rounded than quartz during eolian transport (Pye and Tsoar, 2009)
Quartz and feldspar common (Pye and Tsoar, 2009); minimal to no muscovite (Moorhouse, 1959).	Mostly quartz sand; some feldspars and trace mica (Maithel and Whitmore, 2010; Whitmore and Strom, 2009)	Subaqueous fluid may explain the presence of mica in the absence of a nearby basement source (Anderson et al., 2017)
Interbedded marine carbonates in some sections (Fisher, 1961)	Dolomite cements, clasts, beds, and ooids observed (Cheung et al., 2010; Cheung et al., 2009; Whitmore and Strom, 2009)	Not eolian dune deposition; specific processes yet to be interpreted
Steeply dipping cross-beds: 15-30° (Baars, 1961; McKee, 1945; Noble, 1922); up to 34° (McKee, 1974); 40-60° (Hunt et al., 1995; Santucci and Wall, 1995)	Cross-bed dips notably below the angle of repose (average: ~ 20°; Emery et al., 2011; Reiche, 1938)	Dip angle alone not a diagnostic criterion for depositional fluid (Kocurek and Dott, 1981; Loope, 1984); below-angle-of-repose beds are not likely unmodified grainflow deposits (Maithel et al., 2015); specific processes yet to be interpreted
Slump marks (McKee, 1945)	“Slump marks” on beds dipping at angles below the angle of repose (Maithel et al., 2014)	Possibly not slump features associated with angle-of-repose eolian grainflows; specific processes yet to be interpreted
Rainprints (McKee, 1945)	Some prints oriented in linear bands (Maithel et al., 2014)	Possibly not rainprints; specific processes yet to be interpreted
Distinct grainfall, grainflow, and wind ripple stratification (Blakey and Knepp, 1989; Blakey and Middleton, 1983; Middleton et al., 2003)	Laterally extensive cross-beds with relatively low dip angles and lack of distinct down-dip pinch outs (Maithel et al., 2013, 2015)	Beds described by Maithel et al. (2013, 2015) probably not “normal” eolian grainflows; specific processes yet to be interpreted
Summary	Numerous problems with the eolian model have been observed.	Alternative process models for cross-bed deposition have not yet been developed.

Toward a Better Model

The problems with the current eolian depositional model, therefore, provide a premise for additional research to develop solutions. While new interpretations have been suggested for some features, such as the sand-filled cracks (Whitmore and Strom, 2010a), alternative process models for cross-bed deposition have not been explored. Previous references to eolian dune stratification in the Coconino Sandstone (Blakey and Knepp, 1989; Blakey and Middleton, 1983; Middleton et al., 2003) are brief, so more work must be done to develop depositional models. The goal of this study is to use textures and sedimentary structures in the Coconino Sandstone to better interpret the fine-scale processes that may have deposited its cross-bedding. These processes will serve as a critical piece in the greater puzzle of the formation's depositional environment.

References

- Abbott, L., and Cook, T., 2004, *Hiking the Grand Canyon's Geology*, Seattle, WA, The Mountaineer's Books.
- Alf, R. M., 1968, A spider trackway from the Coconino Formation, Seligman, Arizona: *Bulletin of the Southern California Academy of Sciences*, v. 67, no. 2, p. 125-128.
- Allen, J. R. L., and Banks, N. L., 1972, An interpretation and analysis of recumbent-folded deformed cross-bedding: *Sedimentology*, v. 19, no. 257-283.
- Anderson, C. J., Struble, A., and Whitmore, J. H., 2017, Abrasion resistance of muscovite in aeolian and subaqueous transport experiments: *Aeolian Research*, v. 24, p. 33-37.
- Baars, D. L., 1961, Permian blanket sandstones of Colorado Plateau, *in* Peterson, J. A., and Osmond, J. C., eds., *Geometry of Sandstone Bodies*: Tulsa, Oklahoma, American Association of Petroleum Geologists.
- , 1979, The Permian System, *in* Baars, D. L., ed., *Permianland*, Four Corners Geological Society Guidebook, Ninth Field Conference.

- Bartlett, R., and Elliott, D. K., 2015, Pit-trapping predation strategy: the first record of ant-lion pits in the fossil record: Geological Society of America Abstracts with Programs, v. 47, no. 7, p. 346.
- Billingsley, G. H., and Hampton, H. M., 2000, Geologic Map of the Grand Canyon 30' x 60' Quadrangle, Coconino and Mohave Counties, Northwestern Arizona: United States Geological Survey, scale 1:100,000.
- Blakey, R. C., 1979a, Stratigraphy of the Supai Group (Pennsylvanian-Permian), Mogollon Rim, Arizona, *in* Beus, S. S., and Rawson, R. R., eds., Carboniferous stratigraphy in the Grand Canyon country, northern Arizona and southern Nevada, American Geological Institute, p. 89-104.
- , 1979b, Lower Permian stratigraphy of the southern Colorado Plateau, *in* Baars, D. L., ed., Permianland, Four Corners Geological Society Guidebook, Ninth Field Conference.
- , 1980, Pennsylvanian and early Permian paleogeography, southern Colorado Plateau and vicinity, *in* Fouch, T. D., and Magathan, E. R., eds., Paleozoic paleogeography of the west-central United States: Denver, Colorado, The Rocky Mountain Section, Society of Economic Paleontologists and Mineralogists.
- , 1988, Basin tectonics and erg response: *Sedimentary Geology*, v. 56, p. 127-151.
- , 1990, Stratigraphy and geologic history of Pennsylvanian and Permian rocks, Mogollon Rim region, central Arizona and vicinity: *Geological Society of America Bulletin*, v. 102, p. 1189-1217.
- , 2003, Supai Group and Hermit Formation, *in* Beus, S. S., and Morales, M., ed., *Grand Canyon Geology*: New York, Oxford University Press, p. 136-162.
- Blakey, R. C., and Knepp, R., 1989, Pennsylvanian and Permian geology of Arizona, *in* Jenney, J. P., and Reynolds, S. J., eds., *Arizona Geological Society Digest*, v. 17, p. 313-347.
- Blakey, R. C., and Middleton, L. T., 1983, Permian shoreline eolian complex in central Arizona: dune changes in response to cyclic sealevel changes, *in* Brookfield, M. E., and Ahlbrandt, T. S., eds., *Eolian Sediments and Processes*, Elsevier.
- Braddy, S. J., 1995, The ichnotaxonomy of the invertebrate trackways of the Coconino Sandstone (lower Permian), northern Arizona, *in* Lucas, S. G., and Heckert, A. B., eds., *Early Permian Footprints and Facies*: Albuquerque, New Mexico Museum of Natural History and Science Bulletin No. 6, p. 219-224.
- Brady, L. F., 1939, Tracks in the Coconino Sandstone compared with those of small living arthropods: *Plateau*, v. 12, no. 2, p. 32-34.

- , 1947, Invertebrate tracks from the Coconino Sandstone of northern Arizona: *Journal of Paleontology*, v. 21, no. 5, p. 466-472.
- Brand, L. R., 1979, Field and laboratory studies on the Coconino Sandstone (Permian) vertebrate footprints and their paleoecological implications: *Palaeogeography, Palaeoclimatology, Palaeoecology*, v. 28, p. 25-38.
- , 1996, Variations in salamander trackways resulting from substrate differences: *Journal of Paleontology*, v. 70, no. 6, p. 1004-1010.
- Brand, L. R., and Kramer, J. M., 1996, Underprints of vertebrate and invertebrate trackways in the Permian Coconino Sandstone in Arizona: *Ichnos*, v. 4, p. 225-230.
- Brand, L. R., and Tang, T., 1991, Fossil vertebrate footprints in the Coconino Sandstone (Permian) of northern Arizona: evidence for underwater origin: *Geology*, v. 19, p. 1201-1204.
- Cheung, S., Strom, R., and Whitmore, J. H., 2010, Widespread dolomite in the Coconino Sandstone, Arizona, USA: *Geological Society of America Abstracts with Programs*, v. 42, no. 5, p. 108.
- Cheung, S. P., Strom, R., Whitmore, J. H., and Garner, P. A., 2009, Occurrence of dolomite beds, clasts, ooids, and unidentified microfossils in the Coconino Sandstone, northern Arizona: *Geological Society of America Abstracts with Programs*, v. 41, no. 7, p. 119.
- Citton, P., Sacchi, E., and Nicosia, U., 2012, Sometimes they come back: recovery and reinterpretation of a trackway slab from the Permian Coconino Sandstone of the southwestern United States: *Ichnos*, v. 19, p. 165-174.
- Collinson, J. D., and Thompson, D. B., 1989, *Sedimentary Structures*, Chapman & Hall, 207 p.
- Dake, C. L., 1920, The pre-Moenkopi (pre-Permian?) unconformity of the Colorado Plateau: *Journal of Geology*, v. 28, no. 1, p. 61-74.
- Darton, N. H., 1910, *A Reconnaissance of Parts of Northwestern New Mexico and Northern Arizona*: U.S. Geological Survey Bulletin 435.
- Dunbar, C. O., Baker, A. A., Cooper, G. A., King, P. B., McKee, E. D., Miller, A. K., Moore, R. C., Newell, N. D., Romer, A. S., Sellards, E. H., Skinner, J. W., Thomas, H. D., and Wheeler, H. E., 1960, Correlation of the Permian formations of North America: *Geological Society of America Bulletin*, v. 71, p. 1763-1806.
- Elcock, S., 1993, *A study of the early Permian Coconino Sandstone, Arizona* [BSc thesis]: University of Wolverhampton, 79 p.

- Elston, D. P., and DiPaolo, W. D., 1979, Pennsylvanian-Permian Stratigraphy of the Sedona area and environs, central and northern Arizona, *in* Baars, D. L., ed., Permianland, Four Corners Geological Society Guidebook, Ninth Field Conference.
- Emery, M. K., Maithel, S. A., and Whitmore, J. H., 2011, Can compaction account for lower-than-expected cross-bed dips in the Coconino Sandstone (Permian), Arizona?: Geological Society of America Abstracts with Programs, v. 43, no. 5, p. 430.
- Erickson, B. R., Halvorson, H. E., and Kramer, J. M., 2011, Lower Permian Tracks and Traces in the Science Museum of Minnesota, St. Paul, Minnesota, The Science Museum of Minnesota, Ichnofossils III.
- Fisher, W. L., 1961, Upper Paleozoic and lower Mesozoic stratigraphy of Parashant and Andrus Canyons, Mohave County, Northwestern Arizona [PhD dissertation]: University of Kansas, 345 p.
- Garzanti, E., 2017, The maturity myth in sedimentology and provenance analysis: *Journal of Sedimentary Research*, v. 87, p. 353-365.
- Garzanti, E., Resentini, A., Andò, S., Vezzoli, G., Pereira, A., and Vermeesch, P., 2015, Physical controls on sand composition and relative durability of detrital minerals during ultra-long distance littoral and aeolian transport (Namibia and southern Angola): *Sedimentology*, v. 62, p. 971-996.
- Gilmore, C. W., 1926, Fossil footprints from the Grand Canyon: *Smithsonian Miscellaneous Collections*, v. 77, no. 9, p. 1-41.
- , 1927a, Collecting fossil footprints in the Grand Canyon, Arizona: *Smithsonian Miscellaneous Collections*, v. 78, no. 7, p. 45-48.
- , 1927b, Fossil footprints from the Grand Canyon: second contribution: *Smithsonian Miscellaneous Collections*, v. 80, no. 3, p. 1-78.
- , 1928, Fossil footprints from the Grand Canyon: third contribution: *Smithsonian Miscellaneous Collections*, v. 80, no. 8, p. 1-16.
- Goudie, A. S., and Watson, A., 1981, The shape of desert sand dune grains: *Journal of Arid Environments*, v. 4, p. 185-190.
- Hunt, A. P., Lucas, S. G., and Lockley, M. G., 1995, Paleozoic tracksites of the western United States, *in* Lucas, S. G., and Heckert, A. B., eds., *Early Permian Footprints and Facies: Albuquerque, New Mexico Museum of Natural History and Science Bulletin No. 6*, p. 213-217.

- Hunt, A. P., and Santucci, V. L., 1998a, An identification key to Permian tetrapod tracks from Grand Canyon National Park: National Park Service Paleontological Research, v. 3, p. 97-98.
- , 1998b, Taxonomy and ichnofacies of Permian tetrapod tracks from Grand Canyon national park, Arizona: National Park Service Paleontological Research, v. 3, p. 94-96.
- , 2001, An unusual tetrapod track morphology from the Permian Coconino Sandstone, Grand Canyon national Park, Arizona, *in* Santucci, V. L., and McClelland, L., eds., Proceedings of the 6th Fossil Resource Conference, p. 44-47.
- Johnson, M. R., 1994, Thin section grain size analysis revisited: *Sedimentology*, v. 41, p. 985-999.
- Johnson, P. W., 1962, Water in the Coconino Sandstone for the Snowflake-Hay Hollow area, Navajo county, Arizona: Contributions to the Hydrology of the United States, Geological Survey Water-Supply Paper 1539-S.
- Khalaf, F. I., and Gharib, I. M., 1985, Roundness parameters of quartz grains of recent aeolian sand deposits in Kuwait: *Sedimentary Geology*, v. 45, p. 147-158.
- Kocurek, G., and Dott, R. H., 1981, Distinctions and uses of stratification types in the interpretation of eolian sand: *Journal of Sedimentary Petrology*, v. 51, no. 2, p. 579-595.
- Lockley, M., and Hunt, A. P., 1995, Dinosaur tracks and other fossil footprints of the Western United States, New York, Columbia University Press.
- Lockley, M. G., Loope, D. B., and Brand, L. R., 1992, Comment and reply on "Fossil vertebrate footprints in the Coconino Sandstone (Permian) of northern Arizona: evidence for underwater origin": *Geology*, v. 20, no. 7, p. 666-670.
- Loope, D. B., 1984, Eolian origin of upper Paleozoic sandstones, southeastern Utah: *Journal of Sedimentary Petrology*, v. 54, p. 563-580.
- Lundy, W. L., 1973, The stratigraphy and evolution of the Coconino Sandstone of northern Arizona [MS thesis]: University of Tulsa, 106 p.
- Maithele, S. A., Brand, L., and Whitmore, J. H., 2013, Morphology of avalanche beds in the Coconino Sandstone at Chino Wash, Seligman, Arizona: *Geological Society of America Abstracts with Programs*, v. 45, no. 7, p. 126.
- , 2014, "Ripple Marks," "Slump Features," and "Rainprints" in the Coconino Sandstone near Ash Fork, Arizona: *Geological Society of America Abstracts with Programs*, v. 46, no. 6, p. 768.

- , 2015, Morphological analysis of "grainflow" cross-strata in the Coconino Sandstone (Permian), Arizona: Geological Society of America Abstracts with Programs, v. 47, no. 7, p. 589.
- Maithel, S. A., and Whitmore, J. H., 2010, Textural analysis of the Coconino Sandstone, Chino Point, Arizona: Geological Society of America Abstracts with Programs, v. 42, no. 5, p. 426.
- Marsland, P. S., and Woodruff, J. G., 1937, A study of the effects of wind transportation on grains of several minerals: *Journal of Sedimentary Petrology*, v. 7, no. 1, p. 18-30.
- McKee, E. D., 1934, The Coconino Sandstone - its history and origin: Carnegie Institution of Washington Publication 440, p. 77-115.
- , 1945, Small-scale structures in the Coconino Sandstone of northern Arizona: *Journal of Geology*, v. 53, no. 5, p. 313-325.
- , 1947, Experiments on the development of tracks in fine cross-bedded sand: *Journal of Sedimentary Petrology*, v. 17, no. 1, p. 23-28.
- , 1974, Paleozoic Rocks of Grand Canyon: *Geology of Northern Arizona, Part I*, p. 119-154.
- McKee, E. D., and Bigarella, J. J., 1979, Ancient sandstones considered to be eolian, *in* McKee, E. D., ed., *A Study of Global Sand Seas*: Honolulu, HI, University Press of the Pacific, p. 187-238.
- Middleton, L. T., Elliott, D. K., and Morales, M., 2003, Coconino Sandstone, *in* Beus, S. S., and Morales, M., eds., *Grand Canyon Geology*: New York, Oxford University Press, p. 163-179.
- Miller, F. K., and McKee, E. H., 1971, Thrust and strike-slip faulting in the Plomosa Mountains, southwestern Arizona: *Geological Society of America Bulletin*, v. 82, p. 717-722.
- Millhouse, A. M., 2009, Analysis of trackways in the Permian Coconino Sandstone of Ash Fork and Grand Canyon, Arizona [MS thesis]: Northern Arizona University.
- Moorhouse, W. W., 1959, *The Study of Rocks in Thin Section*, New York, NY, Harper & Row, 514 p.
- Noble, L. F., 1922, A section of the Paleozoic formations of the Grand Canyon at the Bass trail: *U.S. Geological Survey Professional Paper*, v. 131-B, p. 23-73.
- Powers, M. C., 1953, A new roundness scale for sedimentary particles: *Journal of Sedimentary Petrology*, v. 23, no. 2, p. 117-119.

- Pye, K., and Tsoar, H., 2009, *Aeolian Sand and Sand Dunes*, Berlin, Springer-Verlag, 458 p.
- Reiche, P., 1938, An analysis of cross-lamination the Coconino Sandstone: *Journal of Geology*, v. 46, no. 7, p. 905-932.
- Richard, S. M., Reynolds, S. J., Spencer, J. E., and Pearthree, P. A., 2000, *Geologic Map of Arizona: Arizona Geological Survey, Map 35, scale 1:1,000,000.*
- Santucci, V. L., and Wall, W. P., 1995, Climbing up sand dunes in the Permian: new tracksites from Grand Canyon national park, Arizona, *in* Santucci, V. L., and McClelland, L., eds., *National Park Service Paleontological Research Technical Report, Volume 2: Denver, CO, U.S. National Park Service Natural Resources Publication Office*, p. 91-93.
- Sorauf, J. E., 1962, *Structural geology and stratigraphy of the Whitmore area, Mohave County, Arizona [PhD dissertation]: University of Kansas*, 361 p.
- Stokes, W. M. L., 1961, Fluvial and eolian sandstone bodies in Colorado Plateau, *in* Peterson, J. A., and Osmond, J. C., eds., *Geometry of Sandstone Bodies: Tulsa, Oklahoma, American Association of Petroleum Geologists.*
- Stone, P., Howard, K. A., and Hamilton, W., 1983, Correlation of metamorphosed Paleozoic strata of the southeastern Mojave Desert region, California and Arizona: *Geological Society of America Bulletin*, v. 94, p. 1135-1147.
- Sumner, C. D., 1999, *Stratigraphy of the northern depositional margin of the Coconino Sandstone, northern Arizona and southern Utah [MS thesis]: Stephen F. Austin State University*, 161 p.
- Swezey, C., 1998, The identification of eolian sands and sandstones: *C. R. Acad. Sci. Paris, Sciences de la Terre et des planetes / Earth and Planetary Sciences*, v. 327, p. 513-518.
- Twenter, F. R., and Metzger, D. G., 1963, *Geology and Ground Water in Verde Valley - the Mogollon Rim Region, Arizona, Washington, D. C., United States Government Printing Office, Geological Survey Bulletin 1177, 132 p.*
- Wells, N. A., Richards, S. S., Peng, S., Keattch, S. E., Hudson, J. A., and Copsey, C. J., 1993, Fluvial processes and recumbently folded crossbeds in the Pennsylvanian Sharon Conglomerate in Summit county, Ohio, U.S.A.: *Sedimentary Geology*, v. 85, p. 63-83.
- Welton, J. E., 1984, *SEM Petrology Atlas, Tulsa, Oklahoma, The American Association of Petroleum Geologists, The AAPG methods in exploration series, no. 4, 237 p.*

- White, D., 1929, Flora of the Hermit Shale, Grand Canyon, Arizona, Washington, D.C., Carnegie Institution of Washington, Publication 405.
- Whitmore, J. H., Forsythe, G., and Garner, P. A., 2012, Significance of parabolic recumbent folds in Permian rocks, Sedona, Arizona: Geological Society of America Abstracts with Programs, v. 44, no. 7, p. 556.
- Whitmore, J. H., Forsythe, G., Strom, R., and Garner, P. A., 2011, Unusual bedding styles for the Coconino Sandstone (Permian), Arizona: Geological Society of America Abstracts with Programs, v. 43, no. 5, p. 433.
- Whitmore, J. H., and Peters, R. A., 1999, Reconnaissance study of the contact between the Hermit Formation and the Coconino Sandstone, Grand Canyon, Arizona: Geological Society of America Abstracts with Programs, v. 31, no. 7, p. A-235.
- Whitmore, J. H., and Strom, R., 2009, Petrographic analysis of the Coconino Sandstone, Northern and Central Arizona: Geological Society of America Abstracts with Programs, v. 41, no. 7, p. 122.
- , 2010a, Sand injectites at the base of the Coconino Sandstone, Grand Canyon, Arizona (USA): Sedimentary Geology, v. 230, p. 46-59.
- , 2010b, Textural trends in the Coconino Sandstone, central and northern Arizona, USA: Geological Society of America Abstracts with Programs, v. 42, no. 5, p. 428.

CHAPTER TWO

DUNE STRATIFICATION TYPES: FINE-SCALE SEDIMENTATION

PROCESSES AND THEIR DEPOSITS

Cross-bedded sandstone interpretations have historically been based on various petrographic, sedimentological, and paleontological parameters. In 1977, Hunter was the first to characterize fine-scale processes on modern eolian dunes and develop criteria by which these could be recognized in the rock record. Since Hunter's paper (1977), additional studies were conducted on subaqueous bedforms (Hunter, 1985b; Hunter and Kocurek, 1986), and bedding-scale facies, or *dune stratification types*, became a powerful tool for interpreting sandstones (Hunter, 1981; Kocurek and Dott, 1981; Swezey, 1998). The characterization of dune stratification types focuses on *processes over fluids* and provides context for sedimentary data, and should, therefore, be used alongside other criteria to develop models for cross-bed deposition.

Fluids, Processes, and Environments in Cross-Bedded Sandstone Research

To interpret cross-bedded sandstones, we must first distinguish between depositional *fluids*, *processes*, and *environments*. Wind, water, and ice are the primary *fluids* that transport and deposit sediment. Specific transport *processes* may occur within each fluid, and the nature of these processes can vary based on flow velocity, fluid viscosity, surface roughness, and sediment parameters. Furthermore, depositional *environments* may contain multiple sedimentary processes and fluids (figure 1). An “eolian environment,” for example, can refer to a desert with wind-deposited dunes as well as interdunal ponds and other subaqueous facies.

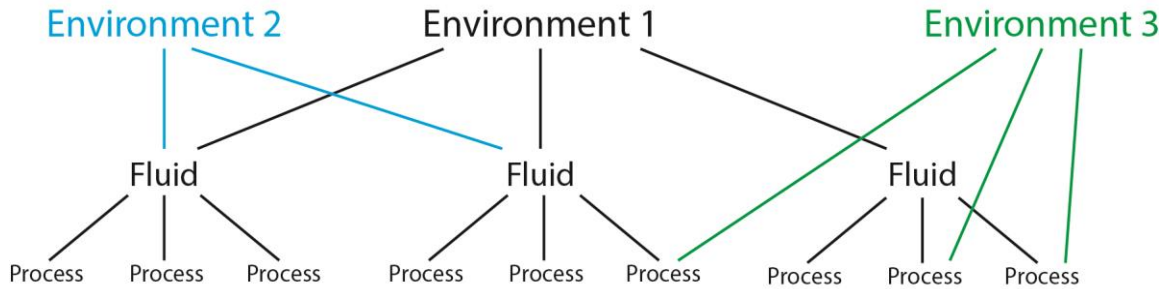


Figure 1: Simplified diagram illustrating the general relationship between sedimentary environments, fluids, and processes. A given environment may include multiple fluids and processes, and some of these fluids and processes can occur in more than one environment.

Select historical papers have fueled debate over whether cross-bedded sandstones were deposited by eolian or subaqueous processes (Freeman and Visher, 1975; McKee, 1934; McKee and Bigarella, 1979; Steidtmann, 1974; Thompson, 1949; Walker and Harms, 1972), citing criteria such as quartz/feldspar/mica composition, grain size, sorting, dip angles, bedding-plane sedimentary structures, and body/trace fossils (when applicable). A more recent study by Maithel et al. (2015) revisited this discussion while characterizing textures and mineral composition in the Permo-Triassic Hopeman Sandstone (Scotland). However, questions arose over the utility of certain data for distinguishing between wind and water transport.

One example of such a criterion is cross-bed dip angle. High angles (at or near the angle of repose for sand: $\sim 30\text{-}34^\circ$) were previously invoked as evidence for eolian deposition, while lower angles were thought to represent subaqueous processes (e.g., McKee, 1934; Freeman and Visher, 1975). When lower-than-expected dips were observed in “eolian” sandstones, the assumed angle reduction was explained by compaction (Glennie, 1972; McKee and Bigarella, 1979; Rittenhouse, 1972; Walker and

Harms, 1972). Eventually, some began to doubt the efficacy of dip angle for interpreting eolian versus subaqueous deposition. According to Kocurek and Dott (1981),

“Foresets formed by [eolian] processes other than avalanching (grainfalls and wind ripple migration) are *necessarily* below the angle of repose. Much of the cross-stratification formed on the lower portions of a dune – that portion of the dune most likely to be preserved – is at angles from less than the angle of repose to near horizontal” (p. 581, emphasis theirs).

Loope (1984) also expressed concern about using dip angle as a diagnostic fluid criterion:

“As a result of the different processes that operate on the lee side of eolian dunes, foreset dip angle and stratification type are likely to vary widely within a single eolian crossbed set... Such variation in foreset dip, stratification type, and deformation style can be seen within many crossbed sets in the Cedar Mesa. Criteria based on these features cannot be used to divide the rocks into distinct genetic units” (p. 576).

Furthermore, others documented experimentally that steep dip angles could be produced on subaqueous bedforms (Hunter, 1985b; Hunter and Kocurek, 1986).

This observed variation in dip angle can be attributed to different *processes* that transport sediment over dune foresets. Angle-of-repose dips are generated by grainflows, which occur on slipfaces in air (figure 2) and underwater, and deposit comparably steep cross-beds in both fluids (since the post-avalanche angle of repose is the same; Allen, 1970; Carrigy, 1970; Hunter, 1985b). Lower-angle dips may suggest that the beds were not deposited by grainflows, or at least not by "normal," unworked grainflows. For this reason, we might expect some lower angles on eolian dunes and some relatively high angles on subaqueous bedforms (e.g., Hunter, 1977; 1985b; Hunter and Kocurek, 1986). Dip angle, therefore, is a useful criterion not for recognizing depositional fluids or environments, but for interpreting *processes*. Defining the interpretive power of dip angle and other sediment parameters will therefore make our sandstone models more robust (table 1).

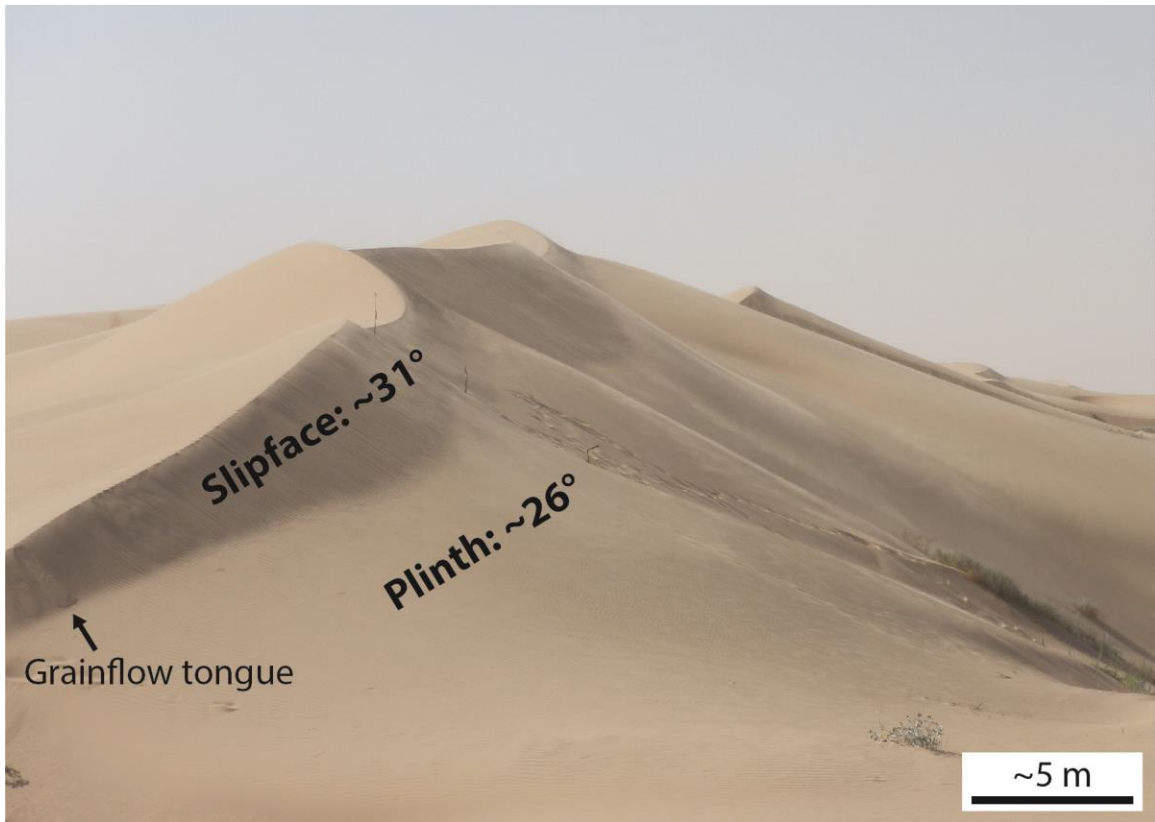


Figure 2: Modern eolian dune in the Algodones Dune Field, at the Imperial Sand Dunes Recreation Area of Southern California. Note the difference in dip angle between the steep, grainflow-dominated slipface and the less-steep plinth (Bagnold, 1954b) on a single foreset. This change in dip comes from a change in the fine-scale depositional processes on the dune: angle-of-repose grainflows on the slipface and wind ripple migration on the plinth. Dip angles were measured by sighting with a Brunton compass in the field.

Table 1: Interpretive scale of common cross-bedded sandstone descriptors

Sedimentological Criterion	Possible Interpretation(s) of the Data
Presence of Mica	Fluid (Anderson et al., 2017); proximity to a micaceous source
Grain Frosting	Fluid; diagenesis (Kuenen and Perdok, 1962; Pye and Tsoar, 2009)
Grain Rounding	Fluid; mineral hardness (Garzanti, 2017; Garzanti et al., 2015)
Grain Size	Process (Allen, 1984; Allen and Narayan, 1964; Hunter, 1977; Hunter and Kocurek, 1986; Kleinhans, 2004); very large grains exclude wind as a fluid (Bagnold, 1954b)
Sorting	Process; poorly sorted sediment may exclude wind as a fluid (Bagnold, 1954b)
Dip Angle	Process (Hunter, 1977, 1985b; Hunter and Kocurek, 1986)
Lateral extent of cross-strata	Process (Buck, 1985); possibly fluid (Hunter, 1985b)
Along-dip cross-bed curvature	Process (Allen, 1965; Hunter, 1985b; Hunter and Kocurek, 1986; Imbrie and Buchanan, 1965)

Each individual parameter is limited in its interpretive scale. Most of the commonly cited cross-bedded sandstone criteria should be used to interpret processes, and may not, on their own, provide evidence for specific depositional fluids.

It is important to note that processes, fluids, and environments do not exist independently: certain processes are often associated with specific fluids and environments. Furthermore, a given fluid constrains the range of processes that may occur and can exclude some environments. Evidence for a fluid or process, therefore, should be used alongside other criteria to develop depositional models. In the dip-angle example above, eolian grainflows should dip at or near the angle of repose. Lower dips

might imply that the beds were not deposited by grainflows, or that they were deposited in another fluid (water) with a different range of allowable processes.

Sorting provides another illustration of this concept. Traditionally, well-sorted sand is used as evidence for eolian deposition due to the narrow distribution of particle sizes transported by the wind (Bagnold, 1954b). While eolian *dune* sand should be generally well sorted, interdunal areas and other facies within eolian environments may contain poorly sorted sediment. Consequently, sorting can be a useful criterion for interpreting depositional *fluid*, as long as the data are placed in their appropriate context. The same holds true for most of the descriptors listed in table 1: invoking certain processes may constrain fluid interpretations (and vice versa), and both have implications for environmental models.

Skepticism over sedimentological criteria may, therefore, result from poor differentiation between environments, fluids, and processes in cross-bedded sandstone research. Many of the early “eolian-versus-subaqueous” sandstone papers presented process-scale data while making fluid- or environment-scale interpretations (table 1). Once certain textures and sedimentary structures were deemed ineffective for distinguishing fluids/environments, interest in the criteria seemed to wane. However, many of these parameters are, *in context*, very useful for interpreting depositional *processes* (Buck, 1985; Kocurek and Dott, 1981; Swezey, 1998).

This is where dune stratification types come in. Differentiating processes at the cross-bed level provides a context for fine-scale data such as dip angle and texture. While individual features have limited interpretive power, building a suite of evidence for processes and fluids can eventually lead to an environment. These fine depositional

processes therefore lay the foundation for larger-scale models, and may serve as an important tool for deciphering cross-bedded sands in the rock record.

Depositional Processes on Dunes

When air or water flows over a dune bedform, sediment is transported and deposited on the foreset by fine-scale processes (figure 3). These processes produce the three primary dune stratification types: grainfall, grainflow, and translant strata/ripple lamination. As sand is discharged over the dune brink, it falls onto the upper foreset in a process called *grainfall*. This grainfall deposition steepens the slope until it reaches the angle of repose, at which point the slope fails in a *grainflow*. In addition to grainfall and grainflow, *ripple migration* may move sand laterally across the foreset or even upslope, depending on flow conditions. The steeply dipping part of the dune foreset where grainflows occur is called the *slipface*, while Bagnold (1954b) defined the lower foreset beneath the slipface as the *plinth* (based on a seif dune profile, but could reasonably apply to other dune morphologies). Cross-beds, which are interpreted as preserved dune foresets, should display the textures and spacial distribution characteristic of each of these processes.

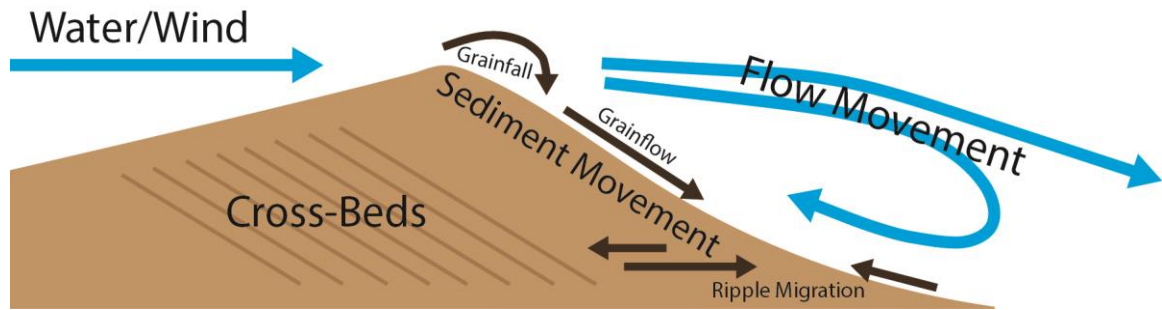


Figure 3: Diagram illustrating flow and grain trajectories over a dune bedform and their theoretical relationship to cross-bed deposition. The fine-scale sediment transport processes deposit characteristic textures and structures that may be preserved in sandstones.

Dune Stratification Types

Recognizing diagnostic parameters of each stratification type may therefore aid in the interpretation of cross-bedded sandstones. Here I review characteristics of grainfall, grainflow, and ripple lamination observed on modern dune bedforms (table 2). By distinguishing features derived from these processes, we will be able to more effectively classify similar deposits in ancient units.

Table 2: Overview of the three primary dune sedimentation processes and their deposits

	Grainfall	Grainflow	Ripple Lamination
Process	Grains settling onto foreset	Angle-of-repose sediment gravity flow	Traction deposition from ripple migration
Distribution	Upper foreset; farther down dip on some subaqueous bedforms (Anderson, 1988; Hunter, 1985a; Hunter and Kocurek, 1986; McDonald and Anderson, 1995; Nickling et al., 2002; Sutton et al., 2013)	Slipface (Hunter, 1977, 1985b; Hunter and Kocurek, 1986)	Commonly plinth (Bagnold, 1954b) but may occur anywhere on foreset (Hunter, 1977)
Texture	Indistinctly laminated (Hunter, 1977)	Massive; faint lamination possible (Hunter, 1977)	Laminated (Hunter, 1977)
Grain Size	Relatively fine-grained (Kocurek and Dott, 1981); may fine down dip, with vertical grading possible (Fryberger and Schenk, 1981)	Relatively coarse-grained (Kocurek and Dott, 1981); coarsens down dip (Allen and Narayan, 1964; Hunter, 1977; Hunter and Kocurek, 1986; Kleinhans, 2004)	Vertical grading within laminae (Kocurek and Dott, 1981)
Porosity	Intermediate (Hunter, 1977)	High (Allen, 1972; Hunter, 1977; Hunter and Kocurek, 1986)	Low (Hunter, 1977)
Dip Angle	Usually below the angle of repose (Hunter, 1977)	At or close to the angle of repose (Hunter, 1977; Hunter and Kocurek, 1986)	Usually below the angle of repose (Hunter, 1977)

Grainfall

Grainfall is deposited as grains are discharged over the brink of the dune and settle onto the lee face. This process generates a “bulge” of sediment a short distance from the dune brink (Anderson, 1988; McDonald and Anderson, 1995; Sutton et al., 2013). Distribution of grainfall depends largely on the nature of the fluid and flow over the bedform: on eolian dunes, grain trajectories place most grainfall deposition (84-99%) within two meters of the brink (Nickling et al., 2002), but this distance may vary with wind speed (Nield et al., 2017). The limited-distance threshold probably suggests that grainfall could be deposited at the base of small dunes, but not at the base of large dunes (Hunter, 1977; Kocurek and Dott, 1981). Theoretically, the same grainfall distribution might be expected on subaqueous dunes under low flow velocities, in which the sand is not carried very far down-dip; however, most of these deposits are often reworked into grainflows and therefore not preserved (Hunter and Kocurek, 1986). Nevertheless, subaqueous grainfall deposition may occur farther down dip due to the greater potential for water to transport sediment, as Hunter and Kocurek (1986) submitted that thin grainfall beds could be preserved between grainflow deposits on the lower lee face of subaqueous bedforms.

Grainfall deposition normally precedes grainflow: sand accumulates on the upper slipface until it reaches the angle of repose and avalanches downslope. Because the build-up of too much grainfall results in grainflow, these beds usually dip at angles below the angle of repose (20-30°), but may dip at higher angles (up to 40°; Hunter, 1977a); generally, they follow the dip of the underlying stratification (McKee et al., 1971).

Texturally, eolian grainfall laminae have been described as internally laminated with thin, parallel lamination and indistinct grain segregation (Hunter, 1977). Since

coarser grains have a shorter trajectory than finer ones, the coarse grains should be deposited closer to the brink, producing a down-dip fining trend (Fryberger and Schenk, 1981). These beds may be finer-grained overall (Kocurek and Dott, 1981) and exhibit an intermediate degree of packing (Hunter, 1977). Kocurek and Dott (1981) suggested that distinguishing between eolian and subaqueous grainfall might be extremely difficult, since grainfall deposits in both fluids may exhibit similar textural characteristics.

Grainflow

Grainflow (also called sandflow or avalanche) beds are deposited as sand accumulates up to its angle of repose (30-34°) and slides down the slipface. Some authors suggest that dispersive pressure from grain interaction plays a critical role in the propagation of these flows (Dasgupta and Manna, 2011; Lowe, 1976, 1979; Mullins and Van Buren, 1979; Stauffer, 1967): an interpretation partly based on earlier work by Bagnold (1954a, 1954b). In a study of small eolian dunes, Hunter (1977) described these deposits as generally massive (non-laminated) cross-beds that dip at relatively high angles of 28-34°, exhibit open grain packing and high porosities, and coarsen down-dip (reverse tangential grading; see Allen, 1984, and Kleinhans, 2004). Eolian avalanches are typically straight (little to no down-dip curvature; Hunter, 1985b), as they are unable to advance on slopes below the angle of repose (Lowe, 1976). These flows are sometimes associated with small-scale deformation structures (Bigarella, 1972; McKee and Bigarella, 1972; McKee et al., 1971).

Hunter (1977) suggested that eolian grainflows are deposited as relatively narrow “tongues” (lenticular in cross section) that may be separated by grainfall laminae (see also Hunter, 1976). The lateral width of these tongues has been described as 20 cm

(McDonald and Anderson, 1996), 5-30 cm (Pye and Tsoar, 2009), and 1-2 m (Sweet, 1992; Sweet et al., 1988). According to Hunter (1977), individual, discrete avalanche tongues may only be deposited on small dunes; on tall slipfaces, several tongues merge to form “composite sandflow cross-strata.” He described these beds in horizontal exposures at both high and low levels on the lee face: at high levels (upper slipface), the grainflow beds had scalloped basal contacts, while those at lower levels had uneven upper contacts (figure 4).

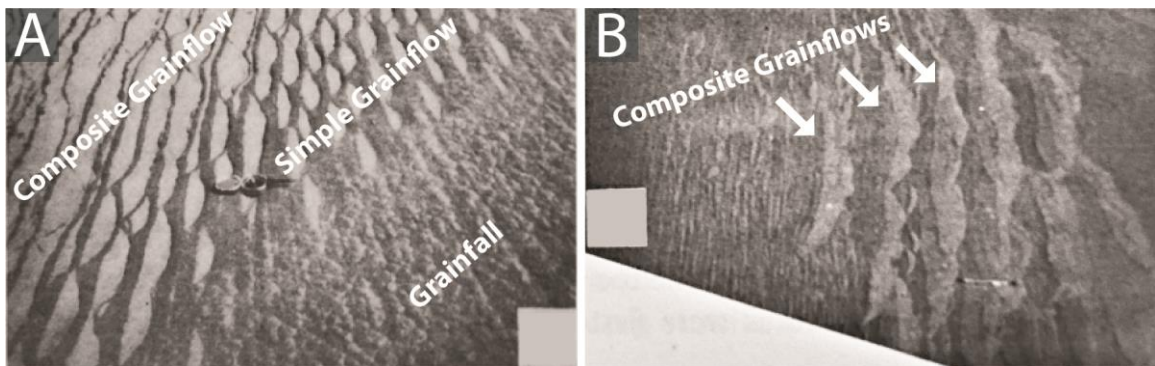


Figure 4: Composite grainflow beds in horizontal exposure at (A) low, and (B) high levels on eolian dunes (images modified from Hunter, 1977, p. 380, figures 8c and d). These photos highlight the unevenness of beds that may form by the merging of several grainflow tongues.

Grainflows on subaqueous bedforms occur by similar processes, but the deposits may differ slightly in their morphologies (Hunter, 1976). Allen (1965) described these processes as they occur on subaqueous sand waves. Under low current velocities, grainfall accumulates on the upper lee face and, upon reaching the angle of repose, slides down the foreset as a grainflow. When additional grainfall accumulates, subsequent grainflows occur. This process, which has been termed *intermittent avalanching*, is comparable to the process of grainflow on eolian dunes. As a result, these deposits may exhibit analogous features: massive internal texture, relatively high dip angles of 26-37°

(average 31°), loosely packed grains and high porosities, reverse tangential grading, and little down-dip curvature (Hunter and Kocurek, 1986). Buck (1985) suggested that the presence of “narrow tongues” did not necessarily imply eolian processes, since intermittent subaqueous avalanching could produce narrow, tongue-like deposits. However, he also proposed that the width of the tongues should increase with increasing flow velocity. Even though beds formed by intermittent subaqueous avalanching may be tongue-shaped, they are usually wider than eolian grainflow deposits (2-3 m wide; Hunter, 1985b; figure 5).

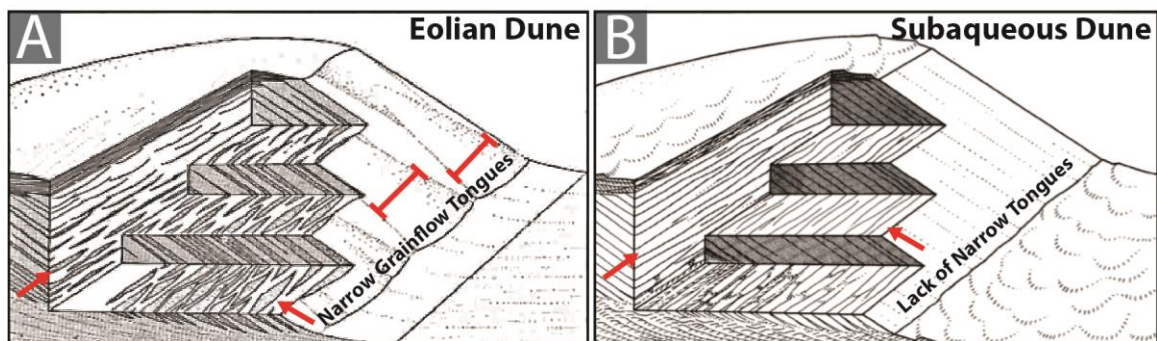


Figure 5: Grainflow deposits depicted in horizontal, vertical, and foreset surface exposures on eolian (A) and subaqueous (B) dunes. Grainflows in dry sand are deposited as relatively narrow “tongues” while their subaqueous counterparts can be significantly wider. The increased lateral width of subaqueous grainflow deposits may be attributed partly to the fluid, but largely to the greater range of flow processes that occur underwater. Figures modified from Hunter (1977), p. 378, figure 7 and Hunter (1985b), p. 892, figure 7.

The Case of Continuous Avalanching

According to Allen (1984), avalanche frequency increases with flow velocity until *continuous avalanching* results. Continuous avalanching occurs when grains continually settle on and slide down the foreset (Allen 1965). These cross-beds are distinctly different from “normal” grainflow deposits on both eolian and subaqueous bedforms.

They may have a massive internal texture, though some authors have suggested that they are laminated (Kocurek and Dott, 1981; Smith, 1972). Stratification has been described as “thin and indistinct” (Hunter and Kocurek, 1986). Smith (1972) proposed that cross-bed dip angle decreases with increasing flow velocity and water depth, so beds deposited by continuous subaqueous avalanching should dip at angles below the angle of repose (Hunter, 1985b; Hunter and Kocurek, 1986). These beds may exhibit slight down-dip curvature (Allen, 1965; Hunter and Kocurek, 1986) and minimal to no reverse tangential grading (Allen, 1965) or even normal tangential grading (Allen, 1984). Instead of forming narrow “avalanche tongues,” the deposits are laterally extensive or “sheetlike” (Buck, 1985).

Hunter (1985b) submitted that, “...Subaqueous cross-strata formed by continuous avalanching may be very difficult to distinguish from those formed by grainfall deposition without avalanching” (p. 893). Since continuous avalanching does not involve failure and gravity flow at the angle of repose, it is not really “avalanching” according to the traditional understanding of grainflow processes. Collinson and Thompson (1989) suggested that, while grainflow is the dominant depositional process under weak currents, grainfall deposition increases with higher flow velocities. The process of continuous avalanching is, accordingly, almost more analogous to grainfall deposition except that it also includes grain movement down the foreset. Allen (1984) called it a, “sustained and general downward flow of grains” (p. 149). This similarity between continuous avalanching and grainfall may explain why beds deposited by continuous avalanching are texturally and structurally different from other avalanche deposits in both eolian and subaqueous settings.

Ripple Lamination

Often called *translatent stratification* (Hunter, 1977; Kocurek and Dott, 1981), the migration of superimposed wind and water ripples can generate parallel lamination on dune foresets. Hunter (1977) described two types of translatent strata in his study of small eolian dunes: subcritically climbing and supercritically climbing. These types are defined by the angle of ripple climb, which may be lower or higher than the angle of the ripple's windward slope ("critical angle"). He also described other "traction" deposits – planebed lamination and rippleform lamination – but these were rare in the dunes that he studied. Translatent strata are commonly observed on the bottomsets and topsets of eolian dunes (Hunter, 1977) and on dune plinths where accretion dominates (Bagnold, 1954b), but may occur anywhere that ripples form. These deposits should usually dip at angles below the angle of repose and have lower porosities than grainfall and grainflow deposits (Hunter, 1977). Ripple laminae may be deposited on underwater bedforms (Allen, 1965; Collinson and Thompson, 1989), but these should exhibit different texture and form from those deposited in air (Kocurek and Dott, 1981). According to Kocurek and Dott (1981), subcritically climbing translatent strata is a uniquely eolian feature and identifying it in sandstones may be the best indicator of eolian deposition; widespread supercritically climbing translatent strata, however, may suggest subaqueous processes.

Dune Shape and Stratification Type Distribution

Modern dunes assume different shapes (McKee, 1966), and evidence for these morphologies might be preserved in cross-bedded sandstones (Bigarella, 1972; Kocurek, 1991). Because each dune type exhibits its own foreset geometry/orientation, we might expect variation in the relative proportions of stratification types deposited (Kocurek and

Dott, 1981). However, while dune shape may determine the distribution of stratification types, their structural characteristics are generally based on the physical processes which deposit them, as noted by Kocurek and Dott (1981); for example, eolian grainflow beds exhibit angle-of-repose dips and, accordingly, are associated with slipfaces. One possible exception is that certain dune types may have longer slipfaces, and if these authors are correct in suggesting that taller slipfaces produce thicker grainflows, then thicker grainflow beds might be expected in preserved deposits of those dune types. The literature, however, does not appear to suggest that *individual* grainflows are wider on large eolian dunes, or that they dip at low angles, exhibit down-dip curvature or lack reverse tangential grading.

Using Stratification Types to Interpret Cross-Bedded Sandstones

The expected characteristics and distribution of the stratification types, therefore, are derived from differing processes and dune morphologies. Recognizing these distinctive textures and sedimentary structures in cross-bedded sandstones may enable the interpretation of fine-scale processes in the rock record (Allen and Narayan, 1964; Buck, 1985; Clemmensen and Abrahamsen, 1983; Hunter, 1981; Kocurek and Dott, 1981; Loope et al., 2012; Narayan, 1971; Romain and Mountney, 2014). However, limits exist in applying modern criteria to ancient deposits. Differences in depositional scales, as well as bedform truncation (Romain and Mountney, 2014), separate preserved cross-strata from most modern analogues. Consequently, modern criteria might have limited utility for *quantitative* process interpretations, but may still generally apply for describing trends. As a result of the contrasting textures, morphologies, and distributions, dune

stratification types may serve as a useful tool for describing reservoir geometries (Howell and Mountney, 2001; Loope et al., 2012; Romain and Mountney, 2014).

References

- Allen, J. R. L., 1965, Sedimentation to the lee of small underwater sand waves: an experimental study: *Journal of Geology*, v. 73, no. 1, p. 95-116.
- , 1970, The avalanching of granular solids on dune and similar slopes: *Journal of Geology*, v. 78, p. 326-351.
- , 1972, Intensity of deposition from avalanches and the loose packing of avalanche deposits: *Sedimentology*, v. 18, p. 105-111.
- , 1984, *Sedimentary Structures: Their Character and Physical Basis*, Amsterdam, Netherlands, Elsevier.
- Allen, J. R. L., and Narayan, J., 1964, Cross-stratified units, some with silt bands, in the Folkestone Beds (Lower Greensand) of Southeast England: *Geologie en Mijnbouw*, v. 43, p. 451-461.
- Anderson, C. J., Struble, A., and Whitmore, J. H., 2017, Abrasion resistance of muscovite in aeolian and subaqueous transport experiments: *Aeolian Research*, v. 24, p. 33-37.
- Anderson, R. S., 1988, The pattern of grainfall deposition in the lee of aeolian dunes: *Sedimentology*, v. 35, p. 175-188.
- Bagnold, R. A., 1954a, Experiments on a gravity-free dispersion of large solid spheres in a Newtonian fluid under shear, *Proceedings of the Royal Society of London A: Mathematical, Physical and Engineering Sciences*, Volume 225, The Royal Society, p. 49-63.
- , 1954b, *The Physics of Blown Sand and Desert Dunes*, Mineola, NY, Dover Publications, Inc., 265 p.
- Bigarella, J. J., 1972, Eolian environments: their characteristics, recognition, and importance, *in* Rigby, J. K., and Hamblin, W. K., eds., *Recognition of Ancient Sedimentary Environments*, Volume 16, Society of Economic Paleontologists and Mineralogists Special Publication, p. 12-62.
- Buck, S. G., 1985, Sand-flow cross strata in tidal sands of the Lower Greensand (Early Cretaceous), Southern England: *Journal of Sedimentary Petrology*, v. 55, no. 6, p. 895-906.

- Carrigy, M. A., 1970, Experiments on the angles of repose of granular materials: *Sedimentology*, v. 14, p. 147-158.
- Clemmensen, L. B., and Abrahamsen, K., 1983, Aeolian stratification and facies association in desert sediments, Arran basin (Permian), Scotland: *Sedimentology*, v. 30, p. 311-339.
- Collinson, J. D., and Thompson, D. B., 1989, *Sedimentary Structures*, Chapman & Hall, 207 p.
- Dasgupta, P., and Manna, P., 2011, Geometrical mechanism of inverse grading in grain-flow deposits: an experimental revelation: *Earth-Science Reviews*, v. 104, p. 186-198.
- Freeman, W. E., and Visher, G. S., 1975, Stratigraphic analysis of the Navajo Sandstone: *Journal of Sedimentary Petrology*, v. 45, no. 3, p. 651-668.
- Fryberger, S. G., and Schenk, C., 1981, Wind sedimentation tunnel experiments on the origins of aeolian strata: *Sedimentology*, v. 28, p. 805-821.
- Garzanti, E., 2017, The maturity myth in sedimentology and provenance analysis: *Journal of Sedimentary Research*, v. 87, p. 353-365.
- Garzanti, E., Resentini, A., Andò, S., Vezzoli, G., Pereira, A., and Vermeesch, P., 2015, Physical controls on sand composition and relative durability of detrital minerals during ultra-long distance littoral and aeolian transport (Namibia and southern Angola): *Sedimentology*, v. 62, p. 971-996.
- Glennie, K. W., 1972, Permian Rotliegendes of northwest Europe interpreted in light of modern desert sedimentation studies: *AAPG Bulletin*, v. 56, no. 6, p. 1048-1071.
- Howell, J., and Mountney, N., 2001, Aeolian grain flow architecture: hard data for reservoir models and implications for red bed sequence stratigraphy: *Petroleum Geoscience*, v. 7, p. 51-56.
- Hunter, R. E., 1976, Comparison of eolian and subaqueous sand-flow cross-strata: *Bulletin of the American Association of Petroleum Geologists*, v. 60, p. 683-684.
- , 1977, Basic types of stratification in small eolian dunes: *Sedimentology*, v. 24, p. 361-387.
- , 1981, Stratification styles in eolian sandstones: some Pennsylvanian to Jurassic examples from the western interior U.S.A., *in* Ethridge, F. G., and Flores, R. M., eds., *Recent and Ancient Nonmarine Depositional Environments: Models for Exploration*: Society of Economic Paleontologists and Mineralogists, Special Publication 31, p. 315-329.

- , 1985a, A kinematic model for the structure of lee-side deposits: *Sedimentology*, v. 32, p. 409-422.
- , 1985b, Subaqueous sand-flow cross strata: *Journal of Sedimentary Petrology*, v. 55, no. 6, p. 886-894.
- Hunter, R. E., and Kocurek, G., 1986, An experimental study of subaqueous slipface deposition: *Journal of Sedimentary Petrology*, v. 56, no. 3, p. 387-394.
- Imbrie, J., and Buchanan, H., 1965, Sedimentary structures in modern carbonate sands of the Bahamas, *in* Middleton, G. V., ed., Primary sedimentary structures and their hydrodynamic interpretation, Volume 12: Tulsa, OK, Society of Economic Paleontologists and Mineralogists, p. 149-172.
- Kleinbans, M. G., 2004, Sorting in grain flows at the lee side of dunes: *Earth-Science Reviews*, v. 65, p. 75-102.
- Kocurek, G., 1991, Interpretation of ancient eolian sand dunes: *Annual Review of Earth and Planetary Sciences*, v. 19, p. 43-75.
- Kocurek, G., and Dott, R. H., 1981, Distinctions and uses of stratification types in the interpretation of eolian sand: *Journal of Sedimentary Petrology*, v. 51, no. 2, p. 579-595.
- Kuenen, P. H., and Perdok, W. G., 1962, Experimental abrasion 5. frosting and defrosting of quartz grains: *Journal of Geology*, v. 70, no. 6, p. 648-658.
- Loope, D. B., 1984, Eolian origin of upper Paleozoic sandstones, southeastern Utah: *Journal of Sedimentary Petrology*, v. 54, p. 563-580.
- Loope, D. B., Elder, J. F., and Sweeney, M. R., 2012, Downslope coarsening in aeolian grainflows of the Navajo Sandstone: *Sedimentary Geology*, v. 265-266, p. 156-162.
- Lowe, D. R., 1976, Grain flow and grain flow deposits: *Journal of Sedimentary Petrology*, v. 46, no. 1, p. 188-199.
- , 1979, Sediment gravity flows: their classification and some problems of application to natural flows and deposits: *SEPM Special Publication*, v. 27, p. 75-82.
- Maithel, S. A., Garner, P. A., and Whitmore, J. H., 2015, Preliminary assessment of the petrology of the Hopeman Sandstone (Permo-Triassic), Moray Firth Basin, Scotland: *Scottish Journal of Geology*, v. 51, no. 2, p. 177-184.
- McDonald, R. R., and Anderson, R. S., 1995, Experimental verification of aeolian saltation and lee side deposition models: *Sedimentology*, v. 42, p. 39-56.

- , 1996, Constraints on eolian grain flow dynamics through laboratory experiments on sand slopes: *Journal of Sedimentary Research*, v. 66, no. 3, p. 642-653.
- McKee, E. D., 1934, *The Coconino Sandstone - its history and origin*: Carnegie Institution of Washington Publication 440, p. 77-115.
- , 1966, Structures of dunes at White Sands National Monument, New Mexico (and a comparison with structures of dunes from other selected areas): *Sedimentology*, v. 7, p. 1-69.
- McKee, E. D., and Bigarella, J. J., 1972, Deformational structures in Brazilian coastal dunes: *Journal of Sedimentary Petrology*, v. 42, no. 3, p. 670-681.
- , 1979, Ancient sandstones considered to be eolian, *in* McKee, E. D., ed., *A Study of Global Sand Seas*: Honolulu, HI, University Press of the Pacific, p. 187-238.
- McKee, E. D., Douglass, J. R., and Rittenhouse, S., 1971, Deformation of lee-side laminae in eolian dunes: *Geological Society of America Bulletin*, v. 82, p. 359-378.
- Mullins, H. T., and Van Buren, H. M., 1979, Modern modified carbonate grain flow deposit: *Journal of Sedimentary Petrology*, v. 49, no. 3, p. 747-752.
- Narayan, J., 1971, Sedimentary structures in the Lower Greensand of the Weald, England, and Bas-Boulonnais, France: *Sedimentary Geology*, v. 6, p. 73-109.
- Nickling, W. G., McKenna Neuman, C., and Lancaster, N., 2002, Grainfall processes in the lee of transverse dunes, Silver Peak, Nevada: *Sedimentology*, v. 49, p. 191-209.
- Nield, J. M., Wiggs, G. F. S., Baddock, M. C., and Hipondoka, M. H. T., 2017, Coupling leeside grainfall to avalanche characteristics in aeolian dune dynamics: *Geology*, v. 45, no. 3, p. 271-274.
- Pye, K., and Tsoar, H., 2009, *Aeolian Sand and Sand Dunes*, Berlin, Springer-Verlag, 458 p.
- Rittenhouse, G., 1972, Cross-bedding dip as a measure of sandstone compaction: *Journal of Sedimentary Petrology*, v. 42, no. 3, p. 682-683.
- Romain, H. G., and Mountney, N. P., 2014, Reconstruction of three-dimensional eolian dune architecture from one-dimensional core data through adoption of analog data from outcrop: *AAPG Bulletin*, v. 98, no. 1, p. 1-22.
- Smith, N. D., 1972, Some sedimentological aspects of planar cross-stratification in a sandy braided river: *Journal of Sedimentary Petrology*, v. 42, no. 3, p. 624-634.

- Stauffer, P. H., 1967, Grain-flow deposits and their implications, Santa Ynez Mountains, California: *Journal of Sedimentary Petrology*, v. 37, no. 2, p. 487-508.
- Steidtmann, J. R., 1974, Evidence for eolian origin of cross-stratification in sandstone of the Casper Formation, Southernmost Laramie Basin, Wyoming: *Geological Society of America Bulletin*, v. 85, p. 1835-1842.
- Sutton, S. L. F., McKenna Neuman, C., and Nickling, W., 2013, Lee slope sediment processes leading to avalanche initiation on an aeolian dune: *Journal of Geophysical Research: Earth Surface*, v. 118, p. 1754-1766.
- Sweet, M. L., 1992, Lee-face airflow, surface processes, and stratification types: their significance for refining the use of eolian cross-strata as paleocurrent indicators: *Geological Society of America Bulletin*, v. 104, p. 1528-1538.
- Sweet, M. L., Nielson, J., Havholm, K., and Farrelley, J., 1988, Algodones dune field of southeastern California: case history of a migrating modern dune field: *Sedimentology*, v. 35, p. 939-952.
- Swezey, C., 1998, The identification of eolian sands and sandstones: *C. R. Acad. Sci. Paris, Sciences de la Terre et des planetes / Earth and Planetary Sciences*, v. 327, p. 513-518.
- Thompson, W. O., 1949, Lyons sandstone of Colorado Front Range: *AAPG Bulletin*, v. 33, no. 1, p. 52-72.
- Walker, T. R., and Harms, J. C., 1972, Eolian origin of flagstone beds, Lyons sandstone (Permian), type area, Boulder county, Colorado: *The Mountain Geologist*, v. 9, no. 2-3, p. 279-288.

CHAPTER THREE
A METHODOLOGY FOR DISAGGREGATION AND TEXTURAL ANALYSIS
OF QUARTZ-CEMENTED SANDSTONES

Abstract

Sandstone textures provide critical information for reservoir modelling and interpreting depositional processes. While loose-sand textures are easy to describe, various authors have developed thin-section and image-analysis techniques to characterize lithified deposits that were assumed impossible to disaggregate successfully. These methods are effective but tedious, and are generally not feasible for processing many samples. We present a new methodology for disaggregating quartz-dominated sandstones cemented by quartz overgrowths, with application to the Permian Coconino Sandstone of northern and central Arizona, USA. Textural parameters of the disaggregated sand were measured using a laser-diffraction particle analyzer. Our average grain sizes from laser analysis are coarser than those from thin section (as expected), but trends from the analyzer correlate well with thin-section results. This strong correlation strengthens the validity of both methods and suggests that disaggregation and whole-particle analysis may effectively replace petrographic techniques in many textural studies. We hope that our methods, which increase the efficiency of grain-size analysis, will expand the potential for collecting textural data from quartz-cemented sandstones.

Introduction

Texture has long served as a useful criterion for interpreting depositional processes in sandy sediment. Textural parameters, which commonly include grain size, sorting, and spatial changes in grain size and sorting, can be used alongside other criteria to develop process and environmental models for these deposits. While the methods used to describe loose sediment textures are relatively straightforward, challenges arise when characterizing original textures in sandstones, which are often strongly cemented and altered by other diagenetic processes. Because of the difficulty in disaggregating these rocks, numerous methodologies for quantifying grain size in thin section have been proposed and discussed (Krumbein, 1935, 1950; Chayes, 1950, 1951; Greenman, 1951; Pelto, 1952; Packham, 1955; Roethlisberger, 1955; Friedman, 1958, 1962, 1965, 1996; Van der Plas, 1962, 1965; Sahu, 1966, 1968a, 1968b; Smith, 1966, 1968; Stauffer, 1966; Rose, 1968; Gray, 1969; Kellerhals et al., 1975; Adams, 1977; Harrell and Eriksson, 1979; Johnson, 1994; Kong et al., 2005). Various authors have characterized sandstone textures from thin sections (Sumner, 1999; Walderhaug and Bjørkum, 2003; Maithel and Whitmore, 2010; Maithel et al., 2015; Maithel et al., 2016), but these methods require manually measuring hundreds to thousands of grains and, accordingly, considerable processing time. Despite their effectiveness, petrographic methods are tedious and not conducive to analyzing many samples. Furthermore, such methods require thin sections, which can be expensive and cumbersome to make in large quantities.

More recent papers have developed image-analysis techniques for describing textures (Mazzullo and Kennedy, 1985; Francus, 1998; Persson, 1998; van den Berg et al., 2002; van den Berg et al., 2003; Seelos and Sirocko, 2005; Fernlund et al., 2007; Resentini et al., 2018), providing a faster alternative to manual grain measurement, but

many rocks are too complex for these techniques to be straightforward. Like petrography, image-analysis methods also commonly require thin sections. Loose-sediment analyses (e.g., via sieve or laser diffraction), therefore, remain the simplest approaches for characterizing textures in sandstones; however, the thin-section and image-analysis methods were developed on the assumption that some rocks cannot be disaggregated (Krumbein, 1935; Friedman, 1958, 1962; Rose, 1968; Kellerhals et al., 1975; Johnson, 1994; Kong et al., 2005).

Loope et al. (2012) successfully collected textural data from disaggregated Navajo Sandstone using laser-diffraction particle analysis. These authors noted that their grainflow beds were relatively weakly cemented and easily disaggregated, unlike many other ancient dune deposits which are well lithified (see p. 158 of their paper). An earlier paper by Freeman and Visher (1975) also reported textural data from the Navajo Sandstone (obtained by sieve analysis), but their presumed disaggregation methods were not described. Others have conducted studies on the “friable” St. Peter Sandstone (Thiel, 1935; Amaral and Pryor, 1977; Mazzullo and Ehrlich, 1983). In these examples, the sandstones were relatively poorly cemented and could be readily disaggregated.

The goal of this study is to develop a protocol for disaggregation and textural analysis of well-cemented sandstones: specifically those composed mostly of quartz grains and cemented by quartz overgrowths. The Permian Coconino Sandstone provides an ideal setting for this project because of its predominantly quartz and feldspar composition and quartz overgrowth cement, which cannot be readily dissolved without dissolving the grains. Paragenetic variation across the formation also broadens the potential application of our methods: while the sandstone is generally well lithified by

quartz overgrowths in most localities, it is more weakly cemented in some of its eastern outcrops near the town of Holbrook (figure 1). Samples that we call weakly or poorly cemented in this chapter are generally friable, while those that are well or strongly cemented are “hard” or non-friable. Porosity estimates (from image analysis) range approximately from 7 to 35%, with the highest porosities associated with “weakly cemented” Holbrook samples; these friable samples are also less likely to contain abundant stylolitic seams.

The Coconino Sandstone (Permian) is a cross-bedded, quartz-rich sandstone that crops out across northern and central Arizona. McKee (1934) described large-scale cross-bedding, quartz-dominated composition, and relatively uniform grain size in the formation, among other features, and interpreted it as an eolian deposit. In most outcrops, the sandstone is well cemented by quartz overgrowths, making it readily quarried for construction purposes, but not easily disaggregated.

McKee (1934) managed to collect textural data from the Coconino Sandstone using disaggregation and sieving methods. To disaggregate the sandstone, he broke his samples on cardboard and checked for remaining aggregated grains under the microscope. Since McKee’s paper (1934), few have attempted to collect quantitative textural data from the formation. Lundy (1973) disaggregated samples with a mortar and pestle for sieve analysis. He took care to avoid grain fracturing; however, he admitted that it probably occurred in some samples. Grain fracturing during the manual disaggregation methods employed by McKee (1934) and Lundy (1973) is not surprising given the well-cemented nature of the sandstone in many localities and the presumed force that would be needed to “crush” these samples. More recent petrographic studies

involved measuring the long axes of individual grains in thin section (Sumner, 1999; Maithel and Whitmore, 2010; Whitmore and Strom, 2010; Maithel et al., 2016), which eliminated fracturing and allowed the grains to be distinguished from surrounding overgrowths where dust rims were visible. These methods are time-consuming, but were used because of the assumption that disaggregating the sandstone would be difficult or impossible (Maithel et al., 2016). Recent methodologies involving high-voltage disaggregation (SELFRAG) have been used on some rocks (e.g., van der Wielen et al., 2013), but the need for a more accessible solution remains.

Our disaggregation methods will therefore broaden the scope and opportunities for sedimentological research on well-cemented sandstones. If textural trends from disaggregation and whole-particle analysis compare favorably to those from thin section, these methods may be able to replace petrographic approaches, saving considerable time and expense required to make thin sections and measure grains. Since textural trends serve as important criteria for distinguishing dune stratification types and interpreting depositional processes in cross-bedded sandstones (Hunter, 1981; Kocurek and Dott, 1981; Clemmensen and Abrahamsen, 1983; Loope, 1984; Kocurek, 1991; Langford and Chan, 1993; Loope et al., 2012; Romain and Mountney, 2014), such methods could be used to better develop process models for cross-bedded deposits. Furthermore, sediment textures may correlate with porosity and permeability (e.g., Ahlbrandt, 1979), and so textural data obtained by these methods might be useful (alongside other parameters) for predicting sandstone reservoir properties (Howell and Mountney, 2001; Loope et al., 2012; Romain and Mountney, 2014).

Methods

Coconino Sandstone samples were collected from outcrops near the towns of Ash Fork, Seligman, and Holbrook, Arizona, and along the Hermit Trail on the South Rim of the Grand Canyon. The sandstone is “strongly cemented” by quartz in most of our outcrops, with the exception of Holbrook, where many samples can be easily crushed by hand (figure 1).

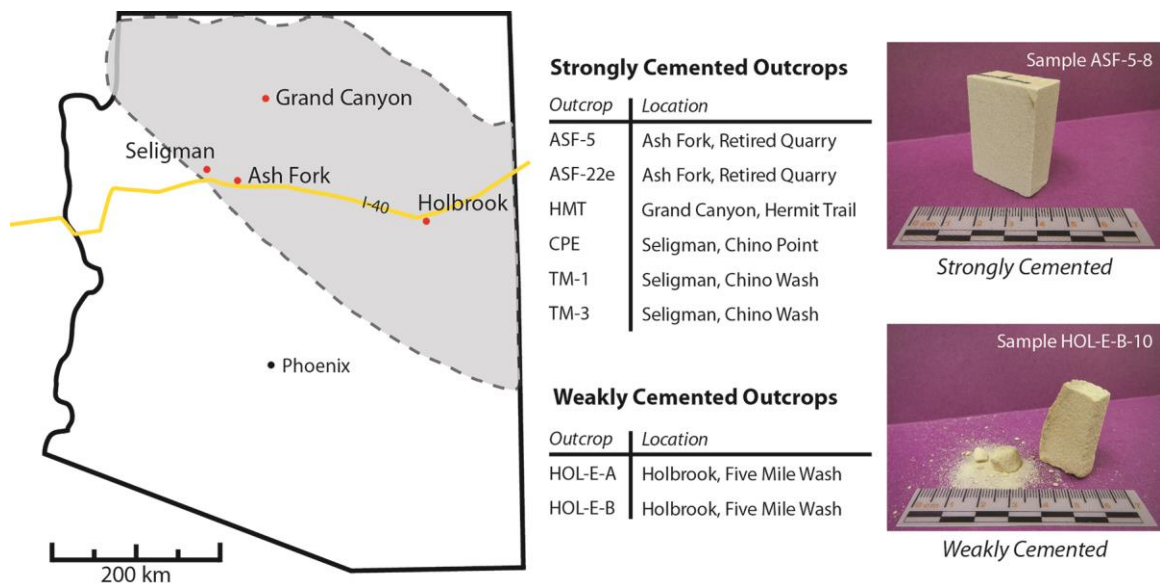


Figure 1: Map and locations where we collected samples with different degrees of cementation. The approximate extent of the contiguous Coconino Sandstone across northern Arizona is marked on the map (McKee, 1934; Blakey, 1988; Blakey and Knepp, 1989; Richard et al., 2000; Middleton et al., 2003). Most of our samples (from Ash Fork, Grand Canyon, and Seligman-area outcrops) are well lithified by quartz-overgrowth cement, but many of those from Holbrook break apart easily by hand. While relatively weak cementation in the Holbrook samples might lend itself better to disaggregation, we sought to develop methods that would disaggregate even strongly cemented sand, which is characteristic of the Coconino Sandstone and numerous other formations.

While the majority of our samples are from the Coconino Sandstone, we also disaggregated several samples from other quartz-dominated sandstone formations. These

include the Tensleep Sandstone (Wyoming, USA), the Penrith Sandstone, and the Bridgnorth Sandstone (England).

Disaggregation Methods

Small pieces of sandstone were disaggregated for laser-diffraction particle analysis (table 1). Samples were cut into thin slices (as thin as ~ 2 mm or less; perpendicular to bedding) using a diamond-blade saw. We chose to use thin slices so that they could be easily crushed (likely related to microfractures produced by sawing), and to represent the vertical grain-size distribution in beds better than breaking off a small piece. For the weakly cemented Holbrook samples, we could generally cut thicker slices (up to ~ 0.5 cm), but the well-lithified Ash Fork, Seligman, and Grand Canyon samples were cut as thinly as possible so that they could be adequately crushed. The sandstone slices were rinsed and crushed in the palm of the hand, and then transferred to 50 mL centrifuge tubes.

Table 1: Workflow of our sandstone-disaggregation and particle-analysis method

1) Break down whole rock sample.

Cut thin slice of sandstone.

Crush as much as possible by hand and rinse.

2) Dissolve carbonate minerals (which may occur as cement).

Crush with glass rod in HCl and let sit overnight.

Centrifuge to rinse out acid.

3) Sonicate to disperse grains in suspension.

Crush again with glass rod and sonicate in sodium hexametaphosphate solution.

4) Isolate sand fraction.

Rinse out suspended fines.

Remove any remaining aggregated pieces.

5) Analyze loose sediment with laser-diffraction particle analyzer.

Concentrated hydrochloric acid was poured over the samples (we used ~ 10 M HCl). After a few hours, more acid was added to each sample, and they were crushed with a glass rod (some were crushed after the initial acid was added). Using a thick glass rod (1 cm diameter, cylindrical) was preferred, as thinner rods tended to break more easily. Samples were then left to sit in hydrochloric acid overnight. The next day, we diluted the hydrochloric acid by adding deionized water to each centrifuge tube, approximately up to the 40 mL line. The tubes were then capped and shaken.

A Beckman Coulter Allegra X-30R centrifuge was used to separate minerals from the acid. Each sample was centrifuged and rinsed ~ 3-6 times with deionized water (4255 x g; 3 minutes/run), and the tubes refilled to the ~ 40 mL line after each run. When the samples were centrifuged for the final time, tubes were refilled to the ~ 40 mL line again in preparation for sonication.

Using a pipette, ~ 6 drops of a sodium hexametaphosphate (NaHMP) solution were added to each sample. The solution was made by dissolving powdered NaHMP in

deionized water to produce an ~ 4% weight/volume concentration (~ 2.13 g/50 mL). Adding 6 drops of this solution to ~ 40 mL water should, after accounting for varying sample volumes, fall roughly within the optimal range of 0.025-0.06 g per 100 cc proposed by Tchillingarian (1952). To eliminate concentration variation, the NaHMP solution could be mixed separately and added to dried samples; however, adding a fixed number of drops to each centrifuge tube saves time and should sufficiently promote dispersion.

The samples (in the dilute NaHMP solution) were then crushed vigorously with a glass rod and sonicated using a QSonica quarter-inch microtip sonicator probe (pulse setting 03 02; 50% amplitude; five minutes). Poorly lithified Holbrook samples were each crushed with the glass rod and sonicated one time, but all others were crushed and sonicated a second time using the same settings.

Sonicated samples were rinsed to eliminate suspended sediment and any fine abraded glass fragments (our glass rods were frosted by the quartz abrasion, presumably incorporating some glass material into the sand). The purpose of this was twofold: 1) remove authigenic and/or detrital clays, broken overgrowths, and other abraded grain and glass fragments, and 2) isolate the sand-size fraction, which makes the data more comparable to thin-section results. Each sample vial was shaken, and the sediment was allowed to settle for ~ 30 seconds (timed with a stopwatch). We then decanted the suspension, taking care to lose as little of the sand fraction as possible. The vials were refilled to the ~ 40 mL line, shaken, and rinsed two additional times (three total rinses).

Initially, some of our samples from the Ash Fork area were sonicated in ~ 25 mL of solution (with ~ 4 drops NaHMP), and were rinsed and refilled *five* times. However,

this resulted in sand adhering to the probe above the water line, which was wiped off and discarded before analysis. We therefore increased the solution level to ~ 40 mL for the remaining samples, which significantly reduced the amount of sediment that stuck to the probe and resulting sample loss. The greater volume of water also allowed us to rinse the samples fewer times.

By this stage, many of the well-cemented samples were not completely disaggregated. Before particle analysis, each sample was poured into a tray and inspected for grain aggregates. If observed, these were removed with tweezers.

The disaggregated Coconino Sandstone sand was analyzed using a Beckman Coulter LS 13 320 laser-diffraction particle analyzer and Universal Liquid Module (ULM; sample density: 2.65 g/mL; fluid: water). We chose to use a laser-diffraction analyzer because of the better efficiency and smaller sample volumes required compared to mechanical sieving. Other methods, such as QEMSCAN (e.g., Speirs et al., 2008) and CCSEM (e.g., Keulen et al., 2008) can be used to obtain grain-size data from loose sediment, but laser diffraction provides an effective and accessible option for analyzing bulk samples.

Lithified-Rock Analysis

We also described textures in selected samples using petrographic methods and compared these with our loose-sand results from the particle analyzer (table 2). The long axes of at least 200 grains were measured from Coconino Sandstone thin-section photos using the FIJI distribution of ImageJ software (Schindelin et al., 2012; Schneider et al., 2012). Grains from non-Coconino Sandstone samples were measured at a different

institution using the Nikon Br software. 150 grains were then randomly selected from each sample and used to calculate descriptive statistics.

Table 2: Samples selected for petrographic analysis

Coconino Sandstone (Well-Cemented Samples)¹	Coconino Sandstone HOL-E-B Samples²	Non-Coconino Sandstone Samples³
ASF-5-24	HOL-E-B-1	ALC-3
ASF-5-14	HOL-E-B-2	COW-2
ASF-22e-F	HOL-E-B-3	COW-3
ASF-22e-H	HOL-E-B-4	KIN-1
HMT-5	HOL-E-B-5	KIN-2
HMT-3	HOL-E-B-6	TEN-1
TM-1-41	HOL-E-B-7	
ASF-5-16	HOL-E-B-8	
TM-1-25	HOL-E-B-9	
TM-3-1	HOL-E-B-11	
TM-3-5	HOL-E-B-12	
ASF-22e-A	HOL-E-B-13	
TM-1-50	HOL-E-B-14	
TM-3-15	HOL-E-B-15	
TM-1-47	HOL-E-B-16	

¹We randomly selected fifteen of the relatively well-cemented Coconino Sandstone samples (all except the HOL outcrops) for petrographic analysis. CPE samples were excluded from this group (due to minimal sample volume and uncertain disaggregation quality), as well as sample HMT-1, which is so strongly bimodal that we would not expect a good correlation with our petrographic methods. ²The HOL samples are weakly cemented overall compared to our other outcrops. We collected petrographic data from fifteen HOL-E-B samples (all except sample HOL-E-B-10, which had a lower-quality thin section due to poor epoxy impregnation). ³Non-Coconino Sandstone samples include the Tensleep Sandstone (ALC, TEN), the Penrith Sandstone (COW), and the Bridgnorth Sandstone (KIN).

Sources of Discrepancy between Results from each Method

Due to the intrinsic differences in methodology, both loose-sand analysis (disaggregation and laser diffraction) and thin-section methods may introduce various sources of “error” into textural data (table 3). We will discuss those that have the potential to affect our particle-analysis results.

Table 3: Sources of discrepancy between petrographic and disaggregated-sediment analyses

Thin Section	Disaggregation and Laser-Diffraction Analysis
Fewer grains measured	Grain fracturing and slicing
Grains measured from a limited number of photos per slide	Sample loss during disaggregation and analysis
Human error in measurement	Removal of aggregated grains
2D plane likely does not slice most grains through their longest axes, resulting in underestimation of grain size	Overgrowths remaining on grains, making them appear larger than they are
Grain edges (dust rims) not always distinct (affecting human error)	Data on partially dissolved grains lost ¹
Grains smaller than 30 μm (standard thin-section thickness) cannot be accurately measured	Clastic rock fragments breaking apart ²
Statistics based on individual grain measurements	Statistics based on grain populations

¹Partially or fully dissolved grains were usually excluded from our thin-section data, but these could be measured in thin section if the original grain edges were distinct. Since these grains would not be measured accurately during disaggregation and laser analysis, they could present a source of discrepancy between the methods. ²Our Coconino Sandstone samples do not contain abundant clastic rock fragments, but where these are present, they could be disaggregated along with the rest of the framework grains.

Grain Fracturing during Disaggregation

One concern in disaggregating quartz-cemented sandstones is the potential for grain fracturing. Broken or sliced grains and overgrowths would be measured as finer particles, making the overall grain-size distribution for each sample artificially finer. Most of our laser-diffraction histograms are positively skewed with distinct fine-grained “tails” even after the suspended sediment was rinsed away. We needed to determine whether these fine fractions reflect the original grain-size distributions or whether they result from grain slicing and/or fracturing that increased the fine fraction of the samples.

Clear evidence for abundant grain fracturing is not apparent in thin sections of disaggregated sand, but it was initially hard to determine whether the finer material represented fractured particles or overgrowth fragments. To test whether the fine tails in our graphs of laser-diffraction data result from fractured or sliced grains, we excluded the finest ~ 10% of sediment from each sample (after rinsing). Grains below the tenth-percentile size were omitted using the “range” setting under “statistic preferences” in the LS software; actual omitted percentages ranged from 7.5 to 12.1%, averaging 9.8% (variation likely due to binning).

When these recalculated average grain sizes (excluding the fines) are correlated with our original averages using a Pearson correlation, the correlation is statistically significant for all locations (table 4). This illustrates that removing the finest sediment fraction still results in a strong correlation with our original data, and any error introduced by grain fracturing likely does not have a large impact on the overall results.

Table 4: Correlation between average grain sizes (ϕ) with and without the fine fraction (finest 10%)

Outcrop	Samples	Pearson	p-value
ASF-5	22	0.987	< 0.0001
ASF-22e	10	0.955	< 0.0001
CPE	8	0.9821	< 0.0001
HMT	5	0.9958	< 0.0001
HOL-E-A	10	0.9974	< 0.0001
HOL-E-B	16	0.9942	< 0.0001
TM-1	12	0.9592	< 0.0001
TM-3	14	0.9959	< 0.0001

Furthermore, while many of our laser-diffraction-analysis histograms appear distinctly fine skewed, we observe similar skewness trends in our thin-section data (figure 2; table 5). Since grain sizes measured in thin sections would not be affected by grain fracturing or broken overgrowths, this positive skew cannot be attributed to those processes. Therefore, the skewness of our thin-section data further confirms that the fine tails in our particle-analysis histograms are probably real, and not entirely an artifact of the disaggregation methodology.

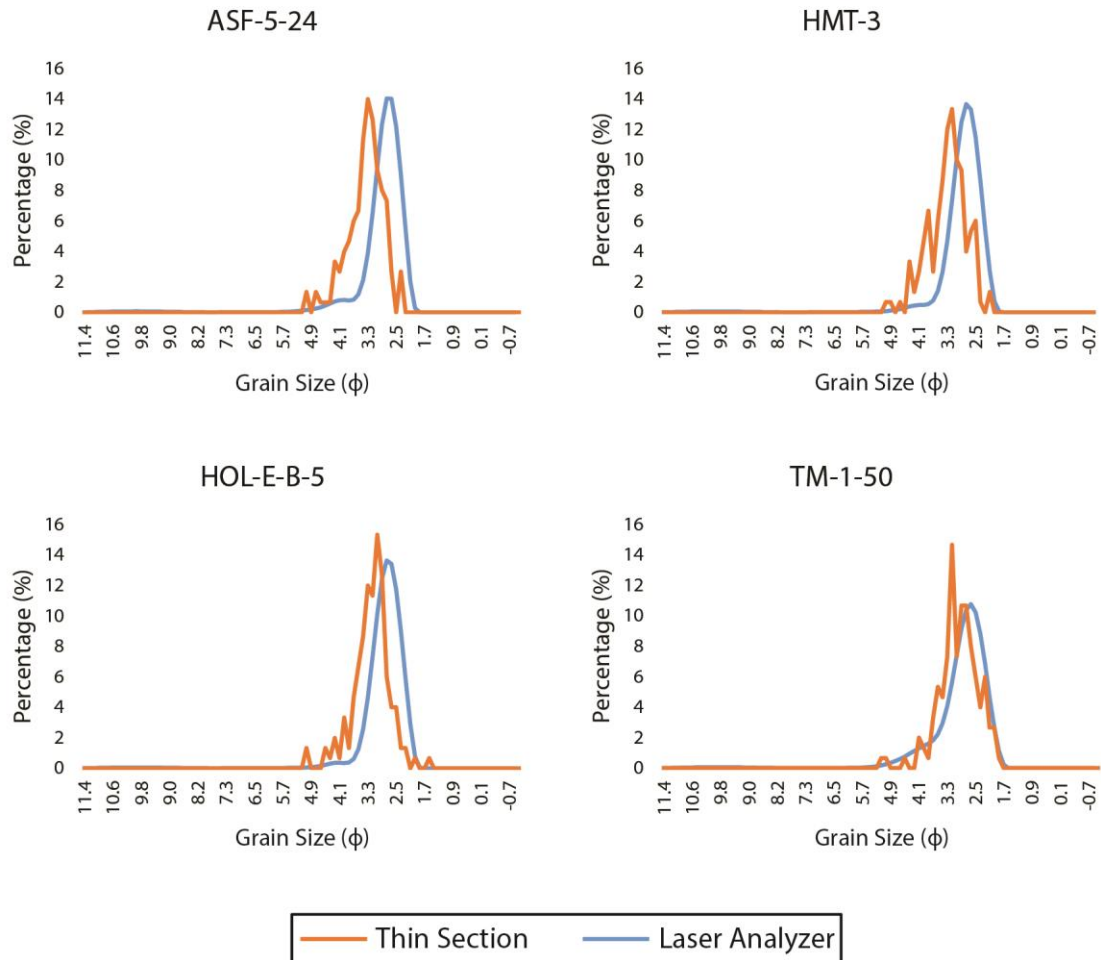


Figure 2: Comparison of thin-section and laser-diffraction-analysis histograms for four samples, one each from Ash Fork (ASF-5), Grand Canyon (HMT), Holbrook (HOL-E-B), and Seligman (TM-1). X-axis values reflect grain-size bins generated by the LS particle-analyzer software (converted from micrometers to phi). The presence of fine tails in both data sets suggests that the fines in the particle-analyzer data are probably real and not from grain fracturing or broken overgrowths produced during disaggregation.

Table 5: Skewness of thin-section data

Sample	Skewness (ϕ)	Sample	Skewness (ϕ)
ASF-5-24	0.81	HOL-E-B-1	0.21
ASF-5-14	0.92	HOL-E-B-2	0.03
ASF-22e-F	0.86	HOL-E-B-3	0.66
ASF-22e-H	1.31	HOL-E-B-4	0.56
HMT-5	0.48	HOL-E-B-5	0.59
HMT-3	0.58	HOL-E-B-6	0.51
TM-1-41	0.33	HOL-E-B-7	0.45
ASF-5-16	0.56	HOL-E-B-8	0.54
TM-1-25	0.28	HOL-E-B-9	0.43
TM-3-1	-0.07	HOL-E-B-11	0.41
TM-3-5	0.19	HOL-E-B-12	0.48
ASF-22e-A	0.69	HOL-E-B-13	0.41
TM-1-50	0.77	HOL-E-B-14	0.65
TM-3-15	0.10	HOL-E-B-15	0.88
TM-1-47	0.91	HOL-E-B-16	0.63
Average	0.58		0.50

During sample disaggregation, we noticed that substantial fines were dispersed into solution by the sonicator probe. Because of the aggressive nature of the sonication, we needed to determine whether this suspended fraction represents authigenic or detrital clays, or whether the framework grains are being abraded into fines. Four samples of loose, predominantly quartz dune sand from the Algodones Dunes (Southern California) were sonicated for different lengths of time and analyzed with the laser-diffraction analyzer after each increment. The samples were rinsed before each analysis to eliminate the suspended fine fraction. Average grain sizes after each time interval fall within two

standard deviations of the mean for a given sample (most fall within one standard deviation), and we find no significant difference between the zero and twenty-minute groups (Wilcoxon signed rank test; $p = 0.125$; $n = 4$; table 6), which suggests that even twenty minutes of sonication does not strongly reduce the average grain size.

Table 6: Mean grain size (ϕ) after time sonicated for four loose-sand samples

	0 min	5 min	10 min	20 min	Mean	Standard Deviation
Sample 1	2.17	2.20	2.19	2.17	2.18	0.01
Sample 2	2.08*	2.11	2.14	2.12	2.11	0.02
Sample 3	2.14	2.19	2.16	2.21*	2.17	0.03
Sample 4	2.15	2.15	2.16	2.16	2.15	0.01

*Designated values are within two standard deviations of the mean for each sample. All unmarked values fall within one standard deviation of the mean.

Correlation between the coarse fraction and average grain size and comparison with thin-section data therefore imply that the fine tails in our laser-analysis histograms are real and not a product of grain fracturing. Cutting thin pieces of sandstone would inevitably slice some grains, and a degree of grain fracturing during disaggregation might be expected; however, we suggest that these “artificial fines” do not significantly affect our results. Furthermore, notable grain and/or overgrowth fracturing probably does not occur during sonication. These tests demonstrate that substantial grain fracturing should not likely occur from our disaggregation methods, strengthening the validity of the methods and resulting particle-analysis data.

Until this point, our discussion of grain fracturing has focused on breakage related to the disaggregation process. However, intragranular microfractures may occur in some quartz sediment (Moss and Green, 1975). These fractures might cause grains that appear whole in thin section to break apart during disaggregation, making the resulting particle-

analysis data artificially fine. Accordingly, sandstones with abundant intragranular microfractures would not lend themselves well to disaggregation and would be better analyzed using petrographic techniques.

Sample Loss

While sample loss might be expected to affect data quality, it would be difficult to meaningfully quantify this variation. Sonicating most of the ASF-5 samples in 25 mL (versus 40 mL) of NaHMP solution did result in some sediment sticking to the probe above the water line. Sample material could also be lost during the initial cutting and rinsing, and in the later centrifuge and rinsing steps. However, once the samples are placed into the centrifuge tubes, sample loss should generally be minimal because they are kept in the same tubes throughout the disaggregation protocol.

Removal of Aggregated Grains

Removing sandstone fragments from disaggregated sediment is essentially a form of sample loss and has the potential to affect the quality of textural data. However, the impact of sample loss due to incomplete disaggregation can be evaluated for individual samples. We observed that four of our TM-1 samples were not well disaggregated after the first attempt. Aggregated grains were removed and the samples were analyzed with the laser-diffraction analyzer, but we suspected that the significant sample loss might strongly affect our results. We therefore re-disaggregated the same samples, cutting new, thinner slices to ensure that they would come apart more effectively. Grain-size averages from the well-disaggregated samples are coarser than their poorly disaggregated counterparts (figure 3). The size differences between poorly and well-disaggregated

samples might be due to natural variation in the rock, or suggest preferential cementation of certain grain sizes (Houseknecht, 1984; McBride, 1989; Walderhaug, 1996). Since removal of preferentially cemented grain sizes may affect particle-size distribution, extraction of too many sandstone pieces could introduce error into textural-analysis results.

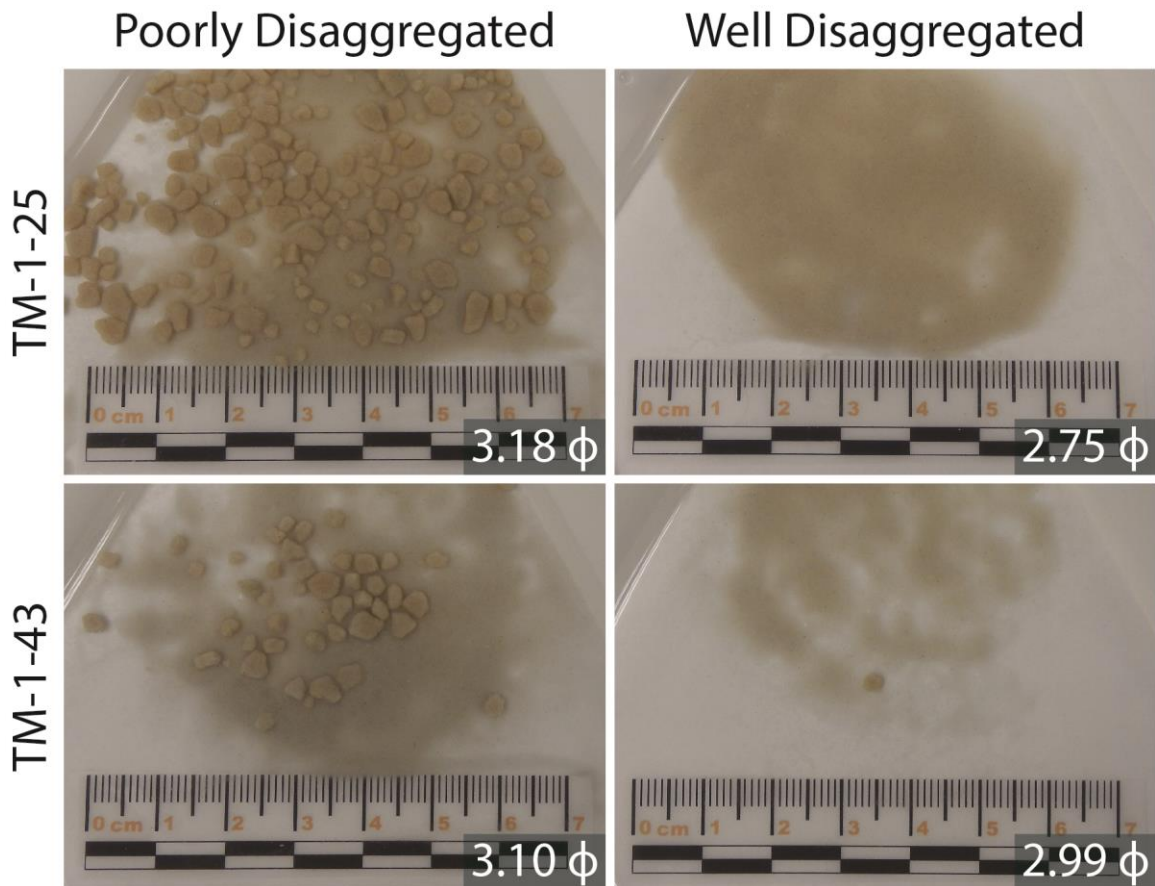


Figure 3: Comparison of average grain sizes (ϕ) for two TM-1 samples: poorly disaggregated at first and reanalyzed after being better disaggregated. Many aggregated grains had to be removed from the poorly disaggregated samples, resulting in significant sample loss. While it is possible that the differences in grain size result from natural variation in the sample or other factors, they also suggest that the removal of too many aggregated grains could introduce error into the particle-analysis results. Two additional TM-1 samples (not pictured) also differ in grain size when better disaggregated (*TM-1-45*: 3.10 ϕ , poorly disaggregated; 2.84 ϕ , well disaggregated; *TM-1-50*: 2.91 ϕ , poorly disaggregated; 2.77 ϕ , well disaggregated).

Overgrowths Remaining on Grains

Thin-section and scanning-electron-microscope (SEM) photos reveal overgrowths remaining on the disaggregated grains (figure 4). Because these overgrowths appear small in thin section (figure 5), we do not expect that they would have a significant impact on our particle-analysis results, except possibly a slight increase in grain size. Our thin-section histograms do compare well with those from the laser-diffraction analyzer (figure 2), with the analyzer grain sizes being slightly coarser overall (as expected). Furthermore, the difference between the medians of our thin-section and laser-diffraction data sets (based on average grain sizes for each sample) is $33.7 \mu\text{m}$, or 4.9ϕ (for all samples analyzed by both methods; $n = 36$). While this difference may be influenced by numerous variables such as natural sample variation and sources of error, it places an approximate size constraint on the overgrowth cement, especially since whole-particle data are already coarser than thin-section measurements. The appearance of overgrowths in thin section, the relatively close agreement of our particle-analysis and thin-section graphs, and the limited difference between medians from each method, therefore support the hypothesis that – at least in our Coconino Sandstone outcrops – overgrowths may only slightly increase the grain size of disaggregated samples.

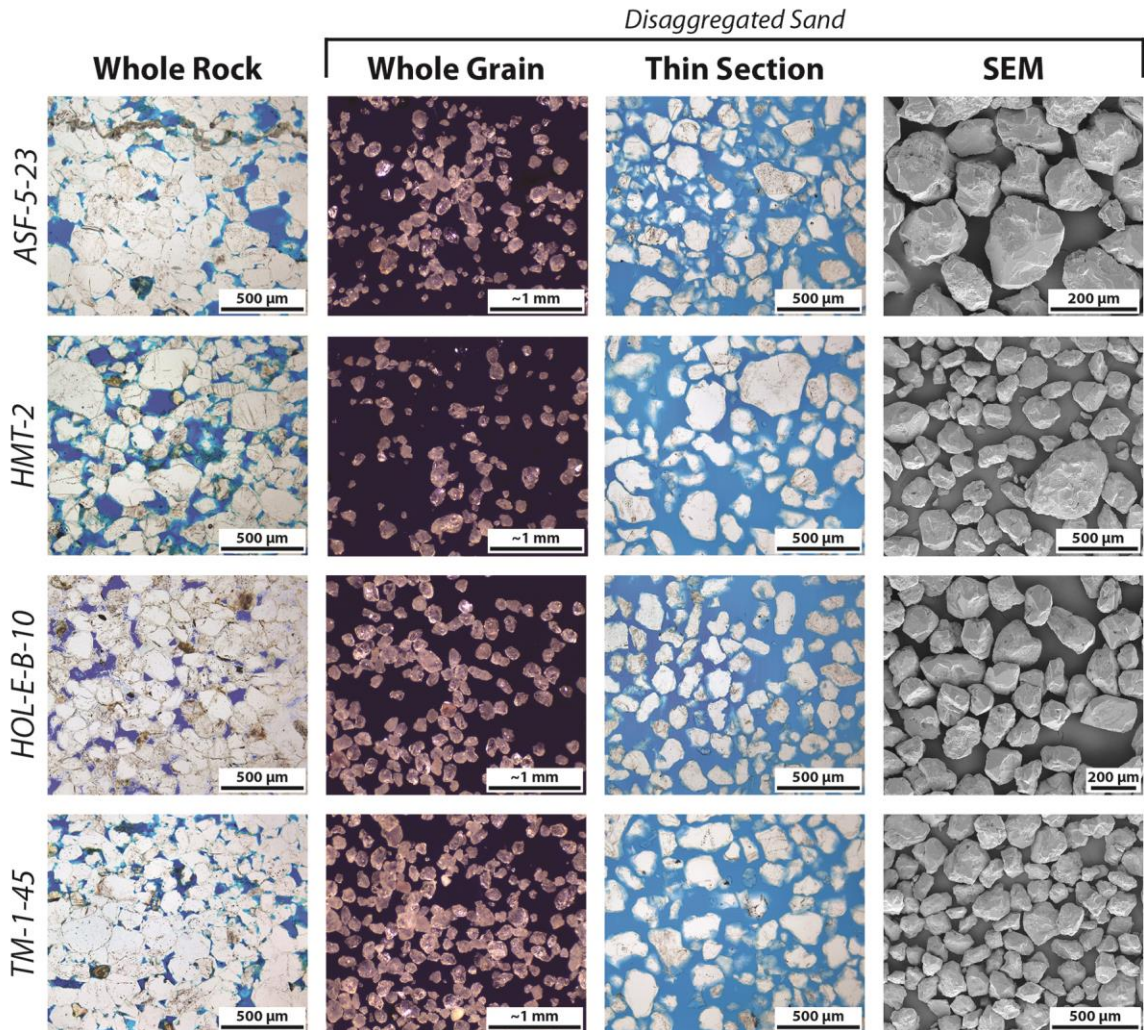


Figure 4: Four Coconino Sandstone samples shown lithified (in thin section; lefthand column) and disaggregated (three righthand columns). Most of the disaggregated grains retain their quartz overgrowths. The Holbrook samples (e.g., HOL-E-B-10), however, are generally less well cemented than the others and can be easily crushed by hand, which may correspond to smaller overgrowths and a different paragenetic history for that area. Thin-section photo brightness and levels were adjusted in Adobe Photoshop, and uneven illumination was corrected with methods similar to those described in Leong et al. (2003). In the HOL-E-B-10 thin-section photo, epoxy coloration was enhanced in Adobe Photoshop due to poor impregnation of that sample.

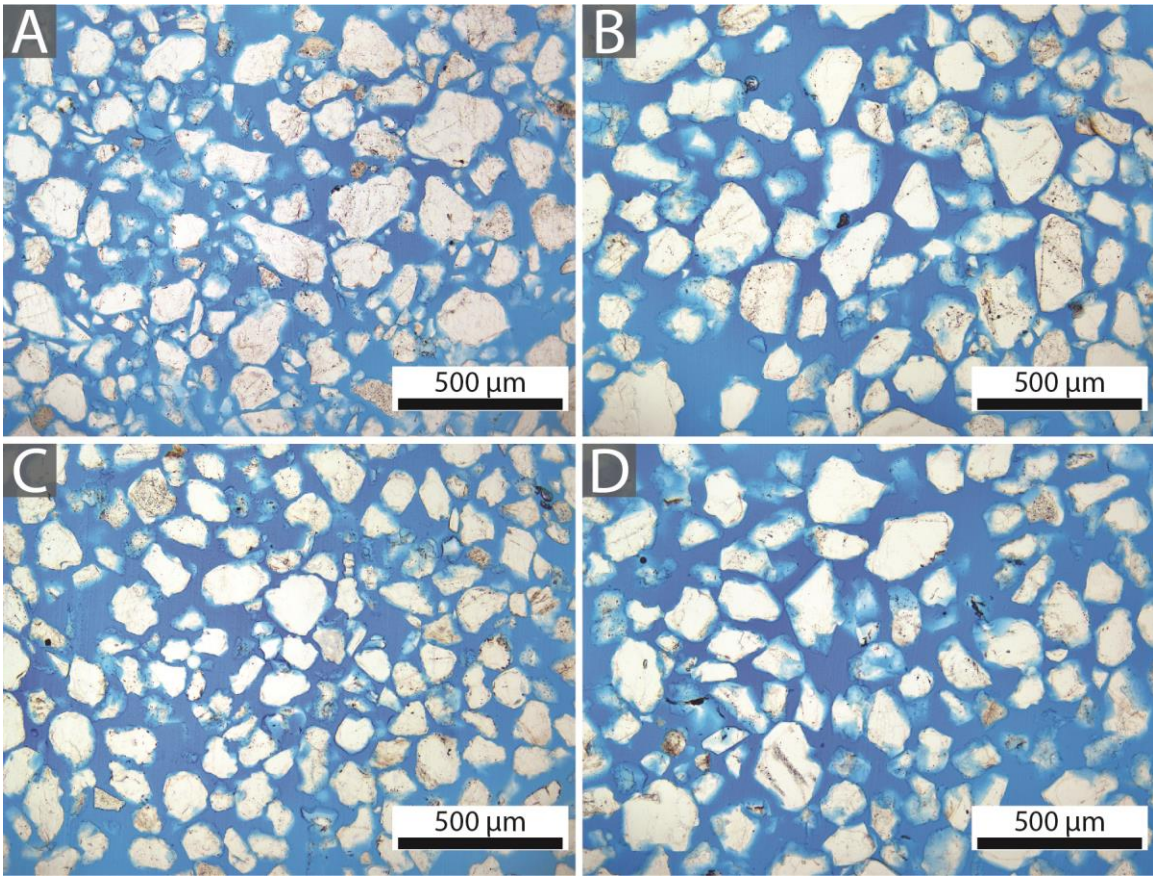


Figure 5: Photos of disaggregated sand in thin section. While distinct overgrowths are visible on many grains, they generally appear small. Brightness, contrast, levels, and uneven illumination were adjusted in Adobe Photoshop. The four samples shown include **A)** ASF-5-23, **B)** HMT-2, **C)** HOL-E-B-10, and **D)** TM-1-45.

Studies have been conducted on quartz overgrowths that required the overgrowths to be isolated from the quartz grains (Lee and Savin, 1985; Brint et al., 1991; Girard and Deynoux, 1991; Graham et al., 1996). Samples were etched in dilute hydrofluoric acid (HF) to preferentially dissolve dust-rim minerals and then sonicated to separate the overgrowths. Such methods might be employed to improve our disaggregation methods, but they would add additional steps and safety precautions for using HF. Since the overgrowths remaining on our disaggregated grains appear small, we therefore suggest that removing the overgrowths is not essential for our samples and probably for many

other formations. However, these additional steps could be taken if the overgrowths are suspected or observed to notably change the size of the sand.

Comparison between Thin-Section and Laser-Particle-Analysis Methods

Our main objective in developing these disaggregation methods was to provide a viable and more efficient alternative to measuring grains in thin section. Average grain sizes from thin-section and whole-grain analysis should not directly compare because of a fundamental difference between the methods: long axes measured in a 2D thin section generally do not represent the true longest axes of the original grains, and should likely underestimate grain size in most cases (e.g., Smith, 1966; Sahu, 1968b; Johnson, 1994). We accordingly find that average grain sizes from our thin sections are finer than those from laser diffraction (figure 6). Methods for converting 2D to 3D grain-size distributions have been developed (e.g., Heilbronner and Barrett, 2014), but these are not straightforward.

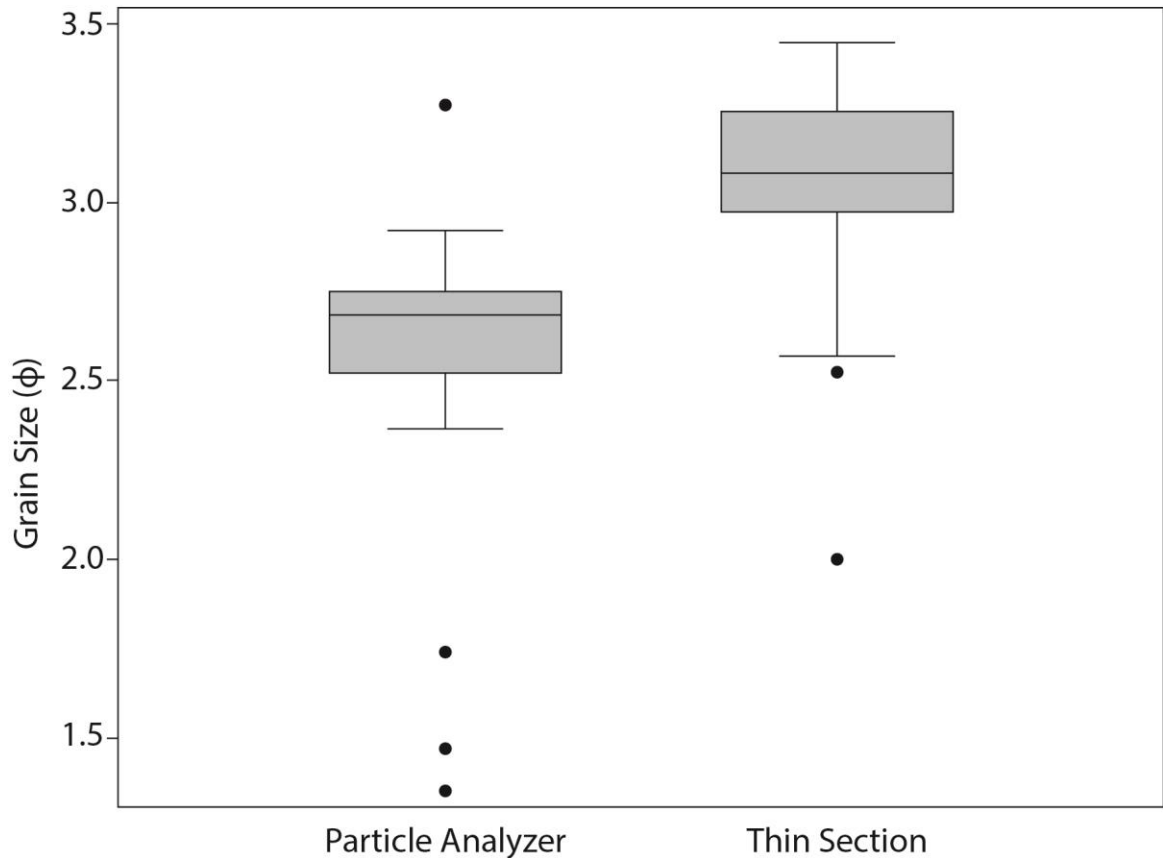


Figure 6: Boxplot comparing grain-size data from laser-diffraction particle analysis and long grain axes in thin section for selected samples. When compared using a two-sample t-test, the average grain sizes from the particle analyzer are coarser overall than those from thin section ($p < 0.0001$; $n = 36$).

While overall grain sizes may differ between the methods, grain-size *trends* should be comparable; e.g., a cross-bed set that exhibits reverse grading from thin-section data should also be inversely graded from particle analysis. We find that average grain sizes from thin section correlate well with those from the particle analyzer (using a Pearson correlation), with statistical significance for all groups included in our analysis (table 7). To determine whether disaggregation quality could affect this correlation, we re-disaggregated and re-analyzed five samples from the non-HOL Coconino Sandstone group (ensuring that they were well disaggregated), and did see an improvement in the correlation for that group (Pearson = 0.7368; $p = 0.0017$; $n = 15$). This observation

further emphasizes the importance of disaggregating samples as fully as possible, and implies that discrepancy between thin-section and particle-analyzer data is partially related to variables such as disaggregation quality and/or grain fracturing. The strong correlation between our thin-section and particle-analyzer data suggests that the average grain sizes from the laser analyzer generally correspond well to those from thin section, which strengthens the validity of both methods for characterizing textural trends.

Table 7: Correlation between average grain sizes (ϕ) from thin-section and laser-diffraction particle analysis

Group	Samples	Pearson	p-value
All Samples	36	0.9002	< 0.0001
HOL-E-B	15	0.9399	< 0.0001
Non-HOL Coconino Sandstone	15	0.5812	0.023
Non-Coconino Sandstone	6	0.9028	0.0137

Mineralogical Constraints

Mineralogical composition may control how sandstones respond to our proposed disaggregation methods. The sandstones used in this study are composed chiefly of quartz and feldspar, with small percentages of clays and heavy minerals. Most are cemented by incomplete quartz overgrowths, but some contain carbonate cement. Our current disaggregation methodology aims to isolate the framework silicate grain fraction by removing carbonate and clay components. Accordingly, the method may not work for characterizing grain size in samples that contain a large percentage of carbonate grains, since these would be dissolved. Even if the HCl dissolution step is skipped, the response of relatively soft carbonate clasts to intense agitation, especially alongside quartz and

feldspar, has not been tested. Therefore, this methodology is probably best used for disaggregation of quartz arenites and feldspathic arenites.

Relative variation in hardness and cleavage among silicate minerals could result in preferential degradation of certain grains during disaggregation. Feldspars – which are softer than quartz and exhibit cleavage – are often partially dissolved in our Coconino Sandstone samples. Even though these were usually not measured in thin section, intact and fragmented feldspars would still be included in particle-analyzer data. Furthermore, the disaggregation methods might crush these feldspars into fines, which would be subsequently removed during the rinsing step.

To determine whether feldspars were removed by the disaggregation and rinsing methods, mineralogy before and after processing was measured by x-ray diffraction (weight percentages were estimated using MDI Jade software). While natural variation within the samples could slightly affect compositional trends, the difference in feldspar content between whole-rock and disaggregated samples is not significant (Wilcoxon signed rank test; $p = 0.1563$; $n = 7$; table 8). Persistence of feldspars in disaggregated sand – along with the strong correlation between associated thin-section and particle-analyzer data – suggests that any feldspar degradation should not significantly affect the results of our methodology.

Table 8: Relative feldspar percentages (%) from x-ray-diffraction analysis of whole-rock and disaggregated samples

Sample	Whole Rock	Disaggregated
ALC-3	15	12
COW-3	16	16
HMT-4	11	10
KIN-1	15	14
KIN-2	23	23
TEN-1	13	10
TM-3-8	9	10
Average	15	14

Relative percentages were calculated based on quartz and the sum of all recognized feldspar phases $\left(\frac{\text{Feldspar}}{\text{Quartz} + \text{Feldspar}} \times 100\right)$. Feldspar phases include K-feldspars, anorthoclase, and a small percentage of plagioclase in one sample.

Conclusions

The overall quality of our particle-analysis results and correlation with thin-section data from the Coconino Sandstone suggest that these disaggregation methods may provide a robust alternative to petrography for characterizing textures in quartz-cemented sandstones. More work could be done to explore methods for successfully removing quartz overgrowths, and for comparing particle-analysis results to long-axis data from additional outcrops. While this study focused on the Coconino Sandstone, the well-lithified nature of most of our samples, compared with some weakly cemented samples, suggests that the methods should work on other quartz-rich sandstone units. Certain steps could be modified to accommodate specific project goals; for example, researchers may choose to skip the rinsing step to include the distribution of clay-size grains. We hope that our disaggregation methods will greatly increase the potential for describing and

interpreting sandstone textures, for both historical and industrial applications of sedimentology.

Acknowledgements

Substantial help was provided by Dr. Kevin Nick on the laboratory work and analyses that were involved in this project. Statistical analyses were conducted by the Research Consulting Group in the Center for Health Research at the Loma Linda University School of Public Health. We thank Loma Linda University and The Geological Society of America (Graduate Student Research Grant, #11232-16) for support and funding, and Calgary Rock and Materials Services Inc. for providing most of our thin sections. Field work and sampling in Grand Canyon National Park was conducted under permit number GRCA-2016-SCI-0033. Ash Fork field work was conducted under a US Forest Service Special Use Permit. We thank Big Boquillas Ranch for access to the Seligman-area outcrops, and Michael Reidhead for access to Five Mile Wash on his land in Holbrook.

References

- Adams, J., 1977, Sieve size statistics from grain measurement: *Journal of Geology*, v. 85, p. 209-227.
- Ahlbrandt, T. S., 1979, Textural parameters of eolian deposits, *in* McKee, E. D., ed., *A Study of Global Sand Seas*: Honolulu, Hawaii, University Press of the Pacific, p. 21-51.
- Amaral, E. J., and Pryor, W. A., 1977, Depositional environment of the St. Peter Sandstone deduced by textural analysis: *Journal of Sedimentary Petrology*, v. 47, no. 1, p. 32-52.
- Blakey, R. C., 1988, Basin tectonics and erg response: *Sedimentary Geology*, v. 56, p. 127-151.

- Blakey, R. C., and Knepp, R., 1989, Pennsylvanian and Permian geology of Arizona, *in* Jenney, J. P., and Reynolds, S. J., eds., *Arizona Geological Society Digest*, v. 17, p. 313-347.
- Brint, J. F., Hamilton, P. J., Haszeldine, R. S., Fallick, A. E., and Brown, S., 1991, Oxygen isotopic analysis of diagenetic quartz overgrowths from the Brent Sands: a comparison of two preparation methods: *Journal of Sedimentary Petrology*, v. 61, no. 4, p. 527-533.
- Chayes, F., 1950, On the bias of grain-size measurements made in thin section: *Journal of Geology*, v. 58, no. 2, p. 156-160.
- , 1951, On the bias of grain-size measurements made in thin section: a reply: *Journal of Geology*, v. 59, no. 3, p. 274-275.
- Clemmensen, L. B., and Abrahamsen, K., 1983, Aeolian stratification and facies association in desert sediments, Arran basin (Permian), Scotland: *Sedimentology*, v. 30, p. 311-339.
- Fernlund, J. M. R., Zimmerman, R. W., and Kragic, D., 2007, Influence of volume/mass on grain-size curves and conversion of image-analysis size to sieve size: *Engineering Geology*, v. 90, p. 124-137.
- Francus, P., 1998, An image-analysis technique to measure grain-size variation in thin sections of soft clastic sediments: *Sedimentary Geology*, v. 121, p. 289-298.
- Freeman, W. E., and Visser, G. S., 1975, Stratigraphic analysis of the Navajo Sandstone: *Journal of Sedimentary Petrology*, v. 45, no. 3, p. 651-668.
- Friedman, G. M., 1958, Determination of sieve-size distribution from thin-section data for sedimentary petrological studies: *Journal of Geology*, v. 66, no. 4, p. 394-416.
- , 1962, Comparison of moment measures for sieving and thin-section data in sedimentary petrological studies: *Journal of Sedimentary Petrology*, v. 32, no. 1, p. 15-25.
- , 1965, In defence of point counting analysis, a discussion: *Sedimentology*, v. 4, p. 247-253.
- , 1996, Thin section grain size analysis revisited: *Sedimentology*, v. 43, p. 189-191.
- Girard, J. P., and Deynoux, M., 1991, Oxygen isotope study of diagenetic quartz overgrowths from the upper Proterozoic quartzites of western Mali, Taoudeni Basin: implications for conditions of quartz cementation: *Journal of Sedimentary Petrology*, v. 61, no. 3, p. 406-418.

- Graham, C. M., Valley, J. W., and Winter, B. L., 1996, Ion microprobe analysis of $^{18}\text{O}/^{16}\text{O}$ in authigenic and detrital quartz in the St. Peter Sandstone, Michigan Basin and Wisconsin Arch, USA: contrasting diagenetic histories: *Geochimica et Cosmochimica Acta*, v. 60, no. 24, p. 5101-5116.
- Gray, N. H., 1969, Grain size-frequency distributions from thin-section data: *Journal of Sedimentary Petrology*, v. 39, no. 4, p. 1598-1599.
- Greenman, N. N., 1951, The mechanical analysis of sediments from thin-section data: *Journal of Geology*, v. 59, no. 5, p. 447-462.
- Harrell, J. A., and Eriksson, K. A., 1979, Empirical conversion equations for thin-section and sieve derived size distribution parameters: *Journal of Sedimentary Petrology*, v. 49, no. 1, p. 273-280.
- Heilbronner, R., and Barrett, S., 2014, *Image Analysis in Earth Sciences; Microstructures and Textures of Earth Materials*, Berlin, Springer-Verlag, 520 p.
- Houseknecht, D. W., 1984, Influence of grain size and temperature on intergranular pressure solution, quartz cementation, and porosity in a quartzose sandstone: *Journal of Sedimentary Petrology*, v. 54, no. 2, p. 348-361.
- Howell, J., and Mountney, N., 2001, Aeolian grain flow architecture: hard data for reservoir models and implications for red bed sequence stratigraphy: *Petroleum Geoscience*, v. 7, p. 51-56.
- Hunter, R. E., 1981, Stratification styles in eolian sandstones: some Pennsylvanian to Jurassic examples from the western interior U.S.A., *in* Ethridge, F. G., and Flores, R. M., eds., *Recent and Ancient Nonmarine Depositional Environments: Models for Exploration*: Society of Economic Paleontologists and Mineralogists, Special Publication 31, p. 315-329.
- Johnson, M. R., 1994, Thin section grain size analysis revisited: *Sedimentology*, v. 41, p. 985-999.
- Kellerhals, R., Shaw, J., and Arora, V. K., 1975, On grain size from thin sections: *Journal of Geology*, v. 83, p. 79-96.
- Keulen, N., Frei, D., Bernstein, S., Hutchison, M. T., Knudsen, C., and Jensen, L., 2008, Fully automated analysis of grain chemistry, size and morphology by CCSEM: examples from cement production and diamond exploration: *Geological Survey of Denmark and Greenland Bulletin*, v. 15, p. 93-96.
- Kocurek, G., 1991, Interpretation of ancient eolian sand dunes: *Annual Review of Earth and Planetary Sciences*, v. 19, p. 43-75.

- Kocurek, G., and Dott, R. H., 1981, Distinctions and uses of stratification types in the interpretation of eolian sand: *Journal of Sedimentary Petrology*, v. 51, no. 2, p. 579-595.
- Kong, M., Bhattacharya, R. N., James, C., and Basu, A., 2005, A statistical approach to estimate the 3D size distribution of spheres from 2D size distributions: *Geological Society of America Bulletin*, v. 117, no. 1/2, p. 244-249.
- Krumbein, W. C., 1935, Thin-section mechanical analysis of indurated sediments: *Journal of Geology*, v. 43, no. 5, p. 482-496.
- , 1950, Grain-size measurements made in thin section: comments: *Journal of Geology*, v. 58, no. 2, p. 160.
- Langford, R. P., and Chan, M. A., 1993, Downwind changes within an ancient dune sea, Permian Cedar Mesa Sandstone, southeast Utah, *in* Pye, K., and Lancaster, N., eds., *Aeolian Sediments: Ancient and Modern*: International Association of Sedimentologists, Special Publication 16, p. 109-126.
- Lee, M., and Savin, S. M., 1985, Isolation of diagenetic overgrowths on quartz sand grains for oxygen isotopic analysis: *Geochimica et Cosmochimica Acta*, v. 49, p. 497-501.
- Leong, F. J. W.-M., Brady, M., and McGee, J. O., 2003, Correction of uneven illumination (vignetting) in digital microscopy images: *Journal of Clinical Pathology*, v. 56, no. 8, p. 619-621.
- Loope, D. B., 1984, Eolian origin of upper Paleozoic sandstones, southeastern Utah: *Journal of Sedimentary Petrology*, v. 54, p. 563-580.
- Loope, D. B., Elder, J. F., and Sweeney, M. R., 2012, Downslope coarsening in aeolian grainflows of the Navajo Sandstone: *Sedimentary Geology*, v. 265-266, p. 156-162.
- Lundy, W. L., 1973, The stratigraphy and evolution of the Coconino Sandstone of northern Arizona [MS thesis]: University of Tulsa, 106 p.
- Maithel, S. A., Brand, L., and Whitmore, J. H., 2016, Using textural trends to interpret cross-bed depositional processes in the Coconino Sandstone (Permian), Arizona: *Geological Society of America Abstracts with Programs*, v. 48, no. 7.
- Maithel, S. A., Garner, P. A., and Whitmore, J. H., 2015, Preliminary assessment of the petrology of the Hopeman Sandstone (Permo-Triassic), Moray Firth Basin, Scotland: *Scottish Journal of Geology*, v. 51, no. 2, p. 177-184.

- Maithel, S. A., and Whitmore, J. H., 2010, Textural analysis of the Coconino Sandstone, Chino Point, Arizona: Geological Society of America Abstracts with Programs, v. 42, no. 5, p. 426.
- Mazzullo, J. M., and Ehrlich, R., 1983, Grain-shape variation in the St. Peter Sandstone: a record of eolian and fluvial sedimentation of an early Paleozoic cratonic sheet sand: *Journal of Sedimentary Petrology*, v. 53, no. 1, p. 105-119.
- Mazzullo, J., and Kennedy, S. K., 1985, Automated measurement of the nominal sectional diameters of individual sedimentary particles: *Journal of Sedimentary Petrology*, v. 55, no. 4, p. 593-595.
- McBride, E. F., 1989, Quartz Cement in Sandstones: A Review: *Earth-Science Reviews*, v. 26, p. 69-112.
- McKee, E. D., 1934, The Coconino Sandstone - its history and origin: Carnegie Institution of Washington Publication 440, p. 77-115.
- Middleton, L. T., Elliott, D. K., and Morales, M., 2003, Coconino Sandstone, *in* Beus, S. S., and Morales, M., eds., *Grand Canyon Geology*: New York, Oxford University Press, p. 163-179.
- Moss, A. J., and Green, P., 1975, Sand and silt grains: predetermination of their formation and properties by microfractures in quartz: *Journal of the Geological Society of Australia*, v. 22, no. 4, p. 485-495.
- Packham, G. H., 1955, Volume-, weight-, and number-frequency analysis of sediments from thin-section data: *Journal of Geology*, v. 63, no. 1, p. 50-58.
- Pelto, C. R., 1952, The mechanical analysis of sediments from thin-section data: a discussion: *Journal of Geology*, v. 60, no. 4, p. 402-406.
- Persson, A. L., 1998, Image analysis of shape and size of fine aggregates: *Engineering Geology*, v. 50, p. 177-186.
- Resentini, A., Andò, S., and Garzanti, E., 2018, Quantifying roundness of detrital minerals by image analysis: sediment transport, shape effects, and provenance implications: *Journal of Sedimentary Research*, v. 88, p. 276-289.
- Richard, S. M., Reynolds, S. J., Spencer, J. E., and Pearthree, P. A., 2000, Geologic Map of Arizona: Arizona Geological Survey, Map 35, scale 1:1,000,000.
- Roethlisberger, H., 1955, An adequate method of grain-size determination in sections: *Journal of Geology*, v. 63, no. 6, p. 579-584.

- Romain, H. G., and Mountney, N. P., 2014, Reconstruction of three-dimensional eolian dune architecture from one-dimensional core data through adoption of analog data from outcrop: *AAPG Bulletin*, v. 98, no. 1, p. 1-22.
- Rose, H. E., 1968, The determination of the grain-size distribution of a spherical granular material embedded in a matrix: *Sedimentology*, v. 10, p. 293-309.
- Sahu, B. K., 1966, Thin-section analysis of sandstones on weight-frequency basis: *Sedimentology*, v. 7, p. 255-259.
- , 1968a, Discussion of the article "grain size measurement in thin section and in grain mount" by R. E. Smith: *Journal of Sedimentary Petrology*, v. 38, no. 1, p. 266-268.
- , 1968b, Thin-section size analysis and the moment problem: *Sedimentology*, v. 10, p. 147-151.
- Schindelin, J., Arganda-Carreras, I., Frise, E., Kaynig, V., Longair, M., Pietzsch, T., Preibisch, S., Rueden, C., Saalfeld, S., Schmid, B., Tinevez, J., White, D. J., Hartenstein, V., Eliceiri, K., Tomancak, P., and Cardona, A., 2012, Fiji: an open-source platform for biological-image analysis: *Nature Methods*, v. 9, no. 7, p. 676-682.
- Schneider, C. A., Rasband, W. S., and Eliceiri, K. W., 2012, NIH Image to ImageJ: 25 years of image analysis: *Nature Methods*, v. 9, no. 7, p. 671-675.
- Seelos, K., and Sirocko, F., 2005, RADIUS – rapid particle analysis of digital images by ultra-high-resolution scanning of thin sections: *Sedimentology*, v. 52, p. 669-681.
- Smith, R. E., 1966, Grain size measurement in thin section and in grain mount: *Journal of Sedimentary Petrology*, v. 36, no. 3, p. 841-843.
- , 1968, Grain size measurement in thin section and in grain mount: reply to comment by Sahu: *Journal of Sedimentary Petrology*, v. 38, no. 1, p. 268-271.
- Speirs, J. C., McGowan, H. A., and Neil, D. T., 2008, Polar eolian sand transport: grain characteristics determined by an automated scanning electron microscope (QEMSCAN®): *Arctic, Antarctic, and Alpine Research*, v. 40, no. 4, p. 731-743.
- Stauffer, P. H., 1966, Thin-section size analysis: a further note: *Sedimentology*, v. 7, p. 261-263.
- Sumner, C. D., 1999, Stratigraphy of the northern depositional margin of the Coconino Sandstone, northern Arizona and southern Utah [MS thesis]: Stephen F. Austin State University, 161 p.

- Tchillingarian, G., 1952, Study of the dispersing agents: *Journal of Sedimentary Petrology*, v. 22, no. 4, p. 229-233.
- Thiel, G. A., 1935, Sedimentary and petrographic analysis of the St. Peter Sandstone: *Geological Society of America Bulletin*, v. 46, p. 559-614.
- van den Berg, E. H., Bense, V. F., and Schlager, W., 2003, Assessing textural variation in laminated sands using digital image analysis of thin sections: *Journal of Sedimentary Research*, v. 73, no. 1, p. 133-143.
- van den Berg, E. H., Meesters, A. G. C. A., Kenter, J. A. M., and Schlager, W., 2002, Automated separation of touching grains in digital images of thin sections: *Computers & Geosciences*, v. 28, p. 179-190.
- Van der Plas, L., 1962, Preliminary note on the granulometric analysis of sedimentary rocks: *Sedimentology*, v. 1, p. 145-157.
- , 1965, In defence of point counting analysis, a reply: *Sedimentology*, v. 4, p. 247-253.
- van der Wielen, K. P., Pascoe, R., Weh, A., Wall, F., and Rollinson, G., 2013, The influence of equipment settings and rock properties on high voltage breakage: *Minerals Engineering*, v. 46-47, p. 100-111.
- Walderhaug, O., 1996, Kinetic modeling of quartz cementation and porosity loss in deeply buried sandstone reservoirs: *AAPG Bulletin*, v. 80, no. 5, p. 731-745.
- Walderhaug, O., and Bjørkum, P. A., 2003, The effect of stylolite spacing on quartz cementation in the lower Jurassic Stø Formation, southern Barents Sea: *Journal of Sedimentary Research*, v. 73, no. 2, p. 146-156.
- Whitmore, J. H., and Strom, R., 2010, Textural trends in the Coconino Sandstone, central and northern Arizona, USA: *Geological Society of America Abstracts with Programs*, v. 42, no. 5, p. 428.

CHAPTER FOUR
CHARACTERIZATION OF CROSS-BED FACIES AND ASSOCIATED
DEPOSITIONAL PROCESSES IN THE PERMIAN COCONINO SANDSTONE
(ARIZONA, USA)

Abstract

Small-scale processes, which include grainflow, grainfall, and ripple migration, transport and deposit sediment on modern dune foresets. In sandstone, the cross-strata produced by these processes can be recognized by sedimentary textures, structures, and facies associations. The Permian Coconino Sandstone (northern and central Arizona, USA) is widely known for its distinctive, large-scale cross-bedding, but little has been published on the fine-scale processes that may have deposited its cross-beds. Furthermore, interpreting such processes in this formation is a challenging task, since individual dune stratification types – grainflow, grainfall, and ripple lamination – are hard to distinguish at the outcrop scale.

We used a suite of textures and sedimentary structures to interpret cross-bed depositional processes in the Coconino Sandstone. Data were collected via a combination of field measurements and laboratory analyses to characterize cross-bedding at multiple scales. We found that most beds are laterally extensive along strike and dip at angles ranging from the mid-teens to mid-twenties. Grain sizes become coarser near the base of several cross-bed sets, but vertical changes in texture vary within a single set. High-resolution scans of thin sections reveal massive and laminated microfacies, and while some inversely graded lamination was observed, laminae contacts are commonly diffuse and grading is difficult to define. Stylolite seams, associated with clay,

muscovite, and quartz-grain dissolution, are also prevalent and mimic textural lamination in some slides. Samples from one cross-bed set contain pores that are much larger than the surrounding framework grains, and these may indicate dissolution of carbonate clasts or cement.

Based on the observed bedding geometry, textural trends, and microfacies, we suggest that the cross-beds are best interpreted as undifferentiable grainfall and grainflow deposits, which may explain why individual stratification types are hard to distinguish in outcrop and thin section. This characterization of fine-scale processes will serve as a critical part of the endeavor to develop and refine larger-scale depositional models for the Coconino Sandstone.

Introduction

Since the 1970s, research on dune stratification has served an important role in the interpretation of cross-bedded sandstones. While some earlier papers recognized fine-scale processes on dune foresets (e.g., Inman et al., 1966; McKee et al., 1971), Hunter (1977) was the first to define criteria for distinguishing grainflow, grainfall/suspension and ripple laminae on modern eolian dunes. Later papers described stratification on subaqueous bedforms (Hunter, 1985b; Hunter and Kocurek, 1986), and these criteria were used to interpret a wide range of cross-bedded deposits (Buck, 1985; Clemmensen and Abrahamsen, 1983; Hunter, 1981; Kocurek, 1991; Kocurek and Dott, 1981; Loope, 1984; Loope et al., 2012; Romain and Mountney, 2014). However, specific depositional processes in some formations, like the Coconino Sandstone, have not been adequately documented.

The Permian Coconino Sandstone is a cross-bedded, quartz-rich unit that extends across northern and central Arizona. Even though the formation is widely known as a classic eolian deposit, little work has been done on its sedimentology since the landmark papers of the 1930s and 40s (McKee, 1934, 1945; Reiche, 1938). Some authors described textural parameters (Elcock, 1993; Fisher, 1961; Johnson, 1962; Lundy, 1973; McKee, 1934, 1945, 1974; Middleton et al., 2003; Reiche, 1938; Sumner, 1999) and noted ripple marks (Elcock, 1993; Lundy, 1973; McKee, 1934, 1945), but only a few have mentioned specific stratification types in the unit. Blakey and Middleton (1983), for example, referred to climbing translational strata (ripple laminae), grainflow, and grainfall in the transition interval between the upper Schnebly Hill Formation and lower Coconino Sandstone. While they provided descriptions and some photos from their study areas, the processes that dominated this transition zone may not explain cross-bed deposition throughout the rest of the formation. Blakey and Knepp (1989) mentioned grainflow and grainfall deposits, and noted these as the “only facies” in the Coconino and Glorieta Sandstones (p. 329 of their paper). Finally, Middleton et al. (2003) suggested that most cross-beds were deposited by wind ripples, and they also mentioned “wedge-shaped” avalanches that were more prevalent in thicker cross-bed sets. More recent studies have described textural trends across the formation (Maithel and Whitmore, 2010; Whitmore and Strom, 2009, 2010), but they did not distinguish specific stratification types. Additional research is therefore needed to characterize fine-scale facies within the Coconino Sandstone and to interpret associated processes. Modelling these processes may help us to understand larger-scale depositional models as well as paleo-dune morphologies and migration (Kocurek and Dott, 1981; Romain and Mountney, 2014).

For some other cross-bedded units, like the Jurassic Navajo Sandstone, stratification types are readily differentiated by texture and weathering patterns in outcrop. Kocurek and Dott (1981) noted this difference in weathering between grainfall and grainflow cross-strata in the Galesville Formation (p. 585 of their paper). The weathering patterns are likely controlled by textural variation between the stratification types and associated differences in porosity and permeability (e.g., Howell and Mountney, 2001; Kertes, 1995; Romain and Mountney, 2014). Such weathering patterns are not characteristic of the Coconino Sandstone (figure 1), however, which makes it challenging to recognize distinct stratification types.

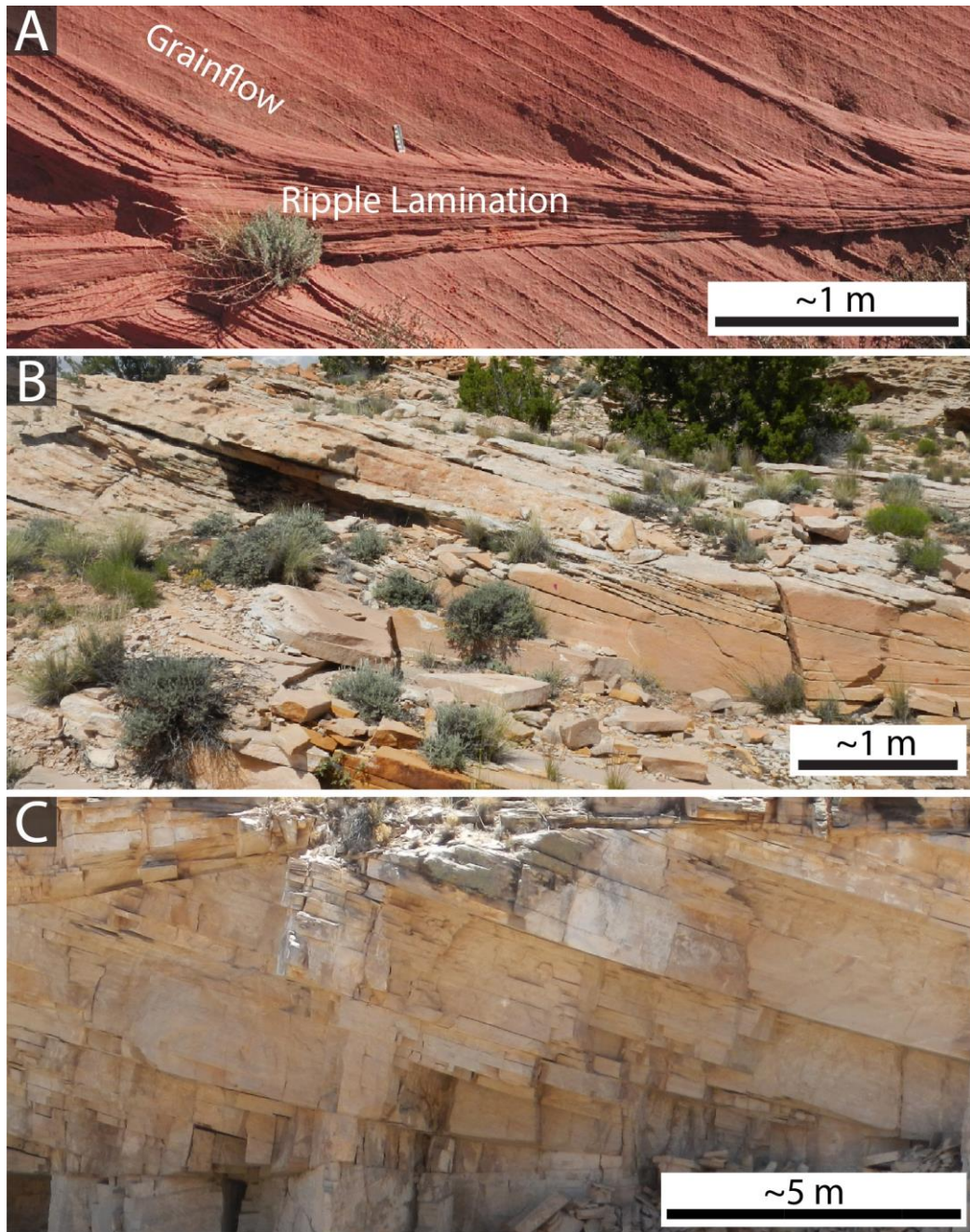


Figure 1: Comparison of outcrop weathering patterns between the Navajo (A) and Coconino (B, C) Sandstones. Cross-beds dip generally toward the right in both photos. A) In the Navajo Sandstone, grainflow cross-beds are commonly distinguishable from more-resistant ripple lamination in outcrop. Photo taken at Coyote Buttes, Utah, by Leonard Brand. B) Weathering patterns in the Coconino Sandstone are usually more homogeneous and do not reveal distinct stratification types. This is most apparent toward the right side of the photo where the cross-beds approach the base of the set. Photo taken near Holbrook, Arizona (HOL-E-B outcrop). C) Another example of homogeneous stratification patterns at a retired quarry in Chino Wash, near Seligman, Arizona (TM outcrop area). Here, the surface rock has been removed by quarrying processes, which might reduce the visibility of any weathering differences between stratification types.

Sedimentological Criteria for Distinguishing Dune Stratification Types

The three main types of dune stratification – grainflow, grainfall/suspension, and ripple laminae – can be identified by various sedimentary textural and structural parameters (Fryberger and Schenk, 1981; Hunter, 1977, 1981; Kocurek and Dott, 1981; Schenk, 1983). These criteria should serve as useful tools for interpreting depositional processes in the Coconino Sandstone, especially in light of the ambiguous weathering patterns that are characteristic of most outcrops.

Grainflow (also called *sandflow* or *avalanche*) processes occur as grains accumulate on the upper foreset of a dune and, upon reaching the angle of repose, flow down the slipface. Modern eolian grainflows typically exhibit a narrow, “tongue-like” shape (Hunter, 1977; McDonald and Anderson, 1996; Pye and Tsoar, 2009; Sweet, 1992; Sweet et al., 1988), dip at angles near the angle of repose, and pinch out sharply at their bases (Hunter, 1977). The high dip angles and sharp “pinch outs” are intrinsically linked to the gravity-driven nature of the grainflow process; Lowe (1976) suggested that grainflows “freeze” on slopes below the angle of repose, and so their deposits should not be expected to extend into low-angle bottomsets. Schenk (1983) specifically noted that grainflow cross-strata do not tangentially approach the dune base. Appropriately, below-angle-of-repose dips in some sandstones have been invoked as evidence for non-grainflow processes (Sneh, 1988). In modern and ancient dune deposits, grainflow cross-strata are usually recognized as texturally massive (lacking fine-scale internal lamination) beds that coarsen down dip (Fryberger and Schenk, 1981; Hunter, 1977; Kocurek and Dott, 1981; Schenk, 1983). Kocurek and Dott (1981) also suggested that these are generally the coarsest of the stratification types in a given dune.

Sources disagree about the mechanism that produces down-dip coarsening in grainflow deposits. Some suggest that this grading develops as a result of dispersive pressure between grains (Kocurek and Dott, 1981; Sallenger, 1979): larger grains exert greater force on surrounding grains and are “pushed” to the top of the flow. They are then moved to the base of the slope more quickly than the finer grains. Many, in fact, define “grainflows” as flows that are maintained through dispersive pressure from grain interaction (Dasgupta and Manna, 2011; Lowe, 1976, 1979; Mullins and Van Buren, 1979; Stauffer, 1967): an interpretation based partially on earlier work done by Bagnold (1954a, 1954b). This dispersive-pressure phenomenon is sometimes called the “Brazil Nut Effect” (Möbius et al., 2001).

Others (Legros, 2002; Middleton, 1970; Reesink and Bridge, 2007, 2009), however, disagree that dispersive pressure can adequately produce the down-dip coarsening observed in grainflow deposits. They submit that kinetic sieving – the process of finer grains percolating downward into pores between coarser grains – may be responsible for this sorting trend. Legros (2002) further suggested the possibility that reverse grading results from an increase in the grain size of the sediment supply. Whether dispersive pressure, kinetic sieving, a combination of the two mechanisms (Collinson and Thompson, 1989; Pye and Tsoar, 2009), or another process is responsible for down-dip coarsening in grainflow deposits, it is generally recognized that these beds do increase in grain size with distance down dip. This trend has been confirmed from cross-beds produced in various depositional settings (Allen, 1965; Allen and Narayan, 1964; Buck, 1985; Dasgupta and Manna, 2011; Dingler and Anima, 1989; Fryberger and Schenk, 1981; Hunter, 1977, 1985b; Imbrie and Buchanan, 1965; Jopling, 1965). Allen

(1984) and Kleinhans (2004) called this down-dip coarsening “reverse tangential grading.” Because grainflow processes are typically expected to produce reverse tangential grading, such coarsening trends in sandstones may suggest a grainflow interpretation for the corresponding cross-beds.

In addition to grainflow processes, grainfall/suspension and ripple migration deposit sediment on dune foresets. Both of these stratification types are thought to be finer-grained than grainflow cross-strata (Kocurek and Dott, 1981).

Grainfall is deposited when grains “fall” onto a dune foreset and are preserved without flowing downslope in a grainflow. Accordingly, these beds should normally dip at angles below and up to the angle of repose (Hunter, 1977). Eolian grainfall is generally deposited close to the dune brink (within 2 m; Nickling et al., 2002), with deposition rates decreasing exponentially with distance from the brink (Hunter, 1985a) or beyond a point of maximum deposition near the brink (Anderson, 1988; McDonald and Anderson, 1995; Sutton et al., 2013). This pattern results from the limited capacity of wind to carry sand-size grains over the foreset. For this reason, grainfall deposits should taper or thin downslope (Schenk, 1983).

Hunter (1977) suggested, based on his study of modern eolian dunes, that grainfall cross-strata may be internally laminated with thin, parallel lamination and indistinct grain segregation. Gradational contacts between experimentally produced grainfall laminae were also described by Schenk (1983), and may help to distinguish grainfall from other laminated deposits. Individual laminae may exhibit normal or reverse vertical grading (depending on wind velocity), and they should generally become

finer with distance down dip as grains progressively settle out of suspension (Fryberger and Schenk, 1981; Schenk, 1983).

Ripple laminae (often called “translatent strata”) are produced by small-scale ripples that migrate over the dune surface. Hunter (1977) described both reverse and normal vertical grading within these laminae, depending on the angle of ripple climb; however, subcritically climbing translatent strata, which are deposited by normal wind ripple migration, characteristically exhibit reverse grading (Kocurek and Dott, 1981; Schenk, 1983) or a lack of grading, but not normal grading (Fryberger and Schenk, 1981). In contrast to grainfall laminae contacts, which may appear diffuse, ripple lamination should be delineated by sharp contacts and repetition throughout the bed (Schenk, 1983).

These textures and sedimentary structures (table 1), when described within the context of individual cross-bed sets, may enable us to interpret cross-bed depositional processes in the Coconino Sandstone.

Table 1: Summary of select criteria for distinguishing dune stratification types

Process	Textures	Sedimentary Structures
<i>Grainflow</i>	-Relatively coarse-grained overall ² -Mostly massive (lacking fine lamination) ^{1,2} -Coarsens down dip ^{1,2}	-Cross-bed dip angles at or near the angle of repose ¹ -Tongue-shaped deposits ¹ -Sharp down-dip “pinch outs” ¹
<i>Grainfall/Suspension</i>	-Finer-grained overall ² -May contain textural laminae ¹ -Fines down dip ^{3,4} -Gradational laminae contacts ⁴ -Normal or reverse vertical grading possible within laminae ^{3,4}	-Dips below and up to the angle of repose possible ¹ -Tapers downslope ^{3,4}
<i>Ripple Migration</i>	-Finer-grained overall ² -Should contain graded laminae ^{1,2} -Reverse grading, sharp contacts, repetition ⁴	-Dips below and up to the angle of repose possible ¹ -Tapers upslope ³

¹Hunter (1977); ²Kocurek and Dott (1981); ³Fryberger and Schenk (1981); ⁴Schenk (1983)

Where stratification types are indistinguishable, textural trends within cross-bed sets may be useful for interpreting the general nature of depositional processes.

Kleinhan (2004) proposed a theoretical model for relating vertical grain-size variation in cross-bedded deposits to grainflow and suspension deposition (this was followed by experimental work; Kleinhan, 2005b). He suggested that grainflow processes should produce fining-upward deposits, while suspension may transport finer sediment to the base of the bedform. Variables such as sorting of the sediment mixture, suspension, and celerity affect the nature of these trends: for example, non-uniform sediment mixtures exhibit greater variation in grain size (figure 2). Others have also linked vertical sorting trends to cross-bed depositional processes (Abdel-Motaleb, 1993, 1994; Blom and Kleinhan, 2006; Blom and Parker, 2004; Blom et al., 2006; Blom et al., 2003; Jopling,

1965; Kleinhans, 2005a, b). Therefore, vertical changes in grain size within our Coconino Sandstone cross-bed sets may help us to interpret which processes dominated sediment deposition on the dune foresets.

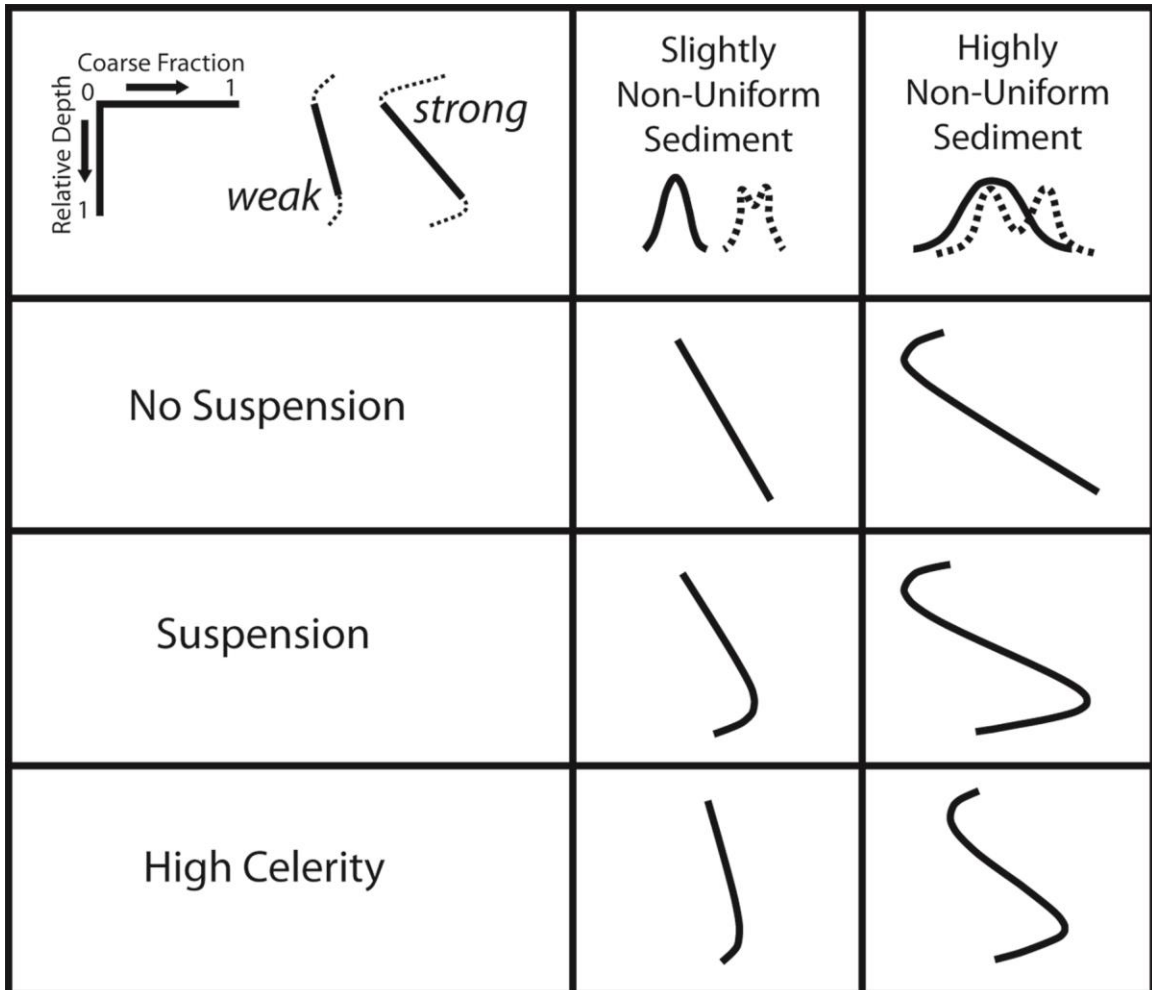


Figure 2: Vertical sorting trends, after Kleinhans (2004), p. 99, figure 10. The graphs illustrate a theoretical change in the coarsest grain fraction with relative depth. Vertical changes in grain size become exaggerated where the sediment mixture is more poorly sorted.

Methods

Coconino Sandstone outcrops were selected for this study from four areas across northern Arizona. Eight cross-bed sets were chosen from these localities: two near the

town of Ash Fork, three near the town of Seligman, two near the town of Holbrook, and one exposed along the Hermit Trail on the South Rim of the Grand Canyon (figure 3). With the exception of Grand Canyon, all of our outcrops were either retired quarries or wash exposures. These were selected because the cross-bedding was well exposed and easily accessible. Bounding surfaces were also studied at several additional locations within these study areas.

It is difficult to determine the exact stratigraphic levels of cross-bed sets in the Coconino Sandstone, especially where a complete section is not exposed. Furthermore, variable cross-bed set geometries may hinder correlation between outcrops. The studied cross-bed set along Hermit Trail (Grand Canyon) is in the bottom half of the section, with its lower bounding surface approximately 29 meters from the basal formation contact. One of the Ash Fork outcrops (ASF-22e), however, is closer to the top of the section: its upper bounding surface is ~ 10.5 m below the contact between the Coconino Sandstone and the overlying Toroweap Formation. While we were not able to measure the stratigraphic positions of all studied outcrops, the cross-bed sets likely represent various vertical intervals within the sandstone.



Figure 3: Maps showing our study areas and specific Coconino Sandstone outcrop locations. **A)** Outcrops were located in four study areas across northern Arizona: near the towns of Ash Fork, Seligman, and Holbrook, and along the Hermit Trail on the South Rim of the Grand Canyon. The grey/tan area on the map marks the approximate subsurface extent of the contiguous Coconino Sandstone (Blakey, 1988; Blakey and Knepp, 1989; McKee, 1934; Middleton et al., 2003; Richard et al., 2000). Outcrops marked with an asterisk (*) in Ash Fork and Holbrook were bounding surface exposures that were not directly related to our primary cross-bed sets. **B)** Ash Fork outcrops were retired quarries located north of the town. **C)** Seligman outcrops were retired quarries in Chino Wash, which is located north of town. The “TM” code for these outcrops was derived from “Trinity Mountain,” which is the name of the surrounding quadrangle. **D)** Holbrook outcrops were cross-bed sets exposed in Five Mile Wash, located south of the town along Highway 77.

Field Methods

Samples were collected at various down-dip positions along cross-beds, and the location of each sample was marked on printed outcrop photo mosaics in the field. Since we wanted to characterize textural trends linked to processes, sampling along individual beds (as in Loope et al., 2012), or interpreted depositional units, would be preferred. However, tracing individual bedding planes over significant distances is often difficult or impossible in the Coconino Sandstone. We therefore sampled at various positions across multiple cross-beds with the goal of describing averaged vertical trends within the sets (as in Kleinhans, 2004). The relative vertical position of each sample was determined from annotated outcrop photo mosaics in Adobe Illustrator (figure 4; table 2). For the ASF-22e, CPE, and HMT outcrops, along-dip distances were measured roughly along a single bed in the field (in HMT, however, the lowermost sample position was not measured in the field, and was estimated later from a trail map). The approximate vertical distance to each sample in these outcrops was calculated from the along-dip distance and dip angle.

This approach for describing relative vertical sample positions worked well for our outcrops, in which cross-beds were commonly difficult to trace along their entire lengths. The method also allowed us to characterize textural changes without reference to upper or lower bounding surfaces, which were not always well exposed. Even where the respective bounding surfaces are visible, accurately measuring along-dip distances can prove challenging where changes in dip angle occur, and obtaining these data from photographs further introduces the variable of apparent dip (if the outcrop face is not exactly parallel to dip direction). Various authors have described vertical grain-size trends within cross-bedded deposits (e.g., Kleinhans, 2004). While our methodology

does not describe grain-size variation within individual depositional units (like in Loope et al., 2012), it provides averaged textural trends across cross-bed sets, which may be useful, alongside other criteria, for interpreting the dominant depositional processes.

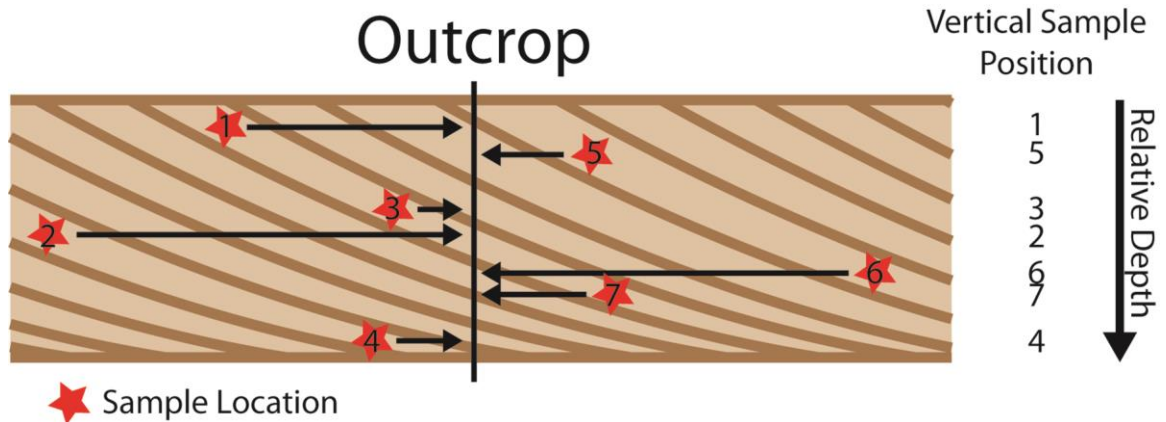


Figure 4: Explanation of relative vertical sample position method. Sample labels, which were originally marked on printed photo mosaics in the field, were horizontally aligned (in Adobe Illustrator) so that their relative positions could be determined.

Table 2: Vertical range sampled within each cross-bed set

Outcrop	Approximate Vertical Distance Sampled (m)
ASF-22e	14.9
ASF-5	23.7
CPE	6.1
HMT	26.2
HOL-E-A	2.1
HOL-E-B	2.9
TM-1 A ₁	4.4
TM-3	9.9

The upper and lower cross-bed set boundaries were not always exposed in our immediate outcrops, but we attempted to sample along as much of the exposed cross-bedding as possible. Accordingly, the sets with substantial vertical distance between samples were thicker in outcrop.

Strike and dip measurements along the cross-beds were recorded, and bedding was described in cliffs and where exposed on bounding surfaces. Most strikes and dips were measured with a standard Brunton compass, but some measurements were taken with the “Clino FieldMove” smartphone application. Structural dip for the formation was measured along the top of the Coconino Sandstone (in Chino Wash, near Seligman) as $\sim 1.5^\circ$ to the east (Leonard Brand, pers. comm.). Furthermore, a regional geologic cross section reveals minimal to no structural dip for the Coconino Sandstone (Blakey, 1988), so we do not expect that this would significantly affect our bedding-plane measurements.

Quarrying operations uncovered many extensive bounding surfaces, especially in the Ash Fork area. We took additional notes and photographs at some of these sites (marked with asterisks in figure 3) even though they were not directly related to our primary eight cross-bed sets. Plants and debris were cleared from exposed bounding surfaces and $1.0 \times 0.5 \text{ m}^2$ grids were marked on the surfaces. The ASF-3 and TM-1 surfaces were photographed from a ladder, and all of the other surfaces were photographed with drones. Identifiable bedding planes were traced along or nearly along strike on these bounding surfaces. The traced lines represent the intersection between the bounding surface and the underlying cross-bedding planes (figure 5), revealing the cross-sectional geometry of the beds.

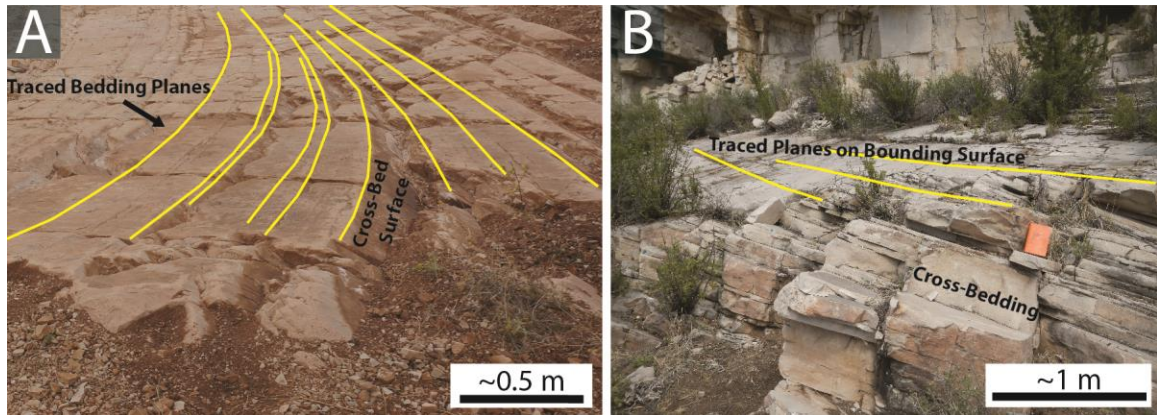


Figure 5: Illustration showing the relationship between traced bedding planes on bounding surfaces and the underlying cross-beds. The traced lines in these photos are two-dimensional representations of bedding planes where they intersect the bounding surfaces. **A)** ASF-4 bounding surface, with cross-beds dipping toward the right side of the photograph. **B)** TM-1 bounding surface, with cross-beds also dipping toward the right.

We stitched photographs of the bounding surfaces into photo mosaics using the “Photomerge” command in Adobe Photoshop (versions Creative Suite 6 and Creative Cloud). The HOL-W-A bounding surface fit into a single drone photograph and was not stitched from multiple images in Photoshop (but was still corrected for geometric distortion). When differences in perspectives (parallax error) and/or size prevented the photos from being stitched automatically, “puppet warp” and other “transform” tools were used to manually fit the images together. Since our grids were originally marked on the outcrops in the field, the size of each grid square was known even if the photos were distorted by the stitching process. Grids were traced in Adobe Illustrator (versions Creative Suite 6 and Creative Cloud) by connecting points that were marked on the bounding surface outcrops, and bedding planes were traced according to notes taken in the field. Some planes were projected across areas where they were not exposed or ambiguous/faint. For the ASF-8 bounding surface, select planes were numbered and traced on printed photos in the field. Most notable planes were traced, but not every

visible bedding plane on the surface was included. For the ASF-3, ASF-4 and HOL-W-A surfaces, all visible bedding planes were traced on printed photos in the field and were later drawn onto the digital photo mosaics. Bedding planes at TM-1 were not traced in the field, but were traced on the stitched images.

Petrographic Methods

Thin sections were made from samples collected at each outcrop. For some of our petrographic images, levels, brightness, and contrast were adjusted in Adobe Photoshop, and uneven illumination was corrected using methods similar to those described in Leong et al. (2003).

The slides were scanned using an Epson Perfection 4990 photo scanner, and scans were enlarged to full-page size so that fine-scale structures and textural changes could be observed. These high-resolution scans provided a detailed picture of the cross-beds, and the relatively larger field of view, along with blue epoxy in the pore space, made sedimentary structures – such as lamination – more visible than with higher magnifications of the petrographic microscope. Many of the thin sections from our HOL outcrops exhibited less contrast between epoxied pores and quartz grains due to variable epoxy coloration (these were not made at the same lab as our other slides). As a result, it was difficult to recognize sedimentary structures in these scans (due to the lower slide quality), and so we did not use them to describe microfacies at the Holbrook locations.

Disaggregation and Grain-Size Analysis

The Coconino Sandstone is well-cemented by quartz overgrowths in most outcrops; however, we were able to successfully disaggregate our samples for whole-

particle analysis. Samples were cut into thin slices using a diamond-blade rock saw and were broken apart (as much as possible) by hand. The crushed samples were placed in hydrochloric acid (to dissolve any carbonate), crushed further with a glass rod, and then rinsed to remove the acid. Rinsed samples were sonicated in a sodium hexametaphosphate solution using a QSonica quarter-inch microtip sonicator probe, and then rinsed a second time to remove suspended fines. At this stage, some of our samples were not completely disaggregated, and so the remaining lithified sandstone pieces were removed with tweezers. Loose Coconino Sandstone sand was analyzed using a Beckman Coulter LS 13 320 laser-diffraction particle analyzer and Universal Liquid Module (ULM). Descriptive statistics for each sample were generated by the LS software program.

Results

Interpreting cross-bed depositional processes requires the delineation of fine-scale facies in sandstone deposits. Textures and sedimentary structures were therefore described within the Coconino Sandstone to develop depositional models for its undeformed cross-bedding.

Sedimentary Structures

Most of the cross-beds in our outcrops dip at angles ranging from the mid-teens to mid-twenties, with an overall average of 19.8° ($n = 135$; figure 6). Within a given set, dip is usually fairly consistent along the cross-beds, but decreases rapidly upon approaching the lower bounding surface (however, these bounding surfaces are covered at ASF-5 and TM-3). Accordingly, the 19.8° average reflects the distribution of most

measurements from the mid-teens to mid-twenties, but does not account for significant changes in dip along a single cross-bed (figure 7).

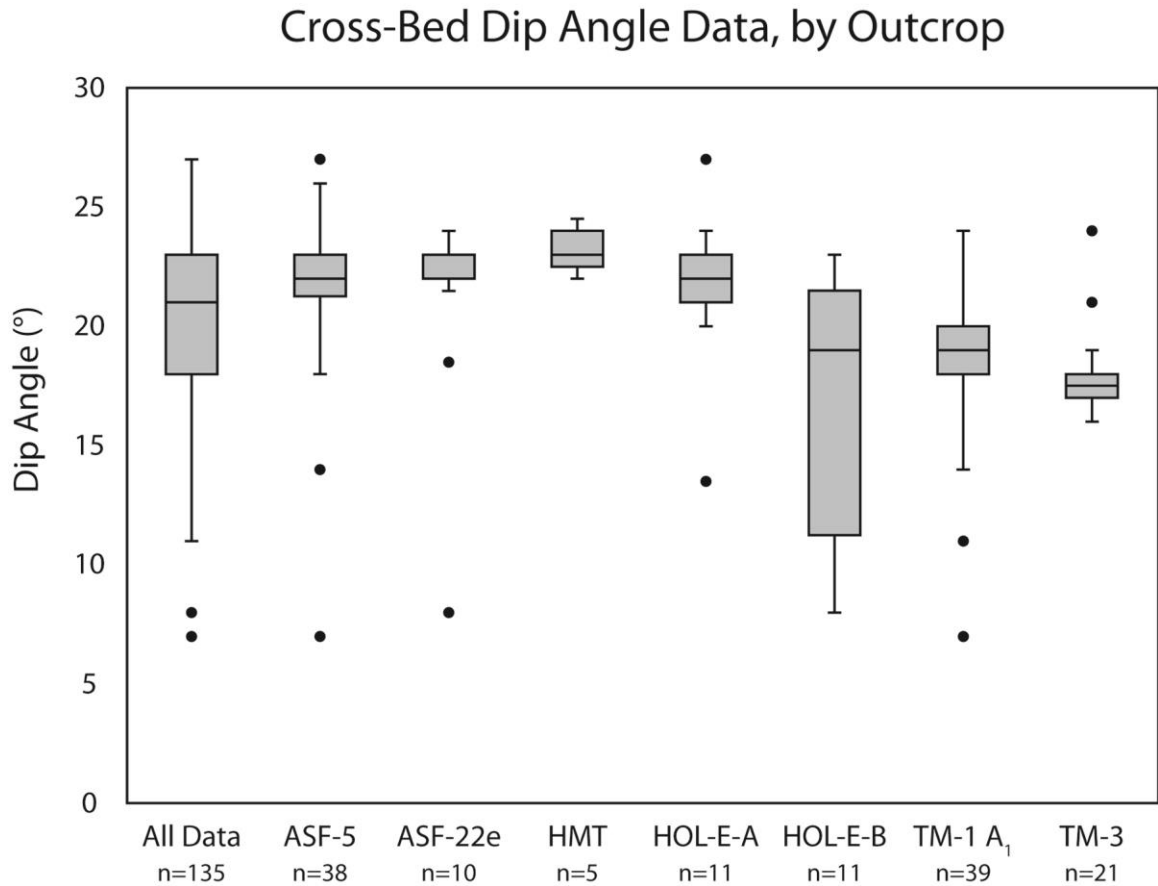


Figure 6: Cross-bed dip angles for all outcrops (except for CPE, where strike and dip measurements were not collected). At these outcrops, most cross-bed dips range from the upper teens to low/mid-twenties (average 19.8° for all samples), with dip remaining relatively constant along most of the length of a given bed.

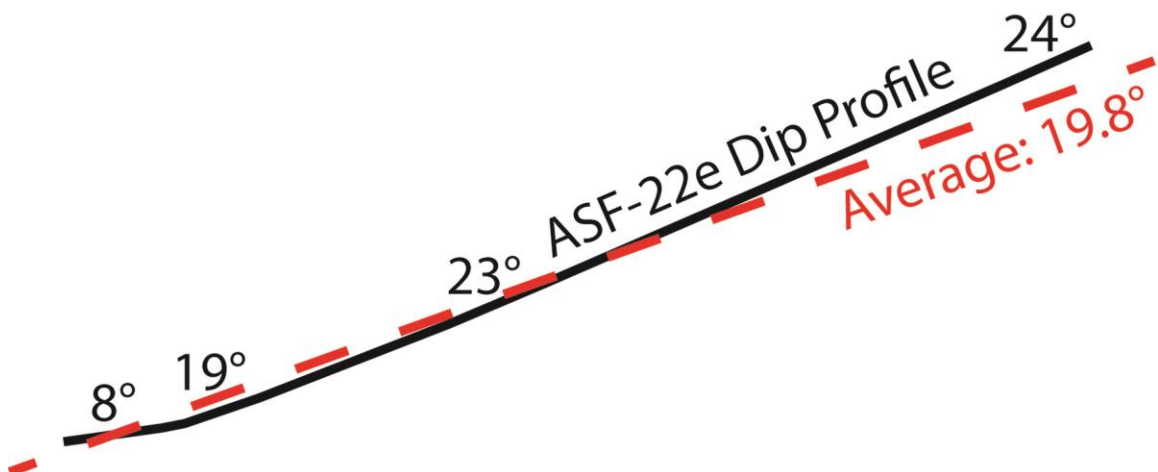


Figure 7: Diagram comparing the ASF-22e cross-bed profile to the average dip for all samples (19.8°). This comparison illustrates that the average alone does not reflect dip-angle variation along individual cross-beds.

While cross-sectional geometries of beds within our designated outcrops are not all directly exposed, many bounding surfaces have been cleared by quarrying operations in our study areas (especially near Ash Fork). These surfaces reveal truncated cross-beds that appear laterally extensive (roughly along strike), generally lacking narrow, “tongue-shaped” structures (figure 8). Variability in quality of the surface exposures prevented us from following some bedding planes over significant distances; despite this, many beds appear to extend for at least several meters, with some up to ten meters or more.

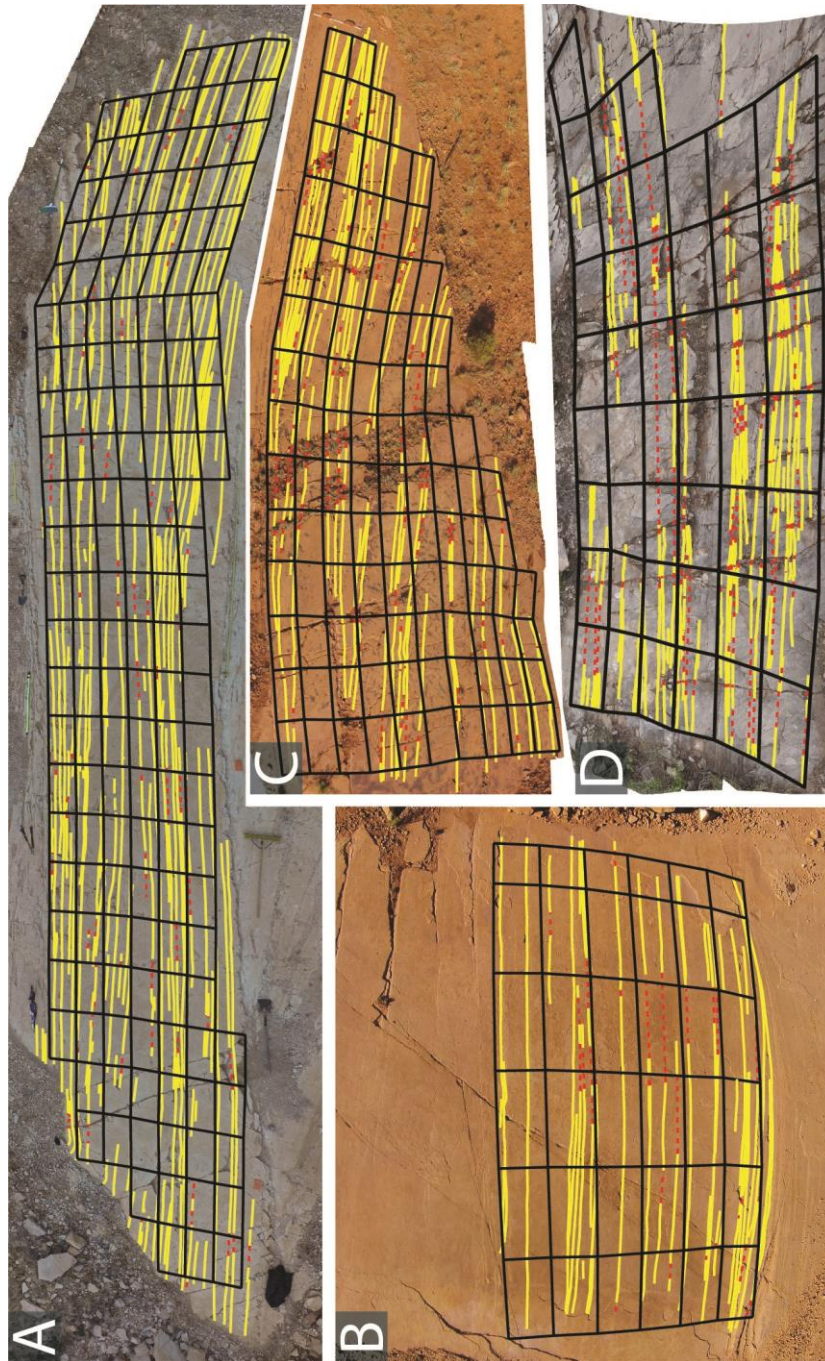


Figure 8: Photo mosaics of bounding surfaces with traced bedding planes. Grid boxes measure 1 x 0.5 m². Bedding planes are traced in yellow with red-dashed lines across areas of poor exposure. These surfaces show underlying cross-beds that are laterally extensive; narrow “tongues,” with lateral pinch outs on both sides, are not characteristic of the bedding geometries that we observed. **A)** Bounding surface in the Ash Fork area (ASF-4). **B)** Surface exposed on the west side of Five Mile Wash, near Holbrook (HOL-W-A). **C)** Ash Fork-area bounding surface (ASF-8). **D)** TM-1 bounding surface, which shows the lateral extent of the TM-1 A₁ cross-beds. Patches of overlying sandstone cover portions of this bounding surface, which limited our ability to follow some bedding planes.

In the studied outcrops, cross-bedding tangentially approaches the lower bounding surfaces without sharp “pinch outs” or other distinct stratification type differentiation (see figure 1). This occurs in contrast to many other dune deposits, in which massive beds pinch out sharply into lamination near the base of their respective cross-bed sets.

Textural Trends

Particle analysis of the disaggregated-and-rinsed sediment reveals, on average, fine sand (Wentworth, 1922) that ranges from well to moderately sorted (Folk and Ward, 1957; table 3). According to Folk (1968), all of our moderately sorted outcrops would be classified as moderately well sorted (on average). Most individual samples are unimodal (with the exception of one distinctly bimodal sample from the HMT outcrop), and many are fine skewed even after the suspended fines were removed.

Table 3: Summary of textural data for each outcrop

Outcrop	Samples	Average Grain Size (ϕ)	Average Standard Deviation of Grain Size	Sorting (Folk and Ward, 1957)
ASF-22e	10	2.87	0.58	Moderately Sorted
ASF-5	22	2.81	0.61	Moderately Sorted
CPE	8	2.89	0.68	Moderately Sorted
HMT	5	2.60	0.69	Moderately Sorted
HOL-E-A	10	2.50	0.39	Well Sorted
HOL-E-B	16	2.56	0.41	Well Sorted
TM-1 A ₁	12	2.87	0.64	Moderately Sorted
TM-3	14	2.75	0.56	Moderately Sorted

Plotting textural data on outcrop photo mosaics does not reveal obvious vertical or lateral trends (figure 9). In some sections of a given cross-bed set, the beds appear to become coarser down dip, but in other areas (moving laterally within the same set), they become finer. When textural trends are described with respect to relative vertical position within each outcrop, we find that some sets are coarser overall near their bases, but others show no significant trend (table 4).



Figure 9: Portions of the TM-3 (A) and HOL-E-A (B) outcrops with average grain-size (ϕ) and dip-angle ($^\circ$) annotations. The black-dashed lines mark the approximate locations of the upper bounding surfaces of the cross-bed sets.

Table 4: Changes in texture with respect to relative vertical position in cross-bed sets

<i>Outcrop</i>	Average Grain Size (ϕ)		Median Grain Size (ϕ)	
	<i>Correlation</i>	<i>p-value</i>	<i>Correlation</i>	<i>p-value</i>
ASF-22e	-0.86159	0.0014	-0.85393	0.0017
ASF-5	0.28975*	0.1909	0.32590*	0.1388
CPE	0.35758	0.3845	0.49971	0.2073
HMT	-0.92064	0.0265	-0.92194	0.0259
HOL-E-A	-0.69478	0.0258	-0.70320	0.0233
HOL-E-B	0.29264	0.2714	0.28347	0.2874
TM-1 A ₁	-0.35213	0.2616	-0.15158	0.6382
TM-3	-0.24396*	0.4006	-0.37582*	0.1854

Marked correlation values (*) were computed via a Spearman correlation due to non-normality. All others were calculated using a Pearson correlation. Note that since phi units are used for average and median grain size, a negative correlation corresponds with a decrease in phi value and therefore an increase in grain size with vertical distance down section.

Since most of our outcrops were not sampled along individual cross-beds, we graphed the textural data with respect to vertical sample position in the style of Kleinhans (2004). This approach reveals trends that are much more complex than Kleinhans' (2004) theoretical model. In our Coconino Sandstone outcrops, grain size (or in this case, the relative distribution of the coarsest grain fraction) does not change vertically in a consistent, predictable manner (figure 10).

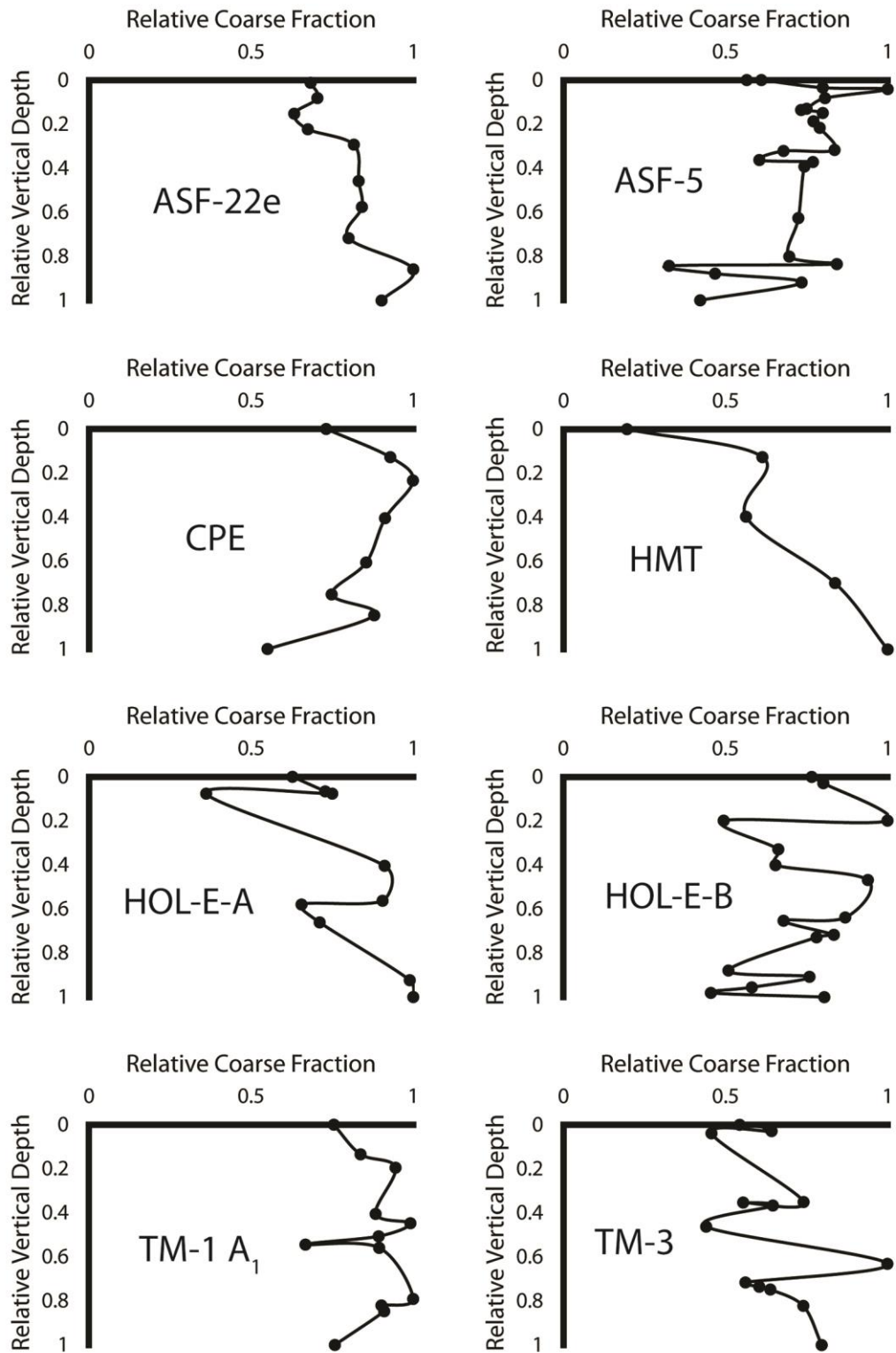


Figure 10: Graphs illustrating the relative change in the coarsest grain fraction with vertical depth, in the style of Kleinhans (2004). Each point represents the relative proportion of sediment in a given sample above the averaged median grain size for that particular outcrop.

We also graphed our data as boxplots in the style of Loope et al. (2012), who described textural changes along grainflow cross-strata in the Jurassic Navajo Sandstone (figure 11). Our data cannot compare directly with theirs, since we did not sample along individual depositional units in most outcrops; however, the graphs still highlight similarities and differences between the studied cross-beds in each sandstone. The grain sizes from Navajo Sandstone grainflows are coarser overall than our Coconino Sandstone data. Most of the cross-beds in the Loope et al. (2012) study coarsen down dip, in that the median grain size at the base is coarser than at the top. However, this coarsening trend is not well developed in many of their beds, and grain sizes vary along slope (the authors describe this variation as “erratic”). All of their Navajo Sandstone samples are well to moderately sorted, but median grain sizes range from fine to coarse sand.

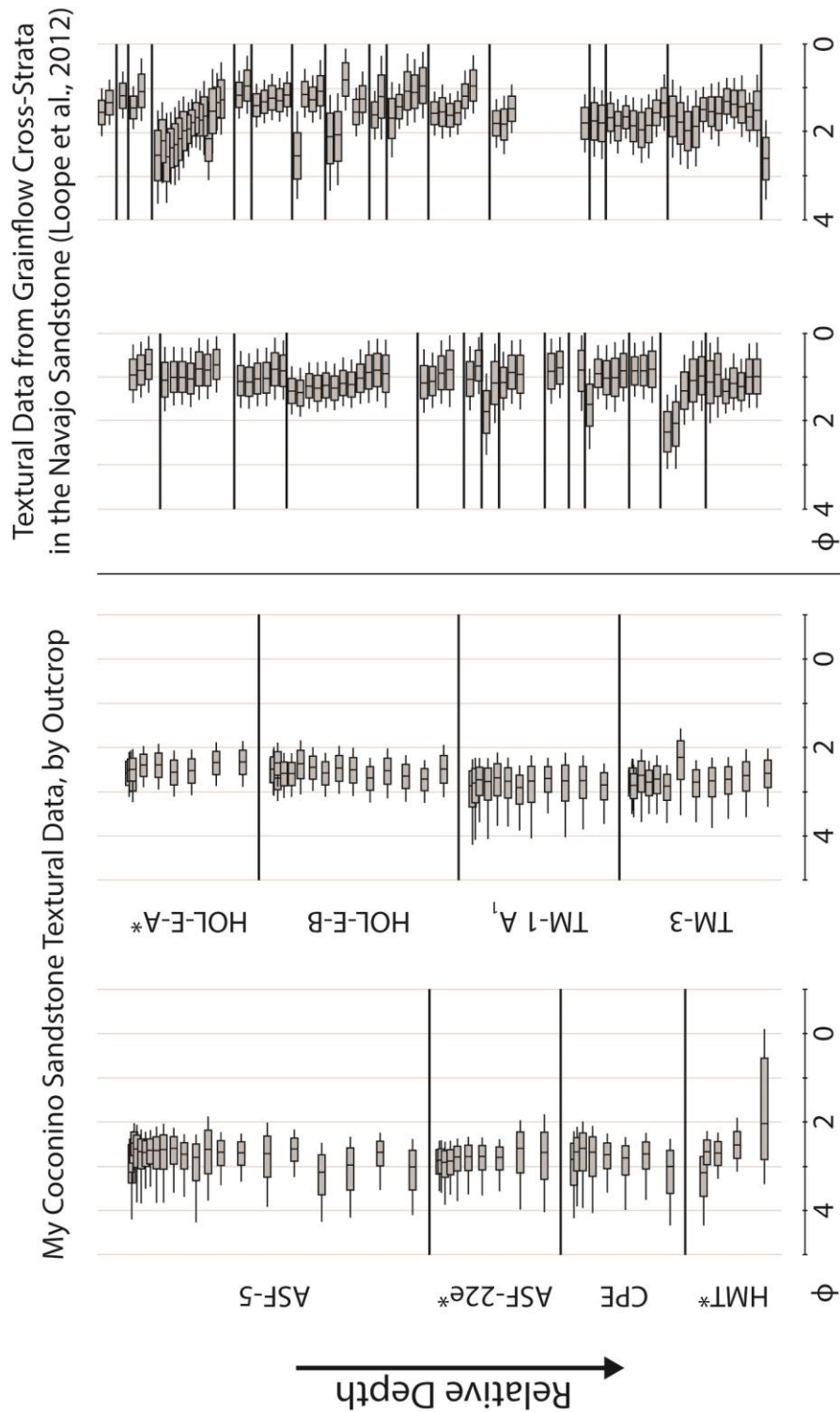


Figure 11: Vertical grain-size variation in our Coconino Sandstone cross-bed sets, graphed in the style of Loope et al. (2012) for comparison with grainflow textural data from the Jurassic Navajo Sandstone. The Navajo Sandstone data were redrawn from Loope et al. (2012), p. 159, figure 5. Error bars extend to the 10th and 90th-percentile values as in the original publication. Coconino Sandstone outcrops marked with an asterisk (*) are statistically coarser near their bases.

Microfacies

High-resolution scans of thin sections reveal a spectrum of massive to distinctly laminated textures, with primary “lamination” here defined by vertical variation in framework grain size, and “massive” beds lacking such variation. Furthermore, some samples exhibit “indistinct lamination,” which appears as vague stratification without sharp, traceable contacts. Even lamina contacts within distinctly laminated samples, however, are often difficult to trace laterally at a close scale.

Normal and reverse vertical grading are observed in individual laminae, with both trends sometimes present within a single sample. However, grading is difficult to define where laminae contacts are indistinct, and some laminations appear as relatively coarse or fine horizons that seem to lack vertical grading altogether. Most of the clearest examples of graded laminae are observed in the TM-1 A₁ cross-bed set (figure 12). This set is relatively thin compared to some of the others that we studied, but the laminae do not show a preferred distribution within the outcrop (figure 13).

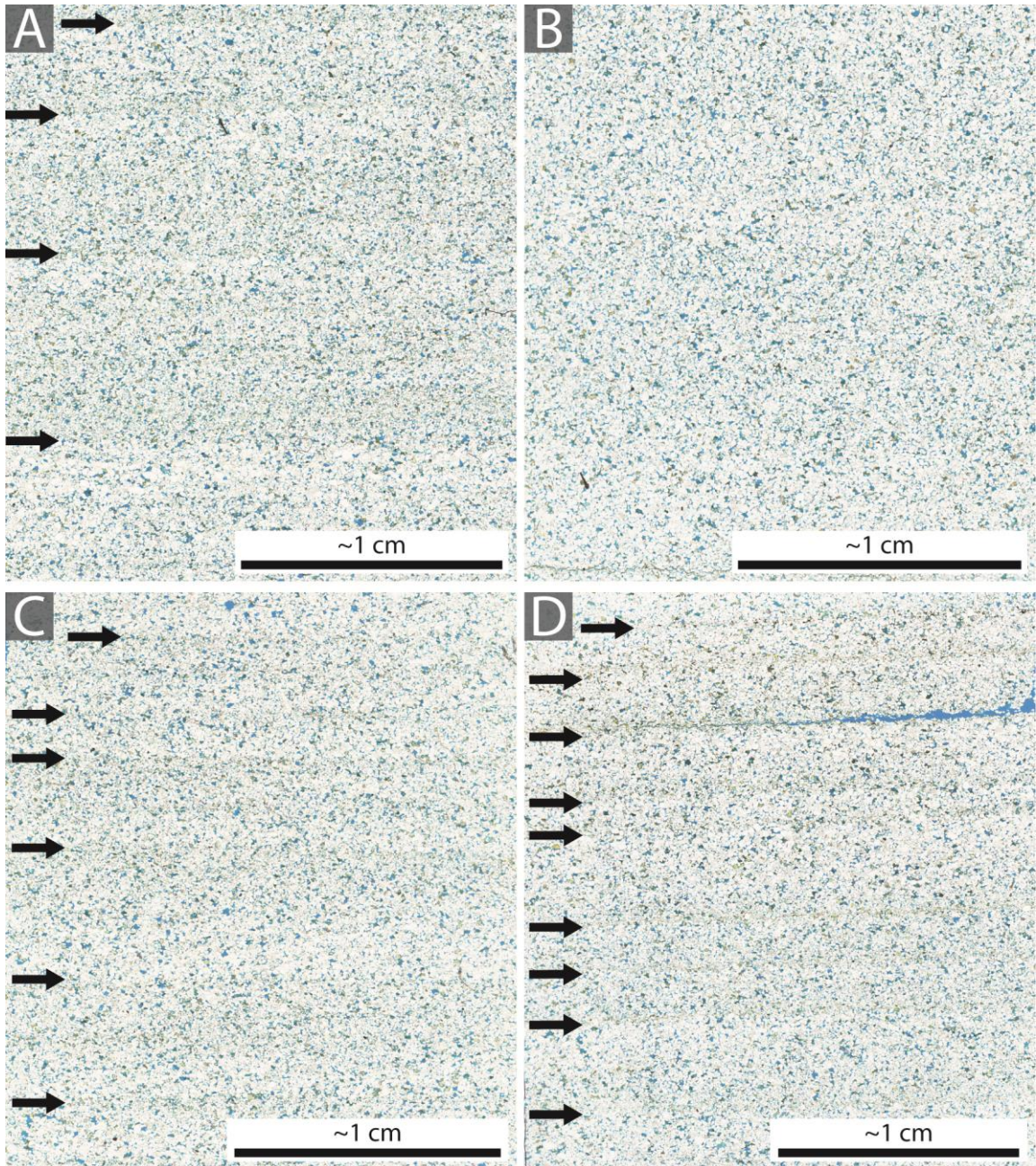


Figure 12: High-resolution scans of four thin sections from the TM-1 A₁ outcrop. This cross-bed set contains some of our best examples of distinctly laminated samples with vertical grading, but the grading style remains difficult to define where laminae contacts are diffuse. Where applicable, laminae contacts have been marked by arrows. All of these samples would be classified as moderately sorted by Folk and Ward (1957). **A)** Possible inversely graded lamination in sample TM-1-48 (standard deviation of grain size: 0.74). Some indistinct/discontinuous stratification is observed between the marked surfaces. **B)** Vague lamination without sharp contacts in sample TM-1-49 (standard deviation of grain size: 0.72). **C)** Distinct lamination with possible normal grading in sample TM-1-26 (standard deviation of grain size: 0.70). **D)** Distinct lamination and possible reverse grading in sample TM-1-50 (standard deviation of grain size: 0.64).

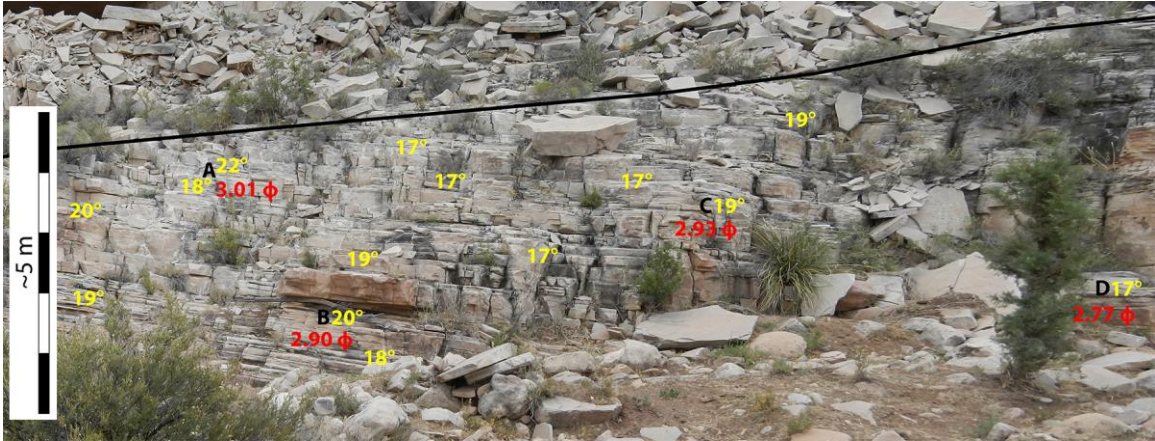


Figure 13: Distribution of dip angles and select textural data across part of the TM-1 A₁ cross-bed set. The black line marks the approximate location of the upper bounding surface. Lettered labels and average grain sizes (ϕ) correspond to the four samples pictured in figure 12. Samples A and D contain inversely graded lamination, B has indistinct stratification, and C exhibits normally graded laminae; the distribution of these facies within the cross-beds shows no distinct correlation with grain size, dip angle, or outcrop position.

In the ASF-22e outcrop, distinctly laminated samples are observed only at the base of a large cross-bed exposure (figure 14). Laminae contacts are irregular and grading appears variable or difficult to define, but grain-size variation is still visible at the centimeter scale. These laminated samples are the coarsest along this particular cross-bed, producing an overall down-dip coarsening trend. We also observe distinctly laminated cross-beds near the bases of the ASF-5 and TM-3 sets. At TM-1, many of our samples exhibit distinct lamination, but it should be noted that this is a relatively thin cross-bed set and may represent the base of a much taller bedform. At ASF-5, which is a thicker set, lamination is observed near the base in addition to other vertical horizons. While distinct lamination therefore occurs near the bottom of large cross-beds, this is not an exclusive rule, as we also observe examples of distinct laminae higher up in the sets.

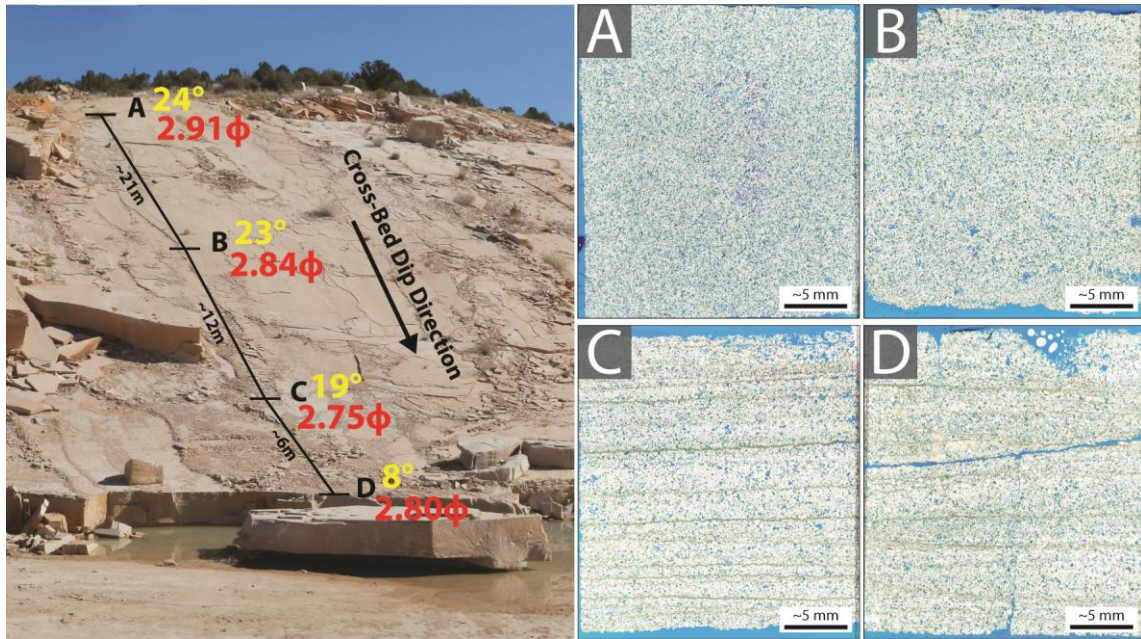


Figure 14: Textures and corresponding dip angles along a single cross-bed at the ASF-22e quarry near Ash Fork. The bed exhibits distinct lamination and lower dips near its base, but the textural change does not correlate with a sharp change in dip angle at the outcrop scale. Approximate along-dip distances between samples (as measured in the field) are shown in meters.

Diagenetic Features

Our thin sections reveal features – stylolite seams and large pores – that were likely produced by diagenetic alteration of the original sediment. These features may mimic depositional textures in some samples and likely relate to original processes, so we need to account for them in our interpretations.

Stylolite seams are observed in many of our Coconino Sandstone samples (figure 15). These clay-rich seams are characterized by a jagged appearance in thin section, and they are commonly associated with micas. Quartz-grain dissolution/truncation is evident along the seams, which favors a diagenetic interpretation. However, the exact relationship between stylolites and original sediment composition/texture is not

completely understood. Scanning-electron-microscope images of a stylolite seam from the ASF-5 outcrop reveal illite with probable detrital textures (figure 16; Welton, 1984).

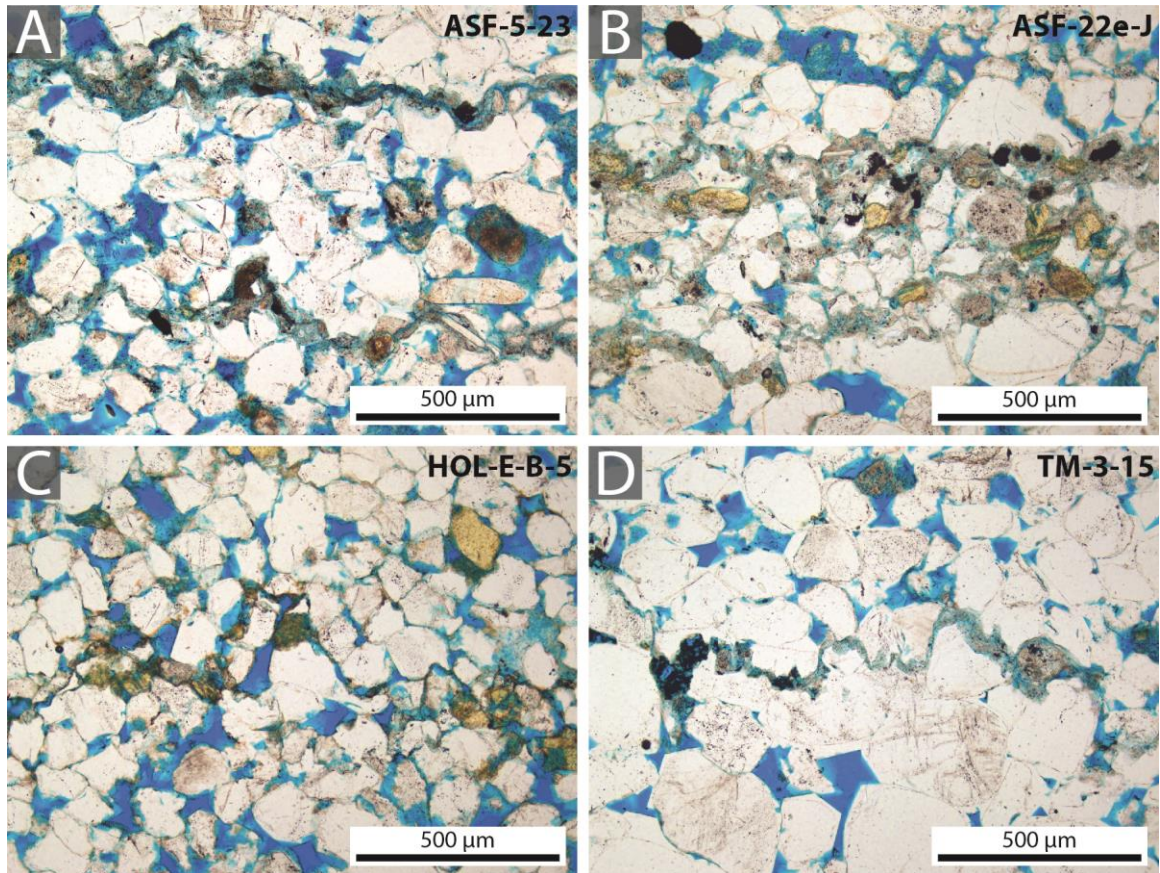


Figure 15: Stylolite seams in Coconino Sandstone thin sections. K-feldspar grains have been stained with sodium cobaltinitrite. All photos were taken at 100x magnification. **A, B)** Stylolite seams in samples from Ash Fork-area outcrops. Note the distinct cross-cutting relationship between the stylolites and quartz grains, which implies that diagenetic processes were involved in producing these structures. Muscovite grains are visible within the stylolite seams in these photos. **C, D)** Stylolites in samples from the HOL-E-B (**C**) and TM-3 (**D**) outcrops that exhibit a characteristic “sutured” morphology.

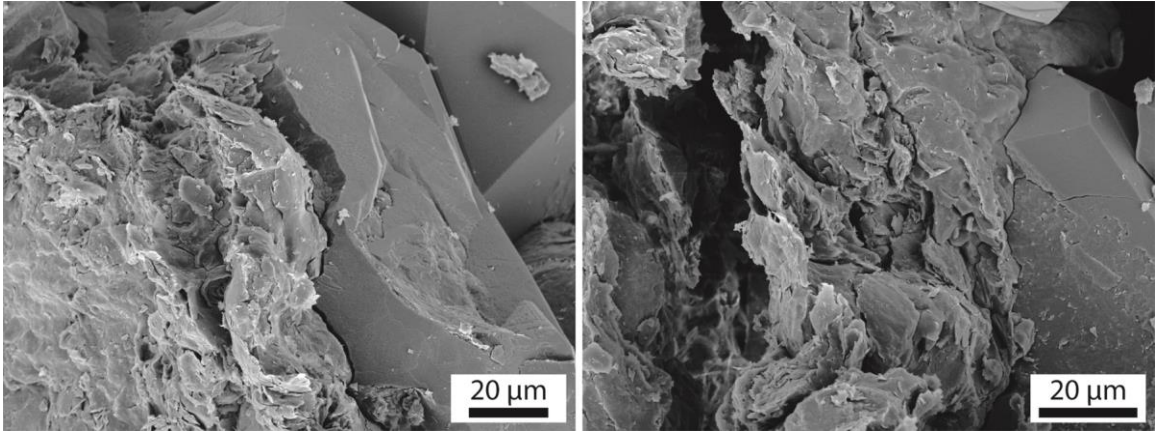


Figure 16: SEM images showing probable detrital illite textures in an ASF-5 stylolite seam. In both images, the contacts between the illite (left) and adjacent quartz (right) indicate that quartz dissolution occurred during stylolite formation.

In hand sample, these seams can look like textural lamination (figure 17). Some of the stylolites do correlate with changes in framework grain size, which may indicate a relationship to depositional processes, but others appear unrelated to framework textures. The lowermost samples in the ASF-22e cross-bed set (figure 14C; D) exhibit both distinct textural laminae and stylolites; within a single sample, certain seams appear to occur along laminae contacts while some pass through otherwise uniform sediment. Despite this variation, most of our samples with repeating stylolite seams also contain textural lamination.

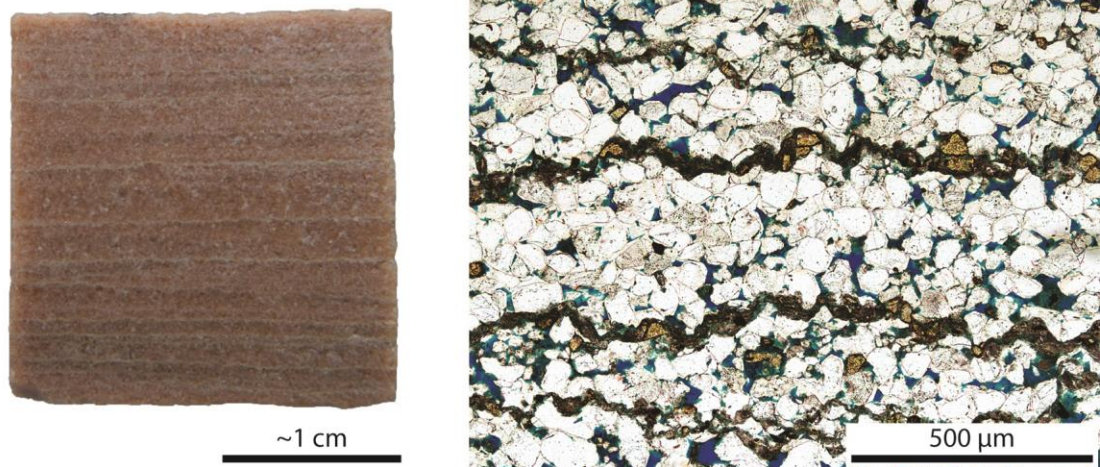


Figure 17: Stylolite seams in hand sample and thin section. These seams can mimic textural laminae in hand samples, but while some appear to correlate with textural laminae contacts (and associated changes in framework grain size), others do not. Sample from the ASF-22e outcrop.

Some of our samples exhibit pore spaces that are much larger than the surrounding sediment (figure 18). The pores vary in shape, and some include “floating” quartz grains (figure 18D). These voids are most conspicuous in samples collected from the ASF-5 outcrop, and they do not show a preferred distribution within that cross-bed set (figure 19). Large pores are visible in cut epoxied surfaces, and in cross section, they are not associated with branching structures or linear trails (figure 20).

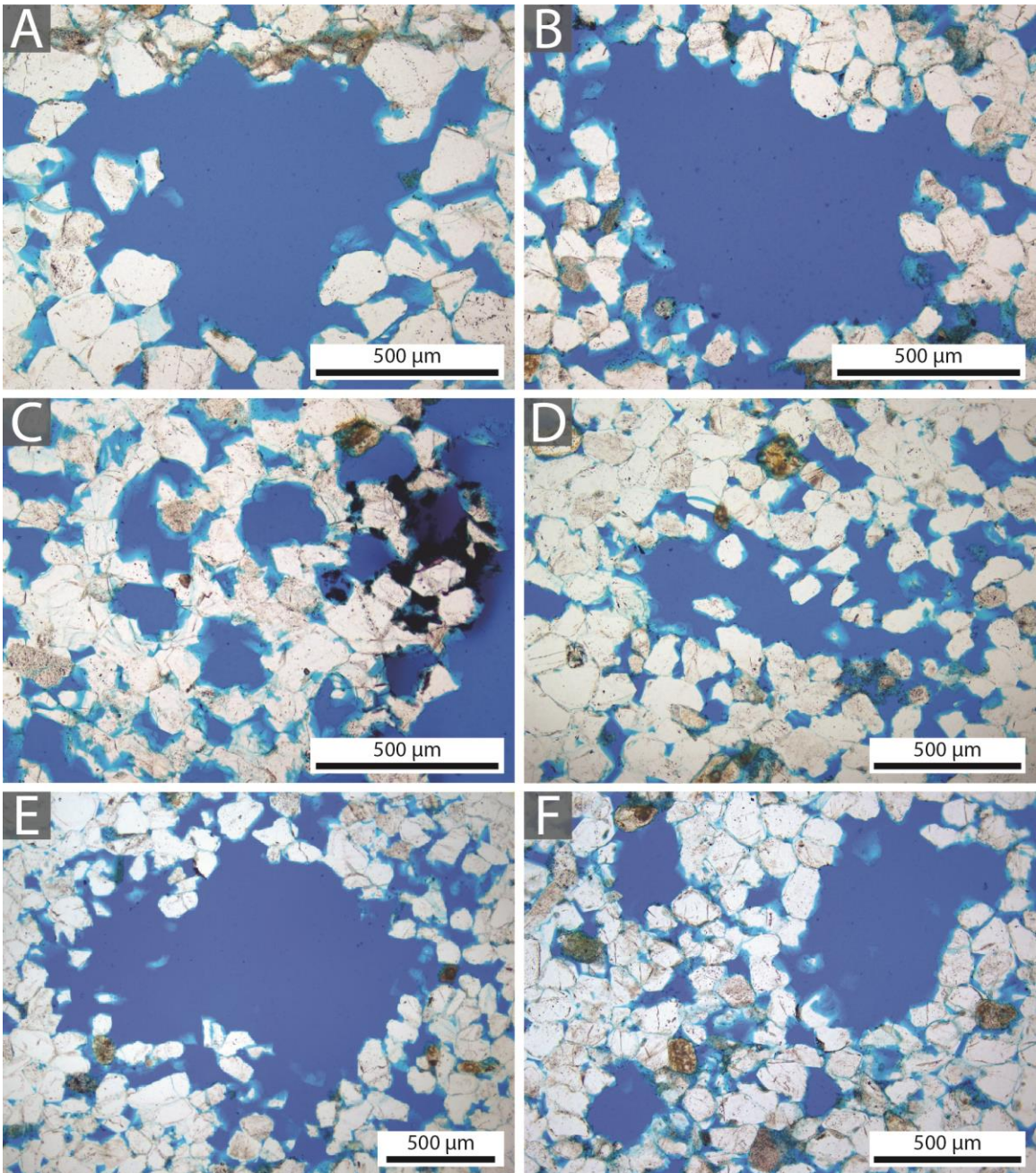


Figure 18: Large pore spaces observed in samples collected at the ASF-5 outcrop (A-F). Figure 18C shows smaller voids associated with intergranular iron carbonate (right; stained dark purple). In D, an open pore space is partially filled with “floating” quartz grains.

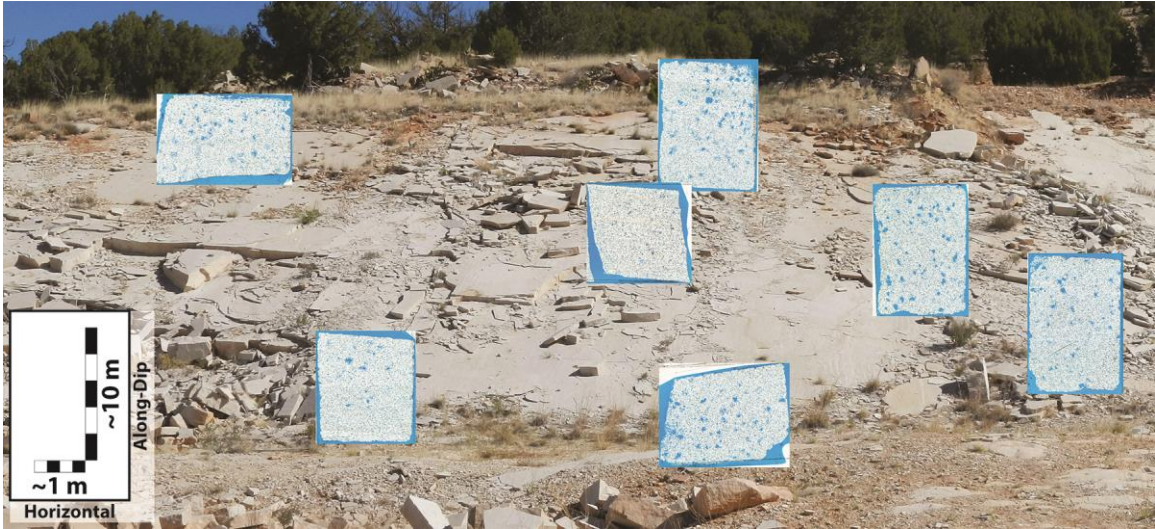


Figure 19: A section of the ASF-5 cross-bed set showing the outcrop distribution of large pores in high-resolution thin-section scans (scan images are not to scale). The pores do not appear to be preferentially distributed along a specific vertical horizon within the cross-bed set. Cross-beds dip toward the viewer.

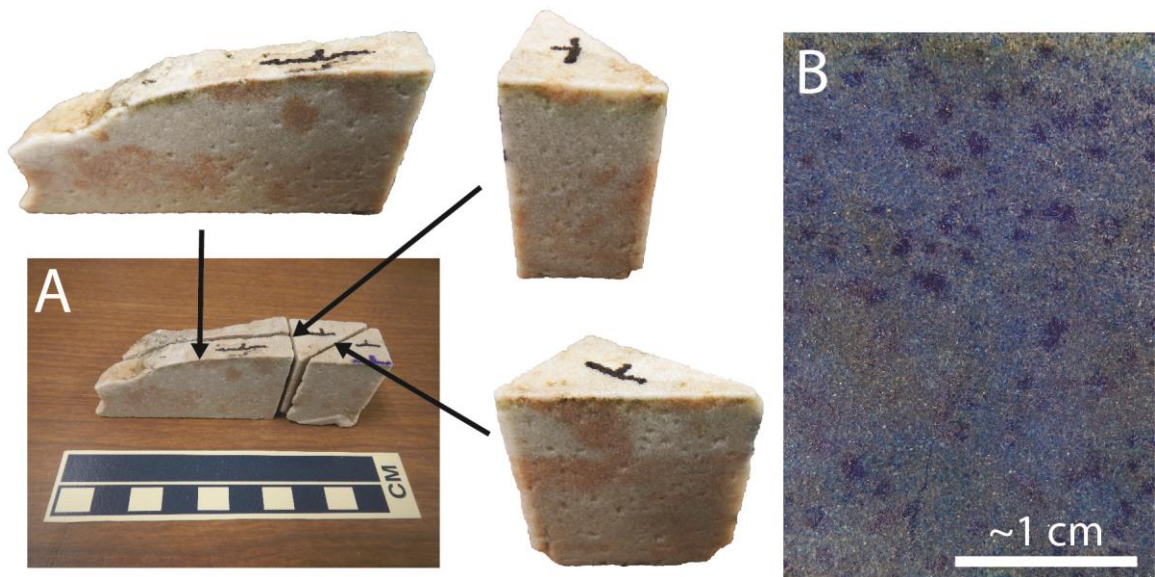


Figure 20: Large pores visible in cut surfaces of an ASF-5 sample (ASF-5-24). Surfaces were moistened with water to enhance contrast. **A)** When the block is cut in multiple directions (strike and dip direction marked on sample), pores are visible in every orientation, and no linear trails or branching structures are observed. Contrast on these block surfaces was further increased using Adobe Photoshop. **B)** Along-dip face of the ASF-5-24 sample which was impregnated with epoxy before it was cut. The pores are visible even on this cut surface, suggesting that they are not surficial features.

While partially dissolved grains are prevalent in the Coconino Sandstone (commonly feldspars), we do not observe remnant dust rims or grain residue within the large pores. However, scanning electron microscopy reveals micro-pitted quartz in association with these samples, which may suggest that carbonate minerals once occupied the voids and were later dissolved (figure 21). Intergranular iron carbonate (figure 18C) and calcite are also present in some of the porous samples (though not directly in conjunction with large pores), which further supports this hypothesis.

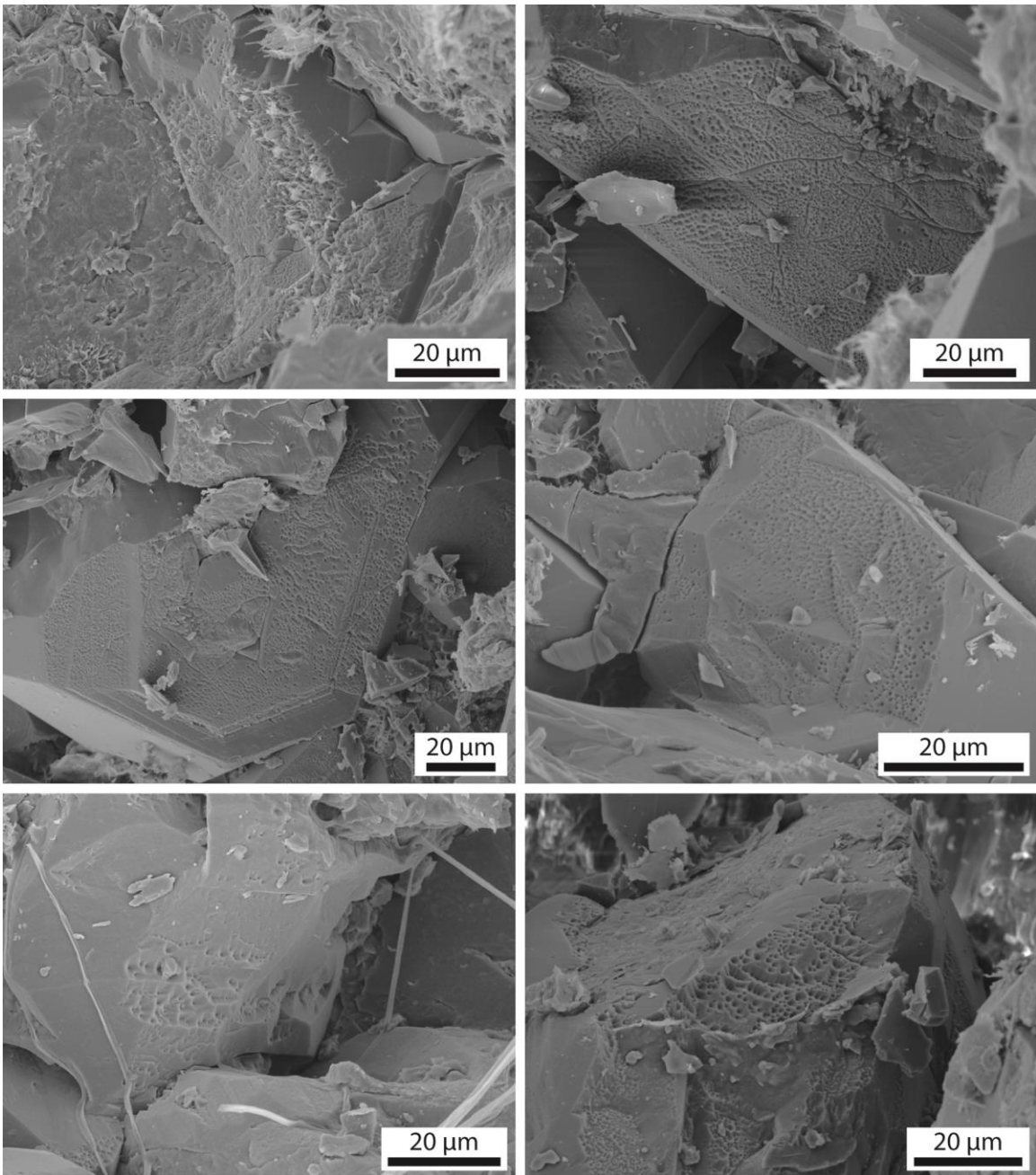


Figure 21: Micro-pitted quartz surfaces observed with the scanning electron microscope in samples containing large pores (from the ASF-5 outcrop). These pits may suggest that carbonate minerals once occupied the voids and were later dissolved.

Discussion

Textural and structural parameters serve as pieces in the greater puzzle of the Coconino Sandstone's depositional model. To best interpret the processes, we must,

therefore, account for all of the variables and evaluate them against existing criteria. While modern analogs may shed light on the ancient depositional processes, notable differences remain.

Sedimentary Structures

In our Coconino Sandstone outcrops, the cross-bedding exhibits morphological characteristics that differ significantly from those of modern grainflow deposits. Instead of narrow, “tongue-shaped” units (figures 22A; 23A), we find the cross-beds to be laterally extensive along strike (figures 22C; 23B). Beds also dip at angles below the angle of repose and do not appear to pinch out sharply at their bases (figures 1; 6). The geometry of the Coconino Sandstone cross-beds therefore suggests that these beds were not deposited by grainflows, or at least not by “normal,” unreworked, eolian grainflows. While compaction has been employed as a mechanism to explain lower-than-expected dip angles in sandstones (Borradaile, 1973; Clemmensen and Abrahamsen, 1983; Hunter, 1981; McKee and Bigarella, 1979; Rittenhouse, 1972; Walker and Harms, 1972), Emery et al. (2011) calculated, based on theoretical initial dip angles and porosity, that compactive processes are probably not sufficient to dramatically reduce cross-bed dips. Even if compaction could explain the relatively low angles, it does not explain the lateral, along-strike extent of the cross-bedding, or the lack of differential weathering and distinct “pinch outs” at the bottom of the sets. Nield et al. (2017) documented an increase in grainflow width at high wind speeds, but even their widest example – 1.13 m – is still narrow compared to the laterally extensive cross-strata in our outcrops. Since the Coconino Sandstone cross-beds do not meet any of these proposed criteria for typical

grainflow deposits, alternative or additional processes are needed to explain their deposition.

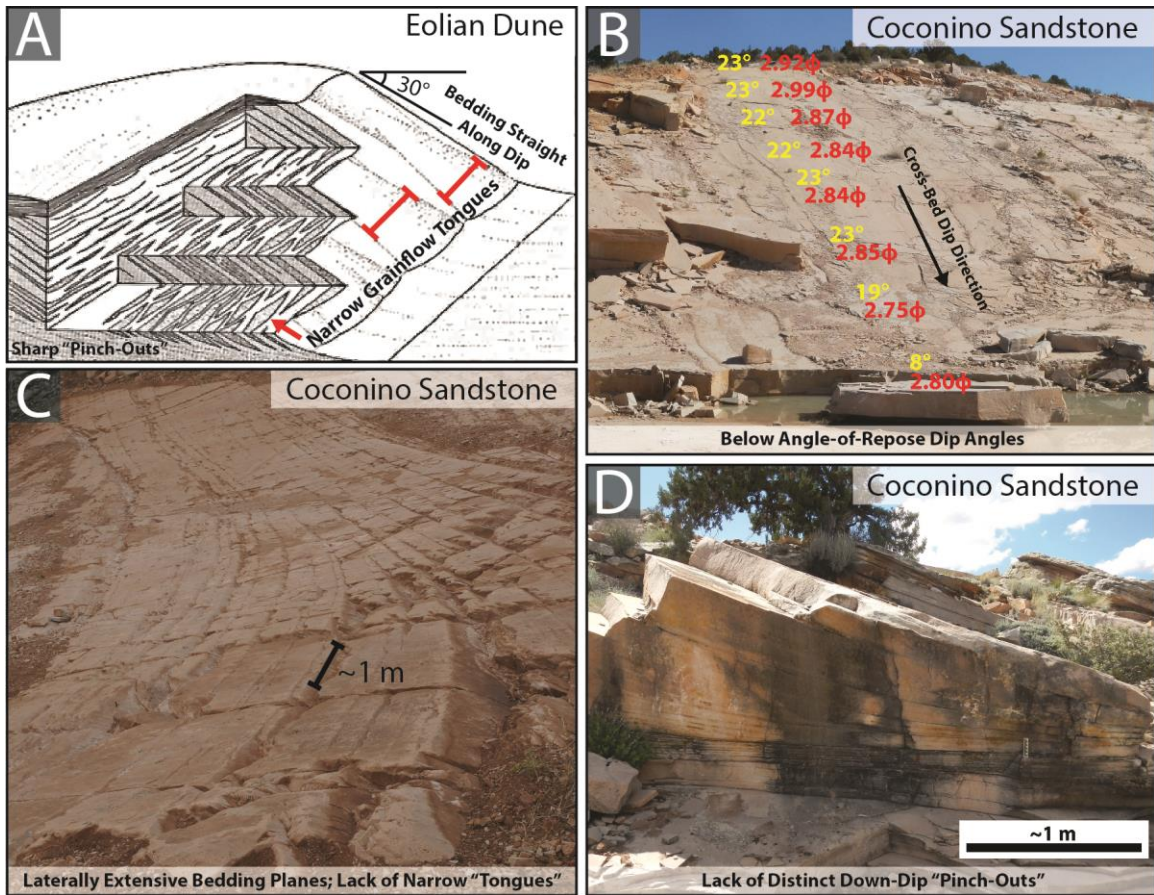


Figure 22: Comparison between expected eolian grainflow morphology and the cross-bedding observed in the Coconino Sandstone. **A)** Diagram of an eolian dune (modified from Hunter, 1977, p. 378, figure 7) showing grainflow deposits that are “tongue shaped” along strike, dip at high angles (near the angle of repose), are straight along dip, and pinch out sharply at their bases. **(B-D)** Photos illustrating cross-bedding styles in the Coconino Sandstone. The beds differ in several ways from modern grainflow deposits, which suggests that they were not deposited solely by typical eolian grainflow processes. **B)** Cross-bed dip angles ($^{\circ}$) and average grain sizes (ϕ) labelled on the ASF-22e outcrop near Ash Fork, Arizona. The dips are all notably below the angle of repose, and decrease further in angle near the base of the set. Cross-beds dip toward the viewer, and roughly 42 meters were measured along dip from the uppermost to the lowermost sample. **C)** Laterally extensive bedding planes in the Coconino Sandstone exposed on the ASF-4 bounding surface (photo taken by Leonard Brand). Narrow, “tongue-shaped” beds, like those deposited by modern eolian grainflows, were not observed. Cross-beds dip toward the right side of the photo. **D)** Cross-bedding approaching the set base at the HOL-E-A outcrop near Holbrook. Distinct grainflow strata do not interfinger with ripple or grainfall lamination, as is observed in other cross-bedded deposits.

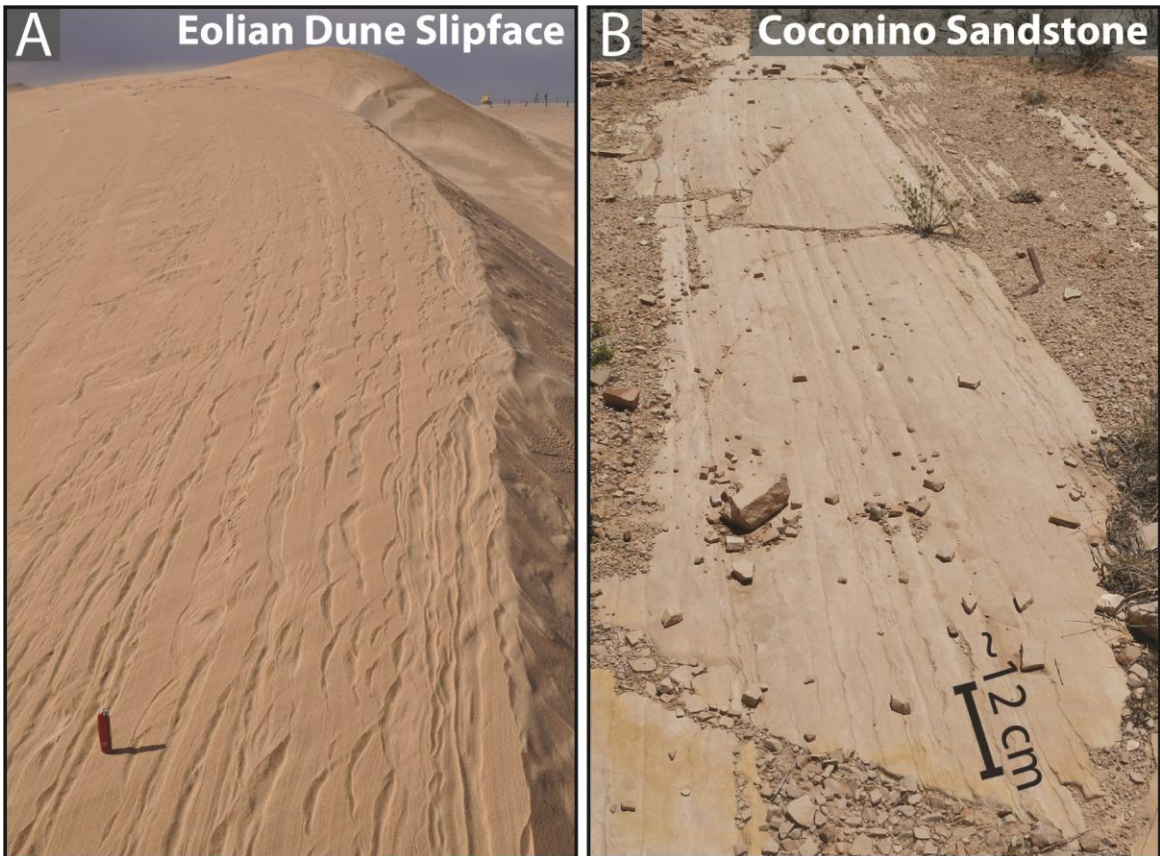


Figure 23: Bounding surface exposures on a modern eolian dune (**A**; Algodones Dunes, Southern California) and in the Coconino Sandstone (**B**), revealing roughly strike-parallel views of truncated cross-bedding. Narrow, “tongue-shaped” beds, which are characteristic of eolian grainflow deposits, are observed in the modern dune, but the Coconino Sandstone cross-bedding is more laterally extensive. Cross-beds dip toward the right in both photos. The sand dune photo (A) was taken by John Whitmore. Pocket knife provided for scale in A.

Textural Trends

According to Kleinhans (2004), vertical textural trends within cross-bedded deposits may indicate the predominance of grainfall or grainflow deposition (figure 2). Our results show more chaotic grain-size variation than Kleinhans' (2004) theoretical model (figure 10), especially for cross-beds that were not sampled along a single bed (all except ASF-22e, CPE, and HMT). While this variation might result from the relative complexity of real rocks versus theoretical models, it may also reflect mixed sampling

between indistinguishable grainflow and grainfall cross-strata or changes in the source sediment size during bedform migration.

In their study of grainflow cross-strata in the Navajo Sandstone, Loope et al. (2012) described “erratic” changes in grain size even along individual beds. These authors proposed several possible explanations for this trend, such as mixed sampling of different flows or of different lateral and vertical horizons within a flow. However, Loope et al. (2012)’s observation of variable grain-size changes – even along single, well-defined cross-beds in the Navajo Sandstone (see figure 1) – matches our observed variation along single cross-beds (ASF-22e, CPE, and HMT outcrops), and may agree with the “erratic” grain-size changes in our vertically sampled cross-bed sets.

A well-sorted sediment mixture may not contain a wide enough range of grain sizes to result in significant sorting trends. The Navajo Sandstone samples in Loope et al.’s study (2012) were well to moderately sorted, with median grain sizes ranging from fine to coarse sand. Our Coconino Sandstone samples are also well to moderately sorted (except for HMT-1, which is poorly sorted), with median grain sizes classified as fine to very fine sand (but most are in the fine sand range; Wentworth, 1922). Within these individual samples, our degree of sorting is comparable to that of Loope et al. (2012), which might suggest that similar coarsening should be expected in our Coconino Sandstone outcrops. However, with a range of fine to coarse sand, it is possible that some of the Navajo Sandstone beds exhibited greater grain-size variation to produce the significant along-dip trends. Still, even with our narrower range of grain sizes, statistically significant coarsening was observed in three outcrops. When our data are compared to that of Loope et al. (2012), the relatively variable trends seem less

anomalous, and the presence of statistically significant coarsening in some outcrops may be sufficient to imply grainflow processes. Nevertheless, other outcrops in our study do not coarsen at all by Loope et al. (2012)'s definition (median at the base of the set coarser than the top). While this may be an artifact of sampling different cross-beds, it may also imply that non-grainflow processes were involved in producing the observed vertical sorting trends.

With the exception of ASF-5, outcrops that exhibit statistically significant down-dip coarsening (ASF-22e, HMT, and HOL-E-A) have slightly steeper average dip angles than others that show weak coarsening or fining trends (figure 6). Beyond this minor difference, the cross-beds do not display other obvious differences in outcrop. It is possible that the slightly steeper average dips, alongside down-dip coarsening, suggest a predominance of grainflow processes in those cross-bed sets. However, all exhibit below-angle-of-repose dips, which would still indicate that additional processes were involved. Since two of these outcrops – ASF-22e and HMT – were sampled roughly along a single bed, it remains possible that this sampling method strengthened a coarsening trend that might have otherwise been ambiguous. However, averaged vertical trends should still indicate coarsening if the cross-bed deposition was predominated by grainflow processes (Kleinhans, 2004).

It should be further noted that the strength of our coarsening trends does not correspond to a greater sampling distance and associated cross-bed set thickness. Of the three outcrops that exhibit vertical coarsening, ASF-22e and HMT are relatively thick sets compared to HOL-E-A (table 2). Conversely, the ASF-5 cross-bed set, which is one of our thickest and most extensively sampled, does not coarsen down dip. Our textural

trends, therefore, are not controlled by set thickness; significant coarsening (or lack thereof) occurs in relatively thin cross-bed sets as well as in thicker cross-stratification.

If vertical coarsening within cross-bed sets may indicate grainflow processes, fining trends might suggest grainfall deposition. One potential problem with this interpretation, however, is that it requires the deposition of grainfall near the base of large dune bedforms. Even though our cross-bed sets vary in thickness and the original bedform heights are not known, some are thick, with more than 15 m of vertical thickness between the uppermost and lowermost samples. If the dunes were only slightly taller than the preserved cross-bedding, grains would still need to be discharged a significant distance down dip to fall out from suspension along the entire length of the foresets. Hunter (1977) did document grainfall laminae at the base of an eolian dune (Hunter, 1977, p. 376, figure 6c). While he did not provide the height of this specific bedform, he noted that dunes in the study area were, “commonly as high as 3 m” (p. 363). Therefore, it is not evident that this example of grainfall deposition at the base of a dune could be applied to larger bedforms. While it has been suggested that wind speed affects the down-dip extent of grainfall deposition (Nield et al., 2017), it remains unclear whether even high speeds could deposit grainfall at the base of very tall dunes like those implied by some Coconino Sandstone cross-bed sets.

Despite these distance constraints, the relatively finer grains near the base of some cross-bed sets (as evidenced by a lack of significant coarsening trends) – in addition to laterally extensive beds and below-angle-of-repose dips – suggest that grainfall is still arguably the best interpretation. Previous authors have invoked grainfall processes to explain some of the cross-bedding in the Coconino Sandstone (Blakey and Knepp, 1989).

Our interpretation, therefore, is consistent with the literature, but does raise questions regarding compatibility with the current understanding of modern eolian processes.

Another possible scenario is that the original dune bedforms were truncated below the slipface (e.g., Kocurek and Dott, 1981; Steidtmann, 1974; Walker and Harms, 1972), and fining or weak-coarsening trends represent grainfall deposition on the dune plinth. This model still introduces the issue of grainfall deposited near the base of relatively large dunes, but might agree with the nature of the cross-bedding and lack of distinct coarsening. Since we do observe statistically significant coarsening in three of our outcrops, we suggest that grainflow processes were probably involved. However, if additional, independent criteria could be developed to recognize otherwise indistinguishable grainfall and grainflow cross-strata, these might be used to refine the process models for the Coconino Sandstone.

Microfacies

The sedimentary structures and textures in our Coconino Sandstone cross-strata – wide lateral extent, low dip angles, lack of distinct pinch outs, and variable textural trends (with coarsening in some outcrops) – therefore appear to suggest that these beds were not deposited exclusively by grainflow processes in dry sand. Cross-beds with these characteristics are sometimes interpreted as wind ripple deposits (Hunter, 1981; Kocurek and Dott, 1981), and such an interpretation has also been invoked for the Coconino Sandstone (Middleton et al., 2003). Ripple deposits may dip at angles below the angle of repose and lack the down-dip coarsening produced by grainflows; however, they should typically exhibit graded internal laminae characteristic of ripple migration. Many of the cross-beds in the Coconino Sandstone do appear laminated, to some degree, in outcrop

and in high-resolution scans. The scans reveal, however, that while some samples contain inversely graded laminae, normal grading also occurs, and in many cases grading is difficult to define due to diffuse laminae contacts. Furthermore, some apparent “laminae” are not defined by changes in framework grain size, but rather by the presence of stylolitic seams (figure 17).

Stylolites occur in carbonate rocks as well as in sandstones (Stockdale, 1943). These are diagenetic features generally believed to be a product of pressure solution (Dunnington, 1954; Stockdale, 1943), but they have been known to mimic primary bedding or lamination (Collinson and Thompson, 1989; Simpson, 1985). In thin section, stylolites may be associated with clays and muscovite. Some authors have suggested that the presence of mica and/or clays promotes stylolite formation (Aharonov and Katsman, 2009; Heald, 1959) or quartz cementation (Oelkers et al., 1996; Walderhaug and Bjørkum, 2003), which may in turn affect porosity/permeability (Bjørkum et al., 1998).

The truncation of quartz grains along these features in our samples likely implies diagenetic processes (Dunnington, 1954), but the exact relationship to depositional lithology remains unclear. Micaceous and *detrital* clays might link stylolites to depositional processes due to sorting associated with the relatively low weight of those grains. Furthermore, many stylolites are oriented roughly parallel to bedding planes (Stockdale, 1943), and some correlate with laminae contacts, possibly indicating a relationship to original processes. Detrital illite may occur along stylolite seams (figure 16), and since the stylolites are commonly observed near the bottom of cross-beds as well as higher up in the sets (e.g., the ASF-5 sample shown in figure 16), any associated detrital clay would not have exhibited a preferential distribution along the dune foreset. Whatever their

relationship to depositional processes, however, laminae defined by stylolitic seams do not represent the textures indicative of wind ripple lamination.

While some cross-beds in the Coconino Sandstone appear laminated in outcrop, therefore, many of these laminae exhibit features that differ from the sharp, repeating, inversely graded lamination commonly associated with ripple deposits (Schenk, 1983). Several of our large cross-bed sets are distinctly laminated at their bases, which might agree with the expected distribution of ripple laminae on a dune plinth; however, distinct lamination is also observed higher up in the cross-beds. This broad distribution alone does not negate a ripple interpretation since ripples commonly migrate across modern dune slipfaces, but they are unlikely to be preserved where frequent grainflows occur. The unpredictable distribution of our laminated samples, along with the indistinct/variable nature of laminae contacts and grading, accordingly suggest that additional or alternative processes may have been involved.

Large Pores

The large pores in some of our ASF-5 samples may provide additional clues for interpreting depositional processes. Even though the pores are diagenetic features, they are most abundant in massive and indistinctly laminated samples, which may imply a connection to specific depositional conditions associated with those beds. Similar pores can be produced by grain plucking during sawing and grinding; however, these were observed in a sample that was epoxied before it was cut (figure 20B), illustrating that they are not an artifact of sample preparation.

Root traces and burrows may produce pore networks within sediment. Retallack (1988) described vertically branching root traces as an important criterion for recognizing

paleosols. Accordingly, if the large pores in our ASF-5 samples are root traces, we would expect to see evidence for vertical branching in at least some cut surfaces – but this is not observed (figure 20A). In our ASF-5 outcrop, beds containing large pores are also not associated with distinct erosional surfaces, clay-rich horizons, or other evidence for paleosols (which would suggest that the foreset slope stabilized long enough for soil development). All of these factors indicate that the large pores in our samples are probably not root traces.

Burrows occur in various forms throughout the rock record, and may produce open voids where infill is not deposited or preserved. We observe these pores on the weathered outcrop and in cut surfaces, but do not see evidence for linear trails. When a single sample is cut in multiple directions (figure 20A), pores are present, but with no extended pathways as relicts of organism movement. Substantial burrowing along certain cross-strata should also disrupt the surface of those beds, but such bioturbation is not observed on the bedding planes (note the upper surface of the slab in figure 20A). These criteria all imply that the large pores occur throughout the samples, and that they are unlikely to represent root traces or burrows.

Since the pores do not contain distinct residue, it is difficult to identify the exact components that might have occupied the voids, but the micro-pitted quartz observed in these samples may point to carbonate minerals (figure 21). These minerals could have been present in the form of grains or cement. If the pores were filled by carbonate cement, it might suggest that they resulted from a depositional process (and were later cemented during diagenesis). Grainflow processes are thought to produce the most porous/permeable dune stratification (Howell and Mountney, 2001; Romain and

Mountney, 2014). Because of the broad distribution of the pores (figure 19), interpreting these beds as grainflow cross-strata would suggest that the grainflows occurred along the foreset and interfingered with other stratification types (that lacked abundant large pores). Since these beds also dip at angles below the angle of repose (figure 6), another process would be required to reduce the dip.

Some Coconino Sandstone samples do contain large carbonate framework grains (figure 24). If the pores at ASF-5 were produced by the dissolution of similar grains, their distribution would indicate a lack of preferred sorting along the cross-beds (figure 19). The specific gravity of dolomite, for example (as in figure 24), is slightly higher than that of quartz and feldspar, which should further promote vertical sorting of large clasts (if the grains were composed of dolomite at the time of deposition). Another possibility is that the pores were once occupied by clay pellets, which were replaced by carbonate and then dissolved. In both cases, interpreting these pores as the byproduct of grain dissolution requires a depositional process to explain why such large clasts were not preferentially sorted within the associated cross-beds.

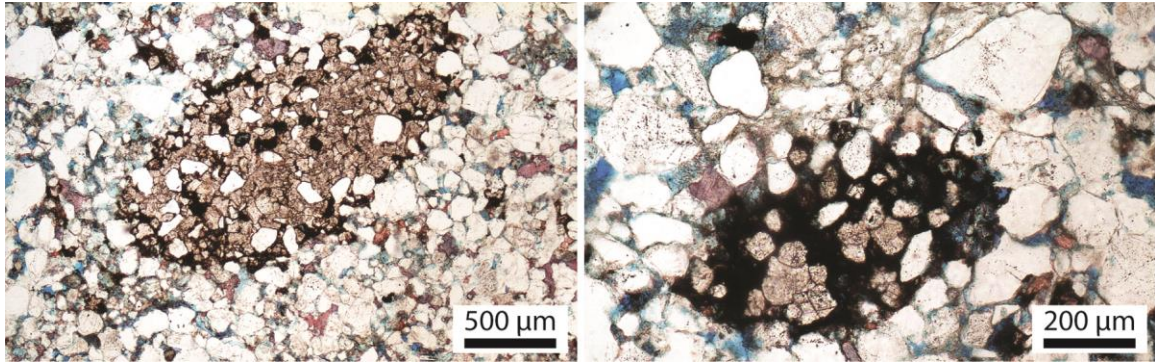


Figure 24: Dolomite clasts along New Hance Trail, Grand Canyon. These clasts are comparable in size to our large pores, and contain quartz grains like some of the pores. Photos provided by John Whitmore.

Dune Morphology and Controls on Stratification Type Distribution

Modern dunes assume different morphologies (McKee, 1966), and these may be reflected in the rock record (Bigarella, 1972; Kocurek, 1991). According to Kocurek and Dott (1981), most thick eolian sandstones were probably deposited by crescentic dunes. McKee (1979) defined “crescentic dunes” as barchan, barchanoid, and transverse bedforms, noting that gradational forms may occur. Some authors, however, suggest that many interpreted transverse bedforms in the rock record may actually represent linear dunes (Bristow et al., 2007; Rubin and Hunter, 1985). Transverse and localized barchan dune morphologies have been suggested for the Coconino Sandstone (McKee, 1945, 1974), and this generally agrees with our field observations. Our primary cross-bed sets do not appear to exhibit dramatic along-strike curvature, but more complex bedding geometries are exposed near our study areas.

Dune morphology may control the relative proportions of stratification types deposited and, consequently, the nature of the preserved cross-bedding (Kocurek and Dott, 1981). However, while dune shape determines the distribution of stratification types, it should have little effect on the structural characteristics of each type (e.g., high

dip angles and relatively narrow width of grainflow deposits) since these are based on their intrinsic depositional processes. Kocurek and Dott (1981) explain this relationship between stratification types and foreset geometry:

“Although it still remains to be documented, the relative abundances of the different stratification types from dune to dune generally can be predicted from knowledge of how each stratification type forms and from the overall structure of dunes. Dunes with abundant slipfaces will be characterized by high percentages of grainflow cross-strata and grainfall laminae. Dunes without slipfaces will be characterized by climbing translent strata” (p. 587).

It follows that predominance of certain stratification types in sandstones may imply specific dune morphologies. The commonly recognized crescentic dune morphology may be associated with grainflow cross-strata, as well as ripple and grainfall laminae (Kocurek and Dott, 1981). While McKee and Tibbitts (1964) described a linear dune structure as consisting of steeply dipping, opposing cross-beds, Breed and Breed (1979) reported lower-angle cross-stratification associated with these bedforms (see also summary in Kocurek and Dott, 1981). The relatively low dip angles, lack of grainflow tongues, indistinct stratification, and variable textural trends observed in our Coconino Sandstone outcrops might suggest that the cross-beds were deposited by accretion during linear dune migration. In this model, however, we would expect most of the cross-beds to exhibit distinct, graded lamination, as the presence of such laminae in some of our samples suggests that the beds contain a wide enough grain-size distribution to promote stratification. The occurrence of both massive and laminated cross-bed facies in our Coconino Sandstone outcrops probably suggests that these beds were not deposited exclusively by ripple migration. Such an interpretation could be made only if the sorting in each cross-bed was too good to form visibly graded laminae, but the prevalent moderate sorting in most of our study areas implies that this is not likely the case.

Cross-Bed Depositional Processes: Undifferentiable Grainflow and Grainfall

Considering the vertical grain-size trends, bedding geometry, and lack of clear ripple lamination, we suggest that the Coconino Sandstone cross-beds consist of grainflow and grainfall deposits, but these are not readily differentiated at outcrop or thin-section scales (table 5). While grainflow beds are expected to coarsen down dip (Hunter, 1977; Kleinhans, 2004), grainfall may exhibit the opposite trend, becoming finer with distance down the foreset (Fryberger and Schenk, 1981). Such an explanation accounts for vertical coarsening in some of our outcrops and a lack of coarsening in others, as well as the random distribution of pores which may have been produced by the dissolution of large carbonate grains. It also predicts that distinct stratification types might be difficult to recognize in outcrop, and that the cross-bedding geometry may differ from that of “typical” grainflow deposits (narrow along strike, angle-of-repose dips, and sharp down-dip pinch outs).

Table 5: Summary of criteria supporting an undifferentiable grainfall/grainflow model

Sedimentary Structures	Textural Trends	Microfacies
Below-angle-of-repose dips	Random vertical changes in grain size: both coarsening and fining trends observed within a single cross-bed set	Massive and laminated textures, with no preferred distribution in most outcrops
Laterally extensive cross-bedding (versus narrow “tongues”)		Normal and reverse grading observed within some laminae, but contacts are commonly diffuse, making grading difficult to define
Lack of sharp grainflow “pinch outs” or other clear stratification type differentiation in outcrop		Indistinct lamination common
		Stylolite seams (and potentially associated detrital illite) at the base of large cross-beds as well as higher up in the sets
		No preferred distribution of large pores (and presumed dissolved grains or cement) in ASF-5 samples

The undifferentiable nature of grainfall and grainflow deposits may result from syndepositional reworking processes (figure 25). Such reworking has been documented for subaqueous bedforms (Reesink and Bridge, 2009), but has not been observed on eolian dunes. While the textures and sedimentary structures presented here fit criteria for grainflow and grainfall, additional study is needed to interpret specific processes that could have reworked the cross-bedding on a large scale.

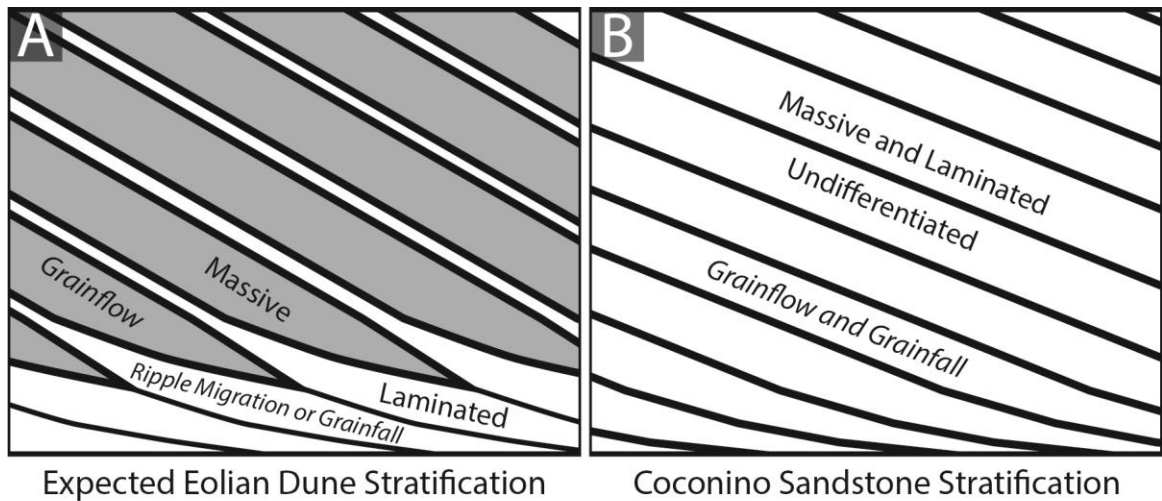


Figure 25: Comparison of dune stratification commonly observed on (A) modern eolian crescentic dunes (and in some sandstones) versus (B) the Coconino Sandstone. Massive grainflow cross-strata in A has been shaded grey to highlight its distinction from the lower-angle grainfall/ripple laminae. The undifferentiated massive and laminated cross-bedding in our Coconino Sandstone outcrops is interpreted to suggest evidence for reworking of grainflow and grainfall deposits.

More work must therefore be done to characterize the nature of these cross-bed facies and associated processes in the Coconino Sandstone. Ideally, the best approach would involve isolated criteria that could better distinguish grainflow and grainfall stratification at the bedding scale. While many diagnostic criteria do exist (e.g., Hunter, 1977; Kocurek and Dott, 1981), these do not readily differentiate sedimentation units in the Coconino Sandstone. Furthermore, the processes that might deposit grainfall near the base of large dunes and rework that grainfall with grainflow strata must be explored and characterized. We hope that this study will prompt additional research on fine-scale processes in the Coconino Sandstone and similar cross-bedded units.

Acknowledgements

Statistical analyses for this project were conducted by the Research Consulting Group in the Center for Health Research at the Loma Linda University School of Public

Health. We thank Loma Linda University and The Geological Society of America (Graduate Student Research Grant, #11232-16) for support and funding, and Calgary Rock and Materials Services Inc. for providing most of the thin sections and the high-resolution scans used in this project. Field work and sampling in Grand Canyon National Park was conducted under permit number GRCA-2016-SCI-0033. Ash Fork field work was conducted under a US Forest Service Special Use Permit. We thank Big Boquillas Ranch for access to the Seligman-area outcrops, and Michael Reidhead for access to Five Mile Wash on his land in Holbrook.

References

- Abdel-Motaleb, M. M. M., 1993, Vertical sorting within dune structure [PhD dissertation]: Colorado State University, 191 p.
- , 1994, Vertical sorting within dune structure, *in* Pugh, C. A., ed., Fundamentals and advancements in hydraulic measurements and experimentation: Buffalo, NY, American Society of Civil Engineers, p. 139-148.
- Aharonov, E., and Katsman, R., 2009, Interaction between pressure solution and clays in stylolite development: insights from modeling: American Journal of Science, v. 309, p. 607-632.
- Allen, J. R. L., 1965, Sedimentation to the lee of small underwater sand waves: an experimental study: Journal of Geology, v. 73, no. 1, p. 95-116.
- , 1984, Sedimentary Structures: Their Character and Physical Basis, Amsterdam, Netherlands, Elsevier.
- Allen, J. R. L., and Narayan, J., 1964, Cross-stratified units, some with silt bands, in the Folkestone Beds (Lower Greensand) of Southeast England: Geologie en Mijnbouw, v. 43, p. 451-461.
- Anderson, R. S., 1988, The pattern of grainfall deposition in the lee of aeolian dunes: Sedimentology, v. 35, p. 175-188.
- Bagnold, R. A., 1954a, Experiments on a gravity-free dispersion of large solid spheres in a Newtonian fluid under shear, Proceedings of the Royal Society of London A:

Mathematical, Physical and Engineering Sciences, Volume 225, The Royal Society, p. 49-63.

- , 1954b, *The Physics of Blown Sand and Desert Dunes*, Mineola, NY, Dover Publications, Inc., 265 p.
- Bigarella, J. J., 1972, Eolian environments: their characteristics, recognition, and importance, *in* Rigby, J. K., and Hamblin, W. K., eds., *Recognition of Ancient Sedimentary Environments*, Volume 16, Society of Economic Paleontologists and Mineralogists Special Publication, p. 12-62.
- Bjørkum, P. A., Oelkers, E. H., Nadeau, P. H., Walderhaug, O., and Murphy, W. M., 1998, Porosity prediction in quartzose sandstones as a function of time, temperature, depth, stylolite frequency, and hydrocarbon saturation: *AAPG Bulletin*, v. 82, no. 4, p. 637-648.
- Blakey, R. C., 1988, Basin tectonics and erg response: *Sedimentary Geology*, v. 56, p. 127-151.
- Blakey, R. C., and Knepp, R., 1989, Pennsylvanian and Permian geology of Arizona, *in* Jenney, J. P., and Reynolds, S. J., eds., *Arizona Geological Society Digest*, v. 17, p. 313-347.
- Blakey, R. C., and Middleton, L. T., 1983, Permian shoreline eolian complex in central Arizona: dune changes in response to cyclic sealevel changes, *in* Brookfield, M. E., and Ahlbrandt, T. S., eds., *Eolian Sediments and Processes*, Elsevier.
- Blom, A., and Kleinhans, M. G., 2006, Modelling sorting over the lee face of individual bed forms, *in* Ferreira, R. M. L., Alves, E. C. T. L., Leal, J. G. A. B., and Cardoso, A. H., eds., *River Flow 2006: Proceedings of the International Conference on Fluvial Hydraulics*, Volume 1: London, UK, Taylor & Francis Group, p. 807-816.
- Blom, A., and Parker, G., 2004, Vertical sorting and the morphodynamics of bed form-dominated rivers: A modeling framework: *Journal of Geophysical Research*, v. 109, p. F02007.
- Blom, A., Parker, G., Ribberink, J. S., and de Vriend, H. J., 2006, Vertical sorting and the morphodynamics of bed-form-dominated rivers: An equilibrium sorting model: *Journal of Geophysical Research*, v. 111, p. F01006.
- Blom, A., Ribberink, J. S., and de Vriend, H. J., 2003, Vertical sorting in bed forms: flume experiments with a natural and a trimodal sediment mixture: *Water Resources Research*, v. 39, no. 2, p. 1025.
- Borradaile, G., 1973, Curves for the determination of compaction using deformed cross-bedding: *Journal of Sedimentary Petrology*, v. 43, no. 4, p. 1160.

- Breed, C. S., and Breed, W. J., 1979, Dunes and other windforms of Central Australia (and a comparison with linear dunes on the Moenkopi Plateau, Arizona), in El-Baz, F., and Warner, D. M., eds., Apollo-Soyuz Test Project, Summary Science Report, Volume 2: Washington, District of Columbia, National Aeronautics and Space Administration (NASA), p. 319-358.
- Bristow, C. S., Duller, G. A. T., and Lancaster, N., 2007, Age and dynamics of linear dunes in the Namib Desert: *Geology*, v. 35, no. 6, p. 555-558.
- Buck, S. G., 1985, Sand-flow cross strata in tidal sands of the Lower Greensand (Early Cretaceous), Southern England: *Journal of Sedimentary Petrology*, v. 55, no. 6, p. 895-906.
- Clemmensen, L. B., and Abrahamsen, K., 1983, Aeolian stratification and facies association in desert sediments, Arran basin (Permian), Scotland: *Sedimentology*, v. 30, p. 311-339.
- Collinson, J. D., and Thompson, D. B., 1989, *Sedimentary Structures*, Chapman & Hall, 207 p.
- Dasgupta, P., and Manna, P., 2011, Geometrical mechanism of inverse grading in grain-flow deposits: an experimental revelation: *Earth-Science Reviews*, v. 104, p. 186-198.
- Dingler, J. R., and Anima, R. J., 1989, Subaqueous grain flows at the head of Carmel Submarine Canyon, California: *Journal of Sedimentary Petrology*, v. 59, no. 2, p. 280-286.
- Dunnington, H. V., 1954, Stylolite development post-dates rock induration: *Journal of Sedimentary Petrology*, v. 24, no. 1, p. 27-49.
- Elcock, S., 1993, A study of the early Permian Coconino Sandstone, Arizona [BSc thesis]: University of Wolverhampton, 79 p.
- Emery, M. K., Maithel, S. A., and Whitmore, J. H., 2011, Can compaction account for lower-than-expected cross-bed dips in the Coconino Sandstone (Permian), Arizona?: *Geological Society of America Abstracts with Programs*, v. 43, no. 5, p. 430.
- Fisher, W. L., 1961, Upper Paleozoic and lower Mesozoic stratigraphy of Parashant and Andrus Canyons, Mohave County, Northwestern Arizona [PhD dissertation]: University of Kansas, 345 p.
- Folk, R. L., 1968, *Petrology of Sedimentary Rocks*, Austin, Texas, Hemphill Publishing Company.

- Folk, R. L., and Ward, W. C., 1957, Brazos River bar: a study in the significance of grain size parameters: *Journal of Sedimentary Petrology*, v. 27, no. 1, p. 3-26.
- Fryberger, S. G., and Schenk, C., 1981, Wind sedimentation tunnel experiments on the origins of aeolian strata: *Sedimentology*, v. 28, p. 805-821.
- Heald, M. T., 1959, Significance of stylolites in permeable sandstones: *Journal of Sedimentary Petrology*, v. 29, no. 2, p. 251-253.
- Howell, J., and Mountney, N., 2001, Aeolian grain flow architecture: hard data for reservoir models and implications for red bed sequence stratigraphy: *Petroleum Geoscience*, v. 7, p. 51-56.
- Hunter, R. E., 1977, Basic types of stratification in small eolian dunes: *Sedimentology*, v. 24, p. 361-387.
- , 1981, Stratification styles in eolian sandstones: some Pennsylvanian to Jurassic examples from the western interior U.S.A., *in* Ethridge, F. G., and Flores, R. M., eds., *Recent and Ancient Nonmarine Depositional Environments: Models for Exploration: Society of Economic Paleontologists and Mineralogists, Special Publication 31*, p. 315-329.
- , 1985a, A kinematic model for the structure of lee-side deposits: *Sedimentology*, v. 32, p. 409-422.
- , 1985b, Subaqueous sand-flow cross strata: *Journal of Sedimentary Petrology*, v. 55, no. 6, p. 886-894.
- Hunter, R. E., and Kocurek, G., 1986, An experimental study of subaqueous slipface deposition: *Journal of Sedimentary Petrology*, v. 56, no. 3, p. 387-394.
- Imbrie, J., and Buchanan, H., 1965, Sedimentary structures in modern carbonate sands of the Bahamas, *in* Middleton, G. V., ed., *Primary sedimentary structures and their hydrodynamic interpretation, Volume 12: Tulsa, OK, Society of Economic Paleontologists and Mineralogists*, p. 149-172.
- Inman, D. L., Ewing, G. C., and Corliss, J. B., 1966, Coastal sand dunes of Guerrero Negro, Baja California, Mexico: *Geological Society of America Bulletin*, v. 77, p. 787-802.
- Johnson, P. W., 1962, Water in the Coconino Sandstone for the Snowflake-Hay Hollow area, Navajo county, Arizona: *Contributions to the Hydrology of the United States, Geological Survey Water-Supply Paper 1539-S*.
- Jopling, A. V., 1965, Laboratory study of the distribution of grain sizes in cross-bedded deposits, *in* Middleton, G. V., ed., *Primary sedimentary structures and their*

- hydrodynamic interpretation, Volume 12: Tulsa, OK, Society of Economic Paleontologists and Mineralogists, p. 53-65.
- Kertes, R. S., 1995, Textural patterns and micro-hydraulic events within major bedforms on a Mississippi River point bar (Bryant Bar) [MS thesis]: University of Cincinnati.
- Kleinhans, M. G., 2004, Sorting in grain flows at the lee side of dunes: *Earth-Science Reviews*, v. 65, p. 75-102.
- , 2005a, Dune-phase fluvial transport and deposition model of gravelly sand, *in* Blum, M. D., Marriott, S. B., and Leclair, S. F., eds., *Fluvial Sedimentology VII*, Volume 35, Blackwell Publishing Ltd, p. 75-97.
- , 2005b, Grain-size sorting in grainflows at the lee side of deltas: *Sedimentology*, v. 52, p. 291-311.
- Kocurek, G., 1991, Interpretation of ancient eolian sand dunes: *Annual Review of Earth and Planetary Sciences*, v. 19, p. 43-75.
- Kocurek, G., and Dott, R. H., 1981, Distinctions and uses of stratification types in the interpretation of eolian sand: *Journal of Sedimentary Petrology*, v. 51, no. 2, p. 579-595.
- Legros, F., 2002, Can dispersive pressure cause inverse grading in grain flows?: *Journal of Sedimentary Research*, v. 72, no. 1, p. 166-170.
- Leong, F. J. W.-M., Brady, M., and McGee, J. O., 2003, Correction of uneven illumination (vignetting) in digital microscopy images: *Journal of Clinical Pathology*, v. 56, no. 8, p. 619-621.
- Loope, D. B., 1984, Eolian origin of upper Paleozoic sandstones, southeastern Utah: *Journal of Sedimentary Petrology*, v. 54, p. 563-580.
- Loope, D. B., Elder, J. F., and Sweeney, M. R., 2012, Downslope coarsening in aeolian grainflows of the Navajo Sandstone: *Sedimentary Geology*, v. 265-266, p. 156-162.
- Lowe, D. R., 1976, Grain flow and grain flow deposits: *Journal of Sedimentary Petrology*, v. 46, no. 1, p. 188-199.
- , 1979, Sediment gravity flows: their classification and some problems of application to natural flows and deposits: *SEPM Special Publication*, v. 27, p. 75-82.
- Lundy, W. L., 1973, The stratigraphy and evolution of the Coconino Sandstone of northern Arizona [MS thesis]: University of Tulsa, 106 p.

- Maithel, S. A., and Whitmore, J. H., 2010, Textural analysis of the Coconino Sandstone, Chino Point, Arizona: Geological Society of America Abstracts with Programs, v. 42, no. 5, p. 426.
- McDonald, R. R., and Anderson, R. S., 1995, Experimental verification of aeolian saltation and lee side deposition models: *Sedimentology*, v. 42, p. 39-56.
- , 1996, Constraints on eolian grain flow dynamics through laboratory experiments on sand slopes: *Journal of Sedimentary Research*, v. 66, no. 3, p. 642-653.
- McKee, E. D., 1934, The Coconino Sandstone - its history and origin: Carnegie Institution of Washington Publication 440, p. 77-115.
- , 1945, Small-scale structures in the Coconino Sandstone of northern Arizona: *Journal of Geology*, v. 53, no. 5, p. 313-325.
- , 1966, Structures of dunes at White Sands National Monument, New Mexico (and a comparison with structures of dunes from other selected areas): *Sedimentology*, v. 7, p. 1-69.
- , 1974, Paleozoic Rocks of Grand Canyon: *Geology of Northern Arizona, Part I*, p. 119-154.
- , 1979, Introduction to a study of global sand seas, *in* McKee, E. D., ed., *A study of global sand seas*: Honolulu, Hawaii, University Press of the Pacific.
- McKee, E. D., and Bigarella, J. J., 1979, Ancient sandstones considered to be eolian, *in* McKee, E. D., ed., *A Study of Global Sand Seas*: Honolulu, HI, University Press of the Pacific, p. 187-238.
- McKee, E. D., Douglass, J. R., and Rittenhouse, S., 1971, Deformation of lee-side laminae in eolian dunes: *Geological Society of America Bulletin*, v. 82, p. 359-378.
- McKee, E. D., and Tibbitts, G. C., 1964, Primary structures of a seif dune and associated deposits in Libya: *Journal of Sedimentary Petrology*, v. 34, no. 1, p. 5-17.
- Middleton, G. V., 1970, Experimental studies related to problems of flysch sedimentation: *Geological Association of Canada Special Paper*, v. 7, p. 253-272.
- Middleton, L. T., Elliott, D. K., and Morales, M., 2003, Coconino Sandstone, *in* Beus, S. S., and Morales, M., eds., *Grand Canyon Geology*: New York, Oxford University Press, p. 163-179.
- Möbius, M. E., Lauderdale, B. E., Nagel, S. R., and Jaeger, H. M., 2001, Size separation of granular particles: *Nature*, v. 414, p. 270.

- Mullins, H. T., and Van Buren, H. M., 1979, Modern modified carbonate grain flow deposit: *Journal of Sedimentary Petrology*, v. 49, no. 3, p. 747-752.
- Nickling, W. G., McKenna Neuman, C., and Lancaster, N., 2002, Grainfall processes in the lee of transverse dunes, Silver Peak, Nevada: *Sedimentology*, v. 49, p. 191-209.
- Nield, J. M., Wiggs, G. F. S., Baddock, M. C., and Hipondoka, M. H. T., 2017, Coupling leeside grainfall to avalanche characteristics in aeolian dune dynamics: *Geology*, v. 45, no. 3, p. 271-274.
- Oelkers, E. H., Bjørkum, P. A., and Murphy, W. M., 1996, A petrographic and computational investigation of quartz cementation and porosity reduction in North Sea sandstones: *American Journal of Science*, v. 296, p. 420-452.
- Pye, K., and Tsoar, H., 2009, *Aeolian Sand and Sand Dunes*, Berlin, Springer-Verlag, 458 p.
- Reesink, A. J. H., and Bridge, J. S., 2007, Influence of superimposed bedforms and flow unsteadiness on formation of cross strata in dunes and unit bars: *Sedimentary Geology*, v. 202, p. 281-296.
- , 2009, Influence of bedform superimposition and flow unsteadiness on the formation of cross strata in dunes and unit bars — Part 2, further experiments: *Sedimentary Geology*, v. 222, p. 274-300.
- Reiche, P., 1938, An analysis of cross-lamination the Coconino Sandstone: *Journal of Geology*, v. 46, no. 7, p. 905-932.
- Retallack, G. J., 1988, *Field Recognition of Paleosols*: Geological Society of America Special Paper 216, p. 1-20.
- Richard, S. M., Reynolds, S. J., Spencer, J. E., and Pearthree, P. A., 2000, *Geologic Map of Arizona*: Arizona Geological Survey, Map 35, scale 1:1,000,000.
- Rittenhouse, G., 1972, Cross-bedding dip as a measure of sandstone compaction: *Journal of Sedimentary Petrology*, v. 42, no. 3, p. 682-683.
- Romain, H. G., and Mountney, N. P., 2014, Reconstruction of three-dimensional eolian dune architecture from one-dimensional core data through adoption of analog data from outcrop: *AAPG Bulletin*, v. 98, no. 1, p. 1-22.
- Rubin, D. M., and Hunter, R. E., 1985, Why deposits of longitudinal dunes are rarely recognized in the geologic record: *Sedimentology*, v. 32, p. 147-157.
- Sallenger, A. H., 1979, Inverse grading and hydraulic equivalence in grain-flow deposits: *Journal of Sedimentary Petrology*, v. 49, no. 2, p. 553-562.

- Schenk, C. J., 1983, Textural and structural characteristics of some experimentally formed eolian strata, *in* Brookfield, M. E., and Ahlbrandt, T. S., eds., *Eolian Sediments and Processes*, Volume 38, Elsevier, p. 41-49.
- Simpson, J., 1985, Stylolite-controlled layering in an homogeneous limestone: pseudo-bedding produced by burial diagenesis: *Sedimentology*, v. 32, p. 495-505.
- Sneh, A., 1988, Permian dune patterns in northwestern Europe challenged: *Journal of Sedimentary Petrology*, v. 58, no. 1, p. 44-51.
- Stauffer, P. H., 1967, Grain-flow deposits and their implications, Santa Ynez Mountains, California: *Journal of Sedimentary Petrology*, v. 37, no. 2, p. 487-508.
- Steidtmann, J. R., 1974, Evidence for eolian origin of cross-stratification in sandstone of the Casper Formation, Southernmost Laramie Basin, Wyoming: *Geological Society of America Bulletin*, v. 85, p. 1835-1842.
- Stockdale, P. B., 1943, Stylolites: primary or secondary?: *Journal of Sedimentary Petrology*, v. 13, no. 1, p. 3-12.
- Sumner, C. D., 1999, Stratigraphy of the northern depositional margin of the Coconino Sandstone, northern Arizona and southern Utah [MS thesis]: Stephen F. Austin State University, 161 p.
- Sutton, S. L. F., McKenna Neuman, C., and Nickling, W., 2013, Lee slope sediment processes leading to avalanche initiation on an aeolian dune: *Journal of Geophysical Research: Earth Surface*, v. 118, p. 1754-1766.
- Sweet, M. L., 1992, Lee-face airflow, surface processes, and stratification types: their significance for refining the use of eolian cross-strata as paleocurrent indicators: *Geological Society of America Bulletin*, v. 104, p. 1528-1538.
- Sweet, M. L., Nielson, J., Havholm, K., and Farrelley, J., 1988, Algodones dune field of southeastern California: case history of a migrating modern dune field: *Sedimentology*, v. 35, p. 939-952.
- Walderhaug, O., and Bjørkum, P. A., 2003, The effect of stylolite spacing on quartz cementation in the lower Jurassic Stø Formation, southern Barents Sea: *Journal of Sedimentary Research*, v. 73, no. 2, p. 146-156.
- Walker, T. R., and Harms, J. C., 1972, Eolian origin of flagstone beds, Lyons sandstone (Permian), type area, Boulder county, Colorado: *The Mountain Geologist*, v. 9, no. 2-3, p. 279-288.
- Welton, J. E., 1984, SEM Petrology Atlas, Tulsa, Oklahoma, The American Association of Petroleum Geologists, The AAPG methods in exploration series, no. 4, 237 p.

- Wentworth, C. K., 1922, A scale of grade and class terms for clastic sediments: *Journal of Geology*, v. 30, no. 5, p. 377-392.
- Whitmore, J. H., and Strom, R., 2009, Petrographic analysis of the Coconino Sandstone, Northern and Central Arizona: *Geological Society of America Abstracts with Programs*, v. 41, no. 7, p. 122.
- , 2010, Textural trends in the Coconino Sandstone, central and northern Arizona, USA: *Geological Society of America Abstracts with Programs*, v. 42, no. 5, p. 428.

CHAPTER FIVE

DISCUSSION AND FUTURE WORK

The interpretation of undifferentiable grainflow and grainfall stratification characterizes fine-scale processes that may explain much of the large-scale, undeformed cross-bedding in the Coconino Sandstone. Textures and sedimentary structures observed in our outcrops exhibit properties of both grainflow and grainfall cross-strata, without exclusively meeting published criteria for a single type. Accordingly, this interpretation suggests that the invoked processes behaved differently from documented examples, since undifferentiated grainflow and grainfall cross-strata, with variable textures and dips consistently below the angle of repose, have not been described on modern eolian dunes.

One possible mechanism to explain this stratification type distribution involves syndepositional reworking of grainflow and grainfall deposits on the dune foreset. When flow separation occurs over dune bedforms, a reverse current moves back up the foreset slope. This return flow may rework newly deposited grainflow beds with sediment simultaneously settling out from suspension (grainfall). Such a model might also allow for traction laminae where ripples migrate across the dune face. Reesink and Bridge (2009) described this potential for syndepositional turbulence to accelerate grainflow deposits toward the bedform trough, therefore reducing their dip angles and affecting grain-size distribution. Kleinhans (2004) also noted that “counterflow” over a dune could reduce the dip of deposited sediment. When combined with Kleinhans' (2004) prediction of relatively fine grainfall deposits near the base of some dunes, this reworking process might explain the textures and sedimentary structures observed in our cross-bedding.

The extreme lateral width, low dip angles and down-dip decrease in dip angle proposed for continuous avalanching deposits may also agree with our Coconino Sandstone cross-bed data; however, it remains uncertain whether a homogeneous movement of grains down a dune foreset would produce distinct massive and laminated textures. Rather, some authors have suggested that beds deposited by continuous avalanching should be laminated (Kocurek and Dott, 1981) or contain “thin and indistinct” bedding (Hunter and Kocurek, 1986). If cross-bedding produced by continuous avalanching is predominantly laminated, then the model does not explain our observation of both massive and laminated textures. Furthermore, some bedding planes in the Coconino Sandstone display trackways (Brand, 1979; Brand and Tang, 1991; Citton et al., 2012; McKee, 1934; McKee and Bigarella, 1979) that appear to indicate at least brief stabilization of the surface sediment. Continuous avalanching is not likely to allow enough time for emplacement of these tracks between deposition of the associated cross-beds. However, the similarity between published criteria for continuous avalanching deposits and our cross-beds is striking, and such an interpretation may not be ruled out for at least some beds within the formation. More study is needed to determine the physical potential for this process to produce similar cross-beds and associated biogenic structures.

It should be noted that the syndepositional reworking processes described here have been documented on subaqueous bedforms, but are not known from eolian dunes. Flow separation occurs over dunes in both air and underwater. While grainflow and grainfall processes occur in both fluids, and subaqueous turbulent reworking has been observed (Reesink and Bridge, 2009), whether such reworking could occur over a wind-

deposited bedform currently remains unclear. The goal of this project was to interpret fine-scale cross-bed facies and associated processes, but additional work must be done to develop larger-scale models that could produce our proposed stratification type distribution.

Future Work

As Reesink and Bridge (2009) note, it is unlikely that their modern observations can be applied directly to ancient deposits without accounting for variations in bedform shape, grain size, and scaling parameters. For this reason, physical sedimentology experiments are needed to explore the range of processes that could promote syndepositional reworking of large-scale cross-beds, and specifically those composed of well to moderately sorted, fine, quartz/feldspar sand. Results from experimental studies must also be scaled appropriately to compare with cross-bed set thicknesses in the Coconino Sandstone. While the original dune heights are unknown, set thicknesses constrain the minimum heights of the bedforms, and so some of our outcrops imply that the dunes were quite tall. It is unclear how the reworking processes described by Reesink and Bridge (2009) would modify cross-bedding on this scale.

With the exception of the lowermost sample at our HMT outcrop (HMT-1), all of our samples are well to moderately sorted. However, poor sorting and even bimodal grain-size distributions have been documented from numerous Coconino Sandstone outcrops (Maithel and Whitmore, 2010; Whitmore and Strom, 2009, 2010). Additional study on the context of poorly sorted samples, and their proximity to the better-sorted cross-beds, would provide helpful insight into sorting trends and associated processes.

Our samples also contain zircons and other trace heavy mineral components (opaque under plane-polarized light), which should exhibit preferential sorting when transported along with quartz and feldspar grains. Most of these minerals are probably not magnetic (due to low magnetic susceptibility values; appendix A), but characterizing their distribution via x-ray diffraction or other methods could add to or refine our process interpretations. Assemblages of zircon, tourmaline, and rutile may be common in “mature” sandstones (Hubert, 1962), so it is possible that the Coconino Sandstone contains enough of these heavy minerals to exhibit distinct sorting trends associated with certain dune sedimentation processes (e.g., grading produced by grainflows).

Finally, low-relief sedimentary structures are prevalent on cross-bedding planes in many of our outcrops. These structures have been previously interpreted as “slump features,” “ripple marks,” and “rainprints” (McKee, 1945), but they exhibit anomalous attributes that should be further investigated (Maithel et al., 2014). They are also typically shallow, and may shed light on related cross-bed depositional and diagenetic processes.

Paleoenvironmental models for sandstone units are based on suites of sedimentary textures, structures, and facies associations. The fine-scale process interpretations proposed in this study provide one piece of the puzzle that should be used, alongside other criteria, to develop a robust depositional model for the Coconino Sandstone.

References

Brand, L. R., 1979, Field and laboratory studies on the Coconino Sandstone (Permian) vertebrate footprints and their paleoecological implications: *Palaeogeography, Palaeoclimatology, Palaeoecology*, v. 28, p. 25-38.

- Brand, L. R., and Tang, T., 1991, Fossil vertebrate footprints in the Coconino Sandstone (Permian) of northern Arizona: evidence for underwater origin: *Geology*, v. 19, p. 1201-1204.
- Citton, P., Sacchi, E., and Nicosia, U., 2012, Sometimes they come back: recovery and reinterpretation of a trackway slab from the Permian Coconino Sandstone of the southwestern United States: *Ichnos*, v. 19, p. 165-174.
- Hubert, J. F., 1962, A zircon-tourmaline-rutile maturity index and the interdependence of the composition of heavy mineral assemblages with the gross composition and texture of sandstones: *Journal of Sedimentary Petrology*, v. 32, no. 3, p. 440-450.
- Hunter, R. E., and Kocurek, G., 1986, An experimental study of subaqueous slipface deposition: *Journal of Sedimentary Petrology*, v. 56, no. 3, p. 387-394.
- Kleinhans, M. G., 2004, Sorting in grain flows at the lee side of dunes: *Earth-Science Reviews*, v. 65, p. 75-102.
- Kocurek, G., and Dott, R. H., 1981, Distinctions and uses of stratification types in the interpretation of eolian sand: *Journal of Sedimentary Petrology*, v. 51, no. 2, p. 579-595.
- Maithel, S. A., Brand, L., and Whitmore, J. H., 2014, "Ripple Marks," "Slump Features," and "Rainprints" in the Coconino Sandstone near Ash Fork, Arizona: *Geological Society of America Abstracts with Programs*, v. 46, no. 6, p. 768.
- Maithel, S. A., and Whitmore, J. H., 2010, Textural analysis of the Coconino Sandstone, Chino Point, Arizona: *Geological Society of America Abstracts with Programs*, v. 42, no. 5, p. 426.
- McKee, E. D., 1934, The Coconino Sandstone - its history and origin: Carnegie Institution of Washington Publication 440, p. 77-115.
- , 1945, Small-scale structures in the Coconino Sandstone of northern Arizona: *Journal of Geology*, v. 53, no. 5, p. 313-325.
- McKee, E. D., and Bigarella, J. J., 1979, Ancient sandstones considered to be eolian, *in* McKee, E. D., ed., *A Study of Global Sand Seas*: Honolulu, HI, University Press of the Pacific, p. 187-238.
- Reesink, A. J. H., and Bridge, J. S., 2009, Influence of bedform superimposition and flow unsteadiness on the formation of cross strata in dunes and unit bars — Part 2, further experiments: *Sedimentary Geology*, v. 222, p. 274-300.
- Whitmore, J. H., and Strom, R., 2009, Petrographic analysis of the Coconino Sandstone, Northern and Central Arizona: *Geological Society of America Abstracts with Programs*, v. 41, no. 7, p. 122.

-, 2010, Textural trends in the Coconino Sandstone, central and northern Arizona, USA:
Geological Society of America Abstracts with Programs, v. 42, no. 5, p. 428.

APPENDIX A

THE PATH TO SANDSTONE DISAGGREGATION: AN ADVENTURE IN METHODOLOGY

"...Thomas Edison tried and failed nearly 2000 times to develop the carbonized cotton-thread filament for the incandescent lightbulb. And when asked about it he said, 'I didn't fail. I found out 2000 ways how not to make a light bulb,' but he only needed to find one way to make it work."

-Benjamin Gates, in the movie "National Treasure"

Disaggregation and loose-particle analysis are the fastest methods for characterizing grain size in sandstones; however, it has long been assumed that some rocks cannot be readily disaggregated (Friedman, 1958, 1962; Johnson, 1994; Kellerhals et al., 1975; Kong et al., 2005; Krumbein, 1935; Rose, 1968). Because we initially believed it would also be impossible to disaggregate the quartz-cemented Coconino Sandstone (Maithel et al., 2016), we employed various whole-rock analysis methods to describe and interpret textural trends and associated processes.

Image Analysis

Two polished Coconino Sandstone samples from the ASF-5 outcrop were photographed for image analysis using scanning electron microscope-cathodoluminescence (SEM-CL). The SEM-CL visually differentiates quartz grains from the surrounding overgrowths and may allow for the collection of textural data by image analysis. However, when images were processed using the FIJI distribution of ImageJ software (Schindelin et al., 2012; Schneider et al., 2012), we found that the grains were not consistently distinguished from the surrounding overgrowths in our samples (figure 1). While SEM-CL and image analysis may allow for the collection of textural data in

some sandstones, these methods appear insufficient for describing grain textures in our Coconino Sandstone samples.

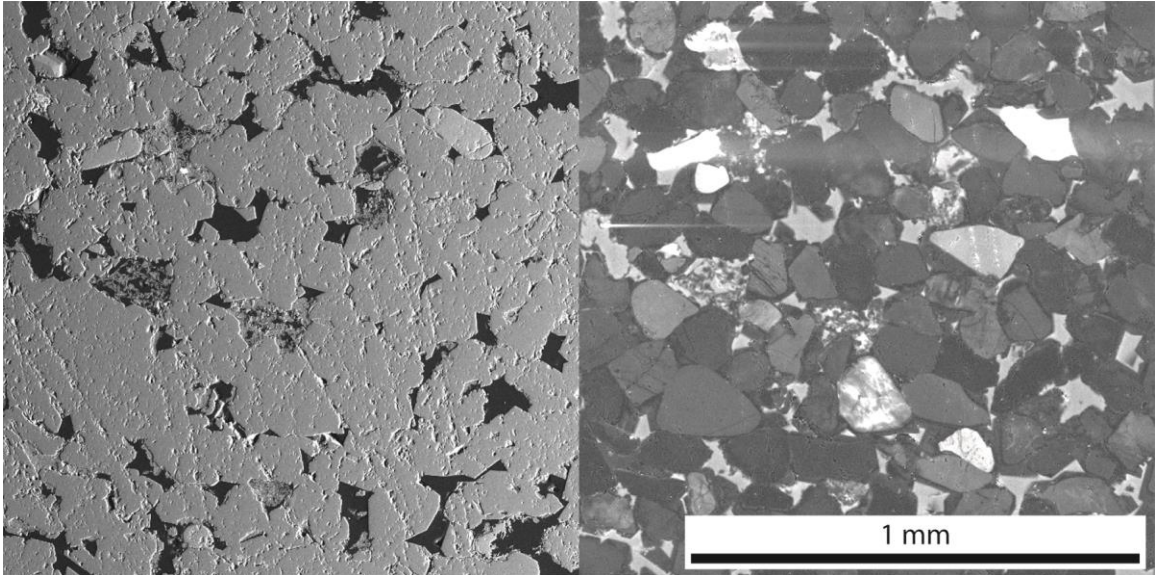


Figure 1: Backscattered-electron (left) and cathodoluminescence (right) images of a Coconino Sandstone sample (ASF-5-26). For both of our imaged samples, contrast between quartz grains and overgrowth cement was not consistent enough (in the SEM-CL image) for straightforward image-analysis techniques.

Petrographic Methods

Thin sections, most of which were cut parallel to strike and perpendicular to bedding, were made from samples collected at our outcrops (table 1). Grains were measured on either isolated thin-section photos or stitched vertical transects (figure 2) using the FIJI distribution of ImageJ software (Schindelin et al., 2012; Schneider et al., 2012) and a Wacom USB tracing pad. All photos were taken at 100x magnification, and the measurement scale in ImageJ was calibrated to ~ 1.56 pixels per micron.

Table 1: Outcrop Names and Location Information

Location	Outcrop Code
Ash Fork	ASF-5
Ash Fork	ASF-22e
Chino Point East ¹	CPE
Chino Wash ¹	TM-1
Chino Wash ¹	TM-3
Hermit Trail ²	HMT
Five Mile Wash ³	HOL-E-A
Five Mile Wash ³	HOL-E-B

¹The Chino Point East and Chino Wash Outcrops are located north of the town of Seligman, Arizona. ²Hermit Trail descends from the South Rim of the Grand Canyon. ³The Five Mile Wash outcrops are located south of the town of Holbrook, Arizona.

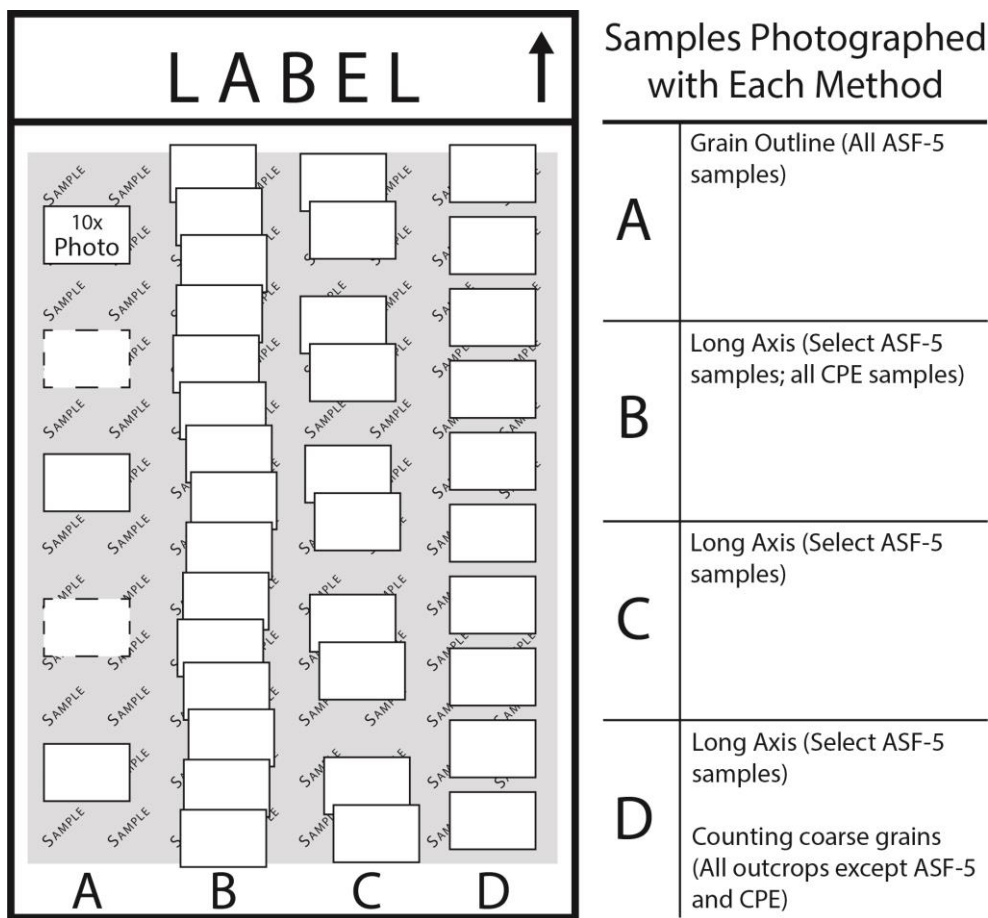


Figure 2: Diagram illustrating the methods used to photograph vertical transects of each thin section. **A)** Isolated photos taken for measuring grain outlines. While we used 2-3 photos from each slide (top, middle, and bottom or top and bottom), an additional two photos could be added in the intermediate positions if desired. Maithel et al. (2015) similarly took up to five photos along slide transects to measure long axes in the Permian-Triassic Hopeman Sandstone (Scotland). **B)** Overlapping photos were taken perpendicular to bedding and then stitched together with the “Photomerge” command in Adobe Photoshop, using the “reposition” layout to avoid or minimize distortion. Stitching a large number of photos provided a better representation of the thin sections, but increased the probability of offset during the stitching process. We identified and corrected this in some transects, but offset remained in others. Grains near obvious offset zones were excluded, so we expect that this would have a minimal, if any, impact on our grain-measurement data. Transects photographed with this method were used to collect long-axis data for all CPE samples and for select samples from ASF-5. **C)** Stitched groups of photos (or in one case, a combination of stitched and isolated photos) were taken from at least five areas along a vertical slide transect. These were used to collect long-axis data from select ASF-5 samples. **D)** Isolated photos were taken along a vertical slide transect. This method was therefore similar to A, but included more photos to better represent the grain-size distribution in the sample. While 8-11 photos were used to collect long-axis data from select ASF-5 samples, ten photos were used for all samples in which coarse grains ($\geq 150 \mu\text{m}$) were counted with the light table and overlay (all outcrops except ASF-5 and CPE).

Tracing Grain Outlines

Outlines of at least 150 quartz grains were traced on 2-3 photos from each thin section in the ASF-5 outcrop. Photos were taken from either the top and bottom or the top, middle, and bottom of the thin section, with the intent of representing vertical grain-size distribution. For two of the samples, grains were measured from five photos, as shown in figure 2A.

Measuring grains from 2-3 photos introduces several potential sources of error. The challenge of measuring 150 grains from only a few photos may have meant that some cement pieces were erroneously measured as grains. Additionally, if only 2-3 photos were used, it is likely that sections of the slides with very large grains (that take up substantial space in the 100x photos) were not adequately represented. While we could have used the same methodology but with more photos, this would add significant time to an already time-consuming approach. Since any grain-shape data obtained from grain outlines were not a vital part of this project, we opted to measure only the long axes of grains.

Measuring Long Axes of Grains

Measuring long grain axes in thin section was still tedious but was faster than tracing grain outlines, therefore allowing us to measure more grains more quickly. We also increased the number of thin-section photos taken from each sample. For two of the outcrops (ASF-5 and CPE), the long axes of at least 170 grains were measured from vertical transects of each thin section (perpendicular to bedding). While a complete transect (figure 2B) covers a larger area and would better represent vertical grain-size variation within individual samples, the stitching process was time consuming and

introduced the possibility of error due to photo offset. We ultimately determined that photographing at least ten areas along a vertical transect from each slide would sufficiently represent the grain-size distribution in the sample (figure 2D). Moreover, since this method was based on number of grains measured, we considered area (number of photos) to be a negligible variable. Textural data from the ASF-5 samples, which were photographed with different methods, were therefore deemed comparable.

Counting Grains $\geq 150 \mu\text{m}$

To expedite textural analysis for the other outcrops, we counted grains with long axes $\geq 150 \mu\text{m}$ on ten printed photos from each thin section using a transparent overlay and a light table (figure 3). The $150 \mu\text{m}$ grain-size threshold was chosen based on the 75th-percentile values from the ASF-5 and CPE long-axis measurements. Since this method was based on a fixed area instead of a fixed number of grains, it was essential for us to use exactly ten photos from each slide (figure 2D) so that the relative number of coarse grains could be compared between samples.

This grain-counting method seemed advantageous over measuring long axes due to the potential for faster analysis. However, several drawbacks to this approach remain. While the method enables a relative comparison of the number of “coarse” grains in each sample, it does not actually provide grain-size data, which limits its potential application. Furthermore, challenges may arise in choosing a threshold value (e.g., $150 \mu\text{m}$) to compare the coarse fractions of very diverse samples.

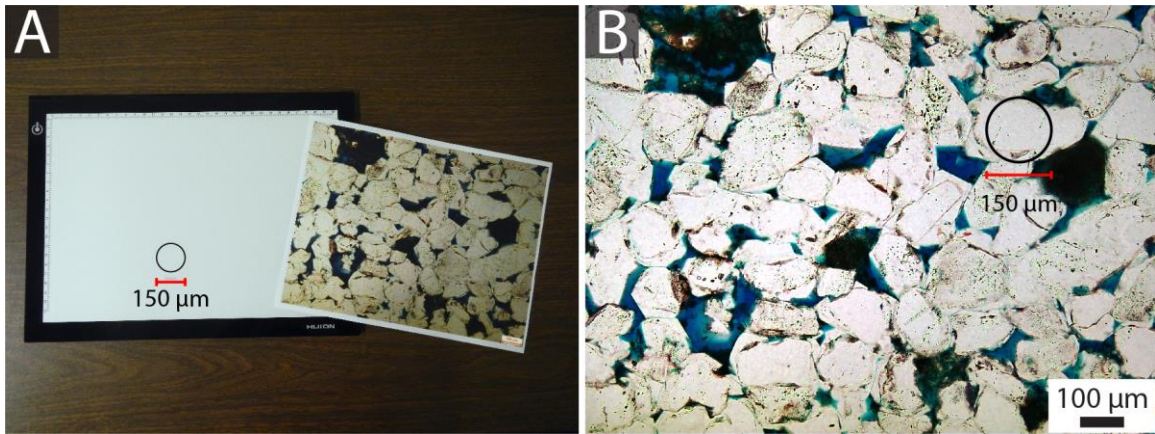


Figure 3: Light table method used for counting the coarsest grains in thin-section photos. **A)** We used a light table and a transparent overlay (with scaled 150 μm circle) to count coarse grains on ten printed photos from each thin section. Brightness/contrast, levels, and uneven illumination in the thin-section images shown here were corrected with Adobe Photoshop methods similar to those described in Leong et al. (2003). **B)** Each printed image was moved over the light table and overlay circle, and grains with long axes roughly $\geq 150 \mu\text{m}$ were counted.

Magnetic Susceptibility

Bulk magnetic susceptibility does not provide grain-size data, but measures the signal of a rock placed in a magnetic field. Because certain magnetic minerals are denser than quartz, we thought that describing the distribution of trace magnetic components might enable us to interpret textural trends and associated processes using a parameter other than grain size. This method involves crushing whole-rock samples, and therefore does not require thin sections. It is also faster than measuring grains. However, while the method might work well for rocks with a higher percentage of magnetic minerals, our Coconino Sandstone samples did not contain enough magnetic material for the results to be useful. The signals were therefore very low, and this approach was ultimately abandoned. Although it did not work for our Coconino Sandstone samples, magnetic susceptibility may enable characterization of trends in units that contain a notable percentage of magnetic minerals.

Disaggregation: A New Hope

The potential for disaggregation – first of our weakly cemented HOL samples, and then the other, well-lithified outcrops – provided hope for a future of expedited textural analysis. While the disaggregation methods that we developed still require multiple steps (which are typically completed over several days), they serve as a much less-tedious alternative to petrographic analyses. Furthermore, the laser-diffraction analyzer includes a larger sample size (compared to, at most, a few hundred grains measured in thin section), therefore making the results more robust. We expect that disaggregation and loose-sediment analysis will provide the best solution for characterizing textures in sandstones, but researchers should evaluate the pros and cons of each method to determine the best option for their specific study.

Acknowledgements

SEM-CL imaging was conducted by Stephanie Mills at the University of Maine.

References

- Friedman, G. M., 1958, Determination of sieve-size distribution from thin-section data for sedimentary petrological studies: *Journal of Geology*, v. 66, no. 4, p. 394-416.
- , 1962, Comparison of moment measures for sieving and thin-section data in sedimentary petrological studies: *Journal of Sedimentary Petrology*, v. 32, no. 1, p. 15-25.
- Johnson, M. R., 1994, Thin section grain size analysis revisited: *Sedimentology*, v. 41, p. 985-999.
- Kellerhals, R., Shaw, J., and Arora, V. K., 1975, On grain size from thin sections: *Journal of Geology*, v. 83, p. 79-96.

- Kong, M., Bhattacharya, R. N., James, C., and Basu, A., 2005, A statistical approach to estimate the 3D size distribution of spheres from 2D size distributions: *Geological Society of America Bulletin*, v. 117, no. 1/2, p. 244-249.
- Krumbein, W. C., 1935, Thin-section mechanical analysis of indurated sediments: *Journal of Geology*, v. 43, no. 5, p. 482-496.
- Leong, F. J. W.-M., Brady, M., and McGee, J. O., 2003, Correction of uneven illumination (vignetting) in digital microscopy images: *Journal of Clinical Pathology*, v. 56, no. 8, p. 619-621.
- Maithel, S. A., Brand, L., and Whitmore, J. H., 2016, Using textural trends to interpret cross-bed depositional processes in the Coconino Sandstone (Permian), Arizona: *Geological Society of America Abstracts with Programs*, v. 48, no. 7.
- Maithel, S. A., Garner, P. A., and Whitmore, J. H., 2015, Preliminary assessment of the petrology of the Hopeman Sandstone (Permo-Triassic), Moray Firth Basin, Scotland: *Scottish Journal of Geology*, v. 51, no. 2, p. 177-184.
- Rose, H. E., 1968, The determination of the grain-size distribution of a spherical granular material embedded in a matrix: *Sedimentology*, v. 10, p. 293-309.
- Schindelin, J., Arganda-Carreras, I., Frise, E., Kaynig, V., Longair, M., Pietzsch, T., Preibisch, S., Rueden, C., Saalfeld, S., Schmid, B., Tinevez, J., White, D. J., Hartenstein, V., Eliceiri, K., Tomancak, P., and Cardona, A., 2012, Fiji: an open-source platform for biological-image analysis: *Nature Methods*, v. 9, no. 7, p. 676-682.
- Schneider, C. A., Rasband, W. S., and Eliceiri, K. W., 2012, NIH Image to ImageJ: 25 years of image analysis: *Nature Methods*, v. 9, no. 7, p. 671-675.

APPENDIX B
OUTCROP GPS COORDINATES

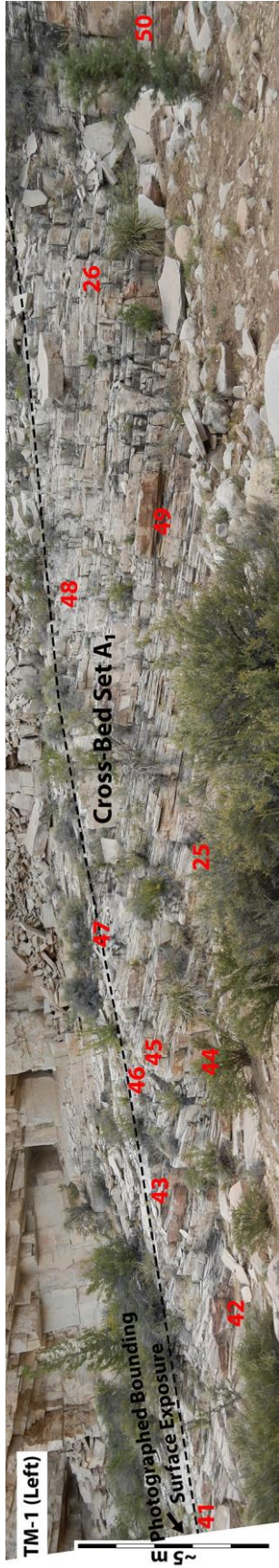
Outcrop	GPS Coordinates	Primary Exposure(s)
ASF-1	35° 19' 28.06" N, 112° 27' 37.51" W	Bounding surface, cross-beds
ASF-2	35° 20' 13.09" N, 112° 27' 8.39" W	Cross-beds
ASF-3	35° 20' 24.18" N, 112° 27' 4.50" W	Bounding surface, cross-beds
ASF-4	35° 17' 11.11" N, 112° 26' 42.68" W	Bounding surface
ASF-5	35° 17' 13.42" N, 112° 26' 38.58" W	Cross-beds
ASF-6	35° 17' 7.22" N, 112° 26' 41.17" W	Bounding surface
ASF-7	35° 16' 46.56" N, 112° 26' 20.15" W	Cross-beds
ASF-8	35° 21' 35.21" N, 112° 28' 47.28" W	Bounding surface
ASF-9	35° 21' 25.88" N, 112° 28' 58.48" W	Bounding surface
ASF-22e	35° 17' 56.36" N, 112° 26' 45.42" W	Cross-beds
CPE	35° 21' 0.60" N, 112° 56' 38.40" W	Cross-beds
HMT	36° 3' 18.50" N, 112° 13' 10.10" W	Cross-beds
HOL-E-A	34° 50' 11.00" N, 110° 8' 37.03" W	Cross-beds
HOL-E-B	34° 50' 9.49" N, 110° 8' 35.48" W	Cross-beds
HOL-W-A	34° 50' 13.24" N, 110° 8' 51.94" W	Bounding surface
HOL-W-B	34° 50' 12.77" N, 110° 8' 52.84" W	Bounding surface
TM-1	35° 23' 8.66" N, 112° 52' 25.00" W	Bounding surface, cross-beds
TM-3	35° 23' 22.50" N, 112° 52' 27.80" W	Cross-beds

APPENDIX C

OUTCROP PHOTO MOSAICS WITH SAMPLE LOCATIONS

Approximate sample locations were marked on printed outcrop photo mosaics in the field. Annotations were later added to the images using Adobe Illustrator.

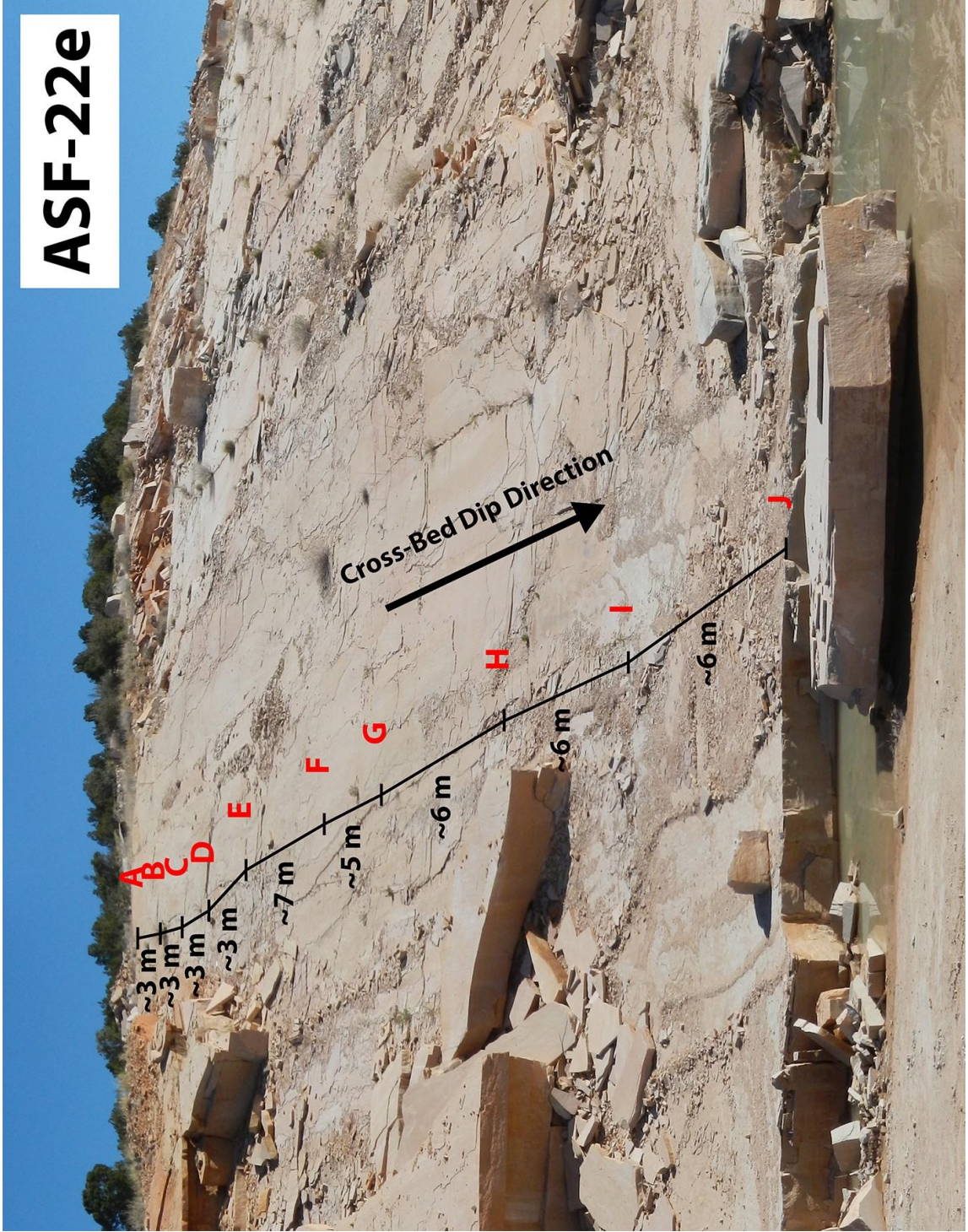




No samples were collected in this area, but strike and dip measurements were recorded.



ASF-22e



APPENDIX D

CROSS-BED DIP-ANGLE DATA

Outcrop	Dip Angle (°)						
ASF-5	7	ASF-22e	23	HMT	22.5	HOL-E-A	21
ASF-5	7	ASF-22e	24	HMT	24.5	HOL-E-A	13.5
ASF-5	14	ASF-22e	23	HMT	23	HOL-E-A	22
ASF-5	22	ASF-22e	21.5	HMT	24	HOL-E-A	23
ASF-5	23	ASF-22e	22	HMT	22	HOL-E-A	24
ASF-5	22	ASF-22e	22	Average	23.2	HOL-E-A	20
ASF-5	24	ASF-22e	23	Minimum	22	HOL-E-A	20
ASF-5	22	ASF-22e	23	Maximum	24.5	HOL-E-A	21
ASF-5	25	ASF-22e	18.5	n	5	HOL-E-A	22
ASF-5	21	ASF-22e	8			HOL-E-A	23
ASF-5	21	Average	20.8			HOL-E-A	27
ASF-5	21	Minimum	8			Average	21.5
ASF-5	23	Maximum	24			Minimum	13.5
ASF-5	22	n	10			Maximum	27
ASF-5	24					n	11
ASF-5	23						
ASF-5	27						
ASF-5	21						
ASF-5	22						
ASF-5	23						
ASF-5	18						
ASF-5	24						
ASF-5	24						
ASF-5	24						
ASF-5	23						
ASF-5	24						
ASF-5	22						
ASF-5	21						
ASF-5	22						
ASF-5	26						
ASF-5	23						
ASF-5	22						
ASF-5	23						
ASF-5	21						
ASF-5	21						
ASF-5	22						
ASF-5	23						
ASF-5	21						
Average	21.5						
Minimum	7						
Maximum	27						
n	38						

Outcrop	Dip Angle (°)	Outcrop	Dip Angle (°)	Outcrop	Dip Angle (°)
HOL-E-B	11.5	TM-1 A ₁ Left	19	TM-3	17
HOL-E-B	20	TM-1 A ₁ Left	20	TM-3	18.5
HOL-E-B	21	TM-1 A ₁ Left	20	TM-3	19
HOL-E-B	8	TM-1 A ₁ Left	16.5	TM-3	21
HOL-E-B	18	TM-1 A ₁ Left	21	TM-3	17
HOL-E-B	11	TM-1 A ₁ Left	20	TM-3	18
HOL-E-B	11	TM-1 A ₁ Left	19	TM-3	17
HOL-E-B	23	TM-1 A ₁ Left	16	TM-3	18
HOL-E-B	19	TM-1 A ₁ Left	17	TM-3	16
HOL-E-B	22	TM-1 A ₁ Left	23.5	TM-3	17
HOL-E-B	22	TM-1 A ₁ Left	23	TM-3	24
Average	17.0	TM-1 A ₁ Left	19.5	TM-3	16
Minimum	8	TM-1 A ₁ Left	21	TM-3	16
Maximum	23	TM-1 A ₁ Left	24	TM-3	21
n	11	TM-1 A ₁ Left	22	TM-3	16
		TM-1 A ₁ Left	18	TM-3	18
		TM-1 A ₁ Left	21	TM-3	18
		TM-1 A ₁ Left	19	TM-3	17
		TM-1 A ₁ Left	20	TM-3	18
		TM-1 A ₁ Left	18	TM-3	18
		TM-1 A ₁ Left	17	TM-3	19
		TM-1 A ₁ Left	18	Average	18.1
		TM-1 A ₁ Left	17	Minimum	16
		TM-1 A ₁ Left	17	Maximum	24
		TM-1 A ₁ Left	19	n	21
		TM-1 A ₁ Left	22		
		TM-1 A ₁ Left	19		
		TM-1 A ₁ Left	17		
		TM-1 A ₁ Left	19		
		TM-1 A ₁ Right	23		
		TM-1 A ₁ Right	11		
		TM-1 A ₁ Right	7		
		TM-1 A ₁ Right	16		
		TM-1 A ₁ Right	18		
		TM-1 A ₁ Right	18		
		TM-1 A ₁ Right	19		
		TM-1 A ₁ Right	14		
		TM-1 A ₁ Right	18		
		TM-1 A ₁ Right	18		
		Average	18.6		
		Minimum	7		
		Maximum	24		
		n	39		

APPENDIX E

PARTICLE-ANALYZER DATA

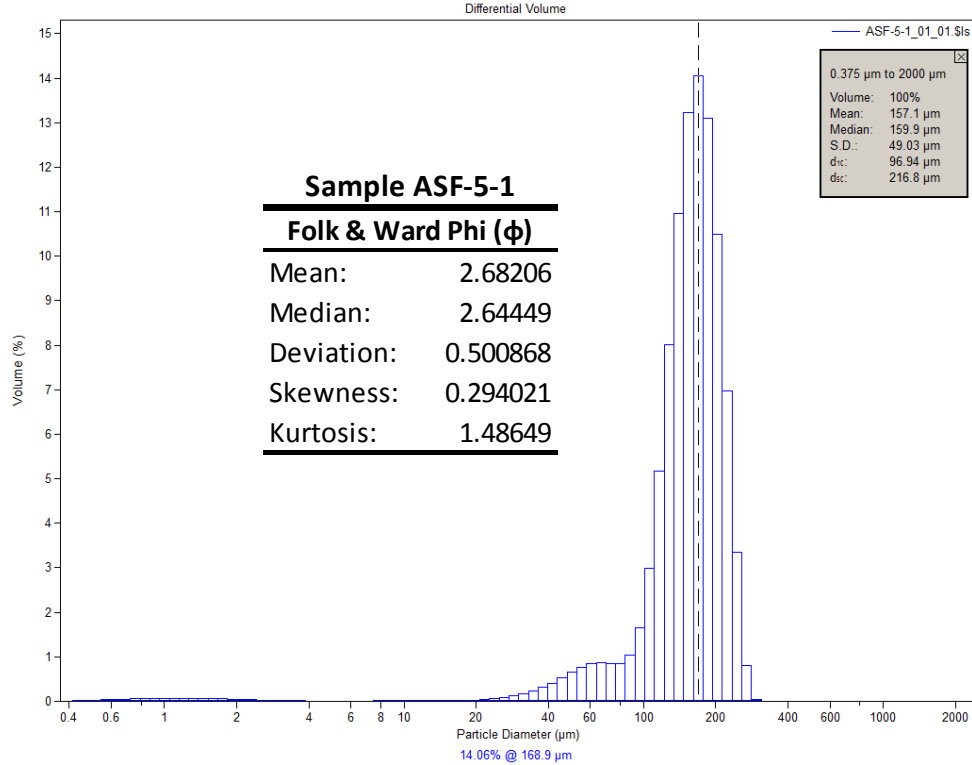
Included particle-analysis data files:

1. Coconino Sandstone data summary tables
2. Coconino Sandstone sample data
3. Poorly disaggregated TM-1 sample data
4. Select re-disaggregated samples for comparison with thin-section data
5. Algodones Dune sand sample data for sonication test

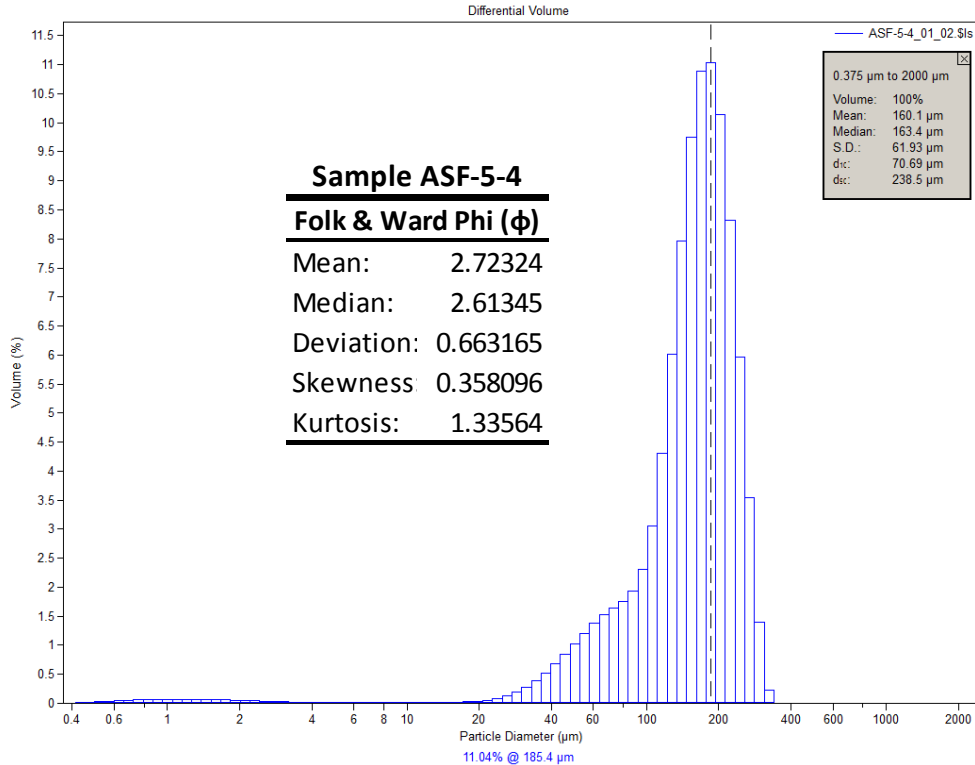
Outcrop	Sample	Average Grain Size (ϕ)	Median Grain Size (ϕ)	Mode Grain Size (ϕ)	Percent at Mode	Standard Deviation (ϕ)	Relative Vertical Distance (m)	Average Grain Size (ϕ) w/o Finest ~10%	Volume % for Average w/o Finest 10%
ASF-22e	A	2.92053	2.87995	2.8	13.48	0.470706	0.166900272	2.84149	90.1
ASF-22e	B	2.91214	2.8667	2.8	13.46	0.494197	1.221567951	2.82432	89.5
ASF-22e	C	2.9854	2.91613	2.8	13.08	0.557993	2.286888838	2.88116	89.6
ASF-22e	D	2.93439	2.8864	2.8	13.29	0.502969	3.352209725	2.85663	90.9
ASF-22e	E	2.86947	2.79737	2.7	14.32	0.540134	4.417530612	2.77257	90.5
ASF-22e	F	2.84098	2.78803	2.7	13.56	0.532694	6.903279349	2.75728	90.7
ASF-22e	G	2.83633	2.78318	2.7	14.07	0.530809	8.678814161	2.75125	90.4
ASF-22e	H	2.85156	2.80724	2.7	14.8	0.49573	10.80945594	2.77146	90.0
ASF-22e	I	2.75114	2.59857	2.4	9.303	0.779296	12.94009771	2.58241	89.9
ASF-22e	J	2.79948	2.69669	2.6	7.573	0.864277	15.07073948	2.62305	89.1
ASF-5	1	2.68206	2.64449	2.6	14.06	0.500868	0.819721255	2.59758	89.2
ASF-5	4	2.72324	2.61345	2.4	11.04	0.663165	1.941760503	2.58426	90.3
ASF-5	5	2.7538	2.65059	2.6	11.07	0.650531	4.43954639	2.6183	90.1
ASF-5	7	3.2268	3.14214	2.8	8.689	0.704686	20.00825714	3.09487	89.8
ASF-5	8	3.11591	3.01949	2.7	9.245	0.677237	23.70732422	2.99011	90.0
ASF-5	9	3.09558	2.97666	2.7	9.172	0.714621	20.84063047	2.9483	89.2
ASF-5	11	2.8235	2.72	2.6	8.687	0.736977	18.99076399	2.68893	90.8
ASF-5	12	2.78312	2.67386	2.6	12.11	0.627582	3.090435697	2.64823	90.0
ASF-5	13	2.68571	2.60126	2.4	12.91	0.558271	7.522657202	2.57098	89.6
ASF-5	14	2.68818	2.64204	2.6	13.61	0.519325	3.545244485	2.60045	89.7
ASF-5	15	2.70845	2.62364	2.4	7.907	0.739668	8.817164204	2.58336	91.1
ASF-5	16	2.73856	2.69153	2.6	13.05	0.525621	3.206302065	2.65419	90.7
ASF-5	17	2.50681	2.48216	2.4	13.91	0.471122	0.986195921	2.4271	88.6
ASF-5	18	3.02127	2.84366	2.7	10.79	0.739789	0	2.86038	90.5
ASF-5	19	2.86729	2.78735	2.7	12.65	0.575873	0	2.75788	90.3
ASF-5	20	2.72329	2.68514	2.6	13.51	0.508423	9.311926911	2.64302	90.1
ASF-5	21	2.80613	2.73274	2.6	13.18	0.541466	7.645848455	2.70427	90.2
ASF-5	23	2.73807	2.6253	2.4	10.45	0.678843	5.148728467	2.59494	90.2
ASF-5	24	2.73107	2.69913	2.7	14.03	0.473779	14.85952868	2.65149	89.2
ASF-5	25	2.64	2.61339	2.6	14.17	0.478337	19.80782165	2.57552	91.1
ASF-5	26	2.74118	2.69099	2.6	13.7	0.517408	21.79619506	2.65524	90.3
ASF-5	27	3.00463	2.80287	2.6	11.53	0.755543	8.616728706	2.81573	89.7
CPE	1	3.00666	2.84864	2.7	9.472	0.760942	0	2.82936	89.0
CPE	2	2.79063	2.67747	2.6	10.78	0.67854	0.776457135	2.65243	90.8
CPE	3	2.74429	2.5979	2.4	9.935	0.747132	1.423504748	2.5822	90.4
CPE	4	2.85268	2.68287	2.4	9.976	0.754335	2.458780928	2.68929	90.7
CPE	5	2.79074	2.7424	2.7	13.02	0.53603	3.67523044	2.6972	89.8
CPE	6	2.93614	2.81369	2.7	12.72	0.621085	4.555215194	2.79327	89.8
CPE	7	2.79751	2.72548	2.6	12.71	0.57036	5.124617093	2.68429	89.4
CPE	8	3.17143	3.00745	2.8	9.445	0.760517	6.056365655	3.0217	90.6
HMT	1	1.79309	2.04058	2.7	4.758	1.37989	26.1577428	1.59271	90.6
HMT	2	2.51951	2.52223	2.6	12.01	0.496531	18.27890461	2.45199	91.5

Outcrop	Sample	Average Grain Size (ϕ)	Median Grain Size (ϕ)	Mode Grain Size (ϕ)	Percent at Mode	Standard Deviation (ϕ)	Relative Vertical Distance (m)	Average Grain Size (ϕ) w/o Finest ~10%	Volume % for Average w/o Finest 10%
HMT	3	2.72571	2.70621	2.7	13.67	0.423714	10.40006641	2.65934	90.7
HMT	4	2.70088	2.67551	2.6	13.3	0.453153	3.309112041	2.62761	90.2
HMT	5	3.2729	3.14994	3.0	9.529	0.706803	0	3.13682	90.6
HOL-E-A	1	2.51167	2.50227	2.4	13.87	0.377973	0.16374269	2.45352	90.9
HOL-E-A	2	2.35077	2.33177	2.3	13.34	0.404134	2.140350877	2.28189	90.3
HOL-E-A	3	2.52526	2.5147	2.4	14.22	0.370972	0.140350877	2.46672	90.7
HOL-E-A	4	2.54271	2.52825	2.4	13.1	0.404702	1.415204678	2.46273	88.2
HOL-E-A	5	2.36	2.34561	2.3	13.79	0.385331	1.976608187	2.30083	91.0
HOL-E-A	7	2.41322	2.3979	2.3	13.09	0.401504	1.204678363	2.33188	88.0
HOL-E-A	8	2.41595	2.403	2.3	14.35	0.367631	0.865497076	2.35277	89.9
HOL-E-A	9	2.57578	2.56569	2.6	12.96	0.407372	1.239766082	2.51931	92.0
HOL-E-A	10	2.59313	2.58112	2.6	13.37	0.398727	0	2.53573	91.8
HOL-E-A	11	2.752	2.73849	2.7	14.87	0.362574	0.16374269	2.70446	92.5
HOL-E-B	1	2.50346	2.48766	2.4	11.67	0.467833	2.899297091	2.43348	91.3
HOL-E-B	2	2.46581	2.45035	2.4	13.91	0.385218	1.851648545	2.41101	92.0
HOL-E-B	3	2.36723	2.35333	2.3	13.66	0.385031	0.576614182	2.30639	90.7
HOL-E-B	4	2.39914	2.36981	2.3	11.54	0.484089	1.356250545	2.30907	89.3
HOL-E-B	5	2.70906	2.69335	2.7	13.66	0.403547	2.550080909	2.6528	91.9
HOL-E-B	6	2.54733	2.52422	2.4	12.49	0.448321	2.631297091	2.47586	90.6
HOL-E-B	7	2.66521	2.64705	2.6	13.43	0.427553	2.769353636	2.58364	88.3
HOL-E-B	8	2.60626	2.59021	2.6	13.55	0.403604	0.954250545	2.54343	91.1
HOL-E-B	9	2.59461	2.5783	2.6	13.86	0.390475	1.892262727	2.53886	91.9
HOL-E-B	10	2.71102	2.6951	2.7	14.45	0.376934	0.576614182	2.63758	88.5
HOL-E-B	11	2.51006	2.49268	2.4	12.56	0.437643	0.081216182	2.42257	88.3
HOL-E-B	12	2.53553	2.52083	2.4	13.37	0.40236	0	2.45928	88.7
HOL-E-B	13	2.60751	2.5943	2.6	13.93	0.383433	1.161341455	2.55356	92.0
HOL-E-B	14	2.48132	2.46854	2.4	12.52	0.426683	2.079046545	2.40587	89.6
HOL-E-B	15	2.73856	2.7185	2.7	14.73	0.387153	2.842444545	2.68432	91.7
HOL-E-B	16	2.52521	2.50833	2.4	12.59	0.428628	2.111535455	2.43765	87.9
TM-1 A ₁	25	2.74573	2.70283	2.6	13.07	0.522964	3.454307494	2.65459	89.4
TM-1 A ₁	26	2.93141	2.80727	2.7	10.65	0.703696	0.585233573	2.78048	90.2
TM-1 A ₁	41	2.8601	2.75707	2.7	9.782	0.724826	3.584359399	2.70739	89.4
TM-1 A ₁	42	2.90455	2.85114	2.7	12.41	0.556477	4.364753455	2.80673	89.8
TM-1 A ₁	43	2.9917	2.91262	2.8	12.04	0.570058	2.375554208	2.8764	89.5
TM-1 A ₁	44	2.8317	2.75308	2.7	10.8	0.644958	3.695324907	2.70827	89.9
TM-1 A ₁	45	2.83999	2.76592	2.7	11.43	0.604441	2.211212887	2.72901	90.6
TM-1 A ₁	46	2.89759	2.77178	2.6	11.31	0.690246	1.767268232	2.75128	90.4
TM-1 A ₁	47	2.80241	2.73217	2.6	12.22	0.56699	0.849220763	2.69826	90.2
TM-1 A ₁	48	3.00658	2.87101	2.7	10.3	0.737995	0	2.85162	90.5
TM-1 A ₁	49	2.90015	2.76301	2.6	10.38	0.718149	2.438679783	2.74939	90.6
TM-1 A ₁	50	2.77074	2.69008	2.6	10.78	0.637388	1.954744581	2.63891	89.2

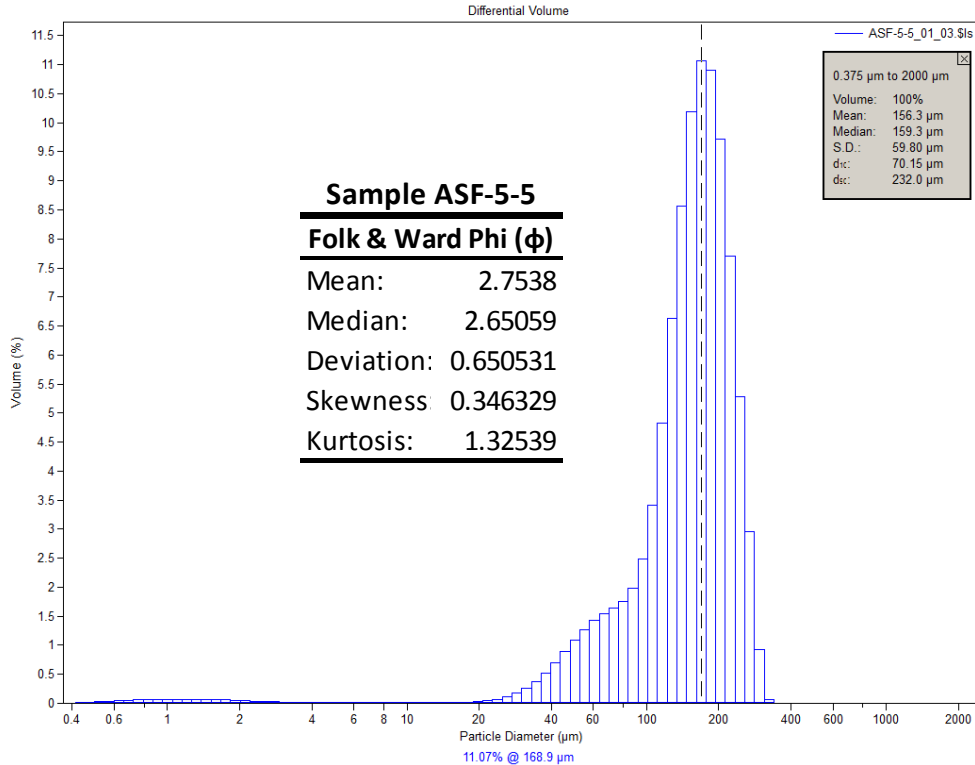
Outcrop	Sample	Average Grain Size (ϕ)	Median Grain Size (ϕ)	Mode Grain Size (ϕ)	Percent at Mode	Standard Deviation (ϕ)	Relative Vertical Distance (m)	Average Grain Size (ϕ) w/o Finest ~10%	Volume % for Average w/o Finest 10%
TM-3	1	2.69494	2.6329	2.6	10.91	0.631687	3.465958934	2.57954	90.2
TM-3	2	2.33812	2.22626	2.0	9.249	0.756764	6.23667425	2.19184	90.4
TM-3	4	2.8289	2.79459	2.7	13.2	0.500367	0	2.75578	91.0
TM-3	5	2.74404	2.71751	2.7	13.94	0.460186	0.289189229	2.66832	89.6
TM-3	6	2.89857	2.85897	2.8	13.25	0.497617	0.385536078	2.81361	89.9
TM-3	7	2.61316	2.59049	2.6	11.97	0.565547	9.88135064	2.52298	89.5
TM-3	8	2.8297	2.75522	2.7	11.83	0.605567	7.269131838	2.7144	90.2
TM-3	9	2.82154	2.78753	2.7	13.13	0.498922	3.486625927	2.73305	88.9
TM-3	10	2.7525	2.7181	2.7	11.94	0.552896	3.624306764	2.66839	90.8
TM-3	11	2.84061	2.7864	2.7	12.57	0.553731	7.073018422	2.74601	90.2
TM-3	12	2.77367	2.72452	2.7	12.27	0.555092	7.392985117	2.67404	89.6
TM-3	13	2.92849	2.87694	2.8	12.89	0.527392	4.57424506	2.83576	90.0
TM-3	14	2.76104	2.72649	2.7	13.26	0.500196	0.137680836	2.67978	90.1
TM-3	15	2.68011	2.63781	2.6	11.43	0.606539	8.129562722	2.57428	89.9



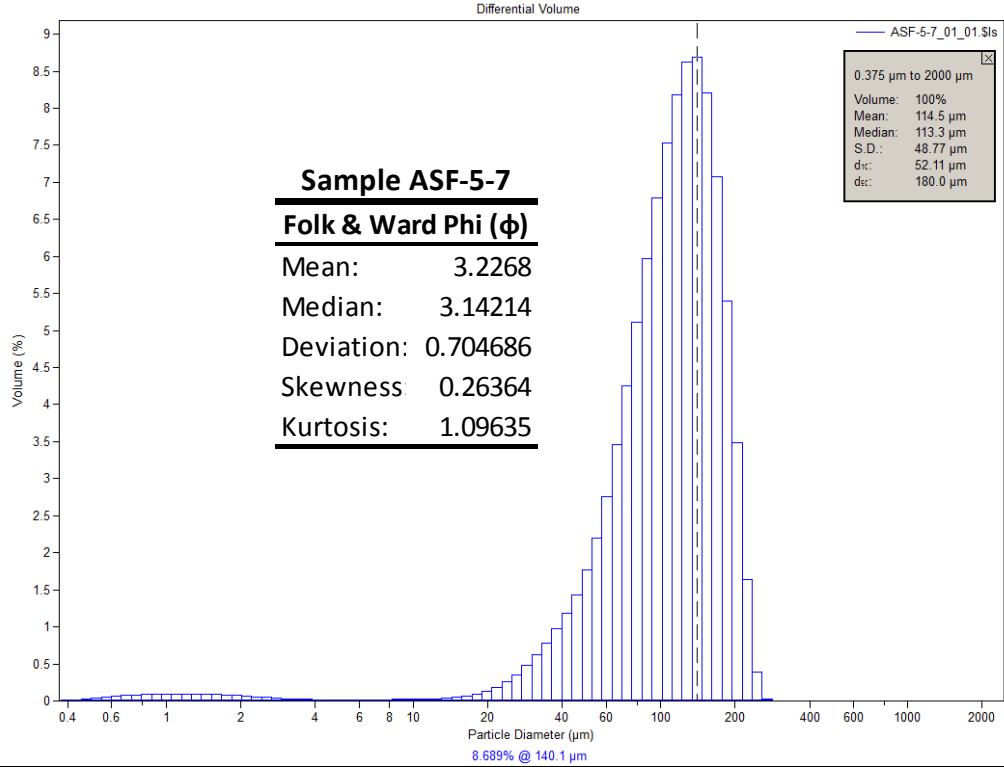
μm	Volume (%)						
0.375198	0.00661633	4.2411	0.00856673	47.9397	0.654316	541.892	0
0.411878	0.0126124	4.65572	0.0078394	52.6264	0.773359	594.869	0
0.452145	0.0212053	5.11087	0.00780456	57.7713	0.855024	653.025	0
0.496347	0.0292589	5.61052	0.00830409	63.4192	0.875133	716.866	0
0.544872	0.0368351	6.15902	0.00920172	69.6192	0.8423	786.949	0
0.59814	0.0438206	6.76114	0.0103387	76.4253	0.840346	863.883	0
0.656615	0.050105	7.42212	0.0115848	83.8969	1.03518	948.338	0
0.720807	0.055538	8.14773	0.0128006	92.0988	1.66219	1041.05	0
0.791275	0.0600417	8.94427	0.0138425	101.103	2.9992	1142.83	0
0.868632	0.0634381	9.81869	0.0146117	110.987	5.18115	1254.55	0
0.953552	0.0656265	10.7786	0.0150228	121.837	8.01647	1377.2	0
1.04677	0.0665017	11.8323	0.0151771	133.748	10.9649	1511.84	0
1.14911	0.066087	12.9891	0.0151977	146.824	13.218	1659.64	0
1.26145	0.0644429	14.2589	0.0155807	161.177	14.0616	1821.89	0
1.38477	0.0616609	15.6529	0.0169056	176.935	13.0988	2000	
1.52015	0.0578707	17.1832	0.0201464	194.232	10.4979		
1.66876	0.0532323	18.863	0.026713	213.221	6.9789		
1.8319	0.0479447	20.7071	0.0379978	234.066	3.35591		
2.011	0.0422272	22.7315	0.0560851	256.948	0.811779		
2.2076	0.0363308	24.9538	0.082694	282.068	0.0461709		
2.42342	0.0305053	27.3934	0.119527	309.644	0		
2.66033	0.0250083	30.0714	0.168715	339.916	0		
2.92042	0.0200624	33.0113	0.231894	373.147	0		
3.20592	0.0158589	36.2385	0.311821	409.626	0		
3.51934	0.0125193	39.7813	0.410566	449.672	0		
3.8634	0.0100944	43.6704	0.527055	493.633	0		



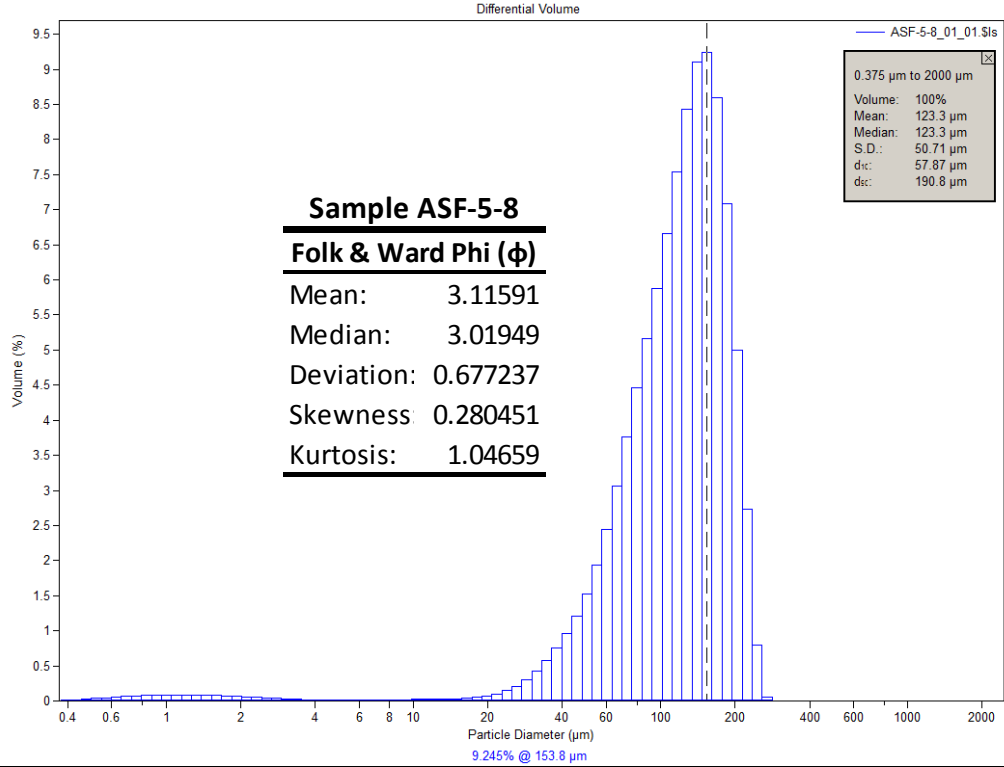
μm	Volume (%)						
0.375198	0.00687064	4.2411	0.013245	47.9397	1.02419	541.892	0
0.411878	0.0131014	4.65572	0.012184	52.6264	1.20552	594.869	0
0.452145	0.022042	5.11087	0.011772	57.7713	1.37717	653.025	0
0.496347	0.0304439	5.61052	0.011853	63.4192	1.52412	716.866	0
0.544872	0.038378	6.15902	0.012292	69.6192	1.63951	786.949	0
0.59814	0.0457334	6.76114	0.012948	76.4253	1.74883	863.883	0
0.656615	0.0524006	7.42212	0.01372	83.8969	1.92794	948.338	0
0.720807	0.0582436	8.14773	0.014507	92.0988	2.31133	1041.05	0
0.791275	0.0631345	8.94427	0.015229	101.103	3.0619	1142.83	0
0.868632	0.0669388	9.81869	0.015849	110.987	4.29942	1254.55	0
0.953552	0.0695323	10.7786	0.016371	121.837	6.01362	1377.2	0
1.04677	0.0708002	11.8323	0.016948	133.748	7.96838	1511.84	0
1.14911	0.0707563	12.9891	0.017771	146.824	9.74607	1659.64	0
1.26145	0.0694517	14.2589	0.019332	161.177	10.8887	1821.89	0
1.38477	0.0669669	15.6529	0.022274	176.935	11.0423	2000	
1.52015	0.0634239	17.1832	0.027775	194.232	10.1425		
1.66876	0.0589755	18.863	0.037729	213.221	8.32446		
1.8319	0.0538166	20.7071	0.05475	234.066	5.96518		
2.011	0.0481659	22.7315	0.082809	256.948	3.54016		
2.2076	0.0422747	24.9538	0.126272	282.068	1.39567		
2.42342	0.0363988	27.3934	0.189629	309.644	0.234743		
2.66033	0.0308004	30.0714	0.276419	339.916	0.007983		
2.92042	0.0257093	33.0113	0.387527	373.147	0		
3.20592	0.0213202	36.2385	0.521878	409.626	0		
3.51934	0.0177572	39.7813	0.67583	449.672	0		
3.8634	0.0150724	43.6704	0.844916	493.633	0		



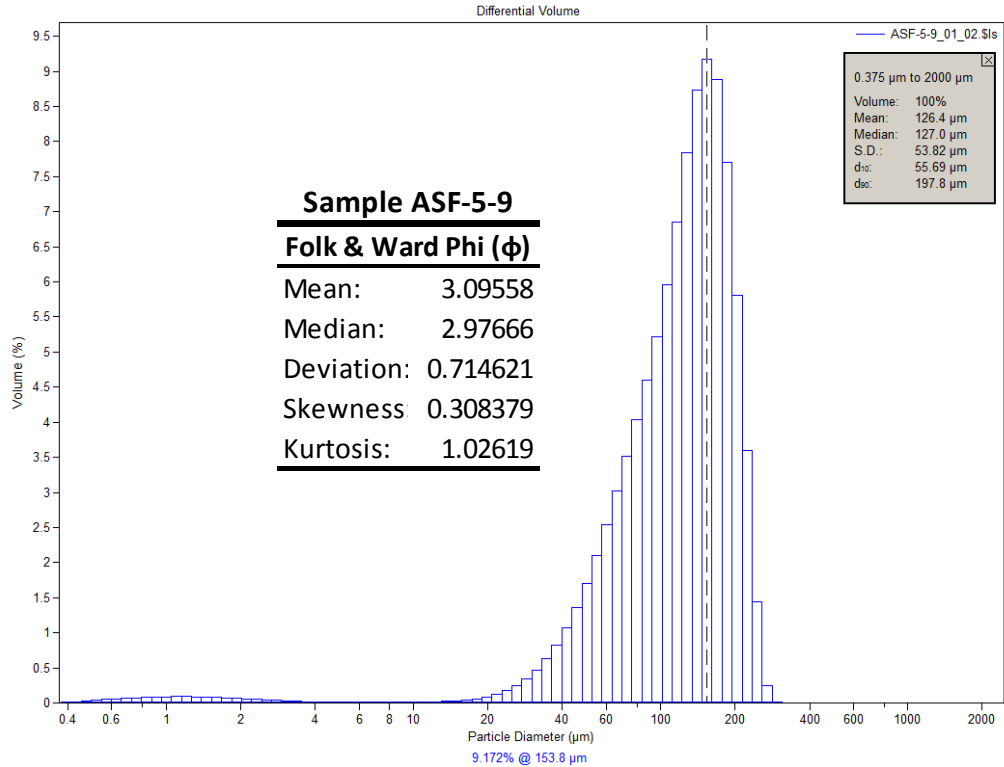
μ m	Volume (%)	μ m	Volume (%)	μ m	Volume (%)	μ m	Volume (%)
0.375198	0.00703793	4.2411	0.009973	47.9397	1.08577	541.892	0
0.411878	0.0134182	4.65572	0.008912	52.6264	1.27357	594.869	0
0.452145	0.0225666	5.11087	0.008528	57.7713	1.43163	653.025	0
0.496347	0.0311511	5.61052	0.008661	63.4192	1.54851	716.866	0
0.544872	0.0392397	6.15902	0.009175	69.6192	1.63569	786.949	0
0.59814	0.046715	6.76114	0.009925	76.4253	1.74721	863.883	0
0.656615	0.0534609	7.42212	0.010808	83.8969	1.98468	948.338	0
0.720807	0.0593349	8.14773	0.011721	92.0988	2.49111	1041.05	0
0.791275	0.0642048	8.94427	0.012579	101.103	3.41232	1142.83	0
0.868632	0.0679307	9.81869	0.013343	110.987	4.82036	1254.55	0
0.953552	0.0703858	10.7786	0.014003	121.837	6.63702	1377.2	0
1.04677	0.0714536	11.8323	0.014684	133.748	8.57137	1511.84	0
1.14911	0.0711557	12.9891	0.01554	146.824	10.1917	1659.64	0
1.26145	0.0695495	14.2589	0.01698	161.177	11.0678	1821.89	0
1.38477	0.0667263	15.6529	0.019547	176.935	10.9091	2000	
1.52015	0.0628191	17.1832	0.024256	194.232	9.72078		
1.66876	0.0579939	18.863	0.03283	213.221	7.70416		
1.8319	0.0524573	20.7071	0.04775	234.066	5.29009		
2.011	0.046441	22.7315	0.072982	256.948	2.9508		
2.2076	0.0402076	24.9538	0.113285	282.068	0.924419		
2.42342	0.0340229	27.3934	0.174071	309.644	0.068229		
2.66033	0.0281563	30.0714	0.260604	339.916	0		
2.92042	0.0228434	33.0113	0.376169	373.147	0		
3.20592	0.0182814	36.2385	0.521876	409.626	0		
3.51934	0.0145949	39.7813	0.694635	449.672	0		
3.8634	0.0118341	43.6704	0.88679	493.633	0		



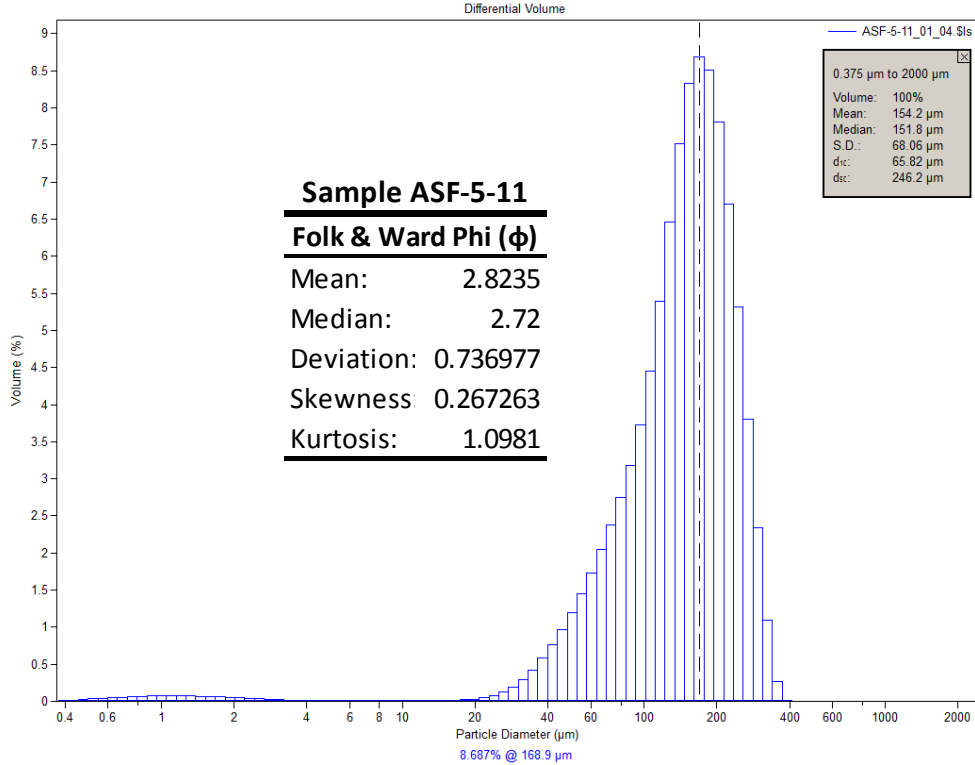
μm	Volume (%)						
0.375198	0.00948726	4.2411	0.014602	47.9397	1.76284	541.892	0
0.411878	0.0180903	4.65572	0.013843	52.6264	2.19653	594.869	0
0.452145	0.0304334	5.11087	0.014027	57.7713	2.76084	653.025	0
0.496347	0.0420304	5.61052	0.014891	63.4192	3.45722	716.866	0
0.544872	0.0529783	6.15902	0.016188	69.6192	4.25909	786.949	0
0.59814	0.0631232	6.76114	0.017723	76.4253	5.11515	863.883	0
0.656615	0.0723144	7.42212	0.01936	83.8969	5.97026	948.338	0
0.720807	0.0803614	8.14773	0.021021	92.0988	6.78697	1041.05	0
0.791275	0.0870862	8.94427	0.022698	101.103	7.53762	1142.83	0
0.868632	0.0922982	9.81869	0.024534	110.987	8.1838	1254.55	0
0.953552	0.0958199	10.7786	0.026932	121.837	8.62539	1377.2	0
1.04677	0.0974821	11.8323	0.030638	133.748	8.68869	1511.84	0
1.14911	0.0972934	12.9891	0.036875	146.824	8.2056	1659.64	0
1.26145	0.0953101	14.2589	0.047356	161.177	7.07141	1821.89	0
1.38477	0.0916308	15.6529	0.06441	176.935	5.40197	2000	
1.52015	0.0864113	17.1832	0.090898	194.232	3.48627		
1.66876	0.0798565	18.863	0.129994	213.221	1.64356		
1.8319	0.0722344	20.7071	0.185034	234.066	0.393984		
2.011	0.0638675	22.7315	0.259188	256.948	0.022433		
2.2076	0.0551319	24.9538	0.355335	282.068	0		
2.42342	0.0464389	27.3934	0.475221	309.644	0		
2.66033	0.0382121	30.0714	0.618753	339.916	0		
2.92042	0.0308472	33.0113	0.784168	373.147	0		
3.20592	0.0246681	36.2385	0.969959	409.626	0		
3.51934	0.0198821	39.7813	1.18123	449.672	0		
3.8634	0.0165531	43.6704	1.43567	493.633	0		



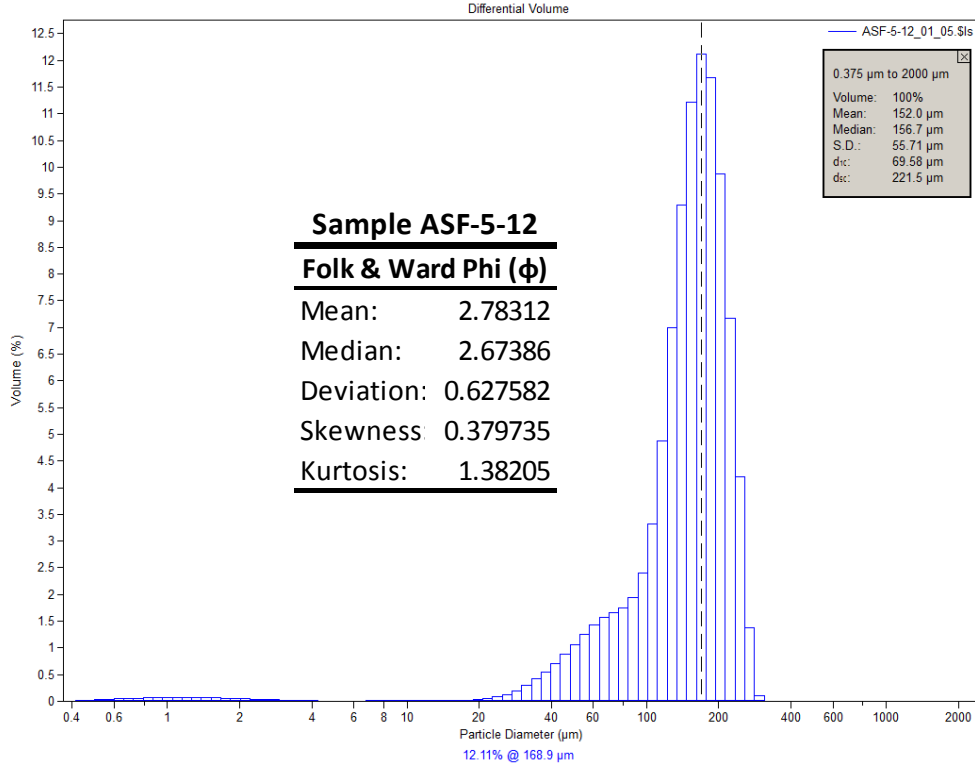
μm	Volume (%)						
0.375198	0.0084825	4.2411	0.013127	47.9397	1.52646	541.892	0
0.411878	0.0161736	4.65572	0.012156	52.6264	1.93318	594.869	0
0.452145	0.027207	5.11087	0.012028	57.7713	2.44912	653.025	0
0.496347	0.0375706	5.61052	0.012528	63.4192	3.0688	716.866	0
0.544872	0.0473509	6.15902	0.013469	69.6192	3.75758	786.949	0
0.59814	0.0564108	6.76114	0.014687	76.4253	4.46727	863.883	0
0.656615	0.0646148	7.42212	0.016079	83.8969	5.16849	948.338	0
0.720807	0.0717951	8.14773	0.017564	92.0988	5.88215	1041.05	0
0.791275	0.077794	8.94427	0.019095	101.103	6.6627	1142.83	0
0.868632	0.0824445	9.81869	0.020688	110.987	7.53732	1254.55	0
0.953552	0.08559	10.7786	0.022456	121.837	8.43141	1377.2	0
1.04677	0.0870855	11.8323	0.024672	133.748	9.1067	1511.84	0
1.14911	0.0869413	12.9891	0.027758	146.824	9.2449	1659.64	0
1.26145	0.0852115	14.2589	0.032416	161.177	8.58938	1821.89	0
1.38477	0.081987	15.6529	0.039695	176.935	7.08366	2000	
1.52015	0.0774067	17.1832	0.051327	194.232	4.99962		
1.66876	0.0716526	18.863	0.069967	213.221	2.73725		
1.8319	0.0649593	20.7071	0.099389	234.066	0.803202		
2.011	0.0576051	22.7315	0.144631	256.948	0.055285		
2.2076	0.0499151	24.9538	0.21105	282.068	0		
2.42342	0.042239	27.3934	0.303289	309.644	0		
2.66033	0.0349395	30.0714	0.423963	339.916	0		
2.92042	0.0283509	33.0113	0.573202	373.147	0		
3.20592	0.0227533	36.2385	0.750643	409.626	0		
3.51934	0.018326	39.7813	0.959195	449.672	0		
3.8634	0.0151354	43.6704	1.21053	493.633	0		



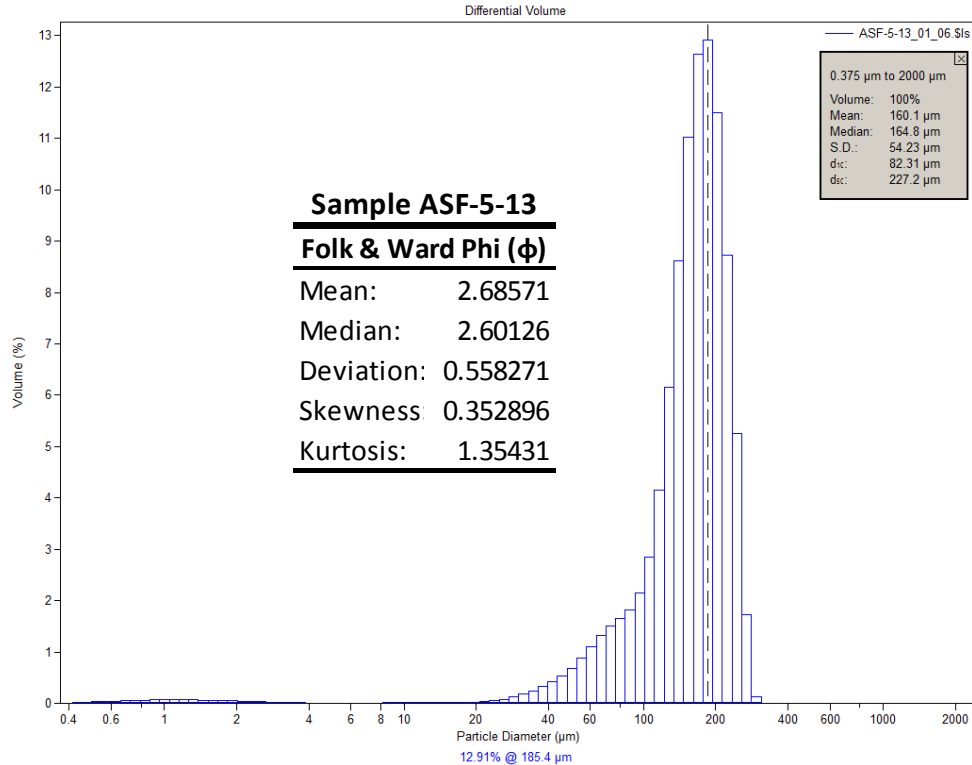
µm	Volume (%)	µm	Volume (%)	µm	Volume (%)	µm	Volume (%)
0.375198	0.00868427	4.2411	0.009923	47.9397	1.69839	541.892	0
0.411878	0.0165642	4.65572	0.008835	52.6264	2.09486	594.869	0
0.452145	0.0278829	5.11087	0.008709	57.7713	2.53881	653.025	0
0.496347	0.0385408	5.61052	0.009305	63.4192	3.01765	716.866	0
0.544872	0.0486322	6.15902	0.010399	69.6192	3.51993	786.949	0
0.59814	0.0580201	6.76114	0.011775	76.4253	4.04301	863.883	0
0.656615	0.0665658	7.42212	0.013261	83.8969	4.59454	948.338	0
0.720807	0.074094	8.14773	0.014696	92.0988	5.21097	1041.05	0
0.791275	0.0804355	8.94427	0.015952	101.103	5.95401	1142.83	0
0.868632	0.0854064	9.81869	0.017009	110.987	6.84948	1254.55	0
0.953552	0.0888303	10.7786	0.018048	121.837	7.84479	1377.2	0
1.04677	0.0905347	11.8323	0.019598	133.748	8.73111	1511.84	0
1.14911	0.0905098	12.9891	0.02256	146.824	9.17182	1659.64	0
1.26145	0.0887889	14.2589	0.028365	161.177	8.88552	1821.89	0
1.38477	0.0854478	15.6529	0.038875	176.935	7.7033	2000	
1.52015	0.0806158	17.1832	0.056359	194.232	5.81009		
1.66876	0.0744726	18.863	0.083216	213.221	3.59102		
1.8319	0.0672604	20.7071	0.121728	234.066	1.43934		
2.011	0.059275	22.7315	0.174787	256.948	0.240627		
2.2076	0.0508683	24.9538	0.24628	282.068	0.008038		
2.42342	0.042425	27.3934	0.341701	309.644	0		
2.66033	0.0343491	30.0714	0.467313	339.916	0		
2.92042	0.0270188	33.0113	0.628069	373.147	0		
3.20592	0.0207577	36.2385	0.827368	409.626	0		
3.51934	0.0157827	39.7813	1.06823	449.672	0		
3.8634	0.0121868	43.6704	1.35638	493.633	0		



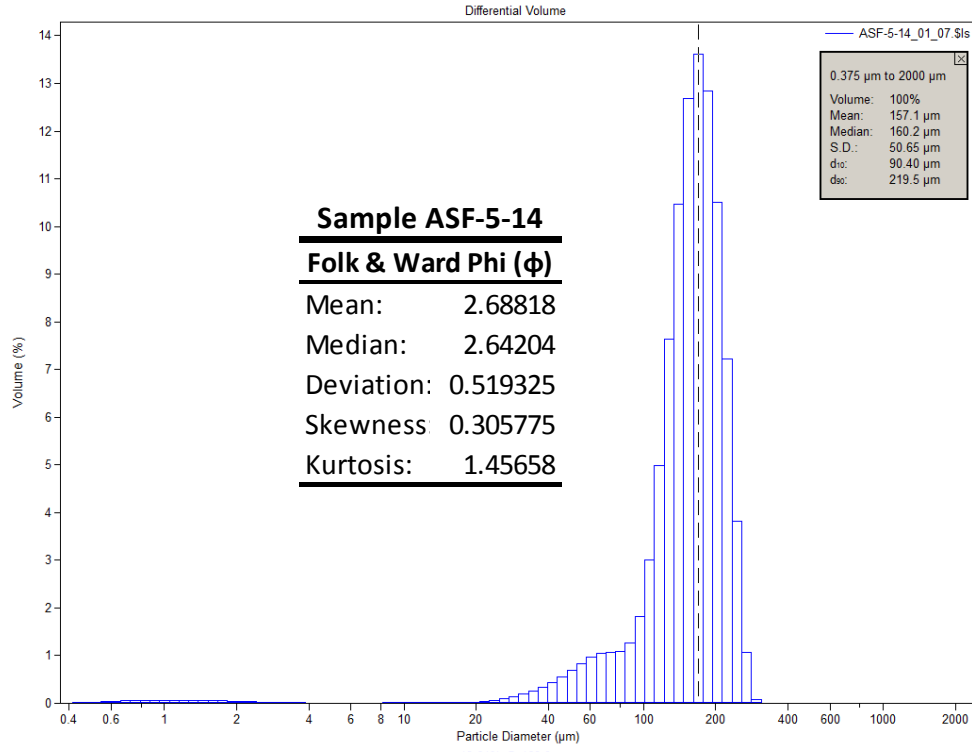
μm	Volume (%)						
0.375198	0.00732624	4.2411	0.008159	47.9397	1.19125	541.892	0
0.411878	0.0139654	4.65572	0.007163	52.6264	1.44498	594.869	0
0.452145	0.0234789	5.11087	0.006892	57.7713	1.72929	653.025	0
0.496347	0.0323947	5.61052	0.007186	63.4192	2.04324	716.866	0
0.544872	0.0407806	6.15902	0.007899	69.6192	2.38305	786.949	0
0.59814	0.0485124	6.76114	0.008894	76.4253	2.75335	863.883	0
0.656615	0.0554681	7.42212	0.010068	83.8969	3.18312	948.338	0
0.720807	0.0614996	8.14773	0.011317	92.0988	3.72918	1041.05	0
0.791275	0.0664682	8.94427	0.012535	101.103	4.45563	1142.83	0
0.868632	0.0702322	9.81869	0.013629	110.987	5.38842	1254.55	0
0.953552	0.0726611	10.7786	0.014531	121.837	6.4645	1377.2	0
1.04677	0.073637	11.8323	0.015257	133.748	7.51986	1511.84	0
1.14911	0.0731861	12.9891	0.015902	146.824	8.32726	1659.64	0
1.26145	0.0713701	14.2589	0.0168	161.177	8.6874	1821.89	0
1.38477	0.0682876	15.6529	0.018567	176.935	8.51053	2000	
1.52015	0.064076	17.1832	0.022428	194.232	7.81375		
1.66876	0.0589086	18.863	0.030516	213.221	6.70378		
1.8319	0.0529981	20.7071	0.046176	234.066	5.31435		
2.011	0.0465881	22.7315	0.074379	256.948	3.79704		
2.2076	0.0399527	24.9538	0.121044	282.068	2.34251		
2.42342	0.0333759	27.3934	0.192031	309.644	1.09383		
2.66033	0.0271452	30.0714	0.291703	339.916	0.266334		
2.92042	0.0215188	33.0113	0.421257	373.147	0.015413		
3.20592	0.0167114	36.2385	0.578843	409.626	0		
3.51934	0.0128607	39.7813	0.760788	449.672	0		
3.8634	0.0100218	43.6704	0.964545	493.633	0		



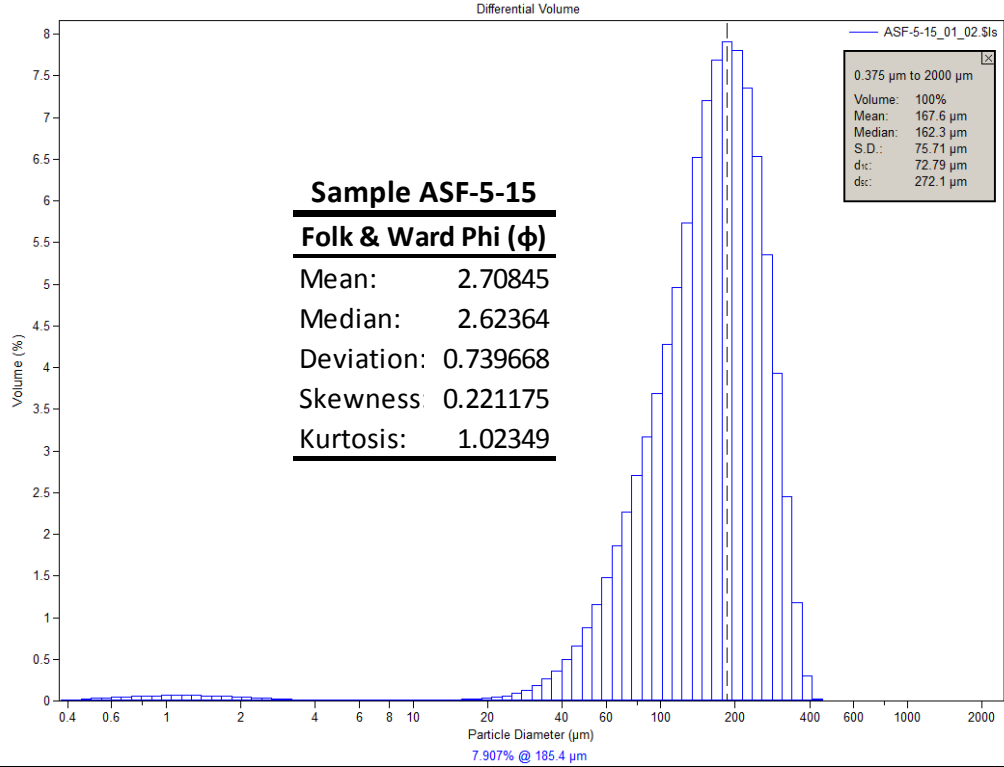
μm	Volume (%)						
0.375198	0.00710392	4.2411	0.00825	47.9397	1.06638	541.892	0
0.411878	0.0135434	4.65572	0.007266	52.6264	1.251	594.869	0
0.452145	0.0227765	5.11087	0.00702	57.7713	1.42357	653.025	0
0.496347	0.0314389	5.61052	0.007348	63.4192	1.56452	716.866	0
0.544872	0.0395994	6.15902	0.008115	69.6192	1.66549	786.949	0
0.59814	0.0471383	6.76114	0.009165	76.4253	1.75649	863.883	0
0.656615	0.0539384	7.42212	0.010382	83.8969	1.9427	948.338	0
0.720807	0.0598547	8.14773	0.011632	92.0988	2.39904	1041.05	0
0.791275	0.0647531	8.94427	0.012778	101.103	3.32887	1142.83	0
0.868632	0.0684904	9.81869	0.013705	110.987	4.88443	1254.55	0
0.953552	0.0709376	10.7786	0.014323	121.837	6.99352	1377.2	0
1.04677	0.0719745	11.8323	0.014705	133.748	9.29781	1511.84	0
1.14911	0.0716198	12.9891	0.015003	146.824	11.2134	1659.64	0
1.26145	0.0699302	14.2589	0.015787	161.177	12.1117	1821.89	0
1.38477	0.066995	15.6529	0.017875	176.935	11.6705	2000	
1.52015	0.0629464	17.1832	0.022776	194.232	9.8708		
1.66876	0.0579497	18.863	0.032908	213.221	7.16404		
1.8319	0.0522139	20.7071	0.051489	234.066	4.20129		
2.011	0.0459746	22.7315	0.083081	256.948	1.37887		
2.2076	0.0395025	24.9538	0.132238	282.068	0.110545		
2.42342	0.0330732	27.3934	0.202928	309.644	3.58E-05		
2.66033	0.0269715	30.0714	0.297608	339.916	0		
2.92042	0.021447	33.0113	0.415812	373.147	0		
3.20592	0.0167148	36.2385	0.555419	409.626	0		
3.51934	0.0129114	39.7813	0.71289	449.672	0		
3.8634	0.0100979	43.6704	0.884566	493.633	0		



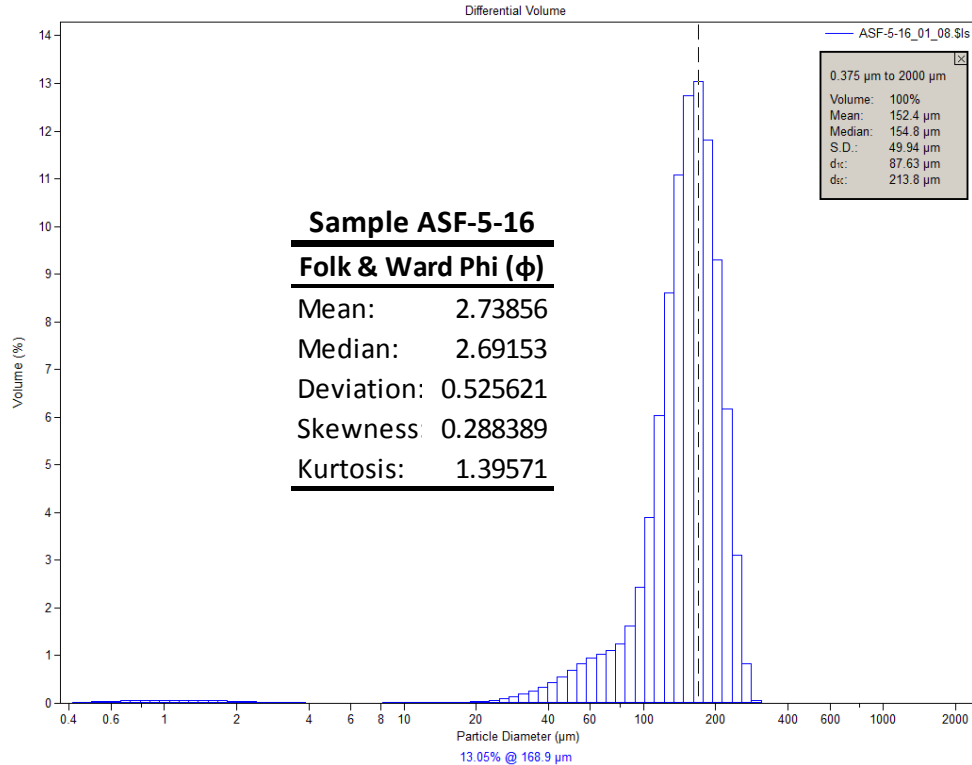
μm	Volume (%)						
0.375198	0.00692541	4.2411	0.005916	47.9397	0.686385	541.892	0
0.411878	0.0131959	4.65572	0.005288	52.6264	0.875465	594.869	0
0.452145	0.0221667	5.11087	0.005325	57.7713	1.09467	653.025	0
0.496347	0.030546	5.61052	0.005864	63.4192	1.31662	716.866	0
0.544872	0.0383897	6.15902	0.006769	69.6192	1.50715	786.949	0
0.59814	0.0455727	6.76114	0.007885	76.4253	1.65288	863.883	0
0.656615	0.0519739	7.42212	0.009089	83.8969	1.81405	948.338	0
0.720807	0.0574495	8.14773	0.010248	92.0988	2.14073	1041.05	0
0.791275	0.0618684	8.94427	0.01123	101.103	2.84701	1142.83	0
0.868632	0.0650983	9.81869	0.011935	110.987	4.16066	1254.55	0
0.953552	0.0670231	10.7786	0.012284	121.837	6.15166	1377.2	0
1.04677	0.067545	11.8323	0.012336	133.748	8.61137	1511.84	0
1.14911	0.0667057	12.9891	0.012185	146.824	11.0212	1659.64	0
1.26145	0.0645872	14.2589	0.012263	161.177	12.6453	1821.89	0
1.38477	0.0613037	15.6529	0.013108	176.935	12.9116	2000	
1.52015	0.0570093	17.1832	0.015761	194.232	11.5078		
1.66876	0.0518869	18.863	0.021794	213.221	8.72052		
1.8319	0.0461566	20.7071	0.033156	234.066	5.25975		
2.011	0.0400567	22.7315	0.052595	256.948	1.72788		
2.2076	0.0338502	24.9538	0.082334	282.068	0.130296		
2.42342	0.027796	27.3934	0.123995	309.644	0		
2.66033	0.0221539	30.0714	0.178166	339.916	0		
2.92042	0.017142	33.0113	0.244333	373.147	0		
3.20592	0.0129432	36.2385	0.323203	409.626	0		
3.51934	0.00966269	39.7813	0.417855	449.672	0		
3.8634	0.0073351	43.6704	0.535736	493.633	0		



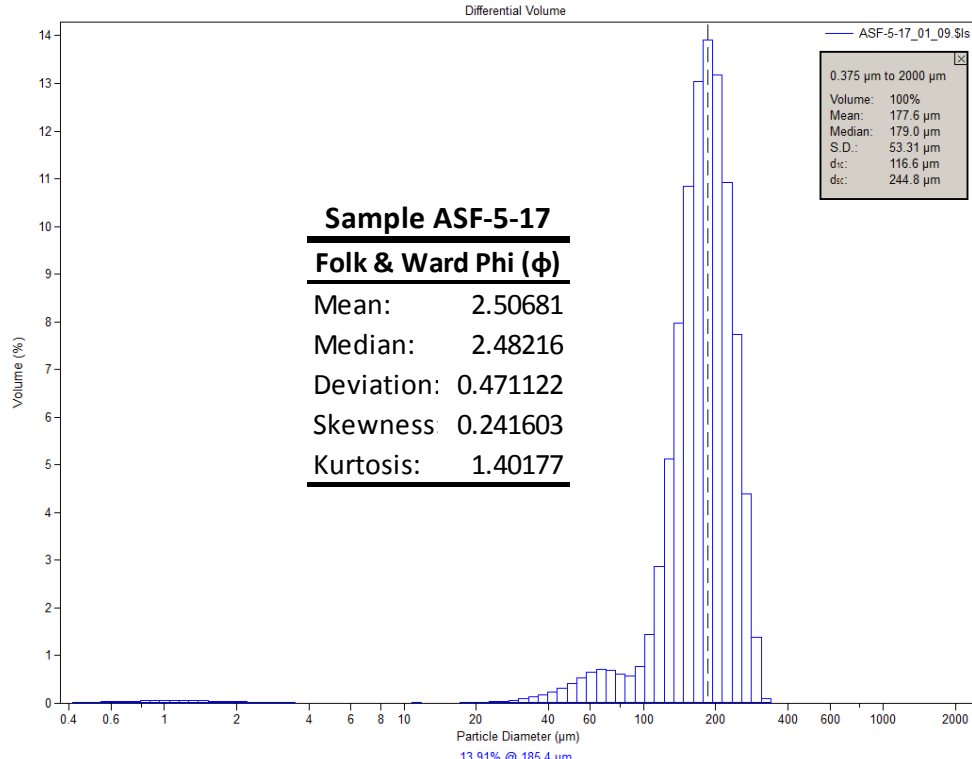
μm	Volume (%)						
0.375198	0.00669758	4.2411	0.006082	47.9397	0.686647	541.892	0
0.411878	0.0127635	4.65572	0.005383	52.6264	0.831662	594.869	0
0.452145	0.0214465	5.11087	0.005347	57.7713	0.960446	653.025	0
0.496347	0.0295658	5.61052	0.005815	63.4192	1.0416	716.866	0
0.544872	0.0371783	6.15902	0.006651	69.6192	1.06587	786.949	0
0.59814	0.0441647	6.76114	0.007702	76.4253	1.08996	863.883	0
0.656615	0.0504096	7.42212	0.008835	83.8969	1.26292	948.338	0
0.720807	0.0557741	8.14773	0.009912	92.0988	1.81072	1041.05	0
0.791275	0.060132	8.94427	0.010785	101.103	2.99894	1142.83	0
0.868632	0.0633533	9.81869	0.011347	110.987	4.9912	1254.55	0
0.953552	0.0653228	10.7786	0.011513	121.837	7.64582	1377.2	0
1.04677	0.0659419	11.8323	0.011386	133.748	10.4647	1511.84	0
1.14911	0.0652453	12.9891	0.011134	146.824	12.6903	1659.64	0
1.26145	0.0633062	14.2589	0.011356	161.177	13.6071	1821.89	0
1.38477	0.0602283	15.6529	0.012794	176.935	12.8414	2000	
1.52015	0.056155	17.1832	0.016685	194.232	10.5013		
1.66876	0.051258	18.863	0.02486	213.221	7.2276		
1.8319	0.0457461	20.7071	0.039213	234.066	3.8109		
2.011	0.0398467	22.7315	0.062128	256.948	1.07698		
2.2076	0.0338148	24.9538	0.095154	282.068	0.072133		
2.42342	0.0279008	27.3934	0.139091	309.644	0		
2.66033	0.0223601	30.0714	0.194357	339.916	0		
2.92042	0.0174085	33.0113	0.260775	373.147	0		
3.20592	0.0132298	36.2385	0.340108	409.626	0		
3.51934	0.00993398	39.7813	0.435623	449.672	0		
3.8634	0.00756249	43.6704	0.551029	493.633	0		



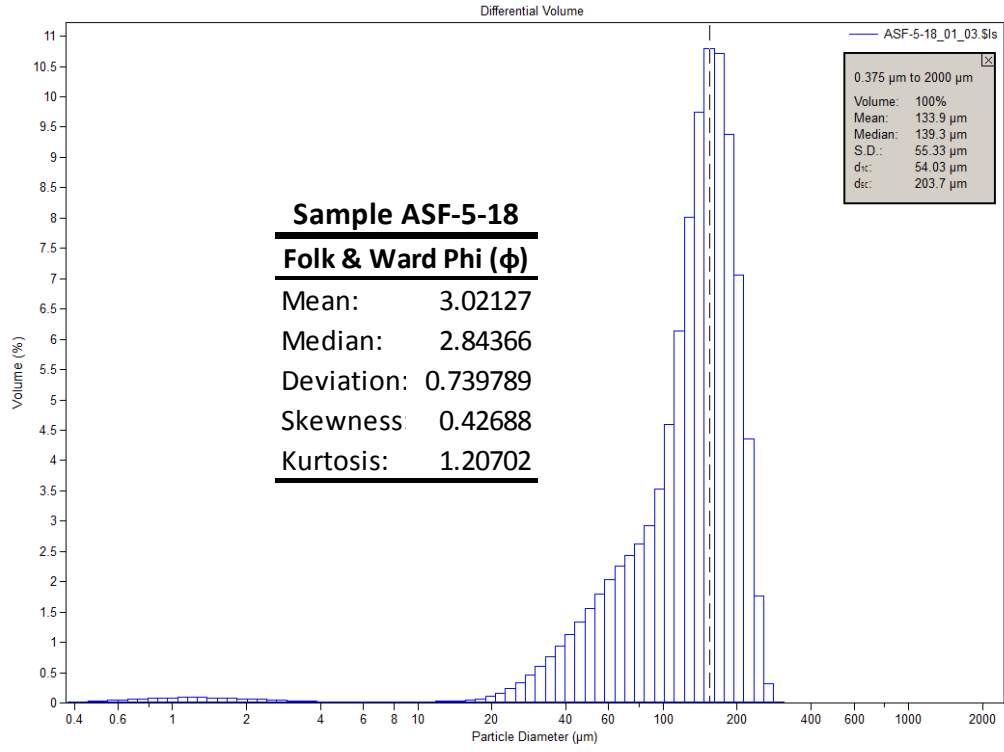
μm	Volume (%)						
0.375198	0.00662651	4.2411	0.008628	47.9397	0.881108	541.892	0
0.411878	0.0126296	4.65572	0.007563	52.6264	1.15221	594.869	0
0.452145	0.0212267	5.11087	0.007113	57.7713	1.47955	653.025	0
0.496347	0.0292747	5.61052	0.007143	63.4192	1.85694	716.866	0
0.544872	0.0368336	6.15902	0.007527	69.6192	2.27111	786.949	0
0.59814	0.0437902	6.76114	0.008144	76.4253	2.70984	863.883	0
0.656615	0.0500346	7.42212	0.008905	83.8969	3.17383	948.338	0
0.720807	0.0554351	8.14773	0.009729	92.0988	3.68419	1041.05	0
0.791275	0.0598703	8.94427	0.010552	101.103	4.2738	1142.83	0
0.868632	0.0632173	9.81869	0.011346	110.987	4.96349	1254.55	0
0.953552	0.0653661	10.7786	0.012139	121.837	5.73504	1377.2	0
1.04677	0.0662192	11.8323	0.013051	133.748	6.5166	1511.84	0
1.14911	0.0658091	12.9891	0.014282	146.824	7.2025	1659.64	0
1.26145	0.0641995	14.2589	0.016172	161.177	7.6901	1821.89	0
1.38477	0.0614851	15.6529	0.019192	176.935	7.9068	2000	
1.52015	0.0577939	17.1832	0.024056	194.232	7.80945		
1.66876	0.053282	18.863	0.031815	213.221	7.35774		
1.8319	0.0481366	20.7071	0.043937	234.066	6.5315		
2.011	0.0425684	22.7315	0.062535	256.948	5.35414		
2.2076	0.0368092	24.9538	0.090248	282.068	3.92613		
2.42342	0.0310976	27.3934	0.130267	309.644	2.45675		
2.66033	0.0256722	30.0714	0.186231	339.916	1.1742		
2.92042	0.0207465	33.0113	0.262145	373.147	0.302044		
3.20592	0.0164978	36.2385	0.362844	409.626	0.018801		
3.51934	0.0130416	39.7813	0.494305	449.672	0		
3.8634	0.0104263	43.6704	0.664171	493.633	0		



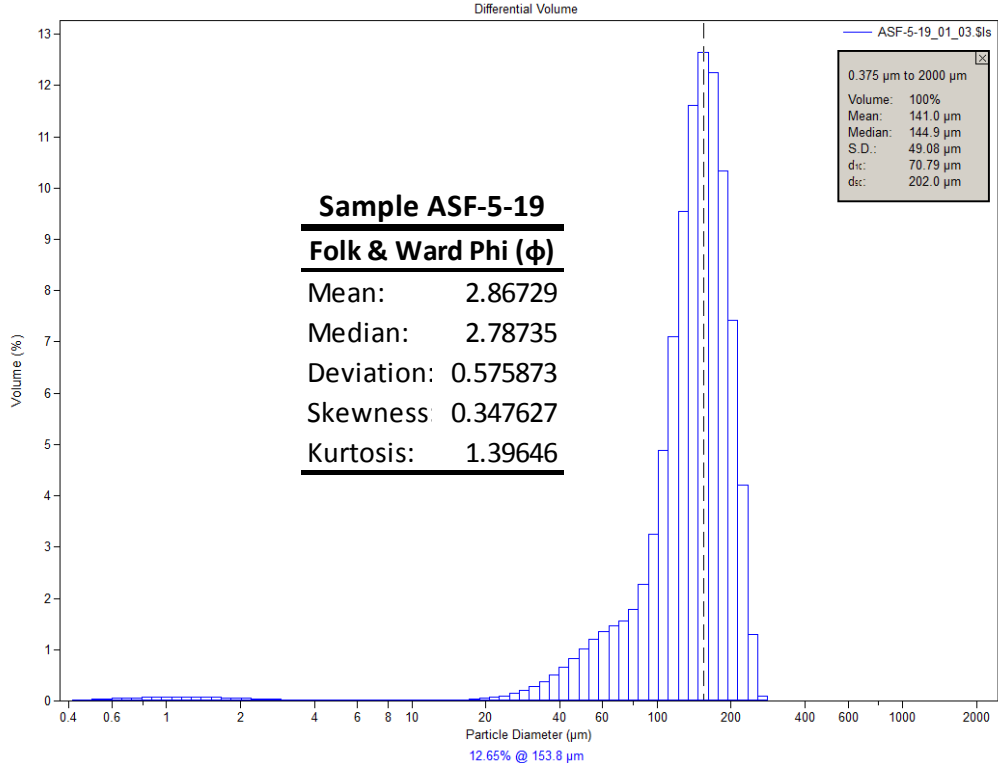
μm	Volume (%)						
0.375198	0.00696224	4.2411	0.006744	47.9397	0.689283	541.892	0
0.411878	0.0132687	4.65572	0.006022	52.6264	0.82827	594.869	0
0.452145	0.0222972	5.11087	0.005973	57.7713	0.949614	653.025	0
0.496347	0.0307423	5.61052	0.006432	63.4192	1.03781	716.866	0
0.544872	0.0386635	6.15902	0.007252	69.6192	1.11054	786.949	0
0.59814	0.0459374	6.76114	0.008278	76.4253	1.25113	863.883	0
0.656615	0.0524437	7.42212	0.009381	83.8969	1.61974	948.338	0
0.720807	0.058039	8.14773	0.010429	92.0988	2.43113	1041.05	0
0.791275	0.0625898	8.94427	0.011299	101.103	3.88821	1142.83	0
0.868632	0.0659615	9.81869	0.011919	110.987	6.0328	1254.55	0
0.953552	0.0680327	10.7786	0.01226	121.837	8.60986	1377.2	0
1.04677	0.0686994	11.8323	0.012481	133.748	11.077	1511.84	0
1.14911	0.0679965	12.9891	0.01282	146.824	12.7393	1659.64	0
1.26145	0.0659987	14.2589	0.01386	161.177	13.0467	1821.89	0
1.38477	0.062814	15.6529	0.016328	176.935	11.814	2000	
1.52015	0.0585916	17.1832	0.021298	194.232	9.30118		
1.66876	0.0535102	18.863	0.030287	213.221	6.16842		
1.8319	0.0477884	20.7071	0.044803	234.066	3.11396		
2.011	0.0416651	22.7315	0.066775	256.948	0.840506		
2.2076	0.035406	24.9538	0.097682	282.068	0.054242		
2.42342	0.029275	27.3934	0.138719	309.644	0		
2.66033	0.0235364	30.0714	0.191223	339.916	0		
2.92042	0.0184164	33.0113	0.256336	373.147	0		
3.20592	0.0141021	36.2385	0.336682	409.626	0		
3.51934	0.0107064	39.7813	0.435394	449.672	0		
3.8634	0.00826667	43.6704	0.554006	493.633	0		



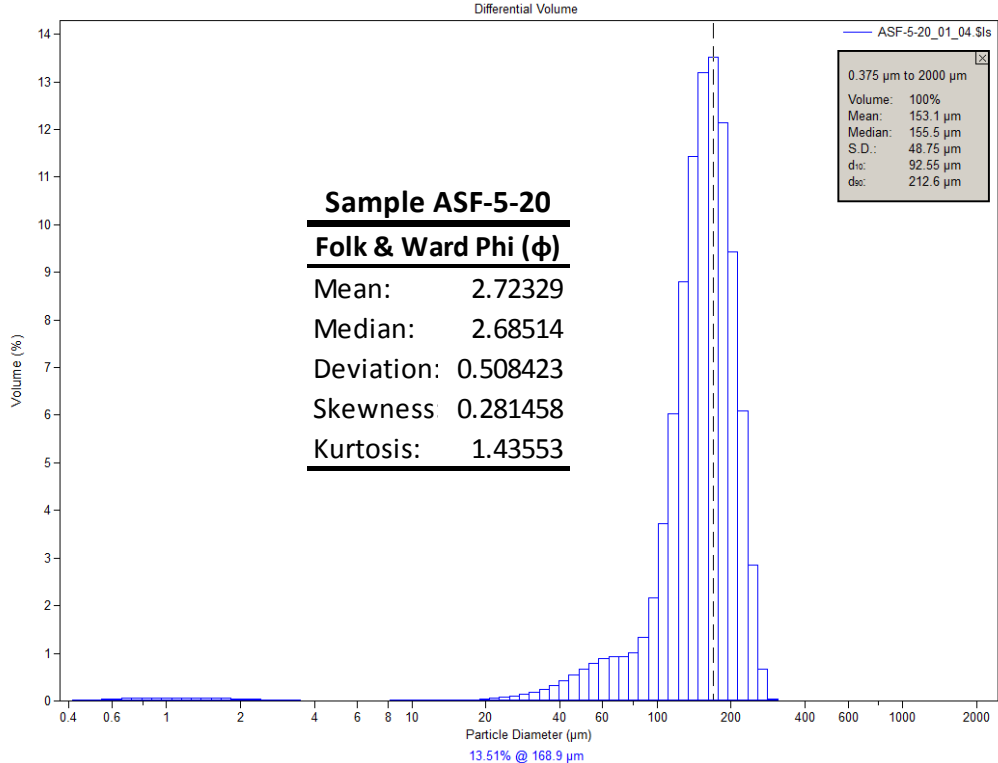
μm	Volume (%)						
0.375198	0.00590346	4.2411	0.005135	47.9397	0.415979	541.892	0
0.411878	0.0112484	4.65572	0.00457	52.6264	0.535851	594.869	0
0.452145	0.0188922	5.11087	0.004576	57.7713	0.645852	653.025	0
0.496347	0.0260278	5.61052	0.005016	63.4192	0.707234	716.866	0
0.544872	0.0327017	6.15902	0.005775	69.6192	0.688407	786.949	0
0.59814	0.0388062	6.76114	0.006715	76.4253	0.610803	863.883	0
0.656615	0.0442376	7.42212	0.007718	83.8969	0.577787	948.338	0
0.720807	0.0488734	8.14773	0.008657	92.0988	0.768212	1041.05	0
0.791275	0.0526024	8.94427	0.0094	101.103	1.43926	1142.83	0
0.868632	0.0553136	9.81869	0.009851	110.987	2.85936	1254.55	0
0.953552	0.0569099	10.7786	0.009929	121.837	5.11563	1377.2	0
1.04677	0.0573117	11.8323	0.009707	133.748	7.96438	1511.84	0
1.14911	0.0565583	12.9891	0.009269	146.824	10.8441	1659.64	0
1.26145	0.0547248	14.2589	0.009017	161.177	13.0459	1821.89	0
1.38477	0.0519113	15.6529	0.009344	176.935	13.913	2000	
1.52015	0.0482538	17.1832	0.01095	194.232	13.1714		
1.66876	0.0439092	18.863	0.014772	213.221	10.9263		
1.8319	0.0390674	20.7071	0.021597	234.066	7.742		
2.011	0.033927	22.7315	0.032617	256.948	4.39692		
2.2076	0.0287095	24.9538	0.048321	282.068	1.38897		
2.42342	0.0236263	27.3934	0.069083	309.644	0.102901		
2.66033	0.0188907	30.0714	0.095566	339.916	0		
2.92042	0.0146786	33.0113	0.128716	373.147	0		
3.20592	0.0111383	36.2385	0.172149	409.626	0		
3.51934	0.00835754	39.7813	0.231012	449.672	0		
3.8634	0.00636524	43.6704	0.311315	493.633	0		



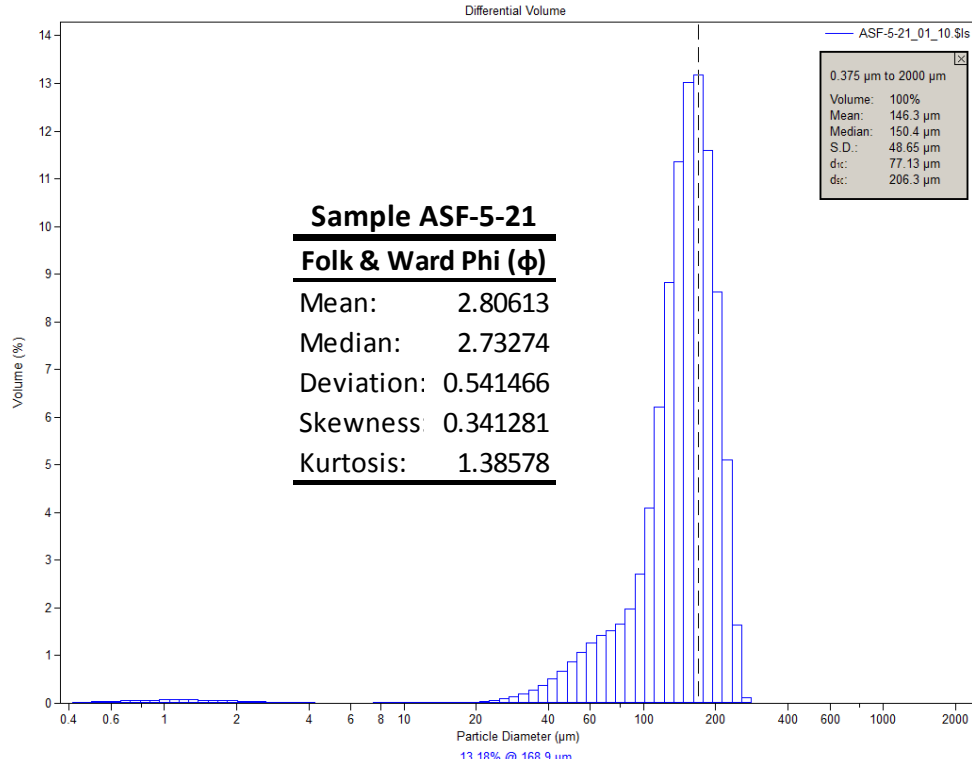
μm	Volume (%)						
0.375198	0.00807545	4.2411	0.018166	47.9397	1.56307	541.892	0
0.411878	0.0154131	4.65572	0.017089	52.6264	1.80242	594.869	0
0.452145	0.0259817	5.11087	0.016968	57.7713	2.0395	653.025	0
0.496347	0.0359867	5.61052	0.017551	63.4192	2.25066	716.866	0
0.544872	0.0455321	6.15902	0.018596	69.6192	2.42856	786.949	0
0.59814	0.0545036	6.76114	0.019849	76.4253	2.61861	863.883	0
0.656615	0.0627837	7.42212	0.021103	83.8969	2.93205	948.338	0
0.720807	0.0702149	8.14773	0.022146	92.0988	3.53547	1041.05	0
0.791275	0.0766425	8.94427	0.022837	101.103	4.59244	1142.83	0
0.868632	0.0818901	9.81869	0.023176	110.987	6.14052	1254.55	0
0.953552	0.0857845	10.7786	0.02343	121.837	8.00567	1377.2	0
1.04677	0.0881466	11.8323	0.024357	133.748	9.75054	1511.84	0
1.14911	0.0889386	12.9891	0.027179	146.824	10.7937	1659.64	0
1.26145	0.0881612	14.2589	0.033947	161.177	10.7202	1821.89	0
1.38477	0.0858521	15.6529	0.047357	176.935	9.37324	2000	
1.52015	0.0821024	17.1832	0.070857	194.232	7.06494		
1.66876	0.0770525	18.863	0.108267	213.221	4.35191		
1.8319	0.0709068	20.7071	0.162813	234.066	1.76772		
2.011	0.0639237	22.7315	0.237529	256.948	0.311407		
2.2076	0.0564265	24.9538	0.334301	282.068	0.011534		
2.42342	0.0487717	27.3934	0.454153	309.644	0		
2.66033	0.0413474	30.0714	0.596836	339.916	0		
2.92042	0.0345199	33.0113	0.759368	373.147	0		
3.20592	0.0286161	36.2385	0.938114	409.626	0		
3.51934	0.0238645	39.7813	1.1304	449.672	0		
3.8634	0.0203836	43.6704	1.33763	493.633	0		



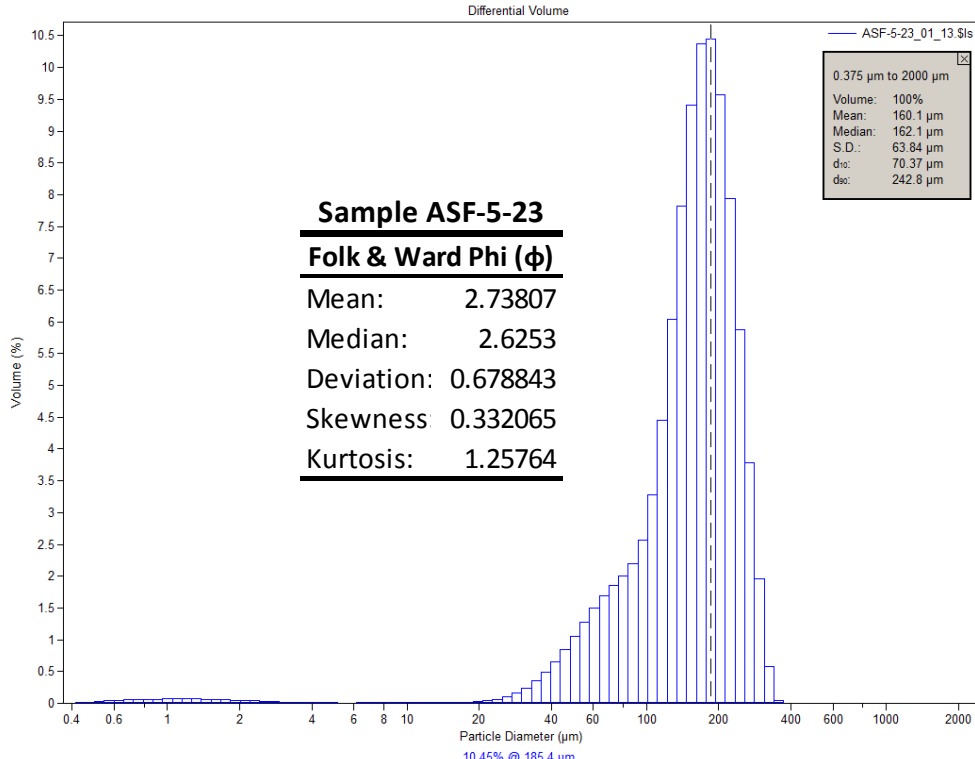
μm	Volume (%)						
0.375198	0.00748994	4.2411	0.011846	47.9397	1.01927	541.892	0
0.411878	0.0142786	4.65572	0.010958	52.6264	1.20051	594.869	0
0.452145	0.0240092	5.11087	0.01077	57.7713	1.34979	653.025	0
0.496347	0.0331334	5.61052	0.011102	63.4192	1.4594	716.866	0
0.544872	0.0417226	6.15902	0.011789	69.6192	1.5658	786.949	0
0.59814	0.0496504	6.76114	0.012665	76.4253	1.77875	863.883	0
0.656615	0.0567931	7.42212	0.013603	83.8969	2.27423	948.338	0
0.720807	0.0629998	8.14773	0.014488	92.0988	3.25897	1041.05	0
0.791275	0.0681308	8.94427	0.015235	101.103	4.88661	1142.83	0
0.868632	0.0720387	9.81869	0.015848	110.987	7.09718	1254.55	0
0.953552	0.0745927	10.7786	0.016413	121.837	9.54217	1377.2	0
1.04677	0.0756739	11.8323	0.01725	133.748	11.6178	1511.84	0
1.14911	0.0753086	12.9891	0.018788	146.824	12.654	1659.64	0
1.26145	0.0735635	14.2589	0.021791	161.177	12.2414	1821.89	0
1.38477	0.0705402	15.6529	0.027203	176.935	10.3339	2000	
1.52015	0.0663841	17.1832	0.03626	194.232	7.41677		
1.66876	0.0612745	18.863	0.050634	213.221	4.20451		
1.8319	0.0554336	20.7071	0.072054	234.066	1.30247		
2.011	0.0491101	22.7315	0.102926	256.948	0.094249		
2.2076	0.0425836	24.9538	0.145814	282.068	0		
2.42342	0.0361378	27.3934	0.203641	309.644	0		
2.66033	0.0300589	30.0714	0.280084	339.916	0		
2.92042	0.0245968	33.0113	0.378528	373.147	0		
3.20592	0.0199578	36.2385	0.50269	409.626	0		
3.51934	0.0162702	39.7813	0.654327	449.672	0		
3.8634	0.0135784	43.6704	0.830116	493.633	0		



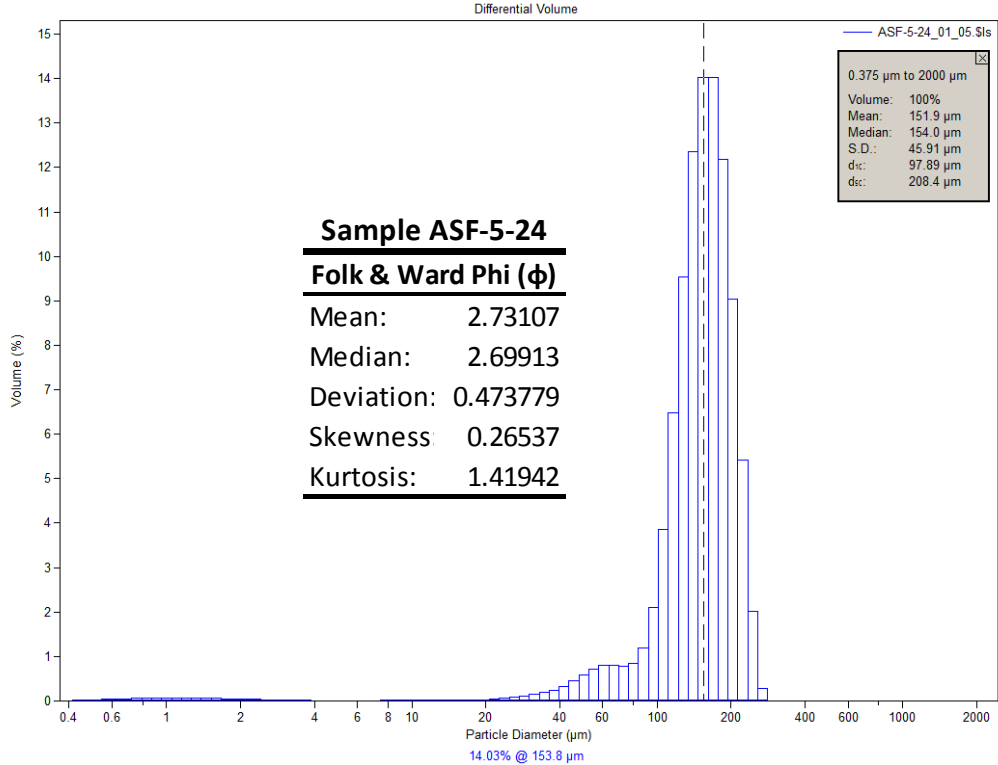
μm	Volume (%)						
0.375198	0.00686695	4.2411	0.006635	47.9397	0.668042	541.892	0
0.411878	0.0130842	4.65572	0.006104	52.6264	0.793619	594.869	0
0.452145	0.0219769	5.11087	0.006209	57.7713	0.884476	653.025	0
0.496347	0.03028	5.61052	0.006783	63.4192	0.922232	716.866	0
0.544872	0.0380481	6.15902	0.007682	69.6192	0.930369	786.949	0
0.59814	0.0451562	6.76114	0.008749	76.4253	1.01018	863.883	0
0.656615	0.0514838	7.42212	0.009857	83.8969	1.34283	948.338	0
0.720807	0.056888	8.14773	0.010884	92.0988	2.16751	1041.05	0
0.791275	0.0612391	8.94427	0.011721	101.103	3.71506	1142.83	0
0.868632	0.0644063	9.81869	0.012334	110.987	6.02178	1254.55	0
0.953552	0.0662763	10.7786	0.012742	121.837	8.79495	1377.2	0
1.04677	0.066754	11.8323	0.013185	133.748	11.4414	1511.84	0
1.14911	0.0658844	12.9891	0.013974	146.824	13.2026	1659.64	0
1.26145	0.063753	14.2589	0.015759	161.177	13.508	1821.89	0
1.38477	0.060476	15.6529	0.019299	176.935	12.1509	2000	
1.52015	0.0562112	17.1832	0.025589	194.232	9.43853		
1.66876	0.0511437	18.863	0.035922	213.221	6.09767		
1.8319	0.0454953	20.7071	0.051345	234.066	2.8564		
2.011	0.039504	22.7315	0.073187	256.948	0.675783		
2.2076	0.0334318	24.9538	0.102363	282.068	0.037787		
2.42342	0.0275341	27.3934	0.139812	309.644	0		
2.66033	0.0220641	30.0714	0.187278	339.916	0		
2.92042	0.0172338	33.0113	0.246964	373.147	0		
3.20592	0.0132151	36.2385	0.322963	409.626	0		
3.51934	0.0101057	39.7813	0.419367	449.672	0		
3.8634	0.00792824	43.6704	0.536691	493.633	0		



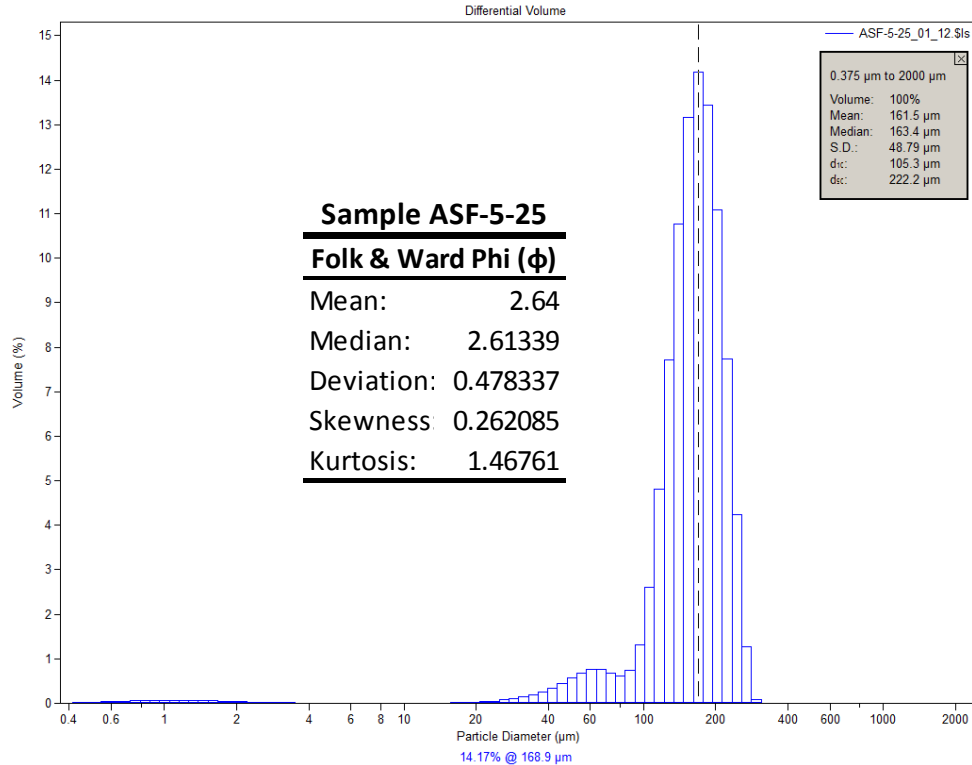
μm	Volume (%)						
0.375198	0.0070574	4.2411	0.008283	47.9397	0.861879	541.892	0
0.411878	0.013454	4.65572	0.007252	52.6264	1.06913	594.869	0
0.452145	0.0226237	5.11087	0.006951	57.7713	1.26441	653.025	0
0.496347	0.0312232	5.61052	0.007212	63.4192	1.41837	716.866	0
0.544872	0.0393202	6.15902	0.007893	69.6192	1.52756	786.949	0
0.59814	0.0467953	6.76114	0.008831	76.4253	1.6627	863.883	0
0.656615	0.0535324	7.42212	0.009894	83.8969	1.98278	948.338	0
0.720807	0.0593875	8.14773	0.010944	92.0988	2.71575	1041.05	0
0.791275	0.0642285	8.94427	0.011838	101.103	4.10214	1142.83	0
0.868632	0.0679161	9.81869	0.012484	110.987	6.21766	1254.55	0
0.953552	0.0703226	10.7786	0.012814	121.837	8.83166	1377.2	0
1.04677	0.0713335	11.8323	0.012952	133.748	11.3639	1511.84	0
1.14911	0.0709701	12.9891	0.013059	146.824	13.0166	1659.64	0
1.26145	0.0692904	14.2589	0.013663	161.177	13.1813	1821.89	0
1.38477	0.0663862	15.6529	0.015389	176.935	11.5904	2000	
1.52015	0.0623892	17.1832	0.019272	194.232	8.63419		
1.66876	0.0574636	18.863	0.0269	213.221	5.09586		
1.8319	0.0518153	20.7071	0.039991	234.066	1.63905		
2.011	0.0456738	22.7315	0.06116	256.948	0.121764		
2.2076	0.039303	24.9538	0.092845	282.068	0		
2.42342	0.0329697	27.3934	0.1375	309.644	0		
2.66033	0.02695	30.0714	0.198086	339.916	0		
2.92042	0.0214862	33.0113	0.277172	373.147	0		
3.20592	0.0167885	36.2385	0.379201	409.626	0		
3.51934	0.0129933	39.7813	0.509107	449.672	0		
3.8634	0.0101636	43.6704	0.670373	493.633	0		



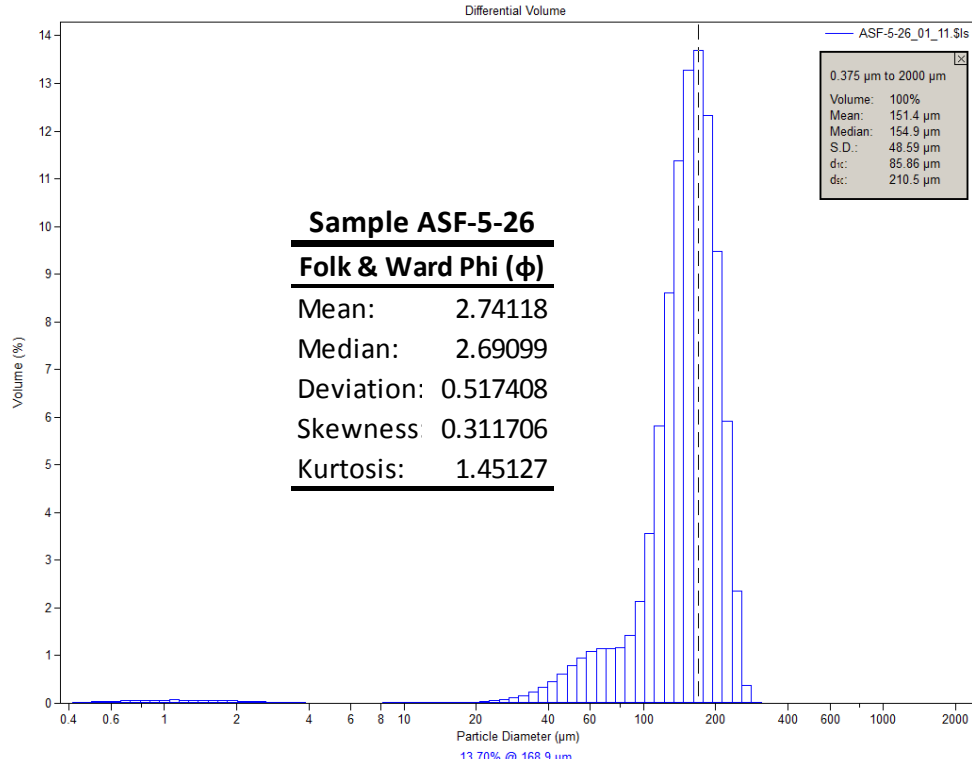
μm	Volume (%)						
0.375198	0.006872	4.2411	0.008522	47.9397	1.05671	541.892	0
0.411878	0.0131027	4.65572	0.007464	52.6264	1.27968	594.869	0
0.452145	0.0220395	5.11087	0.007097	57.7713	1.49888	653.025	0
0.496347	0.0304302	5.61052	0.007266	63.4192	1.69471	716.866	0
0.544872	0.0383425	6.15902	0.007835	69.6192	1.85439	786.949	0
0.59814	0.0456624	6.76114	0.008666	76.4253	1.996	863.883	0
0.656615	0.0522769	7.42212	0.009655	83.8969	2.19201	948.338	0
0.720807	0.0580463	8.14773	0.0107	92.0988	2.57021	1041.05	0
0.791275	0.0628396	8.94427	0.011705	101.103	3.28507	1142.83	0
0.868632	0.0665184	9.81869	0.012602	110.987	4.44892	1254.55	0
0.953552	0.0689546	10.7786	0.013343	121.837	6.03625	1377.2	0
1.04677	0.0700308	11.8323	0.013991	133.748	7.82244	1511.84	0
1.14911	0.0697611	12.9891	0.014623	146.824	9.41004	1659.64	0
1.26145	0.0681974	14.2589	0.015564	161.177	10.38	1821.89	0
1.38477	0.0654234	15.6529	0.017273	176.935	10.4504	2000	
1.52015	0.0615639	17.1832	0.020722	194.232	9.5727		
1.66876	0.0567784	18.863	0.027588	213.221	7.94514		
1.8319	0.0512676	20.7071	0.040349	234.066	5.88266		
2.011	0.0452593	22.7315	0.063002	256.948	3.77976		
2.2076	0.0390145	24.9538	0.100303	282.068	1.96206		
2.42342	0.0328005	27.3934	0.157516	309.644	0.575996		
2.66033	0.0268913	30.0714	0.239513	339.916	0.040689		
2.92042	0.0215281	33.0113	0.349156	373.147	0		
3.20592	0.0169164	36.2385	0.487687	409.626	0		
3.51934	0.0131872	39.7813	0.653957	449.672	0		
3.8634	0.0103974	43.6704	0.845133	493.633	0		



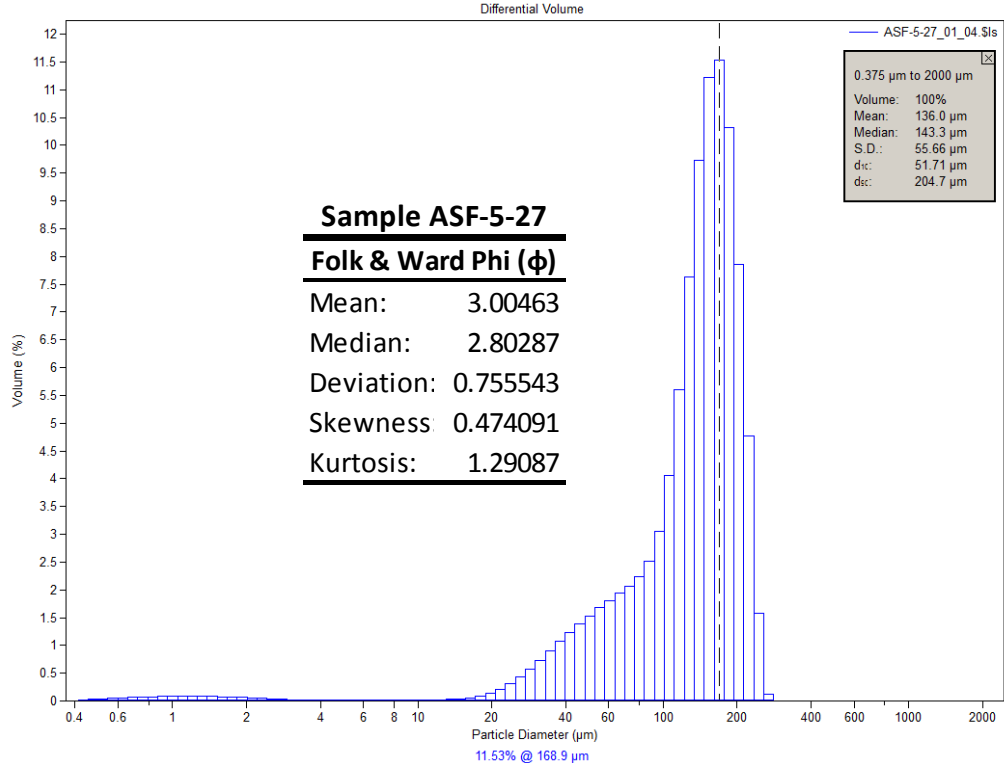
μm	Volume (%)						
0.375198	0.00686641	4.2411	0.008449	47.9397	0.579557	541.892	0
0.411878	0.0130833	4.65572	0.007987	52.6264	0.70814	594.869	0
0.452145	0.021976	5.11087	0.008153	57.7713	0.793524	653.025	0
0.496347	0.0302805	5.61052	0.008777	63.4192	0.809739	716.866	0
0.544872	0.0380521	6.15902	0.009707	69.6192	0.782858	786.949	0
0.59814	0.0451667	6.76114	0.010779	76.4253	0.836424	863.883	0
0.656615	0.0515051	7.42212	0.011854	83.8969	1.18242	948.338	0
0.720807	0.0569255	8.14773	0.012797	92.0988	2.10306	1041.05	0
0.791275	0.0613	8.94427	0.013483	101.103	3.86797	1142.83	0
0.868632	0.0645001	9.81869	0.013865	110.987	6.48002	1254.55	0
0.953552	0.0664138	10.7786	0.013956	121.837	9.54789	1377.2	0
1.04677	0.0669478	11.8323	0.013997	133.748	12.3536	1511.84	0
1.14911	0.0661478	12.9891	0.014299	146.824	14.0293	1659.64	0
1.26145	0.0640996	14.2589	0.015511	161.177	14.0202	1821.89	0
1.38477	0.0609191	15.6529	0.018334	176.935	12.1899	2000	
1.52015	0.0567631	17.1832	0.023612	194.232	9.03605		
1.66876	0.0518145	18.863	0.032357	213.221	5.42076		
1.8319	0.0462936	20.7071	0.045073	234.066	2.02133		
2.011	0.0404345	22.7315	0.062369	256.948	0.277162		
2.2076	0.0344964	24.9538	0.084309	282.068	0.005825		
2.42342	0.0287312	27.3934	0.111154	309.644	0		
2.66033	0.0233892	30.0714	0.144758	339.916	0		
2.92042	0.0186794	33.0113	0.188459	373.147	0		
3.20592	0.0147709	36.2385	0.248981	409.626	0		
3.51934	0.0117603	39.7813	0.333934	449.672	0		
3.8634	0.00966794	43.6704	0.446408	493.633	0		



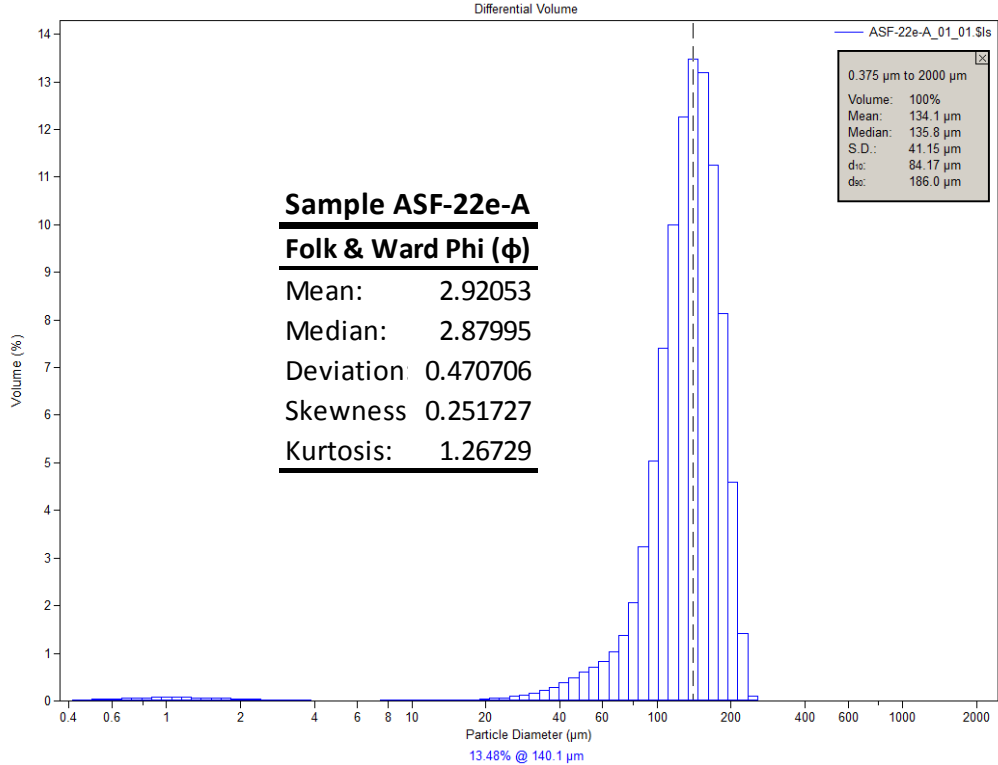
μm	Volume (%)						
0.375198	0.0064363	4.2411	0.005291	47.9397	0.563776	541.892	0
0.411878	0.0122648	4.65572	0.004599	52.6264	0.679984	594.869	0
0.452145	0.0206043	5.11087	0.004535	57.7713	0.756398	653.025	0
0.496347	0.0283961	5.61052	0.004948	63.4192	0.757099	716.866	0
0.544872	0.0356931	6.15902	0.005711	69.6192	0.684412	786.949	0
0.59814	0.042379	6.76114	0.006675	76.4253	0.623083	863.883	0
0.656615	0.0483417	7.42212	0.007713	83.8969	0.747209	948.338	0
0.720807	0.0534476	8.14773	0.008692	92.0988	1.30841	1041.05	0
0.791275	0.0575744	8.94427	0.009478	101.103	2.61107	1142.83	0
0.868632	0.0605986	9.81869	0.009985	110.987	4.81509	1254.55	0
0.953552	0.0624127	10.7786	0.010154	121.837	7.72333	1377.2	0
1.04677	0.0629231	11.8323	0.01012	133.748	10.7716	1511.84	0
1.14911	0.0621691	12.9891	0.01006	146.824	13.1691	1659.64	0
1.26145	0.060226	14.2589	0.010515	161.177	14.1748	1821.89	0
1.38477	0.0571987	15.6529	0.012087	176.935	13.439	2000	
1.52015	0.0532296	17.1832	0.015708	194.232	11.0772		
1.66876	0.0484875	18.863	0.022644	213.221	7.73459		
1.8319	0.0431763	20.7071	0.033947	234.066	4.23229		
2.011	0.0375141	22.7315	0.050989	256.948	1.26566		
2.2076	0.0317439	24.9538	0.074488	282.068	0.089316		
2.42342	0.0261014	27.3934	0.105124	309.644	0		
2.66033	0.0208247	30.0714	0.144137	339.916	0		
2.92042	0.016113	33.0113	0.193364	373.147	0		
3.20592	0.012135	36.2385	0.256933	409.626	0		
3.51934	0.00899167	39.7813	0.339479	449.672	0		
3.8634	0.00672014	43.6704	0.443546	493.633	0		



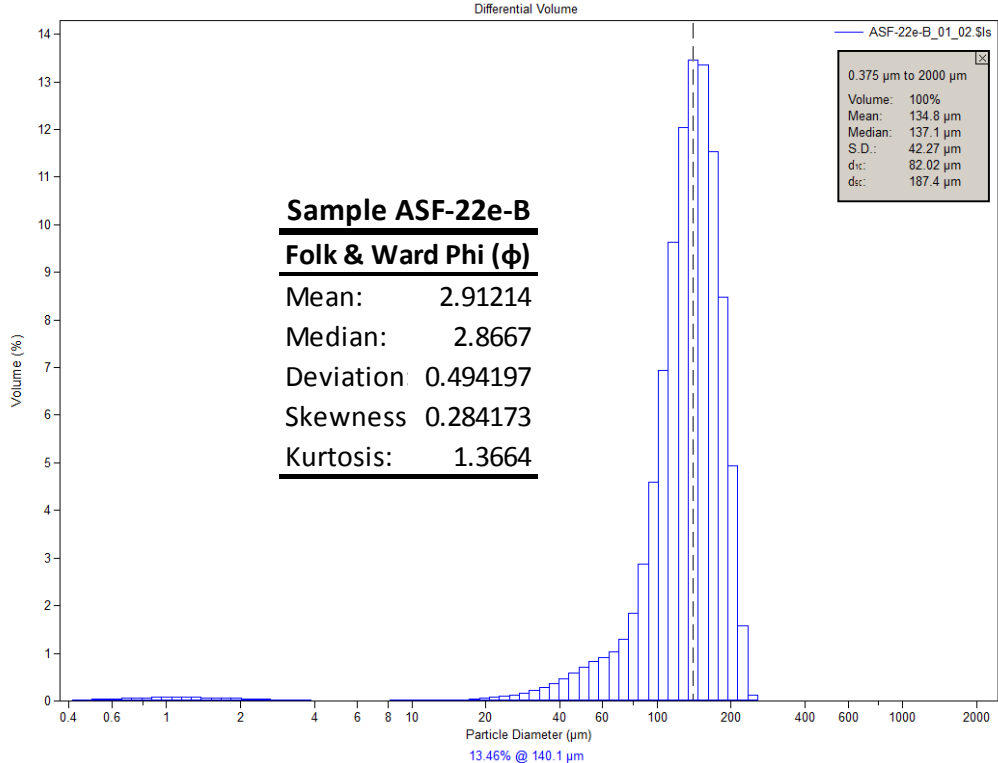
μm	Volume (%)						
0.375198	0.00691056	4.2411	0.007471	47.9397	0.786712	541.892	0
0.411878	0.0131739	4.65572	0.006561	52.6264	0.955482	594.869	0
0.452145	0.0221508	5.11087	0.006345	57.7713	1.08388	653.025	0
0.496347	0.0305665	5.61052	0.006655	63.4192	1.14322	716.866	0
0.544872	0.0384852	6.15902	0.007348	69.6192	1.14173	786.949	0
0.59814	0.0457888	6.76114	0.008265	76.4253	1.17368	863.883	0
0.656615	0.0523609	7.42212	0.009275	83.8969	1.42154	948.338	0
0.720807	0.0580597	8.14773	0.010248	92.0988	2.1298	1041.05	0
0.791275	0.0627521	8.94427	0.011056	101.103	3.56459	1142.83	0
0.868632	0.0663005	9.81869	0.011626	110.987	5.80952	1254.55	0
0.953552	0.0685791	10.7786	0.011906	121.837	8.60982	1377.2	0
1.04677	0.0694745	11.8323	0.012037	133.748	11.374	1511.84	0
1.14911	0.0690101	12.9891	0.012163	146.824	13.2769	1659.64	0
1.26145	0.0672463	14.2589	0.012756	161.177	13.6971	1821.89	0
1.38477	0.0642774	15.6529	0.014328	176.935	12.3256	2000	
1.52015	0.0602397	17.1832	0.017693	194.232	9.47678		
1.66876	0.0553013	18.863	0.024105	213.221	5.92059		
1.8319	0.0496726	20.7071	0.034823	234.066	2.35383		
2.011	0.043586	22.7315	0.051959	256.948	0.369485		
2.2076	0.0373074	24.9538	0.077683	282.068	0.010527		
2.42342	0.0311016	27.3934	0.114647	309.644	0		
2.66033	0.0252403	30.0714	0.166788	339.916	0		
2.92042	0.0199574	33.0113	0.238164	373.147	0		
3.20592	0.015452	36.2385	0.334311	409.626	0		
3.51934	0.0118486	39.7813	0.459626	449.672	0		
3.8634	0.00919681	43.6704	0.613371	493.633	0		



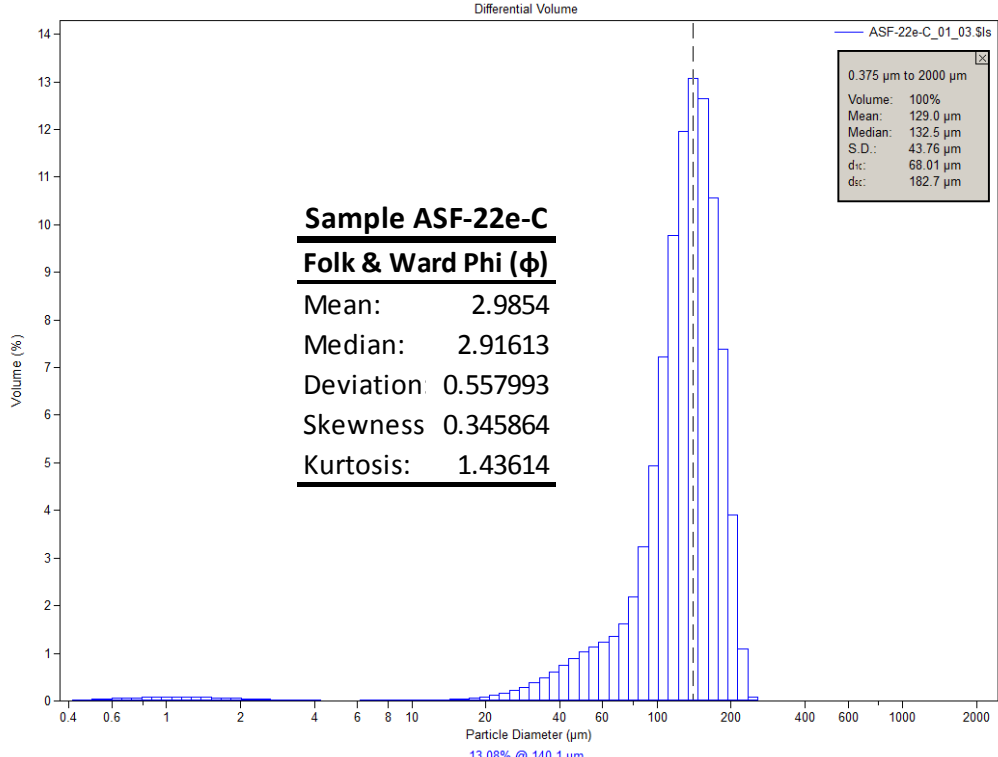
μm	Volume (%)						
0.375198	0.00837365	4.2411	0.010576	47.9397	1.53407	541.892	0
0.411878	0.0159741	4.65572	0.01	52.6264	1.67377	594.869	0
0.452145	0.0268987	5.11087	0.010381	57.7713	1.81001	653.025	0
0.496347	0.0371969	5.61052	0.01144	63.4192	1.94077	716.866	0
0.544872	0.0469618	6.15902	0.012919	69.6192	2.06971	786.949	0
0.59814	0.0560609	6.76114	0.01455	76.4253	2.23214	863.883	0
0.656615	0.0643596	7.42212	0.016122	83.8969	2.51117	948.338	0
0.720807	0.0716844	8.14773	0.01744	92.0988	3.0562	1041.05	0
0.791275	0.0778666	8.94427	0.018414	101.103	4.05423	1142.83	0
0.868632	0.0827216	9.81869	0.019156	110.987	5.60894	1254.55	0
0.953552	0.0860705	10.7786	0.020123	121.837	7.63536	1377.2	0
1.04677	0.0877358	11.8323	0.022387	133.748	9.72656	1511.84	0
1.14911	0.0877023	12.9891	0.027572	146.824	11.2157	1659.64	0
1.26145	0.0859966	14.2589	0.038334	161.177	11.5286	1821.89	0
1.38477	0.0826912	15.6529	0.058116	176.935	10.3173	2000	
1.52015	0.0779165	17.1832	0.091096	194.232	7.85643		
1.66876	0.0718544	18.863	0.1417	213.221	4.77099		
1.8319	0.0647546	20.7071	0.213313	234.066	1.57268		
2.011	0.0569194	22.7315	0.308553	256.948	0.118507		
2.2076	0.0487107	24.9538	0.427739	282.068	0		
2.42342	0.0405173	27.3934	0.56922	309.644	0		
2.66033	0.0327506	30.0714	0.728871	339.916	0		
2.92042	0.0257844	33.0113	0.898903	373.147	0		
3.20592	0.0199425	36.2385	1.07057	409.626	0		
3.51934	0.0154294	39.7813	1.23519	449.672	0		
3.8634	0.0123271	43.6704	1.38891	493.633	0		



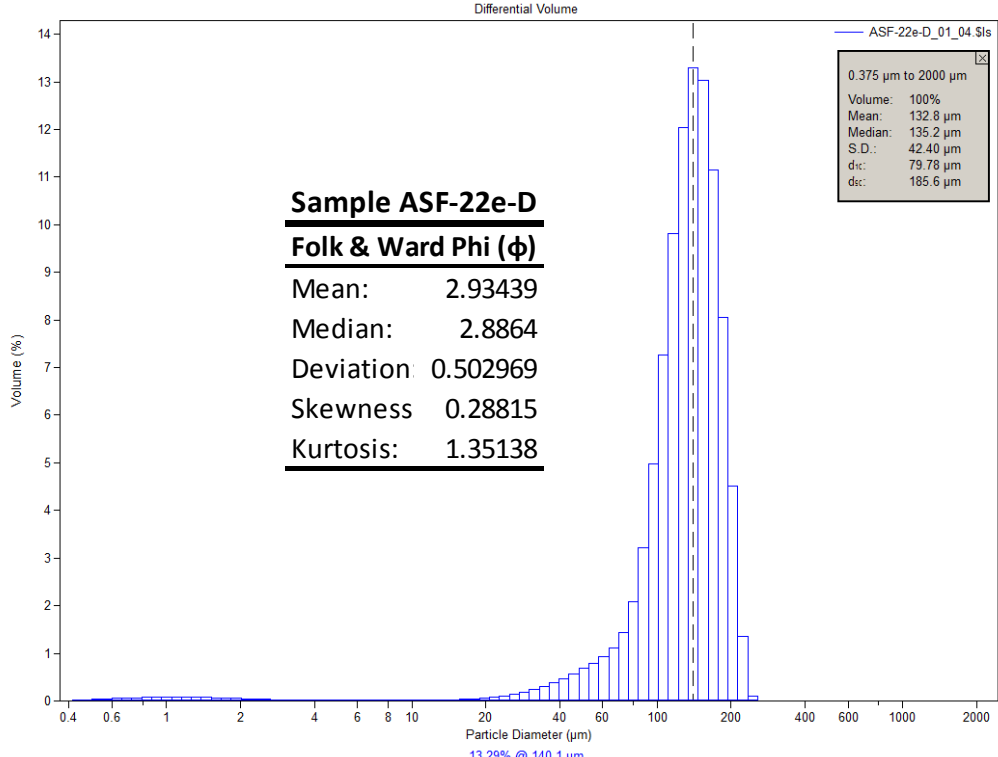
μ m	Volume (%)	μ m	Volume (%)	μ m	Volume (%)	μ m	Volume (%)
0.375198	0.00754948	4.2411	0.006619	47.9397	0.59776	541.892	0
0.411878	0.0143848	4.65572	0.006018	52.6264	0.709993	594.869	0
0.452145	0.0241609	5.11087	0.006141	57.7713	0.835961	653.025	0
0.496347	0.0332888	5.61052	0.006831	63.4192	1.02519	716.866	0
0.544872	0.0418284	6.15902	0.007925	69.6192	1.38216	786.949	0
0.59814	0.0496433	6.76114	0.00927	76.4253	2.06201	863.883	0
0.656615	0.0566008	7.42212	0.010728	83.8969	3.24231	948.338	0
0.720807	0.0625454	8.14773	0.012181	92.0988	5.0449	1041.05	0
0.791275	0.0673347	8.94427	0.013516	101.103	7.40367	1142.83	0
0.868632	0.0708255	9.81869	0.014679	110.987	9.99971	1254.55	0
0.953552	0.0728942	10.7786	0.015692	121.837	12.2549	1377.2	0
1.04677	0.0734352	11.8323	0.016717	133.748	13.483	1511.84	0
1.14911	0.0724973	12.9891	0.018072	146.824	13.1926	1659.64	0
1.26145	0.0701702	14.2589	0.020239	161.177	11.2506	1821.89	0
1.38477	0.0665812	15.6529	0.023911	176.935	8.1301	2000	
1.52015	0.0618974	17.1832	0.029847	194.232	4.59821		
1.66876	0.0563199	18.863	0.038896	213.221	1.4088		
1.8319	0.0500849	20.7071	0.051814	234.066	0.10073		
2.011	0.0434554	22.7315	0.069398	256.948	0		
2.2076	0.0367132	24.9538	0.092842	282.068	0		
2.42342	0.0301457	27.3934	0.123724	309.644	0		
2.66033	0.0240298	30.0714	0.164782	339.916	0		
2.92042	0.0186117	33.0113	0.219637	373.147	0		
3.20592	0.0140839	36.2385	0.291557	409.626	0		
3.51934	0.0105674	39.7813	0.381829	449.672	0		
3.8634	0.00809652	43.6704	0.486737	493.633	0		



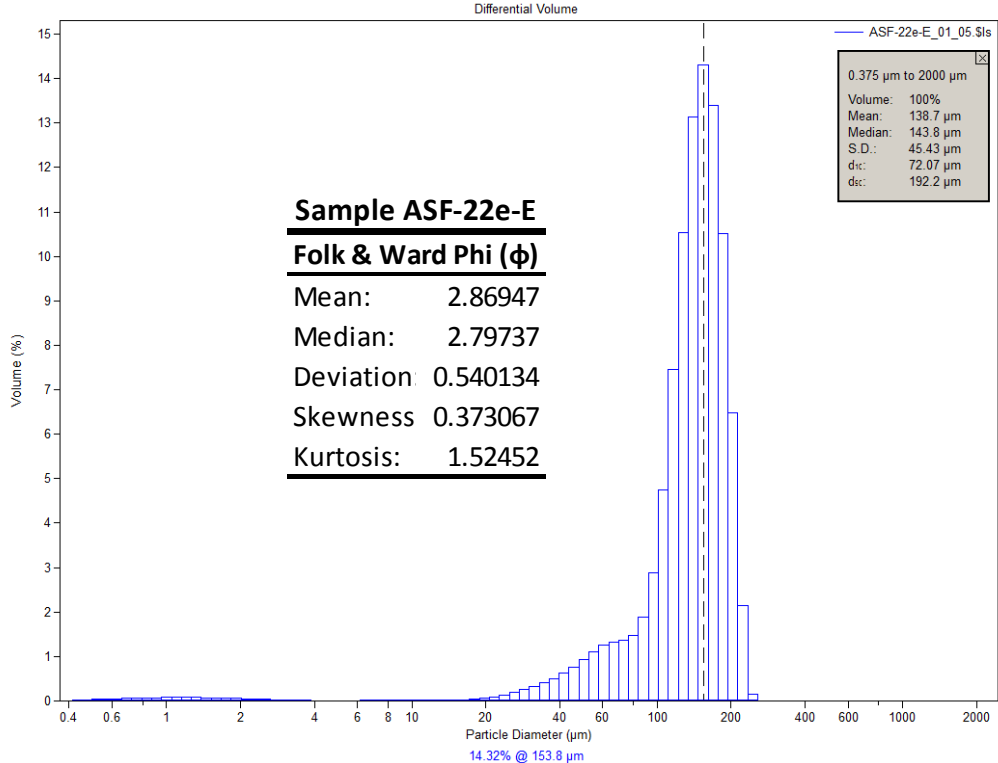
μm	Volume (%)						
0.375198	0.00761546	4.2411	0.007573	47.9397	0.71285	541.892	0
0.411878	0.0145118	4.65572	0.006716	52.6264	0.821772	594.869	0
0.452145	0.0243787	5.11087	0.006541	57.7713	0.918779	653.025	0
0.496347	0.033598	5.61052	0.006894	63.4192	1.04166	716.866	0
0.544872	0.0422319	6.15902	0.007627	69.6192	1.292	786.949	0
0.59814	0.0501442	6.76114	0.008612	76.4253	1.83532	863.883	0
0.656615	0.0572027	7.42212	0.00975	83.8969	2.87746	948.338	0
0.720807	0.0632509	8.14773	0.010972	92.0988	4.59005	1041.05	0
0.791275	0.0681451	8.94427	0.012228	101.103	6.94485	1142.83	0
0.868632	0.0717418	9.81869	0.013539	110.987	9.62901	1254.55	0
0.953552	0.073914	10.7786	0.014997	121.837	12.0473	1377.2	0
1.04677	0.0745534	11.8323	0.01684	133.748	13.4587	1511.84	0
1.14911	0.0737074	12.9891	0.019462	146.824	13.3452	1659.64	0
1.26145	0.0714646	14.2589	0.02346	161.177	11.5316	1821.89	0
1.38477	0.0679494	15.6529	0.029666	176.935	8.47029	2000	
1.52015	0.0633283	17.1832	0.039033	194.232	4.94665		
1.66876	0.0578028	18.863	0.052605	213.221	1.58091		
1.8319	0.0516094	20.7071	0.071228	234.066	0.117062		
2.011	0.0450095	22.7315	0.095708	256.948	0		
2.2076	0.0382848	24.9538	0.126946	282.068	0		
2.42342	0.0317198	27.3934	0.166297	309.644	0		
2.66033	0.0255879	30.0714	0.216536	339.916	0		
2.92042	0.0201282	33.0113	0.281812	373.147	0		
3.20592	0.0155262	36.2385	0.366324	409.626	0		
3.51934	0.011894	39.7813	0.47128	449.672	0		
3.8634	0.00926068	43.6704	0.591296	493.633	0		



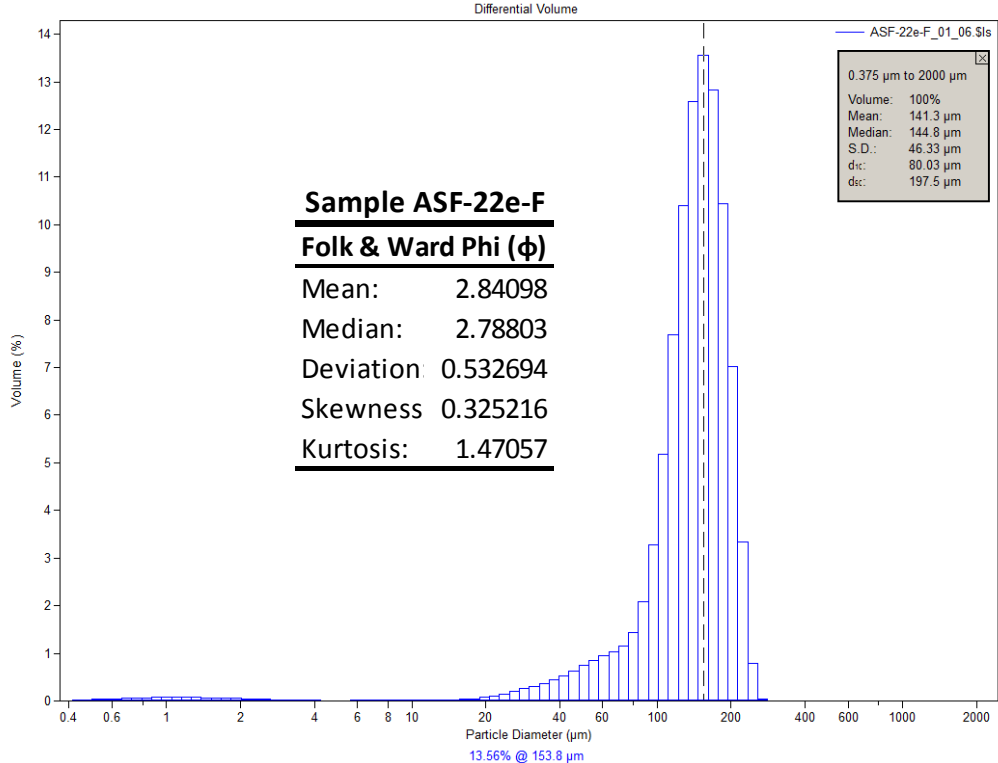
μm	Volume (%)						
0.375198	0.00820336	4.2411	0.009577	47.9397	1.02915	541.892	0
0.411878	0.0156368	4.65572	0.008993	52.6264	1.13938	594.869	0
0.452145	0.0262841	5.11087	0.009143	57.7713	1.23555	653.025	0
0.496347	0.0362547	5.61052	0.009817	63.4192	1.36373	716.866	0
0.544872	0.0456206	6.15902	0.010813	69.6192	1.62658	786.949	0
0.59814	0.0542388	6.76114	0.011961	76.4253	2.1849	863.883	0
0.656615	0.0619678	7.42212	0.013128	83.8969	3.23815	948.338	0
0.720807	0.0686378	8.14773	0.014234	92.0988	4.93109	1041.05	0
0.791275	0.074089	8.94427	0.015258	101.103	7.21705	1142.83	0
0.868632	0.0781585	9.81869	0.016315	110.987	9.76529	1254.55	0
0.953552	0.080697	10.7786	0.017687	121.837	11.9522	1377.2	0
1.04677	0.0815749	11.8323	0.019905	133.748	13.0811	1511.84	0
1.14911	0.0808247	12.9891	0.023781	146.824	12.6376	1659.64	0
1.26145	0.078527	14.2589	0.030388	161.177	10.5621	1821.89	0
1.38477	0.0748037	15.6529	0.041154	176.935	7.39162	2000	
1.52015	0.069827	17.1832	0.057643	194.232	3.90129		
1.66876	0.0638117	18.863	0.08162	213.221	1.08485		
1.8319	0.0570184	20.7071	0.11485	234.066	0.071166		
2.011	0.0497441	22.7315	0.159182	256.948	0		
2.2076	0.0423153	24.9538	0.216807	282.068	0		
2.42342	0.0350683	27.3934	0.289639	309.644	0		
2.66033	0.0283301	30.0714	0.379937	339.916	0		
2.92042	0.0223896	33.0113	0.4891	373.147	0		
3.20592	0.0174683	36.2385	0.615943	409.626	0		
3.51934	0.0136959	39.7813	0.75585	449.672	0		
3.8634	0.0110925	43.6704	0.898175	493.633	0		



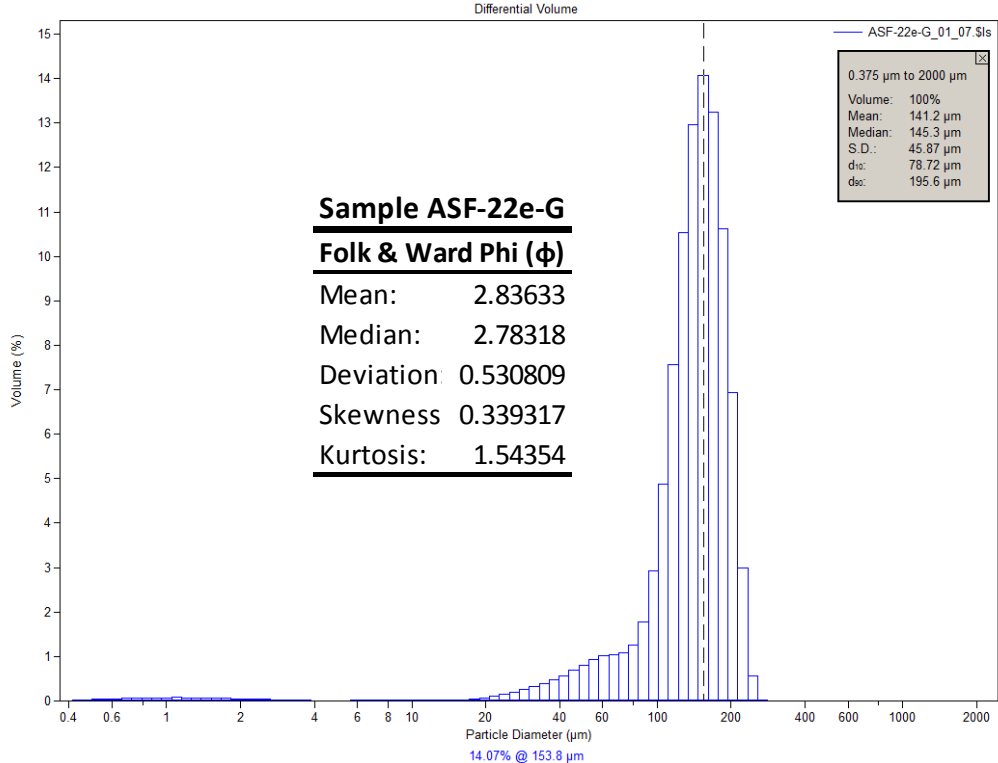
μm	Volume (%)						
0.375198	0.00793547	4.2411	0.012103	47.9397	0.685562	541.892	0
0.411878	0.0151266	4.65572	0.012028	52.6264	0.79776	594.869	0
0.452145	0.0254281	5.11087	0.012774	57.7713	0.922476	653.025	0
0.496347	0.0350777	5.61052	0.014123	63.4192	1.10465	716.866	0
0.544872	0.0441465	6.15902	0.015835	69.6192	1.44349	786.949	0
0.59814	0.0524976	6.76114	0.01768	76.4253	2.09063	863.883	0
0.656615	0.0599961	7.42212	0.019437	83.8969	3.22485	948.338	0
0.720807	0.0664783	8.14773	0.0209	92.0988	4.97072	1041.05	0
0.791275	0.0717934	8.94427	0.021888	101.103	7.27048	1142.83	0
0.868632	0.0757847	9.81869	0.022339	110.987	9.81846	1254.55	0
0.953552	0.0783105	10.7786	0.022369	121.837	12.0481	1377.2	0
1.04677	0.0792446	11.8323	0.022379	133.748	13.2893	1511.84	0
1.14911	0.0786196	12.9891	0.023086	146.824	13.0397	1659.64	0
1.26145	0.0765119	14.2589	0.025491	161.177	11.1477	1821.89	0
1.38477	0.0730366	15.6529	0.030867	176.935	8.06017	2000	0
1.52015	0.0683572	17.1832	0.040513	194.232	4.52122		
1.66876	0.0626775	18.863	0.055642	213.221	1.36276		
1.8319	0.0562456	20.7071	0.077001	234.066	0.095915		
2.011	0.049346	22.7315	0.104941	256.948	0		
2.2076	0.0422925	24.9538	0.139917	282.068	0		
2.42342	0.0354117	27.3934	0.182622	309.644	0		
2.66033	0.0290258	30.0714	0.234895	339.916	0		
2.92042	0.0234249	33.0113	0.299241	373.147	0		
3.20592	0.0188392	36.2385	0.377632	409.626	0		
3.51934	0.0154126	39.7813	0.4707	449.672	0		
3.8634	0.0131863	43.6704	0.575434	493.633	0		



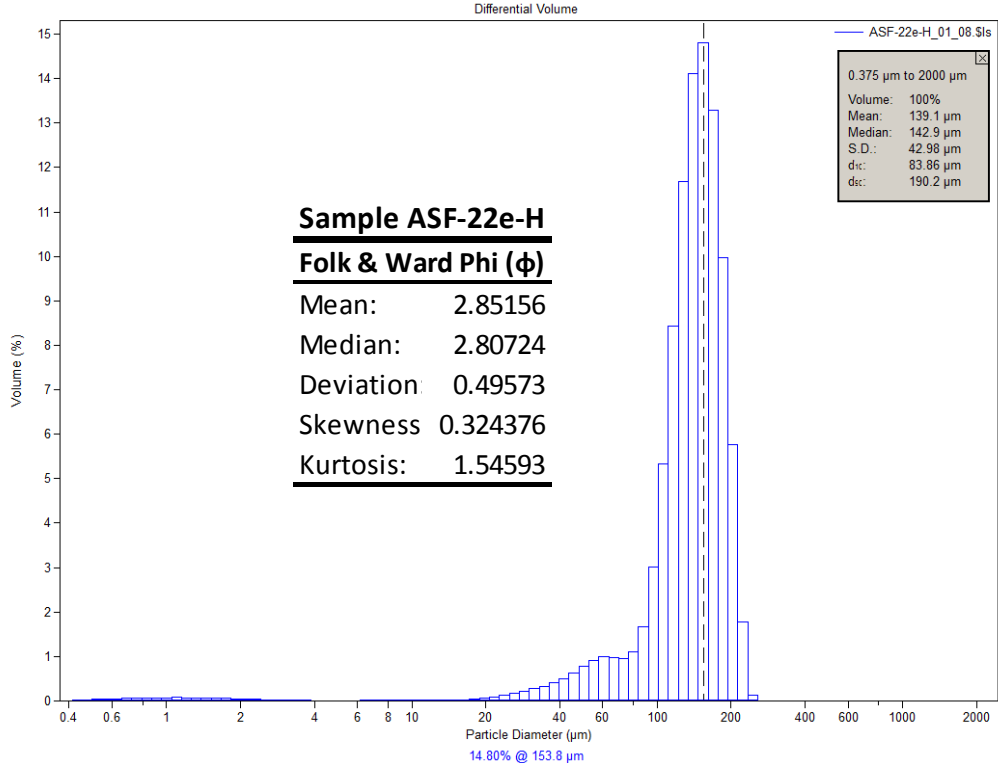
µm	Volume (%)	µm	Volume (%)	µm	Volume (%)	µm	Volume (%)
0.375198	0.00774333	4.2411	0.00801	47.9397	0.939403	541.892	0
0.411878	0.0147651	4.65572	0.008008	52.6264	1.11613	594.869	0
0.452145	0.0248388	5.11087	0.008961	57.7713	1.25823	653.025	0
0.496347	0.0342999	5.61052	0.010619	63.4192	1.33071	716.866	0
0.544872	0.0432236	6.15902	0.01271	69.6192	1.35949	786.949	0
0.59814	0.051479	6.76114	0.014924	76.4253	1.46649	863.883	0
0.656615	0.0589349	7.42212	0.016959	83.8969	1.87586	948.338	0
0.720807	0.0654277	8.14773	0.018488	92.0988	2.89084	1041.05	0
0.791275	0.0708027	8.94427	0.019222	101.103	4.75259	1142.83	0
0.868632	0.0748931	9.81869	0.018999	110.987	7.45266	1254.55	0
0.953552	0.0775447	10.7786	0.017918	121.837	10.5444	1377.2	0
1.04677	0.078612	11.8323	0.016572	133.748	13.1367	1511.84	0
1.14911	0.0781033	12.9891	0.015996	146.824	14.3167	1659.64	0
1.26145	0.0760713	14.2589	0.017918	161.177	13.3944	1821.89	0
1.38477	0.0726109	15.6529	0.024395	176.935	10.5137	2000	
1.52015	0.0678675	17.1832	0.037984	194.232	6.48098		
1.66876	0.0620315	18.863	0.061212	213.221	2.14419		
1.8319	0.0553493	20.7071	0.095239	234.066	0.161491		
2.011	0.0481064	22.7315	0.140301	256.948	0		
2.2076	0.0406342	24.9538	0.195068	282.068	0		
2.42342	0.0332782	27.3934	0.258024	309.644	0		
2.66033	0.0263979	30.0714	0.328694	339.916	0		
2.92042	0.0203154	33.0113	0.408622	373.147	0		
3.20592	0.0153107	36.2385	0.503335	409.626	0		
3.51934	0.0115632	39.7813	0.620485	449.672	0		
3.8634	0.00914545	43.6704	0.766991	493.633	0		



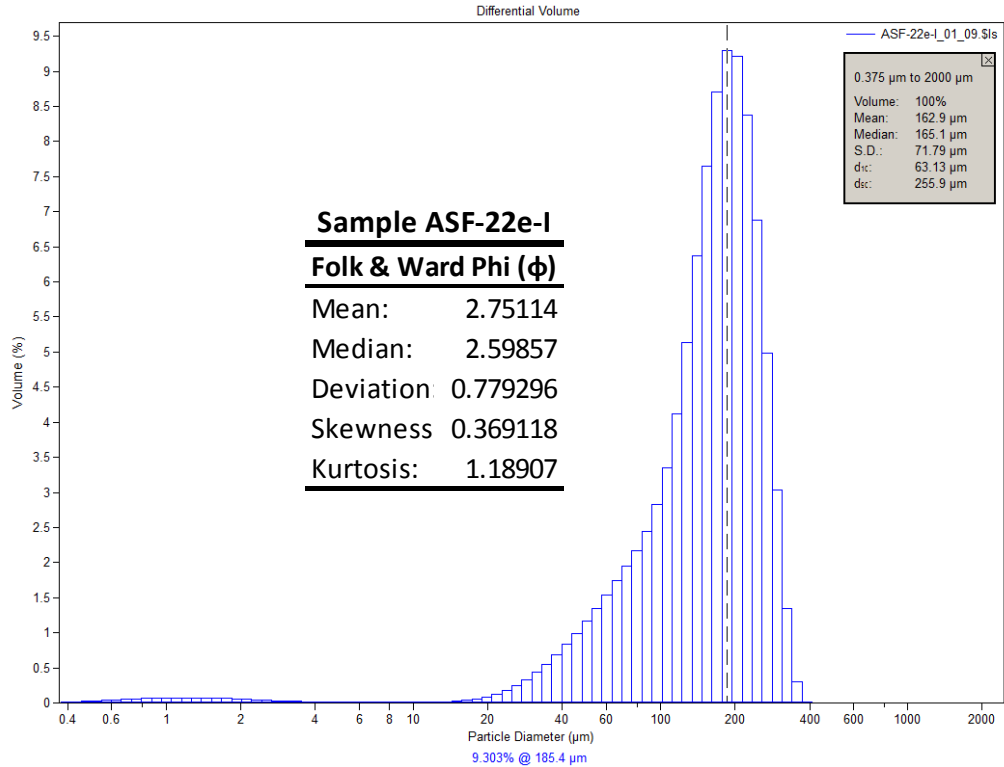
μm	Volume (%)						
0.375198	0.00755266	4.2411	0.009148	47.9397	0.742773	541.892	0
0.411878	0.0143975	4.65572	0.009098	52.6264	0.85697	594.869	0
0.452145	0.0242066	5.11087	0.0099	57.7713	0.955811	653.025	0
0.496347	0.0333994	5.61052	0.011326	63.4192	1.03946	716.866	0
0.544872	0.042045	6.15902	0.013132	69.6192	1.16133	786.949	0
0.59814	0.0500126	6.76114	0.015053	76.4253	1.44516	863.883	0
0.656615	0.057173	7.42212	0.016839	83.8969	2.07808	948.338	0
0.720807	0.0633693	8.14773	0.018234	92.0988	3.28305	1041.05	0
0.791275	0.068454	8.94427	0.019032	101.103	5.18846	1142.83	0
0.868632	0.0722741	9.81869	0.019169	110.987	7.69352	1254.55	0
0.953552	0.0746886	10.7786	0.018827	121.837	10.3922	1377.2	0
1.04677	0.0755717	11.8323	0.018636	133.748	12.5796	1511.84	0
1.14911	0.0749474	12.9891	0.019618	146.824	13.561	1659.64	0
1.26145	0.0728835	14.2589	0.023386	161.177	12.8365	1821.89	0
1.38477	0.0694849	15.6529	0.031901	176.935	10.4488	2000	
1.52015	0.0649045	17.1832	0.047365	194.232	7.02017		
1.66876	0.0593335	18.863	0.071723	213.221	3.34548		
1.8319	0.0530124	20.7071	0.105586	234.066	0.782674		
2.011	0.0462126	22.7315	0.148455	256.948	0.042616		
2.2076	0.0392429	24.9538	0.198347	282.068	0		
2.42342	0.0324211	27.3934	0.253027	309.644	0		
2.66033	0.0260707	30.0714	0.311352	339.916	0		
2.92042	0.0204794	33.0113	0.374023	373.147	0		
3.20592	0.0158889	36.2385	0.444831	409.626	0		
3.51934	0.0124515	39.7813	0.528622	449.672	0		
3.8634	0.0102202	43.6704	0.629012	493.633	0		



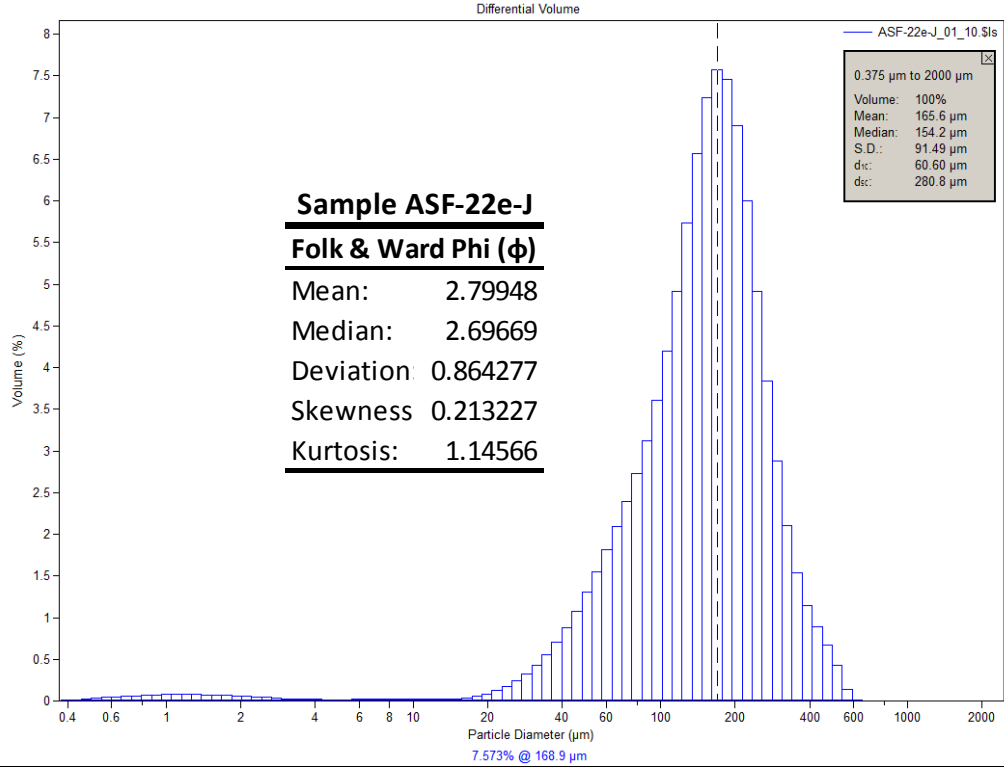
μm	Volume (%)						
0.375198	0.00757069	4.2411	0.008978	47.9397	0.811912	541.892	0
0.411878	0.0144329	4.65572	0.008879	52.6264	0.929014	594.869	0
0.452145	0.0242692	5.11087	0.009622	57.7713	1.01089	653.025	0
0.496347	0.033492	5.61052	0.010974	63.4192	1.04478	716.866	0
0.544872	0.0421714	6.15902	0.012699	69.6192	1.08124	786.949	0
0.59814	0.0501766	6.76114	0.014536	76.4253	1.25446	863.883	0
0.656615	0.0573783	7.42212	0.016248	83.8969	1.77704	948.338	0
0.720807	0.063618	8.14773	0.017592	92.0988	2.92493	1041.05	0
0.791275	0.0687469	8.94427	0.01838	101.103	4.88357	1142.83	0
0.868632	0.0726091	9.81869	0.018566	110.987	7.57309	1254.55	0
0.953552	0.0750617	10.7786	0.018333	121.837	10.542	1377.2	0
1.04677	0.0759735	11.8323	0.018307	133.748	12.9701	1511.84	0
1.14911	0.0753668	12.9891	0.019463	146.824	14.0654	1659.64	0
1.26145	0.0733064	14.2589	0.023386	161.177	13.2523	1821.89	0
1.38477	0.069896	15.6529	0.031988	176.935	10.6315	2000	
1.52015	0.0652884	17.1832	0.047487	194.232	6.92875		
1.66876	0.0596762	18.863	0.071973	213.221	2.99166		
1.8319	0.0533023	20.7071	0.106338	234.066	0.567556		
2.011	0.0464416	22.7315	0.15059	256.948	0.023027		
2.2076	0.039408	24.9538	0.20319	282.068	0		
2.42342	0.0325229	27.3934	0.26226	309.644	0		
2.66033	0.0261144	30.0714	0.326729	339.916	0		
2.92042	0.0204714	33.0113	0.397233	373.147	0		
3.20592	0.0158368	36.2385	0.477726	409.626	0		
3.51934	0.01236	39.7813	0.573124	449.672	0		
3.8634	0.0100911	43.6704	0.686621	493.633	0		



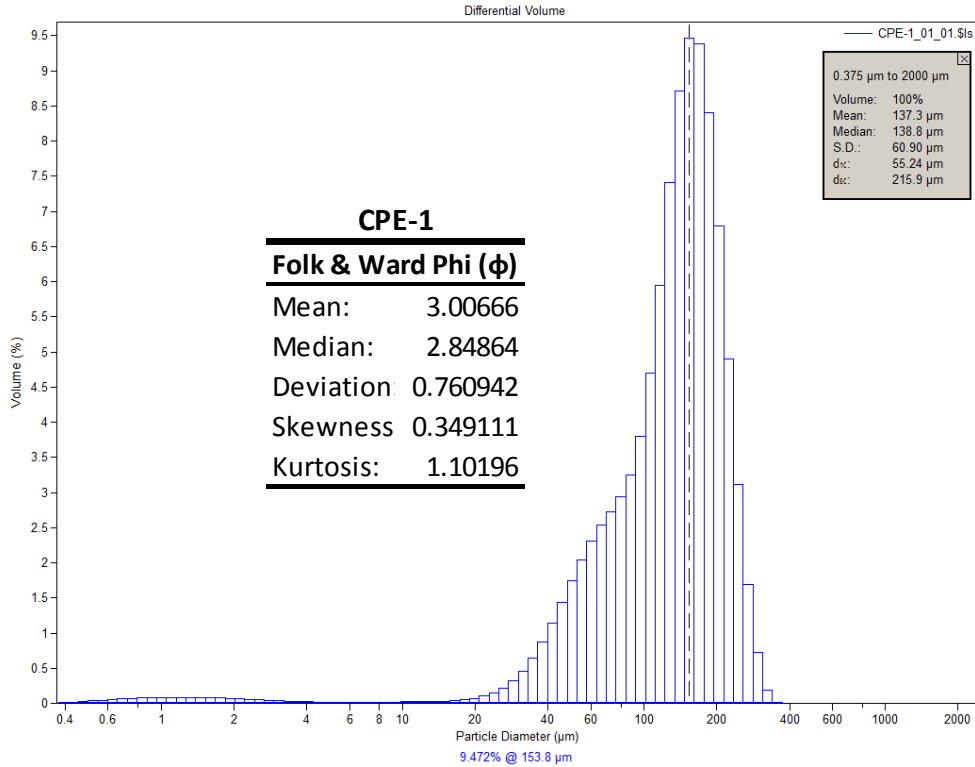
μm	Volume (%)						
0.375198	0.00764309	4.2411	0.008241	47.9397	0.787944	541.892	0
0.411878	0.0145693	4.65572	0.008139	52.6264	0.9208	594.869	0
0.452145	0.0244924	5.11087	0.008868	57.7713	0.991803	653.025	0
0.496347	0.033788	5.61052	0.010189	63.4192	0.981102	716.866	0
0.544872	0.0425241	6.15902	0.011848	69.6192	0.956992	786.949	0
0.59814	0.0505669	6.76114	0.013569	76.4253	1.0958	863.883	0
0.656615	0.0577847	7.42212	0.01509	83.8969	1.66956	948.338	0
0.720807	0.0640169	8.14773	0.016146	92.0988	3.01557	1041.05	0
0.791275	0.0691143	8.94427	0.016526	101.103	5.33086	1142.83	0
0.868632	0.0729207	9.81869	0.016174	110.987	8.44023	1254.55	0
0.953552	0.0752945	10.7786	0.015288	121.837	11.6949	1377.2	0
1.04677	0.076109	11.8323	0.014521	133.748	14.1111	1511.84	0
1.14911	0.0753914	12.9891	0.014889	146.824	14.798	1659.64	0
1.26145	0.073213	14.2589	0.017941	161.177	13.2851	1821.89	0
1.38477	0.0696845	15.6529	0.025533	176.935	9.9623	2000	
1.52015	0.0649636	17.1832	0.039675	194.232	5.77011		
1.66876	0.0592486	18.863	0.062007	213.221	1.78799		
1.8319	0.0527858	20.7071	0.092687	234.066	0.128328		
2.011	0.0458531	22.7315	0.130775	256.948	0		
2.2076	0.0387639	24.9538	0.174183	282.068	0		
2.42342	0.0318388	27.3934	0.22111	309.644	0		
2.66033	0.025403	30.0714	0.272081	339.916	0		
2.92042	0.0197433	33.0113	0.331053	373.147	0		
3.20592	0.0150993	36.2385	0.406443	409.626	0		
3.51934	0.0116199	39.7813	0.507802	449.672	0		
3.8634	0.00935229	43.6704	0.639022	493.633	0		



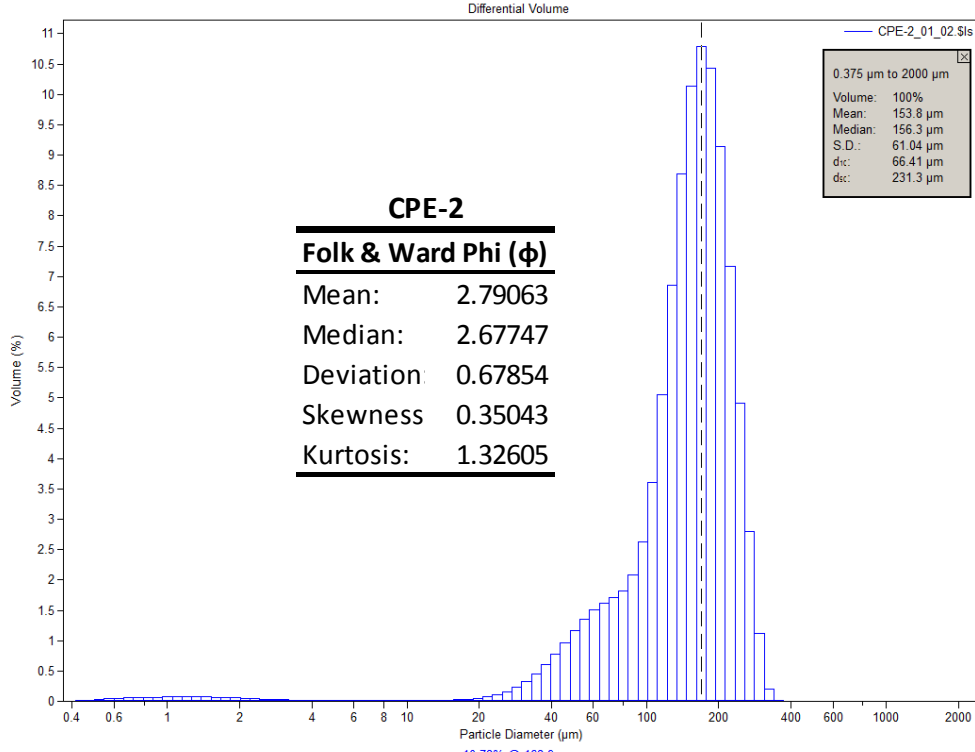
µm	Volume (%)	µm	Volume (%)	µm	Volume (%)	µm	Volume (%)
0.375198	0.0071075	4.2411	0.013781	47.9397	1.16591	541.892	0
0.411878	0.0135577	4.65572	0.013302	52.6264	1.35136	594.869	0
0.452145	0.0228252	5.11087	0.013602	57.7713	1.54384	653.025	0
0.496347	0.0315563	5.61052	0.01445	63.4192	1.7404	716.866	0
0.544872	0.0398296	6.15902	0.015607	69.6192	1.9446	786.949	0
0.59814	0.0475341	6.76114	0.016823	76.4253	2.17145	863.883	0
0.656615	0.0545581	7.42212	0.017871	83.8969	2.44977	948.338	0
0.720807	0.0607592	8.14773	0.018528	92.0988	2.82361	1041.05	0
0.791275	0.0660005	8.94427	0.018643	101.103	3.35609	1142.83	0
0.868632	0.0701339	9.81869	0.018236	110.987	4.11572	1254.55	0
0.953552	0.0730187	10.7786	0.017621	121.837	5.13647	1377.2	0
1.04677	0.0745165	11.8323	0.017563	133.748	6.36917	1511.84	0
1.14911	0.0746241	12.9891	0.019265	146.824	7.64398	1659.64	0
1.26145	0.0733725	14.2589	0.024485	161.177	8.71029	1821.89	0
1.38477	0.070829	15.6529	0.03542	176.935	9.30253	2000	
1.52015	0.0671053	17.1832	0.05456	194.232	9.20911		
1.66876	0.0623527	18.863	0.084236	213.221	8.37443		
1.8319	0.0567736	20.7071	0.126108	234.066	6.88138		
2.011	0.0506081	22.7315	0.181473	256.948	4.98546		
2.2076	0.0441418	24.9538	0.251181	282.068	3.03928		
2.42342	0.0376787	27.3934	0.336055	309.644	1.34774		
2.66033	0.0315376	30.0714	0.436781	339.916	0.303141		
2.92042	0.0260122	33.0113	0.55331	373.147	0.016273		
3.20592	0.0213541	36.2385	0.685147	409.626	0		
3.51934	0.0177314	39.7813	0.831425	449.672	0		
3.8634	0.0152169	43.6704	0.991793	493.633	0		



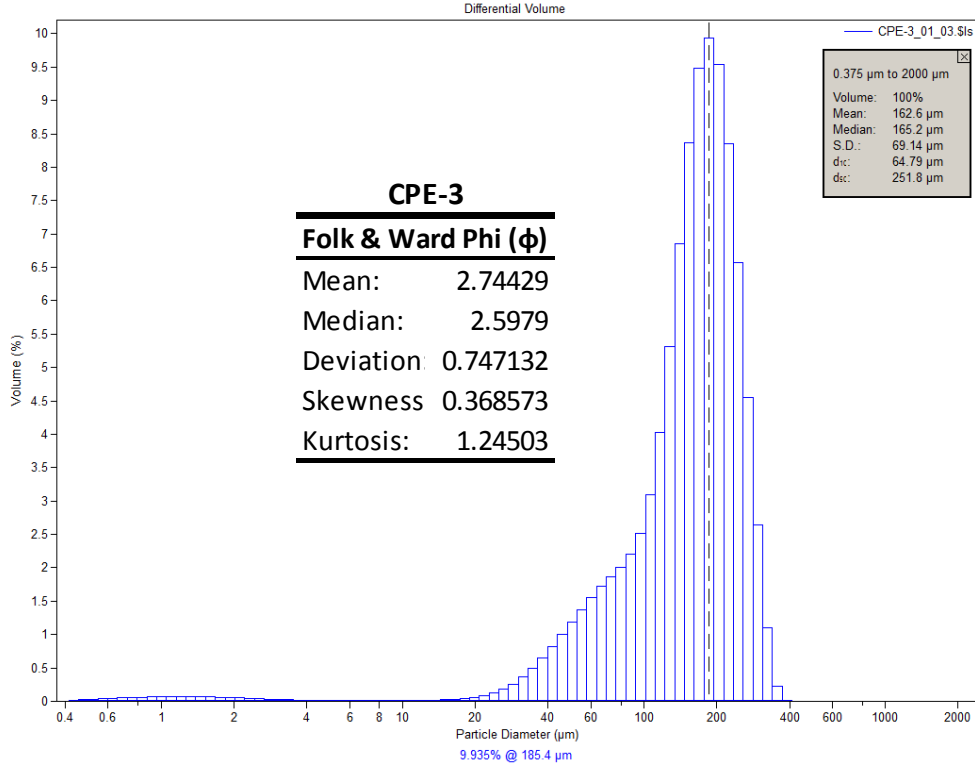
μm	Volume (%)						
0.375198	0.00732683	4.2411	0.016406	47.9397	1.30472	541.892	0.140368
0.411878	0.0139798	4.65572	0.016201	52.6264	1.55297	594.869	0.010282
0.452145	0.0235485	5.11087	0.016825	57.7713	1.81667	653.025	0
0.496347	0.0325821	5.61052	0.018009	63.4192	2.09337	716.866	0
0.544872	0.0411666	6.15902	0.019467	69.6192	2.39069	786.949	0
0.59814	0.0491921	6.76114	0.020911	76.4253	2.72672	863.883	0
0.656615	0.0565461	7.42212	0.022068	83.8969	3.12426	948.338	0
0.720807	0.0630826	8.14773	0.022669	92.0988	3.60681	1041.05	0
0.791275	0.0686601	8.94427	0.022516	101.103	4.19823	1142.83	0
0.868632	0.0731211	9.81869	0.021602	110.987	4.91437	1254.55	0
0.953552	0.0763135	10.7786	0.02026	121.837	5.73411	1377.2	0
1.04677	0.0780848	11.8323	0.019324	133.748	6.56316	1511.84	0
1.14911	0.0784176	12.9891	0.020129	146.824	7.23536	1659.64	0
1.26145	0.0773302	14.2589	0.02452	161.177	7.57321	1821.89	0
1.38477	0.0748783	15.6529	0.034742	176.935	7.46313	2000	
1.52015	0.0711648	17.1832	0.053225	194.232	6.90128		
1.66876	0.0663376	18.863	0.082013	213.221	5.99694		
1.8319	0.0606026	20.7071	0.122364	234.066	4.91966		
2.011	0.0542118	22.7315	0.175296	256.948	3.83836		
2.2076	0.0474707	24.9538	0.242159	282.068	2.8801		
2.42342	0.0407134	27.3934	0.325269	309.644	2.10723		
2.66033	0.0342934	30.0714	0.427797	339.916	1.53726		
2.92042	0.0285425	33.0113	0.552684	373.147	1.14933		
3.20592	0.0237439	36.2385	0.70201	409.626	0.886961		
3.51934	0.0200883	39.7813	0.87688	449.672	0.675485		
3.8634	0.0176551	43.6704	1.07801	493.633	0.426539		



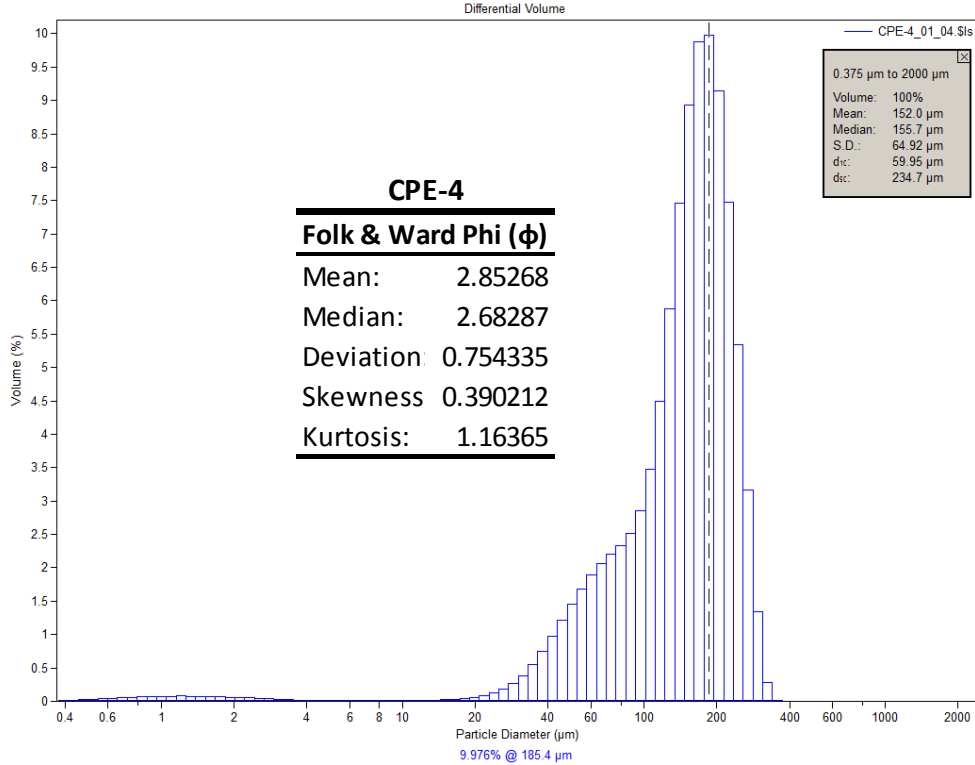
μm	Volume (%)						
0.375198	0.00788457	4.2411	0.017888	47.9397	1.74181	541.892	0
0.411878	0.0150479	4.65572	0.016396	52.6264	2.03733	594.869	0
0.452145	0.0253627	5.11087	0.015721	57.7713	2.30541	653.025	0
0.496347	0.0351227	5.61052	0.015663	63.4192	2.53398	716.866	0
0.544872	0.0444279	6.15902	0.016046	69.6192	2.73008	786.949	0
0.59814	0.0531662	6.76114	0.016708	76.4253	2.93834	863.883	0
0.656615	0.061222	7.42212	0.017551	83.8969	3.25256	948.338	0
0.720807	0.0684424	8.14773	0.018499	92.0988	3.80131	1041.05	0
0.791275	0.0746766	8.94427	0.019522	101.103	4.6962	1142.83	0
0.868632	0.0797568	9.81869	0.02067	110.987	5.951	1254.55	0
0.953552	0.0835146	10.7786	0.022092	121.837	7.405	1377.2	0
1.04677	0.0857819	11.8323	0.024129	133.748	8.71563	1511.84	0
1.14911	0.0865268	12.9891	0.027233	146.824	9.47213	1659.64	0
1.26145	0.0857565	14.2589	0.032165	161.177	9.38108	1821.89	0
1.38477	0.0835146	15.6529	0.039944	176.935	8.40878	2000	
1.52015	0.0798941	17.1832	0.052201	194.232	6.7881		
1.66876	0.0750364	18.863	0.071511	213.221	4.89514		
1.8319	0.0691421	20.7071	0.101584	234.066	3.10942		
2.011	0.0624614	22.7315	0.148082	256.948	1.69093		
2.2076	0.0553004	24.9538	0.218074	282.068	0.729713		
2.42342	0.0479942	27.3934	0.319654	309.644	0.1825		
2.66033	0.0408997	30.0714	0.460625	339.916	0.011675		
2.92042	0.0343489	33.0113	0.645747	373.147	0		
3.20592	0.0286299	36.2385	0.875316	409.626	0		
3.51934	0.0239371	39.7813	1.14322	449.672	0		
3.8634	0.020363	43.6704	1.43743	493.633	0		



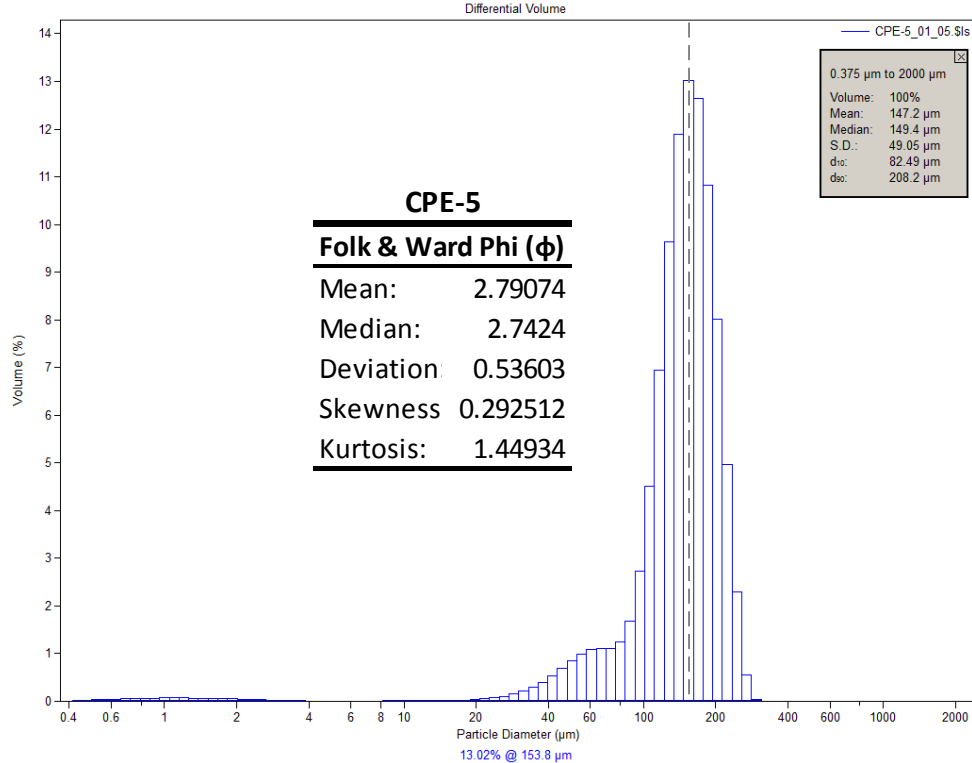
μm	Volume (%)						
0.375198	0.00709686	4.2411	0.011602	47.9397	1.16548	541.892	0
0.411878	0.0135365	4.65572	0.010376	52.6264	1.34874	594.869	0
0.452145	0.0227867	5.11087	0.009884	57.7713	1.50271	653.025	0
0.496347	0.0314976	5.61052	0.00996	63.4192	1.617	716.866	0
0.544872	0.0397467	6.15902	0.010459	69.6192	1.70536	786.949	0
0.59814	0.0474225	6.76114	0.011227	76.4253	1.82587	863.883	0
0.656615	0.0544135	7.42212	0.012161	83.8969	2.08687	948.338	0
0.720807	0.0605773	8.14773	0.013156	92.0988	2.63445	1041.05	0
0.791275	0.0657791	8.94427	0.014132	101.103	3.60678	1142.83	0
0.868632	0.0698728	9.81869	0.015062	110.987	5.05343	1254.55	0
0.953552	0.0727199	10.7786	0.015982	121.837	6.85619	1377.2	0
1.04677	0.0741867	11.8323	0.01711	133.748	8.69347	1511.84	0
1.14911	0.0742735	12.9891	0.018757	146.824	10.1326	1659.64	0
1.26145	0.0730157	14.2589	0.021572	161.177	10.7827	1821.89	0
1.38477	0.0704828	15.6529	0.026438	176.935	10.4312	2000	
1.52015	0.0667871	17.1832	0.03478	194.232	9.14279		
1.66876	0.0620793	18.863	0.048755	213.221	7.16645		
1.8319	0.0565551	20.7071	0.071141	234.066	4.91277		
2.011	0.0504459	22.7315	0.105905	256.948	2.80186		
2.2076	0.0440203	24.9538	0.157356	282.068	1.11226		
2.42342	0.0375606	27.3934	0.229983	309.644	0.2087		
2.66033	0.0313604	30.0714	0.327761	339.916	0.00892		
2.92042	0.0256842	33.0113	0.452597	373.147	0		
3.20592	0.0207598	36.2385	0.604409	409.626	0		
3.51934	0.0167384	39.7813	0.779478	449.672	0		
3.8634	0.013691	43.6704	0.970313	493.633	0		



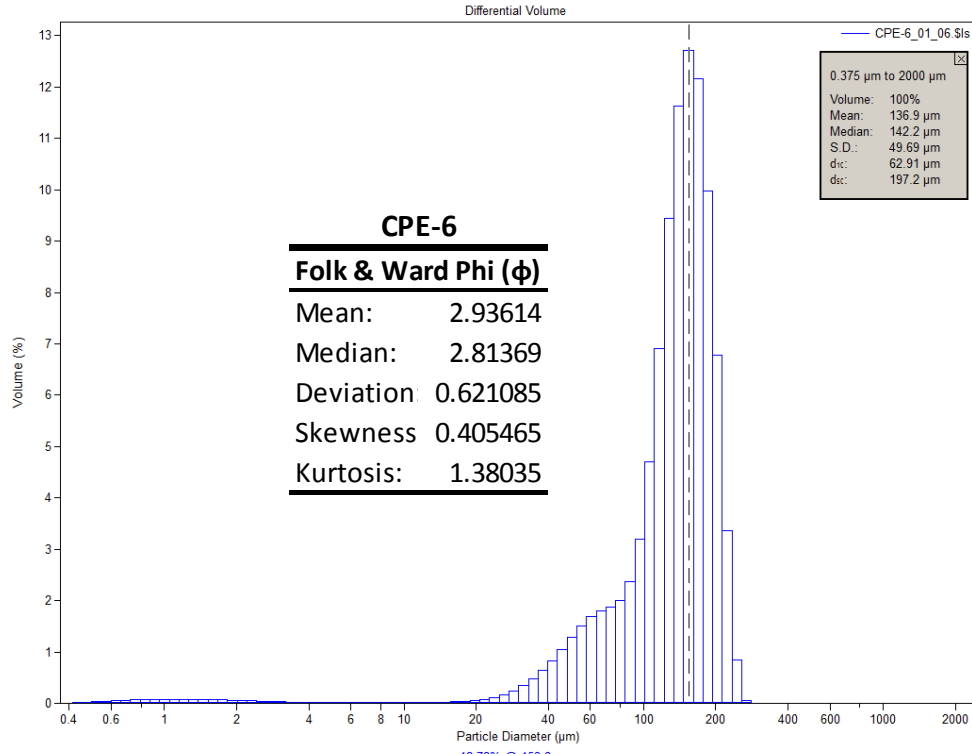
µm	Volume (%)	µm	Volume (%)	µm	Volume (%)	µm	Volume (%)
0.375198	0.00676463	4.2411	0.013594	47.9397	1.18886	541.892	0
0.411878	0.0129065	4.65572	0.012003	52.6264	1.3758	594.869	0
0.452145	0.0217399	5.11087	0.011132	57.7713	1.55519	653.025	0
0.496347	0.030079	5.61052	0.010833	63.4192	1.72001	716.866	0
0.544872	0.0380049	6.15902	0.010975	69.6192	1.86715	786.949	0
0.59814	0.0454179	6.76114	0.011418	76.4253	2.01058	863.883	0
0.656615	0.0522174	7.42212	0.012071	83.8969	2.19902	948.338	0
0.720807	0.0582731	8.14773	0.012847	92.0988	2.52206	1041.05	0
0.791275	0.0634597	8.94427	0.013693	101.103	3.09641	1142.83	0
0.868632	0.0676384	9.81869	0.01462	110.987	4.02273	1254.55	0
0.953552	0.0706762	10.7786	0.01572	121.837	5.31703	1377.2	0
1.04677	0.0724408	11.8323	0.017271	133.748	6.85505	1511.84	0
1.14911	0.0729204	12.9891	0.019668	146.824	8.36062	1659.64	0
1.26145	0.0721333	14.2589	0.023641	161.177	9.48662	1821.89	0
1.38477	0.0701294	15.6529	0.030169	176.935	9.935	2000	
1.52015	0.0669962	17.1832	0.04077	194.232	9.5413		
1.66876	0.0628569	18.863	0.057679	213.221	8.35252		
1.8319	0.0578791	20.7071	0.083812	234.066	6.57558		
2.011	0.0522637	22.7315	0.123234	256.948	4.54543		
2.2076	0.0462526	24.9538	0.180333	282.068	2.63924		
2.42342	0.0401058	27.3934	0.259438	309.644	1.0989		
2.66033	0.0340998	30.0714	0.363715	339.916	0.223706		
2.92042	0.0284919	33.0113	0.493583	373.147	0.010524		
3.20592	0.0235109	36.2385	0.646816	409.626	0		
3.51934	0.0193201	39.7813	0.818135	449.672	0		
3.8634	0.0160112	43.6704	1.0009	493.633	0		



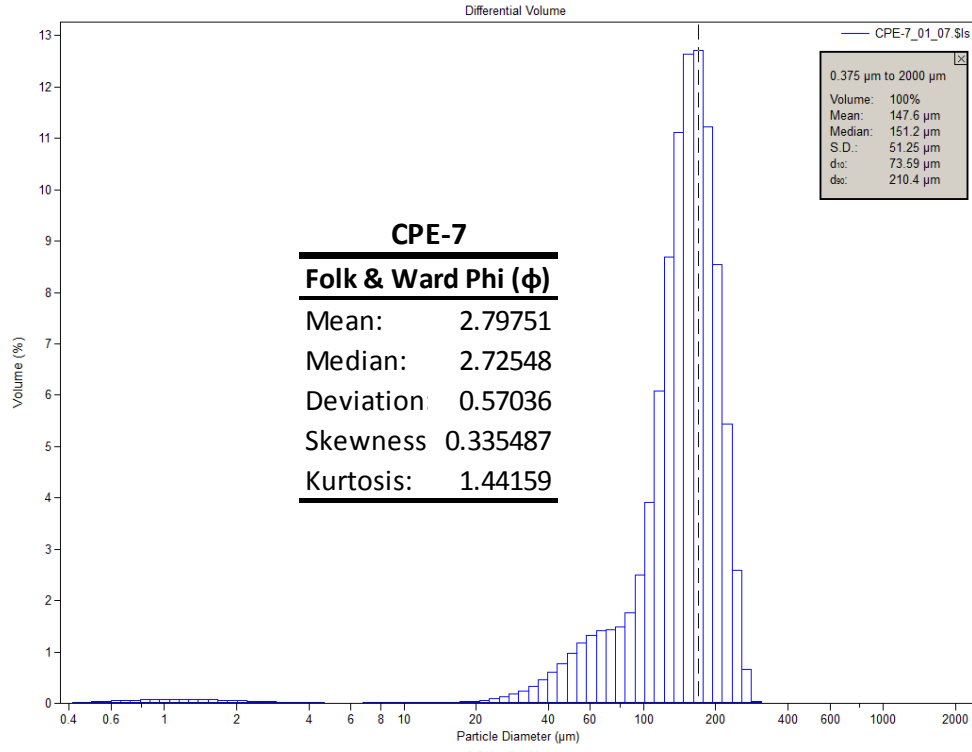
μm	Volume (%)						
0.375198	0.00707487	4.2411	0.014105	47.9397	1.45601	541.892	0
0.411878	0.0135028	4.65572	0.012363	52.6264	1.68736	594.869	0
0.452145	0.0227591	5.11087	0.011411	57.7713	1.89273	653.025	0
0.496347	0.0315188	5.61052	0.01109	63.4192	2.06399	716.866	0
0.544872	0.0398721	6.15902	0.011257	69.6192	2.20307	786.949	0
0.59814	0.0477185	6.76114	0.01176	76.4253	2.33406	863.883	0
0.656615	0.0549552	7.42212	0.012505	83.8969	2.51726	948.338	0
0.720807	0.061445	8.14773	0.013403	92.0988	2.85744	1041.05	0
0.791275	0.0670538	8.94427	0.014397	101.103	3.48171	1142.83	0
0.868632	0.0716302	9.81869	0.015492	110.987	4.48846	1254.55	0
0.953552	0.0750248	10.7786	0.016769	121.837	5.87656	1377.2	0
1.04677	0.0770867	11.8323	0.018491	133.748	7.46926	1511.84	0
1.14911	0.0777861	12.9891	0.021003	146.824	8.93325	1659.64	0
1.26145	0.0771281	14.2589	0.024957	161.177	9.87488	1821.89	0
1.38477	0.0751495	15.6529	0.031195	176.935	9.97568	2000	
1.52015	0.0719312	17.1832	0.041107	194.232	9.13938		
1.66876	0.0675928	18.863	0.056895	213.221	7.47759		
1.8319	0.0623083	20.7071	0.081754	234.066	5.33853		
2.011	0.0562903	22.7315	0.120737	256.948	3.17015		
2.2076	0.049802	24.9538	0.180113	282.068	1.34007		
2.42342	0.0431296	27.3934	0.267152	309.644	0.280648		
2.66033	0.036582	30.0714	0.388542	339.916	0.013919		
2.92042	0.0304483	33.0113	0.547693	373.147	0		
3.20592	0.0249888	36.2385	0.74361	409.626	0		
3.51934	0.0203894	39.7813	0.968923	449.672	0		
3.8634	0.0167571	43.6704	1.21135	493.633	0		



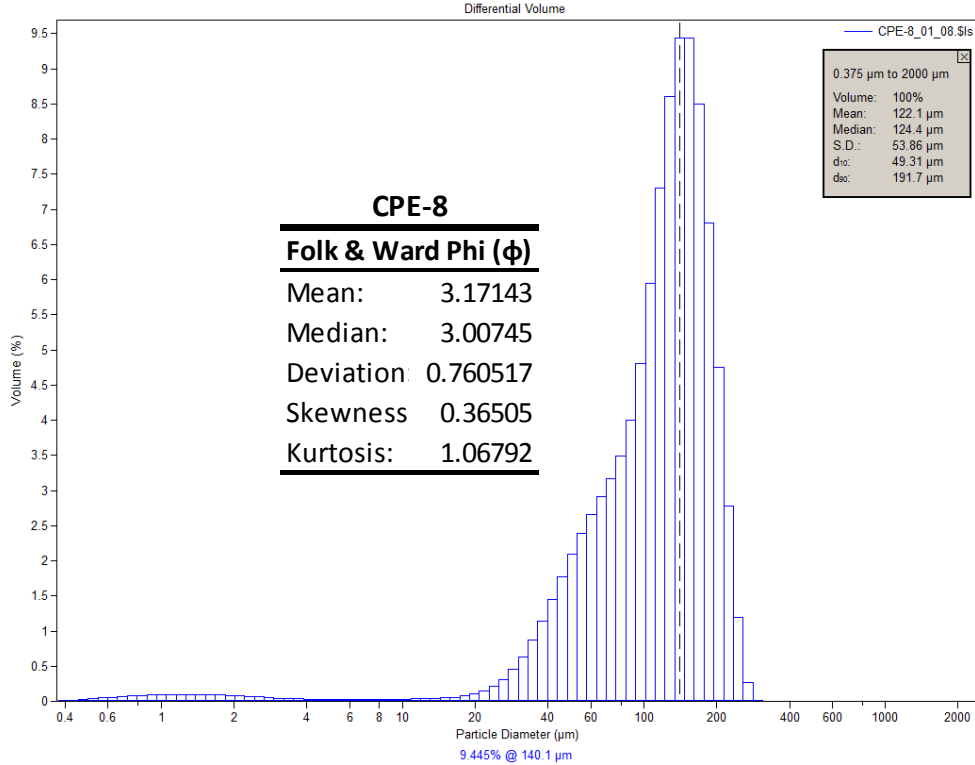
μm	Volume (%)						
0.375198	0.00700425	4.2411	0.008046	47.9397	0.850873	541.892	0
0.411878	0.0133533	4.65572	0.007016	52.6264	0.995973	594.869	0
0.452145	0.022455	5.11087	0.00667	57.7713	1.08567	653.025	0
0.496347	0.0309916	5.61052	0.00684	63.4192	1.10871	716.866	0
0.544872	0.0390299	6.15902	0.007383	69.6192	1.11428	786.949	0
0.59814	0.0464514	6.76114	0.008148	76.4253	1.23822	863.883	0
0.656615	0.0531396	7.42212	0.009022	83.8969	1.69153	948.338	0
0.720807	0.0589513	8.14773	0.009896	92.0988	2.72253	1041.05	0
0.791275	0.0637536	8.94427	0.010679	101.103	4.50541	1142.83	0
0.868632	0.0674065	9.81869	0.011343	110.987	6.95335	1254.55	0
0.953552	0.0697828	10.7786	0.011918	121.837	9.63746	1377.2	0
1.04677	0.0707652	11.8323	0.012632	133.748	11.8872	1511.84	0
1.14911	0.0703759	12.9891	0.013794	146.824	13.0167	1659.64	0
1.26145	0.0686714	14.2589	0.016005	161.177	12.643	1821.89	0
1.38477	0.0657452	15.6529	0.020007	176.935	10.8176	2000	
1.52015	0.0617293	17.1832	0.026768	194.232	8.02109		
1.66876	0.0567902	18.863	0.037583	213.221	4.97385		
1.8319	0.0511362	20.7071	0.053653	234.066	2.30081		
2.011	0.0450013	22.7315	0.076702	256.948	0.562504		
2.2076	0.0386511	24.9538	0.108629	282.068	0.033344		
2.42342	0.0323557	27.3934	0.151962	309.644	0		
2.66033	0.0263902	30.0714	0.21068	339.916	0		
2.92042	0.0209959	33.0113	0.289441	373.147	0		
3.20592	0.0163751	36.2385	0.393783	409.626	0		
3.51934	0.0126563	39.7813	0.526912	449.672	0		
3.8634	0.00988986	43.6704	0.68456	493.633	0		



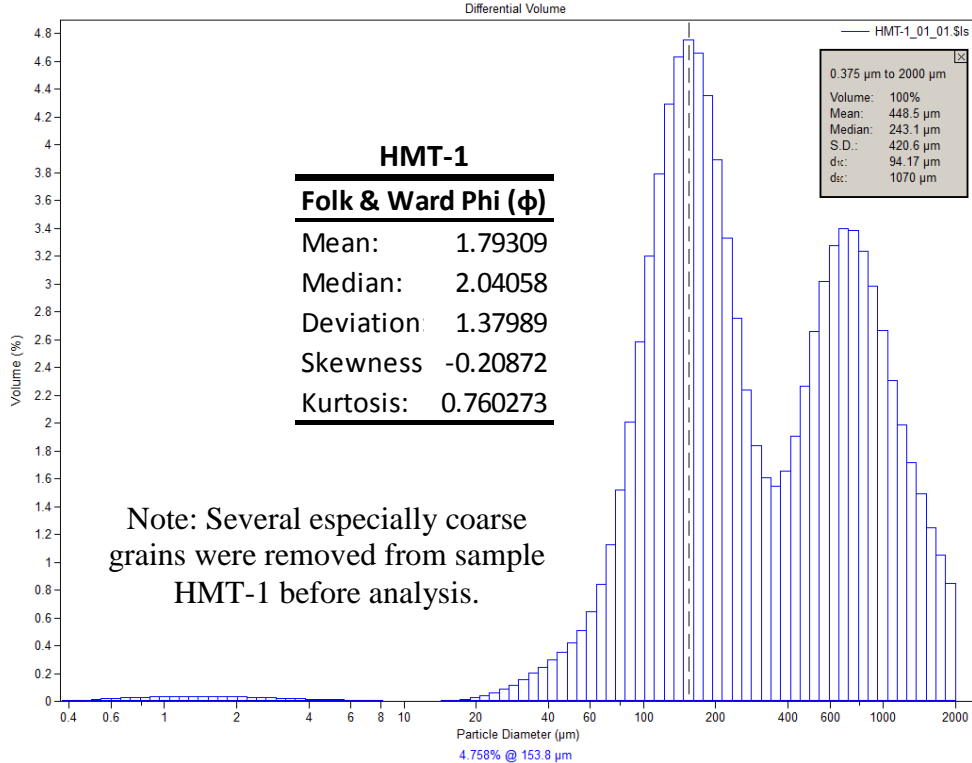
μm	Volume (%)						
0.375198	0.00769727	4.2411	0.014926	47.9397	1.28178	541.892	0
0.411878	0.0146848	4.65572	0.013695	52.6264	1.50269	594.869	0
0.452145	0.0247317	5.11087	0.013252	57.7713	1.68401	653.025	0
0.496347	0.0342098	5.61052	0.013402	63.4192	1.80247	716.866	0
0.544872	0.0432081	6.15902	0.013978	69.6192	1.87707	786.949	0
0.59814	0.0516094	6.76114	0.01481	76.4253	2.00304	863.883	0
0.656615	0.0592951	7.42212	0.015788	83.8969	2.36231	948.338	0
0.720807	0.0661121	8.14773	0.016803	92.0988	3.19729	1041.05	0
0.791275	0.0719125	8.94427	0.017784	101.103	4.70942	1142.83	0
0.868632	0.0765345	9.81869	0.018726	110.987	6.90463	1254.55	0
0.953552	0.0798214	10.7786	0.019697	121.837	9.44443	1377.2	0
1.04677	0.081621	11.8323	0.020982	133.748	11.6356	1511.84	0
1.14911	0.0819223	12.9891	0.022929	146.824	12.7226	1659.64	0
1.26145	0.0807524	14.2589	0.026264	161.177	12.1669	1821.89	0
1.38477	0.0781767	15.6529	0.031886	176.935	9.98225	2000	
1.52015	0.0743089	17.1832	0.041253	194.232	6.77569		
1.66876	0.0693078	18.863	0.056571	213.221	3.36004		
1.8319	0.0633843	20.7071	0.080587	234.066	0.854091		
2.011	0.0567917	22.7315	0.117391	256.948	0.05141		
2.2076	0.0498304	24.9538	0.171325	282.068	0		
2.42342	0.0428176	27.3934	0.24702	309.644	0		
2.66033	0.0360866	30.0714	0.348945	339.916	0		
2.92042	0.0299367	33.0113	0.479947	373.147	0		
3.20592	0.0246258	36.2385	0.641975	409.626	0		
3.51934	0.0203208	39.7813	0.834103	449.672	0		
3.8634	0.0170961	43.6704	1.05138	493.633	0		



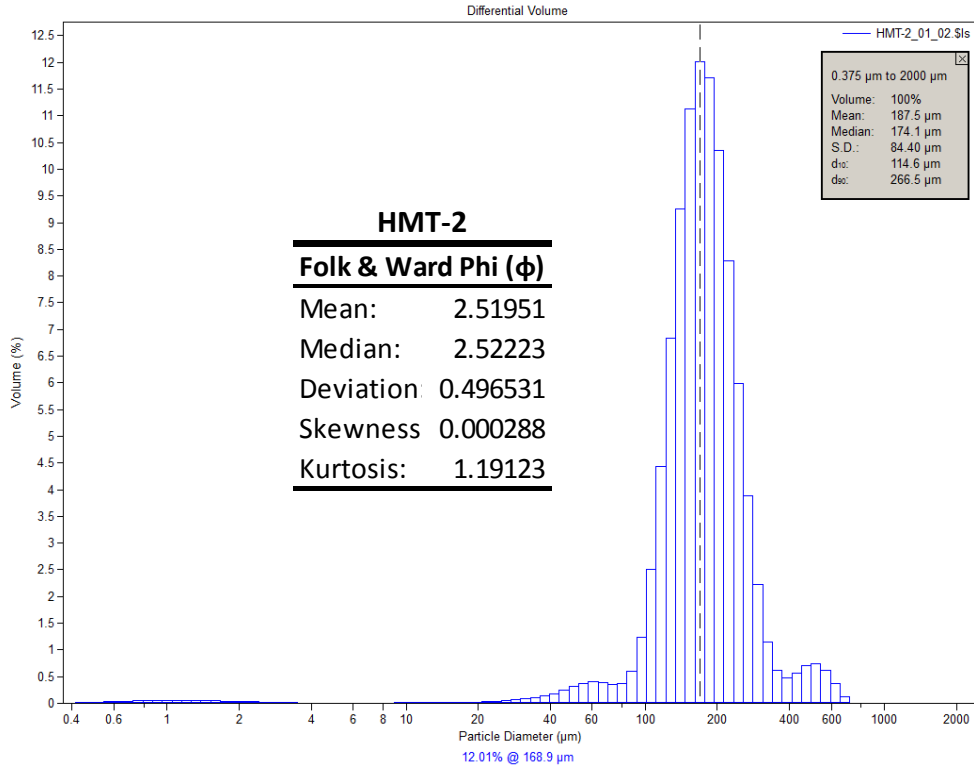
μm	Volume (%)						
0.375198	0.00710151	4.2411	0.009792	47.9397	0.978877	541.892	0
0.411878	0.0135423	4.65572	0.008687	52.6264	1.17349	594.869	0
0.452145	0.0227864	5.11087	0.008306	57.7713	1.32671	653.025	0
0.496347	0.0314764	5.61052	0.008474	63.4192	1.40839	716.866	0
0.544872	0.0396855	6.15902	0.009042	69.6192	1.43032	786.949	0
0.59814	0.0472981	6.76114	0.009847	76.4253	1.48699	863.883	0
0.656615	0.0541996	7.42212	0.010769	83.8969	1.76212	948.338	0
0.720807	0.060246	8.14773	0.011687	92.0988	2.49694	1041.05	0
0.791275	0.0653013	8.94427	0.012503	101.103	3.9202	1142.83	0
0.868632	0.069221	9.81869	0.013178	110.987	6.07915	1254.55	0
0.953552	0.0718691	10.7786	0.013735	121.837	8.68346	1377.2	0
1.04677	0.0731189	11.8323	0.014408	133.748	11.121	1511.84	0
1.14911	0.072978	12.9891	0.015493	146.824	12.6442	1659.64	0
1.26145	0.0714924	14.2589	0.017646	161.177	12.7134	1821.89	0
1.38477	0.0687415	15.6529	0.021651	176.935	11.2189	2000	
1.52015	0.0648486	17.1832	0.028658	194.232	8.54714		
1.66876	0.0599721	18.863	0.040297	213.221	5.43519		
1.8319	0.0543166	20.7071	0.058238	234.066	2.5946		
2.011	0.0481168	22.7315	0.084933	256.948	0.659759		
2.2076	0.0416452	24.9538	0.122794	282.068	0.040599		
2.42342	0.035182	27.3934	0.174638	309.644	0		
2.66033	0.0290186	30.0714	0.244162	339.916	0		
2.92042	0.023412	33.0113	0.335174	373.147	0		
3.20592	0.0185839	36.2385	0.452839	409.626	0		
3.51934	0.0146769	39.7813	0.60123	449.672	0		
3.8634	0.0117538	43.6704	0.779803	493.633	0		



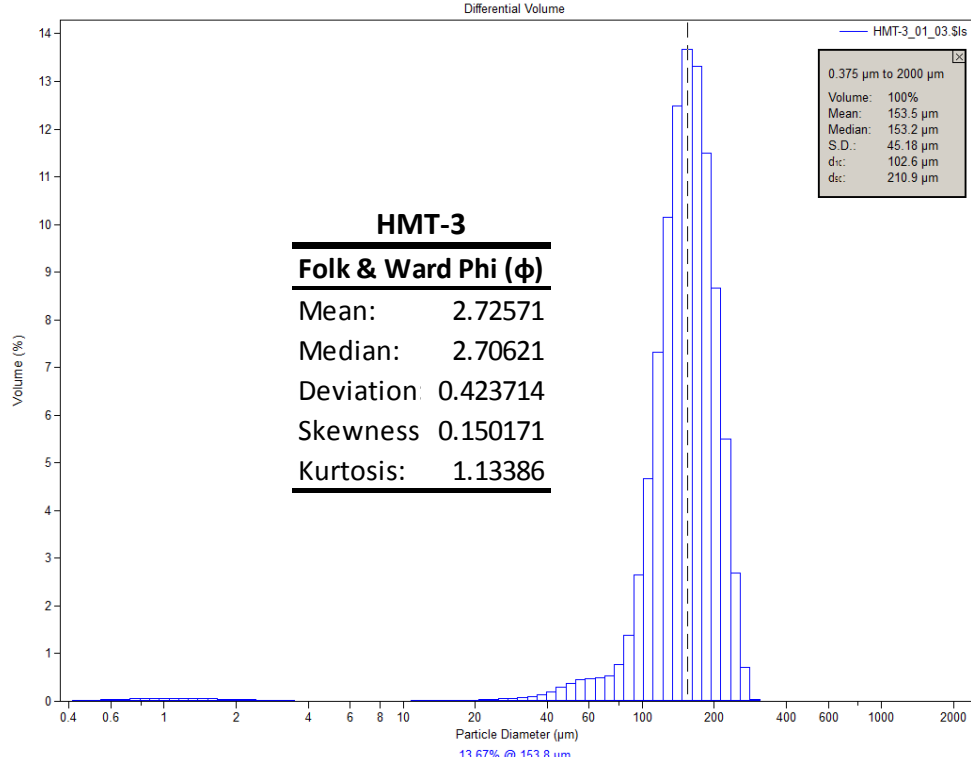
μm	Volume (%)						
0.375198	0.00861562	4.2411	0.027457	47.9397	2.09647	541.892	0
0.411878	0.0164552	4.65572	0.026062	52.6264	2.3956	594.869	0
0.452145	0.0277761	5.11087	0.025607	57.7713	2.66463	653.025	0
0.496347	0.0385491	5.61052	0.02583	63.4192	2.90929	716.866	0
0.544872	0.048902	6.15902	0.026494	69.6192	3.16224	786.949	0
0.59814	0.0587279	6.76114	0.027403	76.4253	3.49377	863.883	0
0.656615	0.0679122	7.42212	0.028436	83.8969	4.00762	948.338	0
0.720807	0.0762945	8.14773	0.029516	92.0988	4.81037	1041.05	0
0.791275	0.0837102	8.94427	0.030638	101.103	5.94504	1142.83	0
0.868632	0.0899672	9.81869	0.031923	110.987	7.30747	1254.55	0
0.953552	0.0948663	10.7786	0.033667	121.837	8.61168	1377.2	0
1.04677	0.0981947	11.8323	0.036429	133.748	9.44482	1511.84	0
1.14911	0.0998771	12.9891	0.040988	146.824	9.44443	1659.64	0
1.26145	0.0998755	14.2589	0.048463	161.177	8.50367	1821.89	0
1.38477	0.0981939	15.6529	0.060374	176.935	6.80535	2000	
1.52015	0.0948907	17.1832	0.078961	194.232	4.7562		
1.66876	0.0900861	18.863	0.107665	213.221	2.78187		
1.8319	0.0839763	20.7071	0.151461	234.066	1.19283		
2.011	0.0768305	22.7315	0.217533	256.948	0.266084		
2.2076	0.0689961	24.9538	0.314642	282.068	0.014497		
2.42342	0.0608763	27.3934	0.451669	309.644	0		
2.66033	0.0529121	30.0714	0.635652	339.916	0		
2.92042	0.0455301	33.0113	0.868458	373.147	0		
3.20592	0.0391029	36.2385	1.14511	409.626	0		
3.51934	0.0338907	39.7813	1.45365	449.672	0		
3.8634	0.0300167	43.6704	1.77695	493.633	0		



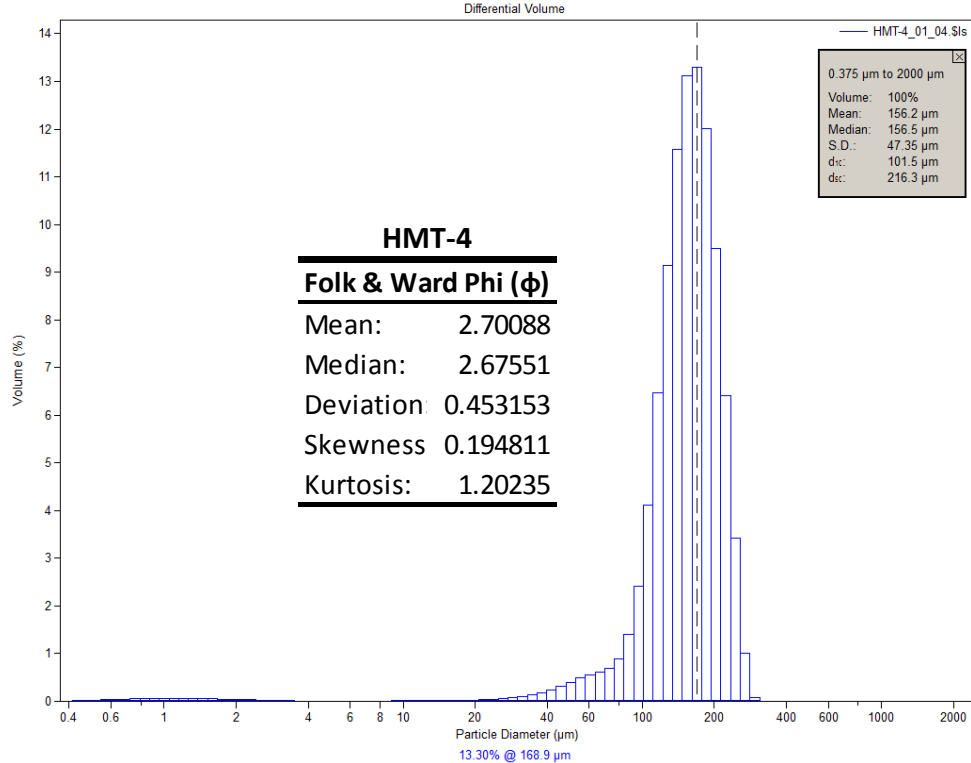
μm	Volume (%)						
0.375198	0.00367131	4.2411	0.014325	47.9397	0.418022	541.892	3.01666
0.411878	0.00660287	4.65572	0.012177	52.6264	0.509521	594.869	3.27489
0.452145	0.00983945	5.11087	0.010239	57.7713	0.643687	653.025	3.39795
0.496347	0.0141348	5.61052	0.008388	63.4192	0.842552	716.866	3.38282
0.544872	0.0176358	6.15902	0.00673	69.6192	1.12841	786.949	3.23753
0.59814	0.0208731	6.76114	0.005094	76.4253	1.51699	863.883	2.98754
0.656615	0.0239216	7.42212	0.003715	83.8969	2.00941	948.338	2.66374
0.720807	0.0270047	8.14773	0.002523	92.0988	2.58547	1041.05	2.3053
0.791275	0.0294602	8.94427	0.001698	101.103	3.20167	1142.83	1.98783
0.868632	0.031523	9.81869	0.001122	110.987	3.79507	1254.55	1.71783
0.953552	0.0331801	10.7786	0.000968	121.837	4.29344	1377.2	1.49506
1.04677	0.0345393	11.8323	0.001273	133.748	4.63008	1511.84	1.24685
1.14911	0.035339	12.9891	0.002415	146.824	4.75827	1659.64	1.05024
1.26145	0.0356355	14.2589	0.00477	161.177	4.66204	1821.89	0.848573
1.38477	0.0354819	15.6529	0.008876	176.935	4.35832	2000	
1.52015	0.0349951	17.1832	0.015438	194.232	3.89326		
1.66876	0.0341741	18.863	0.02538	213.221	3.33337		
1.8319	0.0329438	20.7071	0.039911	234.066	2.7556		
2.011	0.0313702	22.7315	0.059788	256.948	2.23704		
2.2076	0.0295604	24.9538	0.085961	282.068	1.84036		
2.42342	0.0276544	27.3934	0.118504	309.644	1.60521		
2.66033	0.0255374	30.0714	0.157168	339.916	1.54441		
2.92042	0.0232873	33.0113	0.200596	373.147	1.6533		
3.20592	0.0209557	36.2385	0.247201	409.626	1.90858		
3.51934	0.0187292	39.7813	0.296574	449.672	2.26609		
3.8634	0.0164896	43.6704	0.351147	493.633	2.66048		



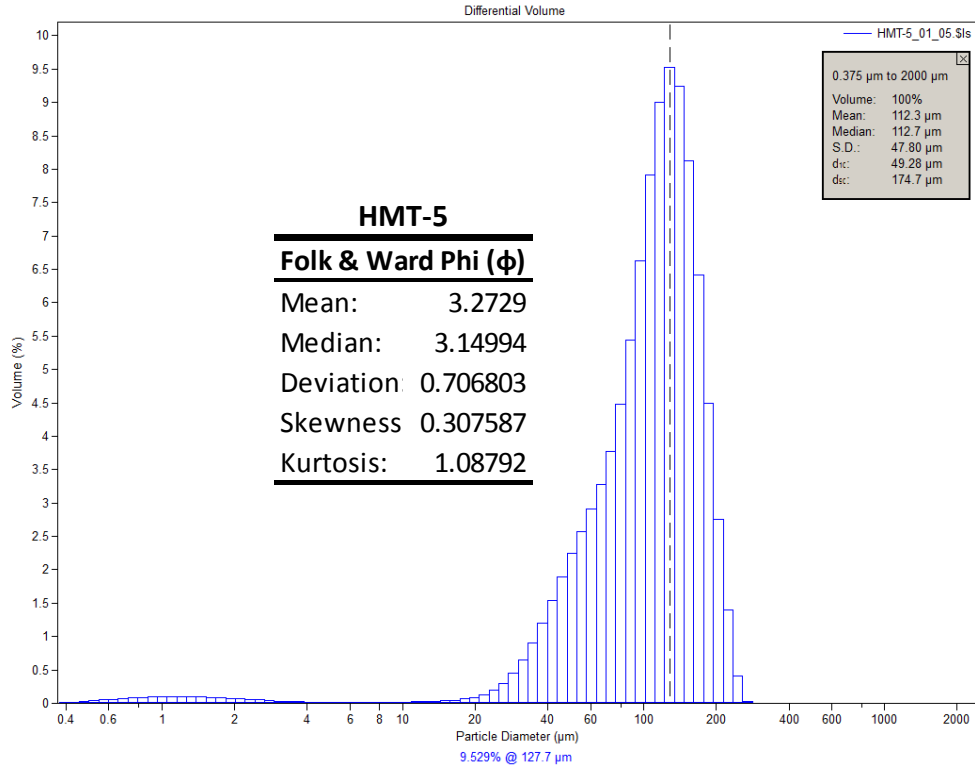
μm	Volume (%)						
0.375198	0.00563273	4.2411	0.00473	47.9397	0.313586	541.892	0.615329
0.411878	0.0107321	4.65572	0.004185	52.6264	0.378711	594.869	0.370721
0.452145	0.0180238	5.11087	0.004202	57.7713	0.410984	653.025	0.115776
0.496347	0.0248293	5.61052	0.004648	63.4192	0.393683	716.866	0.008311
0.544872	0.0311928	6.15902	0.005402	69.6192	0.351089	786.949	0
0.59814	0.0370121	6.76114	0.006326	76.4253	0.369846	863.883	0
0.656615	0.042189	7.42212	0.007298	83.8969	0.592815	948.338	0
0.720807	0.0466073	8.14773	0.0082	92.0988	1.23456	1041.05	0
0.791275	0.0501625	8.94427	0.008927	101.103	2.50392	1142.83	0
0.868632	0.0527496	9.81869	0.009436	110.987	4.44111	1254.55	0
0.953552	0.0542788	10.7786	0.009733	121.837	6.83768	1377.2	0
1.04677	0.054674	11.8323	0.010003	133.748	9.25065	1511.84	0
1.14911	0.0539745	12.9891	0.01048	146.824	11.1289	1659.64	0
1.26145	0.05225	14.2589	0.011642	161.177	12.0136	1821.89	0
1.38477	0.0495952	15.6529	0.013972	176.935	11.7115	2000	
1.52015	0.0461369	17.1832	0.018014	194.232	10.3485		
1.66876	0.0420209	18.863	0.024282	213.221	8.29094		
1.8319	0.0374227	20.7071	0.032791	234.066	5.99716		
2.011	0.0325284	22.7315	0.043459	256.948	3.87991		
2.2076	0.0275437	24.9538	0.055699	282.068	2.22159		
2.42342	0.0226698	27.3934	0.069281	309.644	1.14535		
2.66033	0.0181088	30.0714	0.085143	339.916	0.619113		
2.92042	0.0140345	33.0113	0.105697	373.147	0.482956		
3.20592	0.0105938	36.2385	0.13575	409.626	0.564351		
3.51934	0.00788085	39.7813	0.180329	449.672	0.704057		
3.8634	0.00593295	43.6704	0.241505	493.633	0.743402		



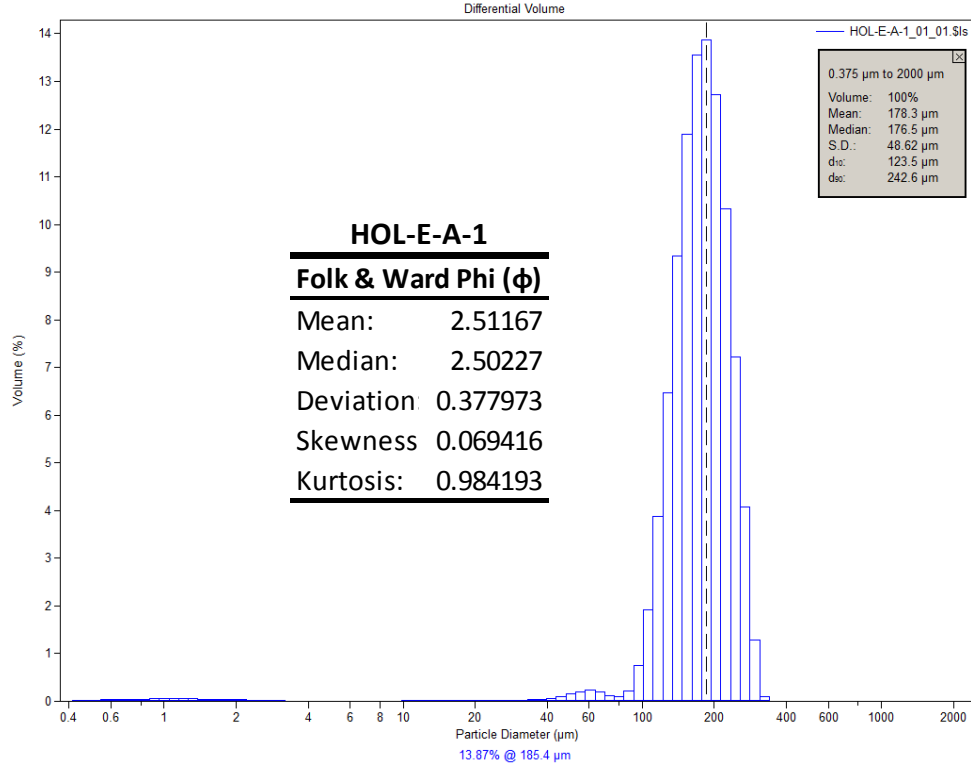
μm	Volume (%)						
0.375198	0.00651797	4.2411	0.004631	47.9397	0.375749	541.892	0
0.411878	0.0124194	4.65572	0.004005	52.6264	0.447459	594.869	0
0.452145	0.0208596	5.11087	0.004024	57.7713	0.481352	653.025	0
0.496347	0.0287399	5.61052	0.004537	63.4192	0.487235	716.866	0
0.544872	0.0361119	6.15902	0.005393	69.6192	0.53477	786.949	0
0.59814	0.0428576	6.76114	0.006435	76.4253	0.762718	863.883	0
0.656615	0.0488626	7.42212	0.007518	83.8969	1.38646	948.338	0
0.720807	0.0539922	8.14773	0.008512	92.0988	2.64947	1041.05	0
0.791275	0.0581233	8.94427	0.009305	101.103	4.67399	1142.83	0
0.868632	0.061133	9.81869	0.009862	110.987	7.32171	1254.55	0
0.953552	0.0629136	10.7786	0.010216	121.837	10.1428	1377.2	0
1.04677	0.0633741	11.8323	0.010579	133.748	12.4779	1511.84	0
1.14911	0.0625562	12.9891	0.011237	146.824	13.6653	1659.64	0
1.26145	0.0605386	14.2589	0.012651	161.177	13.3238	1821.89	0
1.38477	0.0574283	15.6529	0.015282	176.935	11.5047	2000	
1.52015	0.0533698	17.1832	0.019511	194.232	8.65941		
1.66876	0.0485336	18.863	0.025586	213.221	5.50524		
1.8319	0.0431229	20.7071	0.03321	234.066	2.68574		
2.011	0.0373579	22.7315	0.042038	256.948	0.711163		
2.2076	0.0314803	24.9538	0.051769	282.068	0.045583		
2.42342	0.0257312	27.3934	0.063072	309.644	0		
2.66033	0.0203499	30.0714	0.078758	339.916	0		
2.92042	0.0155462	33.0113	0.103629	373.147	0		
3.20592	0.0114942	36.2385	0.144311	409.626	0		
3.51934	0.00830731	39.7813	0.206131	449.672	0		
3.8634	0.00602945	43.6704	0.287514	493.633	0		



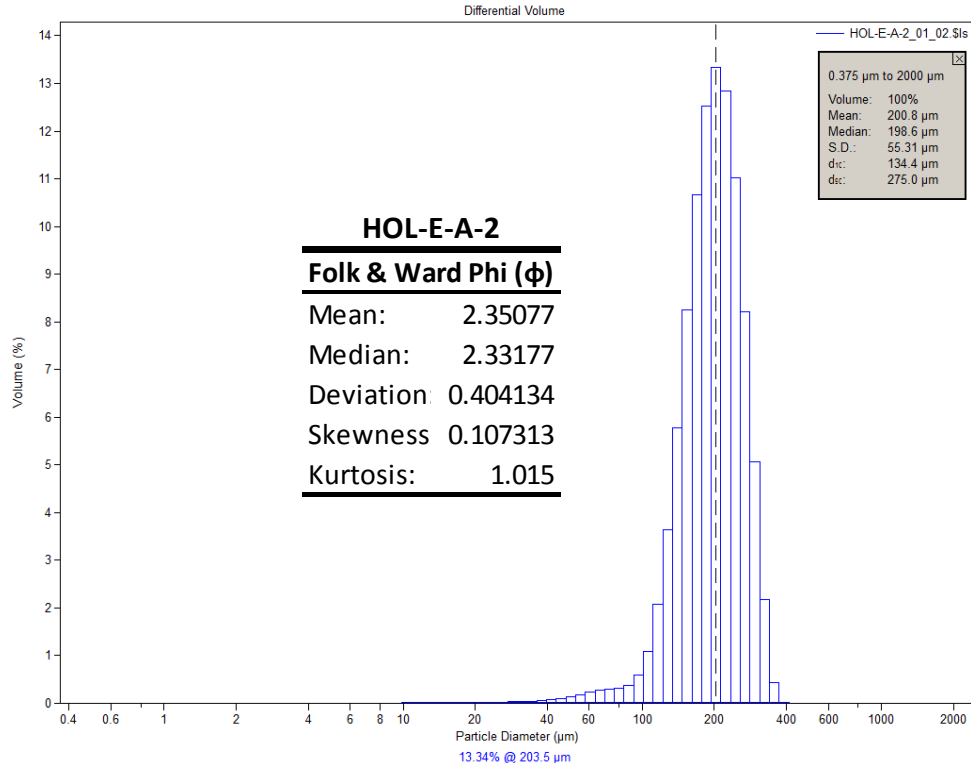
μm	Volume (%)						
0.375198	0.00653049	4.2411	0.00533	47.9397	0.403447	541.892	0
0.411878	0.0124443	4.65572	0.004699	52.6264	0.491899	594.869	0
0.452145	0.0209052	5.11087	0.004726	57.7713	0.561873	653.025	0
0.496347	0.0288103	5.61052	0.005257	63.4192	0.613049	716.866	0
0.544872	0.0362129	6.15902	0.006147	69.6192	0.688859	786.949	0
0.59814	0.0429958	6.76114	0.007239	76.4253	0.893363	863.883	0
0.656615	0.0490453	7.42212	0.008391	83.8969	1.39897	948.338	0
0.720807	0.0542263	8.14773	0.009468	92.0988	2.42193	1041.05	0
0.791275	0.0584162	8.94427	0.010348	101.103	4.1212	1142.83	0
0.868632	0.0614903	9.81869	0.010966	110.987	6.46672	1254.55	0
0.953552	0.0633382	10.7786	0.011313	121.837	9.13957	1377.2	0
1.04677	0.0638677	11.8323	0.011549	133.748	11.5754	1511.84	0
1.14911	0.0631173	12.9891	0.011906	146.824	13.1276	1659.64	0
1.26145	0.0611617	14.2589	0.012849	161.177	13.3048	1821.89	0
1.38477	0.0581058	15.6529	0.014895	176.935	12.0067	2000	
1.52015	0.0540915	17.1832	0.018669	194.232	9.50294		
1.66876	0.0492888	18.863	0.024856	213.221	6.41861		
1.8319	0.0438992	20.7071	0.033781	234.066	3.42936		
2.011	0.0381442	22.7315	0.04578	256.948	1.01379		
2.2076	0.032267	24.9538	0.060827	282.068	0.071327		
2.42342	0.0265105	27.3934	0.07922	309.644	0		
2.66033	0.0211171	30.0714	0.102391	339.916	0		
2.92042	0.0162985	33.0113	0.133072	373.147	0		
3.20592	0.0122316	36.2385	0.175906	409.626	0		
3.51934	0.00903017	39.7813	0.2355	449.672	0		
3.8634	0.00673897	43.6704	0.313237	493.633	0		



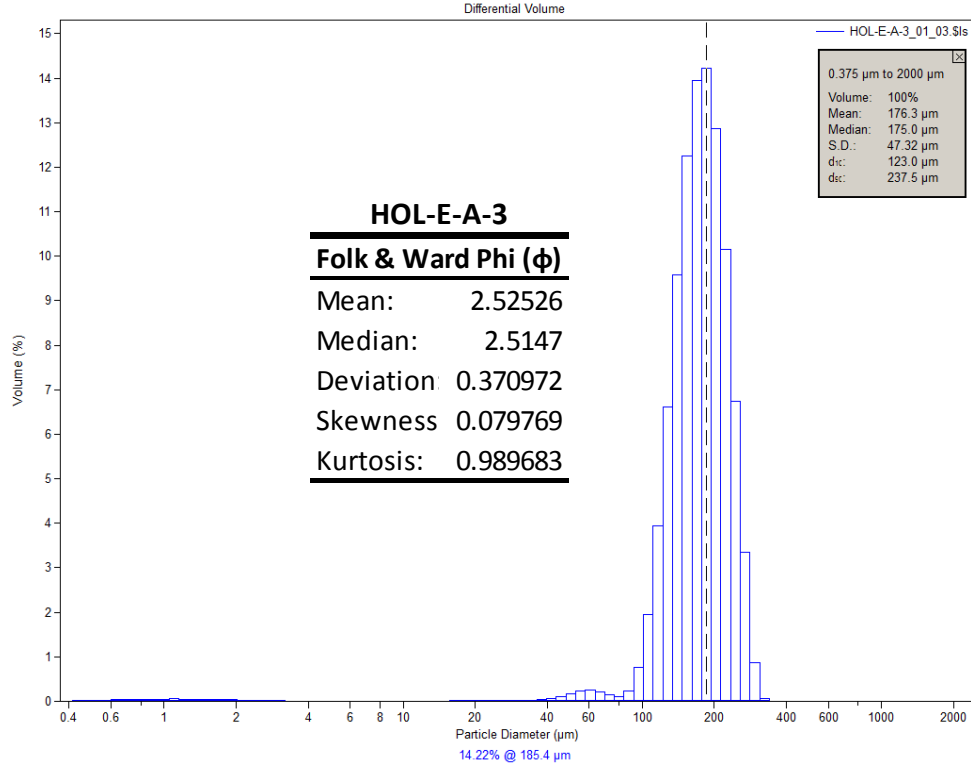
μm	Volume (%)						
0.375198	0.0092362	4.2411	0.014857	47.9397	2.24072	541.892	0
0.411878	0.0176266	4.65572	0.013392	52.6264	2.5733	594.869	0
0.452145	0.0297021	5.11087	0.012891	57.7713	2.90564	653.025	0
0.496347	0.041118	5.61052	0.013104	63.4192	3.28292	716.866	0
0.544872	0.051987	6.15902	0.013797	69.6192	3.77929	786.949	0
0.59814	0.0621741	6.76114	0.014811	76.4253	4.47902	863.883	0
0.656615	0.071539	7.42212	0.016039	83.8969	5.43847	948.338	0
0.720807	0.0798987	8.14773	0.017441	92.0988	6.63533	1041.05	0
0.791275	0.087071	8.94427	0.019	101.103	7.9184	1142.83	0
0.868632	0.0928524	9.81869	0.020784	110.987	8.99786	1254.55	0
0.953552	0.0970415	10.7786	0.022981	121.837	9.52878	1377.2	0
1.04677	0.0994336	11.8323	0.025923	133.748	9.24667	1511.84	0
1.14911	0.0999885	12.9891	0.030233	146.824	8.12305	1659.64	0
1.26145	0.0987126	14.2589	0.036768	161.177	6.41041	1821.89	0
1.38477	0.0956561	15.6529	0.047114	176.935	4.49405	2000	
1.52015	0.0909303	17.1832	0.063728	194.232	2.75887		
1.66876	0.0847072	18.863	0.090586	213.221	1.39497		
1.8319	0.0772328	20.7071	0.13377	234.066	0.405023		
2.011	0.0688211	22.7315	0.201296	256.948	0.028459		
2.2076	0.0598547	24.9538	0.303307	282.068	0		
2.42342	0.0507652	27.3934	0.44967	309.644	0		
2.66033	0.0420038	30.0714	0.648105	339.916	0		
2.92042	0.0340036	33.0113	0.901431	373.147	0		
3.20592	0.0271218	36.2385	1.20381	409.626	0		
3.51934	0.0216024	39.7813	1.54143	449.672	0		
3.8634	0.0175339	43.6704	1.89387	493.633	0		



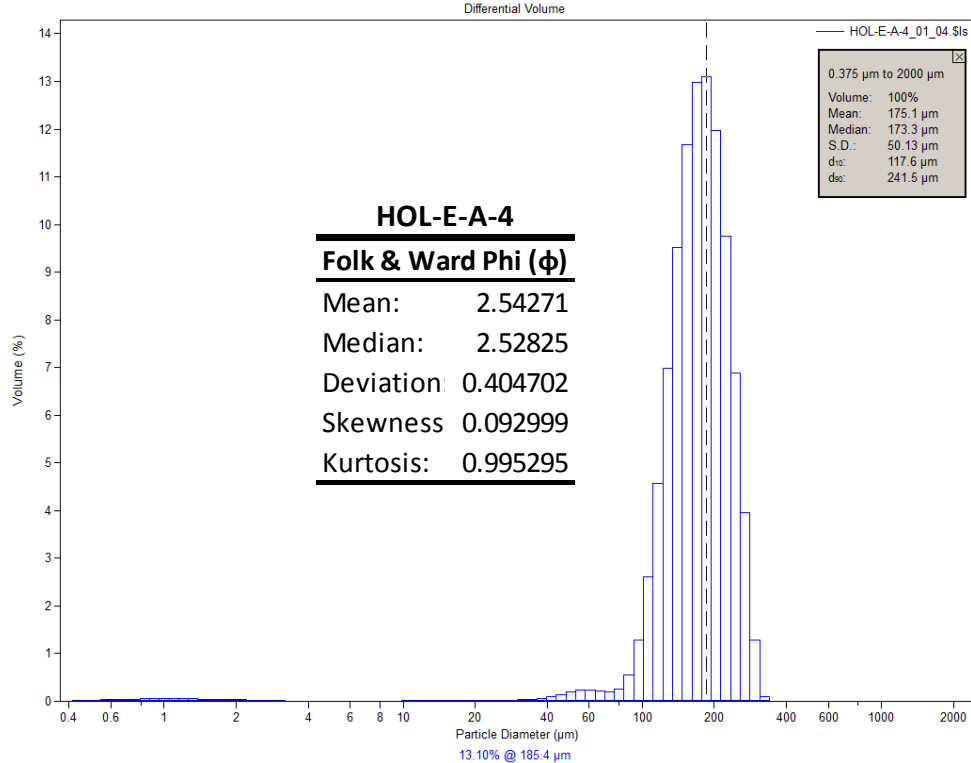
μm	Volume (%)						
0.375198	0.005542	4.2411	0.003029	47.9397	0.153819	541.892	0
0.411878	0.010557	4.65572	0.002598	52.6264	0.206833	594.869	0
0.452145	0.017721	5.11087	0.002768	57.7713	0.229964	653.025	0
0.496347	0.024393	5.61052	0.003431	63.4192	0.198685	716.866	0
0.544872	0.030613	6.15902	0.004473	69.6192	0.125506	786.949	0
0.59814	0.036278	6.76114	0.005756	76.4253	0.096067	863.883	0
0.656615	0.04129	7.42212	0.007136	83.8969	0.222469	948.338	0
0.720807	0.045533	8.14773	0.008472	92.0988	0.743192	1041.05	0
0.791275	0.048906	8.94427	0.009614	101.103	1.92888	1142.83	0
0.868632	0.051309	9.81869	0.010465	110.987	3.87732	1254.55	0
0.953552	0.052655	10.7786	0.010956	121.837	6.47399	1377.2	0
1.04677	0.05288	11.8323	0.011186	133.748	9.34082	1511.84	0
1.14911	0.052028	12.9891	0.011287	146.824	11.8999	1659.64	0
1.26145	0.050176	14.2589	0.011634	161.177	13.562	1821.89	0
1.38477	0.047425	15.6529	0.012552	176.935	13.87	2000	
1.52015	0.043905	17.1832	0.014396	194.232	12.7298		
1.66876	0.039763	18.863	0.017386	213.221	10.3358		
1.8319	0.035174	20.7071	0.021125	234.066	7.22331		
2.011	0.030316	22.7315	0.025059	256.948	4.07886		
2.2076	0.025389	24.9538	0.027929	282.068	1.29058		
2.42342	0.020584	27.3934	0.028998	309.644	0.096019		
2.66033	0.016093	30.0714	0.028911	339.916	0		
2.92042	0.012082	33.0113	0.030243	373.147	0		
3.20592	0.008696	36.2385	0.038428	409.626	0		
3.51934	0.006034	39.7813	0.059805	449.672	0		
3.8634	0.004147	43.6704	0.099116	493.633	0		



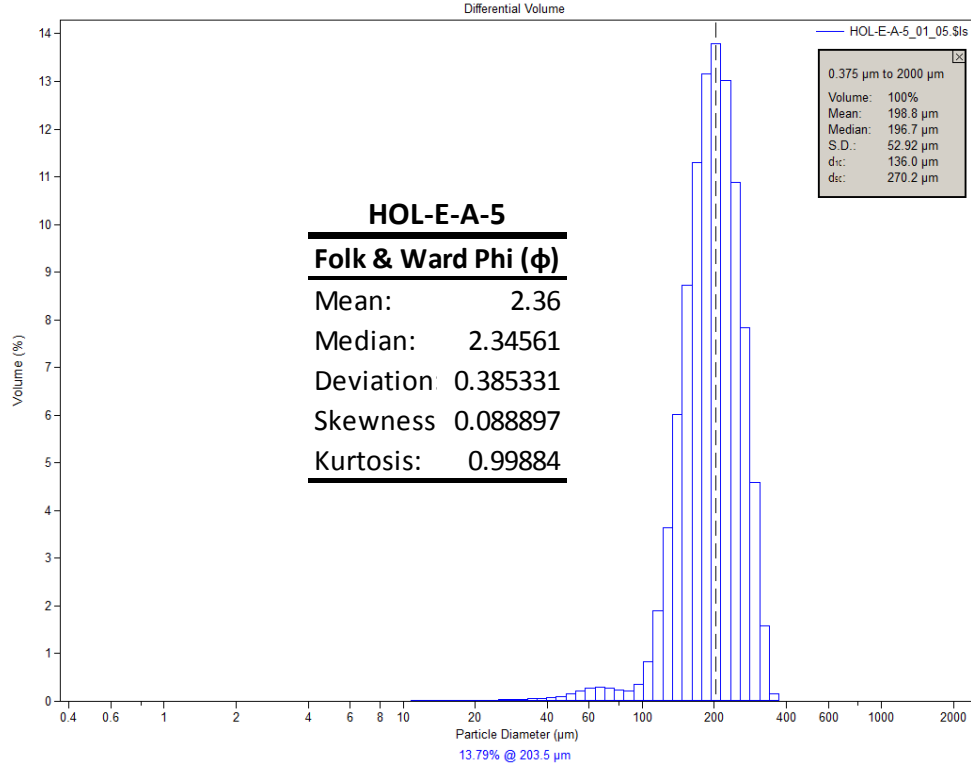
μm	Volume (%)						
0.375198	0	4.2411	0	47.9397	0.128681	541.892	0
0.411878	0	4.65572	4.71E-06	52.6264	0.176033	594.869	0
0.452145	0	5.11087	0.000178	57.7713	0.227545	653.025	0
0.496347	0	5.61052	0.001066	63.4192	0.269434	716.866	0
0.544872	0	6.15902	0.002516	69.6192	0.293082	786.949	0
0.59814	0	6.76114	0.004119	76.4253	0.310259	863.883	0
0.656615	0	7.42212	0.005859	83.8969	0.37445	948.338	0
0.720807	0	8.14773	0.007535	92.0988	0.585492	1041.05	0
0.791275	0	8.94427	0.009026	101.103	1.09313	1142.83	0
0.868632	0	9.81869	0.010165	110.987	2.07595	1254.55	0
0.953552	0	10.7786	0.010882	121.837	3.6437	1377.2	0
1.04677	0	11.8323	0.011165	133.748	5.77035	1511.84	0
1.14911	0	12.9891	0.01111	146.824	8.2441	1659.64	0
1.26145	0	14.2589	0.01099	161.177	10.6579	1821.89	0
1.38477	0	15.6529	0.011105	176.935	12.5231	2000	
1.52015	0	17.1832	0.011928	194.232	13.341		
1.66876	0	18.863	0.013845	213.221	12.8403		
1.8319	0	20.7071	0.017105	234.066	11.0141		
2.011	0	22.7315	0.021847	256.948	8.20351		
2.2076	0	24.9538	0.027649	282.068	5.06782		
2.42342	0	27.3934	0.03405	309.644	2.17568		
2.66033	0	30.0714	0.040567	339.916	0.435451		
2.92042	0	33.0113	0.047406	373.147	0.019421		
3.20592	0	36.2385	0.056254	409.626	0		
3.51934	0	39.7813	0.07007	449.672	0		
3.8634	0	43.6704	0.09315	493.633	0		



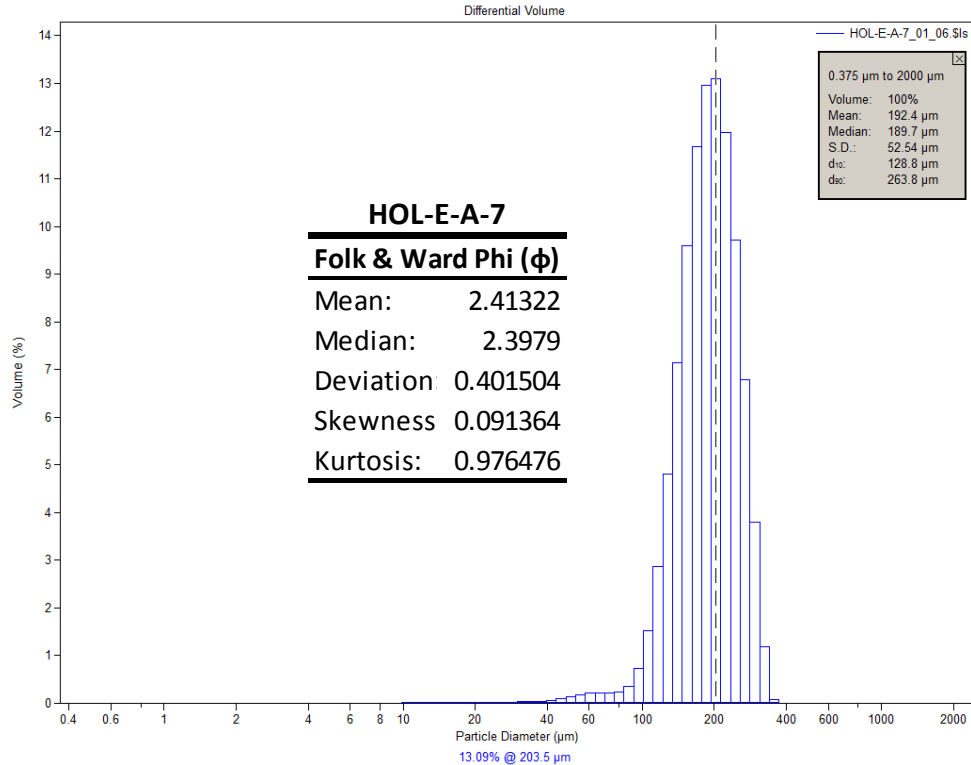
μm	Volume (%)						
0.375198	0.00561716	4.2411	0.002608	47.9397	0.174317	541.892	0
0.411878	0.0106985	4.65572	0.002136	52.6264	0.231418	594.869	0
0.452145	0.017952	5.11087	0.002222	57.7713	0.25551	653.025	0
0.496347	0.0246995	5.61052	0.002754	63.4192	0.22067	716.866	0
0.544872	0.0309788	6.15902	0.003628	69.6192	0.143123	786.949	0
0.59814	0.0366832	6.76114	0.004715	76.4253	0.10872	863.883	0
0.656615	0.0417104	7.42212	0.005882	83.8969	0.231053	948.338	0
0.720807	0.0459448	8.14773	0.00701	92.0988	0.753377	1041.05	0
0.791275	0.0492818	8.94427	0.007971	101.103	1.95399	1142.83	0
0.868632	0.0516225	9.81869	0.008697	110.987	3.94064	1254.55	0
0.953552	0.0528826	10.7786	0.009153	121.837	6.61091	1377.2	0
1.04677	0.0529993	11.8323	0.009466	133.748	9.57582	1511.84	0
1.14911	0.0520242	12.9891	0.009786	146.824	12.2462	1659.64	0
1.26145	0.0500426	14.2589	0.010492	161.177	13.9549	1821.89	0
1.38477	0.0471629	15.6529	0.011883	176.935	14.2173	2000	
1.52015	0.0435237	17.1832	0.014249	194.232	12.8737		
1.66876	0.0392804	18.863	0.017709	213.221	10.1613		
1.8319	0.0346123	20.7071	0.021751	234.066	6.74833		
2.011	0.0297053	22.7315	0.025719	256.948	3.35145		
2.2076	0.0247591	24.9538	0.028346	282.068	0.86697		
2.42342	0.0199631	27.3934	0.02917	309.644	0.053142		
2.66033	0.0155054	30.0714	0.029196	339.916	0		
2.92042	0.011543	33.0113	0.031619	373.147	0		
3.20592	0.00821029	36.2385	0.042413	409.626	0		
3.51934	0.00559266	39.7813	0.068163	449.672	0		
3.8634	0.00372985	43.6704	0.113542	493.633	0		



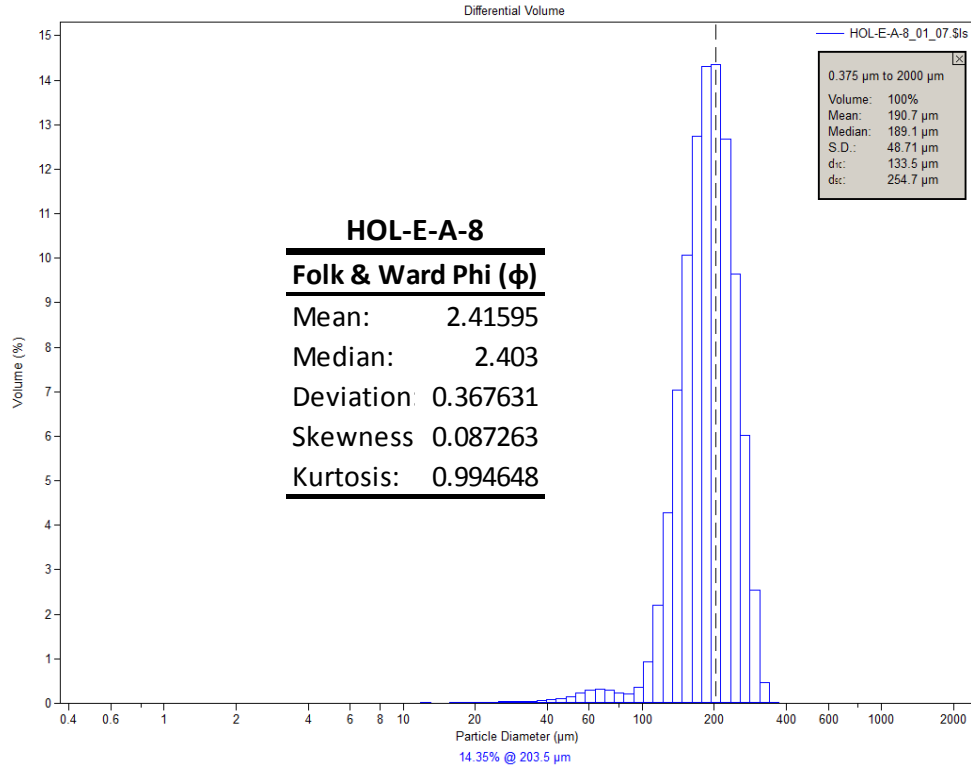
μm	Volume (%)						
0.375198	0.00575031	4.2411	0.003005	47.9397	0.189002	541.892	0
0.411878	0.0109522	4.65572	0.002576	52.6264	0.230196	594.869	0
0.452145	0.0183784	5.11087	0.002732	57.7713	0.24058	653.025	0
0.496347	0.0252879	5.61052	0.003367	63.4192	0.217154	716.866	0
0.544872	0.0317194	6.15902	0.00437	69.6192	0.196362	786.949	0
0.59814	0.0375643	6.76114	0.005607	76.4253	0.262121	863.883	0
0.656615	0.0427183	7.42212	0.006948	83.8969	0.554581	948.338	0
0.720807	0.0470625	8.14773	0.008271	92.0988	1.27802	1041.05	0
0.791275	0.0504909	8.94427	0.009444	101.103	2.60561	1142.83	0
0.868632	0.0529014	9.81869	0.010392	110.987	4.56299	1254.55	0
0.953552	0.0542081	10.7786	0.011067	121.837	6.98942	1377.2	0
1.04677	0.0543452	11.8323	0.011561	133.748	9.52408	1511.84	0
1.14911	0.0533659	12.9891	0.012	146.824	11.6762	1659.64	0
1.26145	0.0513562	14.2589	0.012681	161.177	12.9866	1821.89	0
1.38477	0.0484267	15.6529	0.013851	176.935	13.1018	2000	0
1.52015	0.0447175	17.1832	0.015719	194.232	11.9705		
1.66876	0.0403875	18.863	0.018359	213.221	9.74987		
1.8319	0.0356195	20.7071	0.021387	234.066	6.8782		
2.011	0.0306047	22.7315	0.024422	256.948	3.96125		
2.2076	0.0255469	24.9538	0.026902	282.068	1.28545		
2.42342	0.0206427	27.3934	0.029082	309.644	0.097612		
2.66033	0.0160849	30.0714	0.032733	339.916	0		
2.92042	0.0120384	33.0113	0.040988	373.147	0		
3.20592	0.00864161	36.2385	0.058809	409.626	0		
3.51934	0.00598599	39.7813	0.090656	449.672	0		
3.8634	0.00411205	43.6704	0.136589	493.633	0		



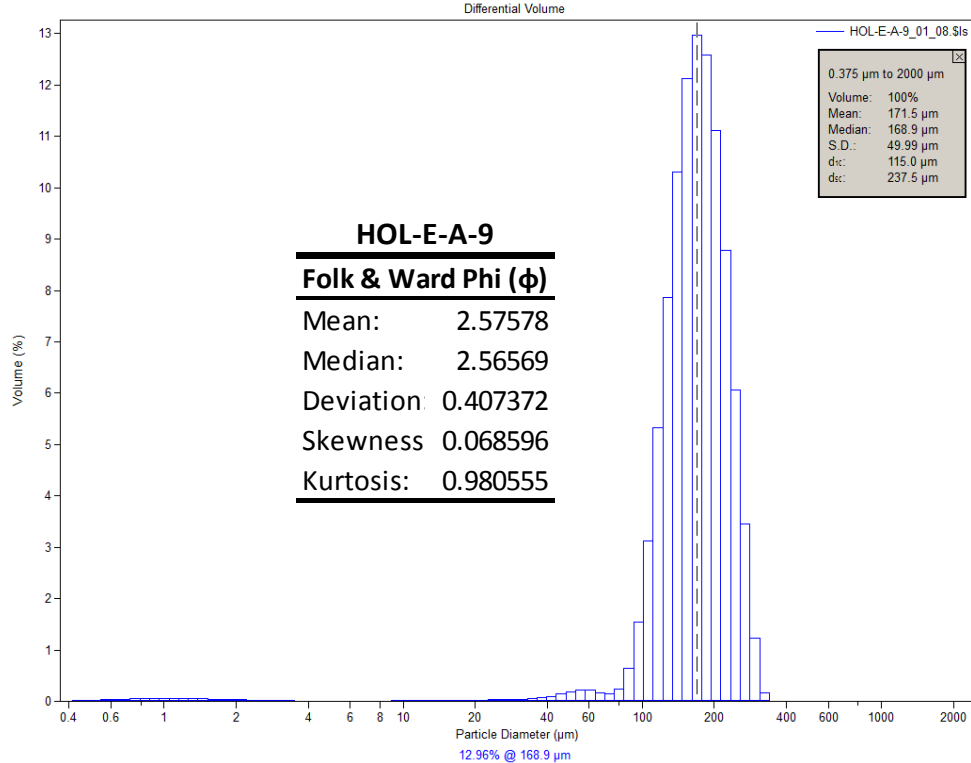
μm	Volume (%)						
0.375198	0	4.2411	0	47.9397	0.153651	541.892	0
0.411878	0	4.65572	9.11E-06	52.6264	0.211991	594.869	0
0.452145	0	5.11087	0.000211	57.7713	0.267878	653.025	0
0.496347	0	5.61052	0.001033	63.4192	0.296787	716.866	0
0.544872	0	6.15902	0.002358	69.6192	0.28072	786.949	0
0.59814	0	6.76114	0.003901	76.4253	0.231267	863.883	0
0.656615	0	7.42212	0.005567	83.8969	0.219777	948.338	0
0.720807	0	8.14773	0.007178	92.0988	0.360411	1041.05	0
0.791275	0	8.94427	0.008593	101.103	0.840306	1142.83	0
0.868632	0	9.81869	0.009667	110.987	1.89504	1254.55	0
0.953552	0	10.7786	0.010327	121.837	3.64287	1377.2	0
1.04677	0	11.8323	0.010601	133.748	6.01788	1511.84	0
1.14911	0	12.9891	0.010604	146.824	8.73353	1659.64	0
1.26145	0	14.2589	0.010676	161.177	11.2923	1821.89	0
1.38477	0	15.6529	0.011158	176.935	13.1501	2000	
1.52015	0	17.1832	0.012561	194.232	13.7934		
1.66876	0	18.863	0.015311	213.221	13.0137		
1.8319	0	20.7071	0.019589	234.066	10.8786		
2.011	0	22.7315	0.025428	256.948	7.82719		
2.2076	0	24.9538	0.03214	282.068	4.58596		
2.42342	0	27.3934	0.03902	309.644	1.57304		
2.66033	0	30.0714	0.045497	339.916	0.151799		
2.92042	0	33.0113	0.05213	373.147	0.000586		
3.20592	0	36.2385	0.061599	409.626	0		
3.51934	0	39.7813	0.078279	449.672	0		
3.8634	0	43.6704	0.107889	493.633	0		



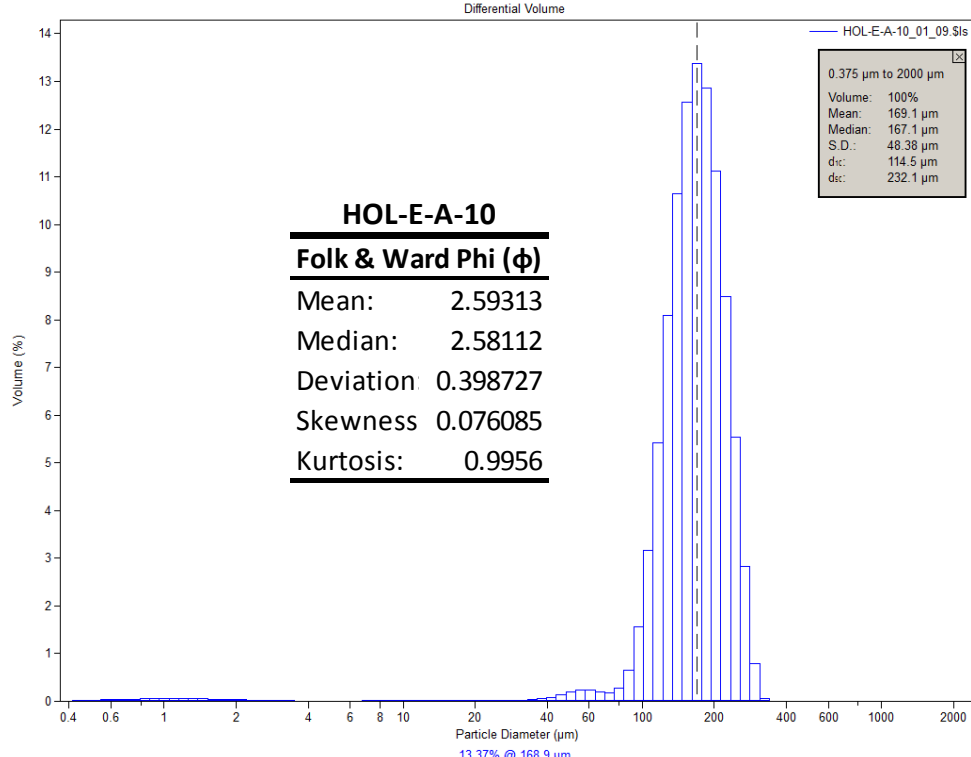
μm	Volume (%)						
0.375198	0	4.2411	0	47.9397	0.134845	541.892	0
0.411878	0	4.65572	2.59E-05	52.6264	0.179586	594.869	0
0.452145	0	5.11087	0.0004	57.7713	0.213809	653.025	0
0.496347	0	5.61052	0.001471	63.4192	0.224614	716.866	0
0.544872	0	6.15902	0.002952	69.6192	0.217798	786.949	0
0.59814	0	6.76114	0.004668	76.4253	0.23411	863.883	0
0.656615	0	7.42212	0.006479	83.8969	0.357626	948.338	0
0.720807	0	8.14773	0.008215	92.0988	0.727476	1041.05	0
0.791275	0	8.94427	0.009722	101.103	1.52105	1142.83	0
0.868632	0	9.81869	0.010869	110.987	2.87651	1254.55	0
0.953552	0	10.7786	0.011582	121.837	4.80406	1377.2	0
1.04677	0	11.8323	0.011901	133.748	7.1512	1511.84	0
1.14911	0	12.9891	0.011937	146.824	9.58912	1659.64	0
1.26145	0	14.2589	0.011995	161.177	11.6729	1821.89	0
1.38477	0	15.6529	0.012363	176.935	12.9609	2000	
1.52015	0	17.1832	0.013408	194.232	13.0937		
1.66876	0	18.863	0.015376	213.221	11.9694		
1.8319	0	20.7071	0.018211	234.066	9.71625		
2.011	0	22.7315	0.021746	256.948	6.78392		
2.2076	0	24.9538	0.025341	282.068	3.79869		
2.42342	0	27.3934	0.028647	309.644	1.18542		
2.66033	0	30.0714	0.031932	339.916	0.087168		
2.92042	0	33.0113	0.036675	373.147	0		
3.20592	0	36.2385	0.046073	409.626	0		
3.51934	0	39.7813	0.064022	449.672	0		
3.8634	0	43.6704	0.093826	493.633	0		



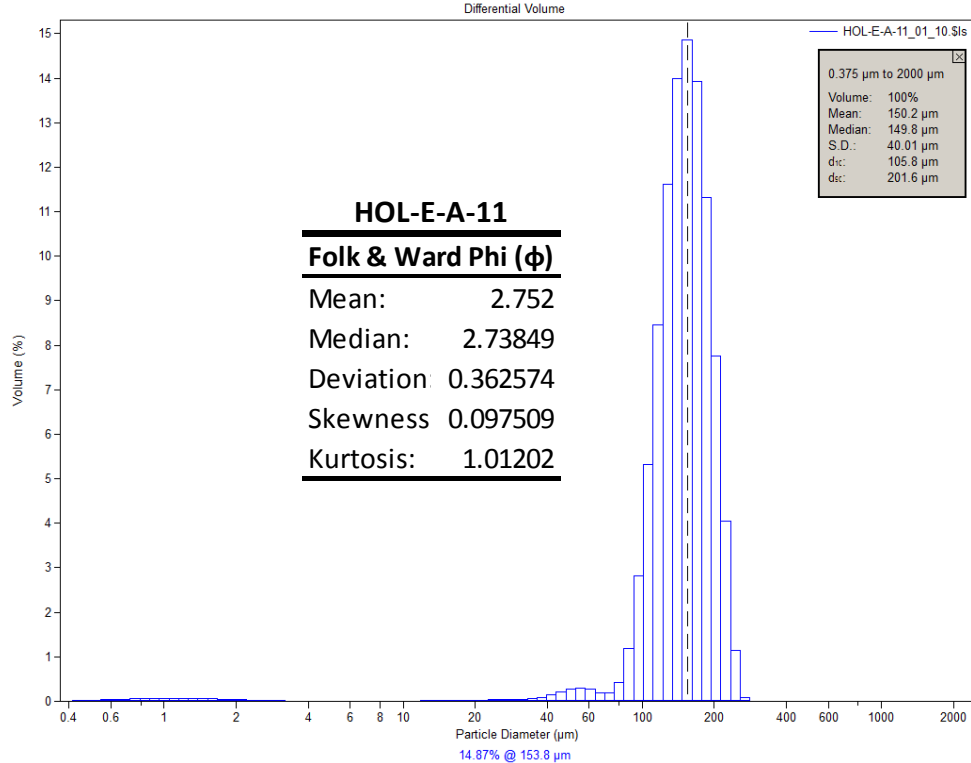
μm	Volume (%)						
0.375198	0	4.2411	0	47.9397	0.158042	541.892	0
0.411878	0	4.65572	2.39E-05	52.6264	0.22601	594.869	0
0.452145	0	5.11087	0.000365	57.7713	0.29172	653.025	0
0.496347	0	5.61052	0.00134	63.4192	0.325389	716.866	0
0.544872	0	6.15902	0.002719	69.6192	0.299467	786.949	0
0.59814	0	6.76114	0.004339	76.4253	0.23265	863.883	0
0.656615	0	7.42212	0.006043	83.8969	0.208976	948.338	0
0.720807	0	8.14773	0.007661	92.0988	0.360917	1041.05	0
0.791275	0	8.94427	0.009027	101.103	0.933739	1142.83	0
0.868632	0	9.81869	0.010007	110.987	2.20121	1254.55	0
0.953552	0	10.7786	0.01051	121.837	4.27901	1377.2	0
1.04677	0	11.8323	0.0106	133.748	7.04604	1511.84	0
1.14911	0	12.9891	0.010405	146.824	10.0722	1659.64	0
1.26145	0	14.2589	0.010334	161.177	12.7371	1821.89	0
1.38477	0	15.6529	0.010791	176.935	14.3202	2000	
1.52015	0	17.1832	0.012321	194.232	14.3487		
1.66876	0	18.863	0.015444	213.221	12.6757		
1.8319	0	20.7071	0.02025	234.066	9.63883		
2.011	0	22.7315	0.026686	256.948	6.02835		
2.2076	0	24.9538	0.033797	282.068	2.54296		
2.42342	0	27.3934	0.040473	309.644	0.473844		
2.66033	0	30.0714	0.046074	339.916	0.01866		
2.92042	0	33.0113	0.051026	373.147	0		
3.20592	0	36.2385	0.058788	409.626	0		
3.51934	0	39.7813	0.074934	449.672	0		
3.8634	0	43.6704	0.10625	493.633	0		



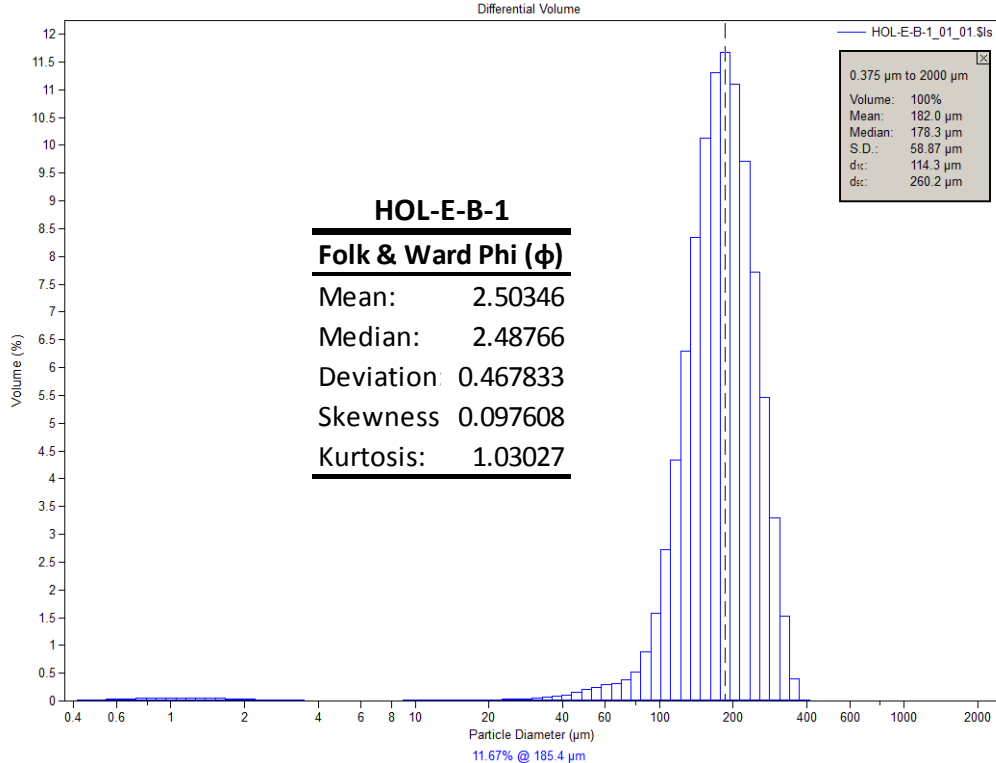
μm	Volume (%)						
0.375198	0.0058416	4.2411	0.003727	47.9397	0.191248	541.892	0
0.411878	0.0111264	4.65572	0.003298	52.6264	0.221532	594.869	0
0.452145	0.0186732	5.11087	0.003455	57.7713	0.21333	653.025	0
0.496347	0.0256983	5.61052	0.004081	63.4192	0.17077	716.866	0
0.544872	0.0322424	6.15902	0.005056	69.6192	0.148676	786.949	0
0.59814	0.0381955	6.76114	0.006243	76.4253	0.244908	863.883	0
0.656615	0.0434531	7.42212	0.00751	83.8969	0.63571	948.338	0
0.720807	0.0478944	8.14773	0.008734	92.0988	1.55181	1041.05	0
0.791275	0.0514118	8.94427	0.009792	101.103	3.12938	1142.83	0
0.868632	0.0539015	9.81869	0.01062	110.987	5.31931	1254.55	0
0.953552	0.0552749	10.7786	0.011197	121.837	7.85946	1377.2	0
1.04677	0.0554637	11.8323	0.011654	133.748	10.3001	1511.84	0
1.14911	0.0545205	12.9891	0.01217	146.824	12.1319	1659.64	0
1.26145	0.05253	14.2589	0.013094	161.177	12.9625	1821.89	0
1.38477	0.0496015	15.6529	0.014725	176.935	12.5894	2000	
1.52015	0.0458768	17.1832	0.017283	194.232	11.1124		
1.66876	0.041515	18.863	0.020814	213.221	8.78969		
1.8319	0.036701	20.7071	0.024826	234.066	6.06493		
2.011	0.0316296	22.7315	0.028765	256.948	3.44917		
2.2076	0.026509	24.9538	0.031897	282.068	1.231		
2.42342	0.0215412	27.3934	0.034379	309.644	0.157449		
2.66033	0.016925	30.0714	0.038073	339.916	0.002749		
2.92042	0.0128302	33.0113	0.046403	373.147	0		
3.20592	0.00939906	36.2385	0.064643	409.626	0		
3.51934	0.00672324	39.7813	0.097136	449.672	0		
3.8634	0.00483981	43.6704	0.142796	493.633	0		



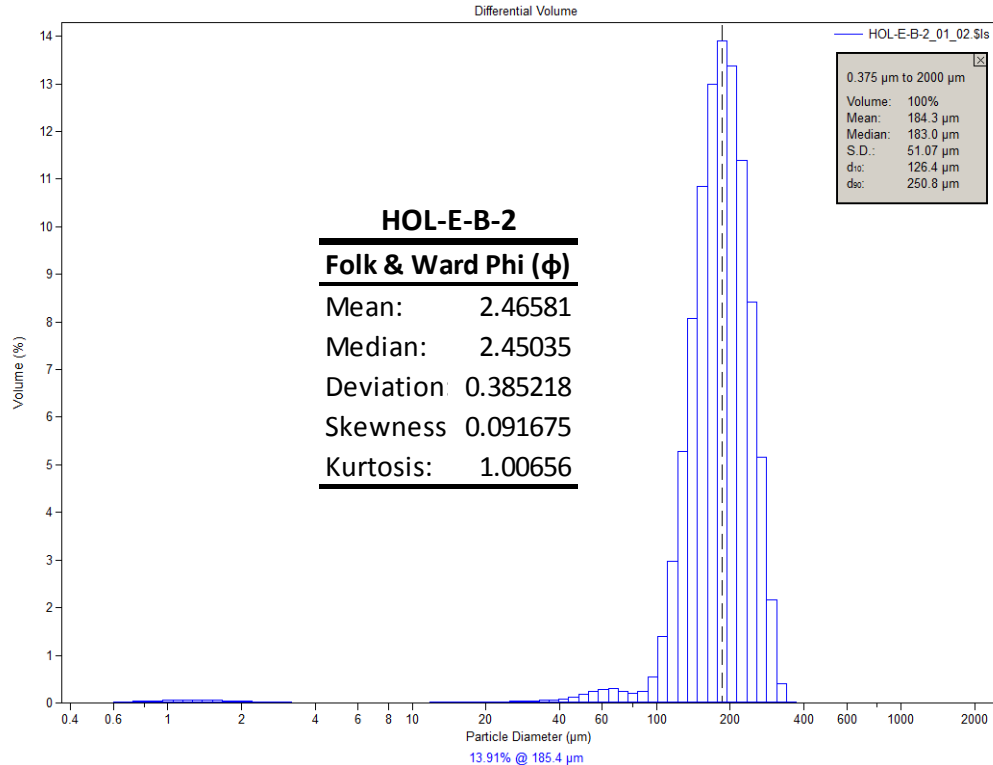
μm	Volume (%)						
0.375198	0.00595524	4.2411	0.007086	47.9397	0.190101	541.892	0
0.411878	0.0113422	4.65572	0.006883	52.6264	0.234142	594.869	0
0.452145	0.0190341	5.11087	0.007244	57.7713	0.240732	653.025	0
0.496347	0.0261924	5.61052	0.008031	63.4192	0.207514	716.866	0
0.544872	0.0328588	6.15902	0.009104	69.6192	0.185348	786.949	0
0.59814	0.0389216	6.76114	0.010311	76.4253	0.274897	863.883	0
0.656615	0.044275	7.42212	0.011512	83.8969	0.651179	948.338	0
0.720807	0.0487972	8.14773	0.012566	92.0988	1.56011	1041.05	0
0.791275	0.0523812	8.94427	0.013344	101.103	3.16262	1142.83	0
0.868632	0.0549231	9.81869	0.013775	110.987	5.42725	1254.55	0
0.953552	0.0563376	10.7786	0.013847	121.837	8.08551	1377.2	0
1.04677	0.0565591	11.8323	0.013715	133.748	10.6524	1511.84	0
1.14911	0.055645	12.9891	0.013582	146.824	12.57	1659.64	0
1.26145	0.0536854	14.2589	0.013853	161.177	13.3742	1821.89	0
1.38477	0.0507959	15.6529	0.014846	176.935	12.8541	2000	
1.52015	0.0471232	17.1832	0.016804	194.232	11.1101		
1.66876	0.0428325	18.863	0.019731	213.221	8.48718		
1.8319	0.0381133	20.7071	0.023021	234.066	5.54577		
2.011	0.0331635	22.7315	0.02594	256.948	2.82561		
2.2076	0.0281949	24.9538	0.027483	282.068	0.786927		
2.42342	0.0234103	27.3934	0.027711	309.644	0.052582		
2.66033	0.0190078	30.0714	0.028565	339.916	0		
2.92042	0.0151542	33.0113	0.033932	373.147	0		
3.20592	0.0119836	36.2385	0.049927	409.626	0		
3.51934	0.00957676	39.7813	0.082415	449.672	0		
3.8634	0.00795416	43.6704	0.132312	493.633	0		



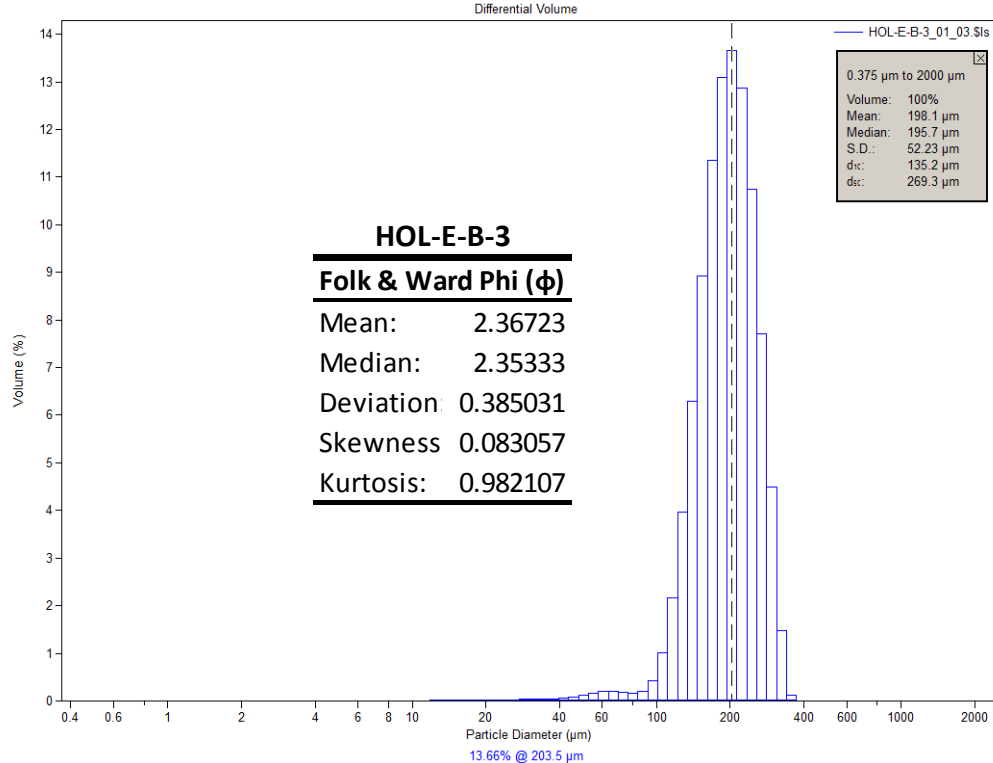
μm	Volume (%)						
0.375198	0.00678915	4.2411	0.003884	47.9397	0.274769	541.892	0
0.411878	0.0129314	4.65572	0.00332	52.6264	0.302714	594.869	0
0.452145	0.0217034	5.11087	0.0034	57.7713	0.266029	653.025	0
0.496347	0.0298702	5.61052	0.003983	63.4192	0.192254	716.866	0
0.544872	0.0374794	6.15902	0.004923	69.6192	0.187365	786.949	0
0.59814	0.0444032	6.76114	0.006064	76.4253	0.418755	863.883	0
0.656615	0.0505199	7.42212	0.007259	83.8969	1.19543	948.338	0
0.720807	0.0556892	8.14773	0.008375	92.0988	2.81123	1041.05	0
0.791275	0.0597852	8.94427	0.009296	101.103	5.32516	1142.83	0
0.868632	0.0626859	9.81869	0.009984	110.987	8.4629	1254.55	0
0.953552	0.0642875	10.7786	0.010475	121.837	11.6207	1377.2	0
1.04677	0.0645094	11.8323	0.010984	133.748	13.9912	1511.84	0
1.14911	0.0634101	12.9891	0.011799	146.824	14.8682	1659.64	0
1.26145	0.0610872	14.2589	0.013351	161.177	13.9216	1821.89	0
1.38477	0.0576676	15.6529	0.016024	176.935	11.315	2000	
1.52015	0.053313	17.1832	0.019964	194.232	7.74924		
1.66876	0.0482111	18.863	0.025023	213.221	4.05947		
1.8319	0.0425758	20.7071	0.030278	234.066	1.13719		
2.011	0.0366362	22.7315	0.034662	256.948	0.075525		
2.2076	0.030636	24.9538	0.037279	282.068	0		
2.42342	0.0248144	27.3934	0.038817	309.644	0		
2.66033	0.0194041	30.0714	0.042949	339.916	0		
2.92042	0.0146064	33.0113	0.055711	373.147	0		
3.20592	0.0105846	36.2385	0.085357	409.626	0		
3.51934	0.00744398	39.7813	0.137819	449.672	0		
3.8634	0.00522166	43.6704	0.208077	493.633	0		



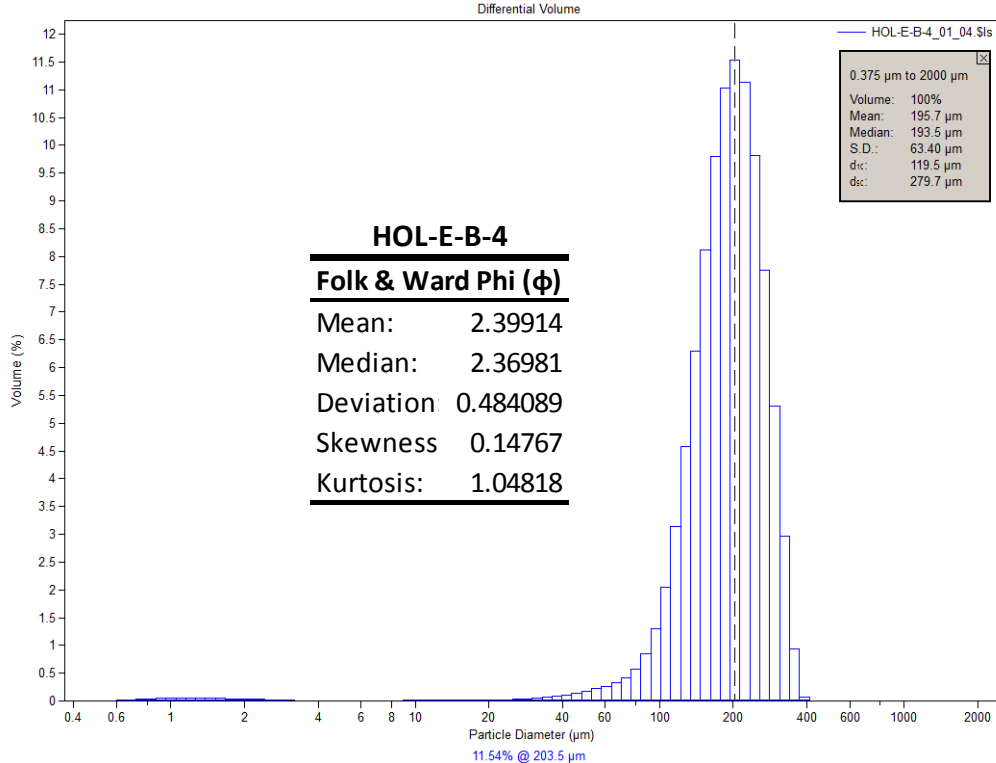
μm	Volume (%)						
0.375198	0.00547747	4.2411	0.003669	47.9397	0.202282	541.892	0
0.411878	0.0104348	4.65572	0.003152	52.6264	0.249454	594.869	0
0.452145	0.0175194	5.11087	0.003197	57.7713	0.287225	653.025	0
0.496347	0.0241242	5.61052	0.003691	63.4192	0.319256	716.866	0
0.544872	0.0302902	6.15902	0.004527	69.6192	0.376024	786.949	0
0.59814	0.0359164	6.76114	0.005581	76.4253	0.525113	863.883	0
0.656615	0.0409059	7.42212	0.006734	83.8969	0.876822	948.338	0
0.720807	0.045146	8.14773	0.007872	92.0988	1.5704	1041.05	0
0.791275	0.048535	8.94427	0.008882	101.103	2.71841	1142.83	0
0.868632	0.0509731	9.81869	0.009691	110.987	4.33748	1254.55	0
0.953552	0.0523738	10.7786	0.010267	121.837	6.30111	1377.2	0
1.04677	0.052668	11.8323	0.010693	133.748	8.34563	1511.84	0
1.14911	0.0518974	12.9891	0.011095	146.824	10.1265	1659.64	0
1.26145	0.050135	14.2589	0.011748	161.177	11.3104	1821.89	0
1.38477	0.0474773	15.6529	0.012915	176.935	11.6665	2000	
1.52015	0.0440495	17.1832	0.014883	194.232	11.1078		
1.66876	0.0399973	18.863	0.017883	213.221	9.71888		
1.8319	0.0354908	20.7071	0.021863	234.066	7.72504		
2.011	0.0307115	22.7315	0.026813	256.948	5.4563		
2.2076	0.0258557	24.9538	0.032538	282.068	3.29191		
2.42342	0.0211163	27.3934	0.039301	309.644	1.53372		
2.66033	0.0166843	30.0714	0.048231	339.916	0.392867		
2.92042	0.012725	33.0113	0.061338	373.147	0.024755		
3.20592	0.00937802	36.2385	0.08181	409.626	0		
3.51934	0.00673491	39.7813	0.112449	449.672	0		
3.8634	0.004837	43.6704	0.15382	493.633	0		



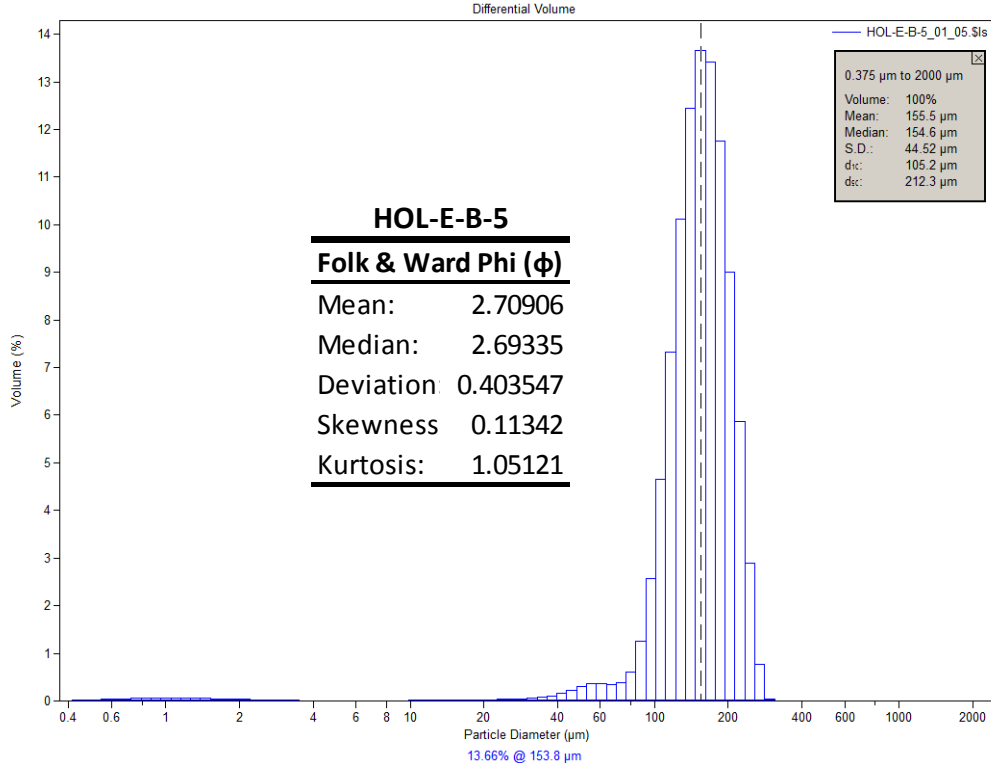
µm	Volume (%)	µm	Volume (%)	µm	Volume (%)	µm	Volume (%)
0.375198	0	4.2411	0.00108	47.9397	0.1795	541.892	0
0.411878	0	4.65572	0.000686	52.6264	0.24378	594.869	0
0.452145	0	5.11087	0.000935	57.7713	0.292345	653.025	0
0.496347	0.000378521	5.61052	0.001755	63.4192	0.296982	716.866	0
0.544872	0.00508721	6.15902	0.003014	69.6192	0.246917	786.949	0
0.59814	0.0156036	6.76114	0.004523	76.4253	0.192892	863.883	0
0.656615	0.0258814	7.42212	0.006101	83.8969	0.23755	948.338	0
0.720807	0.0349975	8.14773	0.007587	92.0988	0.546607	1041.05	0
0.791275	0.0428887	8.94427	0.008816	101.103	1.39184	1142.83	0
0.868632	0.0493007	9.81869	0.009677	110.987	2.9705	1254.55	0
0.953552	0.0540206	10.7786	0.010106	121.837	5.28292	1377.2	0
1.04677	0.0568598	11.8323	0.010215	133.748	8.07866	1511.84	0
1.14911	0.0578487	12.9891	0.010175	146.824	10.8479	1659.64	0
1.26145	0.0570924	14.2589	0.010434	161.177	12.984	1821.89	0
1.38477	0.0547578	15.6529	0.011423	176.935	13.9114	2000	
1.52015	0.0510703	17.1832	0.01366	194.232	13.3664		
1.66876	0.0462965	18.863	0.017602	213.221	11.3978		
1.8319	0.0407375	20.7071	0.023147	234.066	8.42615		
2.011	0.0347053	22.7315	0.029987	256.948	5.15929		
2.2076	0.0285189	24.9538	0.036979	282.068	2.16264		
2.42342	0.0224758	27.3934	0.043077	309.644	0.410212		
2.66033	0.0168539	30.0714	0.048158	339.916	0.016847		
2.92042	0.0118783	33.0113	0.053622	373.147	0		
3.20592	0.00773161	36.2385	0.063945	409.626	0		
3.51934	0.00452097	39.7813	0.085186	449.672	0		
3.8634	0.00230645	43.6704	0.123168	493.633	0		



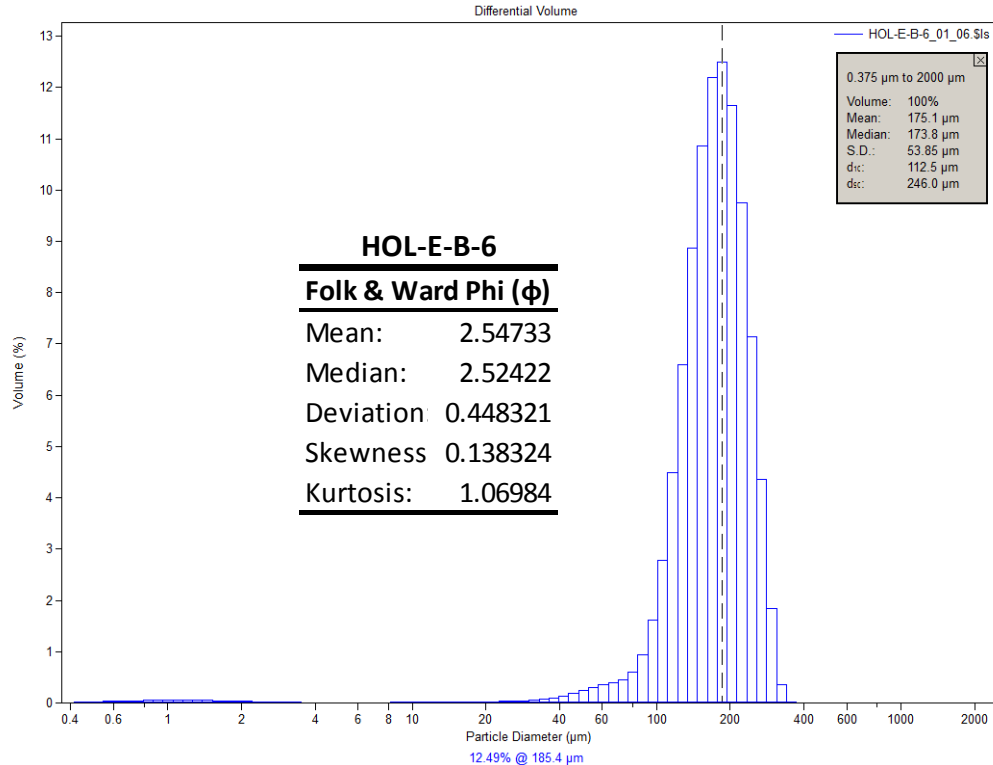
μm	Volume (%)						
0.375198	0	4.2411	0	47.9397	0.121909	541.892	0
0.411878	0	4.65572	1.94E-06	52.6264	0.1661	594.869	0
0.452145	0	5.11087	0.000132	57.7713	0.202185	653.025	0
0.496347	0	5.61052	0.000936	63.4192	0.211288	716.866	0
0.544872	0	6.15902	0.002302	69.6192	0.187737	786.949	0
0.59814	0	6.76114	0.003783	76.4253	0.158426	863.883	0
0.656615	0	7.42212	0.005392	83.8969	0.194563	948.338	0
0.720807	0	8.14773	0.006939	92.0988	0.415894	1041.05	0
0.791275	0	8.94427	0.008316	101.103	1.01088	1142.83	0
0.868632	0	9.81869	0.009374	110.987	2.16699	1254.55	0
0.953552	0	10.7786	0.010071	121.837	3.95933	1377.2	0
1.04677	0	11.8323	0.01043	133.748	6.30294	1511.84	0
1.14911	0	12.9891	0.010586	146.824	8.92036	1659.64	0
1.26145	0	14.2589	0.010847	161.177	11.351	1821.89	0
1.38477	0	15.6529	0.011525	176.935	13.0929	2000	
1.52015	0	17.1832	0.013035	194.232	13.6642		
1.66876	0	18.863	0.015633	213.221	12.8597		
1.8319	0	20.7071	0.0193	234.066	10.7348		
2.011	0	22.7315	0.02379	256.948	7.71113		
2.2076	0	24.9538	0.028294	282.068	4.49681		
2.42342	0	27.3934	0.032193	309.644	1.47296		
2.66033	0	30.0714	0.035274	339.916	0.112642		
2.92042	0	33.0113	0.03866	373.147	0		
3.20592	0	36.2385	0.04527	409.626	0		
3.51934	0	39.7813	0.059043	449.672	0		
3.8634	0	43.6704	0.084291	493.633	0		



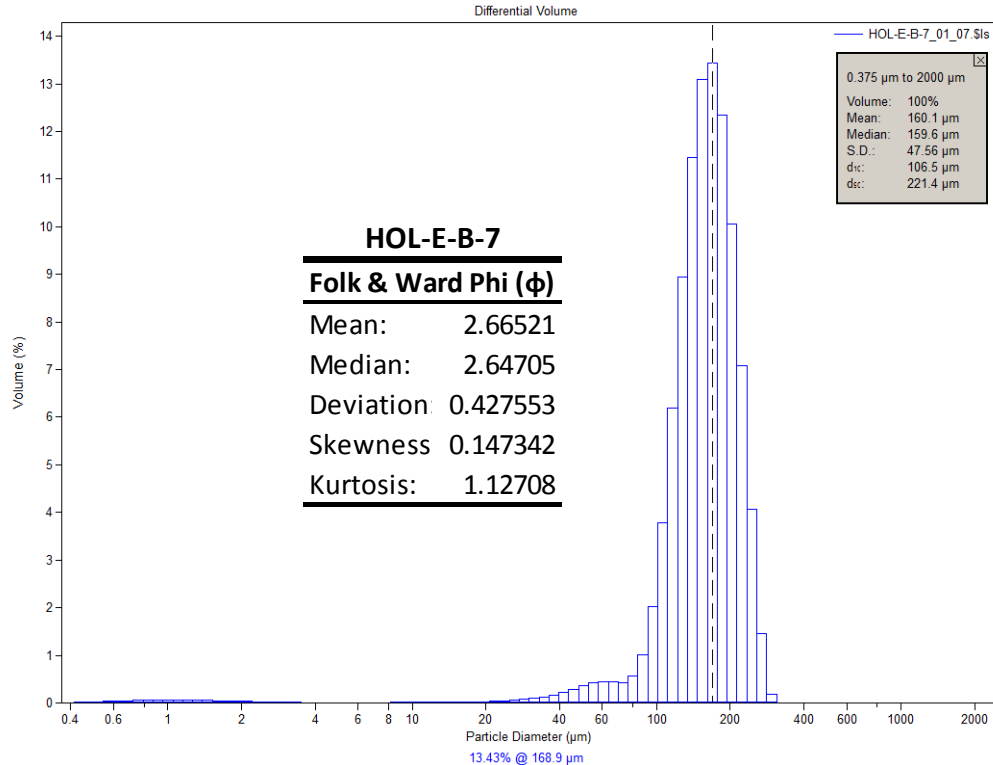
μm	Volume (%)						
0.375198	0	4.2411	0.001167	47.9397	0.174783	541.892	0
0.411878	0	4.65572	0.000913	52.6264	0.218195	594.869	0
0.452145	0	5.11087	0.00126	57.7713	0.268215	653.025	0
0.496347	0.00036027	5.61052	0.002138	63.4192	0.330106	716.866	0
0.544872	0.00484119	6.15902	0.00341	69.6192	0.419794	786.949	0
0.59814	0.0148454	6.76114	0.004909	76.4253	0.571861	863.883	0
0.656615	0.0246116	7.42212	0.006482	83.8969	0.841685	948.338	0
0.720807	0.0332567	8.14773	0.007992	92.0988	1.30706	1041.05	0
0.791275	0.040717	8.94427	0.009298	101.103	2.0524	1142.83	0
0.868632	0.0467487	9.81869	0.010296	110.987	3.13898	1254.55	0
0.953552	0.0511495	10.7786	0.010919	121.837	4.5792	1377.2	0
1.04677	0.0537424	11.8323	0.011204	133.748	6.29477	1511.84	0
1.14911	0.0545635	12.9891	0.011243	146.824	8.1186	1659.64	0
1.26145	0.0537199	14.2589	0.011282	161.177	9.79607	1821.89	0
1.38477	0.0513806	15.6529	0.01159	176.935	11.0246	2000	
1.52015	0.0477687	17.1832	0.01251	194.232	11.5368		
1.66876	0.0431489	18.863	0.014408	213.221	11.1328		
1.8319	0.0378131	20.7071	0.017517	234.066	9.81713		
2.011	0.0320672	22.7315	0.022192	256.948	7.75303		
2.2076	0.0262157	24.9538	0.0286	282.068	5.30666		
2.42342	0.0205445	27.3934	0.037068	309.644	2.96039		
2.66033	0.0153119	30.0714	0.048176	339.916	0.937701		
2.92042	0.0107289	33.0113	0.062591	373.147	0.070345		
3.20592	0.00695645	36.2385	0.081577	409.626	0		
3.51934	0.00409039	39.7813	0.106191	449.672	0		
3.8634	0.00217109	43.6704	0.137186	493.633	0		



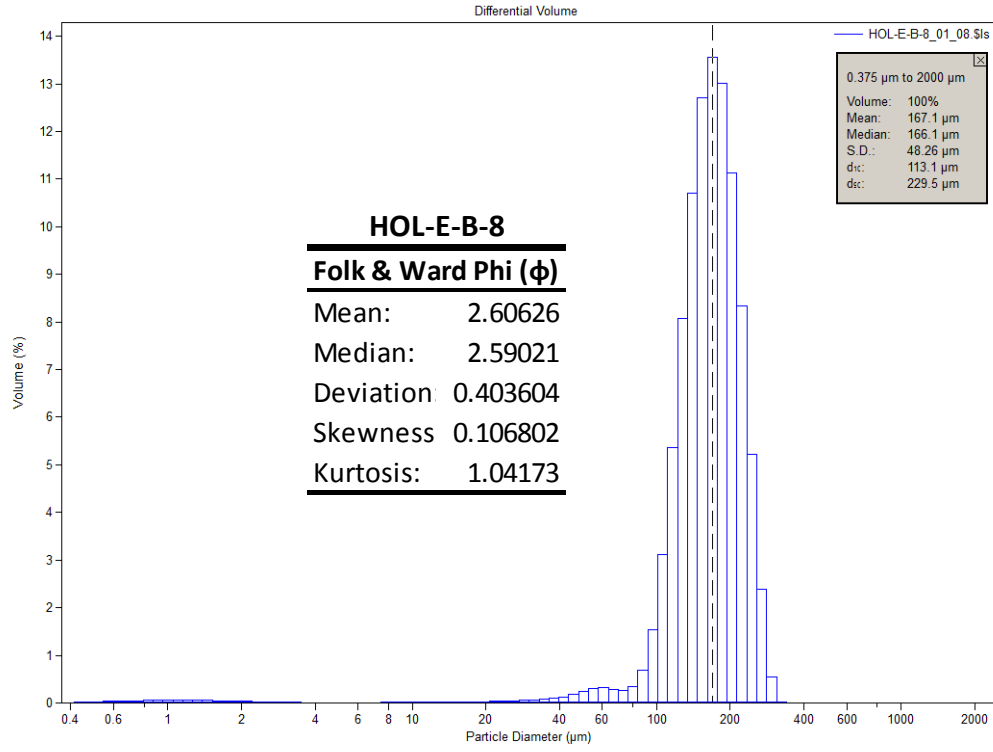
μm	Volume (%)						
0.375198	0.00631852	4.2411	0.00406	47.9397	0.304021	541.892	0
0.411878	0.0120351	4.65572	0.003532	52.6264	0.357109	594.869	0
0.452145	0.0202001	5.11087	0.003625	57.7713	0.36734	653.025	0
0.496347	0.0278032	5.61052	0.004209	63.4192	0.350381	716.866	0
0.544872	0.0348895	6.15902	0.005148	69.6192	0.383889	786.949	0
0.59814	0.041341	6.76114	0.006294	76.4253	0.611312	863.883	0
0.656615	0.0470452	7.42212	0.007504	83.8969	1.2604	948.338	0
0.720807	0.0518724	8.14773	0.008647	92.0988	2.57463	1041.05	0
0.791275	0.0557057	8.94427	0.009594	101.103	4.64944	1142.83	0
0.868632	0.0584335	9.81869	0.010291	110.987	7.31813	1254.55	0
0.953552	0.0599592	10.7786	0.010741	121.837	10.1247	1377.2	0
1.04677	0.0602076	11.8323	0.01112	133.748	12.4426	1511.84	0
1.14911	0.0592328	12.9891	0.011678	146.824	13.6559	1659.64	0
1.26145	0.0571242	14.2589	0.012823	161.177	13.4178	1821.89	0
1.38477	0.0539975	15.6529	0.014943	176.935	11.7463	2000	
1.52015	0.0500013	17.1832	0.018289	194.232	9.01162		
1.66876	0.045306	18.863	0.022925	213.221	5.86019		
1.8319	0.0401084	20.7071	0.02834	234.066	2.89861		
2.011	0.0346178	22.7315	0.033952	256.948	0.763677		
2.2076	0.0290587	24.9538	0.039308	282.068	0.048177		
2.42342	0.023652	27.3934	0.045055	309.644	0		
2.66033	0.0186143	30.0714	0.054162	339.916	0		
2.92042	0.0141345	33.0113	0.071655	373.147	0		
3.20592	0.0103682	36.2385	0.104359	409.626	0		
3.51934	0.00741782	39.7813	0.157682	449.672	0		
3.8634	0.00532372	43.6704	0.229122	493.633	0		



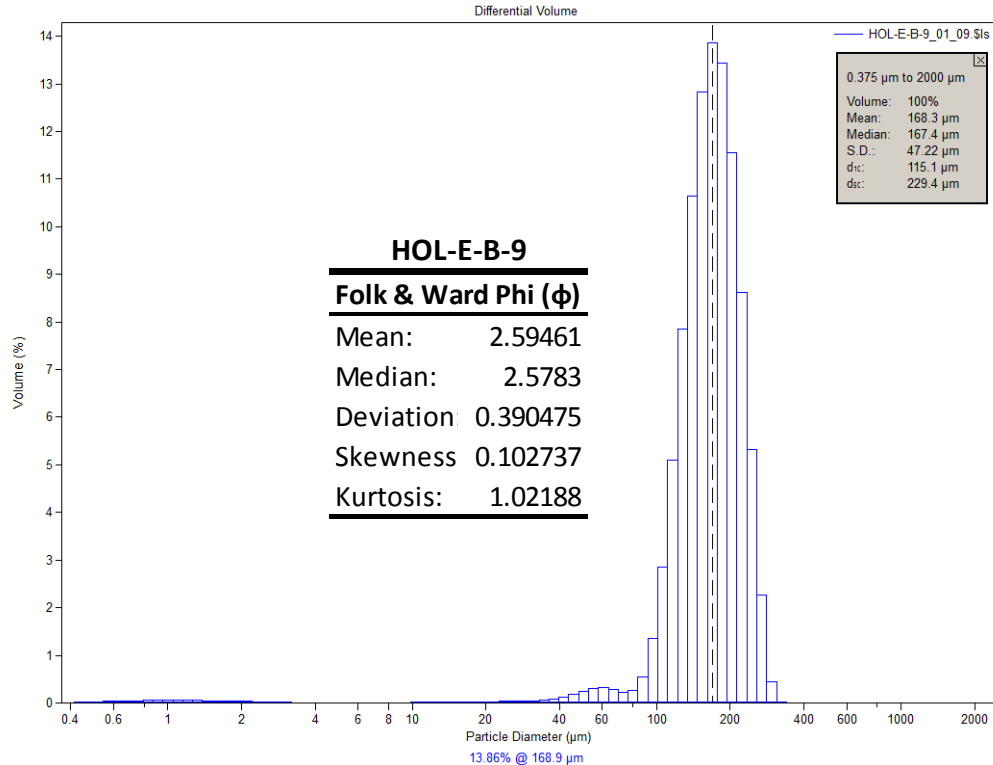
μm	Volume (%)						
0.375198	0.00567882	4.2411	0.004676	47.9397	0.242205	541.892	0
0.411878	0.0108176	4.65572	0.004227	52.6264	0.302541	594.869	0
0.452145	0.0181595	5.11087	0.004359	57.7713	0.354421	653.025	0
0.496347	0.0250008	5.61052	0.004955	63.4192	0.397803	716.866	0
0.544872	0.0313831	6.15902	0.005896	69.6192	0.457738	786.949	0
0.59814	0.0372015	6.76114	0.007046	76.4253	0.601189	863.883	0
0.656615	0.0423558	7.42212	0.008281	83.8969	0.939675	948.338	0
0.720807	0.0467295	8.14773	0.009474	92.0988	1.62213	1041.05	0
0.791275	0.050219	8.94427	0.010499	101.103	2.7898	1142.83	0
0.868632	0.0527221	9.81869	0.011278	110.987	4.4851	1254.55	0
0.953552	0.0541525	10.7786	0.011767	121.837	6.60359	1377.2	0
1.04677	0.0544413	11.8323	0.012051	133.748	8.86534	1511.84	0
1.14911	0.0536351	12.9891	0.012255	146.824	10.8649	1659.64	0
1.26145	0.0518118	14.2589	0.012689	161.177	12.1891	1821.89	0
1.38477	0.0490742	15.6529	0.013639	176.935	12.4889	2000	
1.52015	0.0455536	17.1832	0.015447	194.232	11.6495		
1.66876	0.0414011	18.863	0.018439	213.221	9.75002		
1.8319	0.0367933	20.7071	0.02267	234.066	7.13554		
2.011	0.0319161	22.7315	0.028329	256.948	4.35067		
2.2076	0.0269714	24.9538	0.035354	282.068	1.84464		
2.42342	0.0221557	27.3934	0.044115	309.644	0.365618		
2.66033	0.0176645	30.0714	0.055829	339.916	0.016248		
2.92042	0.013666	33.0113	0.072445	373.147	0		
3.20592	0.0103026	36.2385	0.097401	409.626	0		
3.51934	0.00766641	39.7813	0.13391	449.672	0		
3.8634	0.00579655	43.6704	0.183096	493.633	0		



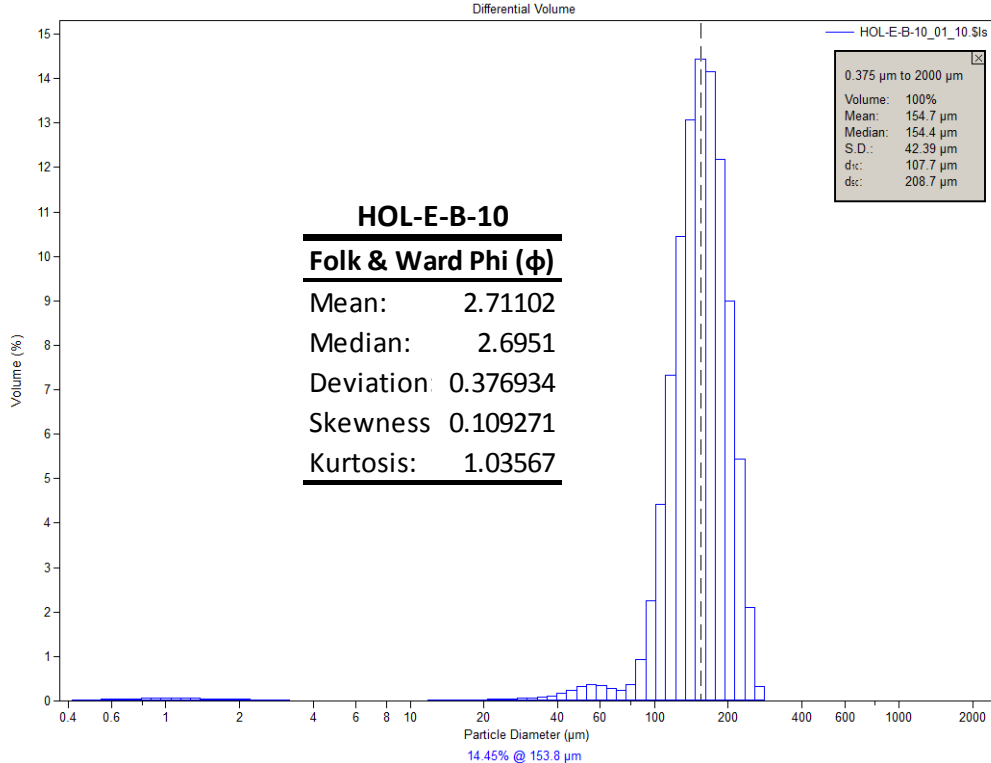
μm	Volume (%)						
0.375198	0.00628442	4.2411	0.004837	47.9397	0.365903	541.892	0
0.411878	0.0119704	4.65572	0.004505	52.6264	0.430031	594.869	0
0.452145	0.0200921	5.11087	0.00481	57.7713	0.454169	653.025	0
0.496347	0.0276559	5.61052	0.00561	63.4192	0.436264	716.866	0
0.544872	0.0347066	6.15902	0.006762	69.6192	0.432092	786.949	0
0.59814	0.0411265	6.76114	0.008105	76.4253	0.559922	863.883	0
0.656615	0.0468037	7.42212	0.00949	83.8969	1.00938	948.338	0
0.720807	0.0516078	8.14773	0.010772	92.0988	2.02865	1041.05	0
0.791275	0.0554237	8.94427	0.011818	101.103	3.7767	1142.83	0
0.868632	0.058137	9.81869	0.012564	110.987	6.19524	1254.55	0
0.953552	0.0596529	10.7786	0.013019	121.837	8.94019	1377.2	0
1.04677	0.0598947	11.8323	0.013381	133.748	11.4427	1511.84	0
1.14911	0.0589166	12.9891	0.013944	146.824	13.0963	1659.64	0
1.26145	0.0568075	14.2589	0.01525	161.177	13.4261	1821.89	0
1.38477	0.0536842	15.6529	0.017859	176.935	12.3426	2000	
1.52015	0.0496963	17.1832	0.022359	194.232	10.0481		
1.66876	0.0450158	18.863	0.029247	213.221	7.07292		
1.8319	0.0398425	20.7071	0.03849	234.066	4.07201		
2.011	0.0343886	22.7315	0.049907	256.948	1.45471		
2.2076	0.0288826	24.9538	0.062942	282.068	0.183547		
2.42342	0.0235476	27.3934	0.077683	309.644	0.003072		
2.66033	0.018604	30.0714	0.095756	339.916	0		
2.92042	0.0142409	33.0113	0.120727	373.147	0		
3.20592	0.0106157	36.2385	0.158324	409.626	0		
3.51934	0.00782725	39.7813	0.213548	449.672	0		
3.8634	0.00591125	43.6704	0.286334	493.633	0		



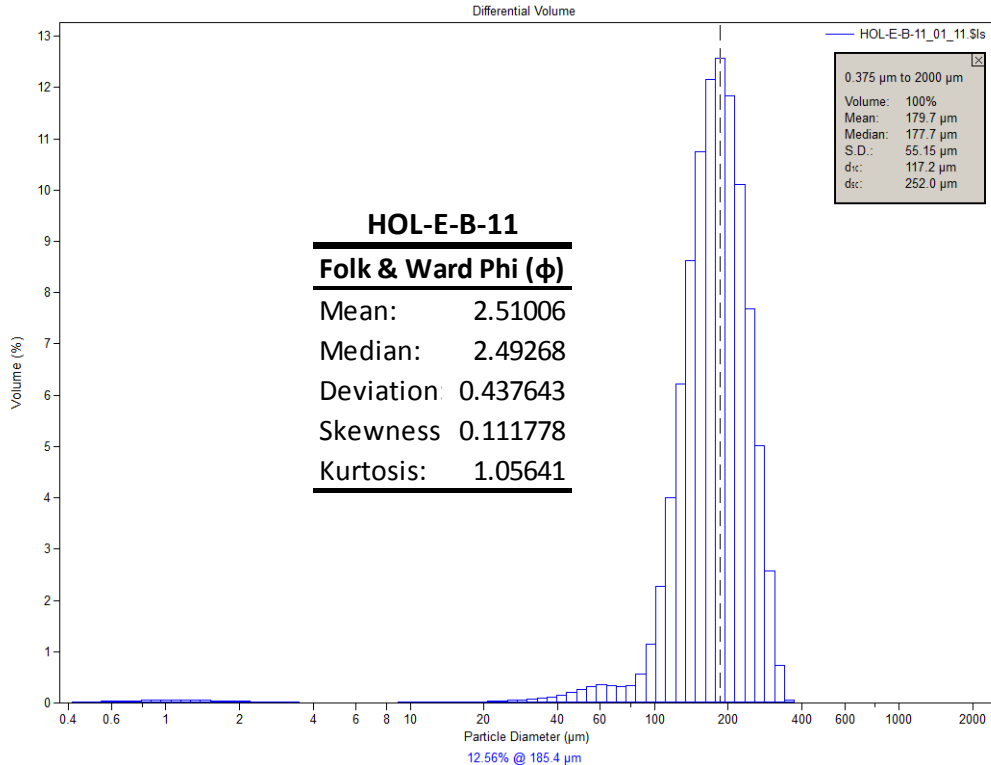
μm	Volume (%)						
0.375198	0.00597446	4.2411	0.005869	47.9397	0.249028	541.892	0
0.411878	0.0113804	4.65572	0.005598	52.6264	0.301942	594.869	0
0.452145	0.0191035	5.11087	0.005955	57.7713	0.319095	653.025	0
0.496347	0.0262984	5.61052	0.006808	63.4192	0.29262	716.866	0
0.544872	0.0330089	6.15902	0.00802	69.6192	0.26673	786.949	0
0.59814	0.0391241	6.76114	0.009437	76.4253	0.341924	863.883	0
0.656615	0.0445386	7.42212	0.010918	83.8969	0.685845	948.338	0
0.720807	0.04913	8.14773	0.012323	92.0988	1.54573	1041.05	0
0.791275	0.0527886	8.94427	0.01352	101.103	3.10763	1142.83	0
0.868632	0.0554083	9.81869	0.014442	110.987	5.36751	1254.55	0
0.953552	0.0568985	10.7786	0.015078	121.837	8.06715	1377.2	0
1.04677	0.0571882	11.8323	0.015597	133.748	10.7104	1511.84	0
1.14911	0.0563279	12.9891	0.01622	146.824	12.7133	1659.64	0
1.26145	0.0544011	14.2589	0.017392	161.177	13.5537	1821.89	0
1.38477	0.0515171	15.6529	0.019508	176.935	13.0028	2000	
1.52015	0.0478174	17.1832	0.022945	194.232	11.1302		
1.66876	0.0434622	18.863	0.027893	213.221	8.3273		
1.8319	0.0386398	20.7071	0.033956	234.066	5.22715		
2.011	0.0335474	22.7315	0.040622	256.948	2.38382		
2.2076	0.0284	24.9538	0.046963	282.068	0.546703		
2.42342	0.0234059	27.3934	0.052867	309.644	0.029568		
2.66033	0.0187728	30.0714	0.059794	339.916	0		
2.92042	0.0146789	33.0113	0.071202	373.147	0		
3.20592	0.0112744	36.2385	0.092903	409.626	0		
3.51934	0.00865587	39.7813	0.130353	449.672	0		
3.8634	0.00686052	43.6704	0.185091	493.633	0		



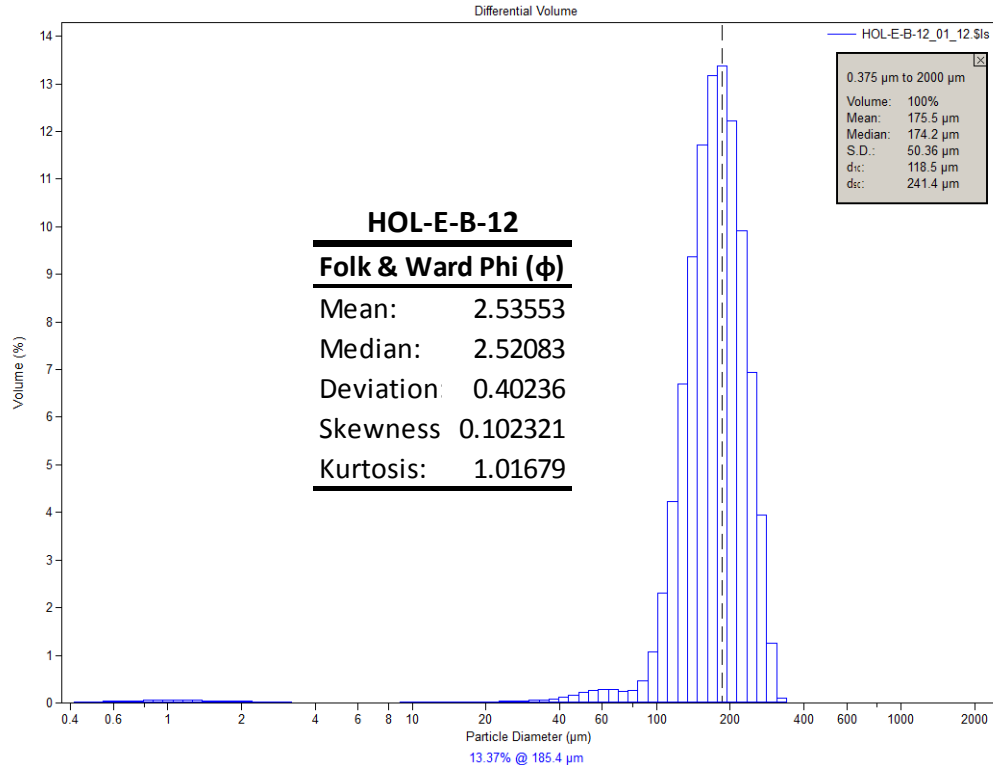
μm	Volume (%)						
0.375198	0.00590354	4.2411	0.003314	47.9397	0.250338	541.892	0
0.411878	0.011244	4.65572	0.002893	52.6264	0.305577	594.869	0
0.452145	0.0188687	5.11087	0.003071	57.7713	0.319845	653.025	0
0.496347	0.0259635	5.61052	0.00373	63.4192	0.280664	716.866	0
0.544872	0.0325686	6.15902	0.00475	69.6192	0.230977	786.949	0
0.59814	0.0385725	6.76114	0.005989	76.4253	0.26965	863.883	0
0.656615	0.0438685	7.42212	0.00731	83.8969	0.555487	948.338	0
0.720807	0.0483344	8.14773	0.00858	92.0988	1.34716	1041.05	0
0.791275	0.0518615	8.94427	0.00967	101.103	2.85422	1142.83	0
0.868632	0.0543445	9.81869	0.010509	110.987	5.10046	1254.55	0
0.953552	0.0556948	10.7786	0.011073	121.837	7.85827	1377.2	0
1.04677	0.0558453	11.8323	0.011511	133.748	10.6377	1511.84	0
1.14911	0.0548496	12.9891	0.012014	146.824	12.8356	1659.64	0
1.26145	0.0527955	14.2589	0.012991	161.177	13.862	1821.89	0
1.38477	0.0497956	15.6529	0.014788	176.935	13.428	2000	
1.52015	0.0459946	17.1832	0.017728	194.232	11.5473		
1.66876	0.0415551	18.863	0.021948	213.221	8.61546		
1.8319	0.0366653	20.7071	0.027006	234.066	5.33003		
2.011	0.0315213	22.7315	0.032395	256.948	2.26617		
2.2076	0.0263342	24.9538	0.037256	282.068	0.439955		
2.42342	0.0213062	27.3934	0.041759	309.644	0.018703		
2.66033	0.0166374	30.0714	0.047725	339.916	0		
2.92042	0.0124971	33.0113	0.059063	373.147	0		
3.20592	0.00902915	36.2385	0.082117	409.626	0		
3.51934	0.00632571	39.7813	0.122568	449.672	0		
3.8634	0.00442694	43.6704	0.181784	493.633	0		



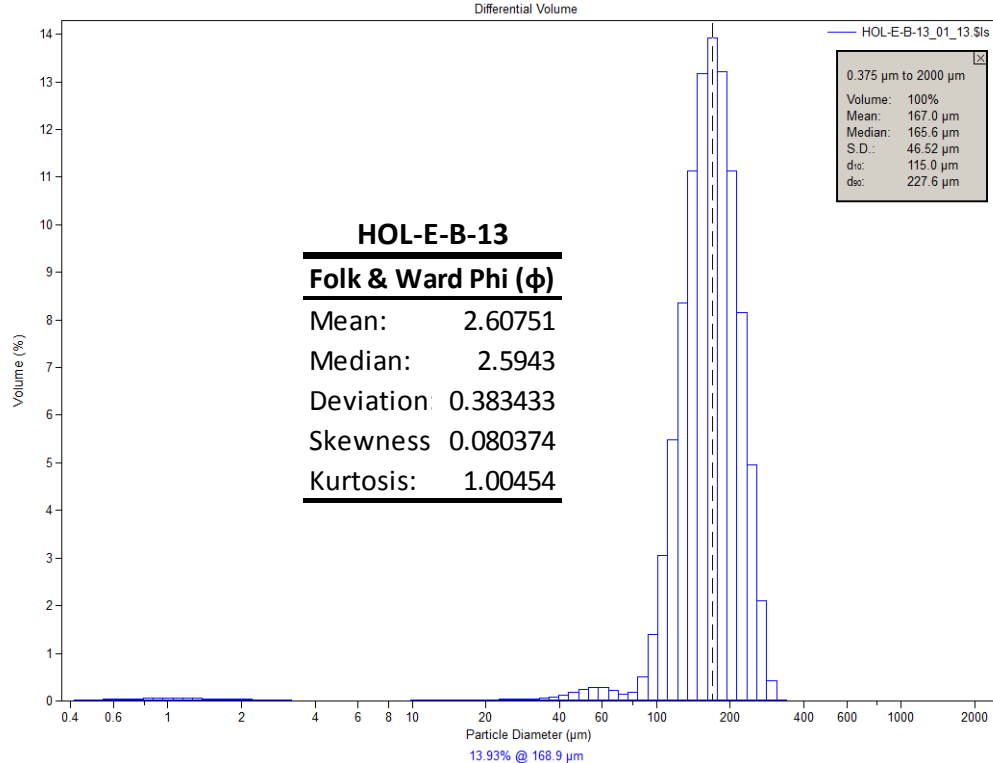
μm	Volume (%)						
0.375198	0.00637443	4.2411	0.003631	47.9397	0.316281	541.892	0
0.411878	0.0121406	4.65572	0.003206	52.6264	0.361628	594.869	0
0.452145	0.0203731	5.11087	0.003403	57.7713	0.3457	653.025	0
0.496347	0.0280331	5.61052	0.004088	63.4192	0.277241	716.866	0
0.544872	0.0351642	6.15902	0.005119	69.6192	0.239038	786.949	0
0.59814	0.0416456	6.76114	0.006342	76.4253	0.375829	863.883	0
0.656615	0.0473626	7.42212	0.007606	83.8969	0.942255	948.338	0
0.720807	0.0521824	8.14773	0.008776	92.0988	2.24777	1041.05	0
0.791275	0.0559886	8.94427	0.009723	101.103	4.43204	1142.83	0
0.868632	0.0586666	9.81869	0.010403	110.987	7.33522	1254.55	0
0.953552	0.0601217	10.7786	0.010838	121.837	10.4549	1377.2	0
1.04677	0.0602791	11.8323	0.011252	133.748	13.0771	1511.84	0
1.14911	0.0591981	12.9891	0.011952	146.824	14.4451	1659.64	0
1.26145	0.0569722	14.2589	0.013439	161.177	14.1535	1821.89	0
1.38477	0.0537237	15.6529	0.016225	176.935	12.1736	2000	
1.52015	0.0496069	17.1832	0.020677	194.232	8.99582		
1.66876	0.0447991	18.863	0.026969	213.221	5.43127		
1.8319	0.0395032	20.7071	0.034514	234.066	2.10749		
2.011	0.0339333	22.7315	0.042486	256.948	0.325007		
2.2076	0.0283189	24.9538	0.04999	282.068	0.009058		
2.42342	0.0228831	27.3934	0.057104	309.644	0		
2.66033	0.0178439	30.0714	0.066609	339.916	0		
2.92042	0.0133892	33.0113	0.083649	373.147	0		
3.20592	0.00967336	36.2385	0.1157	409.626	0		
3.51934	0.00679571	39.7813	0.169179	449.672	0		
3.8634	0.00479168	43.6704	0.241545	493.633	0		



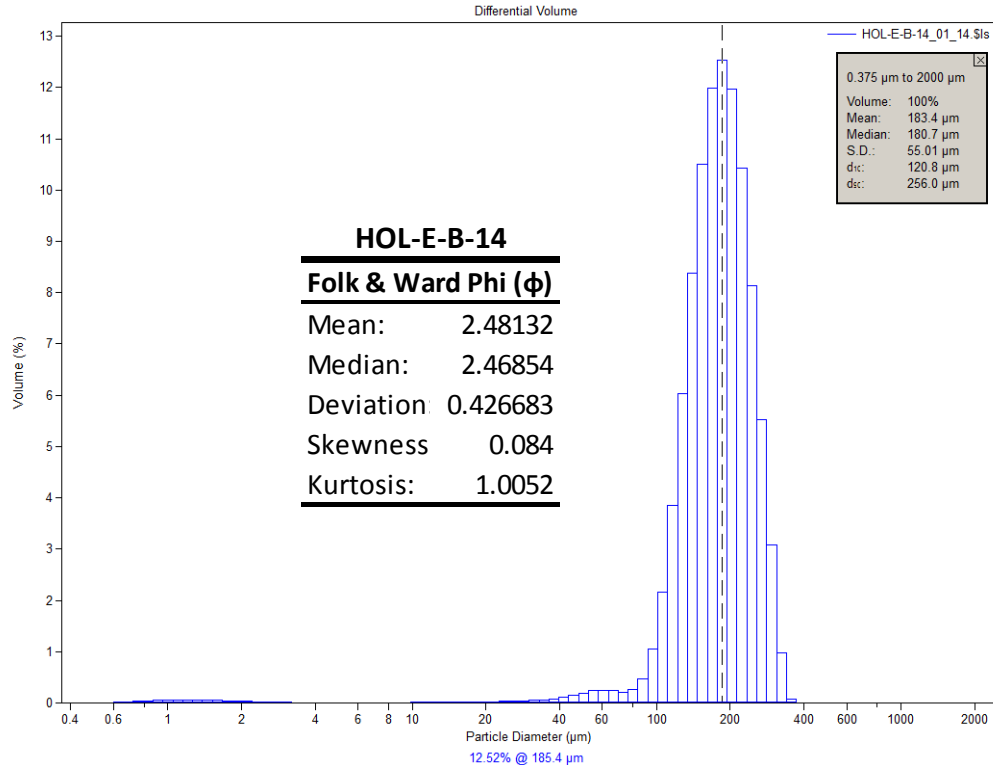
μm	Volume (%)						
0.375198	0.00557594	4.2411	0.003705	47.9397	0.267906	541.892	0
0.411878	0.0106216	4.65572	0.003226	52.6264	0.322044	594.869	0
0.452145	0.0178296	5.11087	0.003338	57.7713	0.348817	653.025	0
0.496347	0.0245449	5.61052	0.00393	63.4192	0.337455	716.866	0
0.544872	0.0308079	6.15902	0.004892	69.6192	0.311474	786.949	0
0.59814	0.036515	6.76114	0.00609	76.4253	0.344529	863.883	0
0.656615	0.0415672	7.42212	0.007396	83.8969	0.559536	948.338	0
0.720807	0.0458507	8.14773	0.008683	92.0988	1.13882	1041.05	0
0.791275	0.0492618	8.94427	0.009823	101.103	2.26519	1142.83	0
0.868632	0.0517013	9.81869	0.010742	110.987	4.00176	1254.55	0
0.953552	0.0530832	10.7786	0.011411	121.837	6.22375	1377.2	0
1.04677	0.0533406	11.8323	0.011959	133.748	8.6182	1511.84	0
1.14911	0.0525198	12.9891	0.012583	146.824	10.7429	1659.64	0
1.26145	0.0506968	14.2589	0.013698	161.177	12.1622	1821.89	0
1.38477	0.0479736	15.6529	0.015735	176.935	12.5629	2000	
1.52015	0.044479	17.1832	0.019172	194.232	11.8375		
1.66876	0.0403625	18.863	0.024424	213.221	10.1105		
1.8319	0.0357963	20.7071	0.031466	234.066	7.6778		
2.011	0.0309623	22.7315	0.04018	256.948	5.00872		
2.2076	0.0260579	24.9538	0.05002	282.068	2.567		
2.42342	0.0212742	27.3934	0.060857	309.644	0.724572		
2.66033	0.0168023	30.0714	0.073649	339.916	0.049114		
2.92042	0.0128066	33.0113	0.090727	373.147	0		
3.20592	0.00942893	36.2385	0.116349	409.626	0		
3.51934	0.00676431	39.7813	0.154701	449.672	0		
3.8634	0.0048591	43.6704	0.207052	493.633	0		



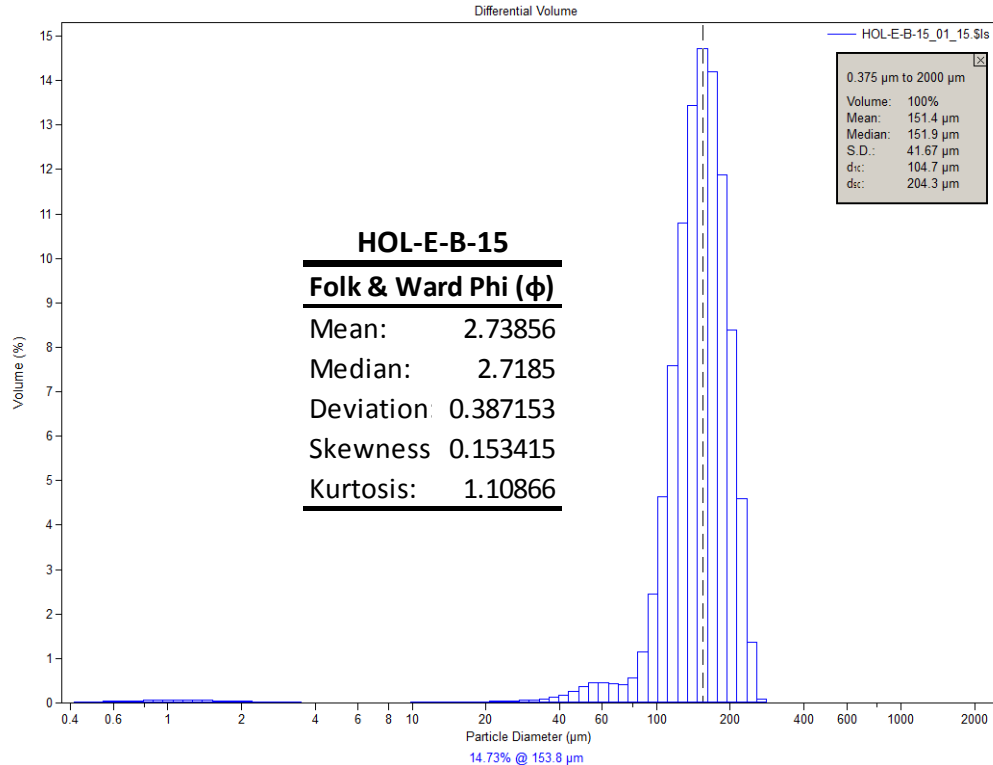
μm	Volume (%)						
0.375198	0.0057527	4.2411	0.003914	47.9397	0.213181	541.892	0
0.411878	0.0109581	4.65572	0.00356	52.6264	0.26441	594.869	0
0.452145	0.0183939	5.11087	0.003825	57.7713	0.289176	653.025	0
0.496347	0.0253201	5.61052	0.004593	63.4192	0.273502	716.866	0
0.544872	0.0317781	6.15902	0.005741	69.6192	0.238746	786.949	0
0.59814	0.0376603	6.76114	0.007124	76.4253	0.262813	863.883	0
0.656615	0.0428642	7.42212	0.008599	83.8969	0.474576	948.338	0
0.720807	0.0472708	8.14773	0.010029	92.0988	1.08237	1041.05	0
0.791275	0.0507738	8.94427	0.011269	101.103	2.30585	1142.83	0
0.868632	0.0532693	9.81869	0.012234	110.987	4.22106	1254.55	0
0.953552	0.0546685	10.7786	0.01288	121.837	6.69898	1377.2	0
1.04677	0.0549021	11.8323	0.013335	133.748	9.37339	1511.84	0
1.14911	0.0540176	12.9891	0.013778	146.824	11.7098	1659.64	0
1.26145	0.0520962	14.2589	0.01463	161.177	13.1786	1821.89	0
1.38477	0.0492432	15.6529	0.01629	176.935	13.3742	2000	
1.52015	0.0455949	17.1832	0.019189	194.232	12.2266		
1.66876	0.0413067	18.863	0.023658	213.221	9.91777		
1.8319	0.036561	20.7071	0.029476	234.066	6.94183		
2.011	0.0315483	22.7315	0.036311	256.948	3.93958		
2.2076	0.0264766	24.9538	0.043261	282.068	1.255		
2.42342	0.0215464	27.3934	0.049864	309.644	0.093884		
2.66033	0.0169587	30.0714	0.056889	339.916	0		
2.92042	0.0128853	33.0113	0.066581	373.147	0		
3.20592	0.00947383	36.2385	0.083679	409.626	0		
3.51934	0.00682195	39.7813	0.113191	449.672	0		
3.8634	0.00497318	43.6704	0.157651	493.633	0		



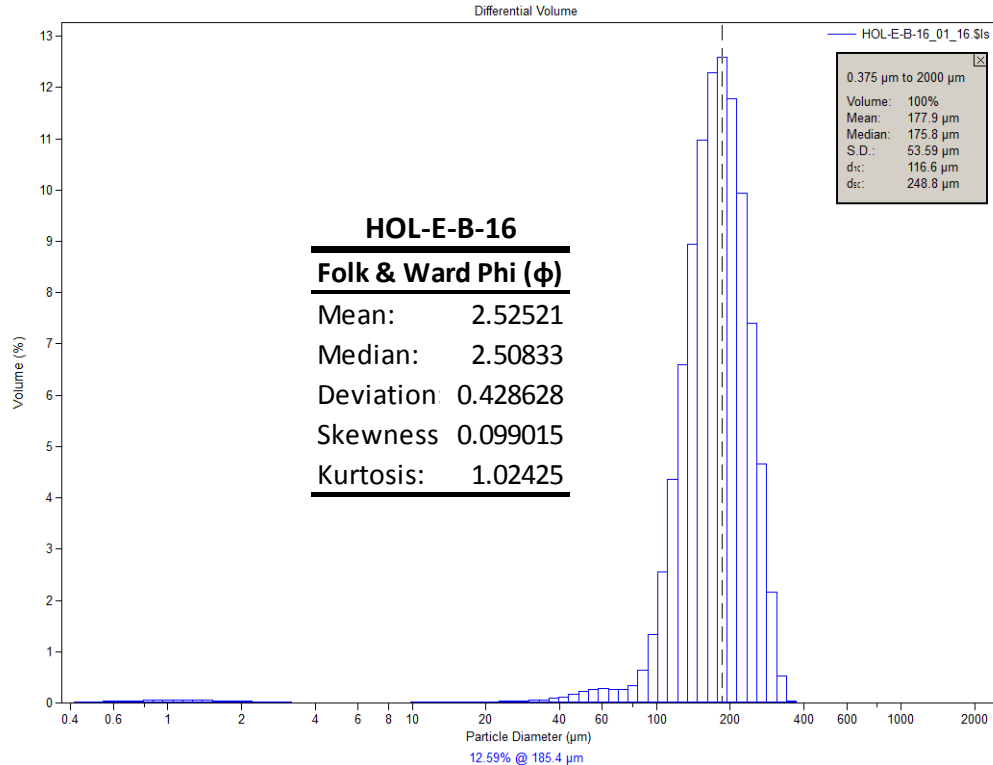
μm	Volume (%)						
0.375198	0.00589828	4.2411	0.003203	47.9397	0.241323	541.892	0
0.411878	0.0112331	4.65572	0.00282	52.6264	0.288751	594.869	0
0.452145	0.0188479	5.11087	0.003026	57.7713	0.285778	653.025	0
0.496347	0.0259297	5.61052	0.003702	63.4192	0.220932	716.866	0
0.544872	0.0325178	6.15902	0.004725	69.6192	0.151465	786.949	0
0.59814	0.0384997	6.76114	0.005952	76.4253	0.185495	863.883	0
0.656615	0.0437688	7.42212	0.007243	83.8969	0.49934	948.338	0
0.720807	0.0482031	8.14773	0.008469	92.0988	1.39369	1041.05	0
0.791275	0.0516935	8.94427	0.009505	101.103	3.06285	1142.83	0
0.868632	0.0541363	9.81869	0.010293	110.987	5.4822	1254.55	0
0.953552	0.055445	10.7786	0.010831	121.837	8.35542	1377.2	0
1.04677	0.055553	11.8323	0.011295	133.748	11.1289	1511.84	0
1.14911	0.054517	12.9891	0.011917	146.824	13.1704	1659.64	0
1.26145	0.052427	14.2589	0.013141	161.177	13.9312	1821.89	0
1.38477	0.0493981	15.6529	0.015352	176.935	13.2094	2000	
1.52015	0.0455758	17.1832	0.018872	194.232	11.1254		
1.66876	0.0411249	18.863	0.023784	213.221	8.14536		
1.8319	0.0362337	20.7071	0.029484	234.066	4.95713		
2.011	0.0310989	22.7315	0.035186	256.948	2.09956		
2.2076	0.0259307	24.9538	0.039743	282.068	0.416236		
2.42342	0.0209306	27.3934	0.043093	309.644	0.018508		
2.66033	0.0162973	30.0714	0.047154	339.916	0		
2.92042	0.0121989	33.0113	0.056261	373.147	0		
3.20592	0.00877717	36.2385	0.077313	409.626	0		
3.51934	0.00612226	39.7813	0.11659	449.672	0		
3.8634	0.00427183	43.6704	0.175104	493.633	0		



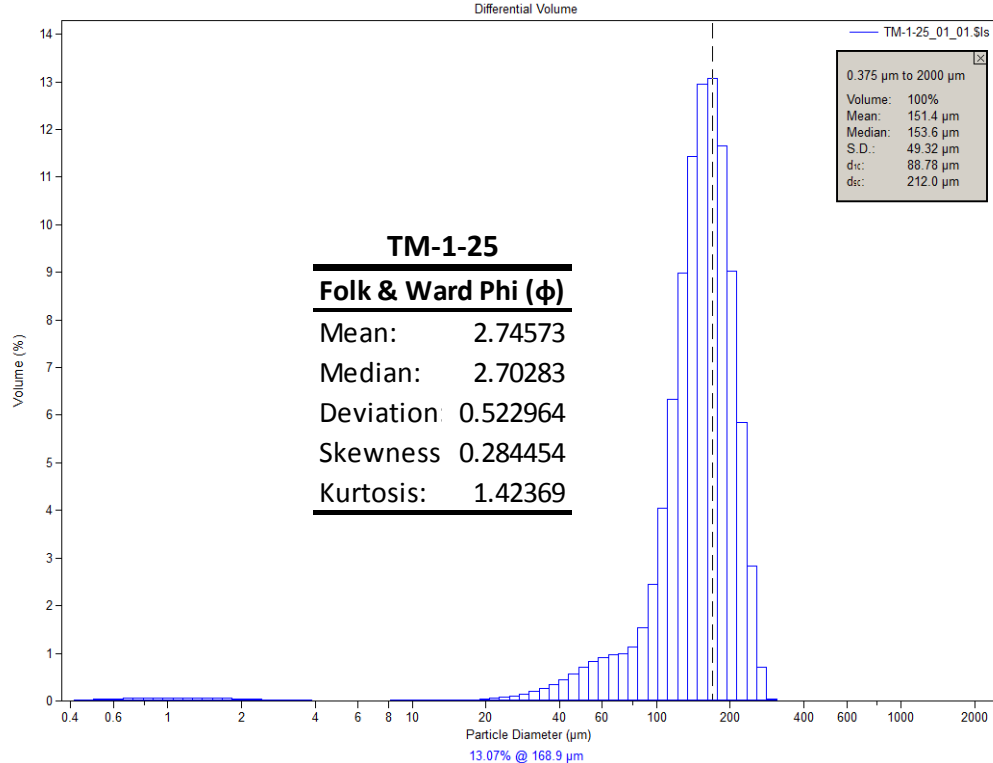
μ m	Volume (%)	μ m	Volume (%)	μ m	Volume (%)	μ m	Volume (%)
0.375198	0	4.2411	0.000551	47.9397	0.196605	541.892	0
0.411878	0	4.65572	0.000315	52.6264	0.237526	594.869	0
0.452145	0	5.11087	0.000682	57.7713	0.253316	653.025	0
0.496347	0.000388291	5.61052	0.001681	63.4192	0.236829	716.866	0
0.544872	0.00521773	6.15902	0.0031	69.6192	0.21476	786.949	0
0.59814	0.0159999	6.76114	0.004744	76.4253	0.255447	863.883	0
0.656615	0.0265258	7.42212	0.006444	83.8969	0.476074	948.338	0
0.720807	0.0358427	8.14773	0.008043	92.0988	1.05662	1041.05	0
0.791275	0.0438821	8.94427	0.009389	101.103	2.16478	1142.83	0
0.868632	0.0503801	9.81869	0.010386	110.987	3.86021	1254.55	0
0.953552	0.0551176	10.7786	0.010988	121.837	6.02786	1377.2	0
1.04677	0.0579035	11.8323	0.011307	133.748	8.38124	1511.84	0
1.14911	0.058774	12.9891	0.011522	146.824	10.5097	1659.64	0
1.26145	0.0578449	14.2589	0.012012	161.177	11.9905	1821.89	0
1.38477	0.0552963	15.6529	0.013143	176.935	12.5242	2000	
1.52015	0.0513682	17.1832	0.015302	194.232	11.9656		
1.66876	0.0463446	18.863	0.018755	213.221	10.4217		
1.8319	0.0405411	20.7071	0.023363	234.066	8.13819		
2.011	0.0342867	22.7315	0.028886	256.948	5.53008		
2.2076	0.0279125	24.9538	0.034745	282.068	3.07909		
2.42342	0.0217282	27.3934	0.040874	309.644	0.975521		
2.66033	0.0160169	30.0714	0.048229	339.916	0.073156		
2.92042	0.011008	33.0113	0.059119	373.147	0		
3.20592	0.00688057	36.2385	0.077444	409.626	0		
3.51934	0.00373515	39.7813	0.106909	449.672	0		
3.8634	0.00162279	43.6704	0.148483	493.633	0		



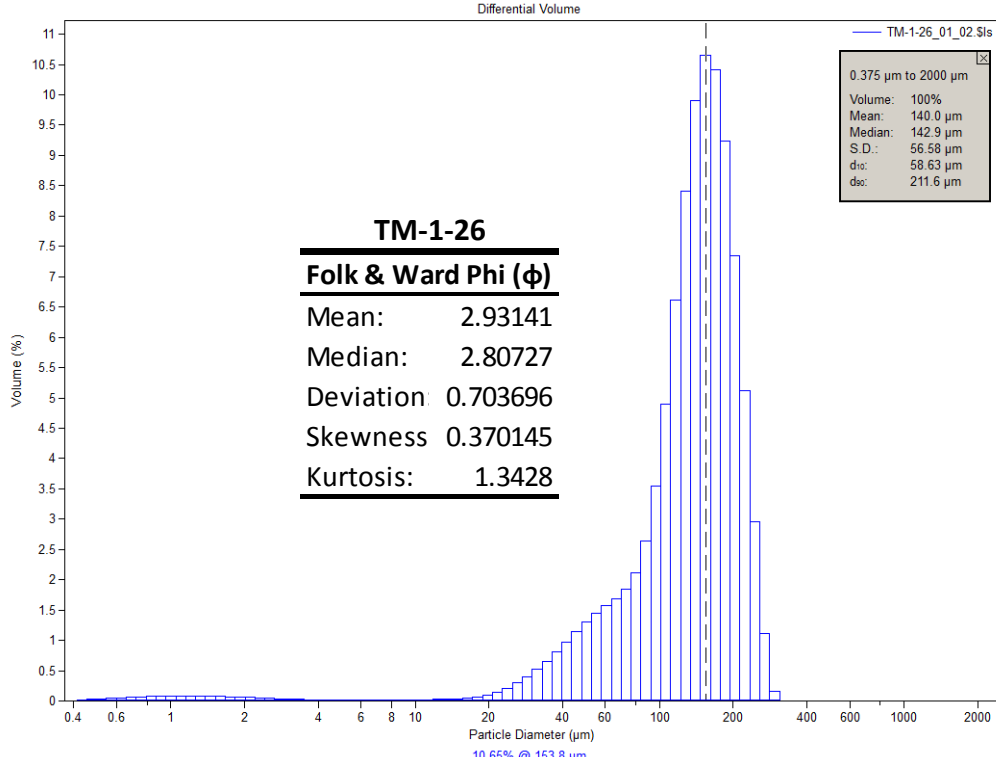
μm	Volume (%)						
0.375198	0.00640565	4.2411	0.005638	47.9397	0.368873	541.892	0
0.411878	0.0122022	4.65572	0.005041	52.6264	0.444556	594.869	0
0.452145	0.0204843	5.11087	0.005068	57.7713	0.464124	653.025	0
0.496347	0.0282023	5.61052	0.00558	63.4192	0.427593	716.866	0
0.544872	0.0354038	6.15902	0.00644	69.6192	0.409415	786.949	0
0.59814	0.0419709	6.76114	0.007496	76.4253	0.564487	863.883	0
0.656615	0.0477911	7.42212	0.008611	83.8969	1.13855	948.338	0
0.720807	0.0527337	8.14773	0.009653	92.0988	2.44067	1041.05	0
0.791275	0.0566825	8.94427	0.010499	101.103	4.64359	1142.83	0
0.868632	0.0595232	9.81869	0.011105	110.987	7.59589	1254.55	0
0.953552	0.0611583	10.7786	0.011481	121.837	10.7869	1377.2	0
1.04677	0.0615115	11.8323	0.011837	133.748	13.4315	1511.84	0
1.14911	0.0606347	12.9891	0.012442	146.824	14.7281	1659.64	0
1.26145	0.0586158	14.2589	0.01378	161.177	14.2076	1821.89	0
1.38477	0.0555695	15.6529	0.016311	176.935	11.8827	2000	
1.52015	0.0516427	17.1832	0.020384	194.232	8.3838		
1.66876	0.0470048	18.863	0.026171	213.221	4.58781		
1.8319	0.0418524	20.7071	0.033091	234.066	1.35715		
2.011	0.0363937	22.7315	0.040444	256.948	0.094503		
2.2076	0.0308538	24.9538	0.047403	282.068	0		
2.42342	0.0254527	27.3934	0.054368	309.644	0		
2.66033	0.0204084	30.0714	0.064514	339.916	0		
2.92042	0.0159091	33.0113	0.083626	373.147	0		
3.20592	0.0121115	36.2385	0.120536	409.626	0		
3.51934	0.00911788	39.7813	0.183131	449.672	0		
3.8634	0.00696711	43.6704	0.270951	493.633	0		



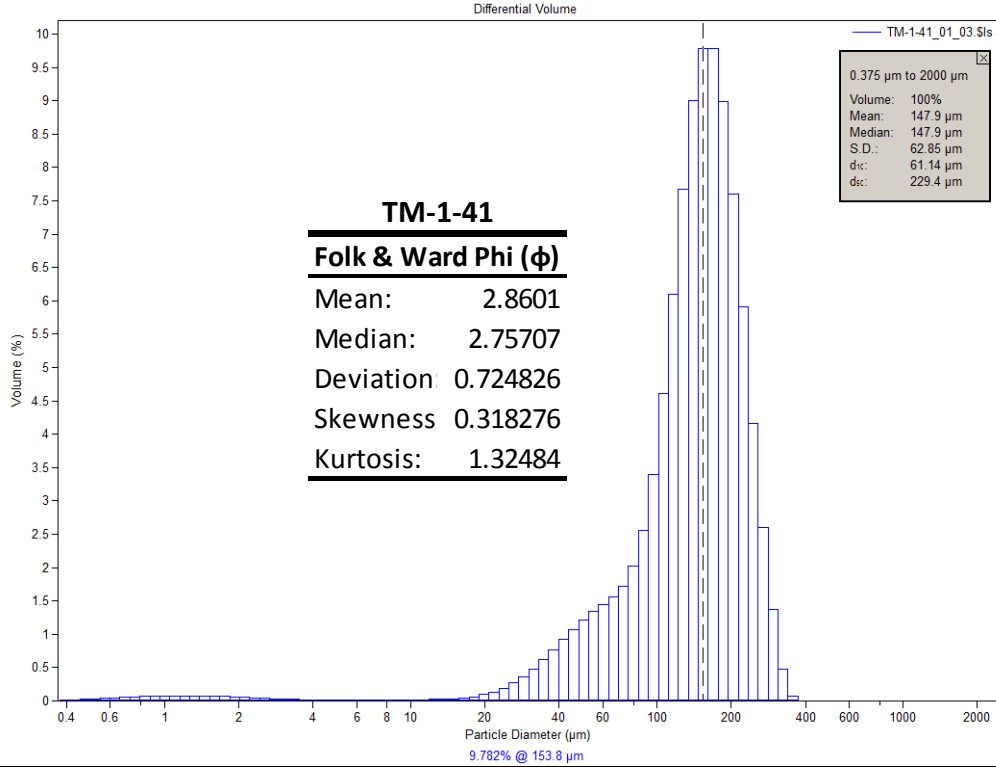
µm	Volume (%)	µm	Volume (%)	µm	Volume (%)	µm	Volume (%)
0.375198	0.00568968	4.2411	0.002887	47.9397	0.21642	541.892	0
0.411878	0.0108374	4.65572	0.002427	52.6264	0.257652	594.869	0
0.452145	0.0181887	5.11087	0.002557	57.7713	0.273094	653.025	0
0.496347	0.0250325	5.61052	0.003172	63.4192	0.261855	716.866	0
0.544872	0.0314085	6.15902	0.004161	69.6192	0.258101	786.949	0
0.59814	0.0372098	6.76114	0.005394	76.4253	0.34035	863.883	0
0.656615	0.042334	7.42212	0.006739	83.8969	0.637904	948.338	0
0.720807	0.0466638	8.14773	0.008072	92.0988	1.3289	1041.05	0
0.791275	0.0500939	8.94427	0.009268	101.103	2.56428	1142.83	0
0.868632	0.0525213	9.81869	0.010255	110.987	4.36837	1254.55	0
0.953552	0.0538608	10.7786	0.011002	121.837	6.59715	1377.2	0
1.04677	0.0540441	11.8323	0.011619	133.748	8.93814	1511.84	0
1.14911	0.0531206	12.9891	0.012269	146.824	10.9699	1659.64	0
1.26145	0.0511723	14.2589	0.013295	161.177	12.2911	1821.89	0
1.38477	0.0483058	15.6529	0.015018	176.935	12.5923	2000	
1.52015	0.0446564	17.1832	0.017748	194.232	11.7768		
1.66876	0.0403795	18.863	0.021686	213.221	9.94239		
1.8319	0.0356539	20.7071	0.026611	234.066	7.39888		
2.011	0.0306684	22.7315	0.032267	256.948	4.65525		
2.2076	0.0256252	24.9538	0.038177	282.068	2.16811		
2.42342	0.0207207	27.3934	0.044481	309.644	0.519535		
2.66033	0.0161485	30.0714	0.052589	339.916	0.029612		
2.92042	0.0120756	33.0113	0.065172	373.147	0		
3.20592	0.00864351	36.2385	0.086441	409.626	0		
3.51934	0.00594707	39.7813	0.119953	449.672	0		
3.8634	0.00403226	43.6704	0.165538	493.633	0		



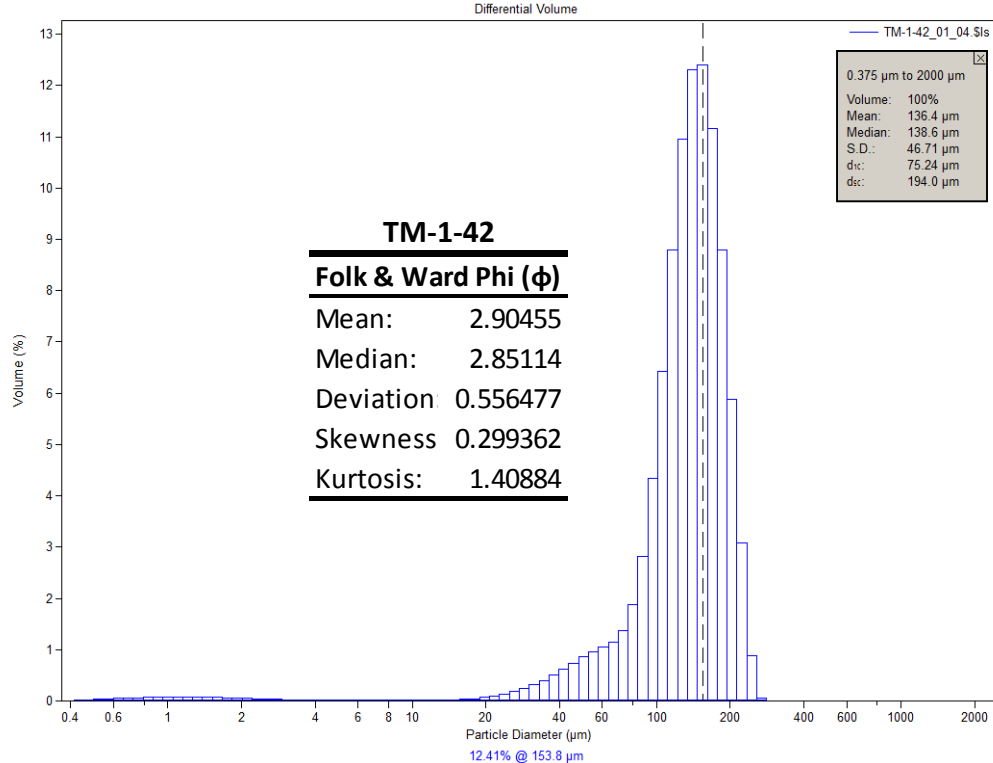
μm	Volume (%)						
0.375198	0.00688834	4.2411	0.007544	47.9397	0.7064	541.892	0
0.411878	0.0131285	4.65572	0.006802	52.6264	0.83088	594.869	0
0.452145	0.0220631	5.11087	0.006723	57.7713	0.920446	653.025	0
0.496347	0.030423	5.61052	0.007144	63.4192	0.965069	716.866	0
0.544872	0.0382678	6.15902	0.00792	69.6192	0.999771	786.949	0
0.59814	0.0454766	6.76114	0.008897	76.4253	1.13194	863.883	0
0.656615	0.0519313	7.42212	0.009947	83.8969	1.54131	948.338	0
0.720807	0.0574904	8.14773	0.01095	92.0988	2.45279	1041.05	0
0.791275	0.0620228	8.94427	0.011801	101.103	4.05641	1142.83	0
0.868632	0.0653961	9.81869	0.012467	110.987	6.3425	1254.55	0
0.953552	0.0674911	10.7786	0.012985	121.837	8.9929	1377.2	0
1.04677	0.0682035	11.8323	0.013604	133.748	11.426	1511.84	0
1.14911	0.0675685	12.9891	0.014668	146.824	12.9485	1659.64	0
1.26145	0.0656587	14.2589	0.016834	161.177	13.0659	1821.89	0
1.38477	0.0625784	15.6529	0.020895	176.935	11.6488	2000	
1.52015	0.0584736	17.1832	0.02786	194.232	9.01554		
1.66876	0.0535197	18.863	0.039011	213.221	5.84731		
1.8319	0.0479305	20.7071	0.055406	234.066	2.82363		
2.011	0.0419394	22.7315	0.078375	256.948	0.712368		
2.2076	0.0358068	24.9538	0.108993	282.068	0.04297		
2.42342	0.0297919	27.3934	0.148527	309.644	0		
2.66033	0.0241538	30.0714	0.199175	339.916	0		
2.92042	0.0191152	33.0113	0.263642	373.147	0		
3.20592	0.0148599	36.2385	0.345956	409.626	0		
3.51934	0.0115001	39.7813	0.449313	449.672	0		
3.8634	0.00907306	43.6704	0.572469	493.633	0		



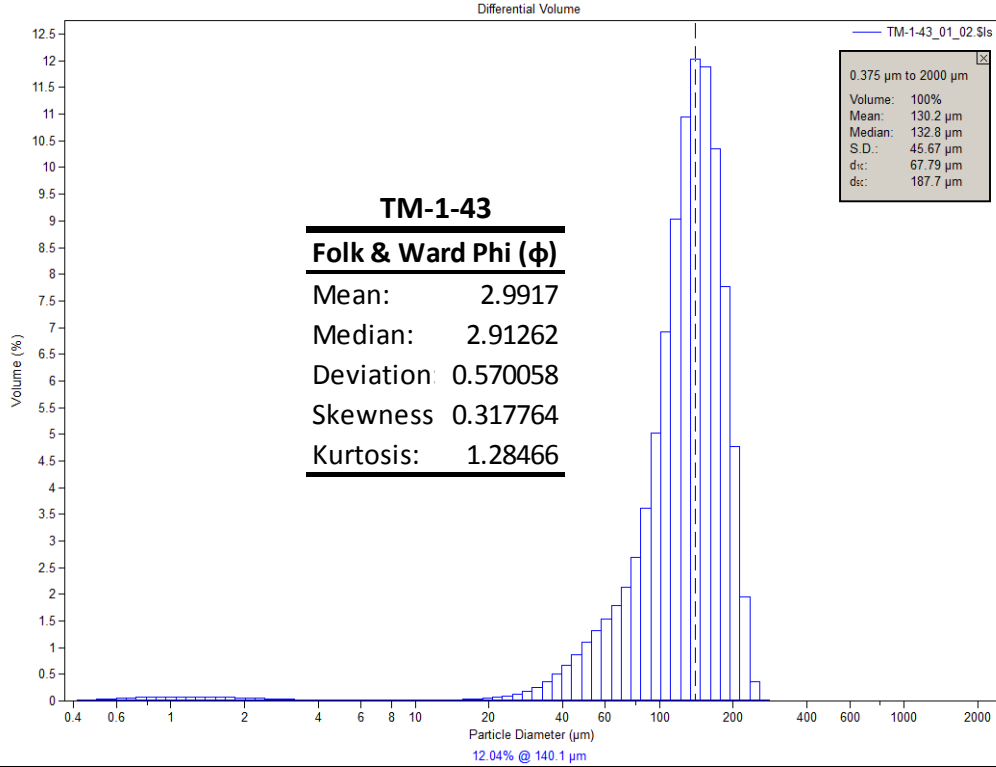
μm	Volume (%)						
0.375198	0.00776945	4.2411	0.016138	47.9397	1.3003	541.892	0
0.411878	0.0148236	4.65572	0.015014	52.6264	1.44792	594.869	0
0.452145	0.0249673	5.11087	0.01475	57.7713	1.57462	653.025	0
0.496347	0.0345406	5.61052	0.015144	63.4192	1.69078	716.866	0
0.544872	0.043635	6.15902	0.015991	69.6192	1.84164	786.949	0
0.59814	0.0521346	6.76114	0.01709	76.4253	2.11662	863.883	0
0.656615	0.0599212	7.42212	0.01828	83.8969	2.64391	948.338	0
0.720807	0.0668426	8.14773	0.01942	92.0988	3.55099	1041.05	0
0.791275	0.0727525	8.94427	0.020422	101.103	4.89851	1142.83	0
0.868632	0.0774893	9.81869	0.021338	110.987	6.60981	1254.55	0
0.953552	0.0808959	10.7786	0.02242	121.837	8.41194	1377.2	0
1.04677	0.0828196	11.8323	0.024284	133.748	9.8978	1511.84	0
1.14911	0.0832444	12.9891	0.027928	146.824	10.651	1659.64	0
1.26145	0.0821957	14.2589	0.034928	161.177	10.4139	1821.89	0
1.38477	0.0797322	15.6529	0.047443	176.935	9.23675	2000	
1.52015	0.0759605	17.1832	0.068216	194.232	7.33882		
1.66876	0.0710324	18.863	0.100448	213.221	5.11898		
1.8319	0.0651504	20.7071	0.147179	234.066	2.96494		
2.011	0.0585631	22.7315	0.211154	256.948	1.10979		
2.2076	0.0515659	24.9538	0.294209	282.068	0.164741		
2.42342	0.0444799	27.3934	0.396923	309.644	0.00437		
2.66033	0.0376432	30.0714	0.518783	339.916	0		
2.92042	0.0313725	33.0113	0.657635	373.147	0		
3.20592	0.0259427	36.2385	0.810258	409.626	0		
3.51934	0.021547	39.7813	0.972549	449.672	0		
3.8634	0.0182812	43.6704	1.1386	493.633	0		



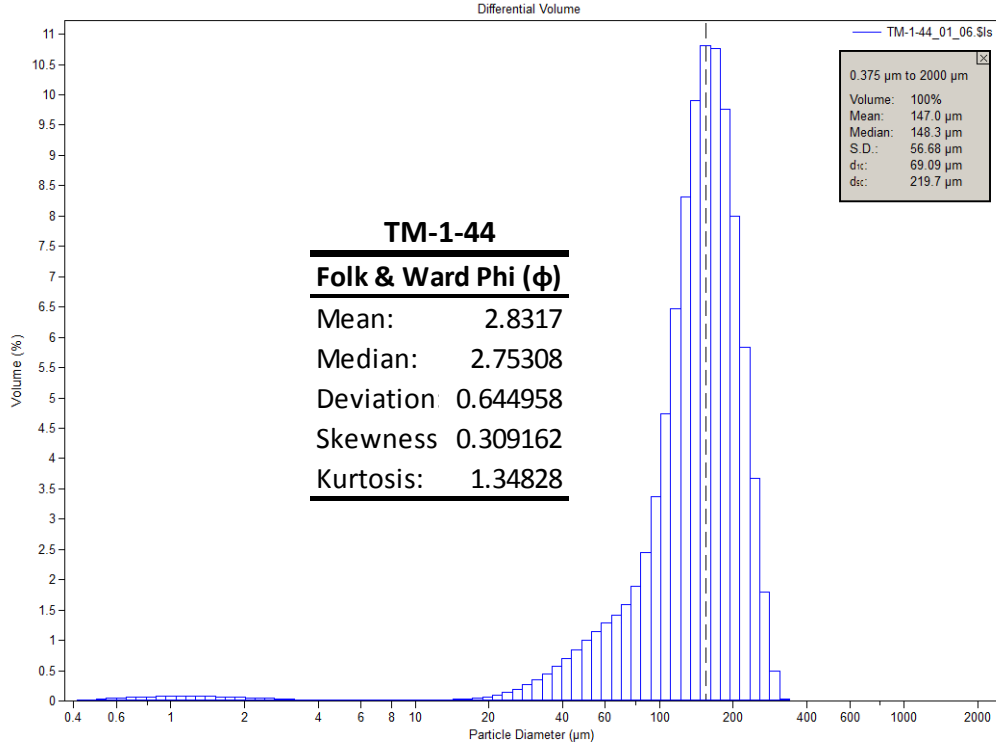
μm	Volume (%)						
0.375198	0.00753484	4.2411	0.013708	47.9397	1.21933	541.892	0
0.411878	0.0143725	4.65572	0.012801	52.6264	1.34348	594.869	0
0.452145	0.0241951	5.11087	0.012677	57.7713	1.45045	653.025	0
0.496347	0.0334466	5.61052	0.013141	63.4192	1.56173	716.866	0
0.544872	0.0422094	6.15902	0.014009	69.6192	1.72679	786.949	0
0.59814	0.0503654	6.76114	0.015105	76.4253	2.0247	863.883	0
0.656615	0.0577956	7.42212	0.016295	83.8969	2.5536	948.338	0
0.720807	0.064349	8.14773	0.017472	92.0988	3.40302	1041.05	0
0.791275	0.069881	8.94427	0.01858	101.103	4.60933	1142.83	0
0.868632	0.0742351	9.81869	0.019689	110.987	6.10182	1254.55	0
0.953552	0.0772631	10.7786	0.021048	121.837	7.67362	1377.2	0
1.04677	0.0788216	11.8323	0.023213	133.748	9.01113	1511.84	0
1.14911	0.0789095	12.9891	0.027072	146.824	9.78212	1659.64	0
1.26145	0.0775625	14.2589	0.033995	161.177	9.77804	1821.89	0
1.38477	0.0748549	15.6529	0.045843	176.935	8.99349	2000	
1.52015	0.0709081	17.1832	0.064971	194.232	7.60738		
1.66876	0.0658849	18.863	0.094188	213.221	5.90898		
1.8319	0.0599973	20.7071	0.136332	234.066	4.16636		
2.011	0.0534998	22.7315	0.194266	256.948	2.60865		
2.2076	0.0466863	24.9538	0.270367	282.068	1.3668		
2.42342	0.0398703	27.3934	0.366157	309.644	0.470651		
2.66033	0.0333738	30.0714	0.482048	339.916	0.065469		
2.92042	0.0274909	33.0113	0.616295	373.147	0.001626		
3.20592	0.0224682	36.2385	0.764889	409.626	0		
3.51934	0.0184684	39.7813	0.921219	449.672	0		
3.8634	0.0155587	43.6704	1.07606	493.633	0		



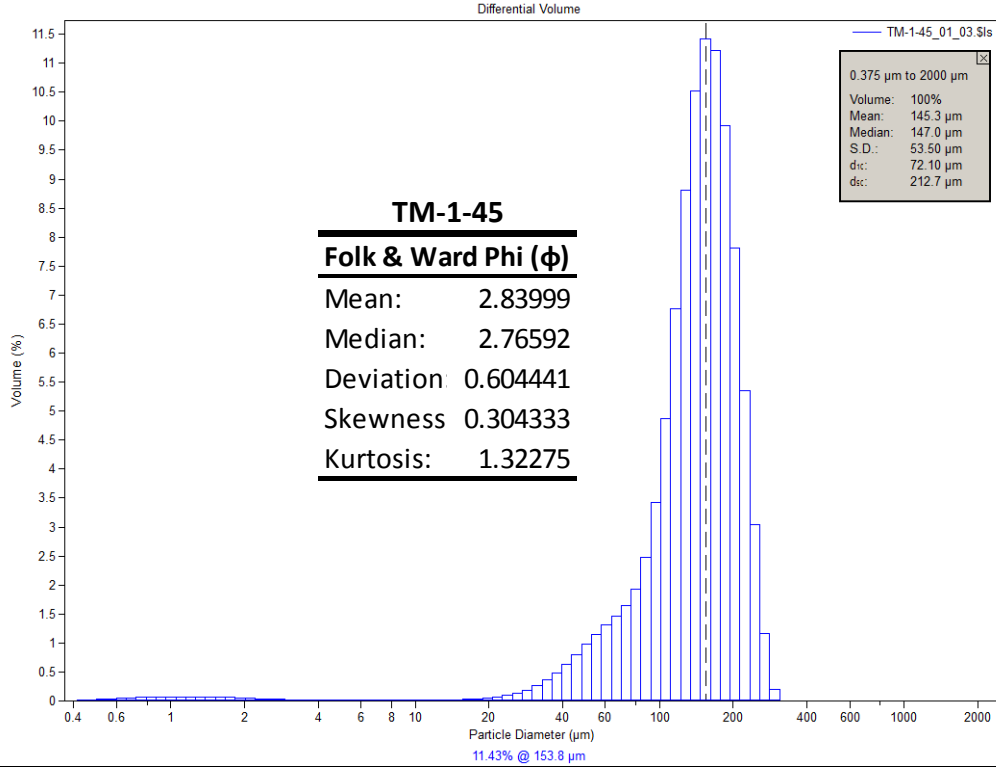
μm	Volume (%)						
0.375198	0.00770685	4.2411	0.011274	47.9397	0.858478	541.892	0
0.411878	0.014694	4.65572	0.010426	52.6264	0.961708	594.869	0
0.452145	0.0247128	5.11087	0.010363	57.7713	1.04807	653.025	0
0.496347	0.0341155	5.61052	0.0109	63.4192	1.1553	716.866	0
0.544872	0.0429769	6.15902	0.011847	69.6192	1.37849	786.949	0
0.59814	0.0511693	6.76114	0.013022	76.4253	1.87138	863.883	0
0.656615	0.0585666	7.42212	0.014267	83.8969	2.81574	948.338	0
0.720807	0.0650135	8.14773	0.015441	92.0988	4.34589	1041.05	0
0.791275	0.070364	8.94427	0.016432	101.103	6.43197	1142.83	0
0.868632	0.0744665	9.81869	0.017231	110.987	8.79578	1254.55	0
0.953552	0.0771804	10.7786	0.017978	121.837	10.9468	1377.2	0
1.04677	0.0783772	11.8323	0.019087	133.748	12.301	1511.84	0
1.14911	0.078076	12.9891	0.021274	146.824	12.4093	1659.64	0
1.26145	0.0763365	14.2589	0.025621	161.177	11.1544	1821.89	0
1.38477	0.0732556	15.6529	0.033599	176.935	8.78503	2000	
1.52015	0.0689724	17.1832	0.046894	194.232	5.88959		
1.66876	0.0636666	18.863	0.067307	213.221	3.07685		
1.8319	0.0575605	20.7071	0.096242	234.066	0.876013		
2.011	0.0509118	22.7315	0.134687	256.948	0.059448		
2.2076	0.0440114	24.9538	0.183339	282.068	0		
2.42342	0.037164	27.3934	0.242711	309.644	0		
2.66033	0.0306774	30.0714	0.314107	339.916	0		
2.92042	0.024833	33.0113	0.399155	373.147	0		
3.20592	0.0198623	36.2385	0.499396	409.626	0		
3.51934	0.0159204	39.7813	0.614391	449.672	0		
3.8634	0.0130685	43.6704	0.738144	493.633	0		



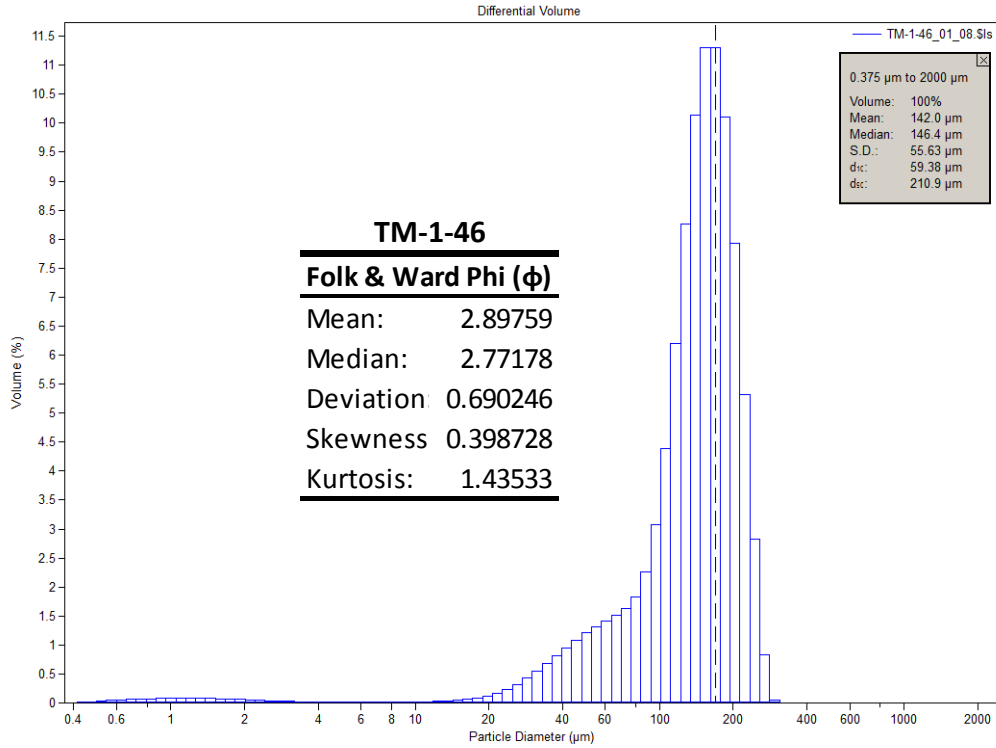
µm	Volume (%)	µm	Volume (%)	µm	Volume (%)	µm	Volume (%)
0.375198	0.0078369	4.2411	0.013249	47.9397	1.09308	541.892	0
0.411878	0.0149429	4.65572	0.012229	52.6264	1.31652	594.869	0
0.452145	0.025136	5.11087	0.011996	57.7713	1.53936	653.025	0
0.496347	0.0347094	5.61052	0.012369	63.4192	1.78464	716.866	0
0.544872	0.0437422	6.15902	0.013164	69.6192	2.12535	786.949	0
0.59814	0.0521074	6.76114	0.014212	76.4253	2.68337	863.883	0
0.656615	0.0596791	7.42212	0.01537	83.8969	3.60881	948.338	0
0.720807	0.0663027	8.14773	0.016517	92.0988	5.02545	1041.05	0
0.791275	0.0718321	8.94427	0.017554	101.103	6.91316	1142.83	0
0.868632	0.0761143	9.81869	0.018458	110.987	9.04042	1254.55	0
0.953552	0.0790079	10.7786	0.019311	121.837	10.9446	1377.2	0
1.04677	0.0803812	11.8323	0.020362	133.748	12.036	1511.84	0
1.14911	0.0802515	12.9891	0.022017	146.824	11.8915	1659.64	0
1.26145	0.0786741	14.2589	0.024857	161.177	10.3541	1821.89	0
1.38477	0.0757397	15.6529	0.029651	176.935	7.76716	2000	
1.52015	0.071583	17.1832	0.037342	194.232	4.76592		
1.66876	0.0663782	18.863	0.0492	213.221	1.9509		
1.8319	0.0603427	20.7071	0.066845	234.066	0.353986		
2.011	0.0537293	22.7315	0.092664	256.948	0.013828		
2.2076	0.0468262	24.9538	0.130121	282.068	0		
2.42342	0.0399387	27.3934	0.183745	309.644	0		
2.66033	0.0333767	30.0714	0.25939	339.916	0		
2.92042	0.0274257	33.0113	0.363297	373.147	0		
3.20592	0.0223233	36.2385	0.500363	409.626	0		
3.51934	0.0182301	39.7813	0.672077	449.672	0		
3.8634	0.0152143	43.6704	0.873669	493.633	0		



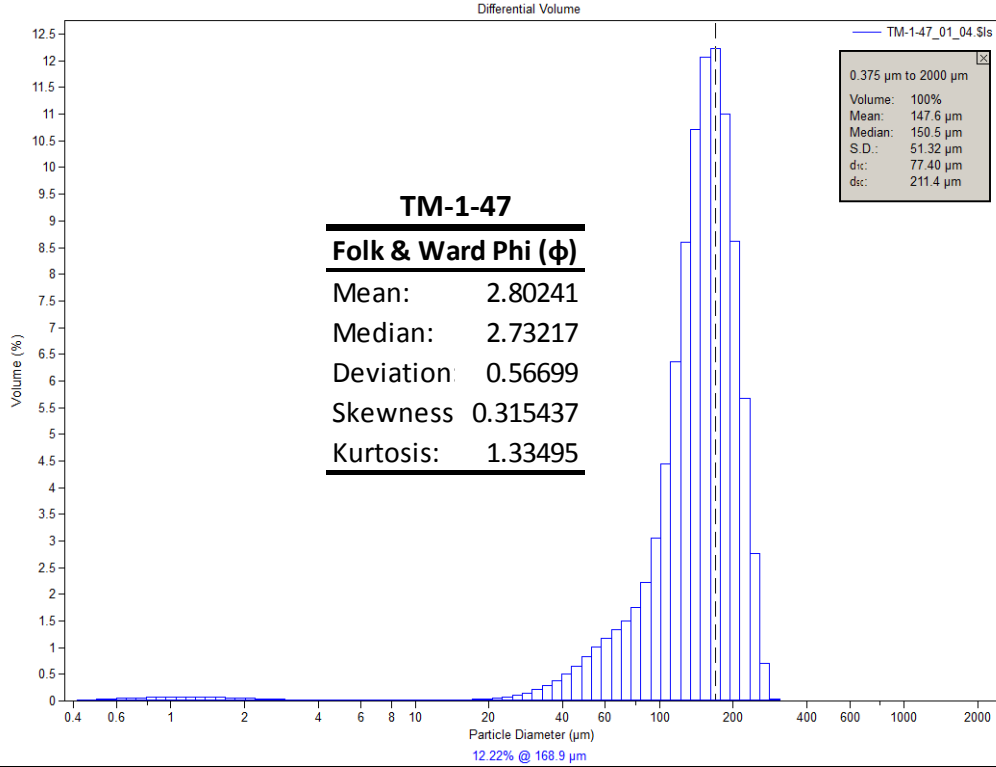
μm	Volume (%)						
0.375198	0.00729186	4.2411	0.014736	47.9397	0.999592	541.892	0
0.411878	0.0139093	4.65572	0.013665	52.6264	1.14694	594.869	0
0.452145	0.0234169	5.11087	0.013378	57.7713	1.28312	653.025	0
0.496347	0.0323747	5.61052	0.0137	63.4192	1.41748	716.866	0
0.544872	0.0408645	6.15902	0.014458	69.6192	1.59293	786.949	0
0.59814	0.0487741	6.76114	0.015475	76.4253	1.89575	863.883	0
0.656615	0.055991	7.42212	0.016605	83.8969	2.44781	948.338	0
0.720807	0.0623727	8.14773	0.017707	92.0988	3.37436	1041.05	0
0.791275	0.0677815	8.94427	0.018666	101.103	4.73904	1142.83	0
0.868632	0.0720715	9.81869	0.019462	110.987	6.47073	1254.55	0
0.953552	0.0751012	10.7786	0.020208	121.837	8.32158	1377.2	0
1.04677	0.0767353	11.8323	0.021294	133.748	9.90106	1511.84	0
1.14911	0.0769727	12.9891	0.023377	146.824	10.8038	1659.64	0
1.26145	0.0758462	14.2589	0.027547	161.177	10.7601	1821.89	0
1.38477	0.0734236	15.6529	0.035254	176.935	9.75505	2000	
1.52015	0.0698153	17.1832	0.048318	194.232	7.99938		
1.66876	0.0651698	18.863	0.068845	213.221	5.83449		
1.8319	0.0596808	20.7071	0.098778	234.066	3.66495		
2.011	0.0535806	22.7315	0.140051	256.948	1.80099		
2.2076	0.0471396	24.9538	0.194283	282.068	0.485973		
2.42342	0.0406471	27.3934	0.262921	309.644	0.031739		
2.66033	0.0344038	30.0714	0.347441	339.916	0		
2.92042	0.0286881	33.0113	0.448683	373.147	0		
3.20592	0.0237397	36.2385	0.566984	409.626	0		
3.51934	0.019725	39.7813	0.701263	449.672	0		
3.8634	0.0167262	43.6704	0.847801	493.633	0		



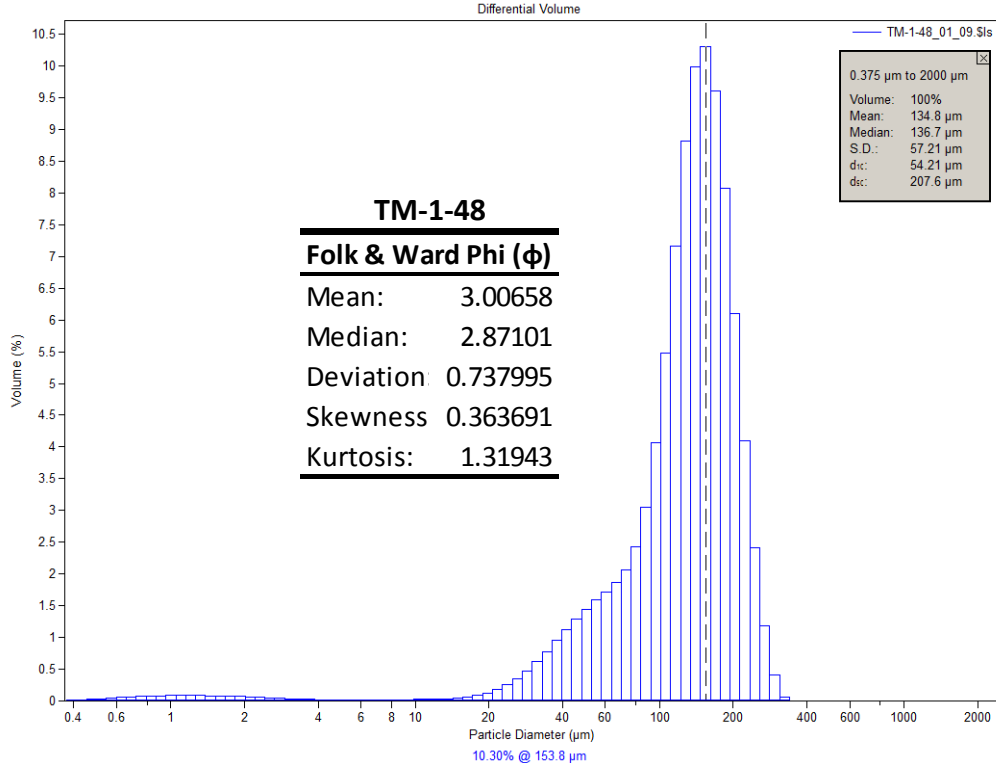
μm	Volume (%)						
0.375198	0.0073129	4.2411	0.011477	47.9397	0.973437	541.892	0
0.411878	0.0139408	4.65572	0.010688	52.6264	1.15096	594.869	0
0.452145	0.0234402	5.11087	0.010589	57.7713	1.31441	653.025	0
0.496347	0.0323465	5.61052	0.011004	63.4192	1.46571	716.866	0
0.544872	0.0407286	6.15902	0.011772	69.6192	1.64258	786.949	0
0.59814	0.0484635	6.76114	0.012736	76.4253	1.93318	863.883	0
0.656615	0.0554301	7.42212	0.013772	83.8969	2.47652	948.338	0
0.720807	0.0614807	8.14773	0.014768	92.0988	3.42704	1041.05	0
0.791275	0.0664781	8.94427	0.015636	101.103	4.87795	1142.83	0
0.868632	0.0702807	9.81869	0.016358	110.987	6.76725	1254.55	0
0.953552	0.0727598	10.7786	0.016996	121.837	8.80179	1377.2	0
1.04677	0.0737981	11.8323	0.017794	133.748	10.5156	1511.84	0
1.14911	0.0734231	12.9891	0.019109	146.824	11.4251	1659.64	0
1.26145	0.0716993	14.2589	0.021555	161.177	11.2172	1821.89	0
1.38477	0.0687255	15.6529	0.025928	176.935	9.92062	2000	
1.52015	0.0646441	17.1832	0.033343	194.232	7.80881		
1.66876	0.0596303	18.863	0.045387	213.221	5.35866		
1.8319	0.0539017	20.7071	0.063986	234.066	3.04567		
2.011	0.0477022	22.7315	0.091846	256.948	1.17147		
2.2076	0.0413074	24.9538	0.132069	282.068	0.20092		
2.42342	0.0349982	27.3934	0.188028	309.644	0.007367		
2.66033	0.029057	30.0714	0.263312	339.916	0		
2.92042	0.0237325	33.0113	0.360777	373.147	0		
3.20592	0.0192281	36.2385	0.482434	409.626	0		
3.51934	0.0156697	39.7813	0.628326	449.672	0		
3.8634	0.0130994	43.6704	0.79482	493.633	0		



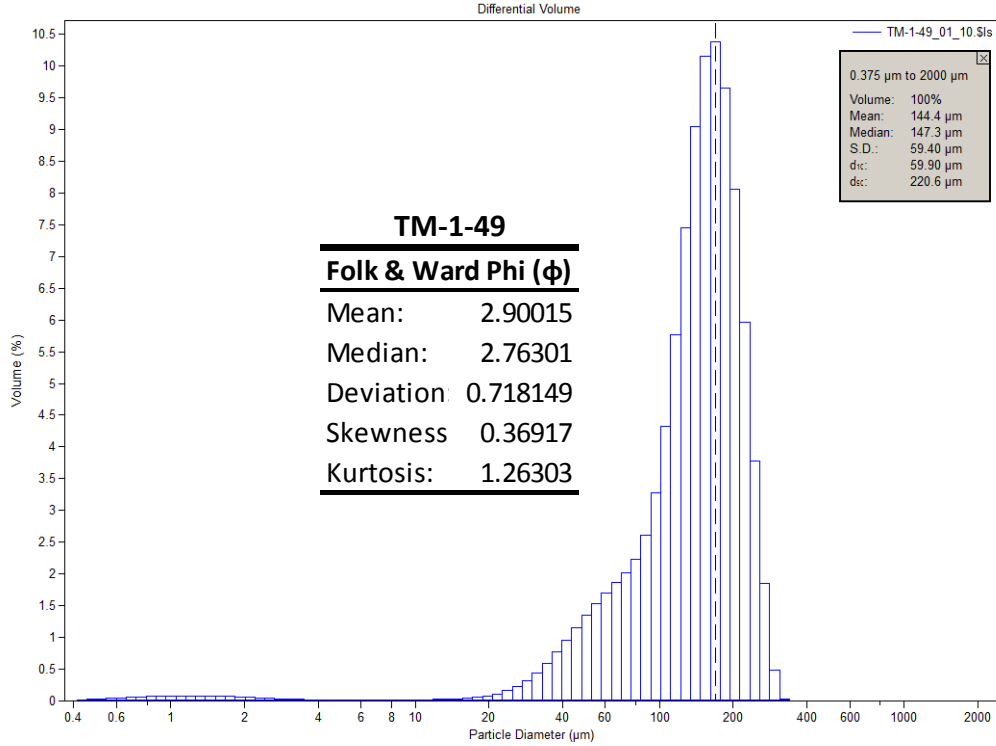
μm	Volume (%)						
0.375198	0.00774779	4.2411	0.01174	47.9397	1.20514	541.892	0
0.411878	0.0147783	4.65572	0.010669	52.6264	1.31696	594.869	0
0.452145	0.024878	5.11087	0.010445	57.7713	1.41719	653.025	0
0.496347	0.03439	5.61052	0.010881	63.4192	1.51008	716.866	0
0.544872	0.0433989	6.15902	0.011814	69.6192	1.62423	786.949	0
0.59814	0.0517825	6.76114	0.013087	76.4253	1.83387	863.883	0
0.656615	0.0594183	7.42212	0.014598	83.8969	2.26647	948.338	0
0.720807	0.0661497	8.14773	0.016279	92.0988	3.07702	1041.05	0
0.791275	0.0718283	8.94427	0.018118	101.103	4.38847	1142.83	0
0.868632	0.0762904	9.81869	0.02024	110.987	6.19398	1254.55	0
0.953552	0.0793812	10.7786	0.022938	121.837	8.26049	1377.2	0
1.04677	0.0809526	11.8323	0.026866	133.748	10.1431	1511.84	0
1.14911	0.0809993	12.9891	0.032985	146.824	11.2969	1659.64	0
1.26145	0.0795572	14.2589	0.042838	161.177	11.3099	1821.89	0
1.38477	0.0766996	15.6529	0.058478	176.935	10.1076	2000	
1.52015	0.0725488	17.1832	0.082539	194.232	7.93245		
1.66876	0.0672694	18.863	0.118178	213.221	5.32455		
1.8319	0.06108	20.7071	0.168374	234.066	2.82907		
2.011	0.0542396	22.7315	0.235996	256.948	0.830579		
2.2076	0.0470543	24.9538	0.322644	282.068	0.058042		
2.42342	0.0398476	27.3934	0.428165	309.644	0		
2.66033	0.0329576	30.0714	0.550206	339.916	0		
2.92042	0.026691	33.0113	0.683282	373.147	0		
3.20592	0.0213111	36.2385	0.820593	409.626	0		
3.51934	0.0169912	39.7813	0.955642	449.672	0		
3.8634	0.0138094	43.6704	1.08423	493.633	0		



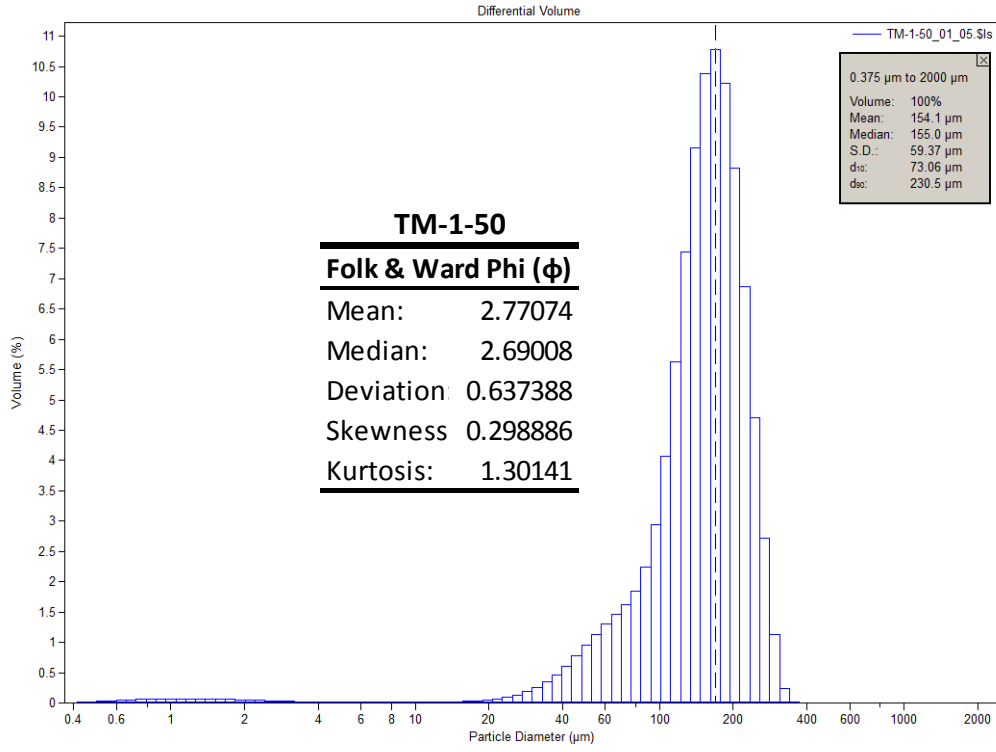
µm	Volume (%)	µm	Volume (%)	µm	Volume (%)	µm	Volume (%)
0.375198	0.00708354	4.2411	0.01237	47.9397	0.825741	541.892	0
0.411878	0.0135044	4.65572	0.011627	52.6264	1.00437	594.869	0
0.452145	0.0227101	5.11087	0.011572	57.7713	1.17758	653.025	0
0.496347	0.0313462	5.61052	0.012034	63.4192	1.33804	716.866	0
0.544872	0.0394814	6.15902	0.012862	69.6192	1.5057	786.949	0
0.59814	0.0469973	6.76114	0.013894	76.4253	1.75357	863.883	0
0.656615	0.0537781	7.42212	0.01501	83.8969	2.21487	948.338	0
0.720807	0.0596814	8.14773	0.016089	92.0988	3.05953	1041.05	0
0.791275	0.0645754	8.94427	0.017031	101.103	4.43838	1142.83	0
0.868632	0.0683218	9.81869	0.017803	110.987	6.36232	1254.55	0
0.953552	0.0707948	10.7786	0.018431	121.837	8.6051	1377.2	0
1.04677	0.0718817	11.8323	0.019123	133.748	10.705	1511.84	0
1.14911	0.0716055	12.9891	0.02015	146.824	12.0647	1659.64	0
1.26145	0.0700263	14.2589	0.022057	161.177	12.2229	1821.89	0
1.38477	0.0672382	15.6529	0.025479	176.935	11	2000	
1.52015	0.063376	17.1832	0.031322	194.232	8.62142		
1.66876	0.0586078	18.863	0.040857	213.221	5.67084		
1.8319	0.0531416	20.7071	0.055469	234.066	2.76696		
2.011	0.0472124	22.7315	0.077257	256.948	0.700258		
2.2076	0.0410853	24.9538	0.108462	282.068	0.042172		
2.42342	0.0350298	27.3934	0.151698	309.644	0		
2.66033	0.0293193	30.0714	0.210208	339.916	0		
2.92042	0.0241931	33.0113	0.287012	373.147	0		
3.20592	0.0198498	36.2385	0.385676	409.626	0		
3.51934	0.0164138	39.7813	0.508925	449.672	0		
3.8634	0.0139306	43.6704	0.656908	493.633	0		



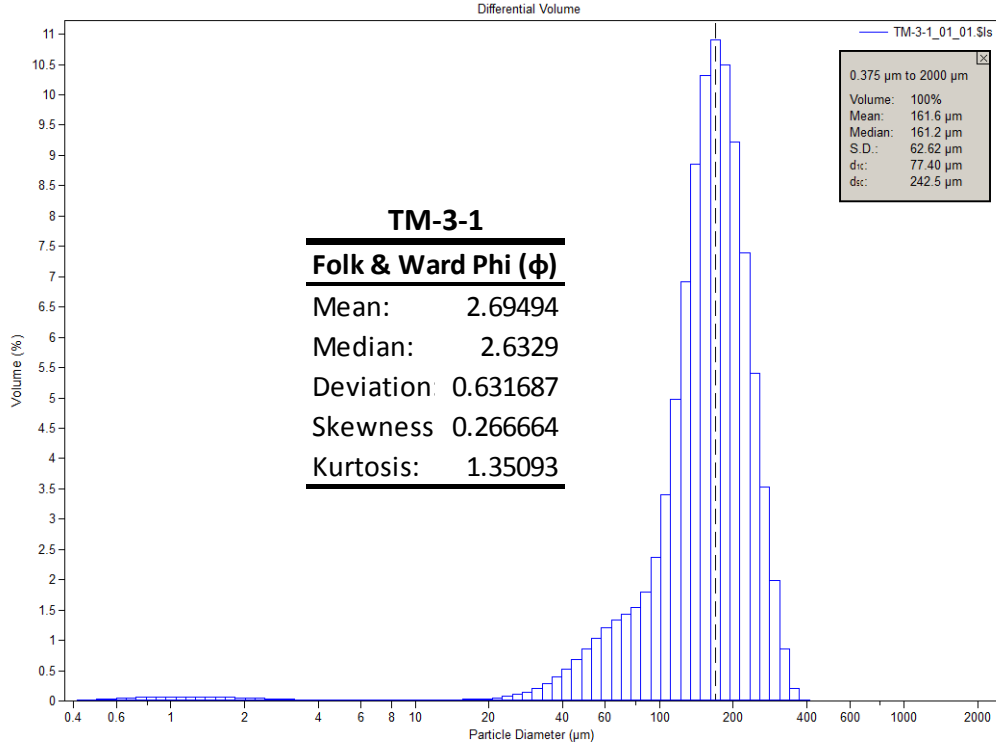
µm	Volume (%)	µm	Volume (%)	µm	Volume (%)	µm	Volume (%)
0.375198	0.0079528	4.2411	0.017015	47.9397	1.44702	541.892	0
0.411878	0.0151757	4.65572	0.015564	52.6264	1.58763	594.869	0
0.452145	0.0255694	5.11087	0.015027	57.7713	1.71855	653.025	0
0.496347	0.0353923	5.61052	0.01522	63.4192	1.86165	716.866	0
0.544872	0.0447427	6.15902	0.01596	69.6192	2.06831	786.949	0
0.59814	0.0535061	6.76114	0.017075	76.4253	2.42744	863.883	0
0.656615	0.0615657	7.42212	0.018443	83.8969	3.05635	948.338	0
0.720807	0.0687692	8.14773	0.019974	92.0988	4.06367	1041.05	0
0.791275	0.074968	8.94427	0.021633	101.103	5.47743	1142.83	0
0.868632	0.0799959	9.81869	0.023528	110.987	7.16642	1254.55	0
0.953552	0.0836913	10.7786	0.02598	121.837	8.81342	1377.2	0
1.04677	0.0858915	11.8323	0.029687	133.748	9.98375	1511.84	0
1.14911	0.0865713	12.9891	0.035763	146.824	10.297	1659.64	0
1.26145	0.0857428	14.2589	0.04592	161.177	9.60646	1821.89	0
1.38477	0.083453	15.6529	0.062518	176.935	8.07693	2000	0
1.52015	0.0797956	17.1832	0.088556	194.232	6.10214		
1.66876	0.07491	18.863	0.12758	213.221	4.10349		
1.8319	0.0689903	20.7071	0.183131	234.066	2.41294		
2.011	0.06228	22.7315	0.258576	256.948	1.18477		
2.2076	0.0550749	24.9538	0.35637	282.068	0.409465		
2.42342	0.0477042	27.3934	0.477262	309.644	0.067816		
2.66033	0.0405193	30.0714	0.619963	339.916	0.002581		
2.92042	0.0338562	33.0113	0.780156	373.147	0		
3.20592	0.0280105	36.2385	0.951	409.626	0		
3.51934	0.0231967	39.7813	1.12428	449.672	0		
3.8634	0.0195293	43.6704	1.2917	493.633	0		



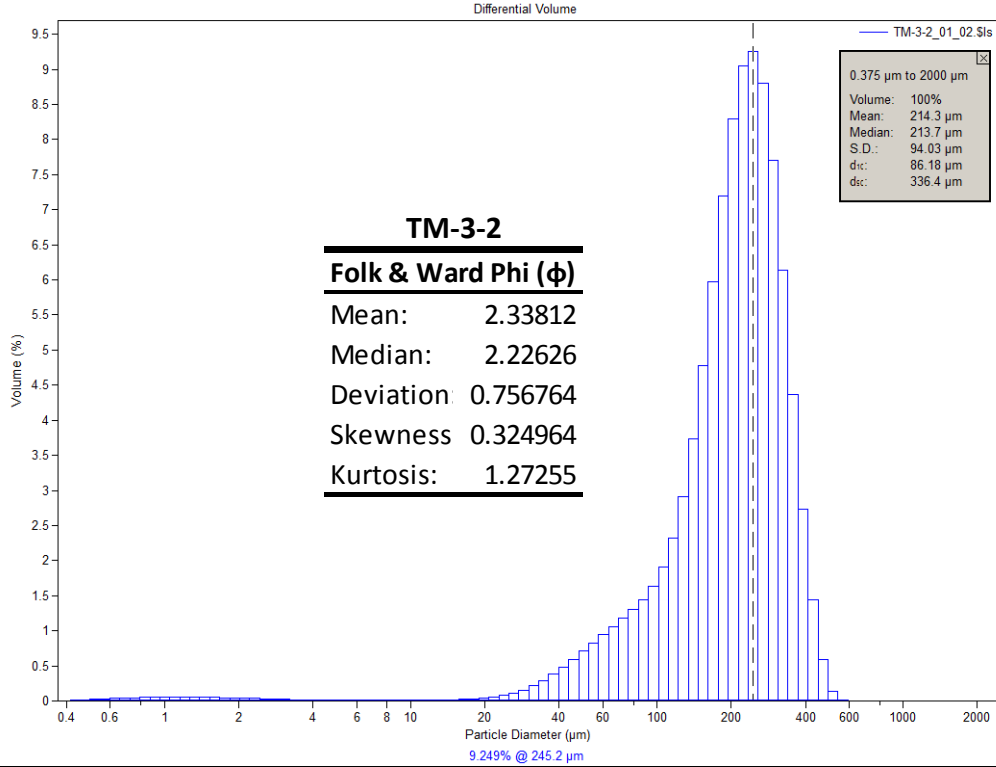
µm	Volume (%)	µm	Volume (%)	µm	Volume (%)	µm	Volume (%)
0.375198	0.00752163	4.2411	0.01451	47.9397	1.34538	541.892	0
0.411878	0.0143502	4.65572	0.012966	52.6264	1.53194	594.869	0
0.452145	0.0241695	5.11087	0.012235	57.7713	1.70343	653.025	0
0.496347	0.0334357	5.61052	0.012152	63.4192	1.85941	716.866	0
0.544872	0.0422376	6.15902	0.012568	69.6192	2.0191	786.949	0
0.59814	0.050463	6.76114	0.013336	76.4253	2.23771	863.883	0
0.656615	0.0579982	7.42212	0.01436	83.8969	2.61391	948.338	0
0.720807	0.0646973	8.14773	0.015565	92.0988	3.27326	1041.05	0
0.791275	0.0704194	8.94427	0.016914	101.103	4.31964	1142.83	0
0.868632	0.0750087	9.81869	0.018457	110.987	5.76416	1254.55	0
0.953552	0.0783157	10.7786	0.020348	121.837	7.45188	1377.2	0
1.04677	0.0801939	11.8323	0.022958	133.748	9.05135	1511.84	0
1.14911	0.0806292	12.9891	0.026807	146.824	10.1458	1659.64	0
1.26145	0.0796461	14.2589	0.032781	161.177	10.3838	1821.89	0
1.38477	0.0773015	15.6529	0.042089	176.935	9.64502	2000	
1.52015	0.0736963	17.1832	0.056527	194.232	8.06232		
1.66876	0.0689732	18.863	0.078683	213.221	5.96187		
1.8319	0.0633249	20.7071	0.111834	234.066	3.77463		
2.011	0.0569824	22.7315	0.160429	256.948	1.84987		
2.2076	0.050223	24.9538	0.229308	282.068	0.492772		
2.42342	0.0433447	27.3934	0.323083	309.644	0.03171		
2.66033	0.0366628	30.0714	0.44482	339.916	0		
2.92042	0.0304693	33.0113	0.593986	373.147	0		
3.20592	0.0250208	36.2385	0.766455	409.626	0		
3.51934	0.0204968	39.7813	0.954813	449.672	0		
3.8634	0.0169925	43.6704	1.15045	493.633	0		



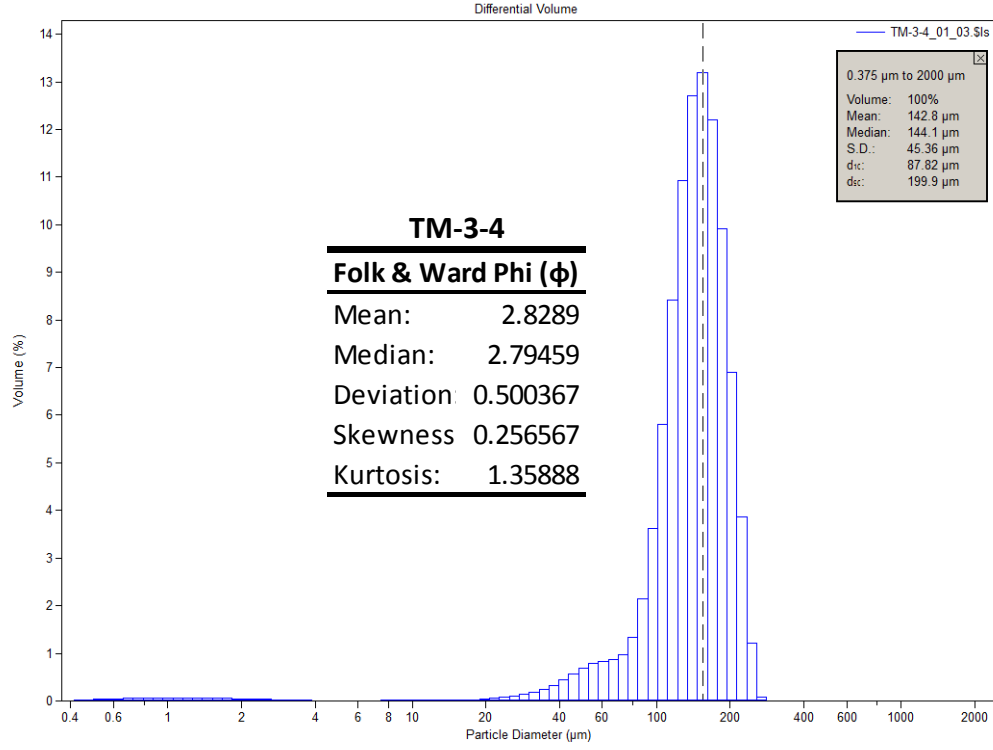
μm	Volume (%)						
0.375198	0.00683518	4.2411	0.011055	47.9397	0.950898	541.892	0
0.411878	0.0130323	4.65572	0.009896	52.6264	1.13143	594.869	0
0.452145	0.0219209	5.11087	0.009425	57.7713	1.30134	653.025	0
0.496347	0.0302673	5.61052	0.009496	63.4192	1.45551	716.866	0
0.544872	0.0381404	6.15902	0.009971	69.6192	1.61378	786.949	0
0.59814	0.0454287	6.76114	0.010705	76.4253	1.83876	863.883	0
0.656615	0.0520231	7.42212	0.011589	83.8969	2.23817	948.338	0
0.720807	0.0577883	8.14773	0.012519	92.0988	2.94709	1041.05	0
0.791275	0.0625985	8.94427	0.013413	101.103	4.0759	1142.83	0
0.868632	0.0663219	9.81869	0.014253	110.987	5.62771	1254.55	0
0.953552	0.0688361	10.7786	0.015094	121.837	7.43576	1377.2	0
1.04677	0.0700297	11.8323	0.016164	133.748	9.15732	1511.84	0
1.14911	0.0699198	12.9891	0.01779	146.824	10.3808	1659.64	0
1.26145	0.068557	14.2589	0.020568	161.177	10.7789	1821.89	0
1.38477	0.066023	15.6529	0.025248	176.935	10.2198	2000	
1.52015	0.0624361	17.1832	0.032905	194.232	8.82591		
1.66876	0.0579456	18.863	0.045042	213.221	6.8657		
1.8319	0.0527402	20.7071	0.063445	234.066	4.7097		
2.011	0.0470327	22.7315	0.090688	256.948	2.72052		
2.2076	0.0410665	24.9538	0.129649	282.068	1.13277		
2.42342	0.0350934	27.3934	0.18362	309.644	0.235302		
2.66033	0.0293722	30.0714	0.25615	339.916	0.011588		
2.92042	0.0241361	33.0113	0.350114	373.147	0		
3.20592	0.0195858	36.2385	0.467865	409.626	0		
3.51934	0.015857	39.7813	0.609727	449.672	0		
3.8634	0.0130162	43.6704	0.773004	493.633	0		



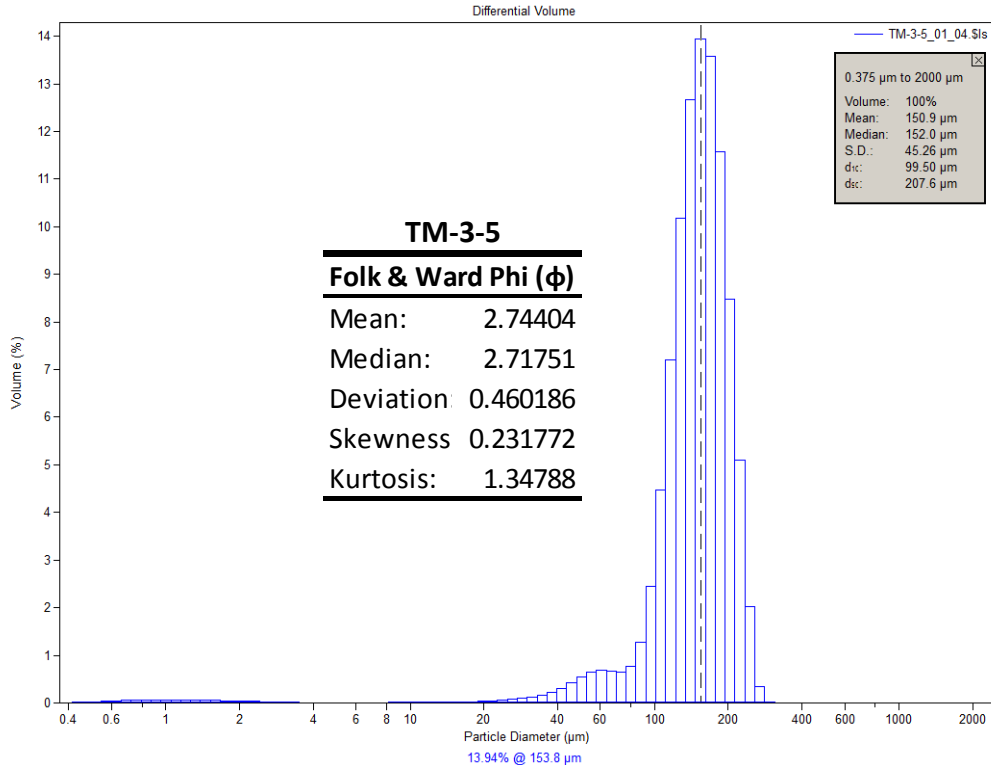
μm	Volume (%)						
0.375198	0.0065498	4.2411	0.013724	47.9397	0.85604	541.892	0
0.411878	0.0124932	4.65572	0.012852	52.6264	1.03939	594.869	0
0.452145	0.0210322	5.11087	0.012704	57.7713	1.20579	653.025	0
0.496347	0.0290762	5.61052	0.013114	63.4192	1.33424	716.866	0
0.544872	0.0366986	6.15902	0.013928	69.6192	1.42793	786.949	0
0.59814	0.043798	6.76114	0.014971	76.4253	1.54238	863.883	0
0.656615	0.0502737	7.42212	0.016103	83.8969	1.79847	948.338	0
0.720807	0.0559968	8.14773	0.017179	92.0988	2.3643	1041.05	0
0.791275	0.0608459	8.94427	0.018082	101.103	3.40264	1142.83	0
0.868632	0.0646876	9.81869	0.018758	110.987	4.97102	1254.55	0
0.953552	0.0673975	10.7786	0.019235	121.837	6.91493	1377.2	0
1.04677	0.0688547	11.8323	0.019727	133.748	8.85824	1511.84	0
1.14911	0.0690591	12.9891	0.020515	146.824	10.3197	1659.64	0
1.26145	0.0680432	14.2589	0.02215	161.177	10.9117	1821.89	0
1.38477	0.0658682	15.6529	0.025236	176.935	10.4995	2000	
1.52015	0.0626355	17.1832	0.030667	194.232	9.21984		
1.66876	0.0584785	18.863	0.039664	213.221	7.40039		
1.8319	0.0535746	20.7071	0.053619	234.066	5.40244		
2.011	0.04813	22.7315	0.074745	256.948	3.53036		
2.2076	0.0423887	24.9538	0.105482	282.068	1.99354		
2.42342	0.0366074	27.3934	0.14889	309.644	0.86142		
2.66033	0.0310563	30.0714	0.208674	339.916	0.198909		
2.92042	0.0259813	33.0113	0.288369	373.147	0.011198		
3.20592	0.0215986	36.2385	0.391943	409.626	0		
3.51934	0.0180568	39.7813	0.522105	449.672	0		
3.8634	0.0154322	43.6704	0.678664	493.633	0		



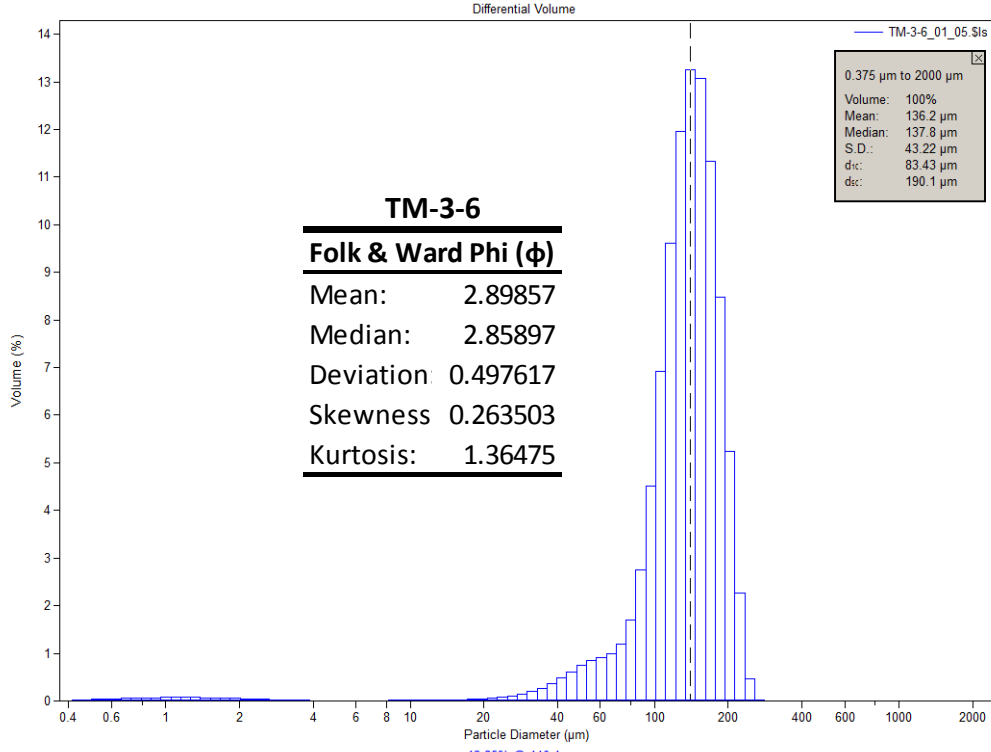
μm	Volume (%)						
0.375198	0.00526917	4.2411	0.013813	47.9397	0.711275	541.892	0.008512
0.411878	0.0100491	4.65572	0.012781	52.6264	0.827166	594.869	0
0.452145	0.0169119	5.11087	0.012254	57.7713	0.943109	653.025	0
0.496347	0.0233698	5.61052	0.01213	63.4192	1.05937	716.866	0
0.544872	0.0294808	6.15902	0.012305	69.6192	1.17704	786.949	0
0.59814	0.0351642	6.76114	0.012668	76.4253	1.30043	863.883	0
0.656615	0.0403404	7.42212	0.013132	83.8969	1.44223	948.338	0
0.720807	0.0449099	8.14773	0.013615	92.0988	1.62898	1041.05	0
0.791275	0.0487804	8.94427	0.014062	101.103	1.90256	1142.83	0
0.868632	0.0518526	9.81869	0.014476	110.987	2.31516	1254.55	0
0.953552	0.0540368	10.7786	0.014933	121.837	2.91743	1377.2	0
1.04677	0.0552473	11.8323	0.015629	133.748	3.74043	1511.84	0
1.14911	0.0554945	12.9891	0.016856	146.824	4.7768	1659.64	0
1.26145	0.0548119	14.2589	0.019071	161.177	5.96878	1821.89	0
1.38477	0.0532562	15.6529	0.022862	176.935	7.19991	2000	
1.52015	0.05091	17.1832	0.029067	194.232	8.29547		
1.66876	0.047879	18.863	0.038854	213.221	9.04439		
1.8319	0.0442948	20.7071	0.053784	234.066	9.24927		
2.011	0.0403094	22.7315	0.076046	256.948	8.7955		
2.2076	0.0360941	24.9538	0.108239	282.068	7.70091		
2.42342	0.0318283	27.3934	0.153204	309.644	6.13271		
2.66033	0.0276954	30.0714	0.213351	339.916	4.373		
2.92042	0.0238637	33.0113	0.28968	373.147	2.72855		
3.20592	0.0204789	36.2385	0.381266	409.626	1.44195		
3.51934	0.0176452	39.7813	0.484925	449.672	0.597152		
3.8634	0.0154207	43.6704	0.596282	493.633	0.141267		



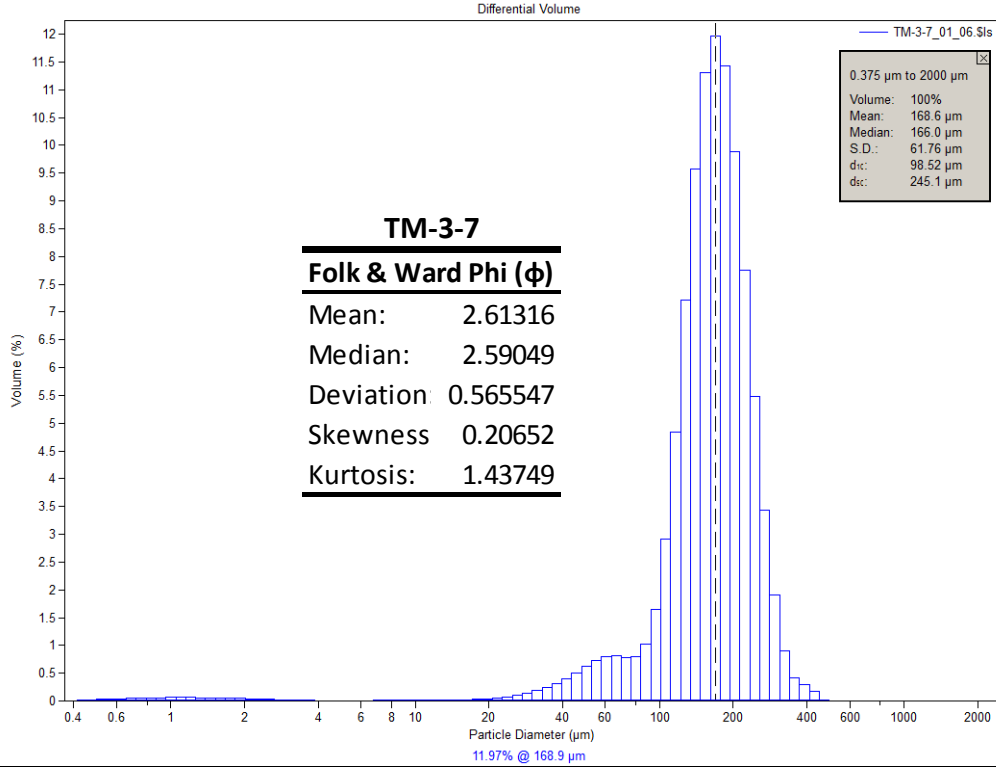
μm	Volume (%)						
0.375198	0.00716223	4.2411	0.008372	47.9397	0.695718	541.892	0
0.411878	0.0136481	4.65572	0.007607	52.6264	0.790293	594.869	0
0.452145	0.0229274	5.11087	0.007496	57.7713	0.838387	653.025	0
0.496347	0.0315976	5.61052	0.00788	63.4192	0.86881	716.866	0
0.544872	0.0397177	6.15902	0.008602	69.6192	0.976702	786.949	0
0.59814	0.0471604	6.76114	0.009509	76.4253	1.32959	863.883	0
0.656615	0.0538028	7.42212	0.010473	83.8969	2.14877	948.338	0
0.720807	0.0594982	8.14773	0.011382	92.0988	3.6292	1041.05	0
0.791275	0.0641147	8.94427	0.012149	101.103	5.80421	1142.83	0
0.868632	0.0675187	9.81869	0.012775	110.987	8.41545	1254.55	0
0.953552	0.0695934	10.7786	0.013348	121.837	10.9355	1377.2	0
1.04677	0.07024	11.8323	0.014146	133.748	12.7165	1511.84	0
1.14911	0.0695042	12.9891	0.015576	146.824	13.1975	1659.64	0
1.26145	0.0674691	14.2589	0.01822	161.177	12.2019	1821.89	0
1.38477	0.064252	15.6529	0.022786	176.935	9.9083	2000	
1.52015	0.0600075	17.1832	0.029959	194.232	6.89964		
1.66876	0.0549209	18.863	0.040482	213.221	3.86914		
1.8319	0.0492112	20.7071	0.054849	234.066	1.21126		
2.011	0.0431177	22.7315	0.073776	256.948	0.089162		
2.2076	0.0369	24.9538	0.098569	282.068	0		
2.42342	0.0308187	27.3934	0.131539	309.644	0		
2.66033	0.0251279	30.0714	0.177155	339.916	0		
2.92042	0.0200504	33.0113	0.240999	373.147	0		
3.20592	0.0157632	36.2385	0.328487	409.626	0		
3.51934	0.0123775	39.7813	0.441116	449.672	0		
3.8634	0.00992693	43.6704	0.57021	493.633	0		



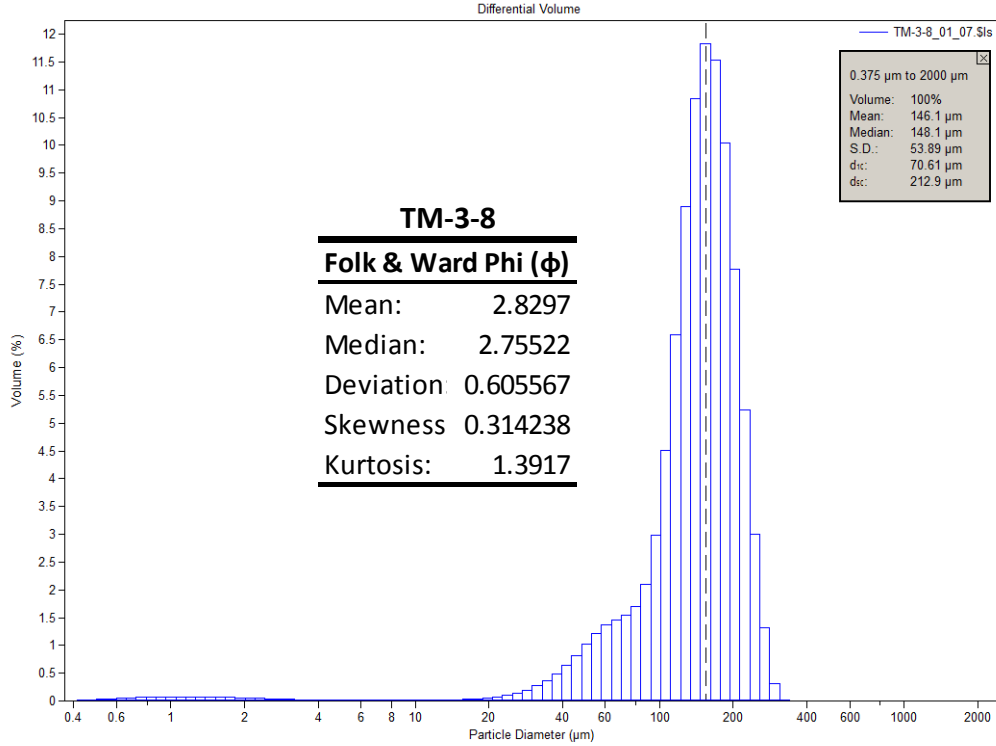
µm	Volume (%)	µm	Volume (%)	µm	Volume (%)	µm	Volume (%)
0.375198	0.00680656	4.2411	0.00668	47.9397	0.540021	541.892	0
0.411878	0.0129681	4.65572	0.00619	52.6264	0.637677	594.869	0
0.452145	0.0217773	5.11087	0.006322	57.7713	0.678721	653.025	0
0.496347	0.0299962	5.61052	0.006914	63.4192	0.658036	716.866	0
0.544872	0.037677	6.15902	0.007813	69.6192	0.638376	786.949	0
0.59814	0.0446951	6.76114	0.008862	76.4253	0.769633	863.883	0
0.656615	0.0509303	7.42212	0.009923	83.8969	1.28121	948.338	0
0.720807	0.0562412	8.14773	0.010868	92.0988	2.45197	1041.05	0
0.791275	0.0605005	8.94427	0.011587	101.103	4.46437	1142.83	0
0.868632	0.0635806	9.81869	0.012056	110.987	7.19686	1254.55	0
0.953552	0.065372	10.7786	0.012325	121.837	10.1706	1377.2	0
1.04677	0.0657855	11.8323	0.012659	133.748	12.6694	1511.84	0
1.14911	0.0648697	12.9891	0.013419	146.824	13.938	1659.64	0
1.26145	0.0627137	14.2589	0.015215	161.177	13.5723	1821.89	0
1.38477	0.0594381	15.6529	0.01872	176.935	11.5806	2000	
1.52015	0.0552008	17.1832	0.024596	194.232	8.48691		
1.66876	0.0501885	18.863	0.033486	213.221	5.09313		
1.8319	0.0446204	20.7071	0.045455	234.066	2.0298		
2.011	0.0387316	22.7315	0.060513	256.948	0.34912		
2.2076	0.0327773	24.9538	0.078558	282.068	0.012369		
2.42342	0.027007	27.3934	0.100227	309.644	0		
2.66033	0.0216643	30.0714	0.128451	339.916	0		
2.92042	0.0169555	33.0113	0.168268	373.147	0		
3.20592	0.0130439	36.2385	0.227222	409.626	0		
3.51934	0.0100252	39.7813	0.311945	449.672	0		
3.8634	0.00791946	43.6704	0.421078	493.633	0		



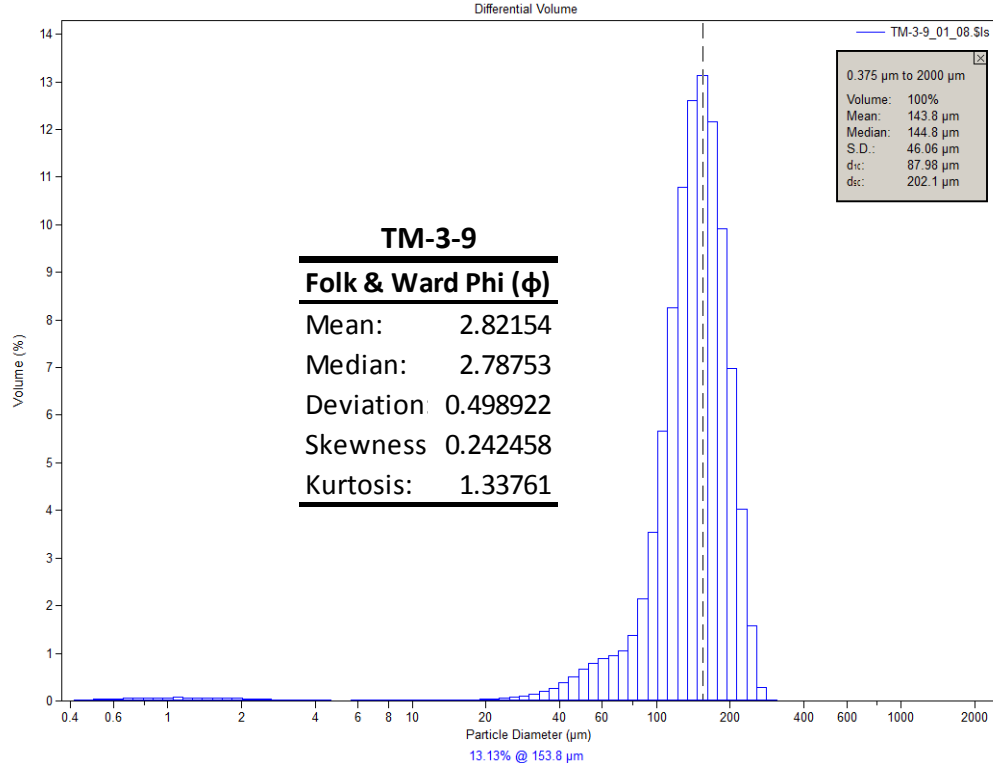
μm	Volume (%)						
0.375198	0.00741661	4.2411	0.007482	47.9397	0.745663	541.892	0
0.411878	0.0141364	4.65572	0.00667	52.6264	0.848456	594.869	0
0.452145	0.0237594	5.11087	0.006579	57.7713	0.916884	653.025	0
0.496347	0.0327677	5.61052	0.00704	63.4192	0.992932	716.866	0
0.544872	0.0412265	6.15902	0.007876	69.6192	1.19348	786.949	0
0.59814	0.0490069	6.76114	0.008927	76.4253	1.70616	863.883	0
0.656615	0.0559822	7.42212	0.010047	83.8969	2.75706	948.338	0
0.720807	0.062001	8.14773	0.011117	92.0988	4.51542	1041.05	0
0.791275	0.0669219	8.94427	0.012034	101.103	6.92078	1142.83	0
0.868632	0.0706011	9.81869	0.012783	110.987	9.60554	1254.55	0
0.953552	0.0729078	10.7786	0.013451	121.837	11.9503	1377.2	0
1.04677	0.0737274	11.8323	0.014299	133.748	13.2543	1511.84	0
1.14911	0.0730917	12.9891	0.015762	146.824	13.0755	1659.64	0
1.26145	0.0710738	14.2589	0.018433	161.177	11.34	1821.89	0
1.38477	0.0677811	15.6529	0.023089	176.935	8.48302	2000	0
1.52015	0.0633636	17.1832	0.030531	194.232	5.23795		
1.66876	0.0580062	18.863	0.041651	213.221	2.26154		
1.8319	0.0519337	20.7071	0.057244	234.066	0.469348		
2.011	0.0453994	22.7315	0.078266	256.948	0.022521		
2.2076	0.0386828	24.9538	0.1063	282.068	0		
2.42342	0.0320735	27.3934	0.143819	309.644	0		
2.66033	0.0258563	30.0714	0.195095	339.916	0		
2.92042	0.0202887	33.0113	0.265585	373.147	0		
3.20592	0.0155771	36.2385	0.360138	409.626	0		
3.51934	0.0118562	39.7813	0.479455	449.672	0		
3.8634	0.00917219	43.6704	0.614746	493.633	0		



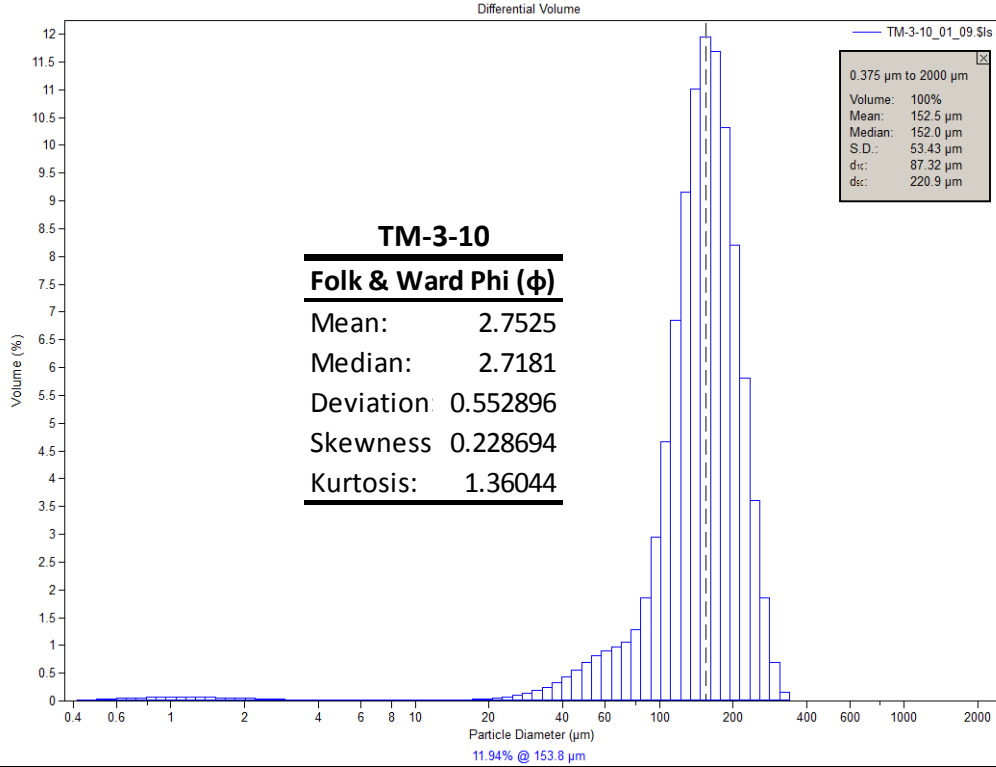
µm	Volume (%)	µm	Volume (%)	µm	Volume (%)	µm	Volume (%)
0.375198	0.00634719	4.2411	0.007069	47.9397	0.620217	541.892	0
0.411878	0.0120973	4.65572	0.006491	52.6264	0.726581	594.869	0
0.452145	0.0203313	5.11087	0.006572	57.7713	0.797149	653.025	0
0.496347	0.0280373	5.61052	0.007162	63.4192	0.810045	716.866	0
0.544872	0.0352708	6.15902	0.00812	69.6192	0.78202	786.949	0
0.59814	0.0419208	6.76114	0.009285	76.4253	0.799025	863.883	0
0.656615	0.0478788	7.42212	0.010523	83.8969	1.01731	948.338	0
0.720807	0.0530147	8.14773	0.011695	92.0988	1.64994	1041.05	0
0.791275	0.0572076	8.94427	0.01268	101.103	2.90633	1142.83	0
0.868632	0.0603351	9.81869	0.013422	110.987	4.83897	1254.55	0
0.953552	0.0622864	10.7786	0.013939	121.837	7.22157	1377.2	0
1.04677	0.0629658	11.8323	0.014455	133.748	9.56927	1511.84	0
1.14911	0.0624029	12.9891	0.015301	146.824	11.3037	1659.64	0
1.26145	0.0606634	14.2589	0.017152	161.177	11.9702	1821.89	0
1.38477	0.0578421	15.6529	0.020808	176.935	11.4361	2000	
1.52015	0.0540718	17.1832	0.027346	194.232	9.89253		
1.66876	0.0495115	18.863	0.038089	213.221	7.74984		
1.8319	0.0443578	20.7071	0.054129	234.066	5.4806		
2.011	0.0388244	22.7315	0.076707	256.948	3.43912		
2.2076	0.0331519	24.9538	0.106467	282.068	1.90078		
2.42342	0.02758	27.3934	0.143963	309.644	0.907547		
2.66033	0.0223514	30.0714	0.19016	339.916	0.418648		
2.92042	0.017676	33.0113	0.246485	373.147	0.297719		
3.20592	0.0137316	36.2385	0.316167	409.626	0.173162		
3.51934	0.0106304	39.7813	0.402463	449.672	0.020003		
3.8634	0.00841749	43.6704	0.505998	493.633	0		



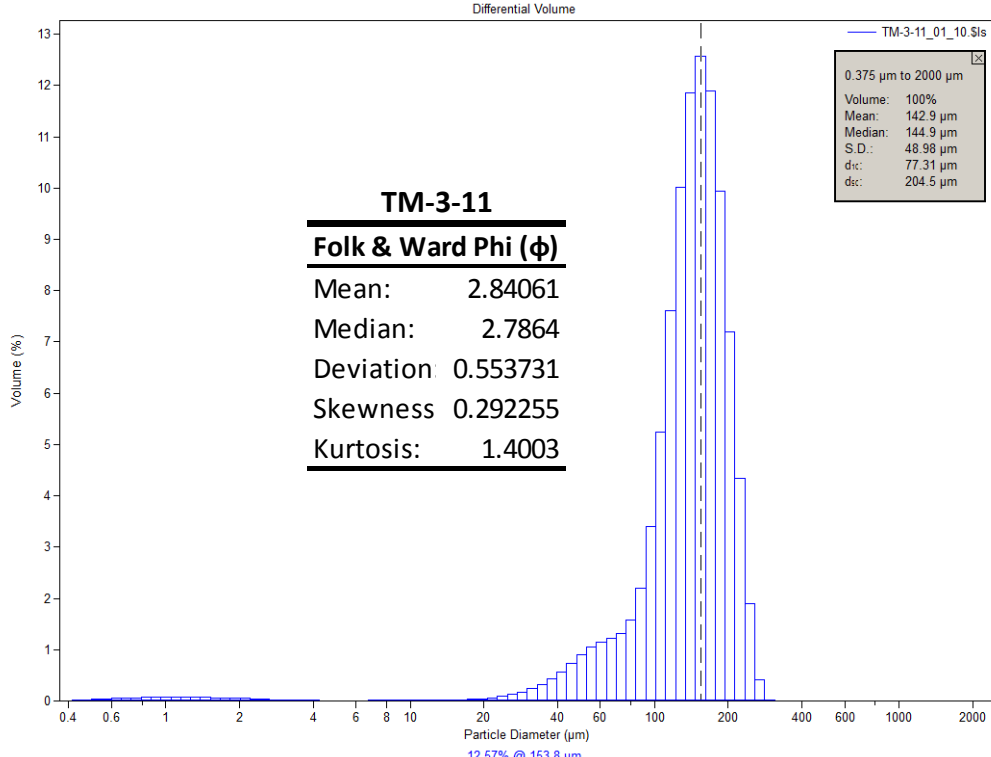
μm	Volume (%)						
0.375198	0.00720369	4.2411	0.015869	47.9397	1.0188	541.892	0
0.411878	0.0137387	4.65572	0.015062	52.6264	1.20989	594.869	0
0.452145	0.0231222	5.11087	0.014974	57.7713	1.36452	653.025	0
0.496347	0.0319519	5.61052	0.015426	63.4192	1.46446	716.866	0
0.544872	0.0403054	6.15902	0.01625	69.6192	1.53837	786.949	0
0.59814	0.048069	6.76114	0.017274	76.4253	1.69143	863.883	0
0.656615	0.0551299	7.42212	0.018363	83.8969	2.1034	948.338	0
0.720807	0.061346	8.14773	0.019383	92.0988	2.98966	1041.05	0
0.791275	0.0665831	8.94427	0.020232	101.103	4.50406	1142.83	0
0.868632	0.0706969	9.81869	0.020885	110.987	6.59225	1254.55	0
0.953552	0.0735535	10.7786	0.021409	121.837	8.90017	1377.2	0
1.04677	0.0750265	11.8323	0.022085	133.748	10.8413	1511.84	0
1.14911	0.0751222	12.9891	0.02331	146.824	11.8325	1659.64	0
1.26145	0.0738856	14.2589	0.025811	161.177	11.5419	1821.89	0
1.38477	0.0713935	15.6529	0.030466	176.935	10.0477	2000	
1.52015	0.0677671	17.1832	0.038475	194.232	7.76597		
1.66876	0.0631628	18.863	0.051445	213.221	5.24081		
1.8319	0.0577838	20.7071	0.071117	234.066	2.99611		
2.011	0.0518631	22.7315	0.099935	256.948	1.31082		
2.2076	0.0456722	24.9538	0.140504	282.068	0.309752		
2.42342	0.039493	27.3934	0.195859	309.644	0.017876		
2.66033	0.0336161	30.0714	0.269762	339.916	0		
2.92042	0.0283015	33.0113	0.365998	373.147	0		
3.20592	0.0237684	36.2385	0.488951	409.626	0		
3.51934	0.0201594	39.7813	0.641483	449.672	0		
3.8634	0.017534	43.6704	0.821659	493.633	0		



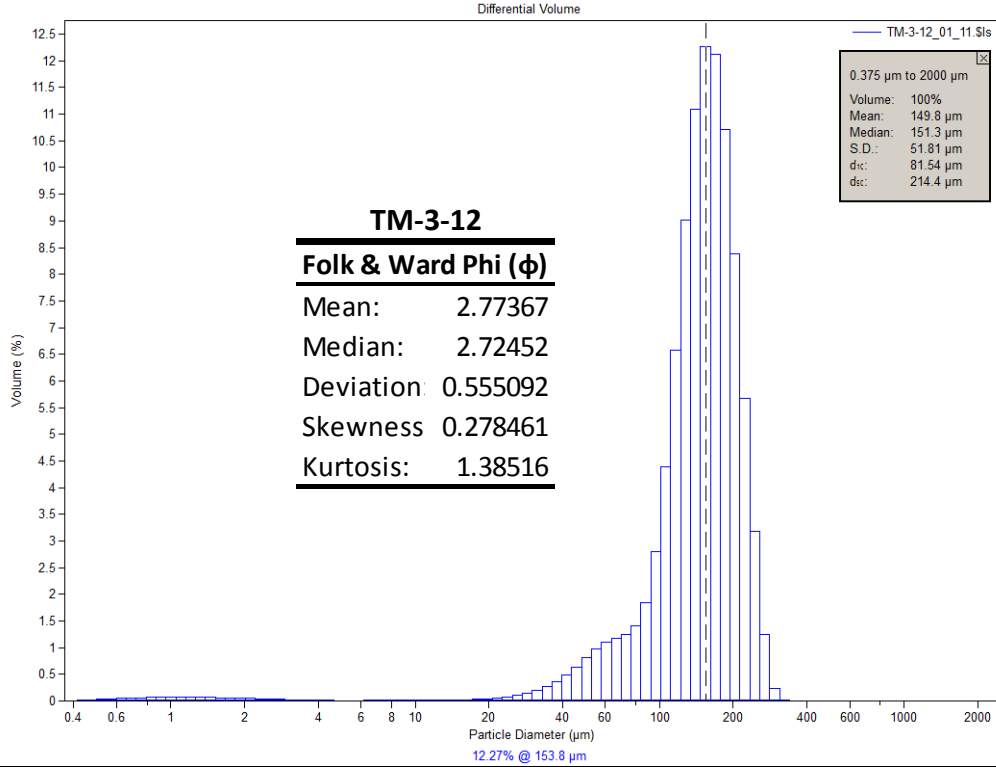
µm	Volume (%)	µm	Volume (%)	µm	Volume (%)	µm	Volume (%)
0.375198	0.00706742	4.2411	0.010572	47.9397	0.662431	541.892	0
0.411878	0.0134725	4.65572	0.009783	52.6264	0.792888	594.869	0
0.452145	0.0226505	5.11087	0.009691	57.7713	0.88318	653.025	0
0.496347	0.0312525	5.61052	0.01013	63.4192	0.945613	716.866	0
0.544872	0.0393445	6.15902	0.01093	69.6192	1.05917	786.949	0
0.59814	0.0468069	6.76114	0.011925	76.4253	1.38316	863.883	0
0.656615	0.053523	7.42212	0.012971	83.8969	2.13929	948.338	0
0.720807	0.0593501	8.14773	0.013933	92.0988	3.54157	1041.05	0
0.791275	0.0641574	8.94427	0.014702	101.103	5.65575	1142.83	0
0.868632	0.0678083	9.81869	0.01525	110.987	8.24839	1254.55	0
0.953552	0.07018	10.7786	0.015634	121.837	10.7903	1377.2	0
1.04677	0.0711625	11.8323	0.016104	133.748	12.6088	1511.84	0
1.14911	0.0707827	12.9891	0.017013	146.824	13.1262	1659.64	0
1.26145	0.0691048	14.2589	0.018894	161.177	12.1589	1821.89	0
1.38477	0.0662262	15.6529	0.022344	176.935	9.91299	2000	
1.52015	0.062283	17.1832	0.027916	194.232	6.9757		
1.66876	0.0574441	18.863	0.036165	213.221	4.03432		
1.8319	0.0519161	20.7071	0.047289	234.066	1.58159		
2.011	0.0459312	22.7315	0.061694	256.948	0.280559		
2.2076	0.0397498	24.9538	0.080258	282.068	0.010865		
2.42342	0.033639	27.3934	0.105016	309.644	0		
2.66033	0.0278666	30.0714	0.140547	339.916	0		
2.92042	0.0226729	33.0113	0.193354	373.147	0		
3.20592	0.0182559	36.2385	0.271276	409.626	0		
3.51934	0.0147457	39.7813	0.379823	449.672	0		
3.8634	0.0121933	43.6704	0.515517	493.633	0		



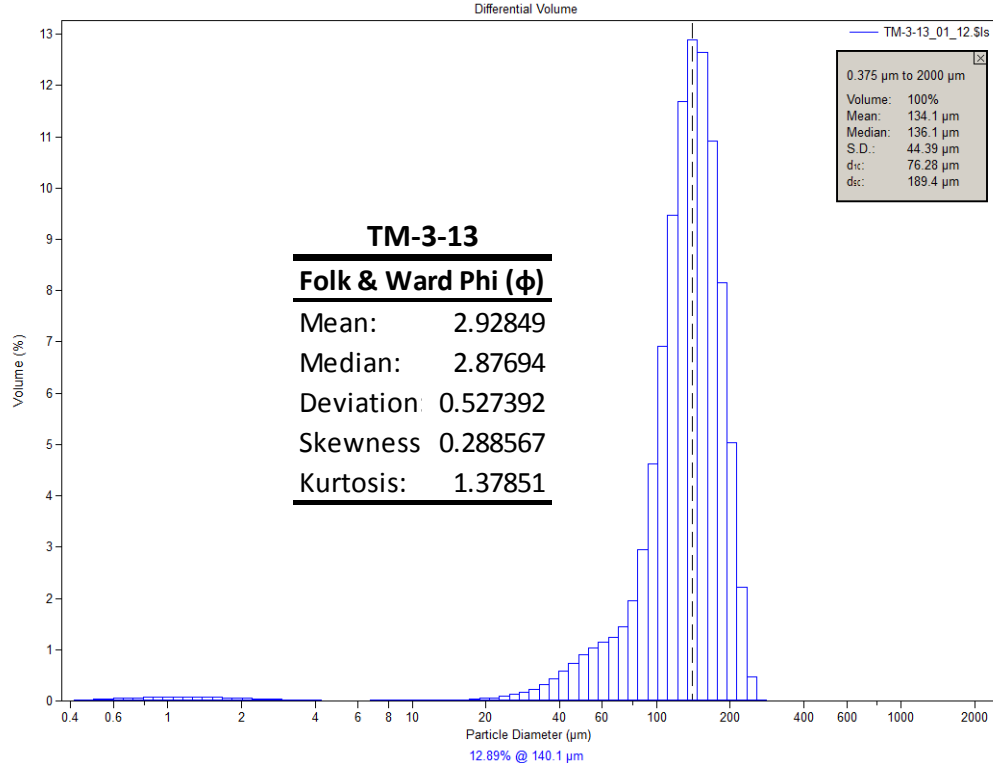
µm	Volume (%)	µm	Volume (%)	µm	Volume (%)	µm	Volume (%)
0.375198	0.00688777	4.2411	0.009675	47.9397	0.699485	541.892	0
0.411878	0.0131287	4.65572	0.00893	52.6264	0.820897	594.869	0
0.452145	0.0220682	5.11087	0.008858	57.7713	0.907602	653.025	0
0.496347	0.0304403	5.61052	0.009298	63.4192	0.964525	716.866	0
0.544872	0.0383073	6.15902	0.010094	69.6192	1.05014	786.949	0
0.59814	0.0455509	6.76114	0.011088	76.4253	1.28897	863.883	0
0.656615	0.0520558	7.42212	0.012146	83.8969	1.85986	948.338	0
0.720807	0.057683	8.14773	0.013146	92.0988	2.95314	1041.05	0
0.791275	0.0623036	8.94427	0.013991	101.103	4.6605	1142.83	0
0.868632	0.0657859	9.81869	0.014662	110.987	6.85286	1254.55	0
0.953552	0.0680114	10.7786	0.015229	121.837	9.15051	1377.2	0
1.04677	0.0688753	11.8323	0.015947	133.748	11.0129	1511.84	0
1.14911	0.0684096	12.9891	0.01718	146.824	11.9446	1659.64	0
1.26145	0.0666803	14.2589	0.019514	161.177	11.6868	1821.89	0
1.38477	0.0637881	15.6529	0.023635	176.935	10.3193	2000	
1.52015	0.0598707	17.1832	0.030336	194.232	8.20664		
1.66876	0.0550966	18.863	0.040539	213.221	5.81492		
1.8319	0.0496714	20.7071	0.055007	234.066	3.60312		
2.011	0.043823	22.7315	0.074779	256.948	1.85263		
2.2076	0.0378054	24.9538	0.101076	282.068	0.701981		
2.42342	0.0318763	27.3934	0.135785	309.644	0.14777		
2.66033	0.0262929	30.0714	0.182204	339.916	0.008279		
2.92042	0.0212827	33.0113	0.244617	373.147	0		
3.20592	0.017033	36.2385	0.328077	409.626	0		
3.51934	0.0136638	39.7813	0.435548	449.672	0		
3.8634	0.0112207	43.6704	0.563655	493.633	0		



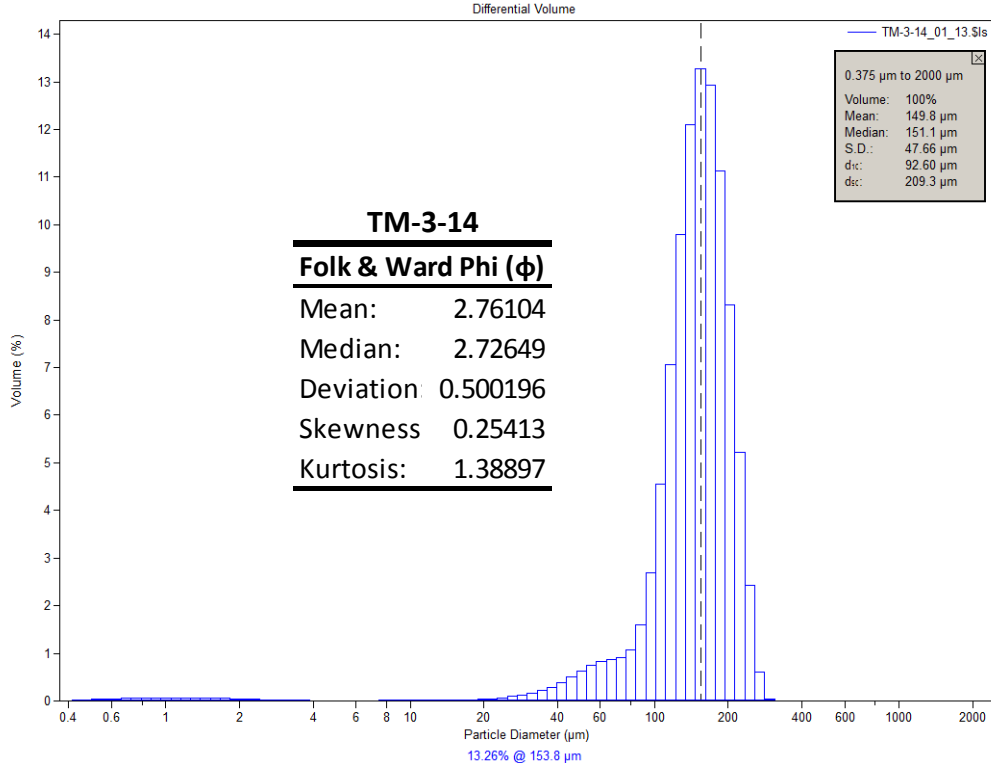
μm	Volume (%)						
0.375198	0.00730918	4.2411	0.009327	47.9397	0.897706	541.892	0
0.411878	0.0139326	4.65572	0.008235	52.6264	1.04712	594.869	0
0.452145	0.0234216	5.11087	0.007863	57.7713	1.15329	653.025	0
0.496347	0.0323117	5.61052	0.008054	63.4192	1.22149	716.866	0
0.544872	0.0406698	6.15902	0.008656	69.6192	1.31595	786.949	0
0.59814	0.0483717	6.76114	0.009516	76.4253	1.57612	863.883	0
0.656615	0.0552958	7.42212	0.010503	83.8969	2.20092	948.338	0
0.720807	0.0612958	8.14773	0.011504	92.0988	3.39335	1041.05	0
0.791275	0.0662346	8.94427	0.012422	101.103	5.24728	1142.83	0
0.868632	0.0699732	9.81869	0.013243	110.987	7.60192	1254.55	0
0.953552	0.0723849	10.7786	0.014036	121.837	10.0101	1377.2	0
1.04677	0.0733588	11.8323	0.015076	133.748	11.8577	1511.84	0
1.14911	0.0729243	12.9891	0.016773	146.824	12.57	1659.64	0
1.26145	0.0711501	14.2589	0.019798	161.177	11.8907	1821.89	0
1.38477	0.0681383	15.6529	0.025013	176.935	9.93991	2000	
1.52015	0.0640297	17.1832	0.03345	194.232	7.20524		
1.66876	0.0589988	18.863	0.046404	213.221	4.34664		
1.8319	0.0532569	20.7071	0.065104	234.066	1.90085		
2.011	0.0470397	22.7315	0.091133	256.948	0.422725		
2.2076	0.0406096	24.9538	0.126394	282.068	0.022522		
2.42342	0.0342347	27.3934	0.173448	309.644	0		
2.66033	0.0281829	30.0714	0.236376	339.916	0		
2.92042	0.0226942	33.0113	0.320071	373.147	0		
3.20592	0.0179682	36.2385	0.429756	409.626	0		
3.51934	0.0141389	39.7813	0.567925	449.672	0		
3.8634	0.0112644	43.6704	0.729224	493.633	0		



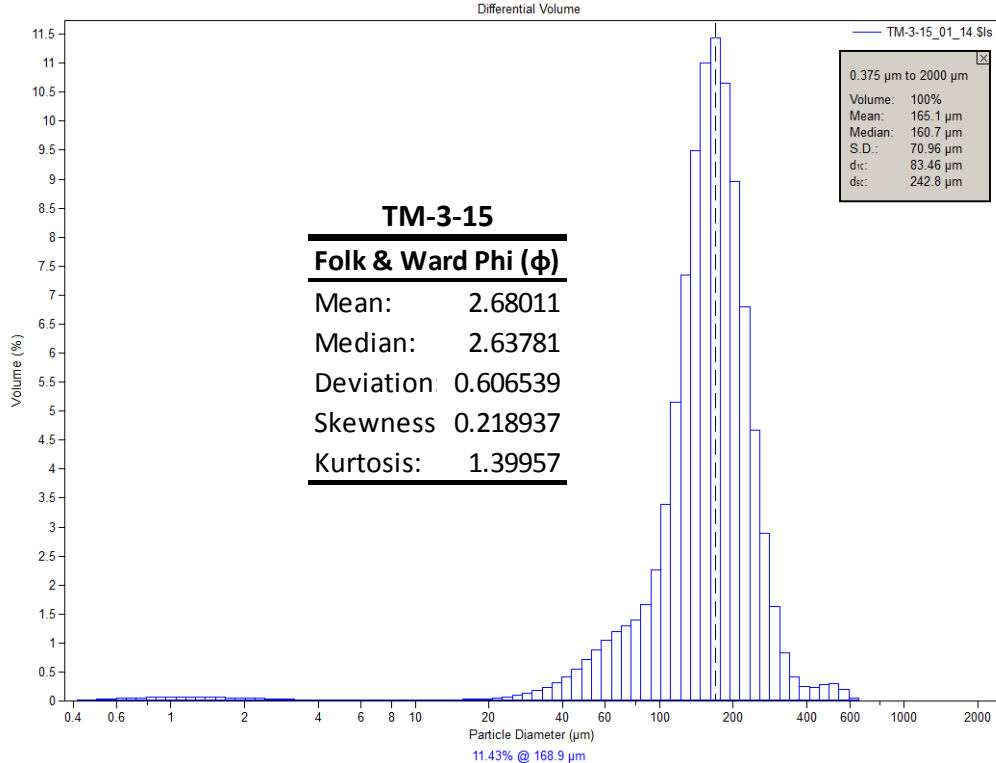
μm	Volume (%)						
0.375198	0.00701644	4.2411	0.009666	47.9397	0.808385	541.892	0
0.411878	0.0133748	4.65572	0.008774	52.6264	0.970277	594.869	0
0.452145	0.0224852	5.11087	0.008573	57.7713	1.09613	653.025	0
0.496347	0.0310219	5.61052	0.008899	63.4192	1.17275	716.866	0
0.544872	0.0390496	6.15902	0.009598	69.6192	1.23798	786.949	0
0.59814	0.0464492	6.76114	0.010505	76.4253	1.40358	863.883	0
0.656615	0.0531036	7.42212	0.011487	83.8969	1.85177	948.338	0
0.720807	0.0588717	8.14773	0.012414	92.0988	2.79807	1041.05	0
0.791275	0.063622	8.94427	0.013181	101.103	4.39258	1142.83	0
0.868632	0.0672195	9.81869	0.013759	110.987	6.58003	1254.55	0
0.953552	0.0695415	10.7786	0.014205	121.837	9.00823	1377.2	0
1.04677	0.0704802	11.8323	0.014782	133.748	11.1017	1511.84	0
1.14911	0.0700638	12.9891	0.015864	146.824	12.2683	1659.64	0
1.26145	0.0683575	14.2589	0.018106	161.177	12.1317	1821.89	0
1.38477	0.0654596	15.6529	0.022283	176.935	10.7181	2000	
1.52015	0.061507	17.1832	0.029362	194.232	8.37542		
1.66876	0.0566686	18.863	0.040508	213.221	5.6728		
1.8319	0.0511511	20.7071	0.056719	234.066	3.17567		
2.011	0.0451841	22.7315	0.079302	256.948	1.24117		
2.2076	0.0390253	24.9538	0.109581	282.068	0.232167		
2.42342	0.0329353	27.3934	0.149488	309.644	0.010014		
2.66033	0.0271772	30.0714	0.202355	339.916	0		
2.92042	0.0219827	33.0113	0.27275	373.147	0		
3.20592	0.0175457	36.2385	0.366763	409.626	0		
3.51934	0.013992	39.7813	0.489384	449.672	0		
3.8634	0.0113731	43.6704	0.640183	493.633	0		



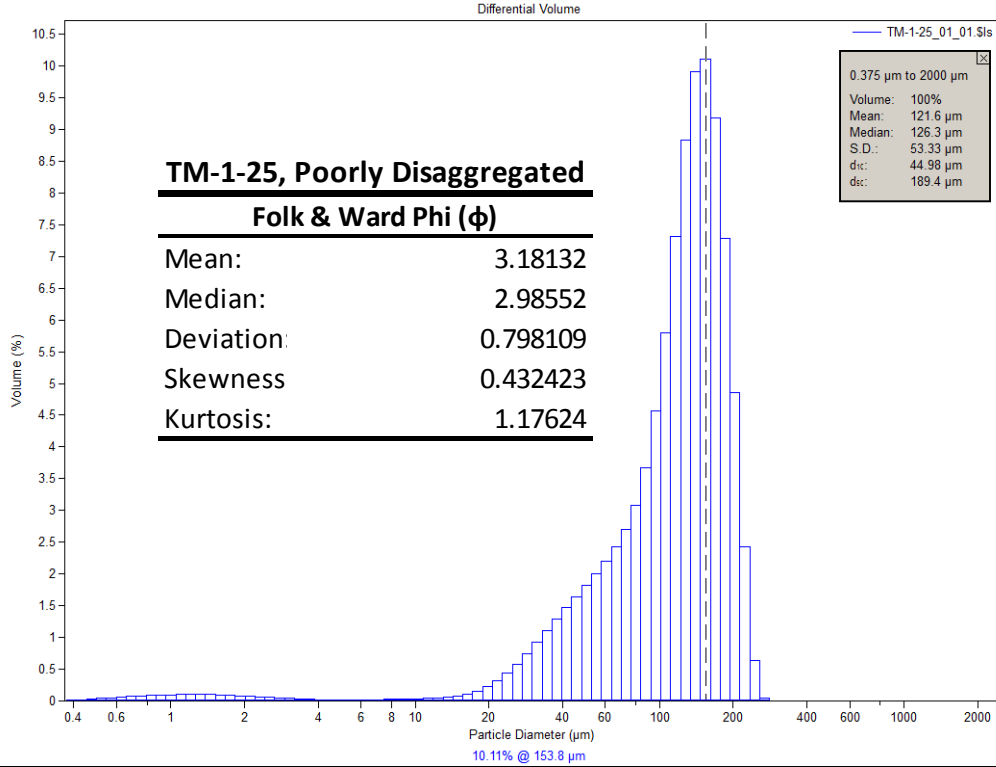
μm	Volume (%)						
0.375198	0.00767687	4.2411	0.009173	47.9397	0.903161	541.892	0
0.411878	0.0146344	4.65572	0.008188	52.6264	1.04034	594.869	0
0.452145	0.0246038	5.11087	0.007948	57.7713	1.14106	653.025	0
0.496347	0.0339473	5.61052	0.008277	63.4192	1.24079	716.866	0
0.544872	0.0427358	6.15902	0.008998	69.6192	1.44955	786.949	0
0.59814	0.0508391	6.76114	0.009945	76.4253	1.94795	863.883	0
0.656615	0.0581294	7.42212	0.01098	83.8969	2.95273	948.338	0
0.720807	0.0644507	8.14773	0.011985	92.0988	4.62789	1041.05	0
0.791275	0.0696586	8.94427	0.012867	101.103	6.9206	1142.83	0
0.868632	0.0736035	9.81869	0.013617	110.987	9.47728	1254.55	0
0.953552	0.0761485	10.7786	0.014339	121.837	11.6933	1377.2	0
1.04677	0.0771716	11.8323	0.015316	133.748	12.8907	1511.84	0
1.14911	0.0766995	12.9891	0.017023	146.824	12.6486	1659.64	0
1.26145	0.0747998	14.2589	0.020112	161.177	10.9208	1821.89	0
1.38477	0.0715764	15.6529	0.025464	176.935	8.14553	2000	
1.52015	0.0671748	17.1832	0.034056	194.232	5.03228		
1.66876	0.0617793	18.863	0.047034	213.221	2.20835		
1.8319	0.0556145	20.7071	0.065534	234.066	0.477799		
2.011	0.0489369	22.7315	0.09093	256.948	0.024312		
2.2076	0.0420325	24.9538	0.125303	282.068	0		
2.42342	0.0351997	27.3934	0.17162	309.644	0		
2.66033	0.028735	30.0714	0.23467	339.916	0		
2.92042	0.0229087	33.0113	0.320415	373.147	0		
3.20592	0.0179399	36.2385	0.434134	409.626	0		
3.51934	0.0139738	39.7813	0.576928	449.672	0		
3.8634	0.0110642	43.6704	0.74017	493.633	0		



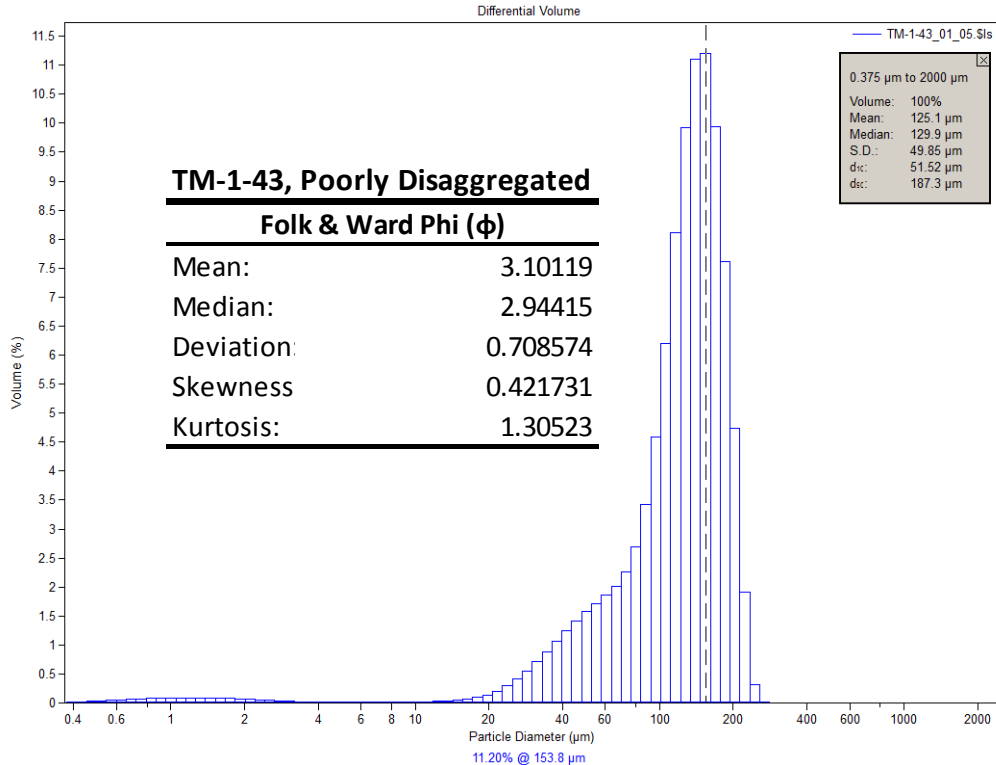
μm	Volume (%)						
0.375198	0.00688076	4.2411	0.007553	47.9397	0.636875	541.892	0
0.411878	0.0131136	4.65572	0.006922	52.6264	0.758132	594.869	0
0.452145	0.0220369	5.11087	0.006974	57.7713	0.837907	653.025	0
0.496347	0.0303846	5.61052	0.007543	63.4192	0.869484	716.866	0
0.544872	0.0382158	6.15902	0.008471	69.6192	0.90424	786.949	0
0.59814	0.0454097	6.76114	0.009591	76.4253	1.07511	863.883	0
0.656615	0.0518483	7.42212	0.010756	83.8969	1.59005	948.338	0
0.720807	0.0573903	8.14773	0.011829	92.0988	2.69492	1041.05	0
0.791275	0.0619057	8.94427	0.012688	101.103	4.55298	1142.83	0
0.868632	0.065262	9.81869	0.013289	110.987	7.06496	1254.55	0
0.953552	0.067341	10.7786	0.013667	121.837	9.79902	1377.2	0
1.04677	0.0680396	11.8323	0.014064	133.748	12.0922	1511.84	0
1.14911	0.0673934	12.9891	0.014824	146.824	13.2639	1659.64	0
1.26145	0.0654741	14.2589	0.016562	161.177	12.9321	1821.89	0
1.38477	0.062388	15.6529	0.019991	176.935	11.1332	2000	
1.52015	0.0582786	17.1832	0.025944	194.232	8.32555		
1.66876	0.053322	18.863	0.035391	213.221	5.21966		
1.8319	0.0477296	20.7071	0.048938	234.066	2.43765		
2.011	0.0417357	22.7315	0.06733	256.948	0.597623		
2.2076	0.0355999	24.9538	0.091152	282.068	0.035321		
2.42342	0.029583	27.3934	0.121469	309.644	0		
2.66033	0.0239462	30.0714	0.160978	339.916	0		
2.92042	0.0189169	33.0113	0.213775	373.147	0		
3.20592	0.0146832	36.2385	0.285941	409.626	0		
3.51934	0.0113629	39.7813	0.38274	449.672	0		
3.8634	0.00899759	43.6704	0.503458	493.633	0		



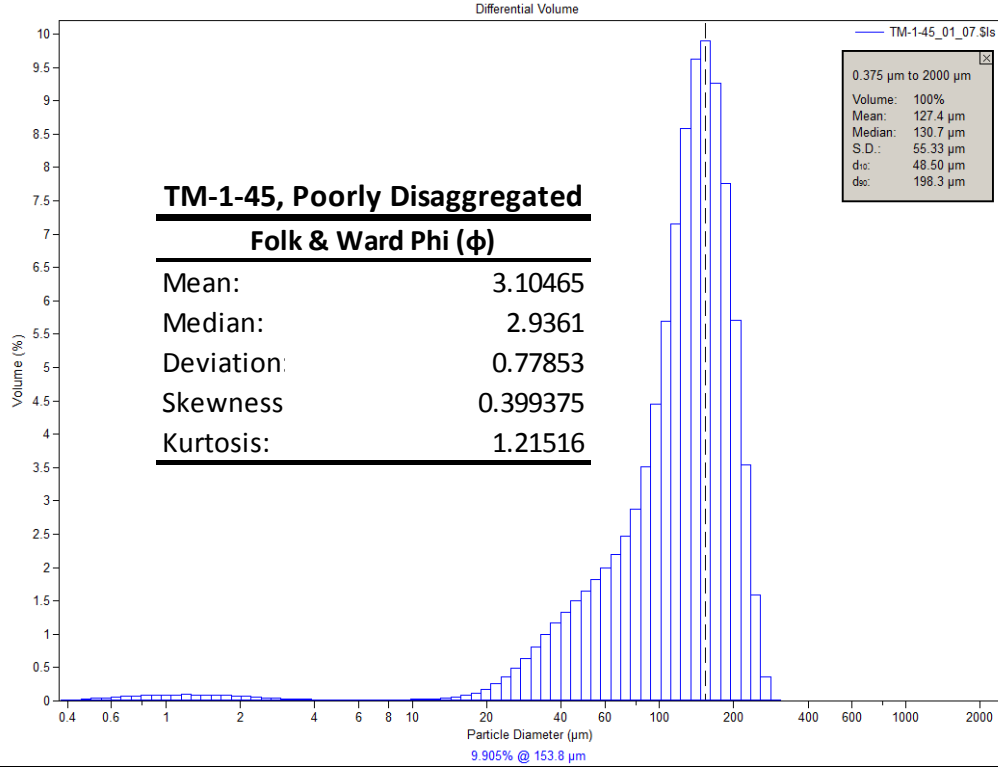
μm	Volume (%)						
0.375198	0.00654092	4.2411	0.01597	47.9397	0.707552	541.892	0.198482
0.411878	0.0124732	4.65572	0.015294	52.6264	0.882751	594.869	0.057128
0.452145	0.0209892	5.11087	0.015275	57.7713	1.05325	653.025	0.003473
0.496347	0.0289981	5.61052	0.015742	63.4192	1.19121	716.866	0
0.544872	0.0365706	6.15902	0.016544	69.6192	1.28991	786.949	0
0.59814	0.0436035	6.76114	0.017513	76.4253	1.40168	863.883	0
0.656615	0.049996	7.42212	0.018523	83.8969	1.65901	948.338	0
0.720807	0.0556208	8.14773	0.019438	92.0988	2.25815	1041.05	0
0.791275	0.0603597	8.94427	0.020157	101.103	3.39847	1142.83	0
0.868632	0.0640863	9.81869	0.020638	110.987	5.15555	1254.55	0
0.953552	0.0666842	10.7786	0.02091	121.837	7.34196	1377.2	0
1.04677	0.0680434	11.8323	0.021194	133.748	9.48899	1511.84	0
1.14911	0.0681745	12.9891	0.021752	146.824	11.0036	1659.64	0
1.26145	0.0671206	14.2589	0.023136	161.177	11.4296	1821.89	0
1.38477	0.0649524	15.6529	0.025901	176.935	10.6585	2000	
1.52015	0.0617788	17.1832	0.030884	194.232	8.95361		
1.66876	0.0577379	18.863	0.039168	213.221	6.79446		
1.8319	0.0530084	20.7071	0.051825	234.066	4.66483		
2.011	0.0477936	22.7315	0.070572	256.948	2.89731		
2.2076	0.0423327	24.9538	0.096897	282.068	1.62851		
2.42342	0.0368722	27.3934	0.132569	309.644	0.834915		
2.66033	0.031671	30.0714	0.179796	339.916	0.414334		
2.92042	0.0269601	33.0113	0.240868	373.147	0.252978		
3.20592	0.0229395	36.2385	0.319851	409.626	0.24077		
3.51934	0.0197403	39.7813	0.421572	449.672	0.286697		
3.8634	0.017422	43.6704	0.550538	493.633	0.297352		



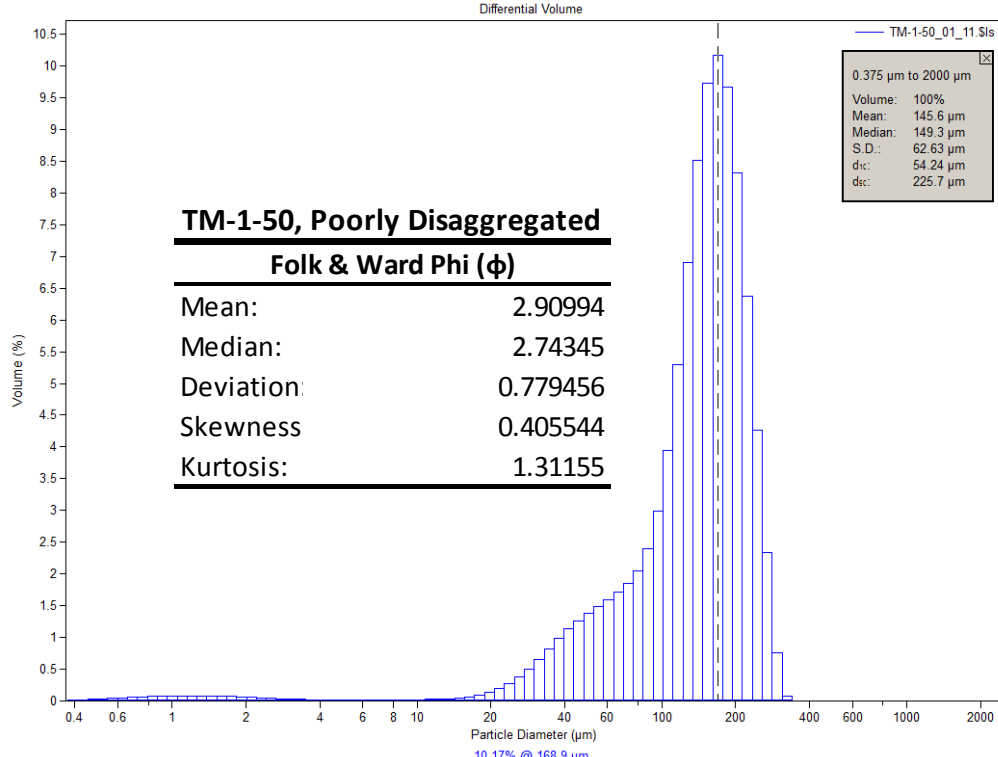
μm	Volume (%)						
0.375198	0.00883357	4.2411	0.017885	47.9397	1.8218	541.892	0
0.411878	0.0168731	4.65572	0.01669	52.6264	2.00603	594.869	0
0.452145	0.0284861	5.11087	0.016809	57.7713	2.2026	653.025	0
0.496347	0.0395423	5.61052	0.017969	63.4192	2.42247	716.866	0
0.544872	0.0501718	6.15902	0.019893	69.6192	2.69549	786.949	0
0.59814	0.0602631	6.76114	0.022321	76.4253	3.08096	863.883	0
0.656615	0.0696947	7.42212	0.025064	83.8969	3.67008	948.338	0
0.720807	0.0782946	8.14773	0.028	92.0988	4.5619	1041.05	0
0.791275	0.0858863	8.94427	0.031127	101.103	5.80176	1142.83	0
0.868632	0.0922588	9.81869	0.034708	110.987	7.31407	1254.55	0
0.953552	0.0971928	10.7786	0.039418	121.837	8.83235	1377.2	0
1.04677	0.10045	11.8323	0.046574	133.748	9.91085	1511.84	0
1.14911	0.101939	12.9891	0.058224	146.824	10.1114	1659.64	0
1.26145	0.101607	14.2589	0.077387	161.177	9.18907	1821.89	0
1.38477	0.0994427	15.6529	0.108023	176.935	7.28624	2000	
1.52015	0.095499	17.1832	0.154876	194.232	4.86106		
1.66876	0.0898948	18.863	0.222943	213.221	2.42059		
1.8319	0.0828341	20.7071	0.316214	234.066	0.629951		
2.011	0.0746043	22.7315	0.436785	256.948	0.039055		
2.2076	0.0655849	24.9538	0.58333	282.068	0		
2.42342	0.0562222	27.3934	0.750673	309.644	0		
2.66033	0.0470149	30.0714	0.930965	339.916	0		
2.92042	0.0384591	33.0113	1.11511	373.147	0		
3.20592	0.0310054	36.2385	1.29616	409.626	0		
3.51934	0.0249922	39.7813	1.47202	449.672	0		
3.8634	0.0206113	43.6704	1.64545	493.633	0		



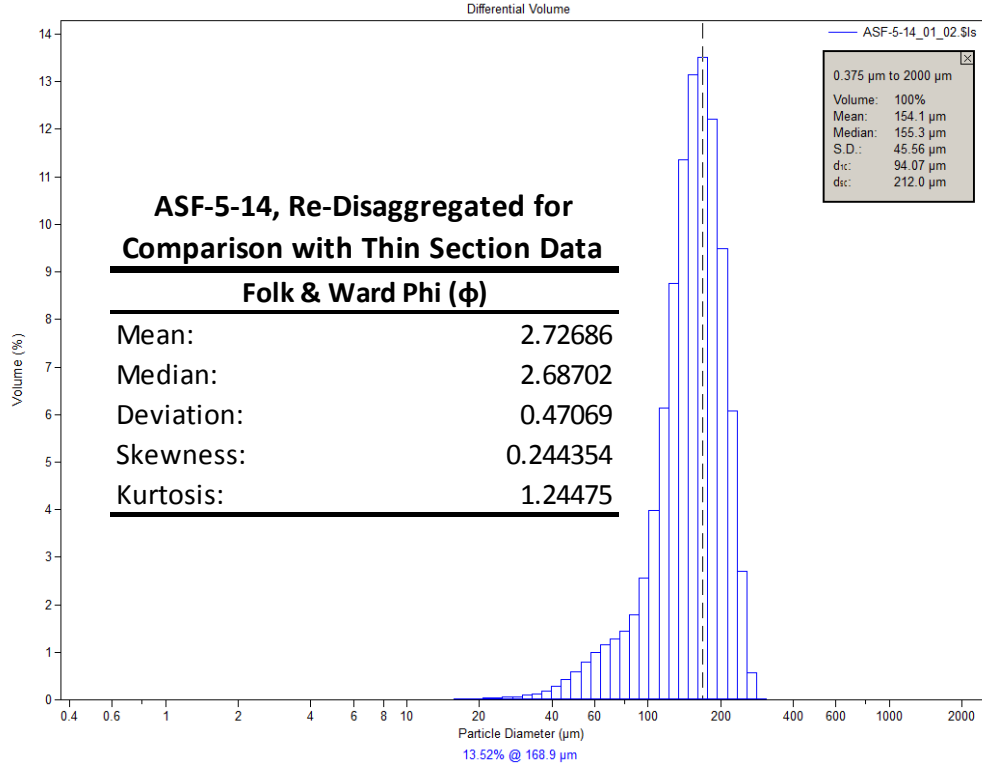
μm	Volume (%)						
0.375198	0.00856258	4.2411	0.011332	47.9397	1.57194	541.892	0
0.411878	0.0163371	4.65572	0.010272	52.6264	1.71699	594.869	0
0.452145	0.0275164	5.11087	0.010253	57.7713	1.85768	653.025	0
0.496347	0.0380658	5.61052	0.011047	63.4192	2.01946	716.866	0
0.544872	0.048084	6.15902	0.012423	69.6192	2.26364	786.949	0
0.59814	0.0574403	6.76114	0.01416	76.4253	2.68939	863.883	0
0.656615	0.0660005	7.42212	0.016079	83.8969	3.42659	948.338	0
0.720807	0.0735918	8.14773	0.018029	92.0988	4.59474	1041.05	0
0.791275	0.0800455	8.94427	0.019914	101.103	6.20629	1142.83	0
0.868632	0.0851745	9.81869	0.021802	110.987	8.10846	1254.55	0
0.953552	0.0887961	10.7786	0.024022	121.837	9.92244	1377.2	0
1.04677	0.0907306	11.8323	0.027365	133.748	11.1035	1511.84	0
1.14911	0.0909522	12.9891	0.033203	146.824	11.1966	1659.64	0
1.26145	0.089483	14.2589	0.04371	161.177	9.94483	1821.89	0
1.38477	0.0863846	15.6529	0.061975	176.935	7.60481	2000	
1.52015	0.0817745	17.1832	0.091921	194.232	4.73269		
1.66876	0.0758242	18.863	0.138037	213.221	1.90722		
1.8319	0.0687687	20.7071	0.204525	234.066	0.322362		
2.011	0.0608988	22.7315	0.294736	256.948	0.011004		
2.2076	0.0525645	24.9538	0.410307	282.068	0		
2.42342	0.0441505	27.3934	0.55031	309.644	0		
2.66033	0.0360625	30.0714	0.711148	339.916	0		
2.92042	0.0286852	33.0113	0.886237	373.147	0		
3.20592	0.0223508	36.2385	1.06703	409.626	0		
3.51934	0.0172942	39.7813	1.24541	449.672	0		
3.8634	0.0136279	43.6704	1.41501	493.633	0		



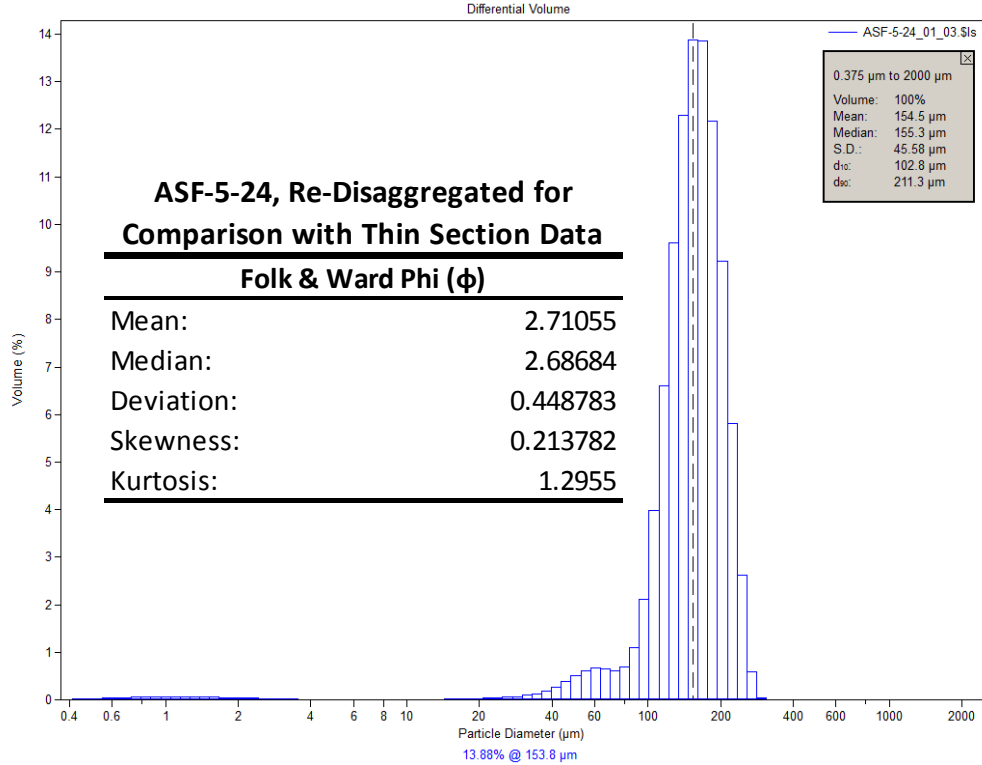
μm	Volume (%)						
0.375198	0.00866927	4.2411	0.015197	47.9397	1.65328	541.892	0
0.411878	0.0165443	4.65572	0.013564	52.6264	1.81484	594.869	0
0.452145	0.02788	5.11087	0.012951	57.7713	1.99099	653.025	0
0.496347	0.0385994	5.61052	0.013146	63.4192	2.19845	716.866	0
0.544872	0.0488105	6.15902	0.013955	69.6192	2.47359	786.949	0
0.59814	0.058389	6.76114	0.015206	76.4253	2.8834	863.883	0
0.656615	0.0672065	7.42212	0.016794	83.8969	3.5153	948.338	0
0.720807	0.0750936	8.14773	0.018666	92.0988	4.44733	1041.05	0
0.791275	0.0818851	8.94427	0.020851	101.103	5.69757	1142.83	0
0.868632	0.0873949	9.81869	0.023572	110.987	7.15981	1254.55	0
0.953552	0.0914374	10.7786	0.027341	121.837	8.5881	1377.2	0
1.04677	0.0938255	11.8323	0.033163	133.748	9.62304	1511.84	0
1.14911	0.0945231	12.9891	0.042651	146.824	9.90463	1659.64	0
1.26145	0.0935343	14.2589	0.058259	161.177	9.26376	1821.89	0
1.38477	0.0909028	15.6529	0.083342	176.935	7.76076	2000	
1.52015	0.0867265	17.1832	0.122029	194.232	5.71185		
1.66876	0.0811538	18.863	0.17884	213.221	3.53482		
1.8319	0.0744011	20.7071	0.257727	234.066	1.59134		
2.011	0.0667416	22.7315	0.361477	256.948	0.364063		
2.2076	0.0585127	24.9538	0.49071	282.068	0.019904		
2.42342	0.0500929	27.3934	0.643041	309.644	0		
2.66033	0.0418882	30.0714	0.812791	339.916	0		
2.92042	0.0342883	33.0113	0.990907	373.147	0		
3.20592	0.0276351	36.2385	1.16768	409.626	0		
3.51934	0.0221731	39.7813	1.33645	449.672	0		
3.8634	0.0180285	43.6704	1.49652	493.633	0		



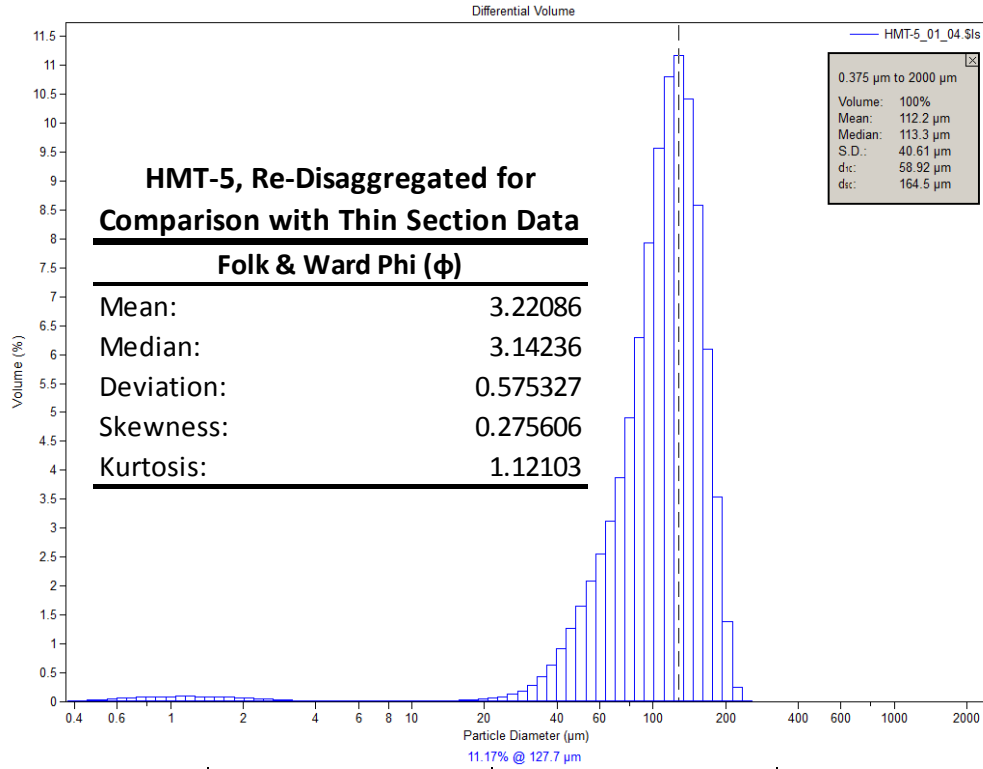
μm	Volume (%)						
0.375198	0.00776097	4.2411	0.015684	47.9397	1.38495	541.892	0
0.411878	0.0148065	4.65572	0.014312	52.6264	1.49304	594.869	0
0.452145	0.0249372	5.11087	0.013732	57.7713	1.59923	653.025	0
0.496347	0.0344958	5.61052	0.013764	63.4192	1.71175	716.866	0
0.544872	0.0435732	6.15902	0.014254	69.6192	1.84808	786.949	0
0.59814	0.0520528	6.76114	0.015064	76.4253	2.05091	863.883	0
0.656615	0.0598168	7.42212	0.016131	83.8969	2.39776	948.338	0
0.720807	0.0667133	8.14773	0.017433	92.0988	2.99718	1041.05	0
0.791275	0.0725953	8.94427	0.019033	101.103	3.95077	1142.83	0
0.868632	0.0773017	9.81869	0.021145	110.987	5.29026	1254.55	0
0.953552	0.0806779	10.7786	0.024178	121.837	6.91014	1377.2	0
1.04677	0.0825706	11.8323	0.028892	133.748	8.52127	1511.84	0
1.14911	0.0829681	12.9891	0.03636	146.824	9.72925	1659.64	0
1.26145	0.0818956	14.2589	0.048228	161.177	10.17	1821.89	0
1.38477	0.079414	15.6529	0.06666	176.935	9.66366	2000	0
1.52015	0.0756331	17.1832	0.094522	194.232	8.31359		
1.66876	0.0707042	18.863	0.135413	213.221	6.37796		
1.8319	0.0648329	20.7071	0.193234	234.066	4.26669		
2.011	0.0582675	22.7315	0.272216	256.948	2.33752		
2.2076	0.0513028	24.9538	0.375419	282.068	0.762439		
2.42342	0.0442558	27.3934	0.503568	309.644	0.075494		
2.66033	0.0374593	30.0714	0.653329	339.916	0.00049		
2.92042	0.031218	33.0113	0.816001	373.147	0		
3.20592	0.0257937	36.2385	0.97963	409.626	0		
3.51934	0.0213603	39.7813	1.13214	449.672	0		
3.8634	0.0179977	43.6704	1.26683	493.633	0		



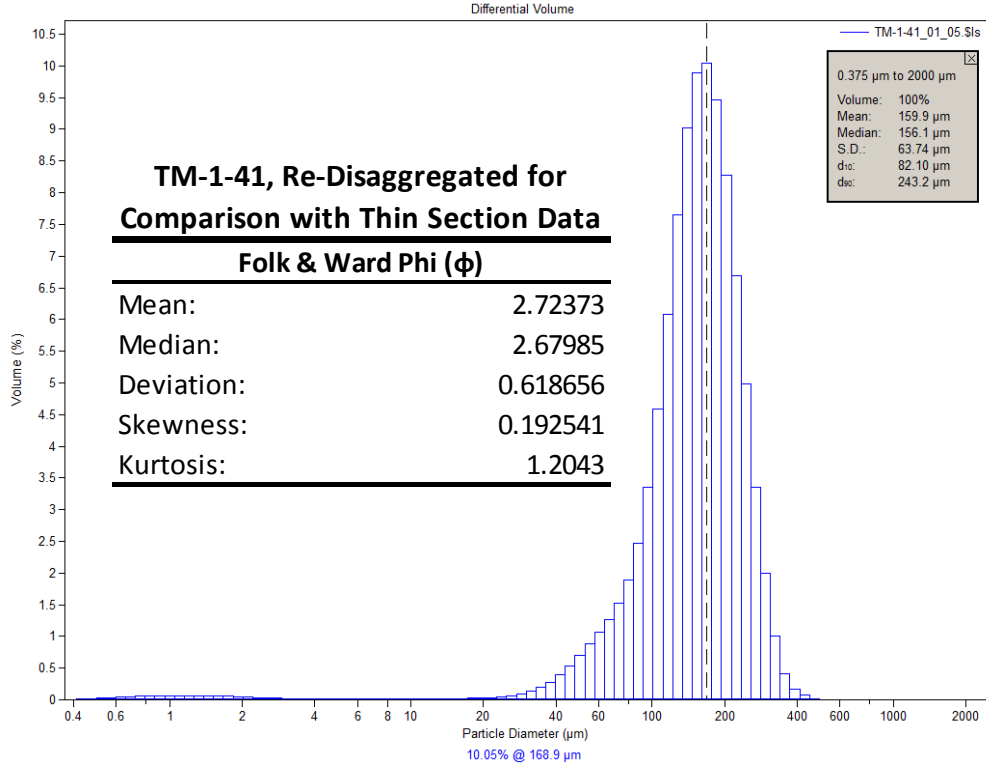
μm	Volume (%)						
0.375198	0	4.2411	0	47.9397	0.597634	541.892	0
0.411878	0	4.65572	0	52.6264	0.800566	594.869	0
0.452145	0	5.11087	0	57.7713	0.997393	653.025	0
0.496347	0	5.61052	0	63.4192	1.15744	716.866	0
0.544872	0	6.15902	0	69.6192	1.2801	786.949	0
0.59814	0	6.76114	0	76.4253	1.43849	863.883	0
0.656615	0	7.42212	0	83.8969	1.7941	948.338	0
0.720807	0	8.14773	0	92.0988	2.56815	1041.05	0
0.791275	0	8.94427	0	101.103	3.99005	1142.83	0
0.868632	0	9.81869	0	110.987	6.13285	1254.55	0
0.953552	0	10.7786	0	121.837	8.76777	1377.2	0
1.04677	0	11.8323	0	133.748	11.3566	1511.84	0
1.14911	0	12.9891	0	146.824	13.142	1659.64	0
1.26145	0	14.2589	0.001184	161.177	13.5212	1821.89	0
1.38477	0	15.6529	0.011301	176.935	12.2132	2000	
1.52015	0	17.1832	0.022085	194.232	9.48484		
1.66876	0	18.863	0.025771	213.221	6.07141		
1.8319	0	20.7071	0.031433	234.066	2.70975		
2.011	0	22.7315	0.039561	256.948	0.575527		
2.2076	0	24.9538	0.051291	282.068	0.027914		
2.42342	0	27.3934	0.068089	309.644	0		
2.66033	0	30.0714	0.09287	339.916	0		
2.92042	0	33.0113	0.131325	373.147	0		
3.20592	0	36.2385	0.191844	409.626	0		
3.51934	0	39.7813	0.285548	449.672	0		
3.8634	0	43.6704	0.42076	493.633	0		



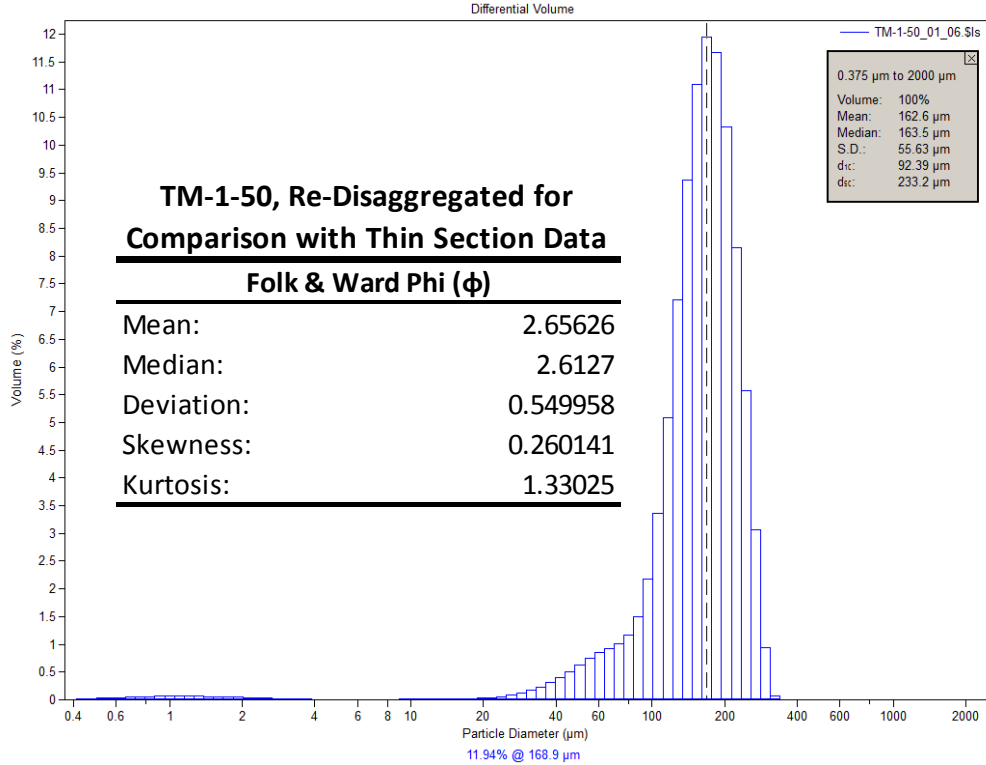
µm	Volume (%)	µm	Volume (%)	µm	Volume (%)	µm	Volume (%)
0.375198	0.00659664	4.2411	0.004496	47.9397	0.50589	541.892	0
0.411878	0.0125678	4.65572	0.003866	52.6264	0.615327	594.869	0
0.452145	0.021103	5.11087	0.003822	57.7713	0.667701	653.025	0
0.496347	0.0290629	5.61052	0.004214	63.4192	0.649019	716.866	0
0.544872	0.0364966	6.15902	0.004903	69.6192	0.609991	786.949	0
0.59814	0.0432822	6.76114	0.005743	76.4253	0.688102	863.883	0
0.656615	0.0493014	7.42212	0.006607	83.8969	1.09862	948.338	0
0.720807	0.0544162	8.14773	0.007377	92.0988	2.1207	1041.05	0
0.791275	0.0585019	8.94427	0.00795	101.103	3.97391	1142.83	0
0.868632	0.061434	9.81869	0.008298	110.987	6.60659	1254.55	0
0.953552	0.0631053	10.7786	0.008453	121.837	9.60595	1377.2	0
1.04677	0.0634293	11.8323	0.008639	133.748	12.2892	1511.84	0
1.14911	0.0624545	12.9891	0.009143	146.824	13.8781	1659.64	0
1.26145	0.0602696	14.2589	0.010466	161.177	13.8687	1821.89	0
1.38477	0.0569922	15.6529	0.013117	176.935	12.177	2000	
1.52015	0.0527798	17.1832	0.017557	194.232	9.22621		
1.66876	0.0478148	18.863	0.02418	213.221	5.80625		
1.8319	0.0423121	20.7071	0.032826	234.066	2.62271		
2.011	0.0365006	22.7315	0.043359	256.948	0.58839		
2.2076	0.0306278	24.9538	0.055708	282.068	0.030961		
2.42342	0.024934	27.3934	0.070911	309.644	0		
2.66033	0.0196524	30.0714	0.092521	339.916	0		
2.92042	0.0149792	33.0113	0.126583	373.147	0		
3.20592	0.0110702	36.2385	0.181766	409.626	0		
3.51934	0.00801698	39.7813	0.265884	449.672	0		
3.8634	0.0058405	43.6704	0.37875	493.633	0		



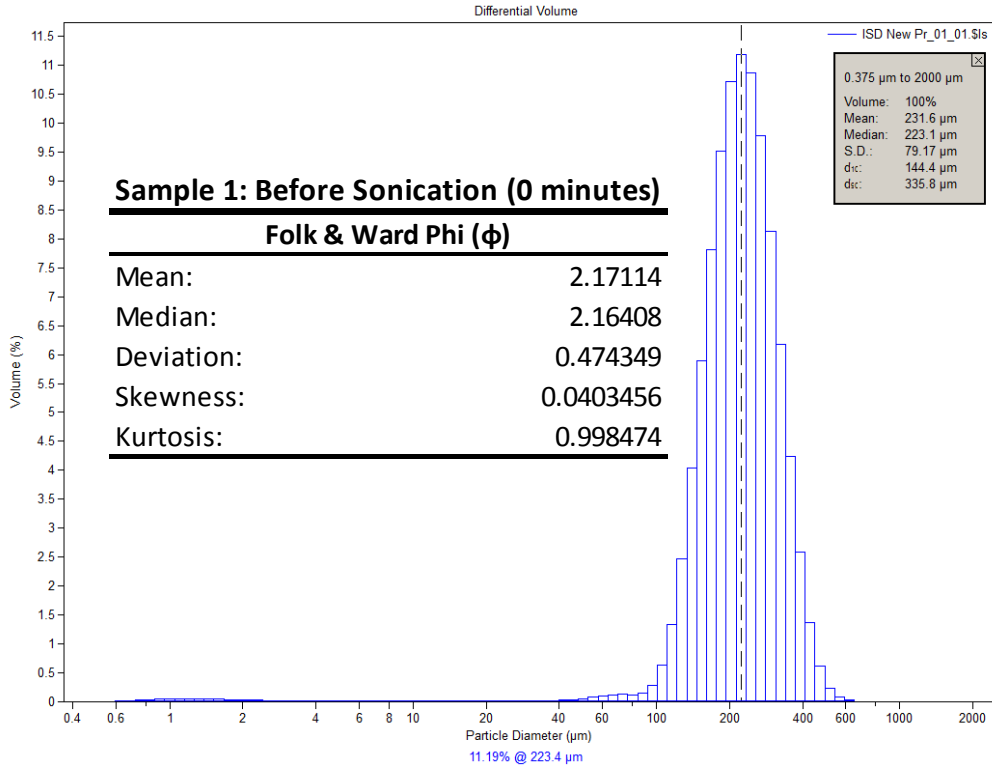
μ m	Volume (%)	μ m	Volume (%)	μ m	Volume (%)	μ m	Volume (%)
0.375198	0.00880672	4.2411	0.010494	47.9397	1.65607	541.892	0
0.411878	0.0168015	4.65572	0.009096	52.6264	2.0858	594.869	0
0.452145	0.0282899	5.11087	0.008533	57.7713	2.56042	653.025	0
0.496347	0.0391188	5.61052	0.008575	63.4192	3.12826	716.866	0
0.544872	0.0493849	6.15902	0.008986	69.6192	3.87796	786.949	0
0.59814	0.058951	6.76114	0.00961	76.4253	4.91214	863.883	0
0.656615	0.0676754	7.42212	0.010309	83.8969	6.28728	948.338	0
0.720807	0.0753791	8.14773	0.011018	92.0988	7.92533	1041.05	0
0.791275	0.0818872	8.94427	0.011682	101.103	9.57152	1142.83	0
0.868632	0.0870082	9.81869	0.012349	110.987	10.8038	1254.55	0
0.953552	0.0905572	10.7786	0.013191	121.837	11.1711	1377.2	0
1.04677	0.0923533	11.8323	0.014473	133.748	10.4215	1511.84	0
1.14911	0.0923799	12.9891	0.0167	146.824	8.58683	1659.64	0
1.26145	0.0906689	14.2589	0.020268	161.177	6.10034	1821.89	0
1.38477	0.0872958	15.6529	0.02583	176.935	3.53927	2000	
1.52015	0.0823933	17.1832	0.033926	194.232	1.38098		
1.66876	0.0761504	18.863	0.045403	213.221	0.244197		
1.8319	0.068819	20.7071	0.062009	234.066	0.009526		
2.011	0.0607099	22.7315	0.086604	256.948	0		
2.2076	0.0521843	24.9538	0.12529	282.068	0		
2.42342	0.0436418	27.3934	0.186903	309.644	0		
2.66033	0.0354835	30.0714	0.283964	339.916	0		
2.92042	0.0280906	33.0113	0.431459	373.147	0		
3.20592	0.0217631	36.2385	0.641476	409.626	0		
3.51934	0.0167041	39.7813	0.920532	449.672	0		
3.8634	0.0129713	43.6704	1.26359	493.633	0		



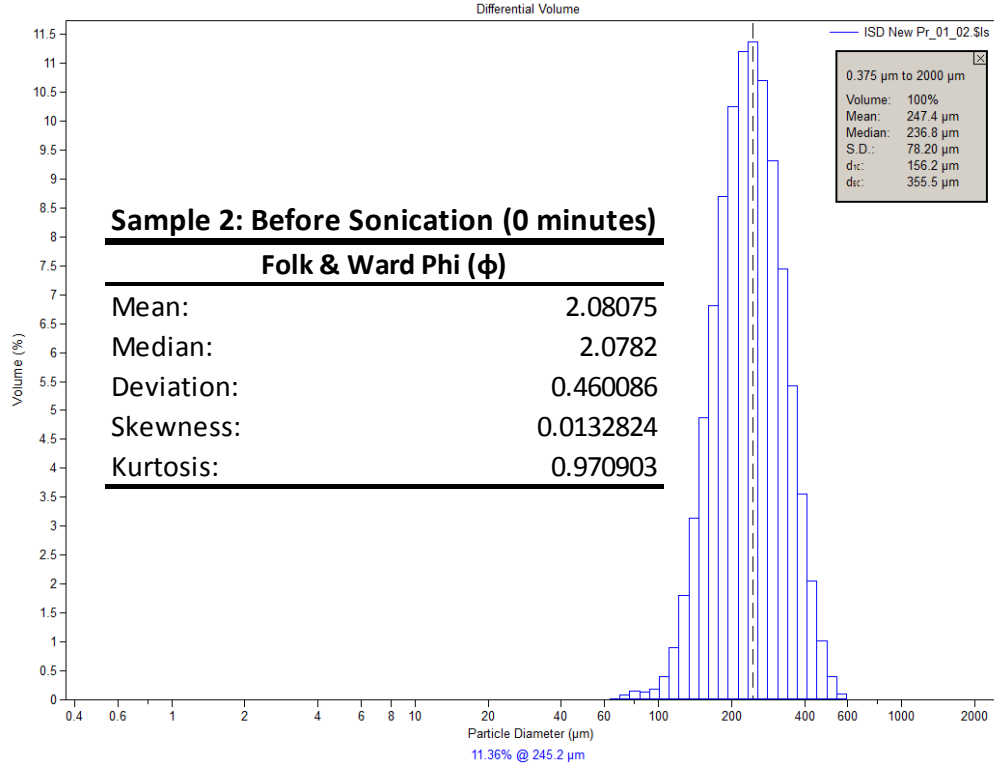
μm	Volume (%)						
0.375198	0.00663808	4.2411	0.009938	47.9397	0.706904	541.892	0
0.411878	0.0126568	4.65572	0.00911	52.6264	0.88563	594.869	0
0.452145	0.0212886	5.11087	0.008913	57.7713	1.07021	653.025	0
0.496347	0.029392	5.61052	0.009188	63.4192	1.26972	716.866	0
0.544872	0.0370318	6.15902	0.009783	69.6192	1.52075	786.949	0
0.59814	0.0440978	6.76114	0.010556	76.4253	1.89191	863.883	0
0.656615	0.0504805	7.42212	0.01139	83.8969	2.47545	948.338	0
0.720807	0.0560454	8.14773	0.012182	92.0988	3.36011	1041.05	0
0.791275	0.0606658	8.94427	0.012849	101.103	4.58272	1142.83	0
0.868632	0.064209	9.81869	0.013365	110.987	6.07895	1254.55	0
0.953552	0.0665522	10.7786	0.01378	121.837	7.65684	1377.2	0
1.04677	0.0675834	11.8323	0.014265	133.748	9.02677	1511.84	0
1.14911	0.0673186	12.9891	0.015068	146.824	9.89251	1659.64	0
1.26145	0.0658105	14.2589	0.016546	161.177	10.0497	1821.89	0
1.38477	0.0631427	15.6529	0.019062	176.935	9.46785	2000	
1.52015	0.0594402	17.1832	0.022998	194.232	8.27211		
1.66876	0.0548607	18.863	0.028825	213.221	6.68668		
1.8319	0.0496009	20.7071	0.037122	234.066	4.97633		
2.011	0.043886	22.7315	0.04908	256.948	3.35146		
2.2076	0.0379696	24.9538	0.066703	282.068	2.00103		
2.42342	0.0321135	27.3934	0.09328	309.644	1.0088		
2.66033	0.0265797	30.0714	0.133742	339.916	0.4045		
2.92042	0.021601	33.0113	0.194	373.147	0.171963		
3.20592	0.0173671	36.2385	0.280073	409.626	0.072989		
3.51934	0.0139974	39.7813	0.39582	449.672	0.008292		
3.8634	0.0115333	43.6704	0.540298	493.633	0		



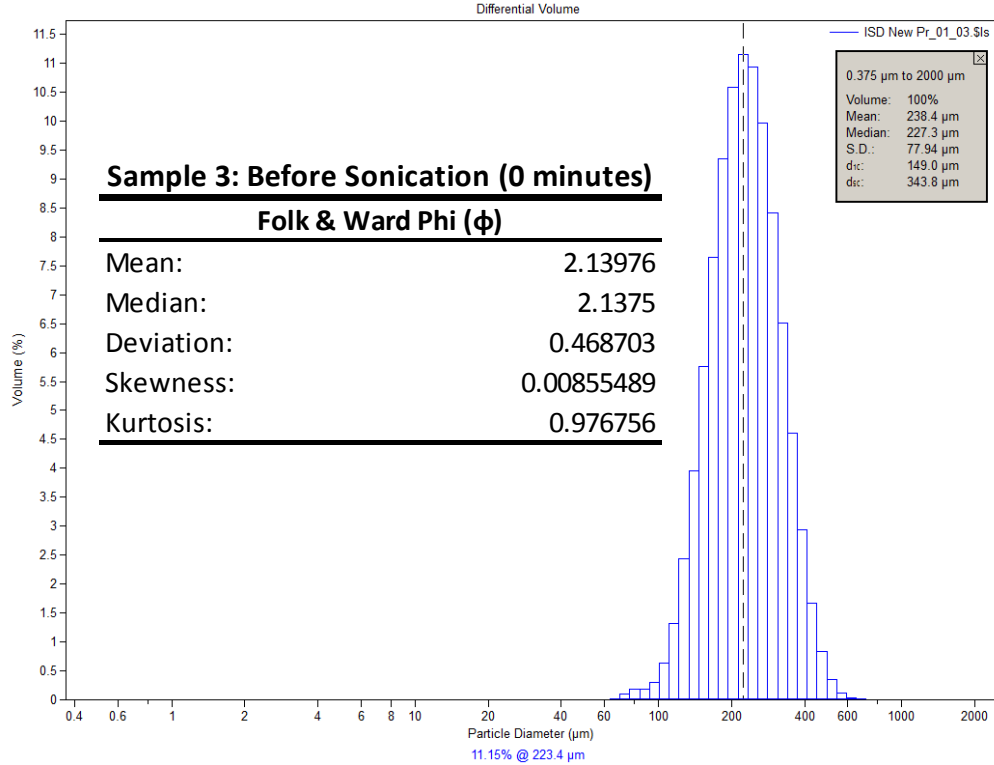
μm	Volume (%)						
0.375198	0.00649503	4.2411	0.005481	47.9397	0.631755	541.892	0
0.411878	0.0123798	4.65572	0.004684	52.6264	0.749331	594.869	0
0.452145	0.0208085	5.11087	0.004521	57.7713	0.850862	653.025	0
0.496347	0.0286996	5.61052	0.004838	63.4192	0.930661	716.866	0
0.544872	0.0361103	6.15902	0.005501	69.6192	1.01037	786.949	0
0.59814	0.0429269	6.76114	0.006369	76.4253	1.15926	863.883	0
0.656615	0.0490378	7.42212	0.007327	83.8969	1.49706	948.338	0
0.720807	0.0543076	8.14773	0.008264	92.0988	2.18405	1041.05	0
0.791275	0.0586121	8.94427	0.009086	101.103	3.36978	1142.83	0
0.868632	0.0618216	9.81869	0.009752	110.987	5.09443	1254.55	0
0.953552	0.0638208	10.7786	0.010273	121.837	7.21326	1377.2	0
1.04677	0.0645061	11.8323	0.010818	133.748	9.36733	1511.84	0
1.14911	0.0639048	12.9891	0.011609	146.824	11.0868	1659.64	0
1.26145	0.0620814	14.2589	0.013119	161.177	11.9415	1821.89	0
1.38477	0.0591312	15.6529	0.015884	176.935	11.6776	2000	
1.52015	0.0551883	17.1832	0.020677	194.232	10.3368		
1.66876	0.0504179	18.863	0.028574	213.221	8.15017		
1.8319	0.0450213	20.7071	0.04071	234.066	5.56785		
2.011	0.0392223	22.7315	0.0588	256.948	3.06849		
2.2076	0.0332709	24.9538	0.084544	282.068	0.943911		
2.42342	0.0274174	27.3934	0.119957	309.644	0.068555		
2.66033	0.021914	30.0714	0.167388	339.916	0		
2.92042	0.0169779	33.0113	0.228813	373.147	0		
3.20592	0.0127907	36.2385	0.306531	409.626	0		
3.51934	0.00946348	39.7813	0.401426	449.672	0		
3.8634	0.00703853	43.6704	0.511807	493.633	0		



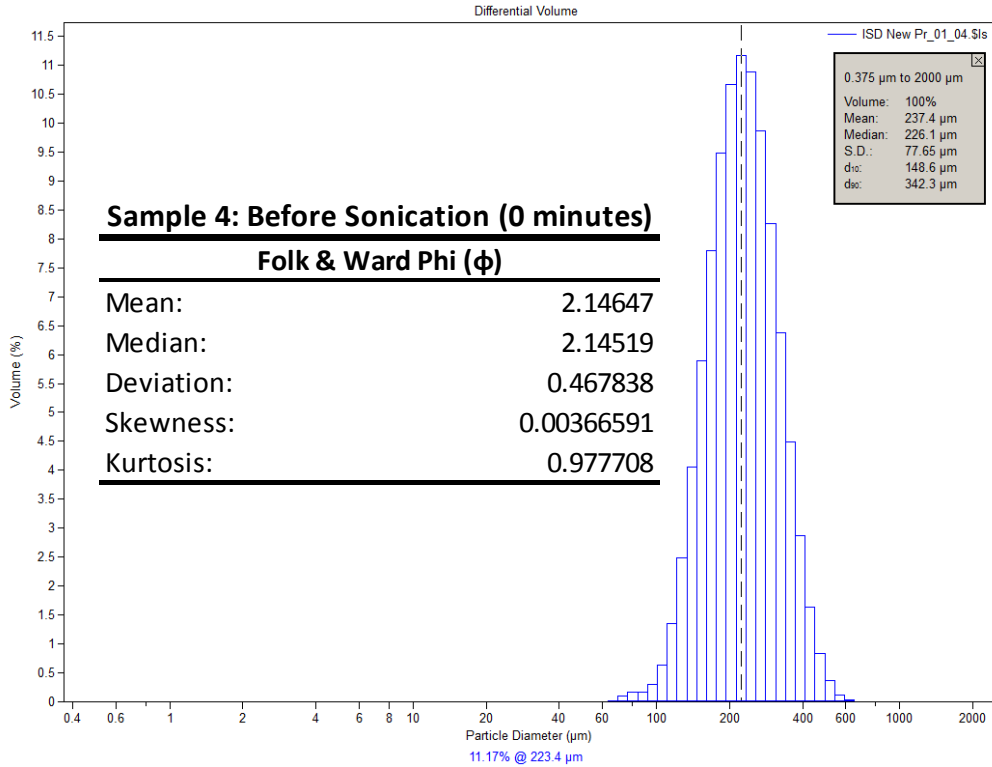
μm	Volume (%)	μm	Volume (%)	μm	Volume (%)	μm	Volume (%)
0.375198	0	4.2411	0.0167394	47.9397	0.0513866	541.892	0.084235
0.411878	0	4.65572	0.0174538	52.6264	0.0755187	594.869	0.0288726
0.452145	0	5.11087	0.0184645	57.7713	0.102125	653.025	0.0030263
0.496347	0.000326117	5.61052	0.0196204	63.4192	0.121332	716.866	0
0.544872	0.00438054	6.15902	0.0207926	69.6192	0.125515	786.949	0
0.59814	0.0134208	6.76114	0.0218627	76.4253	0.123872	863.883	0
0.656615	0.0222149	7.42212	0.0227347	83.8969	0.153313	948.338	0
0.720807	0.0299567	8.14773	0.0233155	92.0988	0.284509	1041.05	0
0.791275	0.0365916	8.94427	0.0235397	101.103	0.634587	1142.83	0
0.868632	0.0419104	9.81869	0.0233849	110.987	1.3356	1254.55	0
0.953552	0.0457548	10.7786	0.0228719	121.837	2.47113	1377.2	0
1.04677	0.0480015	11.8323	0.0221171	133.748	4.03152	1511.84	0
1.14911	0.048725	12.9891	0.0212433	146.824	5.88969	1659.64	0
1.26145	0.0480673	14.2589	0.0204771	161.177	7.81327	1821.89	0
1.38477	0.046224	15.6529	0.0199461	176.935	9.51349	2000	0
1.52015	0.0434349	17.1832	0.0197935	194.232	10.7088		
1.66876	0.0399661	18.863	0.0200342	213.221	11.1912		
1.8319	0.0360968	20.7071	0.020517	234.066	10.8686		
2.011	0.0320997	22.7315	0.021152	256.948	9.78869		
2.2076	0.0282296	24.9538	0.021592	282.068	8.1337		
2.42342	0.0247053	27.3934	0.0217348	309.644	6.17764		
2.66033	0.0217034	30.0714	0.0215668	339.916	4.23783		
2.92042	0.0193441	33.0113	0.0213677	373.147	2.57988		
3.20592	0.0176903	36.2385	0.0222694	409.626	1.36755		
3.51934	0.0167466	39.7813	0.0259085	449.672	0.622012		
3.8634	0.01646	43.6704	0.0347911	493.633	0.233796		



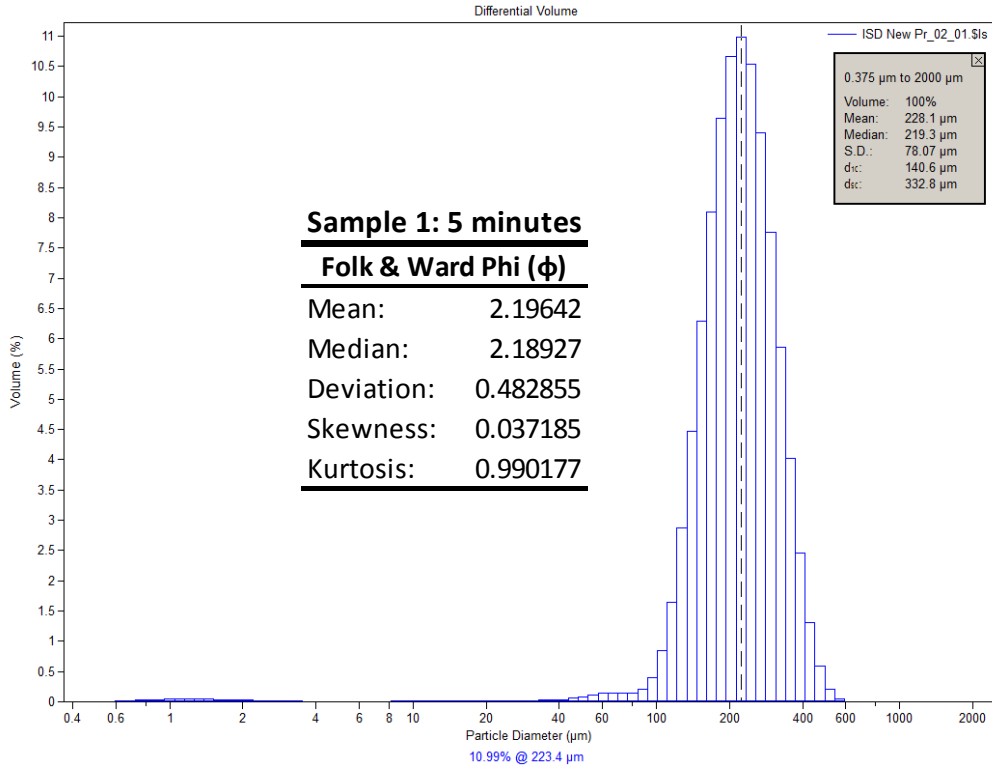
μm	Volume (%)						
0.375198	0	4.2411	0	47.9397	0	541.892	0.094937
0.411878	0	4.65572	0	52.6264	0	594.869	0.005911
0.452145	0	5.11087	0	57.7713	0	653.025	0
0.496347	0	5.61052	0	63.4192	0.00968829	716.866	0
0.544872	0	6.15902	0	69.6192	0.0894912	786.949	0
0.59814	0	6.76114	0	76.4253	0.147318	863.883	0
0.656615	0	7.42212	0	83.8969	0.13504	948.338	0
0.720807	0	8.14773	0	92.0988	0.190388	1041.05	0
0.791275	0	8.94427	0	101.103	0.399802	1142.83	0
0.868632	0	9.81869	0	110.987	0.89485	1254.55	0
0.953552	0	10.7786	0	121.837	1.80143	1377.2	0
1.04677	0	11.8323	0	133.748	3.14501	1511.84	0
1.14911	0	12.9891	0	146.824	4.87045	1659.64	0
1.26145	0	14.2589	0	161.177	6.80702	1821.89	0
1.38477	0	15.6529	0	176.935	8.69791	2000	0
1.52015	0	17.1832	0	194.232	10.2513		
1.66876	0	18.863	0	213.221	11.1981		
1.8319	0	20.7071	0	234.066	11.3606		
2.011	0	22.7315	0	256.948	10.6948		
2.2076	0	24.9538	0	282.068	9.30991		
2.42342	0	27.3934	0	309.644	7.44664		
2.66033	0	30.0714	0	339.916	5.4236		
2.92042	0	33.0113	0	373.147	3.55139		
3.20592	0	36.2385	0	409.626	2.05392		
3.51934	0	39.7813	0	449.672	1.01763		
3.8634	0	43.6704	0	493.633	0.402855		



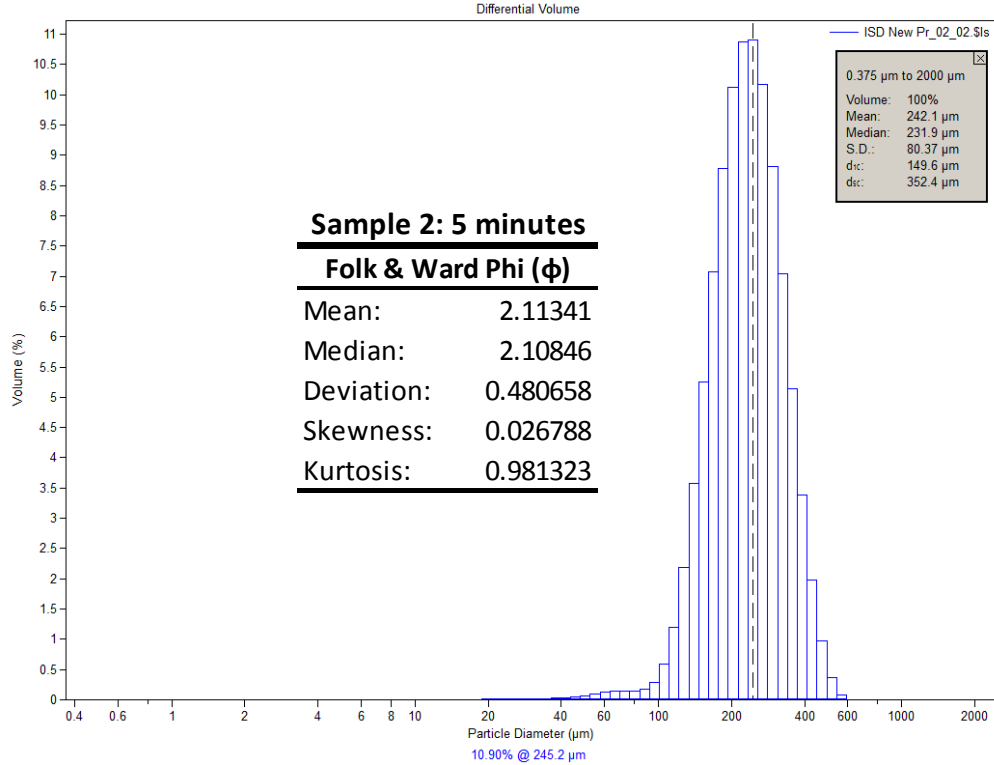
µm	Volume (%)	µm	Volume (%)	µm	Volume (%)	µm	Volume (%)
0.375198	0	4.2411	0	47.9397	0	541.892	0.118281
0.411878	0	4.65572	0	52.6264	0	594.869	0.031183
0.452145	0	5.11087	0	57.7713	0	653.025	0.008873
0.496347	0	5.61052	0	63.4192	0.0117394	716.866	0.001051
0.544872	0	6.15902	0	69.6192	0.107896	786.949	0
0.59814	0	6.76114	0	76.4253	0.182627	863.883	0
0.656615	0	7.42212	0	83.8969	0.190235	948.338	0
0.720807	0	8.14773	0	92.0988	0.307331	1041.05	0
0.791275	0	8.94427	0	101.103	0.641727	1142.83	0
0.868632	0	9.81869	0	110.987	1.31883	1254.55	0
0.953552	0	10.7786	0	121.837	2.43144	1377.2	0
1.04677	0	11.8323	0	133.748	3.94932	1511.84	0
1.14911	0	12.9891	0	146.824	5.76015	1659.64	0
1.26145	0	14.2589	0	161.177	7.64898	1821.89	0
1.38477	0	15.6529	0	176.935	9.34645	2000	0
1.52015	0	17.1832	0	194.232	10.5856		
1.66876	0	18.863	0	213.221	11.1513		
1.8319	0	20.7071	0	234.066	10.9369		
2.011	0	22.7315	0	256.948	9.96784		
2.2076	0	24.9538	0	282.068	8.40533		
2.42342	0	27.3934	0	309.644	6.51498		
2.66033	0	30.0714	0	339.916	4.60098		
2.92042	0	33.0113	0	373.147	2.93112		
3.20592	0	36.2385	0	409.626	1.66519		
3.51934	0	39.7813	0	449.672	0.829173		
3.8634	0	43.6704	0	493.633	0.355551		



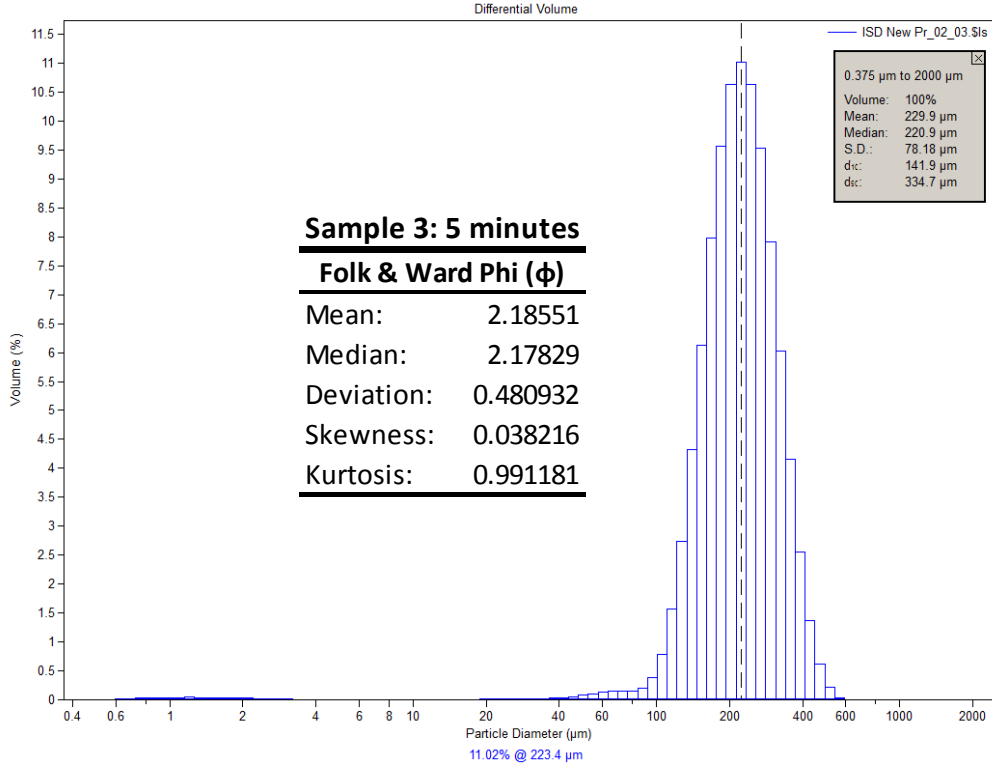
μm	Volume (%)						
0.375198	0	4.2411	0	47.9397	0	541.892	0.123388
0.411878	0	4.65572	0	52.6264	0	594.869	0.026505
0.452145	0	5.11087	0	57.7713	0	653.025	0.001652
0.496347	0	5.61052	0	63.4192	0.0110004	716.866	0
0.544872	0	6.15902	0	69.6192	0.100227	786.949	0
0.59814	0	6.76114	0	76.4253	0.166232	863.883	0
0.656615	0	7.42212	0	83.8969	0.172211	948.338	0
0.720807	0	8.14773	0	92.0988	0.292519	1041.05	0
0.791275	0	8.94427	0	101.103	0.641143	1142.83	0
0.868632	0	9.81869	0	110.987	1.34545	1254.55	0
0.953552	0	10.7786	0	121.837	2.49512	1377.2	0
1.04677	0	11.8323	0	133.748	4.0526	1511.84	0
1.14911	0	12.9891	0	146.824	5.89479	1659.64	0
1.26145	0	14.2589	0	161.177	7.79526	1821.89	0
1.38477	0	15.6529	0	176.935	9.47725	2000	0
1.52015	0	17.1832	0	194.232	10.6722		
1.66876	0	18.863	0	213.221	11.1725		
1.8319	0	20.7071	0	234.066	10.8871		
2.011	0	22.7315	0	256.948	9.85813		
2.2076	0	24.9538	0	282.068	8.26409		
2.42342	0	27.3934	0	309.644	6.37365		
2.66033	0	30.0714	0	339.916	4.48862		
2.92042	0	33.0113	0	373.147	2.86276		
3.20592	0	36.2385	0	409.626	1.63563		
3.51934	0	39.7813	0	449.672	0.829888		
3.8634	0	43.6704	0	493.633	0.360127		



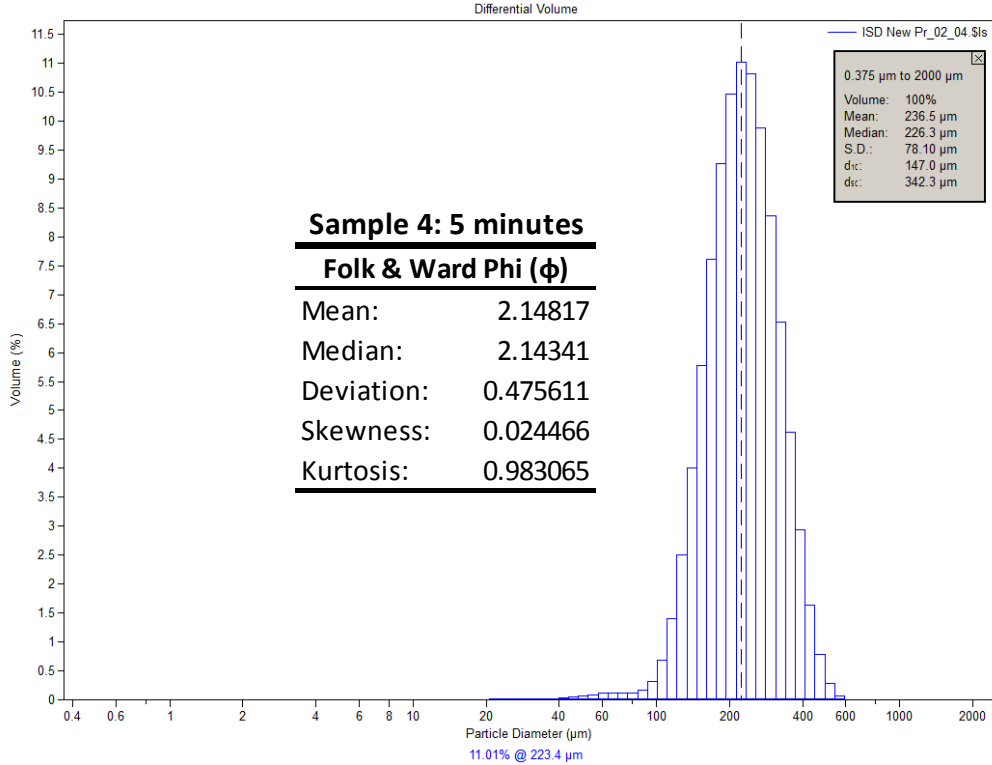
μ m	Volume (%)	μ m	Volume (%)	μ m	Volume (%)	μ m	Volume (%)
0.375198	0	4.2411	0.00498271	47.9397	0.082072	541.892	0.045128
0.411878	0	4.65572	0.00471943	52.6264	0.111476	594.869	0.002647
0.452145	0	5.11087	0.00485806	57.7713	0.136222	653.025	0
0.496347	0.000285456	5.61052	0.00529166	63.4192	0.146773	716.866	0
0.544872	0.00383576	6.15902	0.00592048	69.6192	0.14256	786.949	0
0.59814	0.0117598	6.76114	0.00664664	76.4253	0.144869	863.883	0
0.656615	0.0194891	7.42212	0.00738737	83.8969	0.201276	948.338	0
0.720807	0.0263236	8.14773	0.00806737	92.0988	0.393708	1041.05	0
0.791275	0.032215	8.94427	0.00861921	101.103	0.839928	1142.83	0
0.868632	0.0369748	9.81869	0.00900984	110.987	1.64874	1254.55	0
0.953552	0.0404506	10.7786	0.00922945	121.837	2.87039	1377.2	0
1.04677	0.0425133	11.8323	0.00935241	133.748	4.46381	1511.84	0
1.14911	0.0432025	12.9891	0.00946676	146.824	6.28394	1659.64	0
1.26145	0.0426156	14.2589	0.00976274	161.177	8.10042	1821.89	0
1.38477	0.0408958	15.6529	0.0103857	176.935	9.64382	2000	0
1.52015	0.0382289	17.1832	0.0114844	194.232	10.6643		
1.66876	0.034828	18.863	0.0131206	213.221	10.9859		
1.8319	0.0309252	20.7071	0.015129	234.066	10.5453		
2.011	0.0267554	22.7315	0.0173172	256.948	9.40814		
2.2076	0.0225485	24.9538	0.0192414	282.068	7.75932		
2.42342	0.0185127	27.3934	0.0207176	309.644	5.86589		
2.66033	0.0148295	30.0714	0.0219957	339.916	4.01663		
2.92042	0.0116398	33.0113	0.024028	373.147	2.45187		
3.20592	0.00904001	36.2385	0.0288616	409.626	1.30604		
3.51934	0.00707597	39.7813	0.0389356	449.672	0.587538		
3.8634	0.00573928	43.6704	0.056551	493.633	0.209496		



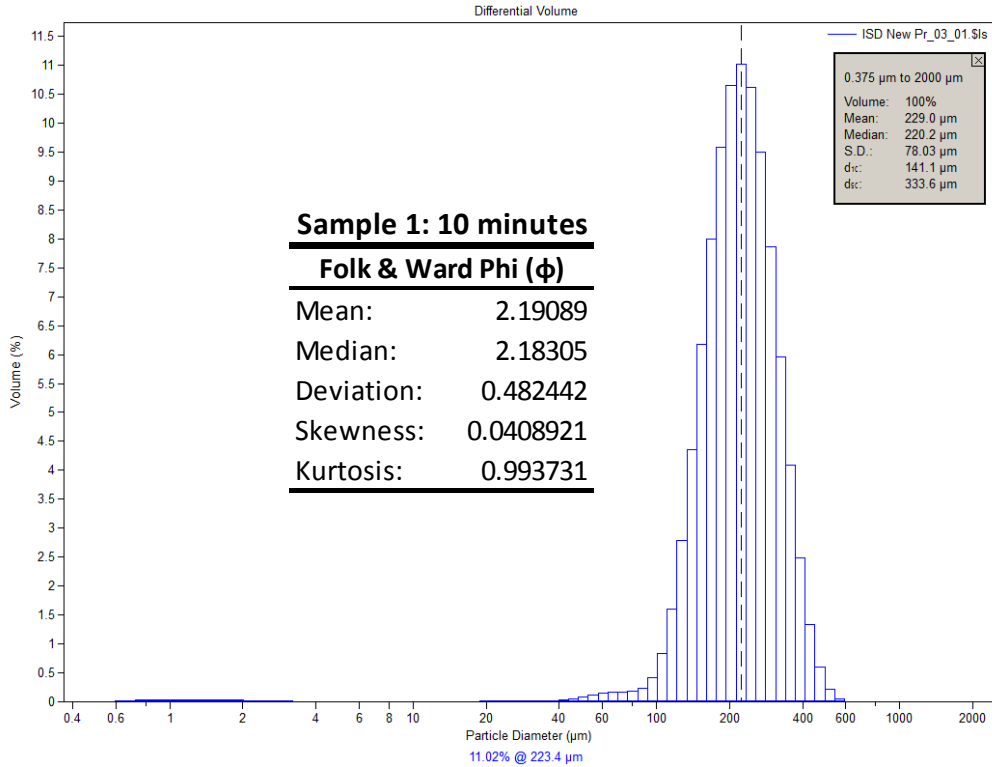
μm	Volume (%)	μm	Volume (%)	μm	Volume (%)	μm	Volume (%)
0.375198	0	4.2411	0	47.9397	0.066821	541.892	0.07554
0.411878	0	4.65572	0	52.6264	0.09353	594.869	0.003853
0.452145	0	5.11087	1.05E-05	57.7713	0.120534	653.025	0
0.496347	0	5.61052	0.000215549	63.4192	0.138875	716.866	0
0.544872	0	6.15902	0.000952413	69.6192	0.14305	786.949	0
0.59814	0	6.76114	0.00200288	76.4253	0.142706	863.883	0
0.656615	0	7.42212	0.00315557	83.8969	0.171221	948.338	0
0.720807	0	8.14773	0.0043509	92.0988	0.289771	1041.05	0
0.791275	0	8.94427	0.00543554	101.103	0.59576	1142.83	0
0.868632	0	9.81869	0.00632705	110.987	1.20229	1254.55	0
0.953552	0	10.7786	0.00692127	121.837	2.19005	1377.2	0
1.04677	0	11.8323	0.0072327	133.748	3.56949	1511.84	0
1.14911	0	12.9891	0.00728172	146.824	5.25767	1659.64	0
1.26145	0	14.2589	0.00724779	161.177	7.07794	1821.89	0
1.38477	0	15.6529	0.00730008	176.935	8.78899	2000	
1.52015	0	17.1832	0.00768122	194.232	10.1307		
1.66876	0	18.863	0.00860975	213.221	10.8802		
1.8319	0	20.7071	0.0101089	234.066	10.9004		
2.011	0	22.7315	0.0122	256.948	10.1736		
2.2076	0	24.9538	0.0145498	282.068	8.81389		
2.42342	0	27.3934	0.0168864	309.644	7.04213		
2.66033	0	30.0714	0.0191059	339.916	5.14357		
2.92042	0	33.0113	0.0215267	373.147	3.38926		
3.20592	0	36.2385	0.0254798	409.626	1.97373		
3.51934	0	39.7813	0.03288	449.672	0.980498		
3.8634	0	43.6704	0.0461233	493.633	0.370329		



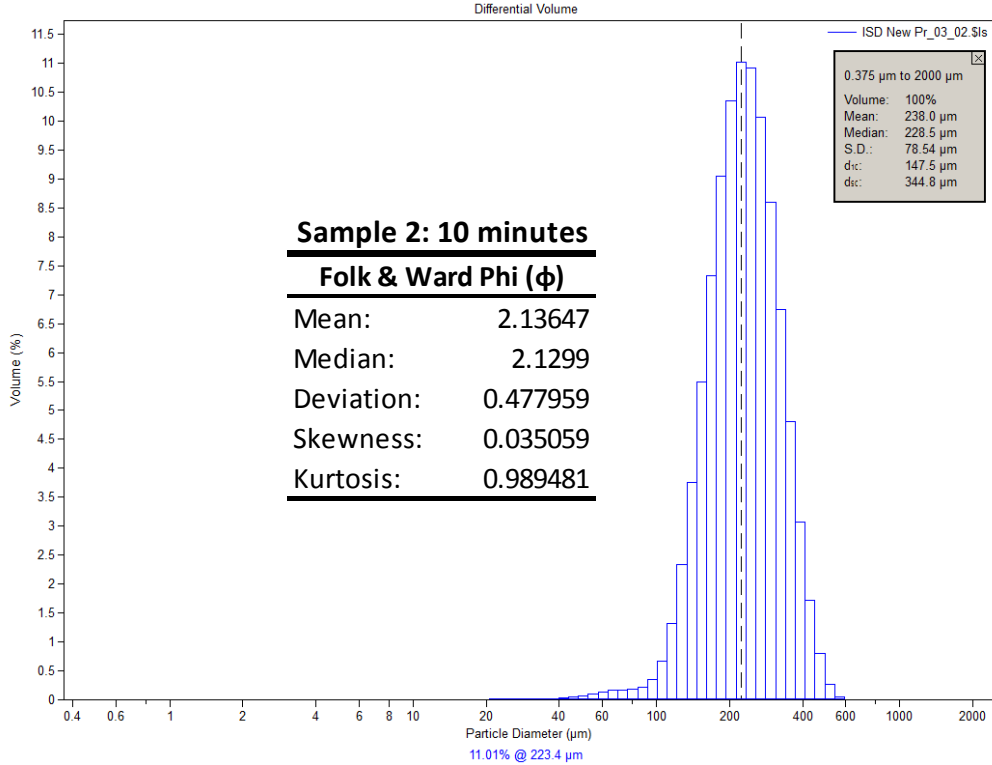
μm	Volume (%)	μm	Volume (%)	μm	Volume (%)	μm	Volume (%)
0.375198	0	4.2411	0.0033781	47.9397	0.077164	541.892	0.041322
0.411878	0	4.65572	0.00310664	52.6264	0.10655	594.869	0.002087
0.452145	0	5.11087	0.00322312	57.7713	0.133299	653.025	0
0.496347	0.000281762	5.61052	0.0036208	63.4192	0.147929	716.866	0
0.544872	0.0037859	6.15902	0.00420047	69.6192	0.148037	786.949	0
0.59814	0.0116047	6.76114	0.00486471	76.4253	0.151302	863.883	0
0.656615	0.0192244	7.42212	0.00553009	83.8969	0.201897	948.338	0
0.720807	0.0259502	8.14773	0.00612129	92.0988	0.377288	1041.05	0
0.791275	0.0317314	8.94427	0.00657173	101.103	0.792489	1142.83	0
0.868632	0.0363796	9.81869	0.00684796	110.987	1.56169	1254.55	0
0.953552	0.0397421	10.7786	0.00694033	121.837	2.7457	1377.2	0
1.04677	0.0416914	11.8323	0.00691976	133.748	4.31523	1511.84	0
1.14911	0.0422686	12.9891	0.00686878	146.824	6.13402	1659.64	0
1.26145	0.041572	14.2589	0.00697384	161.177	7.97406	1821.89	0
1.38477	0.0397479	15.6529	0.00737629	176.935	9.56191	2000	0
1.52015	0.0369836	17.1832	0.0082368	194.232	10.6387		
1.66876	0.0334944	18.863	0.00965205	213.221	11.0189		
1.8319	0.029514	20.7071	0.0115168	234.066	10.631		
2.011	0.0252787	22.7315	0.0137185	256.948	9.53408		
2.2076	0.0210196	24.9538	0.0158742	282.068	7.9092		
2.42342	0.0169448	27.3934	0.01779	309.644	6.01925		
2.66033	0.0132355	30.0714	0.019596	339.916	4.15453		
2.92042	0.0100306	33.0113	0.0220005	373.147	2.5582		
3.20592	0.00742561	36.2385	0.026786	409.626	1.37429		
3.51934	0.00546317	39.7813	0.0362224	449.672	0.621579		
3.8634	0.00413194	43.6704	0.0527104	493.633	0.214227		



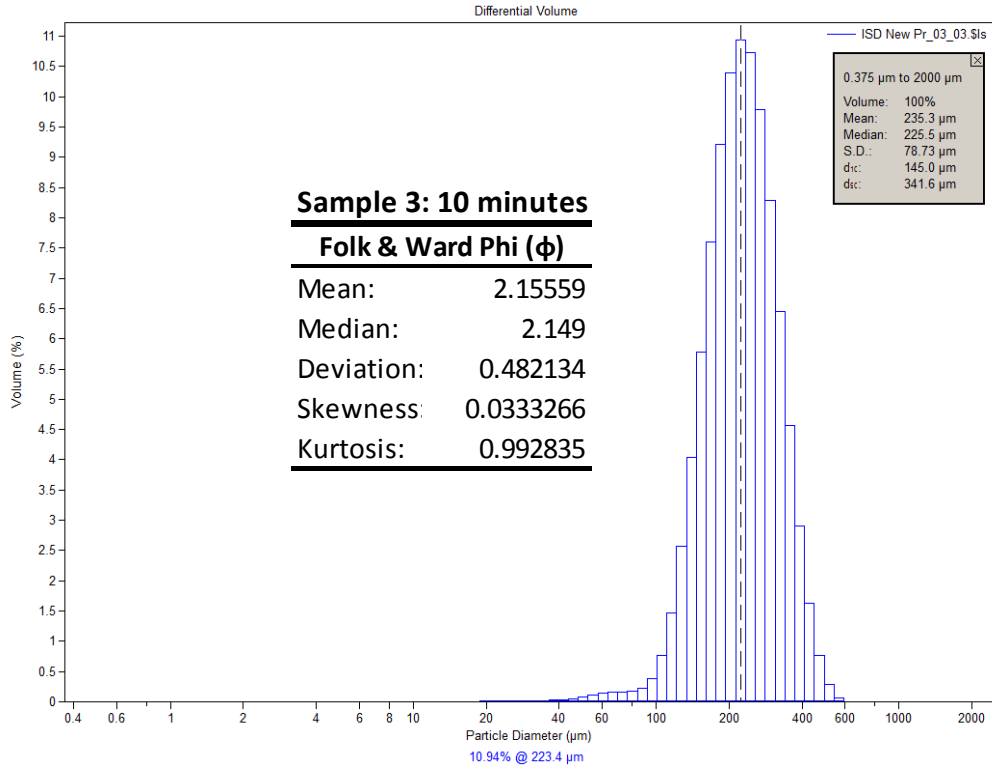
μm	Volume (%)	μm	Volume (%)	μm	Volume (%)	μm	Volume (%)
0.375198	0	4.2411	0	47.9397	0.063241	541.892	0.060321
0.411878	0	4.65572	0	52.6264	0.08871	594.869	0.003362
0.452145	0	5.11087	1.02E-06	57.7713	0.111897	653.025	0
0.496347	0	5.61052	9.29E-05	63.4192	0.123694	716.866	0
0.544872	0	6.15902	0.000706495	69.6192	0.121151	786.949	0
0.59814	0	6.76114	0.001733	76.4253	0.119912	863.883	0
0.656615	0	7.42212	0.00280168	83.8969	0.159886	948.338	0
0.720807	0	8.14773	0.00392654	92.0988	0.312412	1041.05	0
0.791275	0	8.94427	0.004945	101.103	0.687576	1142.83	0
0.868632	0	9.81869	0.0057866	110.987	1.39775	1254.55	0
0.953552	0	10.7786	0.00633937	121.837	2.50899	1377.2	0
1.04677	0	11.8323	0.00662922	133.748	4.00681	1511.84	0
1.14911	0	12.9891	0.00666811	146.824	5.7771	1659.64	0
1.26145	0	14.2589	0.00664775	161.177	7.61511	1821.89	0
1.38477	0	15.6529	0.00672509	176.935	9.26315	2000	
1.52015	0	17.1832	0.00713277	194.232	10.4634		
1.66876	0	18.863	0.00806597	213.221	11.014		
1.8319	0	20.7071	0.00949057	234.066	10.8127		
2.011	0	22.7315	0.0113777	256.948	9.88196		
2.2076	0	24.9538	0.0133194	282.068	8.36999		
2.42342	0	27.3934	0.0150306	309.644	6.52087		
2.66033	0	30.0714	0.0164745	339.916	4.62438		
2.92042	0	33.0113	0.0181411	373.147	2.9408		
3.20592	0	36.2385	0.0216046	409.626	1.64243		
3.51934	0	39.7813	0.0289305	449.672	0.777718		
3.8634	0	43.6704	0.0424498	493.633	0.285657		



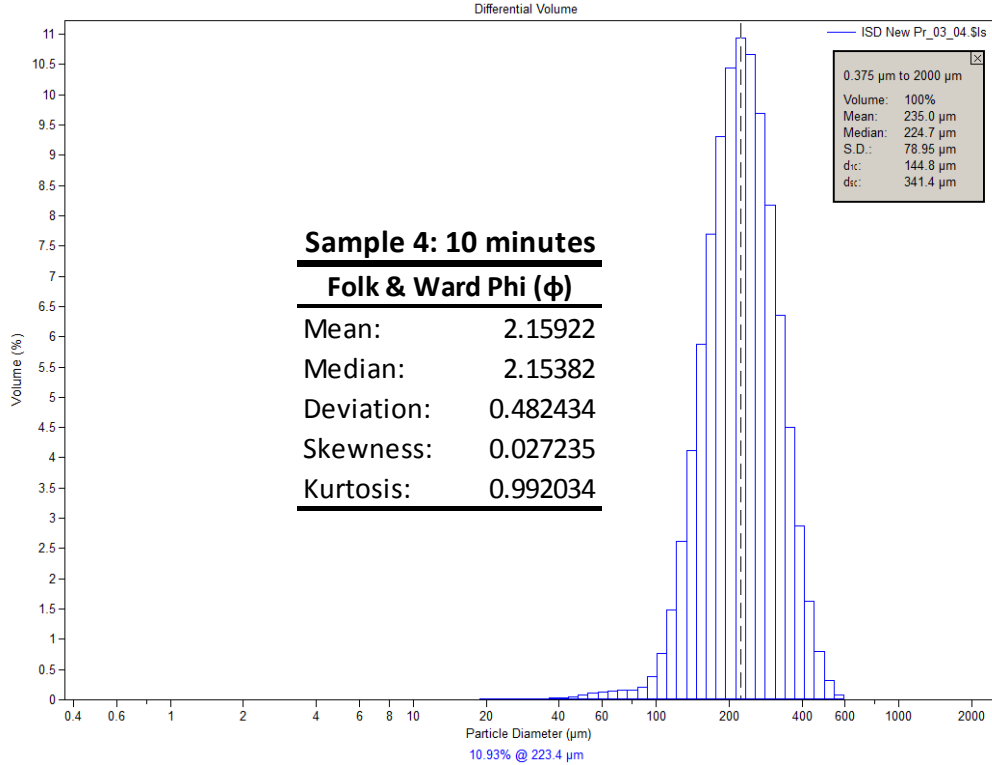
μm	Volume (%)	μm	Volume (%)	μm	Volume (%)	μm	Volume (%)
0.375198	0	4.2411	0.0030459	47.9397	0.082551	541.892	0.044981
0.411878	0	4.65572	0.00272692	52.6264	0.116244	594.869	0.002639
0.452145	0	5.11087	0.00279422	57.7713	0.14772	653.025	0
0.496347	0.000276295	5.61052	0.00314426	63.4192	0.167098	716.866	0
0.544872	0.00371262	6.15902	0.00368118	69.6192	0.171618	786.949	0
0.59814	0.0113812	6.76114	0.00430998	76.4253	0.178727	863.883	0
0.656615	0.0188576	7.42212	0.00494827	83.8969	0.233241	948.338	0
0.720807	0.0254619	8.14773	0.00552194	92.0988	0.412824	1041.05	0
0.791275	0.031145	8.94427	0.0059641	101.103	0.830972	1142.83	0
0.868632	0.0357221	9.81869	0.00623985	110.987	1.60152	1254.55	0
0.953552	0.0390436	10.7786	0.00633604	121.837	2.78545	1377.2	0
1.04677	0.0409825	11.8323	0.00631711	133.748	4.35313	1511.84	0
1.14911	0.0415766	12.9891	0.00625787	146.824	6.16805	1659.64	0
1.26145	0.0409204	14.2589	0.00633402	161.177	8.00244	1821.89	0
1.38477	0.039154	15.6529	0.00667473	176.935	9.58281	2000	
1.52015	0.0364586	17.1832	0.00742454	194.232	10.6499		
1.66876	0.0330427	18.863	0.00866069	213.221	11.0173		
1.8319	0.0291339	20.7071	0.0102608	234.066	10.613		
2.011	0.0249628	22.7315	0.0121032	256.948	9.4978		
2.2076	0.0207559	24.9538	0.013829	282.068	7.85485		
2.42342	0.0167177	27.3934	0.015322	309.644	5.95199		
2.66033	0.0130277	30.0714	0.0168546	339.916	4.08301		
2.92042	0.00982444	33.0113	0.0193318	373.147	2.49407		
3.20592	0.00720445	36.2385	0.0247557	409.626	1.32794		
3.51934	0.00521325	39.7813	0.0356436	449.672	0.595856		
3.8634	0.00384373	43.6704	0.0545964	493.633	0.210667		



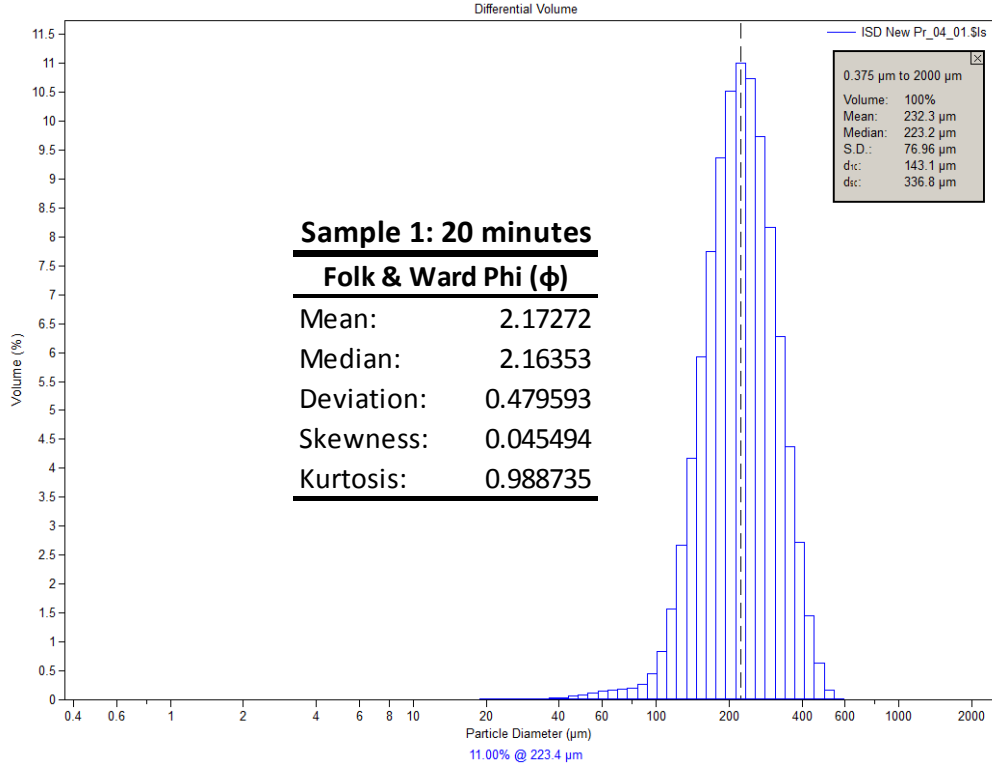
μm	Volume (%)	μm	Volume (%)	μm	Volume (%)	μm	Volume (%)
0.375198	0	4.2411	0	47.9397	0.074699	541.892	0.044437
0.411878	0	4.65572	0	52.6264	0.105785	594.869	0.001685
0.452145	0	5.11087	0	57.7713	0.137454	653.025	0
0.496347	0	5.61052	4.56E-05	63.4192	0.160603	716.866	0
0.544872	0	6.15902	0.000527834	69.6192	0.169996	786.949	0
0.59814	0	6.76114	0.00143953	76.4253	0.175949	863.883	0
0.656615	0	7.42212	0.00237687	83.8969	0.21346	948.338	0
0.720807	0	8.14773	0.00338759	92.0988	0.346699	1041.05	0
0.791275	0	8.94427	0.00433179	101.103	0.674897	1142.83	0
0.868632	0	9.81869	0.0051418	110.987	1.31216	1254.55	0
0.953552	0	10.7786	0.00571526	121.837	2.33921	1377.2	0
1.04677	0	11.8323	0.00605966	133.748	3.76266	1511.84	0
1.14911	0	12.9891	0.00617683	146.824	5.4911	1659.64	0
1.26145	0	14.2589	0.00621873	161.177	7.33595	1821.89	0
1.38477	0	15.6529	0.0063207	176.935	9.04314	2000	
1.52015	0	17.1832	0.00669018	194.232	10.3432		
1.66876	0	18.863	0.00751867	213.221	11.0118		
1.8319	0	20.7071	0.00881887	234.066	10.9207		
2.011	0	22.7315	0.0106303	256.948	10.0701		
2.2076	0	24.9538	0.0126751	282.068	8.5974		
2.42342	0	27.3934	0.0147878	309.644	6.74445		
2.66033	0	30.0714	0.0170163	339.916	4.81115		
2.92042	0	33.0113	0.0198656	373.147	3.07182		
3.20592	0	36.2385	0.0248749	409.626	1.71356		
3.51934	0	39.7813	0.0341597	449.672	0.801237		
3.8634	0	43.6704	0.0502483	493.633	0.26967		



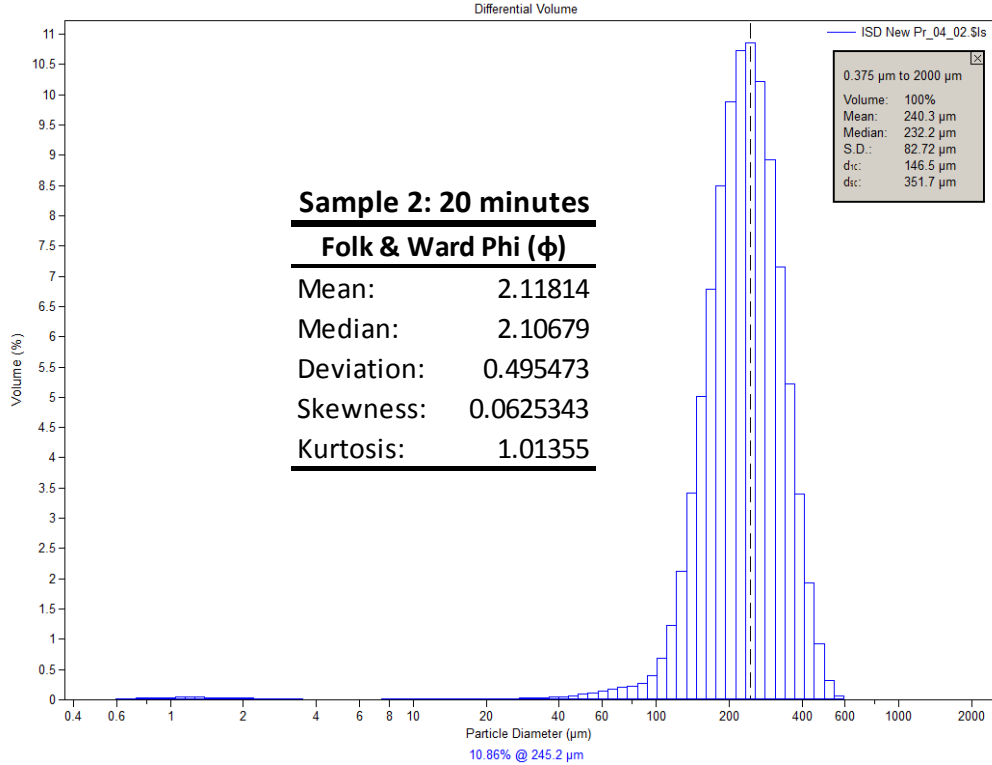
μ m	Volume (%)	μ m	Volume (%)	μ m	Volume (%)	μ m	Volume (%)
0.375198	0	4.2411	0	47.9397	0.078953	541.892	0.062985
0.411878	0	4.65572	0	52.6264	0.109115	594.869	0.003658
0.452145	0	5.11087	1.76E-06	57.7713	0.137976	653.025	0
0.496347	0	5.61052	0.000106384	63.4192	0.157058	716.866	0
0.544872	0	6.15902	0.00073699	69.6192	0.163777	786.949	0
0.59814	0	6.76114	0.00177576	76.4253	0.173103	863.883	0
0.656615	0	7.42212	0.00286847	83.8969	0.2249	948.338	0
0.720807	0	8.14773	0.00401856	92.0988	0.389272	1041.05	0
0.791275	0	8.94427	0.00506351	101.103	0.769784	1142.83	0
0.868632	0	9.81869	0.00593395	110.987	1.47487	1254.55	0
0.953552	0	10.7786	0.00652019	121.837	2.57059	1377.2	0
1.04677	0	11.8323	0.00684672	133.748	4.04437	1511.84	0
1.14911	0	12.9891	0.00692514	146.824	5.78603	1659.64	0
1.26145	0	14.2589	0.00693594	161.177	7.59568	1821.89	0
1.38477	0	15.6529	0.00702952	176.935	9.21928	2000	0
1.52015	0	17.1832	0.00742278	194.232	10.4005		
1.66876	0	18.863	0.00830742	213.221	10.9375		
1.8319	0	20.7071	0.00966687	234.066	10.7278		
2.011	0	22.7315	0.0115217	256.948	9.79459		
2.2076	0	24.9538	0.0135727	282.068	8.28723		
2.42342	0	27.3934	0.0156846	309.644	6.44992		
2.66033	0	30.0714	0.0179987	339.916	4.57051		
2.92042	0	33.0113	0.0211408	373.147	2.90602		
3.20592	0	36.2385	0.0267691	409.626	1.62518		
3.51934	0	39.7813	0.0369896	449.672	0.772973		
3.8634	0	43.6704	0.0540638	493.633	0.288414		



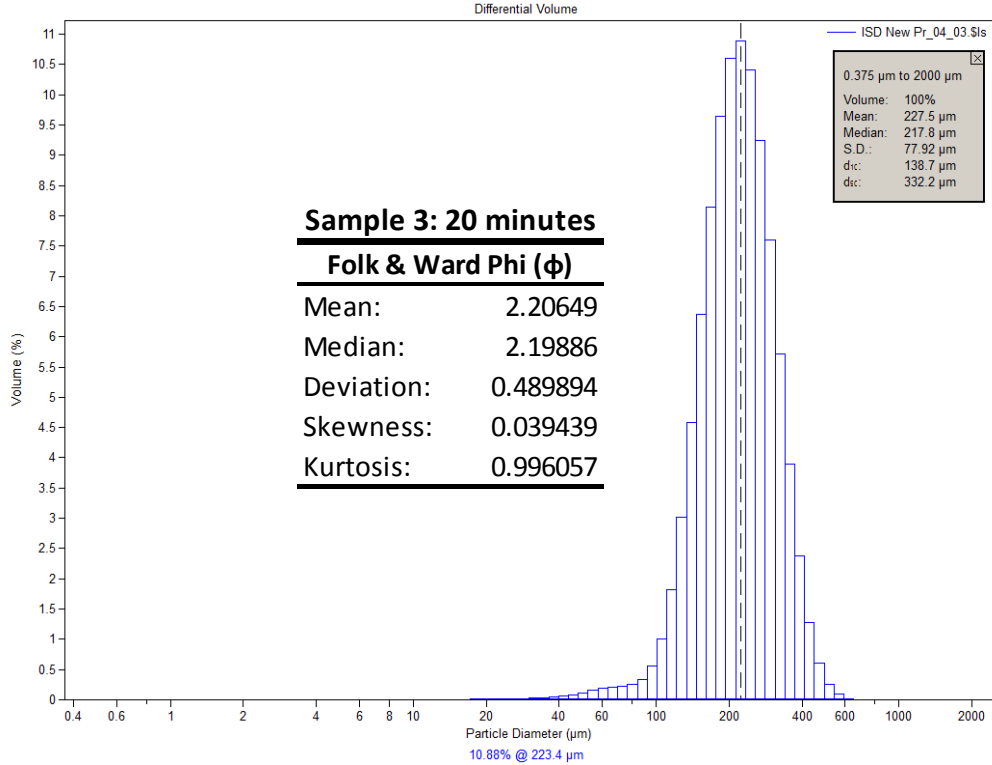
μm	Volume (%)	μm	Volume (%)	μm	Volume (%)	μm	Volume (%)
0.375198	0	4.2411	0	47.9397	0.075889	541.892	0.07818
0.411878	0	4.65572	0	52.6264	0.105264	594.869	0.005072
0.452145	0	5.11087	1.50E-06	57.7713	0.133192	653.025	0
0.496347	0	5.61052	0.000103343	63.4192	0.151027	716.866	0
0.544872	0	6.15902	0.00071577	69.6192	0.156092	786.949	0
0.59814	0	6.76114	0.00169321	76.4253	0.163777	863.883	0
0.656615	0	7.42212	0.00271878	83.8969	0.214839	948.338	0
0.720807	0	8.14773	0.00380061	92.0988	0.381314	1041.05	0
0.791275	0	8.94427	0.00478894	101.103	0.770287	1142.83	0
0.868632	0	9.81869	0.00562163	110.987	1.4925	1254.55	0
0.953552	0	10.7786	0.00619196	121.837	2.61318	1377.2	0
1.04677	0	11.8323	0.00652954	133.748	4.11497	1511.84	0
1.14911	0	12.9891	0.00663374	146.824	5.87925	1659.64	0
1.26145	0	14.2589	0.0066839	161.177	7.69643	1821.89	0
1.38477	0	15.6529	0.00680375	176.935	9.30542	2000	0
1.52015	0	17.1832	0.00721009	194.232	10.4497		
1.66876	0	18.863	0.0080788	213.221	10.9349		
1.8319	0	20.7071	0.00939105	234.066	10.6719		
2.011	0	22.7315	0.0111788	256.948	9.69922		
2.2076	0	24.9538	0.0131335	282.068	8.17619		
2.42342	0	27.3934	0.0151265	309.644	6.3496		
2.66033	0	30.0714	0.0172799	339.916	4.49981		
2.92042	0	33.0113	0.0201924	373.147	2.87329		
3.20592	0	36.2385	0.0254947	409.626	1.62662		
3.51934	0	39.7813	0.0352466	449.672	0.796455		
3.8634	0	43.6704	0.051707	493.633	0.319308		



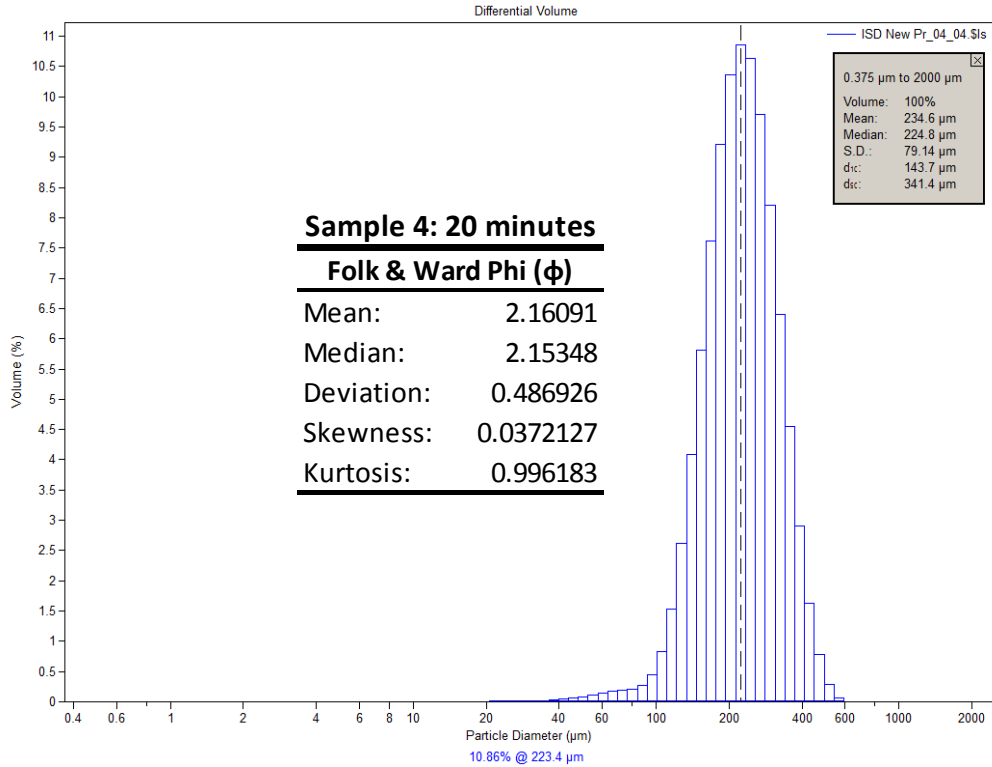
μm	Volume (%)	μm	Volume (%)	μm	Volume (%)	μm	Volume (%)
0.375198	0	4.2411	0	47.9397	0.085533	541.892	0.011269
0.411878	0	4.65572	0	52.6264	0.118127	594.869	0
0.452145	0	5.11087	2.56E-05	57.7713	0.150291	653.025	0
0.496347	0	5.61052	0.000374178	63.4192	0.174068	716.866	0
0.544872	0	6.15902	0.00129752	69.6192	0.187384	786.949	0
0.59814	0	6.76114	0.00245578	76.4253	0.205304	863.883	0
0.656615	0	7.42212	0.00372044	83.8969	0.268074	948.338	0
0.720807	0	8.14773	0.00498085	92.0988	0.446399	1041.05	0
0.791275	0	8.94427	0.00609074	101.103	0.842701	1142.83	0
0.868632	0	9.81869	0.00695022	110.987	1.5646	1254.55	0
0.953552	0	10.7786	0.00746934	121.837	2.67834	1377.2	0
1.04677	0	11.8323	0.00766395	133.748	4.17027	1511.84	0
1.14911	0	12.9891	0.00757988	146.824	5.92693	1659.64	0
1.26145	0	14.2589	0.00740948	161.177	7.74262	1821.89	0
1.38477	0	15.6529	0.0073353	176.935	9.35748	2000	0
1.52015	0	17.1832	0.00760125	194.232	10.5109		
1.66876	0	18.863	0.00840221	213.221	11.001		
1.8319	0	20.7071	0.00974299	234.066	10.7301		
2.011	0	22.7315	0.0116338	256.948	9.73074		
2.2076	0	24.9538	0.0137926	282.068	8.16439		
2.42342	0	27.3934	0.016101	309.644	6.28314		
2.66033	0	30.0714	0.018746	339.916	4.38132		
2.92042	0	33.0113	0.0224267	373.147	2.71541		
3.20592	0	36.2385	0.028862	409.626	1.45218		
3.51934	0	39.7813	0.0402132	449.672	0.63498		
3.8634	0	43.6704	0.0587649	493.633	0.166862		



μm	Volume (%)	μm	Volume (%)	μm	Volume (%)	μm	Volume (%)
0.375198	0	4.2411	0.00498537	47.9397	0.091765	541.892	0.056614
0.411878	0	4.65572	0.00496127	52.6264	0.119672	594.869	0.00236
0.452145	0	5.11087	0.00529961	57.7713	0.151582	653.025	0
0.496347	0.000279546	5.61052	0.00588742	63.4192	0.181718	716.866	0
0.544872	0.00375544	6.15902	0.00662152	69.6192	0.205085	786.949	0
0.59814	0.0115079	6.76114	0.00740442	76.4253	0.226829	863.883	0
0.656615	0.0190534	7.42212	0.00815718	83.8969	0.272757	948.338	0
0.720807	0.025699	8.14773	0.00880693	92.0988	0.395834	1041.05	0
0.791275	0.0313932	8.94427	0.00929424	101.103	0.679668	1142.83	0
0.868632	0.0359488	9.81869	0.00958898	110.987	1.22813	1254.55	0
0.953552	0.0392173	10.7786	0.00968651	121.837	2.12873	1377.2	0
1.04677	0.0410778	11.8323	0.00965325	133.748	3.41003	1511.84	0
1.14911	0.0415785	12.9891	0.00956537	146.824	5.01258	1659.64	0
1.26145	0.0408258	14.2589	0.00959082	161.177	6.78244	1821.89	0
1.38477	0.0389742	15.6529	0.00986008	176.935	8.4929	2000	0
1.52015	0.036217	17.1832	0.0105553	194.232	9.88591		
1.66876	0.0327759	18.863	0.0118388	213.221	10.7269		
1.8319	0.0288878	20.7071	0.0137881	234.066	10.8557		
2.011	0.0247904	22.7315	0.0165716	256.948	10.2259		
2.2076	0.0207133	24.9538	0.0201573	282.068	8.92523		
2.42342	0.0168609	27.3934	0.024599	309.644	7.15979		
2.66033	0.0134084	30.0714	0.0299611	339.916	5.21965		
2.92042	0.0104862	33.0113	0.0363523	373.147	3.4012		
3.20592	0.00817866	36.2385	0.0444343	409.626	1.93227		
3.51934	0.00651516	39.7813	0.0552152	449.672	0.920834		
3.8634	0.00547152	43.6704	0.0703862	493.633	0.321205		



μm	Volume (%)	μm	Volume (%)	μm	Volume (%)	μm	Volume (%)
0.375198	0	4.2411	0	47.9397	0.116163	541.892	0.089948
0.411878	0	4.65572	0	52.6264	0.153328	594.869	0.017271
0.452145	0	5.11087	0	57.7713	0.188788	653.025	0.000798
0.496347	0	5.61052	0	63.4192	0.21491	716.866	0
0.544872	0	6.15902	0	69.6192	0.231292	786.949	0
0.59814	0	6.76114	0	76.4253	0.256887	863.883	0
0.656615	0	7.42212	0	83.8969	0.3382	948.338	0
0.720807	0	8.14773	0	92.0988	0.553851	1041.05	0
0.791275	0	8.94427	0	101.103	1.01196	1142.83	0
0.868632	0	9.81869	0	110.987	1.81748	1254.55	0
0.953552	0	10.7786	0	121.837	3.0225	1377.2	0
1.04677	0	11.8323	0	133.748	4.58833	1511.84	0
1.14911	0	12.9891	0	146.824	6.37194	1659.64	0
1.26145	0	14.2589	0.000746265	161.177	8.14464	1821.89	0
1.38477	0	15.6529	0.006959	176.935	9.63906	2000	
1.52015	0	17.1832	0.0128061	194.232	10.609		
1.66876	0	18.863	0.0133656	213.221	10.884		
1.8319	0	20.7071	0.0142054	234.066	10.4072		
2.011	0	22.7315	0.0153894	256.948	9.24988		
2.2076	0	24.9538	0.0173882	282.068	7.59898		
2.42342	0	27.3934	0.0204687	309.644	5.72094		
2.66033	0	30.0714	0.0250495	339.916	3.90125		
2.92042	0	33.0113	0.0321498	373.147	2.37815		
3.20592	0	36.2385	0.0430558	409.626	1.2813		
3.51934	0	39.7813	0.0597837	449.672	0.608458		
3.8634	0	43.6704	0.0840412	493.633	0.258117		



μm	Volume (%)	μm	Volume (%)	μm	Volume (%)	μm	Volume (%)
0.375198	0	4.2411	0	47.9397	0.086113	541.892	0.058562
0.411878	0	4.65572	0	52.6264	0.118488	594.869	0.003105
0.452145	0	5.11087	1.13E-05	57.7713	0.151356	653.025	0
0.496347	0	5.61052	0.000229574	63.4192	0.176725	716.866	0
0.544872	0	6.15902	0.000959075	69.6192	0.191563	786.949	0
0.59814	0	6.76114	0.00191772	76.4253	0.209367	863.883	0
0.656615	0	7.42212	0.00296392	83.8969	0.268949	948.338	0
0.720807	0	8.14773	0.00403159	92.0988	0.439638	1041.05	0
0.791275	0	8.94427	0.00498616	101.103	0.822834	1142.83	0
0.868632	0	9.81869	0.00575084	110.987	1.52669	1254.55	0
0.953552	0	10.7786	0.00622776	121.837	2.61879	1377.2	0
1.04677	0	11.8323	0.00644261	133.748	4.08678	1511.84	0
1.14911	0	12.9891	0.00640548	146.824	5.81836	1659.64	0
1.26145	0	14.2589	0.00630784	161.177	7.61039	1821.89	0
1.38477	0	15.6529	0.0062848	176.935	9.20744	2000	
1.52015	0	17.1832	0.00658944	194.232	10.3564		
1.66876	0	18.863	0.00742094	213.221	10.8632		
1.8319	0	20.7071	0.00881907	234.066	10.6349		
2.011	0	22.7315	0.0108815	256.948	9.70167		
2.2076	0	24.9538	0.0133714	282.068	8.21297		
2.42342	0	27.3934	0.0162042	309.644	6.40407		
2.66033	0	30.0714	0.0195	339.916	4.55116		
2.92042	0	33.0113	0.0237901	373.147	2.90274		
3.20592	0	36.2385	0.0305991	409.626	1.62653		
3.51934	0	39.7813	0.0418988	449.672	0.774923		
3.8634	0	43.6704	0.0599693	493.633	0.284701		

APPENDIX F

THIN-SECTION LONG-AXIS DATA

Included thin-section data files:

1. Long-axis data summary table
2. All long-axis measurements from each sample
 - a. The 150 randomly selected measurements used for calculations are shaded grey.

Sample	Average Grain Size (ϕ)	Median (ϕ)	Standard Deviation (ϕ)	Skewness (ϕ)
ASF-5-24	3.313366365	3.245011564	0.521701789	0.805394365
ASF-5-14	3.275397077	3.235086461	0.579977397	0.9203958
ASF-22e-F	3.281114521	3.178586177	0.534349879	0.863290184
ASF-22e-H	3.332598751	3.207616431	0.528223813	1.312945617
HMT-5	3.447800964	3.376175104	0.477543671	0.483104068
HMT-3	3.234890225	3.168926106	0.543175104	0.578848004
TM-1-41	3.086425248	3.0508651	0.650118309	0.327287069
ASF-5-16	3.193437617	3.137904256	0.493912816	0.556149589
TM-1-25	3.13898683	3.130674665	0.413438239	0.275961509
TM-3-1	2.997199619	2.984754105	0.562284556	-0.066341634
TM-3-5	3.154960477	3.115796082	0.481625464	0.192406244
ASF-22e-A	3.439440499	3.367468217	0.456819083	0.691712675
TM-1-50	2.913091423	2.889478751	0.566945232	0.767681822
TM-3-15	3.010646331	3.004235943	0.441459818	0.100766883
TM-1-47	3.281928949	3.14296185	0.550927077	0.910491979
HOL-E-B-1	2.970002996	2.977698038	0.56805657	0.213569436
HOL-E-B-2	2.95948312	2.983663688	0.454493765	0.032107311
HOL-E-B-3	2.871637537	2.828498968	0.580083176	0.65889267
HOL-E-B-4	2.875528251	2.836846055	0.572518842	0.560740174
HOL-E-B-5	3.138654282	3.09835859	0.520221987	0.590201691
HOL-E-B-6	3.094087431	3.070879893	0.556630727	0.511173724
HOL-E-B-7	3.163526551	3.101953971	0.509830167	0.453460418
HOL-E-B-8	3.057572687	3.007341493	0.499852422	0.536105058
HOL-E-B-9	3.074966147	3.010807503	0.557400051	0.426118697
HOL-E-B-11	3.04714406	3.018575805	0.544814726	0.408294279
HOL-E-B-12	3.031071373	3.003535432	0.530230955	0.475554999
HOL-E-B-13	3.038558743	3.028264113	0.533991099	0.412724996
HOL-E-B-14	2.97879538	2.930063484	0.508390884	0.649537451
HOL-E-B-15	3.292301806	3.174611817	0.526264775	0.875537248
HOL-E-B-16	3.010242366	2.983959386	0.558472141	0.630845473
ALC-3	3.217479223	3.207161456	0.611138819	0.228149207
COW-2	2.000914868	1.991372546	0.582775694	0.155127972
COW-3	2.964026643	2.994252181	0.631774494	0.157665826
KIN-1	2.569281089	2.652678309	0.966751037	0.043411774
KIN-2	2.524258516	2.473953452	0.794436975	0.087805496
TEN-1	3.314116536	3.247157097	0.532836883	0.726812411

ASF-5-24 (μm)

31.4691	113.2458	97.6087	123.4053	108.7139	134.3648
134.6535	116.3916	141.0562	100.238	166.1778	66.7067
91.9151	104.9796	80.3842	54.105	91.633	62.6568
69.0911	98.3259	125.0592	125.7146	158.1983	126.7562
61.7052	93.9163	66.8175	111.932	42.2737	127.1123
96.593	55.2064	71.2548	116.1831	125.8534	141.0621
93.4843	120.2278	119.75	97.9449	119.556	128.7712
99.328	90.7204	154.8711	59.6705	232.2778	87.6238
105.6662	108.1511	89.4501	96.3033	87.2643	191.8895
59.1205	37.6244	146.3238	140.0975	71.9578	93.24
213.0868	135.226	102.5401	117.0043	50.1477	87.071
137.4757	106.5338	120.4122	126.9247	108.5209	83.1482
74.428	75.0219	134.2746	106.418	91.6487	93.4513
107.4822	112.6638	76.7359	283.8926	139.7524	136.1527
94.5464	55.2994	166.4545	125.1314	93.1695	127.0606
104.7856	124.2615	102.9181	161.2839	81.7025	33.8471
97.4907	116.1389	80.2307	111.26	104.0221	82.6948
60.4912	64.5243	138.035	90.6298	133.9928	134.8974
104.3475	133.0927	159.1307	160.9791	96.3843	155.3876
94.3092	131.8473	65.6793	77.6938	92.5433	155.5092
113.0625	108.3694	148.9168	154.2409	97.9113	115.7047
168.854	83.1581	124.8684	53.0814	65.8355	117.8651
85.2347	203.3274	133.3395	149.0988	129.1885	89.8214
75.2844	57.9765	106.8226	123.6	116.9762	131.1708
100.1088	39.9755	95.6504	107.059	48.9242	115.1351
48.1239	166.6778	110.66	58.0898	125.6427	119.1084
94.874	86.1268	84.1723	93.7586	92.3166	103.8086
96.461	78.0394	56.3884	66.3268	105.263	74.6788
103.6005	108.7271	124.9227	97.438	96.0619	
113.0025	146.7711	122.2461	109.0648	132.5002	
73.4807	131.7616	105.007	178.9598	55.9017	
149.9849	158.3217	125.7407	113.2731	107.74	
105.2864	107.5873	135.112	102.8402	152.3714	
197.4401	89.7665	156.5219	115.4291	137.9099	
82.4958	119.6951	84.2309	118.7144	100.5246	
119.8975	126.97	100.8389	97.2523	108.0618	
67.9971	91.2893	151.5114	166.4212	94.7439	
199.4733	101.9936	66.9158	109.7652	91.7025	
144.0127	120.3098	78.4176	123.8574	88.4987	
117.3987	118.5897	146.8718	87.2596	79.7813	
39.7488	134.1812	87.7456	74.1875	100.2052	
154.4007	147.8673	144.3902	71.9692	35.5581	
53.3247	116.8321	52.8059	158.4112	112.0549	
32.2621	131.9719	80.1051	166.6975	72.8206	
167.6414	110.139	152.8991	119.0324	56.0045	
112.8496	132.5808	102.9739	43.2158	177.0171	
77.6911	94.1413	120.2158	82.1139	155.2672	
124.3788	72.9756	111.7023	122.1251	62.578	
116.1831	94.9519	186.2828	54.1543	94.874	
107.761	95.36	135.0512	166.8145	86.5978	
43.8529	115.1886	100.7043	114.6791	79.5957	
117.0271	73.0769	69.1744	93.5985	94.2286	

ASF-5-14 (µm)

97.0048	111.1805	45.1639	48.7559	86.6713
80.7234	75.5133	88.9156	151.3323	136.555
150.6137	96.5207	103.4676	64.4223	53.9567
91.4243	144.4628	83.9841	72.9813	139.2738
101.3145	164.8383	126.9376	41.4491	103.8264
137.8384	95.2263	160.8208	99.4602	116.8321
41.6716	88.501	103.6045	113.3456	169.0097
35.4018	151.7214	61.4449	118.1158	84.1796
80.8938	134.7512	91.6756	113.4905	48.3539
44.725	84.8796	153.5213	66.7806	83.6311
36.7403	57.0549	87.1889	72.6172	101.2516
77.5879	72.7783	124.7779	136.749	30.6756
110.234	29.9023	87.7737	69.9511	202.0218
67.6943	125.4315	149.6572	134.4902	124.5175
88.9918	241.7483	54.3059	77.4872	115.8289
95.2953	138.1555	111.9375	86.091	188.7121
118.2983	110.8696	99.9445	137.6072	137.2648
137.8429	96.5143	171.619	167.7541	114.4011
99.1913	259.2788	106.066	83.0889	124.4878
116.5627	117.5456	173.1636	166.0937	116.2804
109.0215	62.4466	39.8984	101.8	106.157
131.7959	92.39	133.7963	136.4722	98.4804
128.2596	187.6575	208.8012	124.8684	81.4885
164.0888	175.2827	139.7568	128.1875	135.6023
103.8382	114.2573	142.93	120.3508	112.1337
124.3656	106.4817	49.259	49.8889	209.8985
133.9989	135.1242	146.9054	89.008	54.9415
101.3753	100.8389	120.2432	87.6167	38.7012
182.6023	88.8532	153.2145	116.3228	153.295
111.0752	222.8825	89.4156	64.7182	125.5576
35.1397	125.8763	197.7697	89.4891	91.1181
88.1637	134.9142	57.3673	72.2769	63.5424
109.7072	115.5288	104.3298	129.1026	142.2687
108.4016	108.3959	117.8511	83.205	62.8728
80.2537	144.4116	111.0752	108.6742	90.6547
88.2779	104.4419	99.7696	127.5512	85.5907
110.139	76.3144	91.3613	135.3354	101.2841
100.8124	22.252	76.7653	61.971	113.3184
98.2172	99.8129	106.3427	105.8391	37.728
90.5391	101.8	168.6726	95.6182	136.3864
168.1358	115.655	84.6275	136.785	113.6063
120.4258	128.7824	157.6975	198.7221	137.157
112.3899	80.0769	124.2747	110.1464	62.9675
94.7613	98.1795	71.6832	133.9268	52.3133
178.0217	87.2596	152.119	101.276	75.2489
85.1503	119.9403	109.7072	126.7514	141.7377
90.9308	96.461	124.4399	39.1393	94.0824
83.8568	151.739	51.0572	122.8447	122.9867
56.7588	120.6934	135.7719	32.7488	
99.5655	153.3861	69.5535	34.556	
173.211	108.2423	72.6964	141.0621	
77.5217	82.933	168.591	52.7085	

ASF-22e-F (μm)

172.6014	92.7518	84.8603	127.926	142.2456	87.8416
130.494	96.5398	66.1034	43.0825	107.0532	87.3796
135.0253	126.1518	106.3813	70.0011	129.3364	78.9893
50.7869	87.5417	102.231	121.5619	126.3748	165.2118
109.1627	141.1189	120.1201	78.5747	127.1301	168.0478
125.6672	53.9757	113.8394	56.8926	163.1911	109.6323
130.7708	143.967	86.3007	69.7776	151.7945	144.3447
111.5642	148.3112	110.8085	58.3333	142.0534	125.3037
184.0648	51.9191	95.4784	85.907	49.4712	81.5792
180.9646	101.8606	134.4902	93.3457	86.8797	186.3192
141.4678	115.0601	125.0592	120.39	127.5786	79.5828
114.0269	113.4688	112.2692	88.5845	71.4851	96.094
70.8558	88.8462	99.4417	80.1282	156.8628	
136.6167	138.0588	163.9986	128.0849	91.8279	
80.6419	73.4527	133.3719	140.1195	103.1394	
144.3006	108.0884	64.9179	107.105	137.4862	
63.8617	152.5008	27.5939	60.1677	112.693	
83.4934	163.5872	122.5483	69.21	72.7162	
148.8974	107.8467	137.977	165.3709	135.001	
111.6673	172.3298	42.1374	85.0054	47.5441	
89.9014	129.0437	118.9426	116.0416	145.2245	
65.0854	82.4111	111.7244	70.7165	125.8844	
132.9027	175.4034	112.9516	98.2465	53.8156	
139.9625	86.5764	49.4878	135.9896	98.4366	
203.7867	103.5073	112.1135	39.8572	36.4427	
143.0651	106.6533	92.3722	51.6811	86.1101	
119.5904	109.0366	105.8178	109.5104	87.9491	
126.3227	46.8651	188.4572	154.9175	129.0358	
89.388	49.6247	123.0402	98.9757	76.43	
99.3176	133.0881	55.7987	138.3487	122.0645	
97.1402	126.5015	127.3078	51.6811	203.1171	
76.516	91.8369	69.4471	132.8177	113.9746	
99.8129	73.8822	82.9924	101.9311	94.5594	
68.6377	107.8086	91.1069	136.9111	115.4985	
120.1252	111.6287	75.7387	113.4959	94.3201	
98.72	45.6255	43.3345	93.5897	130.9231	
36.8297	96.2073	114.706	95.0146	133.6904	
175.1608	151.2943	55.0685	105.4755	110.012	
81.7729	106.607	166.3038	106.6224	123.7329	
118.034	110.0848	78.5747	107.266	84.5182	
138.6632	51.0572	73.7625	67.8216	51.2219	
123.5601	44.9861	91.5411	54.4608	161.4901	
145.1184	163.4967	132.731	71.9578	147.7491	
91.422	65.5384	198.0479	116.0752	110.139	
101.7152	107.74	109.7521	112.5653	124.2747	
184.144	139.1734	162.1998	182.8362	88.3616	
73.9961	125.7228	120.9383	93.5656	117.2954	
116.5363	115.9902	136.6167	147.3815	75.6655	
141.0621	129.6156	125.5691	94.405	189.4423	
95.2263	83.5328	133.4873	146.4081	36.9856	
113.2731	113.0552	77.5217	71.4765	62.3774	
124.2499	98.1942	107.082	90.2572	92.8271	

ASF-22e-H (µm)

168.5312	99.852	151.7296	163.9823	85.95	83.0963
145.6413	121.9314	54.728	107.9515	107.5128	52.2976
89.7848	110.4426	116.3228	98.8511	79.704	53.7277
128.1554	135.3111	123.0452	113.3456	136.8391	138.7017
39.8726	104.2352	142.966	137.2828	110.7027	102.942
75.7089	53.0543	150.6751	121.7139	142.3091	94.4311
84.3552	140.5484	148.1449	108.0618	133.3534	145.6864
44.0819	114.8939	114.1476	75.3498	99.4107	84.2748
122.9383	123.0135	98.7367	128.5284	103.6184	132.5048
90.4573	112.4265	96.094	106.9898	112.152	135.2579
66.5495	64.7436	73.251	105.1282	74.0711	122.3402
72.7981	98.5263	108.3959	83.4245	42.7906	101.4847
100.6492	27.8311	123.6	138.1243	137.634	116.5504
44.4901	103.8382	82.2763	133.7533	145.3942	86.8489
134.8548	108.9234	97.3199	123.8441	63.8617	103.2927
121.4672	88.7236	83.9915	111.3412	149.4965	121.1725
68.142	97.9113	112.0549	150.7515	105.6215	142.5817
86.5764	96.1325	48.094	103.4676	128.4421	132.5823
103.2131	162.7763	157.9904	124.4399	117.1938	152.2689
106.1028	83.1779	147.136	59.5913	105.6312	96.5398
67.3046	90.2117	153.0334	152.3134	87.5675	88.7213
101.9311	146.3589	77.0645	124.321	120.3508	114.1314
134.0173	150.9081	117.2306	99.6254	108.0656	98.2465
153.2387	130.7519	160.0075	109.5104	134.8594	125.9106
27.3846	117.9487	130.0003	191.7192	63.926	114.0125
116.6314	95.7084	124.1473	76.8081	32.9988	100.8877
29.4941	86.1649	116.0416	106.0331	105.9769	91.1362
63.7587	85.3359	143.9684	68.9363	61.1936	133.2902
82.8586	106.0001	84.8966	143.717	124.6577	229.8043
159.7916	153.5481	79.0569	42.8769	110.853	
119.0531	35.2622	136.0697	93.8813	99.6089	
113.5502	73.9961	70.2706	146.1665	129.3935	
184.26	148.6032	119.3513	134.5604	135.7477	
124.5406	112.3625	84.3527	66.0288	106.1899	
75.7089	129.1026	107.7419	92.5589	144.869	
90.3027	78.7105	140.874	106.711	117.9766	
74.2843	115.9884	50.6573	57.1772	59.839	
111.7244	111.0918	112.0915	101.8182	115.5999	
75.8716	118.3053	125.0411	31.5669	153.13	
126.1453	82.5929	88.8277	90.5663	165.6279	
112.7185	133.1668	76.0906	99.0691	131.9408	
95.7105	108.9857	114.2555	82.1339	55.3291	
84.3138	130.6057	112.0915	61.1936	119.3685	
35.1397	71.3384	83.4442	85.8544	61.2339	
125.8404	86.1578	140.7018	142.6725	148.9788	
146.8634	95.5322	124.8684	116.5134	150.1711	
93.9053	160.519	131.0784	125.2807	141.9564	
89.1233	125	117.4355	120.489	119.8512	
108.096	62.8336	55.9495	62.3412	145.0475	
83.5795	120.8975	96.9031	132.3015	110.3849	
97.0154	136.1044	126.0916	110.8993	87.5182	
122.9232	97.9449	142.2745	128.0287	140.858	

HMT-5 (μm)

97.758	108.1226	73.9961	109.2925	66.4011
62.578	90.9647	107.0282	148.9788	104.817
145.5566	62.578	81.9335	74.8245	75.9013
111.053	52.2701	96.8649	94.1282	121.896
134.1965	111.1214	99.1934	87.1818	118.7992
96.3268	50.6775	86.4411	222.579	78.5747
120.2073	98.4115	104.0221	120.185	55.0424
124.4878	62.6535	79.6137	245.5538	137.9874
66.2772	127.5126	120.3576	44.7801	93.6885
163.2515	128.3733	75.2434	62.578	137.1855
76.9658	60.0788	86.0719	49.4255	97.4549
104.6463	87.2172	92.9045	94.7439	64.7563
89.3329	85.0078	56.795	125.7848	82.1739
86.1959	73.2286	98.2465	66.716	51.2059
56.2936	122.0645	72.5238	105.2532	93.004
114.6451	153.5066	94.0365	77.0645	167.2733
89.25	48.5024	73.3939	81.5918	39.354
86.5764	109.142	101.276	108.2593	58.164
99.5717	65.0096	31.6643	91.6016	114.4442
102.8082	75.7089	69.9218	60.3858	100.9427
123.8839	83.3949	91.9263	75.7387	41.2504
105.878	174.4438	107.0743	34.1252	124.1357
88.8069	151.7187	102.4438	69.8718	94.2853
43.1777	61.7018	73.0797	34.1914	57.4282
104.2056	74.428	128.7584	116.5768	53.7583
51.6016	98.8116	172.7787	101.6789	60.0138
111.9026	89.1233	70.9196	109.2624	85.907
130.5318	119.9335	114.6737	44.2075	148.5991
113.722	71.0035	110.5857	37.8422	67.676
110.3235	95.1853	114.0269	49.8725	146.9054
54.9378	110.7064	67.9759	99.4107	129.0007
113.2749	62.8728	89.2707	80.1308	107.034
82.3537	99.8232	96.188	57.4639	54.5889
142.2095	70.9225	123.1053	83.0271	102.6482
116.381	97.6065	43.5756	63.6974	40.4862
127.1123	76.15	167.4538	106.0408	138.4512
96.2926	84.9837	59.0996	113.3456	43.6651
81.6824	55.1617	115.0011	112.8369	112.9516
133.612	95.6933	51.4261	129.7614	82.4933
84.3552	131.1661	96.0298	91.6487	91.3051
159.5987	119.048	101.5373	106.3813	
161.6923	110.556	114.7508	121.4722	
84.7731	77.7229	84.9087	95.6933	
115.0172	61.7018	41.7898	106.2247	
110.6916	58.6425	110.556	111.7464	
217.4674	151.506	97.4907	61.7518	
82.1739	81.2283	174.2376	69.8718	
114.1908	126.7741	88.4011	132.8718	
113.3184	97.7475	99.0691	45.3274	
99.0691	76.9338	128.7329	70.4078	
61.5518	97.6907	96.6929	99.39	
94.4072	35.0167	59.3979	44.7801	

HMT-3 (μm)

115.976	110.621	107.5415	163.376	125.7015	155.0434
133.4396	128.3285	110.8974	128.3605	193.7086	
123.6	84.5182	116.1124	143.8256	167.4501	
90.4028	155.156	89.6084	86.6334	141.6565	
107.574	69.1387	105.2298	143.2015	140.6902	
73.5701	74.5494	91.81	122.8781	99.359	
41.0707	117.0903	94.8588	101.3429	97.7916	
117.7971	58.1393	77.5429	174.3696	75.1095	
177.8601	237.3258	155.7428	86.0504	21.0272	
171.7961	77.4262	60.2564	86.4149	83.582	
180.0928	63.202	103.2529	76.9044	104.8248	
142.2629	73.743	74.3838	50.4092	70.3757	
54.9378	121.2234	163.2603	190.3889	87.3984	
91.0617	177.8277	113.077	133.3842	73.7207	
135.3536	100.6308	101.3429	139.5023	138.0931	
120.4105	102.5721	125.793	125.0411	104.4164	
122.3402	120.6508	102.4138	140.9397	189.893	
88.9733	32.9178	51.5578	118.0114	100.2667	
173.7614	74.193	107.6331	99.5139	149.4085	
98.7928	94.3898	91.2781	141.0752	135.2245	
74.8025	139.3372	129.8263	76.3063	79.5957	
89.8008	131.9657	76.8055	110.621	53.3131	
48.7559	165.6242	139.7965	51.0934	74.4942	
64.016	92.1518	128.9784	47.5959	80.4169	
122.2495	117.6767	117.5946	212.2269	63.3287	
92.3366	121.386	64.9938	131.0768	70.6991	
103.9015	137.3202	141.5753	136.1934	110.5486	
116.0469	170.5176	97.6065	97.3283	76.5402	
154.551	157.2095	97.0175	125.0115	105.8022	
189.7826	70.329	110.1539	63.4486	163.6939	
52.3055	93.7499	129.5395	87.3772	91.5209	
111.4795	140.4958	142.0722	82.7147	200.4976	
121.5872	146.0779	114.4352	100.9162	78.5747	
109.885	176.9277	125.1495	165.7891	108.3769	
160.0306	105.1946	180.9578	30.9424	97.7601	
98.3259	67.5879	162.1846	173.3023	73.3351	
59.5913	133.2902	127.3045	64.4669	121.6886	
90.6955	120.6934	69.8277	131.0016	63.926	
103.0158	181.0577	97.438	118.0775	82.0162	
120.4378	148.1712	133.9375	130.9466	117.9383	
78.9529	33.1665	141.9926	93.5305	77.5879	
105.382	53.9567	65.9634	100.1519	178.7312	
48.2305	244.5729	161.8257	149.6929	72.6398	
136.3954	51.3821	114.6594	120.2261	136.4421	
125.6966	114.6594	104.9169	121.9129	124.7779	
117.5666	69.6155	99.4664	115.2421	105.2786	
125.7211	193.1956	124.4399	149.734	140.0021	
104.2529	204.5525	123.8524	153.1421	137.6714	
92.3477	179.8999	129.6917	145.7047	197.62	
63.5133	71.7977	169.1846	38.075	117.0833	
144.595	179.8645	151.3961	136.8526	98.8947	
144.208	76.2497	130.8713	55.7987	123.5601	

TM-1-41 (μm)

63.3416	103.1812	110.7769	131.4993	126.1274
100.9183	138.469	219.1342	84.5814	137.2888
244.7106	74.1043	98.5951	98.1942	119.7878
210.9159	237.1015	136.1059	119.556	123.2054
116.1654	63.4486	122.0342	113.7726	103.9984
126.8858	32.7488	142.9142	196.2805	175.6375
107.6942	74.0711	148.3334	257.1568	60.7454
60.0309	113.5267	118.4649	83.1111	66.568
86.9175	169.0947	147.667	100.2483	58.8209
186.5682	89.9014	73.1781	50.2623	200.4351
65.8886	99.9445	57.621	201.0257	102.7262
137.0806	94.6832	83.0097	132.7558	170.0495
165.479	311.6684	284.153	76.2362	141.0052
88.9803	122.2327	99.1271	57.7813	141.9333
104.5049	106.5974	63.293	302.613	118.4389
63.8714	124.7038	126.3081	276.1876	154.113
244.446	106.188	89.3052	112.2729	117.825
69.5653	133.6796	91.4333	98.3614	155.2103
151.9136	130.5082	229.9433	123.8375	43.4245
146.855	225.3795	38.2473	95.6182	50.2868
93.1695	70.4691	262.6399	107.082	72.5747
126.3406	115.0458	135.1516	71.8521	123.6
105.3098	132.8795	137.2529	186.5043	157.2814
162.8357	134.4382	149.2145	107.4268	66.333
115.0172	160.3653	219.0207	80.0333	131.7616
92.9752	131.3774	257.7537	129.6156	143.9927
55.8539	70.606	119.4391	67.6578	116.9446
173.8645	170.0761	55.1878	175.6516	228.9287
152.9058	98.4449	99.3486	136.6483	107.8086
98.8802	91.6016	130.568	67.109	72.2513
224.2326	233.01	196.6194	118.5499	89.25
127.8721	135.039	96.1154	110.4891	187.1938
185.3939	170.7224	107.1204	187.1806	101.276
163.2641	57.2813	57.1197	237.1708	105.909
52.8331	160.0319	195.0583	121.3233	
137.1046	117.4407	108.3637	85.3431	
123.4786	106.5434	63.7555	143.9855	
106.035	40.1346	169.8186	79.7375	
39.1236	104.1563	125.2036	142.3279	
84.5474	124.5703	58.2205	122.853	
103.7907	297.7507	217.0201	145.9203	
214.3797	138.1555	202.7202	217.9157	
88.5845	172.1008	99.7367	192.0383	
107.2794	187.5173	122.7091	101.9231	
161.6974	198.0811	119.3789	270.7504	
104.2884	165.2827	173.5049	110.4817	
116.441	263.5738	139.7436	90.53	
165.3449	122.8447	121.0996	117.6767	
93.5305	130.7755	113.4108	132.731	
63.3287	121.9129	119.4339	58.3333	
67.2099	102.3234	108.8706	94.0649	
119.2463	43.5945	123.9569	35.7713	

ASF-5-16 (µm)

117.5456	124.9227	103.6897	122.1402	142.3669
195.3204	60.0309	145.6017	164.4478	207.7418
62.9381	106.4797	210.233	193.4507	87.5417
126.983	113.3329	87.2596	123.3037	111.8052
148.0145	160.6943	149.2599	66.8175	98.3614
122.5583	107.3732	112.7075	84.3868	157.6832
195.4529	89.296	102.9839	128.0271	162.2112
152.0461	156.2381	103.1812	173.4445	47.0576
197.2964	113.3456	62.6108	37.2678	53.8462
94.5877	86.3007	96.6993	65.7231	168.9987
151.1761	137.3367	56.3884	147.5821	214.395
84.2693	133.4704	79.3009	126.404	114.498
72.8517	49.861	144.161	75.2489	104.2332
114.9797	120.8397	87.2643	124.712	33.8532
106.066	125.3414	98.7263	131.4993	175.8012
110.8993	62.3675	139.4802	131.9906	93.5305
155.5699	84.6542	159.4132	75.0027	120.4378
154.3501	133.3888	114.7436	194.4802	79.7813
116.9411	80.8099	82.7147	91.1542	115.4718
85.4514	144.5097	109.9317	98.6867	114.4065
147.4415	61.0625	167.8459	149.085	117.2289
100.2565	63.6716	173.4919	103.8086	115.607
117.5317	104.1879	57.31	82.7395	113.235
127.2028	117.6313	154.1877	181.4657	76.8723
49.5957	149.0671	111.2987	116.9569	87.7456
130.2734	117.6086	161.2839	89.9311	101.4219
125.8387	84.0355	101.3753	37.5589	101.4462
78.7105	70.437	152.4846	131.3618	99.2928
102.0681	116.2114	77.0192	140.2191	47.2841
107.6561	141.9622	150.3953	91.9084	51.7804
106.6744	159.6553	106.2421	173.7369	124.2499
163.8244	141.324	146.8075	170.1377	167.9255
113.8646	157.4224	126.3406	127.7717	100.0185
94.5985	47.7123	145.9963	166.4261	172.0112
75.5921	108.7498	93.8813	156.2052	184.7867
113.0679	121.1606	44.5962	73.9711	118.1315
61.9013	100.7288	94.8718	77.5032	108.2043
102.518	92.9045	143.134	146.5708	72.9137
157.8772	115.8981	172.8845	126.868	111.7611
170.7163	131.7413	123.7644	142.1878	132.4583
55.3291	123.6249	141.7116	117.369	90.7204
102.9839	123.3454	183.6122	122.2344	202.3246
148.1324	72.5379	86.5764	57.6674	
86.0146	234.1429	185.2431	36.9411	
86.2936	101.4361	119.2463	141.8927	
88.2523	119.5491	104.1642	122.4158	
41.8045	87.3302	39.8984	118.1784	
83.609	96.3268	76.1985	99.7573	
54.491	146.0892	107.6942	131.4493	
102.6282	125.1643	94.6333	127.3303	
62.4466	117.3637	145.1184	159.079	
166.7308	114.1908	160.9179	111.4906	

TM-1-25 (μm)

74.6727	143.0005	156.3051	83.4986	101.5495	98.5911
150.9122	127.0489	63.0816	101.5495	126.5616	134.8837
77.82	155.2688	110.9493	113.8005	96.2478	59.7668
132.9831	88.6585	110.6004	101.713	158.7306	106.9196
75.0289	183.0677	81.6452	169.4831	113.6463	79.3967
132.8338	121.5483	107.0378	165.8935	83.7808	94.5053
88.5451	111.6816	93.6622	123.5774	158.9284	72.226
124.3788	113.6804	107.8315	120.4279	58.5517	82.8735
154.4244	109.4718	122.6371	162.3972	95.0989	106.2189
117.9921	108.4393	68.8923	117.2935	167.3512	121.2149
92.371	150.6021	113.8646	66.7543	230.4921	68.6017
147.4707	142.488	137.8694	56.1832	147.4373	58.7261
160.7678	102.9196	155.2077	244.0811	55.4568	127.1696
126.3406	132.4816	125.6875	107.8448	102.5841	72.719
112.7786	104.2569	74.9266	66.5241	119.6642	132.2385
156.3565	105.0852	89.6084	123.7993	76.8376	114.2393
71.9676	70.092	118.7992	87.1983	119.7758	133.1807
238.5657	90.8019	108.1019	35.7036	114.8484	69.0617
92.8757	101.5373	107.5226	91.9553	93.1695	90.1479
92.5433	150.2313	63.8617	46.3138	112.516	126.4251
84.3213	72.6546	101.9251	77.3174	161.9359	155.097
171.5507	136.4542	135.911	154.2316	119.1498	
128.0483	110.498	114.4873	119.4748	162.537	
142.4969	117.9766	156.4116	146.3162	93.3973	
129.399	112.7687	179.9851	97.9491	174.7592	
83.0293	73.8516	117.0412	88.4708	116.9661	
150.3108	149.6337	85.7754	209.644	121.1928	
84.8143	128.9035	88.2704	114.8295	122.8066	
115.1351	141.4112	109.7351	158.0735	142.6301	
47.6477	177.2716	79.4665	64.4223	104.0221	
146.3012	71.2347	95.2368	45.4043	116.2205	
156.9022	149.3356	84.8568	58.2766	114.8885	
143.0852	108.0107	149.1001	89.7477	100.0037	
177.9605	142.7146	195.8328	82.1625	90.1684	
108.6311	141.8927	152.2519	79.8219	137.6573	
81.1296	132.7431	112.6456	93.1036	65.2322	
83.21	117.1439	73.4695	84.6542	92.4856	
89.6566	126.6371	102.9201	126.1127	66.333	
144.0291	162.7473	95.4093	104.0666	134.9074	
137.1282	81.7391	183.2252	90.699	175.7943	
137.0776	143.6025	84.6326	165.0702	154.9228	
132.7018	86.9388	160.0574	77.7652	99.4334	
133.5769	132.3683	113.3184	115.0297	132.3573	
117.3777	104.1879	139.6331	118.1384	106.1826	
92.2325	73.5701	113.5466	120.873	98.0853	
66.1779	62.3463	98.3781	99.1048	106.0176	
118.7213	122.1738	121.7191	86.3888	69.4973	
100.3466	137.634	126.4986	103.8558	124.226	
108.5001	205.9847	98.7179	110.4538	90.7363	
142.712	95.9763	78.4511	79.4918	117.0472	
152.4954	89.8453	78.8696	118.5326	95.3059	
65.6793	158.7377	90.7473	102.6211	70.4078	

TM-3-1 (µm)

82.7075	169.9566	111.4394	137.1202
98.6615	148.9168	273.6965	103.6446
199.4111	121.8751	73.965	151.7064
121.9829	80.9849	100.3318	55.2457
119.9904	216.0027	257.0988	146.735
84.4771	228.7918	89.4501	106.9743
56.8231	190.8358	131.1485	161.4389
47.0085	162.0622	157.5736	87.7724
174.7545	136.4955	85.4872	616.2399
193.9719	163.5565	82.3357	177.6668
77.3256	115.8269	76.6996	110.5608
158.3482	95.8028	51.9894	71.9423
282.3994	140.5717	123.8019	46.5008
150.5293	92.4856	72.7099	51.9191
140.8805	106.9879	122.1266	120.2823
99.6744	97.4546	50.0201	136.2008
102.0572	227.1399	163.4715	103.4329
93.581	94.598	92.5606	108.1458
115.8995	323.1131	92.8757	143.8591
153.3992	116.1293	91.1329	182.5342
158.6017	48.3869	92.9111	111.1111
90.6869	158.4589	108.3179	125.3937
157.9417	166.2344	138.0759	87.8015
111.5344	298.7323	209.3755	68.8286
82.5705	158.5649	170.4802	118.5541
112.5255	83.5205	137.256	132.7898
138.3718	152.1512	145.2991	138.6224
150.2451	106.7692	128.4471	109.6718
134.7422	107.3798	124.637	87.5724
122.6518	97.4696	64.3471	102.7491
185.0738	255.0448	54.8675	136.8189
71.9423	99.502	156.2397	109.3917
146.2763	129.695	189.2617	127.6369
143.5618	90.1497	101.7776	132.4235
129.4244	122.5118	133.4675	156.9325
108.3854	80.8766	127.6112	99.2999
168.6708	96.1111	218.4325	195.8179
103.6305	147.011	243.6917	83.9915
221.3296	128.5608	136.2303	70.8371
180.2142	152.1295	376.1033	133.5359
128.8757	91.5528	65.8785	87.0327
126.1777	68.9082	130.7441	246.1672
95.6349	251.2951	152.6664	149.0467
204.629	126.4784	124.798	109.355
162.1906	172.0647	243.4037	93.6356
154.3108	90.6144	136.672	167.1831
89.8453	108.7924	52.1858	141.6562
91.935	139.9858	131.549	122.473
109.5218	166.2827	140.6626	
117.4522	105.6654	126.2472	
90.7795	127.4536	54.7609	
137.6307	124.9647	150.0116	

TM-3-5 (μm)

124.226	32.7139	151.4534	96.6984	112.6456	82.9456
54.0898	103.6305	89.8453	86.1935	93.6356	73.6086
137.3518	115.5143	115.4985	188.4417	113.8678	87.6516
93.8538	122.4133	53.3281	77.2264	72.0437	109.8316
138.854	116.0632	410.1647	98.8686	146.0138	105.7794
70.3819	122.5654	129.0853	134.4165	145.362	45.6125
89.3561	100.9126	116.7692	144.5253	87.9968	355.3583
57.8425	55.3646	96.0351	104.014	88.0508	84.1826
121.4066	77.5191	126.6804	259.5055	66.1662	96.585
113.6495	121.0964	115.0676	135.2319	120.5401	137.7368
153.2229	92.7065	139.7351	127.3275	134.7205	175.5323
149.6679	59.9815	108.1729	81.6407	89.4215	123.908
121.024	41.1057	111.1111	72.1653	138.8856	156.7625
130.0775	128.768	129.2493	155.3817	101.4757	157.981
101.7094	132.3683	116.0632	102.6246	100.441	
131.9261	159.041	131.4601	94.0326	130.0859	
90.4046	150.0116	98.5281	101.7991	140.9609	
84.1132	141.3981	108.1965	104.375	75.5238	
86.4263	110.7093	153.6014	174.6625	137.0749	
176.764	127.7656	128.6147	112.6034	96.5812	
86.6584	194.7687	155.5861	126.1951	111.1407	
161.8005	84.4771	102.4394	102.1716	102.1966	
80.2236	138.7804	152.1752	74.6335	160.9586	
133.689	90.7433	98.2906	135.3129	124.1407	
114.5586	137.256	113.3406	94.2654	99.2374	
113.0824	121.3856	148.4943	105.2706	194.1752	
219.6199	97.1355	67.8667	120.0512	100.6154	
124.6135	221.0621	58.483	187.6403	138.9408	
107.3016	170.583	126.8446	76.5423	69.4888	
166.5636	80.3601	165.4547	136.1579	110.0309	
97.6793	140.7041	120.0269	167.541	135.9834	
87.4848	88.0383	109.355	90.3278	115.2928	
119.4932	123.0116	103.6446	153.5348	140.1345	
100.9741	103.7115	92.5369	146.5631	104.3505	
115.2199	104.0982	289.9755	176.5987	108.9098	
115.8679	119.7344	191.5751	110.5244	96.244	
95.0718	94.6367	100.6154	56.2871	103.8382	
104.5988	126.4986	65.9007	140.7949	72.0437	
61.9643	93.1663	132.655	153.7797	84.2867	
81.8061	91.935	124.8741	107.1789	68.8074	
85.4872	93.7253	94.2538	121.2862	120.8639	
115.953	90.3278	84.3733	80.5145	132.52	
201.4938	171.797	111.3082	75.7267	105.281	
113.8646	146.3811	106.865	106.1551	131.2599	
140.1006	122.8155	159.5546	126.0792	71.8965	
113.8069	130.7441	125.766	129.4554	94.4744	
163.7639	97.5296	103.7432	192.264	136.9043	
115.7007	140.9738	92.9779	105.0309	142.7734	
127.5224	66.2324	185.5961	79.0217	260.155	
149.6923	88.1005	135.2724	118.1869	121.3705	
108.7118	113.7555	74.3197	84.1132	92.7065	
158.627	64.9179	107.638	128.7396	102.2252	

ASF-22e-A (µm)

121.1416	52.2208	114.9819	122.7024
101.713	148.0114	67.9312	119.7069
124.0377	115.4732	101.4649	79.1741
65.5227	132.9822	54.7676	68.8021
89.4501	70.5063	93.5732	109.2146
134.305	113.8422	63.6164	144.9518
124.7775	104.277	104.7662	90.8559
129.0117	101.9927	133.2813	102.1394
125.9314	131.2154	164.9573	117.927
92.7025	82.906	153.6799	85.1618
111.3246	110.6565	96.8984	73.1506
131.2154	116.6565	104.6232	84.3733
88.4357	115.0676	96.0351	87.3302
79.8585	120.1729	108.6681	149.9604
131.6683	67.6241	105.9346	71.9219
70.7391	60.4365	81.5915	121.9619
102.7065	79.2479	62.4868	120.3157
58.6514	30.8167	85.8538	134.8262
121.3585	107.492	132.644	102.9941
132.9657	79.6845	109.0439	67.3046
83.7127	50.4563	117.9766	117.62
87.9346	41.7493	102.9338	95.5814
101.0862	144.0799	89.8372	127.0604
134.1472	63.9428	90.2023	70.9608
47.2024	82.6898	123.6602	96.9699
100.9561	109.6152	113.2503	60.7379
50.4925	114.8261	91.3931	91.3571
109.3015	68.6001	97.049	126.7841
69.6516	86.0833	50.0858	214.7358
56.3455	69.5729	107.2982	129.8752
112.746	82.2691	80.4918	75.9098
144.366	76.0684	62.7434	129.9876
76.1596	64.4719	149.9263	90.7272
97.3196	113.3792	92.5369	102.1966
141.0464	66.9182	58.4705	111.8483
127.6713	66.5789	94.9334	64.0741
108.4797	117.2935	119.7192	59.8352
102.8664	85.406	136.7228	107.0528
111.734	90.1497	74.2951	96.5963
95.4973	74.7509	60.6296	70.3404
92.45	68.2477	106.6734	107.7771
77.0417	84.4944	153.9055	88.6791
114.5969	142.1992	68.0602	71.356
101.4649	69.9864	95.7303	183.4242
96.887	59.6885	81.4167	111.2622
132.52	91.5209	98.3909	132.9822
59.4616	147.0185	60.4908	143.3886
133.5113	66.2104	92.454	
98.7355	113.0308	113.6784	
124.3289	65.945	64.4379	
34.7076	63.5302	73.2504	
86.7932	96.7324	106.3476	

TM-1-50 (μm)

191.9141	187.3043	239.2881	119.4253
232.3293	91.0487	142.1632	124.6457
130.9507	82.7119	100.4083	104.8719
116.9942	83.9621	102.9196	29.515
184.0784	139.8292	146.4035	60.8341
234.3471	104.822	118.0219	64.5441
116.8317	258.3461	200.9002	198.0935
169.1898	172.6009	209.9939	126.3686
131.0928	174.9028	103.4329	125.4869
194.6993	79.1233	164.9542	182.9979
188.042	151.096	155.3817	174.4197
134.5604	60.3458	262.2275	115.4732
116.4402	113.4533	107.7906	124.4111
138.8146	89.0422	132.4207	149.2671
169.0602	87.6308	111.9005	99.513
66.6557	81.6407	65.372	232.649
204.9073	70.1324	80.3828	146.7549
193.7741	233.3474	113.8807	249.7739
118.8772	116.1831	101.0831	99.7634
100.5246	114.3192	125.7137	121.4359
114.8643	150.4298	149.4847	124.1424
144.5279	142.6506	158.4267	120.5401
160.7792	112.8238	100.0037	163.7679
153.3349	102.0478	58.3455	156.4943
190.0772	164.924	87.4389	102.7704
114.4948	103.3163	101.7417	110.6922
83.5904	218.3639	132.389	160.5771
44.1788	110.6749	119.2208	119.3219
136.9283	168.1699	133.9882	78.6743
125.1126	151.9244	228.2333	101.144
86.3629	124.5741	92.0581	304.321
259.0693	239.5	131.951	112.795
95.6807	94.8872	141.9035	98.1753
151.0573	180.0196	101.5579	143.7956
124.6164	165.1365	149.103	109.4551
110.3591	58.0261	117.62	82.9236
149.3576	137.1202	145.2237	104.3505
194.9938	246.9072	154.9652	86.1554
112.5645	222.8918	121.8421	172.398
172.1008	161.1287	94.1569	246.8074
171.3883	118.9877	199.1673	194.8855
221.6198	28.103	135.3453	164.9418
169.4163	114.7508	228.5146	79.9225
189.9764	155.0341	171.984	260.155
86.5978	101.292	153.0374	121.4858
145.1281	135.3696	135.8158	
115.7047	115.3878	260.8586	
125.105	120.4643	94.6714	
281.813	232.2248	122.95	
229.2998	286.6754	201.3995	
189.9706	32.7927	110.7324	
152.5132	114.9279	115.627	

TM-3-15 (μm)

120.0269	180.0743	42.5809	121.1446	96.1871
136.8589	177.749	151.6197	129.9736	330.8399
154.7858	63.9428	123.967	126.3831	77.7825
103.5459	70.3248	70.4078	111.1407	114.1082
73.8464	153.8675	162.8357	74.8876	146.1763
102.8237	133.2484	145.791	189.8129	95.7418
133.2155	143.5999	209.2813	116.3178	213.2412
105.6965	96.0351	182.8521	124.226	124.2877
120.0543	122.1146	136.391	191.2946	87.5349
125.2071	111.9886	62.3053	131.574	130.6127
128.9579	132.0395	153.3753	98.2348	91.1329
95.302	119.6703	180.6555	129.4244	102.8237
150.2451	158.6063	139.4106	112.3598	85.7304
108.6513	123.163	116.167	65.2994	122.5684
86.0366	93.08	82.38	155.2947	129.9736
97.8437	131.353	116.6565	196.3004	110.2862
103.9297	109.3015	126.5217	123.7665	176.087
167.8633	131.4184	104.6232	170.4802	125.6875
159.5569	315.7134	113.9961	128.8219	
88.4151	112.3078	106.1069	180.2993	
139.2533	151.598	107.7059	61.9643	
97.4509	163.6032	73.8464	76.5341	
108.2471	117.094	285.7974	118.9877	
135.7764	141.3981	113.2116	168.4108	
95.4896	117.1439	187.3336	128.8446	
147.1799	151.381	124.1407	163.5697	
101.31	81.6452	109.355	158.1035	
154.4551	128.4357	164.3717	89.3684	
116.3806	112.5255	189.9764	94.9026	
199.1673	142.3969	127.9428	201.771	
125.1283	165.878	200.0018	87.1124	
122.5118	157.5921	87.7807	104.2209	
88.4316	89.3684	127.1438	115.1406	
95.8218	108.1796	69.0194	100.9452	
137.239	196.7391	128.4357	181.8606	
148.2185	204.1733	110.4682	123.0354	
150.5754	135.129	82.4864	84.1696	
76.4707	141.6252	230.9148	54.1236	
137.5856	138.8304	100.2954	121.6561	
116.7191	106.327	139.6933	149.1202	
123.1363	126.7496	211.2149	110.9697	
146.1763	187.5616	197.4673	93.5185	
177.4622	112.8496	133.0371	100.1061	
127.0144	99.0458	109.8715	141.8906	
101.032	120.879	122.4104	150.4977	
158.7306	121.1898	98.5281	121.6261	
97.5445	160.1852	121.1416	122.7352	
169.7932	142.027	102.926	67.1797	
231.5782	84.2867	93.229	115.1406	
84.1305	86.8815	126.6862	197.872	
85.5384	65.6341	109.0707	163.5251	
93.1977	144.4748	76.2267	121.0783	

TM-1-47 (μm)

32.7586	113.6985	53.4325	146.6703	135.0268	81.0885
132.0528	137.8384	84.2699	47.0576	105.709	41.6793
74.4032	131.9968	94.4241	51.9683	181.2301	135.5718
111.4316	128.0712	114.9583	73.0307	103.547	147.5665
126.0231	125.6999	29.1727	123.9788	148.514	132.5544
119.0982	123.0919	82.2763	115.1565	123.4636	128.5444
126.059	115.7704	100.0021	71.356	129.3538	110.303
92.6853	108.2539	120.6168	71.9235	144.6305	193.7086
36.0599	153.7633	129.5348	100.2565	69.5676	110.6805
110.8478	135.0454	100.084	86.8631	75.6437	104.032
138.5149	152.0359	114.5586	104.8954	124.5389	96.3033
111.7797	128.245	68.0454	127.8428	120.5401	96.2862
119.4748	127.8215	84.8966	32.9178	40.1192	104.0162
133.5359	82.9104	116.7723	31.9343	127.0863	125.8518
115.5618	174.6427	48.094	73.9961	151.5114	118.914
77.8787	81.4405	128.2877	91.1091	119.9403	117.6697
125.0805	181.5835	92.3121	100.7134	193.6375	149.513
130.7755	97.0154	103.6045	80.0184	117.1728	90.6346
58.9744	152.5978	165.225	39.3122	88.9751	87.2007
106.4403	48.7348	48.1154	192.0779	110.2732	99.6254
113.2513	167.4974	153.1018	92.0263	125.6476	77.3256
98.9964	68.4818	114.1476	95.6826	148.7981	90.8087
73.6761	166.8539	114.0633	90.872	159.1307	105.6604
43.0968	113.6804	41.2852	133.2917	71.5707	157.4808
149.583	124.4463	152.4105	64.9629	212.9046	238.2654
39.1078	137.0323	110.4072	60.2189	180.2467	45.5264
73.046	150.5919	124.4845	124.1289	180.9	113.3329
135.2625	128.9482	169.3365	144.7654	185.0878	113.5337
113.1632	128.4501	82.2114	183.6715	115.2082	125.7456
59.8081	104.6267	123.1604	126.1951	112.3625	123.0769
212.7398	66.1842	148.386	137.9338	175.6467	
76.3416	107.5415	140.1345	73.5241	101.8969	
164.344	54.0898	122.1402	104.1263	124.2407	
71.6172	206.3844	173.1541	176.2198	144.5438	
111.0881	79.9225	176.1316	185.0264	164.1827	
81.1347	100.3118	125.9517	156.1766	75.2331	
103.4457	52.0614	115.8981	96.2478	143.0981	
144.4925	119.6581	96.156	90.3278	51.9389	
79.7968	84.343	125.7456	149.6723	139.8979	
179.0345	83.7808	52.1442	67.5393	156.4024	
113.5981	148.0769	56.4867	125.6557	132.1508	
84.1796	144.3774	106.128	67.2123	97.4907	
118.6434	103.9905	111.0363	82.6128	159.8456	
99.3486	74.3866	129.6697	130.3948	100.1314	
123.3254	111.7023	83.6827	100.7145	83.538	
99.0691	71.4506	181.73	151.632	69.8662	
114.8134	98.3948	100.902	97.1243	129.0485	
117.4355	76.1068	109.7259	100.0402	200.8938	
56.8617	96.5398	49.5086	65.7453	99.8099	
102.4438	121.9719	107.7686	70.5536	61.4077	
81.2966	85.9381	106.923	123.5774	92.5369	
62.2323	193.8496	138.3718	147.2518	139.6619	

HOL-E-B-1 (μm)

104.277	55.9943	119.1994	127.1868	137.7024
64.7563	119.4748	105.9967	194.2485	156.5596
96.5963	102.0536	145.3142	251.3751	87.5349
64.4889	67.57	189.2308	155.3229	157.1348
142.0579	72.3321	113.4823	165.1432	178.3951
124.2877	126.059	281.9593	111.2721	123.967
91.3091	197.5228	82.5129	163.1673	89.3561
170.0683	110.9828	137.482	80.3828	136.1445
134.902	58.7012	121.1416	140.5795	233.9744
221.3939	66.5625	173.5737	180.9424	235.3782
143.7448	190.3298	155.5579	142.9142	104.5953
122.3059	151.7064	122.8898	189.8475	142.0579
118.2147	203.5983	109.7118	76.6043	
88.5348	124.4399	132.0146	142.2429	
112.2297	105.6965	216.678	173.1756	
120.9273	63.8617	242.9531	116.9067	
252.6274	77.7778	106.3991	181.9148	
157.0162	93.581	48.0537	79.579	
223.5218	117.8682	90.2954	157.5457	
132.7623	222.1729	127.2931	134.8106	
68.5095	112.4378	100.9452	237.7436	
175.0385	254.1496	162.0419	89.7477	
124.2583	147.9201	218.9936	157.87	
225.9548	125.4898	196.4344	109.0874	
100.8149	179.0389	175.7694	122.5207	
124.1701	72.6697	77.9326	140.8805	
204.4522	120.343	147.7026	185.478	
134.0982	132.2551	170.0253	206.1832	
210.8046	182.2137	178.657	194.9018	
99.5717	219.1404	73.0307	93.1938	
158.2451	60.0788	148.4254	122.8066	
57.2139	54.3324	93.2839	73.5092	
109.7817	115.4099	107.0528	279.8855	
147.8657	162.1433	172.0647	77.8482	
119.2086	125.7079	57.7066	130.4644	
143.274	84.6111	131.3684	127.5512	
139.5677	102.0249	95.898	209.8495	
84.7534	172.7299	68.5734	136.1525	
74.0045	108.1019	131.2773	204.7307	
76.7757	166.5066	195.5675	96.7184	
164.4983	90.2104	141.7103	119.0737	
80.6867	207.5727	107.7228	50.1659	
145.7008	249.0247	221.4187	95.1793	
155.6964	218.071	213.0178	95.4896	
205.9847	141.955	138.5565	86.0323	
135.9942	124.3201	126.6025	205.0659	
158.2467	338.3633	64.4719	116.4183	
143.1949	227.0627	126.7063	123.7694	
103.5882	143.1413	120.2823	107.2982	
161.1967	108.2539	171.882	195.0985	
213.3416	124.5431	144.2536	174.2186	
140.296	81.5011	87.483	197.0563	

HOL-E-B-2 (μm)

185.7063	86.4432	161.2578	167.3665
143.9657	140.3819	119.6703	50.896
141.3387	101.7238	156.7275	110.6796
163.8464	176.2363	55.9943	114.5841
131.7266	166.728	113.7523	128.208
107.9092	294.1785	109.8947	206.1265
108.9534	116.4057	100.2772	118.7388
164.4272	67.57	65.7842	251.4535
118.7327	55.0005	178.892	56.9259
166.3157	139.5154	79.1972	200.5216
111.1144	118.4617	158.4174	116.5218
132.0838	110.4682	171.6502	80.3601
127.0087	113.7266	209.6127	132.6219
189.1749	157.1465	102.9196	108.6008
115.8396	102.6246	121.896	177.3829
256.8913	145.0677	152.4078	157.9556
144.0291	99.7513	158.4681	118.5295
92.5132	205.7132	111.8091	164.9595
112.6974	127.8342	79.6845	142.8987
157.4135	110.6796	93.1977	76.999
110.2531	162.2694	116.9067	135.3453
228.4419	84.6197	151.8676	138.0759
122.9136	145.4499	81.681	234.7068
251.1846	145.1281	141.0489	155.2547
245.323	82.3091	186.6088	85.3204
88.9259	108.7622	86.3882	69.7564
142.8808	220.377	87.685	244.3428
98.0562	81.2371	89.7802	89.9672
151.2072	149.5726	114.6256	151.096
106.923	100.5246	122.3745	240.2257
121.3705	120.8881	113.9288	174.8025
121.1446	114.6001	167.076	109.8316
247.3499	94.8756	153.7155	199.6893
127.7628	205.3133	111.6228	132.2579
227.4227	104.7349	126.3484	116.9661
99.3992	130.5456	156.4476	82.0691
68.4295	135.4856	133.0179	138.0203
107.3424	97.8996	124.8127	257.2323
126.4986	123.7222	143.521	111.2031
101.0139	105.5478	117.6417	120.7187
69.2255	166.7171	165.9309	97.5445
192.3742	158.4589	110.6136	109.9412
160.5837	157.7473	153.5848	129.847
193.3684	94.1142	120.437	121.3705
134.0982	138.4431	128.768	163.8107
113.9288	164.2739	146.3362	107.005
277.0287	58.2766	112.4183	153.2801
164.9661	137.3119	94.6598	145.6632
125.7602	135.1725	159.1581	
100.0329	103.2491	73.2953	
168.5387	158.0157	89.8453	
121.7221	194.7405	249.7087	

HOL-E-B-3 (μm)

304.6382	141.0904	113.147	213.7846	116.9411	176.0456	165.4437
89.707	135.013	113.8005	112.3956	120.5401	160.0506	173.203
148.3072	139.3398	44.4773	91.4051	220.7793	101.6807	126.5073
164.9905	137.7846	126.2674	99.8392	151.8989	61.9643	133.6234
134.8722	185.7613	97.8548	225.2911	108.264	138.0811	149.9531
283.807	224.0637	181.4101	99.5461	109.0874	225.0656	204.629
148.3466	269.2905	151.3689	112.3956	99.4543	116.503	112.2916
119.2453	186.6069	128.8446	139.4289	184.2688	68.2959	219.53
222.3159	266.6845	85.7645	188.0594	74.4032	204.8235	85.6622
143.3886	145.796	89.5806	74.5993	100.146	257.299	89.8087
223.6787	215.9148	203.8654	131.3155	47.6568	136.672	99.8099
126.5563	219.2603	127.382	62.399	184.2867	169.9501	138.8935
213.1361	110.3127	130.7916	198.9747	93.4911	128.8446	160.0369
122.7828	68.3814	127.6455	201.1473	159.9844	101.0175	72.3473
141.3387	129.3538	172.4802	179.7475	154.8896	133.358	187.1795
138.2952	48.7479	190.5906	183.9812	106.7418	159.7742	108.21
144.1103	154.8519	176.5118	162.5752	122.5565	207.1711	178.7122
109.8814	196.8282	131.4851	160.1578	174.0172	110.021	96.4942
146.5008	223.0949	144.8712	119.7344	116.9192	65.193	81.2101
165.7965	248.2946	135.2319	159.9753	108.8796	171.4267	94.1413
161.9562	99.1821	124.9443	182.1556	165.468	205.1514	146.7325
75.548	58.6514	109.8049	146.4035	92.3473	235.0816	170.448
219.8974	92.0581	91.8157	143.1949	136.0801	105.1317	
38.6982	217.7073	233.4444	176.2198	152.2232	192.9013	
103.1642	159.7742	132.4814	35.5498	216.2545	166.1289	
212.3807	123.3911	163.659	133.5578	202.2953	51.3532	
156.2327	199.5136	174.5014	160.2125	134.305	188.5618	
157.6477	153.979	151.3689	194.1752	72.226	80.8359	
118.9632	200.7892	57.0349	111.9886	103.3623	58.3267	
150.3691	219.2304	237.6453	151.0912	154.552	216.6696	
191.0405	136.3697	127.5224	221.1215	127.2931	155.7949	
113.8646	195.8739	188.3137	147.2196	74.4375	183.7607	
197.7483	184.8467	105.3191	117.7038	100.5101	151.858	
110.64	171.797	174.4616	176.1306	93.8226	106.8068	
142.8271	110.8775	212.1484	68.0441	179.2041	160.1669	
273.1582	222.265	187.1951	143.8972	103.3623	103.9788	
170.8205	179.9526	54.8742	146.1114	232.0965	245.5864	
160.8678	213.2988	78.4511	141.749	125.1283	69.067	
99.2374	112.8238	177.5311	125.2071	68.8923	209.9452	
80.0047	207.2716	167.6543	228.6528	109.2045	183.2432	
90.9725	62.3229	126.0792	250.3267	113.7266	136.2866	
92.5014	69.6516	102.4394	111.9495	143.9886	143.6533	
88.6585	106.5089	130.4224	96.5812	113.9288	114.3959	
194.2203	64.1254	127.3848	98.324	215.4151	104.445	
89.4215	98.0674	51.5449	150.6263	175.372	112.9887	
134.4355	171.3244	70.8165	117.0035	80.655	178.3132	
164.6026	78.6371	164.9595	139.6723	57.2713	99.5461	
94.968	233.2143	120.9606	184.3798	228.0434	76.1452	
140.4677	125.9517	169.3645	125.6439	121.3224	151.5739	
135.9646	78.5674	232.8193	95.1831	187.4505	147.9324	
186.509	114.0633	88.9423	132.5034	134.7855	168.6383	
140.3428	141.8906	138.2847	132.5475	105.4335	129.238	

HOL-E-B-4 (μm)

74.3786	59.3694	109.0707	143.4192	174.7879
297.3696	104.4345	230.1051	110.8149	156.4009
192.3077	74.7509	199.5045	95.9704	59.3694
126.6025	163.23	197.5617	186.1149	144.4141
132.9932	118.2147	159.3072	53.9072	
140.9738	245.3706	102.1144	99.6744	
181.8887	135.9082	164.4272	100.3318	
120.4643	47.2024	76.4707	161.4141	
165.8318	125.943	57.3351	161.7396	
212.0382	139.5913	137.6175	57.4242	
103.7045	103.8136	151.87	115.5618	
179.1062	213.9724	214.3323	183.7428	
185.541	101.7776	193.2777	84.4815	
128.5608	126.8648	61.8995	100.3537	
99.6744	90.3278	129.695	165.9309	
230.8088	239.5008	81.3584	170.6087	
63.3402	127.0604	80.2919	127.697	
175.4283	171.7013	164.1115	110.531	
105.1664	103.9788	217.3731	63.7884	
215.8403	109.9911	136.1767	92.6552	
113.0824	267.5104	112.005	126.4293	
214.7409	141.749	208.6906	166.7806	
202.7281	112.0539	198.6476	118.4617	
114.3384	138.4615	184.465	168.4303	
90.9403	184.1895	137.9488	93.772	
177.1294	125.7456	300.8403	30.3148	
215.7167	188.6935	136.6506	206.1832	
100.3318	202.8722	75.799	110.3193	
228.581	161.9743	96.4147	143.9556	
96.7172	71.3253	143.6126	182.7102	
106.2617	63.5302	141.2844	190.3663	
183.5936	98.8686	172.8209	140.4677	
233.1846	120.5401	172.8779	208.5225	
233.1517	170.4694	118.6558	171.8289	
136.241	152.5539	188.6122	48.5978	
111.1801	110.1072	139.2008	141.1939	
40.542	164.4805	179.7271	251.0974	
70.3663	170.1048	173.0637	122.1714	
147.8509	160.2877	151.6317	208.3963	
97.6082	107.9227	83.5424	140.3506	
107.6855	203.1601	164.3606	132.28	
198.9086	94.8217	56.2871	229.0407	
173.8597	167.4189	98.5133	116.5469	
157.9162	120.7913	111.6653	29.3724	
207.453	149.1814	159.8382	230.1432	
221.4731	137.3119	162.4606	253.4588	
194.2203	237.3115	182.7881	94.0715	
168.4802	208.2964	203.0324	251.4535	
140.3428	96.8192	97.0942	167.2093	
100.2371	96.2744	125.7573	204.479	
246.8192	89.446	64.715	172.2726	
50.6874	112.937	147.4947	111.9952	

HOL-E-B-5 (μm)

119.768	138.253	116.2425	66.9182
156.9232	114.5841	98.1121	98.6134
103.9297	65.7287	80.2236	117.2468
137.4369	109.4551	76.0876	149.4554
137.8742	226.7278	101.7525	109.9147
65.3161	47.7486	97.0942	89.5195
122.4133	51.6369	122.4133	123.3437
65.2322	108.2235	72.8504	72.6948
118.3876	105.1664	104.9578	117.6014
211.4707	89.8128	187.4155	108.893
153.001	113.9159	106.8068	122.1056
97.8586	90.1497	52.9777	130.3468
147.5096	87.1795	131.6267	139.7325
123.6129	129.1051	162.8357	81.309
78.0216	92.6277	77.9841	140.1136
132.1059	116.4183	122.7024	110.8643
145.5503	84.0089	131.1012	104.277
160.249	158.3989	46.2566	72.6496
88.6791	133.4675	111.5245	116.8317
103.3623	146.7624	135.5718	91.177
92.5014	131.1597	108.4157	137.6175
154.7599	362.0483	91.9151	103.7045
95.302	133.607	114.7338	137.0749
140.1345	66.3812	100.7895	114.4725
208.2105	122.4014	130.0775	101.2234
97.6755	83.5205	131.9593	128.3077
108.5874	164.4605	145.603	179.1531
132.0921	139.1457	145.8035	44.5183
182.7741	129.5767	80.3828	85.8964
78.6743	67.2123	87.0621	169.4745
117.4895	148.4943	90.0727	157.3416
155.1295	103.0756	163.429	142.8271
99.0163	102.1537	144.4258	95.7303
188.8908	140.322	116.0034	114.9406
101.713	32.7586	78.9292	98.3946
137.4555	125.2071	142.9575	189.8783
161.8637	112.8205	141.1939	103.1394
110.996	32.037	164.7623	75.7267
133.2813	117.9487	54.056	164.4228
115.0581	52.9983	101.5477	153.5277
131.6406	97.9369	179.2122	201.7112
142.9575	95.7608	143.6304	162.71
108.3988	94.8718	130.8335	54.3928
110.5608	213.9528	85.1361	132.6853
154.8047	193.9587	95.5776	70.6668
101.3641	138.451	102.9941	129.695
139.0958	63.3748	75.3156	77.6697
113.5048	117.1065	85.2047	104.305
88.9916	256.9581	49.7271	152.4054
186.413	133.3689	86.329	112.3793
132.9822	132.5227	164.1115	146.5756
174.5872	118.954	169.0018	

HOL-E-B-6 (μm)

120.1729	89.008	81.8819	98.2757	199.7387
173.359	121.6681	66.4087	60.5391	196.4139
106.9606	154.604	88.7655	116.5218	172.1156
107.6923	131.8264	183.87	167.541	88.0383
207.5956	137.0749	232.3796	155.2947	176.8405
86.5319	94.4241	164.4983	178.0118	223.7162
137.3757	132.9877	103.6869	165.6356	164.1048
142.3763	121.217	163.0777	65.6786	230.6267
100.2918	135.8625	122.8066	84.8869	158.3205
112.6456	224.2853	111.3246	152.4461	111.4164
191.6837	100.3318	136.883	144.9115	194.3406
105.9346	78.8598	40.533	115.7986	216.2055
135.8141	66.4966	130.4224	96.6077	121.4157
127.6941	163.4446	156.3484	142.9907	220.3421
102.3716	169.9492	130.494	118.1127	104.4345
147.6853	144.019	108.183	161.5272	87.0621
76.1883	70.3819	27.5633	138.9776	93.3347
109.7351	44.1145	245.894	129.0627	118.0354
187.0389	110.8643	200.0073	189.5144	187.6686
55.8179	102.4073	74.951	123.3437	
140.5145	96.2478	189.1362	195.2762	
150.67	80.7794	85.8326	132.4897	
104.0982	115.4353	144.1635	156.3075	
104.5569	102.9232	135.3885	116.6565	
128.7311	148.4943	59.7619	66.6721	
95.715	175.8961	80.4736	118.8772	
152.2232	159.6644	170.4694	189.3293	
158.4335	69.5256	150.4977	108.3988	
167.218	48.3794	143.0852	101.2451	
162.5842	138.1896	107.8448	182.8521	
220.6138	117.8527	113.3277	90.6346	
146.4035	123.7665	170.6707	99.9744	
76.9468	82.734	116.6659	192.4007	
117.4677	125.8531	106.3957	80.2236	
101.9497	126.464	228.549	128.6942	
70.3975	71.4532	183.1155	104.3785	
188.2089	117.2935	126.5073	155.98	
100.146	233.9446	203.9371	109.0037	
96.9549	99.4433	129.9595	121.8151	
107.638	77.9841	87.5975	131.3962	
79.1925	60.0545	79.5607	167.7131	
109.2146	105.3503	167.7393	283.0854	
69.6516	99.5864	126.1632	115.4479	
94.3119	127.6283	112.1614	89.0613	
102.7527	85.4701	120.343	167.4189	
190.7209	52.6596	160.0825	73.4247	
91.5967	134.9372	149.9531	56.8103	
186.1483	124.9735	51.6369	150.3618	
102.8237	270.0976	165.1255	162.6179	
234.4842	227.299	69.7511	55.5556	
78.4278	125.2479	62.2525	147.8435	
114.8134	65.8342	131.8707	184.3144	

HOL-E-B-7 (μm)

142.5688	76.185	113.0279	57.0549	91.5658
127.3078	90.2117	139.6083	133.3041	149.0988
81.9235	99.2679	56.6719	86.2936	82.2114
148.0811	94.7006	181.3151	151.9136	117.7761
122.6773	141.324	150.8305	258.3747	200.3551
135.0055	147.4415	65.5133	123.8109	177.7041
124.1705	122.7727	121.4113	109.5104	83.7195
169.5631	119.8307	75.9338	75.5921	122.3973
124.5967	105.5495	62.8238	120.8975	114.1908
136.5279	175.5615	111.5403	99.5139	175.5954
89.8557	193.6216	196.3046	139.8626	95.3901
50.7424	181.3865	63.5424	83.7269	122.1402
138.4155	148.8505	136.6528	108.2745	89.2845
80.7234	214.9807	117.4197	172.5217	66.1282
114.5572	111.5458	132.2891	80.3842	129.0485
134.9416	110.5932	90.4414	232.4052	111.3135
82.6028	129.5395	84.9256	150.4008	145.4789
79.7581	109.7072	84.3552	192.0137	140.074
76.8055	157.4472	107.9001	105.9711	148.635
140.8522	153.4316	124.9392	120.7887	180.9646
98.8511	154.7158	157.182	220.9122	99.8232
140.5031	89.5603	106.2054	147.699	96.9667
163.6324	139.3269	122.8965	143.0866	103.3026
137.9457	106.607	60.4742	121.6075	171.7686
197.2547	148.5991	187.6268	186.4415	144.2536
64.8989	212.2269	44.3792	133.7349	147.3313
99.3507	114.2267	62.9708	99.7861	231.8502
162.6235	145.7837	188.1473	73.8516	123.1186
71.7605	122.3872	106.43	148.2378	48.2135
140.677	69.8836	119.8992	136.3834	129.5459
65.9509	88.5845	62.2422	114.5716	114.5357
161.9361	128.4901	109.142	77.4554	160.1307
118.9789	78.3311	144.8505	144.5509	151.3689
127.0622	65.6512	85.2347	89.2891	85.09
109.9616	87.1724	161.5703	102.952	143.8485
65.0222	168.7371	37.4438	175.5849	102.3917
69.7158	84.3138	127.9372	120.0499	126.2544
78.4491	90.2299	109.7371	188.4626	179.3154
190.5356	77.1418	57.6246	110.6916	44.3467
122.9383	168.3861	110.4817	111.509	185.2032
181.2958	147.3537	111.5403	150.1547	86.7566
98.5471	108.9461	115.5305	109.5385	134.7999
74.6926	93.4074	111.8401	84.2748	110.2415
55.6623	111.0752	169.6685	167.6009	117.057
79.9614	159.569	121.6261	106.1493	97.21
219.2739	92.0424	88.0658	241.9759	103.6679
137.822	157.6988	94.0715	162.9769	189.3469
62.8728	131.0016	166.6975	157.182	41.8634
144.3731	113.8159	116.7054	205.7782	
133.4211	145.0589	173.4919	145.3433	
85.5475	123.2054	179.8451	122.7376	
195.5202	87.7737	61.465	80.4736	

HOL-E-B-8 (μm)

187.7426	144.0799	80.0047	92.5961	180.6879
173.4622	137.9488	205.6475	88.2455	124.6018
91.6445	134.1227	148.7204	96.1073	169.8018
117.0971	139.5154	76.3751	148.7523	99.2116
148.7401	57.8275	122.3059	111.9789	112.5645
144.9392	77.6274	159.9273	73.37	31.5198
103.56	62.7434	178.18	87.5724	83.1699
75.664	196.3358	200.6527	107.2062	149.3796
113.0178	125.7602	83.433	118.3444	72.4078
95.1332	97.6793	124.2848	44.1228	100.1496
148.514	122.3745	134.2724	144.5279	163.2188
96.1605	82.0691	164.2739	144.7274	131.6267
188.8096	145.0198	122.9136	51.6369	117.7286
178.5834	155.5203	199.5704	144.161	113.2116
175.6467	87.7058	101.9927	170.1907	80.1826
105.2706	194.9393	137.8614	133.0481	107.3016
161.7576	51.3461	108.6277	150.7403	
74.2016	195.0985	162.3144	209.4453	
114.4948	146.4335	76.7615	140.3819	
124.4463	201.2054	89.9062	147.9028	
103.8453	140.8598	114.4725	103.8382	
153.6276	130.2655	83.4636	137.5192	
109.9147	133.4702	118.9877	162.7459	
151.5739	89.8087	105.1838	178.7633	
136.6078	111.5082	178.3378	157.323	
128.1054	218.4191	114.6447	133.5578	
146.4559	148.2087	147.9645	173.1671	
96.2288	109.7351	102.742	183.2033	
125.6672	69.0194	135.6284	121.572	
233.8384	191.8075	130.6798	174.2081	
120.5401	223.3126	42.0978	85.0073	
132.4648	130.9702	141.584	79.4136	
100.0146	96.4904	96.1111	84.6542	
84.3906	125.7573	82.5129	125.7602	
52.9983	203.9729	113.3438	73.787	
106.6563	170.1198	119.4137	66.1276	
82.0913	110.3756	136.8483	92.2325	
44.1228	160.9245	129.4752	162.132	
140.5587	111.2294	53.2459	116.4057	
123.908	138.4642	123.9316	76.3033	
102.4964	97.4696	197.6282	78.5767	
158.7858	62.3873	150.1211	113.5723	
116.167	175.4637	77.2878	151.9662	
132.3131	78.5674	151.4534	83.752	
134.7422	78.9893	141.4214	148.8751	
123.7665	178.6815	90.4692	139.151	
70.3819	196.399	101.9927	95.7608	
102.8664	141.4214	117.3215	172.3468	
105.1421	88.3117	188.8889	191.4415	
228.4531	136.2303	99.8501	237.6084	
90.0037	150.6045	136.7521	210.5064	
67.543	119.4045	109.9412	102.2395	

HOL-E-B-9 (μm)

130.8167	220.7247	109.3516	179.6682	143.9556
87.3511	173.1249	109.8049	121.7311	88.8601
55.6607	123.1007	114.137	146.4559	35.9076
43.5897	145.7234	138.3058	119.1994	151.7545
99.1785	115.2357	142.6762	113.4533	120.8155
98.1567	111.626	144.7072	130.7916	145.2489
134.3594	105.807	133.8501	123.9434	105.7379
132.2883	170.5487	127.6112	165.9529	198.9912
162.8984	105.9553	143.9607	124.7102	107.0801
112.2785	162.0892	64.9629	133.0371	125.5334
80.4736	93.413	119.8167	170.0425	138.5037
152.743	156.7275	122.2342	77.9795	122.464
191.0405	82.4465	96.7172	214.5452	199.444
247.081	50.781	76.2027	143.9607	132.1059
63.0686	99.8501	84.7232	114.0313	138.1393
135.2616	206.4947	102.1144	96.7286	110.4649
81.0525	165.3841	235.0816	106.9743	74.8681
252.9828	120.6431	166.3398	132.1667	123.4118
110.7093	56.4426	59.2462	157.5736	157.6755
146.4958	133.4702	128.5608	133.4784	
235.6821	77.6274	91.7401	130.2851	
115.2199	99.0421	94.5633	143.029	
102.6531	142.1992	100.9452	100.3791	
184.5778	212.0657	86.9991	233.7353	
157.4367	108.183	119.2086	90.7473	
135.3831	154.7599	60.7078	81.5512	
50.4925	70.6306	81.8061	45.0404	
96.5358	93.0329	146.1713	165.0812	
100.3901	160.7792	128.2877	188.2089	
68.4241	62.4868	80.2236	107.7906	
118.4617	218.0878	60.5391	176.0456	
157.1348	217.9772	103.7608	170.859	
133.1634	188.0827	101.8852	147.7669	
41.1146	230.3272	149.4945	210.404	
141.6072	142.3148	184.1082	134.6093	
129.6105	101.2343	218.0878	87.7058	
109.8316	53.019	165.3487	211.5587	
121.8901	108.6681	131.1736	146.5756	
94.3777	228.2323	134.1908	123.9316	
79.8585	119.6703	127.2127	41.6267	
261.1541	47.3183	159.424	160.4882	
196.2855	88.7779	81.484	176.6607	
69.9028	160.7406	197.8812	133.1579	
139.3031	61.5444	104.7767	128.9692	
141.504	149.8873	113.5466	222.0726	
136.5945	119.2668	136.8189	98.643	
193.2153	149.8946	149.3772	56.2871	
127.3762	129.695	93.2564	89.1924	
124.0612	136.4768	47.8174	127.7628	
138.2028	124.073	158.122	80.9939	
116.644	128.0626	115.9656	103.9929	
144.5885	151.0017	233.2206	159.0134	

HOL-E-B-11 (μm)

89.5806	105.3226	88.4151	103.5459	226.6505
89.89	151.6317	163.2904	141.8906	134.1908
207.06	179.8308	109.0439	134.3404	153.915
182.354	80.6595	65.4781	249.2827	175.3887
81.1291	225.2911	128.5608	114.8738	96.8531
181.1905	64.0627	90.4409	84.6111	153.8295
148.6786	79.4918	95.2138	116.4183	125.2246
123.1274	108.1121	214.0185	109.7916	68.4241
119.771	64.9629	98.6615	75.606	135.7334
75.6833	52.3256	213.2868	160.4677	154.2113
55.9291	130.1673	107.1142	242.1384	101.7202
86.0875	167.4712	68.4295	105.8795	142.5379
155.9636	115.8396	180.5848	239.6594	73.3301
67.6241	166.8091	97.0942	128.4471	100.0037
135.7334	179.2693	93.6941	108.1121	142.4687
184.902	80.4918	61.4256	197.6596	43.4218
165.867	134.7096	126.2443	80.9127	134.4083
182.918	45.3636	135.9404	82.8487	144.0291
134.0573	121.3796	135.6903	164.5405	109.355
160.8224	213.3074	160.9472	86.5319	
110.4914	135.9834	149.8167	97.9146	
127.6684	117.8899	110.1006	118.2147	
211.3204	165.8384	112.7071	162.9679	
111.1111	117.8868	239.4688	149.4652	
106.5089	58.1322	123.6749	175.7029	
96.3237	120.5249	165.9309	140.0562	
226.3667	80.2919	118.258	79.6112	
172.387	86.6668	187.119	224.181	
128.9239	82.9236	47.0396	66.2159	
131.0928	51.6016	88.3696	132.1805	
124.4463	82.9764	165.9529	151.4775	
119.184	134.7855	156.0713	140.8287	
152.2519	130.0073	108.3854	122.27	
142.0064	186.0658	98.2348	100.3246	
135.8974	213.5897	146.8494	61.9643	
104.1087	57.8804	186.6303	93.08	
105.4993	90.1051	180.4047	115.0676	
86.6584	183.8581	102.4002	119.6398	
169.5434	80.9443	201.979	93.3152	
138.1578	120.4643	103.789	151.9374	
64.1026	151.3569	161.945	120.4431	
108.8125	64.2335	92.6947	201.9121	
116.644	163.1964	122.27	94.1413	
119.5023	131.635	206.6768	84.8266	
205.4307	59.5905	122.8066	91.5528	
147.0408	143.0111	192.7384	164.0402	
124.798	169.7781	183.1235	145.475	
169.5197	86.5319	124.9647	114.8007	
111.2622	145.6632	127.0087	239.6655	
110.64	74.2065	139.931	90.3924	
136.7628	214.3579	100.3537	109.4318	
255.3325	112.4183	137.7342	94.5324	

HOL-E-B-12 (μm)

178.9185	63.0295	124.9885	89.1371	155.8167
154.137	117.4355	162.1301	74.0516	45.877
242.1313	126.8211	148.7981	145.2245	95.2112
108.0599	148.3749	159.3925	119.8924	108.6534
118.1941	47.4532	111.0085	106.157	127.5899
96.2926	193.1286	162.2821	158.0736	166.7363
92.0268	201.8905	140.449	198.0199	160.1102
140.1444	104.5953	137.8071	92.3166	108.2954
233.6826	311.6004	102.966	97.8777	182.3985
92.0246	152.2419	86.1554	139.7803	
209.5615	62.4992	111.1805	104.8875	
138.7136	86.1983	122.9851	86.9459	
140.6668	222.0171	125.1599	176.5906	
139.2089	116.211	55.0723	163.7341	
178.0021	85.3431	158.7221	138.6113	
100.2483	146.0245	164.1639	215.1785	
69.4914	57.8665	147.8881	105.7304	
122.2091	153.8675	110.6897	133.6058	
148.5313	108.4666	139.3741	98.4303	
226.6051	143.8556	75.6655	108.7271	
120.0071	169.683	123.9436	162.073	
215.5572	128.4309	135.9216	101.5272	
90.6411	96.9476	136.5625	139.6553	
130.8964	67.0171	74.193	211.6247	
81.4204	136.406	85.2781	50.1559	
82.5754	81.7151	112.108	96.3502	
132.4009	95.8757	190.4235	70.7484	
123.3037	130.3979	234.1666	93.2466	
132.0482	113.4905	117.0324	188.1298	
97.9616	71.2433	208.1466	134.806	
111.8732	123.0586	140.3905	107.0801	
90.2572	122.1251	119.2325	150.3625	
141.584	166.3829	119.6677	100.1683	
107.5033	106.8669	89.1602	162.3922	
199.4816	104.4164	171.6669	139.1749	
157.6991	124.3738	126.8923	171.9347	
66.6697	162.3517	117.0271	105.9012	
41.3698	97.6991	119.1963	138.7521	
122.6438	76.2201	114.3292	151.0564	
144.4713	85.1817	244.6957	89.9654	
41.1507	140.8682	167.3752	132.6489	
143.3162	82.1139	118.0219	131.7023	
174.1007	155.4431	191.29	160.9179	
71.4276	151.3106	82.7122	161.3921	
124.4003	127.6028	175.4877	177.8739	
184.5998	136.6949	130.5428	175.5708	
127.68	110.647	224.6427	124.3474	
174.9659	120.4804	133.9268	86.8134	
136.803	90.1388	213.8808	137.9159	
44.8764	177.5687	157.8499	149.5624	
79.3345	243.969	115.1886	166.2779	
184.406	112.2893	128.6435	72.6653	

HOL-E-B-13 (μm)

184.2232	119.0324	176.9974	113.5267	111.1214
92.0514	174.9072	138.1882	125.1446	85.8711
122.4476	252.5787	116.2026	154.1037	109.2045
67.8667	193.3856	169.8331	109.2624	141.5504
108.7857	162.5376	141.4983	169.534	88.1847
51.7994	157.9058	106.6571	83.5904	
240.6921	102.6442	91.4333	215.3283	
117.1692	99.8232	117.9435	95.332	
68.2317	116.3806	123.908	181.5912	
146.7823	84.0404	59.6701	142.8509	
54.2786	79.8128	106.8376	117.825	
132.4567	121.9719	156.8044	99.0163	
145.362	170.4994	190.4666	132.3885	
240.1999	94.0584	70.5157	46.1583	
121.0045	177.7861	171.6333	143.1209	
84.1284	62.2323	117.5548	133.7533	
129.2041	141.132	142.4687	97.5558	
48.7254	114.3799	127.8521	125.2775	
193.1926	108.4925	151.1353	169.2356	
86.0146	109.3527	194.818	77.4872	
192.1752	81.1853	181.9148	102.9839	
104.6758	162.5894	77.5217	130.3443	
187.1463	111.9503	156.8628	132.0342	
137.9695	119.1994	84.8215	151.7257	
50.1441	116.4657	114.2267	186.1592	
99.4873	260.9204	160.6406	116.0522	
107.9515	119.2928	204.5233	130.7692	
133.635	115.0154	56.2092	41.7898	
179.0574	109.0874	94.1151	57.3096	
140.5177	126.6862	120.6508	121.0249	
95.1853	105.4346	176.1888	91.9553	
205.5854	150.6263	146.1039	97.3496	
97.6255	99.4417	149.4847	85.3552	
68.6975	110.2732	142.7146	102.2395	
96.2478	162.6235	87.7058	73.1472	
149.48	213.1842	92.3077	105.9312	
188.3001	139.4315	130.5456	111.9397	
65.2994	87.0663	46.7993	70.0333	
85.7394	188.7786	123.5601	102.0214	
117.9017	152.2136	186.7732	166.4989	
79.5285	129.9876	127.1398	64.8989	
159.7685	64.4892	158.6731	108.9706	
83.923	163.3308	159.3502	115.4637	
105.5106	65.5506	153.2708	120.2739	
151.8893	122.7024	79.4794	123.5734	
117.4677	140.449	107.034	85.8155	
127.9388	53.85	41.1507	139.3918	
285.9477	156.9767	102.229	103.6184	
112.018	213.3622	118.685	191.9274	
154.6826	114.7722	193.2021	118.5187	
101.8121	146.6534	97.4509	109.1627	
179.4597	139.8817	224.8692	173.3592	

HOL-E-B-14 (μm)

130.4751	62.2232	209.1242	69.8061
128.7348	183.3806	189.6805	152.5331
61.5919	159.6784	210.6411	74.1031
119.8735	70.2793	122.464	166.1198
96.7588	203.3668	146.8594	174.5286
49.3678	109.8049	93.3778	121.8859
110.9474	213.053	157.3871	92.8071
145.2853	63.6982	131.8818	209.4389
57.1808	122.0817	152.0623	140.302
79.2853	145.0475	141.4412	131.7772
226.4917	123.9983	169.5413	79.579
177.2989	130.8335	120.7104	206.0326
137.1921	120.2739	197.2341	129.5887
84.7879	160.3744	183.0821	193.2021
148.856	207.4741	103.0898	182.4691
125.7079	182.4441	169.9911	123.0062
82.2314	98.3614	104.1228	147.9423
127.8023	99.4873	214.051	239.0649
131.5852	138.7942	130.4448	162.5022
82.7097	157.6408	167.3643	133.3349
285.7361	99.7243	126.5217	117.0035
133.3719	68.8684	139.0597	129.4018
100.236	235.9927	108.7153	122.9849
91.8952	47.0085	106.2325	94.9064
188.0594	160.5433	142.1531	160.4793
128.4565	142.9617	125.9448	234.7983
121.837	112.3826	146.9683	91.4051
170.7135	78.9165	136.4148	217.4542
120.1799	114.8134	114.8743	72.2058
124.4845	117.7552	135.7695	120.9606
91.8714	165.6356	52.611	223.1454
101.8852	146.3842	133.9592	137.1921
132.8751	149.0781	104.6934	102.6922
102.504	142.3091	136.7127	143.3275
161.5023	183.5046	71.4945	157.6187
153.8168	166.8791	179.6845	161.5935
100.1603	91.1542	202.6006	196.2741
171.7482	184.5196	84.7232	142.9575
95.1918	116.0699	158.7325	109.546
94.3777	205.0302	146.0739	133.6316
126.8446	229.1835	142.9601	131.0638
108.5975	169.2902	146.0872	212.2568
162.9769	193.6411	184.6332	93.4091
61.7018	46.6576	169.8754	83.2983
87.3845	181.8023	107.4138	109.2756
135.4082	124.1473	128.8477	222.129
167.3425	125.7456	211.3873	
98.5096	125.7456	97.1825	
207.9335	74.6348	84.1826	
134.1663	93.9716	74.3393	
60.4505	153.1233	148.7278	
127.3119	147.9971	136.2266	

HOL-E-B-15 (μm)

58.3861	153.649	75.1457	159.3163
96.8034	99.1232	88.9916	49.3631
115.4732	74.0587	69.45	130.9702
123.471	60.2488	116.9692	129.2919
132.731	97.0387	122.2342	127.4536
45.4043	85.3431	88.1171	35.926
79.6157	166.3135	150.5463	141.2301
95.715	110.1636	127.3771	188.5308
112.6456	85.2519	114.9819	69.3849
104.7767	114.2617	119.2135	163.697
68.2317	99.2679	57.4532	82.5129
86.5764	77.0038	190.8453	100.0584
118.9426	124.9297	126.5217	72.9706
55.9291	131.9968	120.3712	107.0562
94.1142	127.8856	129.9736	99.0442
173.7593	143.6884	49.5505	187.0409
53.678	177.5502	138.9622	59.9267
102.143	86.1554	131.7515	64.6924
88.9751	153.0583	117.7659	74.8876
94.8217	133.7955	108.8998	140.6963
103.7045	118.8157	141.4983	105.909
136.2839	71.6778	109.1242	46.4556
100.084	124.8331	144.4173	138.451
116.9442	137.737	71.0842	45.5645
152.3701	94.3506	72.2513	115.1083
162.0103	175.5823	140.756	196.7762
106.7247	138.035	175.3887	94.4396
27.5716	78.6046	96.1871	181.5235
125.7799	161.2012	121.4427	80.3828
161.997	157.2095	68.8319	112.2818
134.6473	35.416	51.6299	89.8453
87.2855	134.2642	111.4689	62.7434
138.8364	129.8977	60.7759	62.5335
84.8697	136.4018	112.5872	117.2468
128.7311	99.4543	145.4323	47.0576
121.1446	105.05	96.887	36.98
139.9728	103.4329	94.9108	166.2278
124.2407	73.2146	98.5471	50.8385
111.9397	150.5878	128.3605	145.1113
58.2766	130.1842	116.4057	113.0824
106.3716	91.5967	47.0396	139.0538
158.6731	155.6964	143.9657	101.5621
147.3523	65.6786	39.3534	46.225
69.5046	172.6407	66.3812	179.1205
115.6249	51.1077	97.668	73.7959
68.5095	79.6653	81.048	96.7739
64.1826	57.5675	70.4804	81.1291
128.8134	106.4574	99.3808	59.9815
111.341	158.0735	133.913	119.6677
103.4329	95.9437	116.0947	
140.634	53.239	69.2255	
128.2051	59.9084	150.9727	

HOL-E-B-16 (µm)

143.6101	34.6127	164.7149	112.9752
86.4896	123.2667	130.6323	216.393
197.6282	143.9242	216.9324	130.9256
206.4947	88.5753	136.0693	114.3959
89.495	71.1047	125.8386	208.6538
123.2934	97.9092	151.869	230.0162
121.911	142.1427	128.3816	92.7784
169.6007	111.796	141.9756	161.7837
123.1303	163.429	95.8821	94.7765
128.8095	87.8639	51.9587	121.599
151.381	122.2969	80.9443	304.4187
150.7403	167.0847	316.5914	96.2212
157.5457	126.3081	209.3755	162.5338
118.6773	143.2969	160.686	100.0913
105.7207	171.1537	158.8308	91.2251
130.0522	95.7277	125.8008	67.6366
152.6257	143.1031	242.253	147.4848
150.5293	117.5796	72.6738	75.335
177.9441	40.3439	217.2303	77.5944
117.5719	84.3625	123.7777	144.2496
160.761	65.0728	73.9057	119.6398
135.5356	175.1449	120.2278	229.353
121.3301	125.6439	156.7928	177.0799
92.062	289.3715	107.0425	69.3625
160.5678	136.907	176.087	63.0454
254.5689	61.1873	139.3031	108.0309
116.2393	76.3063	149.5751	93.1036
236.3445	134.8831	122.8155	217.7358
119.6123	105.9553	112.2785	92.1255
184.2768	204.8805	149.1732	50.8475
53.9546	133.3772	91.2251	111.1407
126.4871	43.5237	165.6665	94.3932
64.0741	50.3644	196.3097	179.78
119.2453	271.838	139.3582	155.9604
58.6514	137.3544	173.9773	138.8054
153.106	144.2395	60.5964	108.3955
182.9779	123.4621	156.4904	172.3404
108.5874	163.4446	176.0144	158.8755
172.6834	149.5531	135.5599	147.9645
105.8935	114.5203	91.0367	167.6195
219.4252	95.0718	121.2591	77.6938
148.9168	62.4166	108.3348	68.0763
151.1275	56.795	140.8598	125.8518
131.4907	217.5478	113.8448	98.1125
149.9027	102.4394	193.0659	129.926
79.8356	114.0313	110.021	88.4151
112.1255	114.4693	123.8461	97.4959
84.2693	112.5452	104.3691	53.8733
112.9097	125.8386	125.1633	129.9848
92.3591	173.2852	41.7055	113.7266
85.6238	93.7253	142.3455	62.5747
154.3794	115.4859	145.8962	

ALC-03 (µm)

73.63	131.62	78.74	92.02	34.9	163.01	120.19	127.91	128.85	91.01	131.7
90.12	104.27	141.63	57.23	119.39	115.41	173.62	115.15	54.46	193.76	77.77
109.45	87.3	122.58	239.25	63.4	111.53	68.56	144.54	76.69	207.18	32.33
96.15	159.42	115.55	80.41	172.84	149.41	127.91	100.39	200.63	160.8	83.1
170.76	172.66	52.78	232.46	90.84	54.97	97.61	109.86	145.65	96.67	238.2
67.68	140.17	250.04	146.4	96.46	173.36	133.78	110.51	157.11	100.27	73.8
186.69	54.66	170.47	56.56	108.27	107.28	110.4	113.02	164.26	56.25	176.9
49.01	119.35	153.25	60.33	91.28	110.85	82.82	297.49	104.34	90.4	166.75
243.9	215.36	128.87	63.84	112.26	168.48	136.97	151.33	239.75	110.55	
61.66	134.67	106.74	81.9	137.56	57.49	119.36	123.8	109.29	95.05	
159.94	72.42	120.78	183.14	157.93	106.48	93.27	101.25	98.29	160.15	
65.57	93.29	145.25	135.84	102.93	142.42	196.64	58.29	77.01	183.04	
240.11	177.88	126.58	91.21	79.86	134.2	99.36	92.39	23.34	124.53	
102.71	237.01	88.25	82.11	138.91	85.33	139.04	71.81	135.16	150.18	
81.7	70.56	147.24	68.35	137.56	143.62	139.86	193.68	102.93	144.04	
91.64	107.77	92.05	95.25	171.37	118.03	142.4	74.81	141.16	208.59	
183.21	91.92	94.85	106.36	78.14	162.95	187.94	72.3	43.5	146.61	
104.34	47.08	103.51	138.4	149.05	124.11	67.98	77.17	161.97	136.56	
123.93	153.84	65.13	33.29	78.7	115.47	135.26	184.07	136.79	92.12	
95.05	126.25	97.35	207.55	112.03	73.4	141.77	165.94	110.66	126.69	
93.74	116.52	67.55	82.82	51.1	109.41	148.85	102.17	59.62	137.49	
125.83	115.22	104.64	114.18	86.07	91.83	95.58	161.19	108.97	83.23	
81.49	132.91	231.17	135.56	82.63	135.96	98.42	170.68	91.91	172.81	
90.31	76.98	79.69	138.85	79.02	69.2	64.35	67.28	117.53	68.99	
82.63	108.23	205.94	198.99	69.78	161.76	113.75	124.74	117	157.29	
122.29	87.3	177.52	101.08	87.63	133.96	125.01	68.15	93.14	118.34	
187.11	257.67	151.86	52.78	208.86	106.34	49.85	86.76	112.55	101.48	
99.01	159.54	108.43	116.91	126.5	132.04	100.7	91.96	107.79	105.81	
91.28	212.57	274.52	103.45	65.8	134.99	119.96	180.06	215.77	139.27	
30.95	121.92	108.33	96.16	122.96	87.51	65.58	189.8	112.85	99.02	
62.25	122.77	115.33	73.86	132.76	79.55	107.17	179.27	74.65	42.99	
61.57	45.78	124.95	61.56	61.35	135.36	123.56	85.36	186.11	114.34	
52.71	109.56	60.01	169.44	96.32	98.78	161.58	148.16	83.73	129.09	
74.89	78.12	97.67	88.79	105.27	123.05	84.72	170.68	92.17	102.89	
158.84	29.67	172.97	100.21	113.83	98.2	54.97	110.21	158.68	111.58	
160.13	72.72	110.13	183.08	72.72	122.2	85.61	138.7	127.68	40.95	
85.07	117.91	65.06	156.12	56.79	98.69	209.57	114.86	258.26	103.8	
88.93	136.69	68.21	55.63	109.38	79.58	27.91	110.59	57.34	110.09	
58.43	146.06	104.3	166.95	84.6	88.21	48.45	124.87	113.22	60.57	
187.97	135.07	63.69	83.38	117.85	113.09	192.4	152.86	98.98	151.52	
90.86	145.2	104.83	108.37	226.92	145.1	58.36	113.5	190.66	100.63	
58.43	54.2	90.77	83.1	117.71	62.25	57.16	140.63	210.99	112.91	
148.36	114.14	121.35	89.78	41.41	166.49	100.9	52.16	85.61	63.53	
88.79	156.9	59.49	58.43	63.7	132.16	96.14	150.03	94.74	198.02	
52.15	62.41	176.89	154.16	205.71	151.36	99.54	140.04	123.92	160.11	
169.65	109.41	115.27	65.45	71.79	161.88	106.38	53.53	59.92	98.92	
163.3	222.64	350.75	155.43	121.95	46.42	108.4	121.91	49.01	81.91	
90.89	130.28	126.53	84.6	145.2	53.58	102.97	100.63	113.64	137.41	
142.13	140.94	114.97	249.34	91.05	105.93	90.04	117.7	81.18	101.7	
101.41	83.68	78.94	120.75	107.41	146.08	99.54	75.39	189.05	251.37	
111	104.08	203.28	64.49	94.44	186.16	85.4	147.07	84.35	107.48	
104.12	100.23	59.24	129.98	99.77	106.15	257.46	67.86	171.83	170.05	

COW-02A (µm)

247	164	155	215	233	138	299	232
282	298	177	150	178	198	219	199
175	240	150	299	177	265	153	230
214	295	589	234	332	325	242	143
175	387	403	221	332	282	370	222
277	168	443	169	645	234	296	396
438	350	177	396	477	125	121	396
309	296	251	286	215	252	208	144
88	250	515	238	224	100	416	329
161	175	242	306	392	224	260	211
360	510	264	370	149	344	189	188
365	356	241	142	131	409	290	224
511	231	102	166	346	361	255	332
309	151	256	151	161	151	358	145
165	344	249	269	236	100	246	216
447	221	111	256	256	233	218	459
177	186	204	204	211	519	75	350
260	216	414	280	622	595	155	307
330	187	188	531	540	415	289	355
213	442	260	184	524	349	235	244
305	261	99	456	358	319	252	147
137	198	299	411	340	368	160	266
501	251	121	213	302	349	258	196
106	162	228	200	315	256	231	220
223	335	396	241	409	135	349	182
215	208	252	380	345	260	377	214
225	236	138	550	264	441	153	543
322	206	308	262	389	380	245	412
279	443	216	147	393	235	309	269
292	215	336	177	186	254	360	163
238	214	298	197	150	141	251	262
240	224	433	352	215	270	227	520
234	305	187	489	205	549	387	368
291	129	359	132	311	138	202	343
274	388	357	116	251	349	311	316
103	138	264	260	318	281	260	194
197	96	437	236	376	250	196	296
363	300	368	151	341	235	252	132
320	180	265	277	289	243	326	560
343	155	860	140	126	206	301	421
172	223	244	180	240	418	180	121
251	334	534	686	427	169	248	315
168	402	315	195	169	163	292	89
242	207	274	228	177	207	295	321
303	255	298	211	257	208	146	120
230	316	310	193	133	445	350	563
263	201	301	338	145	129	149	348
121	203	376	163	215	203	101	510
328	287	237	265	199	163	406	417
394	132	307	316	218	157	396	
198	253	324	295	237	294	148	
254	437	183	208	443	208	279	

COW-3A (µm)

206	156	329	255	203	105	214	261	113	180	163
74	76	96	78	152	104	130	93	178	167	211
107	156	133	117	221	115	190	221	232	215	217
233	75	88	145	121	197	81	77	36	199	122
121	102	125	147	92	143	182	208	364	87	108
91	67	74	88	173	96	84	129	106	149	211
153	160	121	239	196	179	73	154	87	213	235
160	113	105	249	234	189	89	77	114	239	142
148	189	180	98	67	157	150	113	105	228	165
108	99	67	72	202	104	56	62	85	202	183
134	128	72	107	159	170	214	125	157	98	188
93	231	174	137	61	76	69	139	200	159	62
84	67	85	172	268	83	150	230	177	74	91
134	158	220	101	67	341	182	115	92	136	94
92	212	109	120	87	67	116	134	147	60	149
98	226	194	63	140	102	176	150	91	155	170
187	166	139	124	205	79	165	95	185	82	99
124	227	382	263	184	64	189	119	161	136	93
122	148	73	171	58	223	101	112	248	153	117
211	108	83	84	99	177	88	143	183	145	76
69	79	76	210	93	127	145	45	200	71	195
202	130	47	99	111	148	189	119	89	82	48
113	51	173	74	81	181	161	237	88	150	109
377	123	121	220	44	144	128	131	162	178	50
50	260	70	75	155	138	138	112	335	123	56
162	131	173	189	148	186	127	69	132	234	137
150	96	113	127	209	64	177	52	403	110	211
234	258	129	52	243	61	180	199	165	131	139
166	41	209	241	183	106	160	148	254	137	78
233	166	117	46	198	89	73	176	108	201	368
77	95	79	160	111	63	185	53	227	71	139
199	85	75	167	89	137	66	156	92	121	77
220	121	124	151	64	112	353	128	222	83	149
209	110	70	154	59	136	128	59	173	157	171
225	37	160	152	91	89	124	127	103	88	235
88	178	164	183	257	110	160	81	169	101	298
67	71	124	100	79	79	245	117	226	285	45
116	103	106	178	87	400	135	94	140	99	131
122	158	174	107	105	109	307	89	72	97	249
136	119	184	101	105	155	33	166	68	135	107
119	141	152	133	196	155	173	140	108	137	87
145	171	162	127	345	152	81	43	96	125	146
257	123	134	146	155	150	171	52	166	186	140
184	124	170	221	173	142	242	88	125	73	216
103	70	171	124	67	334	97	76	105	229	86
91	205	125	132	256	86	71	151	126	253	
98	209	162	213	115	133	127	152	204	181	
120	196	103	237	124	259	130	136	50	88	
74	139	167	159	128	125	95	337	246	185	
291	126	78	62	103	124	97	100	253	202	
179	258	183	114	125	160	182	143	110	169	
104	148	209	192	120	323	247	194	93	152	

KIN-01B (µm)

549.34	252.29	429.81	43.93	207.3	90.59	301.08	100.91	49.7	98.9
484.63	98.73	108.56	254.14	25.58	102.87	259.89	65.88	59.04	451.01
99.41	166.28	290.72	277.82	61.42	87.86	329.66	304.19	103.65	114.69
119.12	129.15	319.27	121.09	147.31	179.21	31.96	202.97	63.08	117.68
345.07	249.99	303.16	81.14	109.02	363.64	121.47	220.49	71.8	157.3
71.66	122.84	192.07	90.4	139.37	274.17	68.27	31.54	261.53	81.71
371.46	40.36	93.67	316.49	108.93	134.07	449.68	69.77	415.09	395.56
696.82	106.73	485.69	272.1	259.44	67.63	167.38	63.08	40.45	135.41
101.53	170.03	281.76	51.49	424.44	94.87	160.83	70.29	149.16	387.81
192.85	348.34	75.11	334.49	174.34	202.61	159.81	63.98	109.93	72.07
93.02	107.82	417.69	145.49	114.69	97.1	104.04	106.23	70.95	171.34
284.28	277.64	166.66	128.29	493.1	523.22	141.91	121.34	132.06	302.77
149.8	150.34	213.78	241.36	560.32	372.74	502.55	151.66	326.04	
108.68	443.52	138.86	193.04	118.89	133.49	263.44	369.76	255.8	
56.43	134.39	358.54	105.97	79.1	118.78	238.46	132.89	246.83	
52	204.44	456.05	106.07	471.84	75.11	166.28	85.23	82.12	
102.91	100.51	429.17	351.39	119.23	111.14	251.72	347.85	70.95	
137.36	496.18	63.35	146.38	97.3	121.89	715	325.95	235.82	
395.49	58.92	294.55	138.12	473.72	478.88	158.15	430.46	108.68	
62.07	69.96	248.94	241.29	106.82	109.05	77.91	238.23	263.13	
80.27	97.3	91.76	50.96	74.94	109.69	87.44	178.5	239.32	
82.57	569.47	483.23	120.54	121.89	75.11	158.38	170.41	278.84	
154.18	333.69	52.32	155.25	62.23	268.85	128.29	62.87	595.58	
96.86	371.03	119.31	208.09	245.82	80.1	59.66	181.78	256.22	
576.83	474.96	109.05	589.38	105.22	309.05	129.02	317.84	113.81	
64.65	148.01	108.68	170.88	274.45	105.44	67.83	421.32	447.3	
432.39	85.9	171.11	107.48	107.48	85.58	194.23	93.95	54.94	
574.78	139.85	164.83	108.47	240.66	100.64	149.71	194.19	313.3	
83.21	331.39	257.08	96.13	89.7	123.41	246.47	187.33	70.53	
287.01	43.93	296.75	101.7	286.36	89.7	85.43	423.5	76	
208.01	48.75	129.15	214.72	103.17	137.17	342.22	168.26	310.48	
128.6	158.66	292.34	276.69	170.8	219.64	96.55	328.29	399.62	
84.48	236.56	243.07	293.4	38.76	41.42	264.19	70.95	142.7	
215.09	279.48	370.56	334.14	479.43	91.65	317.91	65.88	217.19	
54.33	47.51	191.49	128.29	63.82	80.77	392.3	171.75	610.61	
150	131.81	37.27	186.51	535.36	88.46	144.91	120.45	370.38	
156.6	235.61	149.36	74.4	133.69	102.22	224.38	284.43	349.03	
149.11	230.8	107.54	271.21	73.09	100.34	101.83	66.68	78.21	
90	265.45	211.85	181.17	153.5	59.66	114.22	224.03	215.09	
178.14	264.08	379.1	147.65	210.08	130.59	252.33	117.85	375.4	
497.09	426.51	154.22	89.21	223.6	54.33	240.21	67.38	104.04	
224.39	132.29	170.19	100.91	227.3	118.55	114.08	55.66	600.75	
159.39	147.99	84.13	397.78	641.64	165.25	314.58	65.42	47.15	
146.56	87.44	141.01	617.59	46.01	168.28	34.76	183.3	150.34	
177.47	70.95	198.82	239.21	38.85	209.19	77.73	81.14	259.56	
123.84	173.26	176.36	312.49	88.91	126.22	67.23	173.82	162.98	
332.88	330.51	136.66	115.36	364.79	89.25	130.36	412.96	229.86	
119.12	229.38	303.74	238.62	399.32	200.32	127.25	199.37	102.22	
156.11	103.49	178.29	312.06	176.18	125	200.17	71.09	99.04	
269.99	86.63	143.06	116.99	61.42	136.95	110.6	101.07	96.13	
150.07	71.47	75.25	266.99	640.5	79.81	400.73	131.76	149.16	
263.13	54.33	582.79	116.99	167.66	134.17	56.67	98.4	163.2	

KIN-02B (μm)

274	61	85	337	325	233	22	142	125	80	107	195
260	253	234	163	227	127	74	77	88	53	122	486
258	158	126	202	289	470	384	406	160	377	234	175
144	234	148	62	712	326	48	134	112	82	100	355
250	151	123	142	156	127	323	227	184	377	463	154
190	73	271	444	112	66	142	150	294	748	115	87
475	355	361	355	69	142	129	298	124	190	370	388
176	184	173	275	68	312	243	282	185	112	165	248
353	78	210	343	102	177	191	247	106	116	74	265
319	187	243	130	75	191	224	325	226	274	486	153
69	355	281	193	241	576	166	534	176	29	160	252
200	80	105	100	448	185	805	84	166	226	168	97
301	221	113	443	78	172	146	100	658	229	80	85
252	289	204	168	200	166	238	212	113	182	108	655
171	319	240	281	235	410	105	387	76	201	72	144
188	186	394	159	168	120	323	294	262	398	53	101
389	129	186	123	81	161	114	198	142	181	224	166
97	82	98	156	618	258	126	125	376	325	87	169
499	176	88	400	163	335	275	198	51	142	95	294
174	79	119	241	485	215	174	99	109	405	116	140
520	70	141	92	170	424	166	181	116	309	146	149
167	257	216	74	209	381	387	147	127	61	93	337
364	160	549	156	149	177	694	132	162	123	74	77
94	240	88	141	141	352	353	489	127	111	125	334
158	269	109	216	193	130	239	99	300	378	210	77
224	255	172	203	228	269	255	320	229	314	80	348
179	267	136	245	153	205	429	77	382	287	542	
270	105	202	110	201	157	231	383	485	53	87	
390	198	253	112	267	229	718	65	74	191	63	
591	249	334	261	118	269	281	195	245	318	195	
144	230	181	117	221	207	72	470	178	161	160	
114	104	60	150	191	196	144	178	48	224	199	
87	171	232	427	273	108	153	136	298	195	175	
167	113	68	373	105	238	55	139	76	102	187	
230	245	136	243	185	194	456	101	486	107	101	
151	205	163	332	61	158	334	511	63	609	373	
168	148	136	261	128	551	356	61	195	93	141	
76	195	156	145	219	279	48	231	332	381	164	
341	205	589	287	417	389	214	54	131	78	206	
121	77	116	259	124	165	124	216	250	223	103	
265	61	231	242	337	283	177	193	766	71	102	
184	71	115	94	271	86	284	92	594	111	170	
130	236	175	232	344	294	386	70	161	86	292	
160	90	171	413	103	127	191	209	187	223	356	
244	129	65	47	37	387	142	522	113	80	123	
320	375	44	230	406	87	110	311	250	190	158	
191	121	487	260	204	394	158	230	132	355	216	
231	85	80	131	180	355	74	181	233	86	180	
184	554	476	89	156	184	341	150	403	180	165	
109	308	90	455	95	270	87	199	79	64	136	
73	276	343	381	128	311	96	385	274	66	265	
64	87	429	53	262	773	154	192	582	88	217	

TEN-01 (µm)

179.89	70.67	92.01	96.77	128.87	111.23	100.32	96.23	67.8	89.64
108.9	137.12	108.67	62.77	75.91	109.69	112.74	106.65	117.31	85.82
62.56	81.68	68.23	112.87	116.41	87.97	128.55	114.34	91.37	137.49
65.14	134.2	31.1	79.94	105.48	97.67	96.49	102.56	74.31	106.58
102.25	96.67	111.68	93.19	180.75	89.28	79.92	72.25	130.79	94.56
49.69	120.73	75.21	104.16	79.99	101.02	142.7	84.23	128.42	176.7
131.74	90.27	148.1	79.86	111.94	93.5	146.43	70.49	63.8	142.42
99.94	48.75	100.19	89.07	111.23	112.62	127.05	81.51	108.4	113.53
113.63	144.08	70.97	73.12	124.49	32.11	77.99	114.34	116.12	38.54
61.29	102.91	180.8	67.68	111.63	129.28	84.52	64.99	93.07	94.3
114.68	109.75	93.99	93.5	122.62	62.77	87.68	73.69	74.7	84.22
88.77	62.97	63	69.99	73.71	187.12	79.37	66.22	76.64	95.1
69.3	137.03	89.33	129.89	110.74	99.35	53.96	107.98	138.11	82.33
92.56	82.63	118.12	90.84	141.69	62.97	106.56	87.73	191.24	101.88
118.89	86.95	63.38	74.44	77.99	63	67.49	90.59	103.29	49.46
67.98	114.56	126.41	102.49	87.96	138.53	93	89.82	143.45	79.75
95.85	96.66	112.96	84.52	114.68	127.36	97.4	88.08	126.76	100.71
103.32	89.8	80.65	105.77	52.51	78.63	129.41	88.06	104.61	231.84
57.99	106.93	212.9	81.42	104.72	103.51	110.96	115.34	68.1	67.98
98.6	136.24	108.69	74.19	129.5	105.22	93.05	135.03	73.63	101.53
128.76	125.77	86.41	139.9	153.12	83.83	111.47	129.41	87.3	87.94
144.93	126.25	54.23	33.54	113.66	132.91	54.92	134.99	141.03	144.46
137.77	163.66	117.2	157.19	97.14	201.12	73.97	118.37	81.04	69.51
75.84	112.02	106.55	135.96	99.08	153.4	157.23	148.06	87.06	131.93
114.05	102.34	66.47	88.48	67.28	129.13	51.62	139.68	163.94	57.84
77.67	173.63	108.87	93.32	147.99	139.64	120.3	162.25	84.07	41.72
113.57	64.21	102.87	147.71	106.12	105.4	97.49	172.13	131.74	91.51
120.73	120.28	81.85	96.89	62.71	155.9	87	41.92	106.52	78.94
102.83	91.69	91.48	105.69	108.31	39.88	75.08	129.76	134.99	92.05
112.74	67.08	126.81	87.35	80	106.06	76.71	107.38	67.28	98.48
118.56	135.82	166.35	47.43	92.46	92.1	98.74	96.38	51.38	114.02
61.9	100.15	122.31	122.05	78.04	175.6	70.62	35.21	83.68	110.67
177.3	80.94	129.68	126.41	145.37	70.99	98.27	44.01	79.58	77.71
94.74	23.32	163.63	53.09	70.14	106.55	111.3	46.73	124.37	65.99
36.61	76.82	111	99.79	118.83	127.91	104.12	80.52	116.41	
105.68	147.93	77.35	130.96	156.9	76.35	220.71	124.22	71.21	
114.98	120.45	70.01	136.76	329.62	76.33	54.54	47.08	94.19	
119.35	149.59	203.05	110.24	119.7	154.02	80.59	178.81	146.25	
213.16	69.15	119.88	80.84	82.98	119.88	113.48	94.7	150.81	
110.78	98.74	101.07	153.76	106.15	69.54	78.04	197.44	179.37	
96.55	69.78	63.3	104.78	89.61	128.61	63.4	109.61	159.15	
124.33	150.03	36.71	64.99	105.8	110.91	143.59	31.85	39.15	
146.79	145.64	144.37	94.52	121.54	167.32	118.98	100.63	44.16	
83.15	79.58	73.31	82.63	175.12	103.88	112.87	97.06	180.45	
131.7	119.08	123.87	78.52	117.21	89.79	114.14	156.46	118.28	
97.27	89.53	95.44	87.06	120.99	109.14	52.31	114.14	127.58	
66.22	109.77	96.03	53.06	56.79	54.19	87.13	88.31	71.02	
163.81	87.51	165.69	83.23	84.42	113.81	169.76	128.02	96.84	
159.54	120.53	90.81	88.15	96.14	102.5	73.46	101.97	127.23	
166.04	104.96	72.71	139.9	78.26	176.31	72.36	93.74	142.75	
67.21	252.91	94.52	108.07	97.86	158.21	330.41	83.68	106.03	
126.21	135.84	132.63	80.8	100.44	110.33	81.4	82.77	53.88	

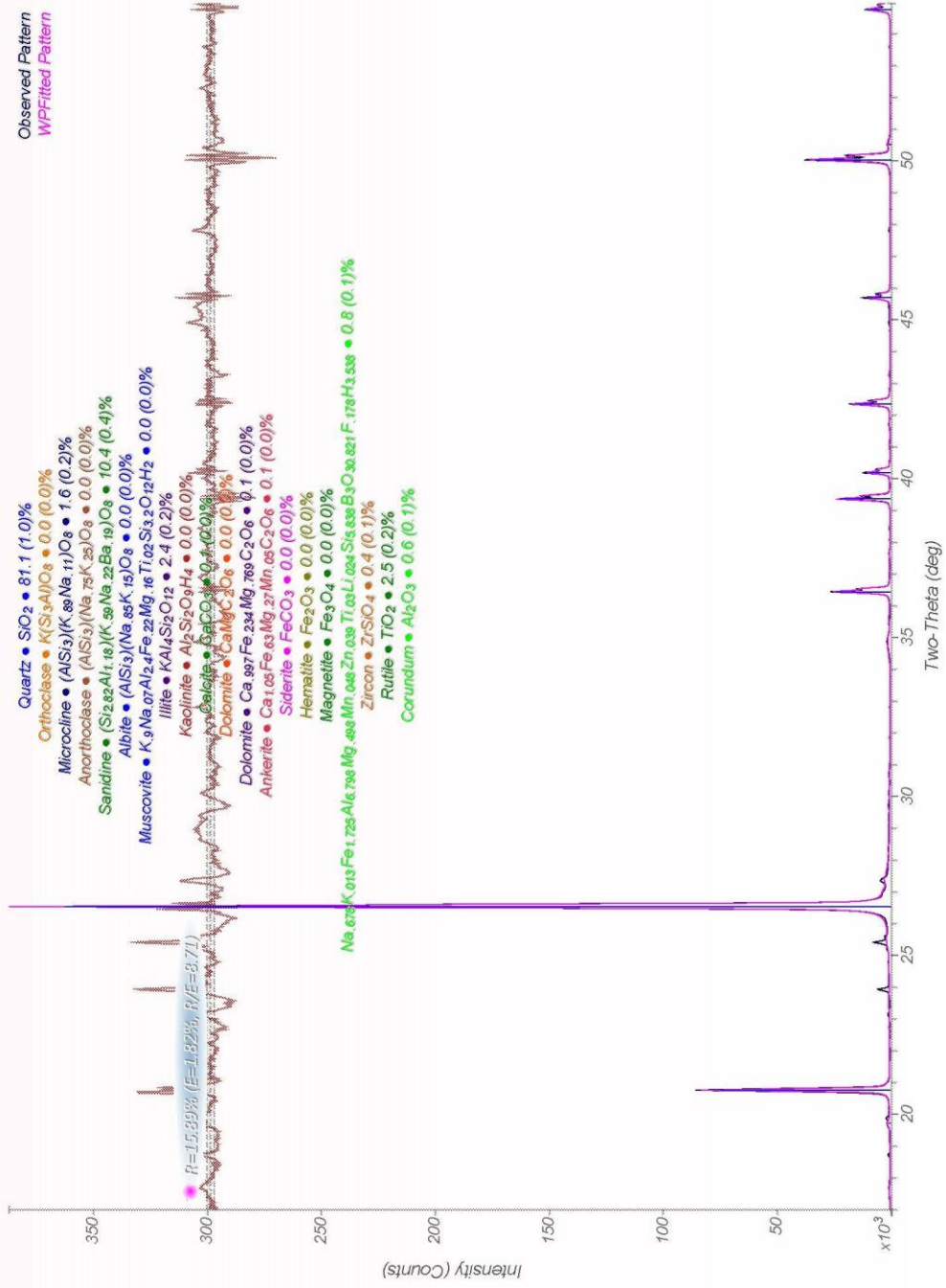
APPENDIX G

X-RAY-DIFFRACTION DATA

Included x-ray-diffraction data files:

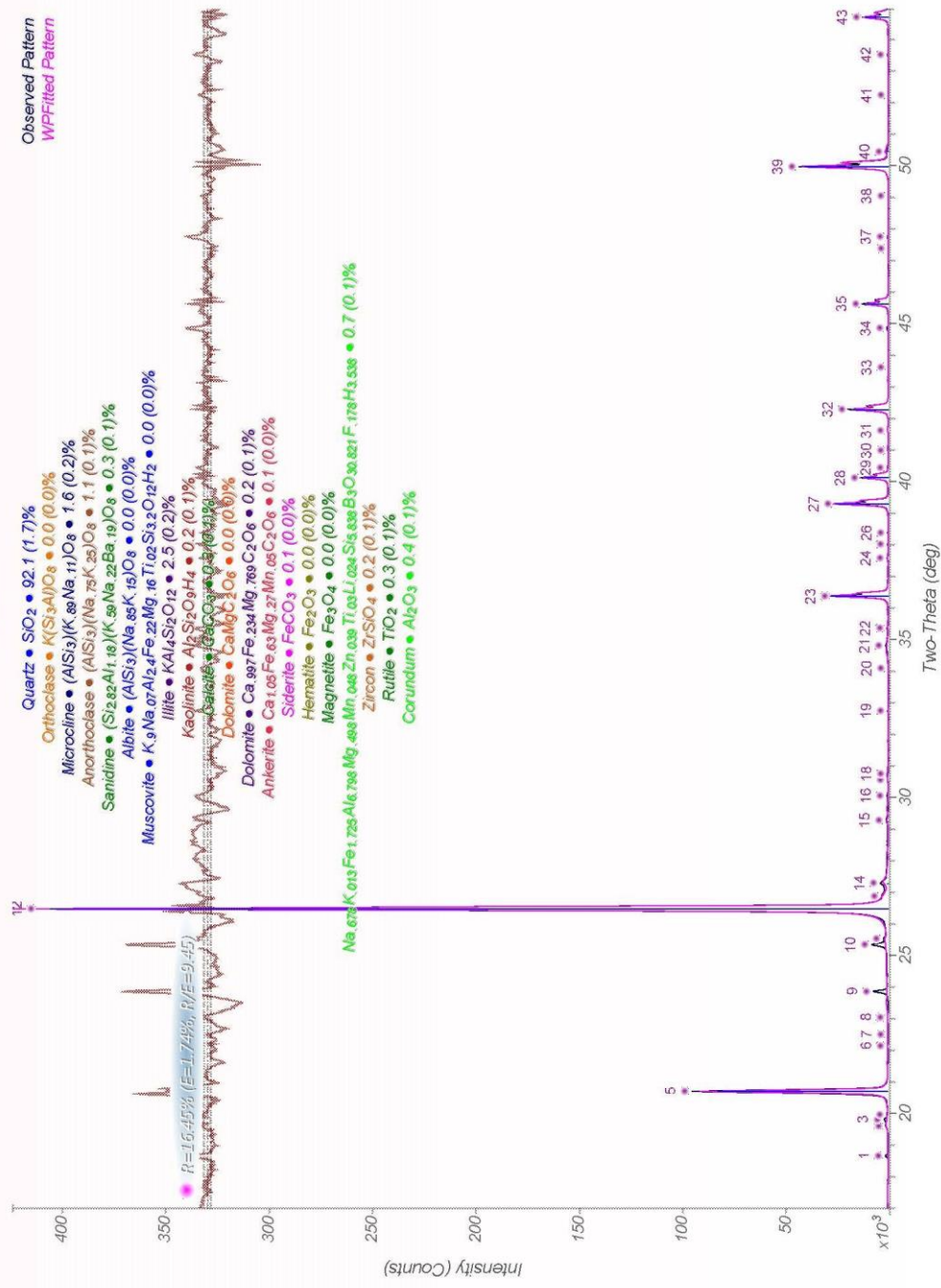
1. Coconino Sandstone samples
2. Whole-Rock (WR) and Disaggregated (D) samples for comparison
 - a. Includes both Coconino and Non-Coconino Sandstones

ASF-5-8

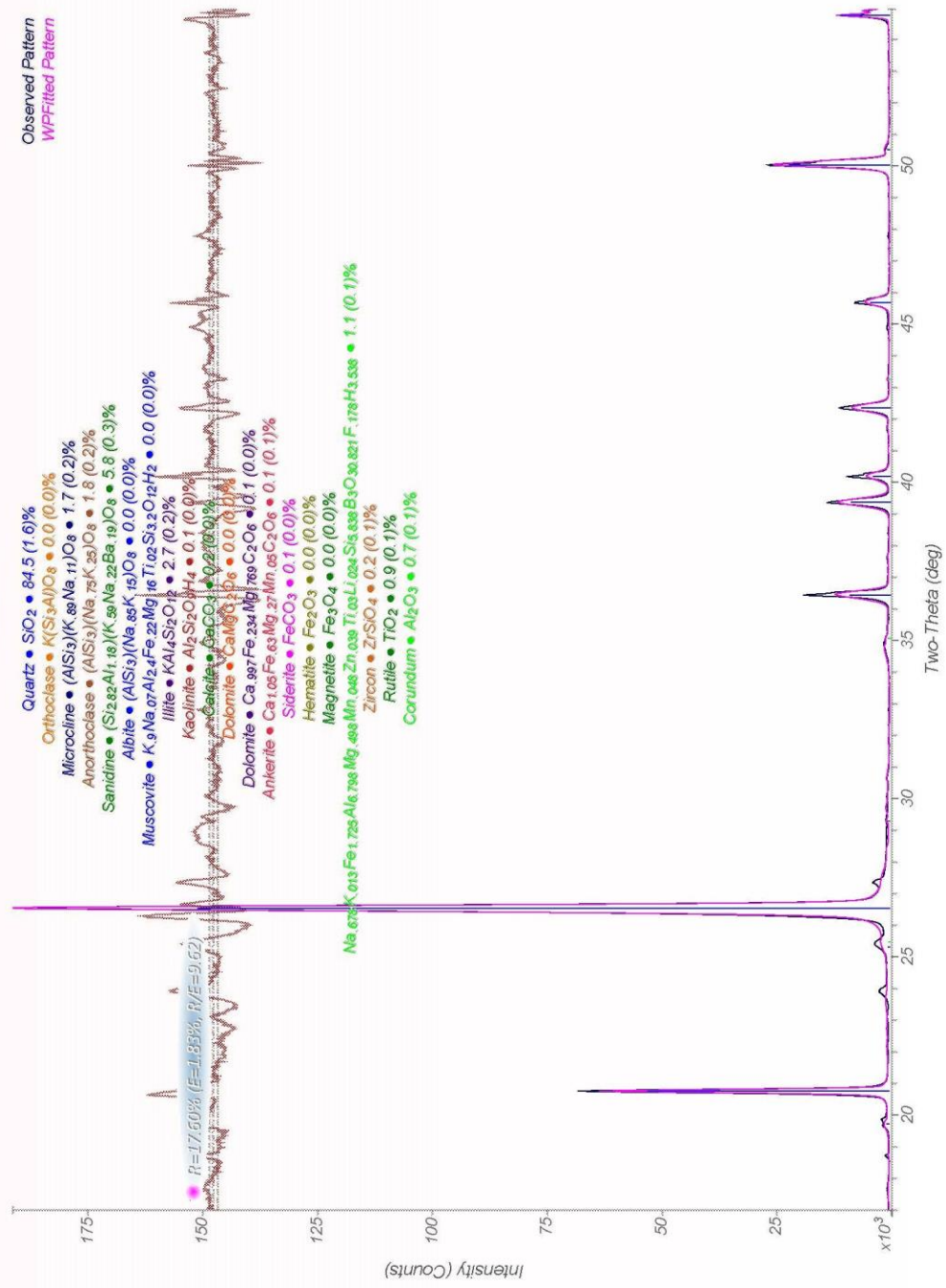


ASF-5-8_exported

ASF-5-24

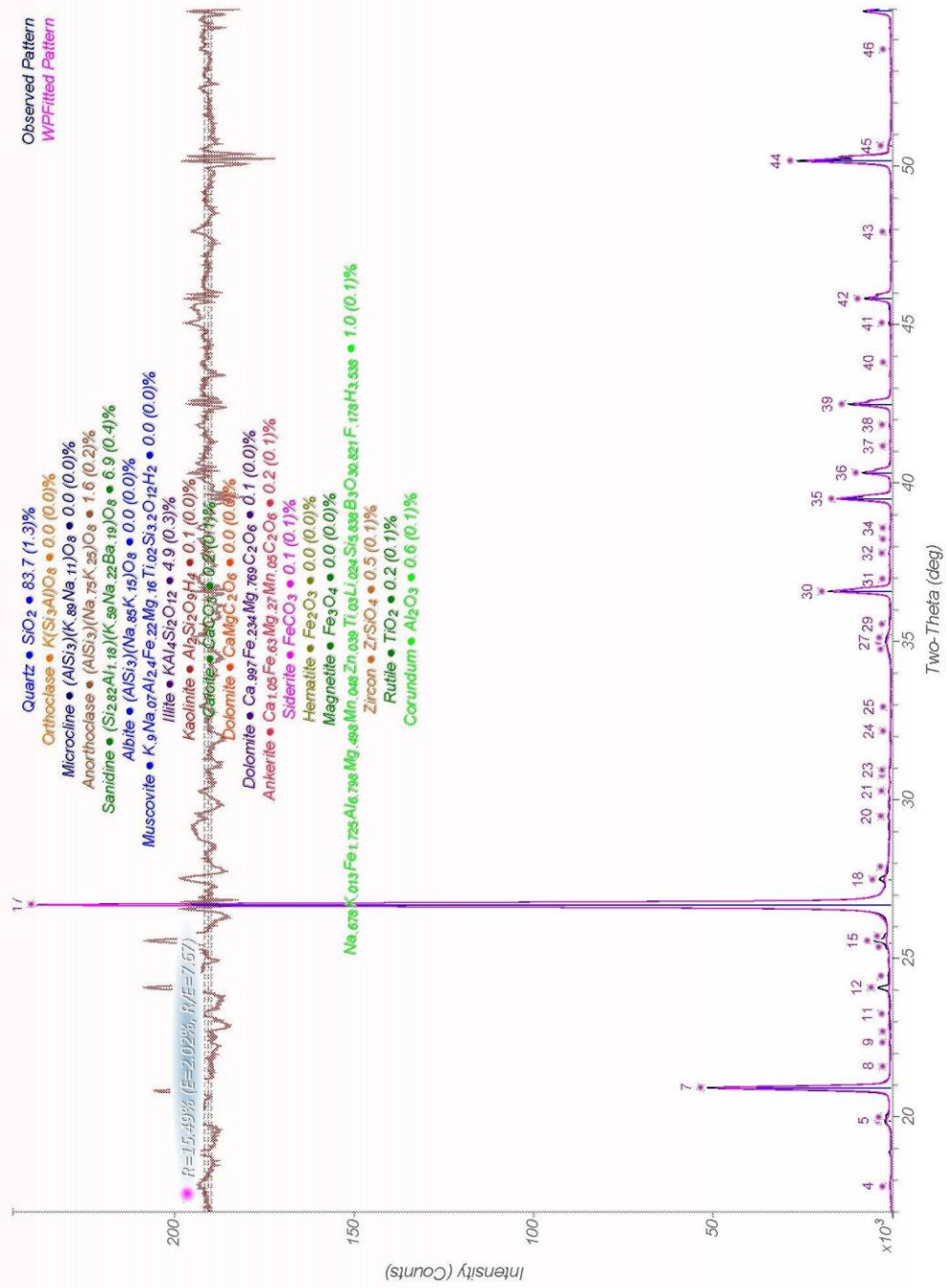


ASF-22e-A

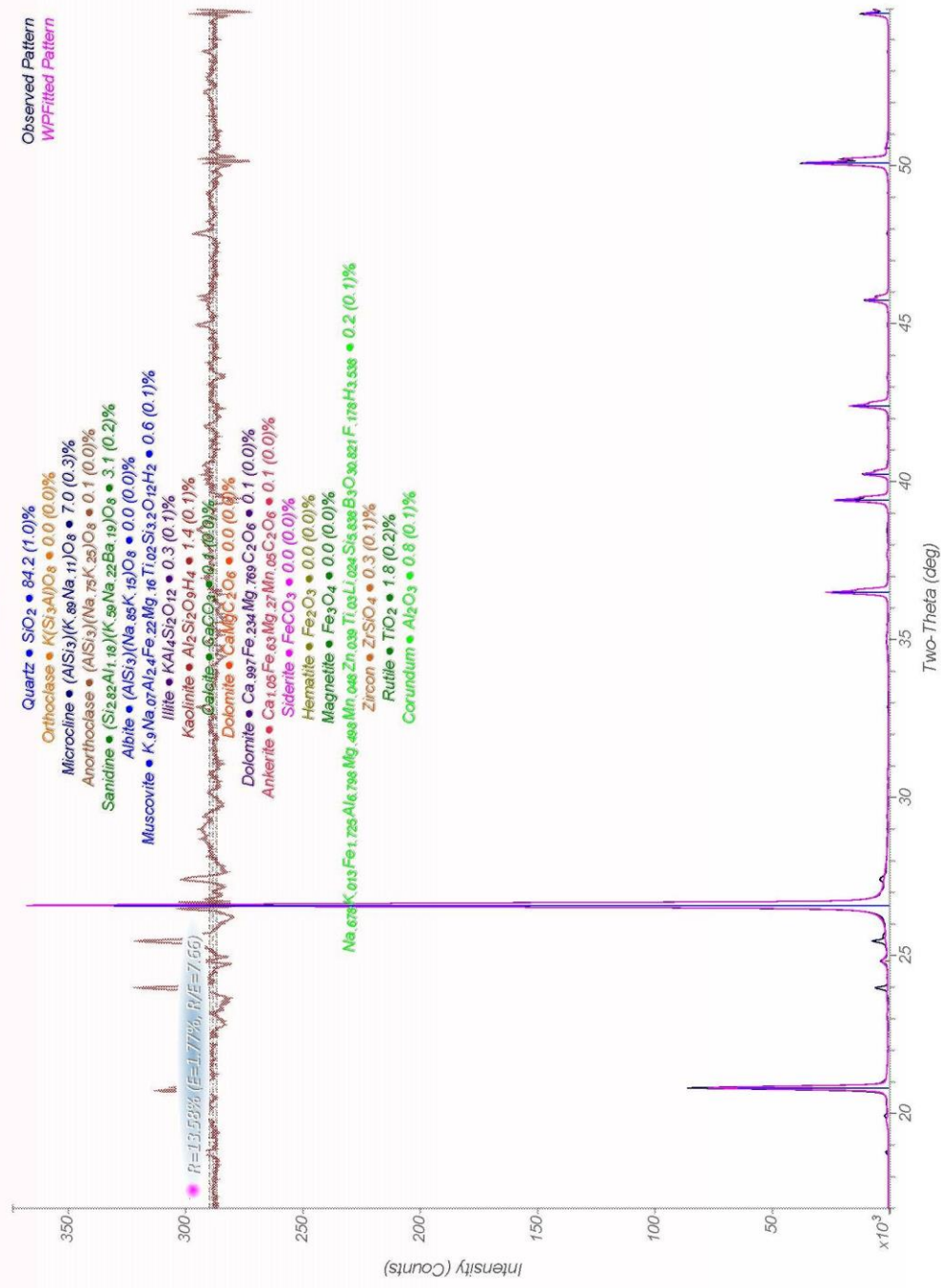


ASF-22e-A_exported

ASF-22e-J

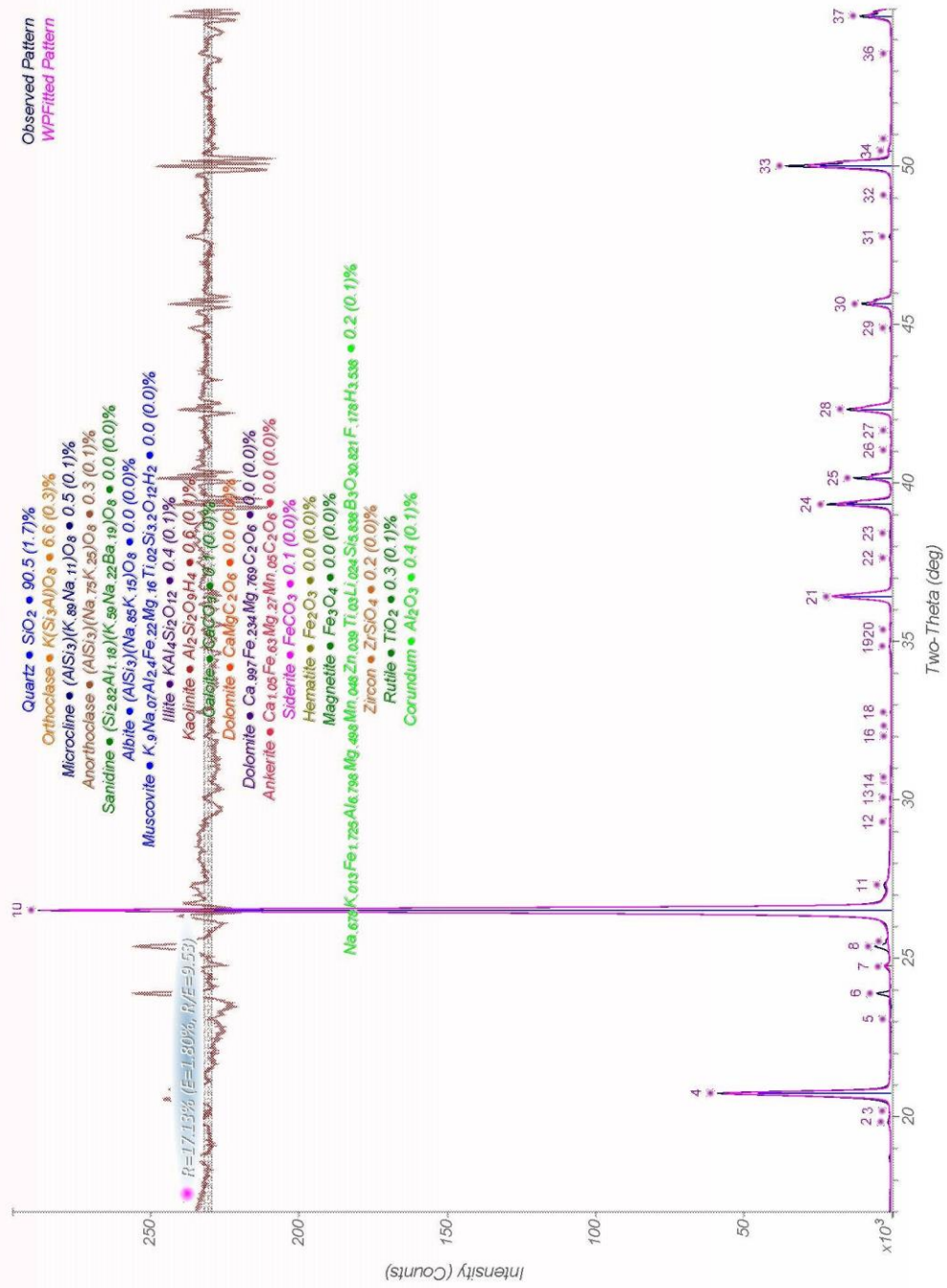


HMT-4

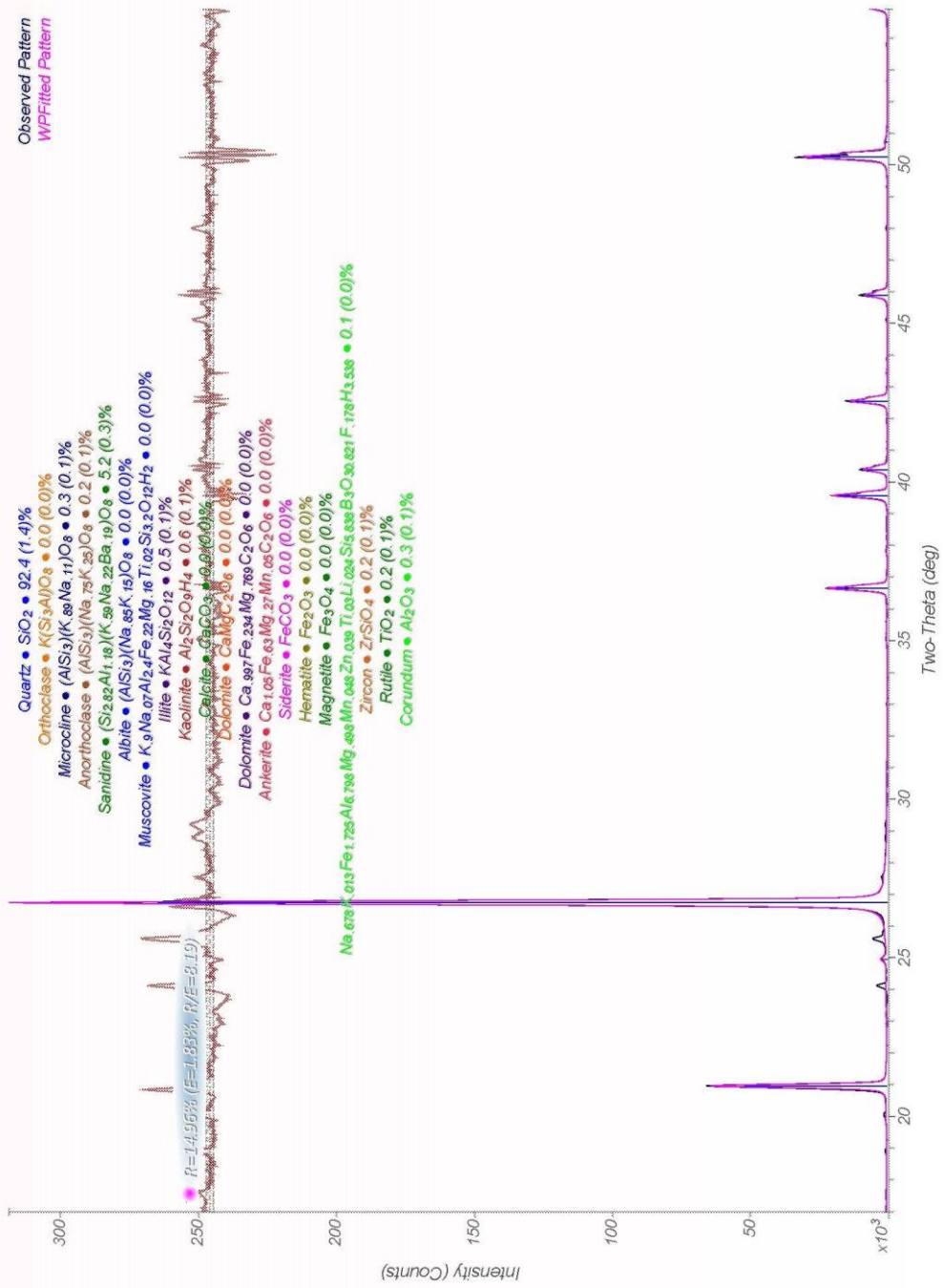


HMT-4-WR

HOL-E-A-4

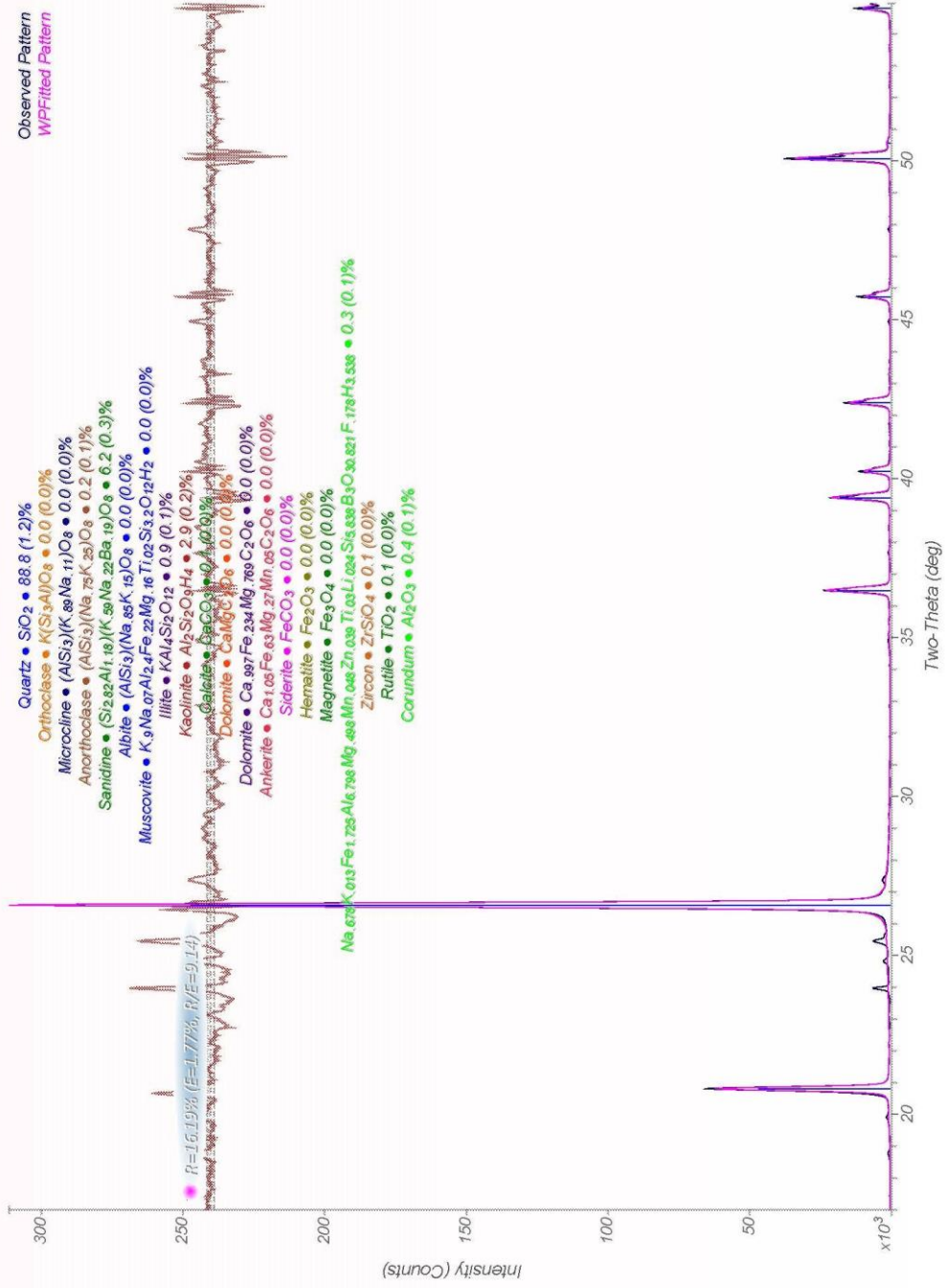


HOL-E-B-1



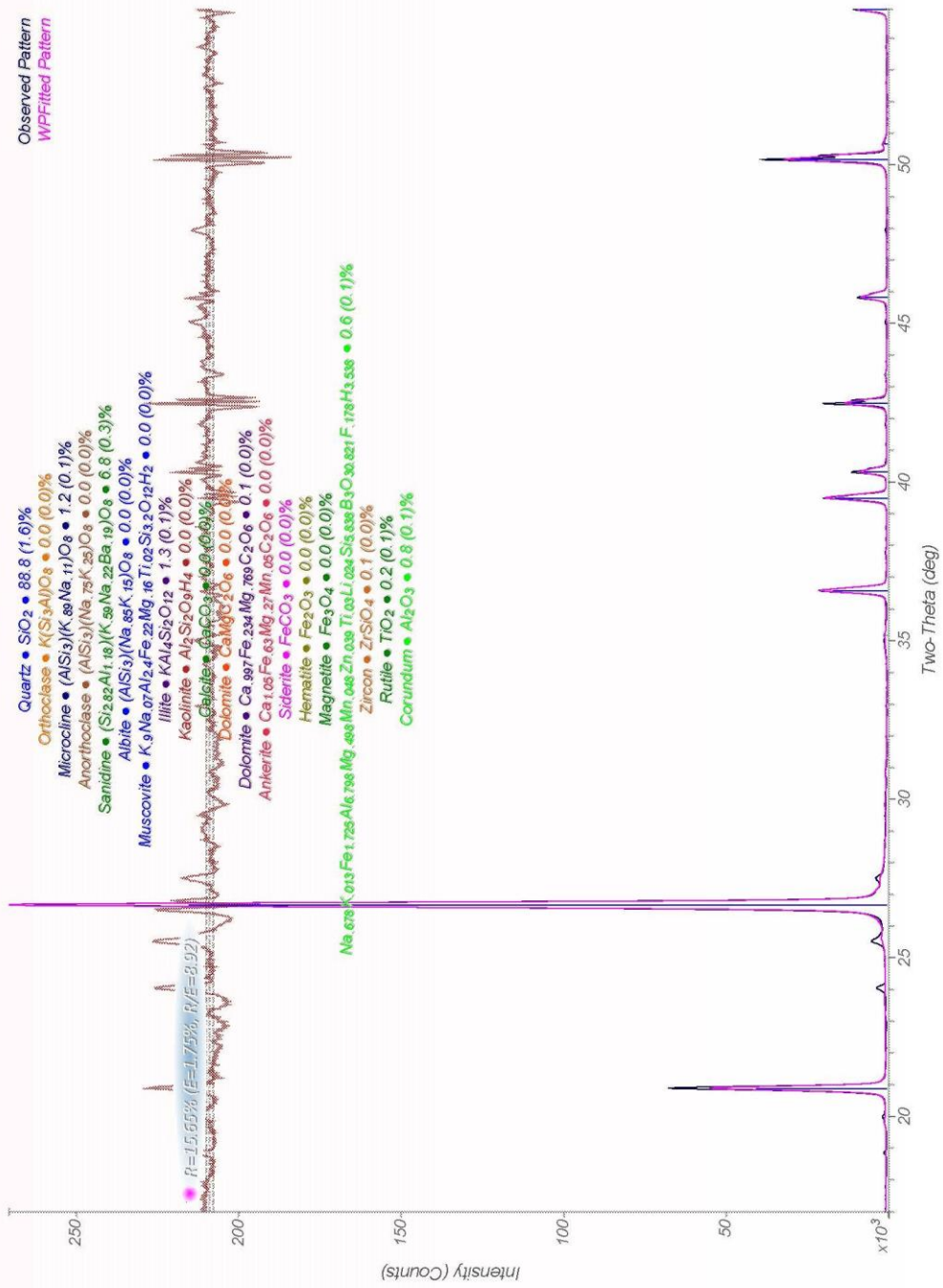
HOL-E-B-1_exported

HOL-E-B-10



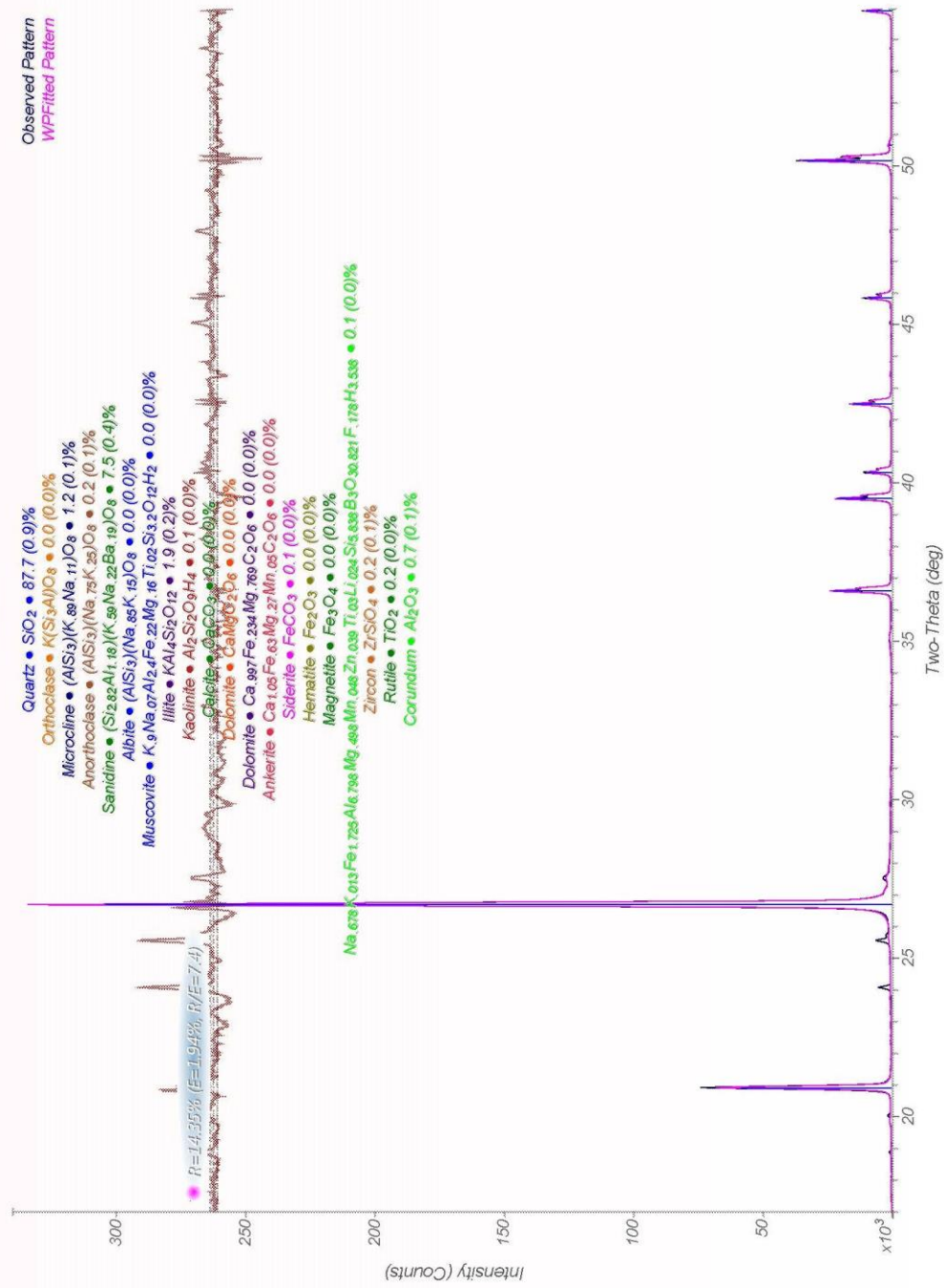
Loma Linda University

TM-1-26



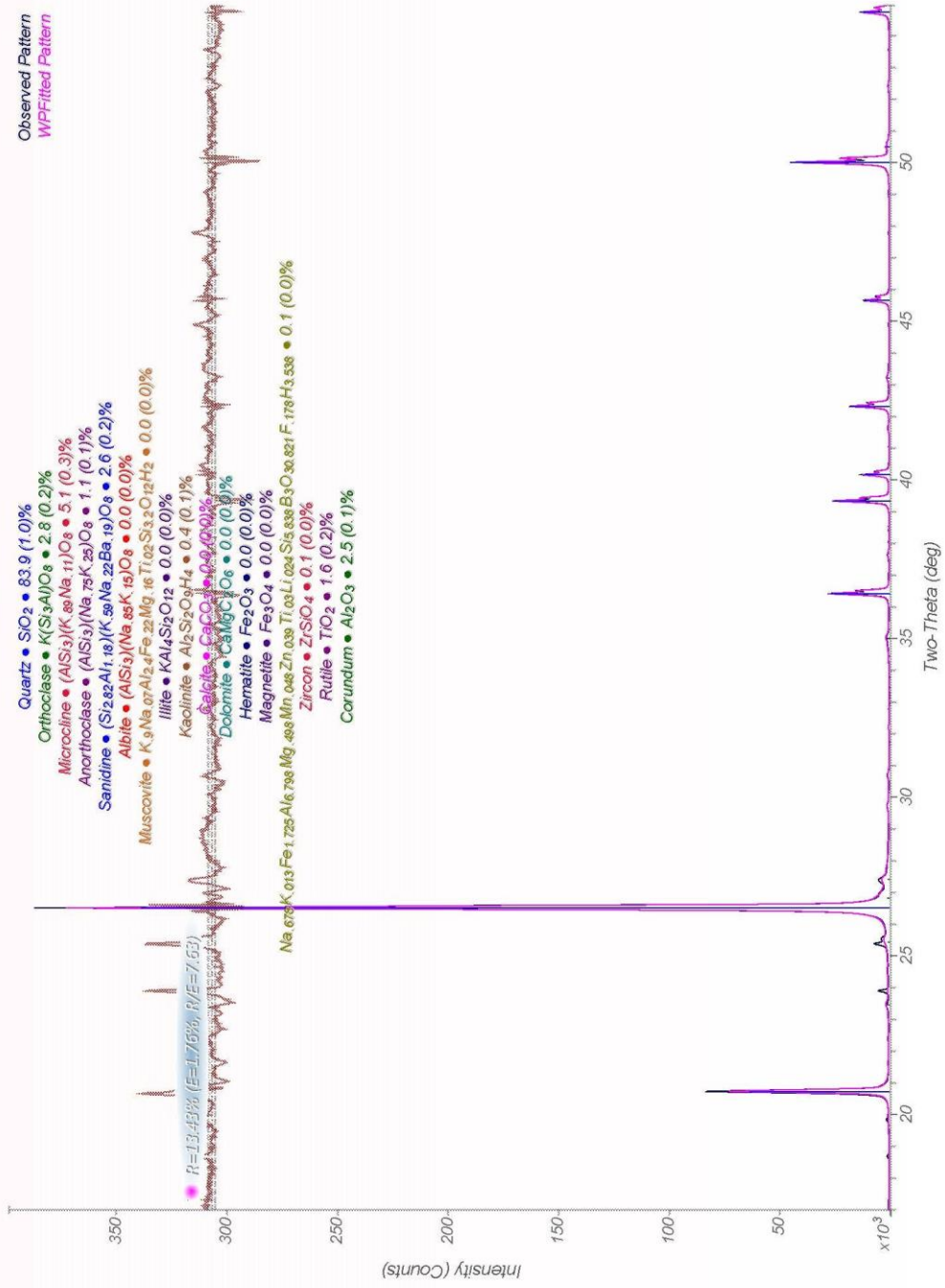
TM-1-26_exp.rtd

TM3-3-8

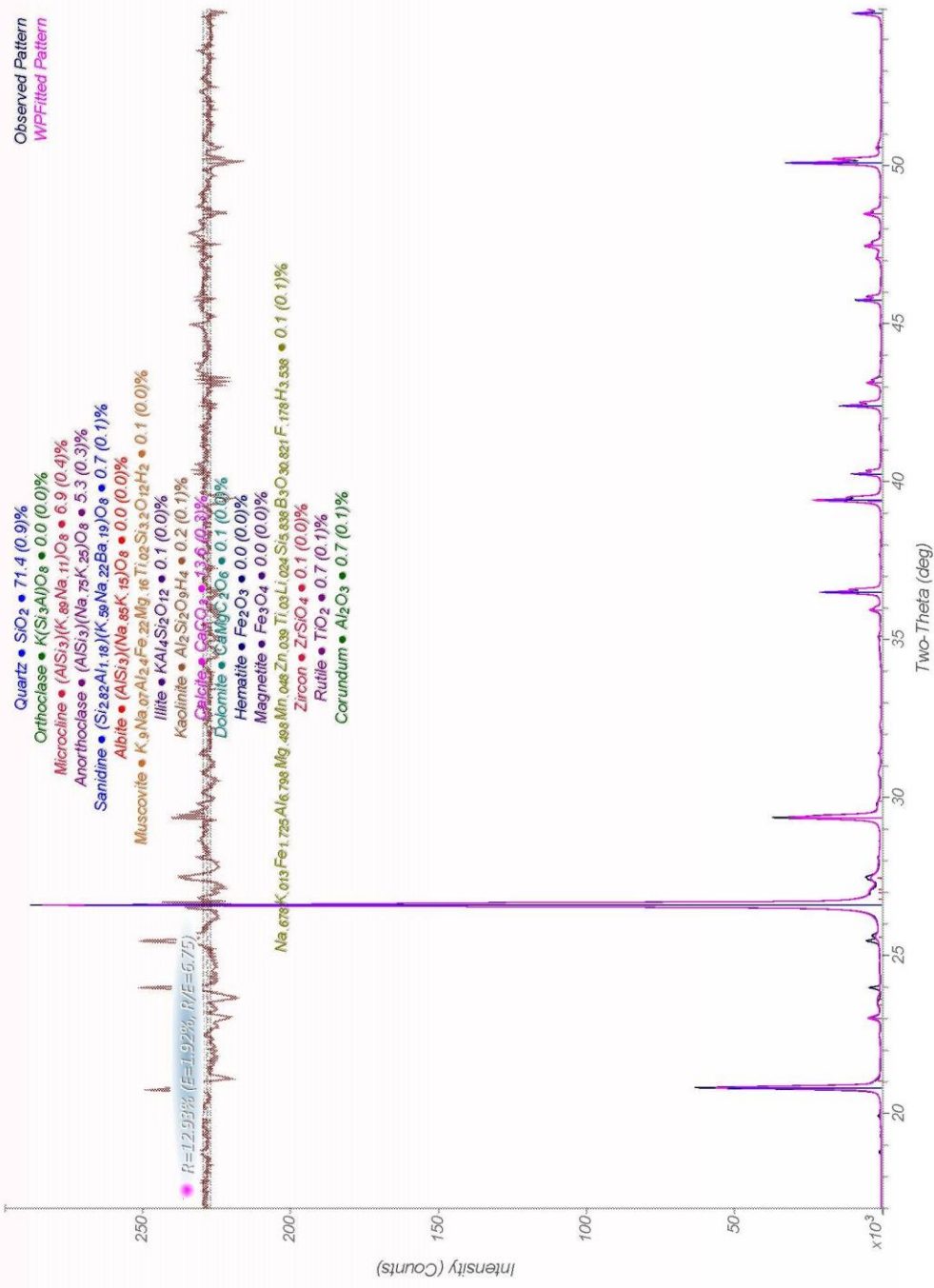


TM3-8-WR

ALC-03-D

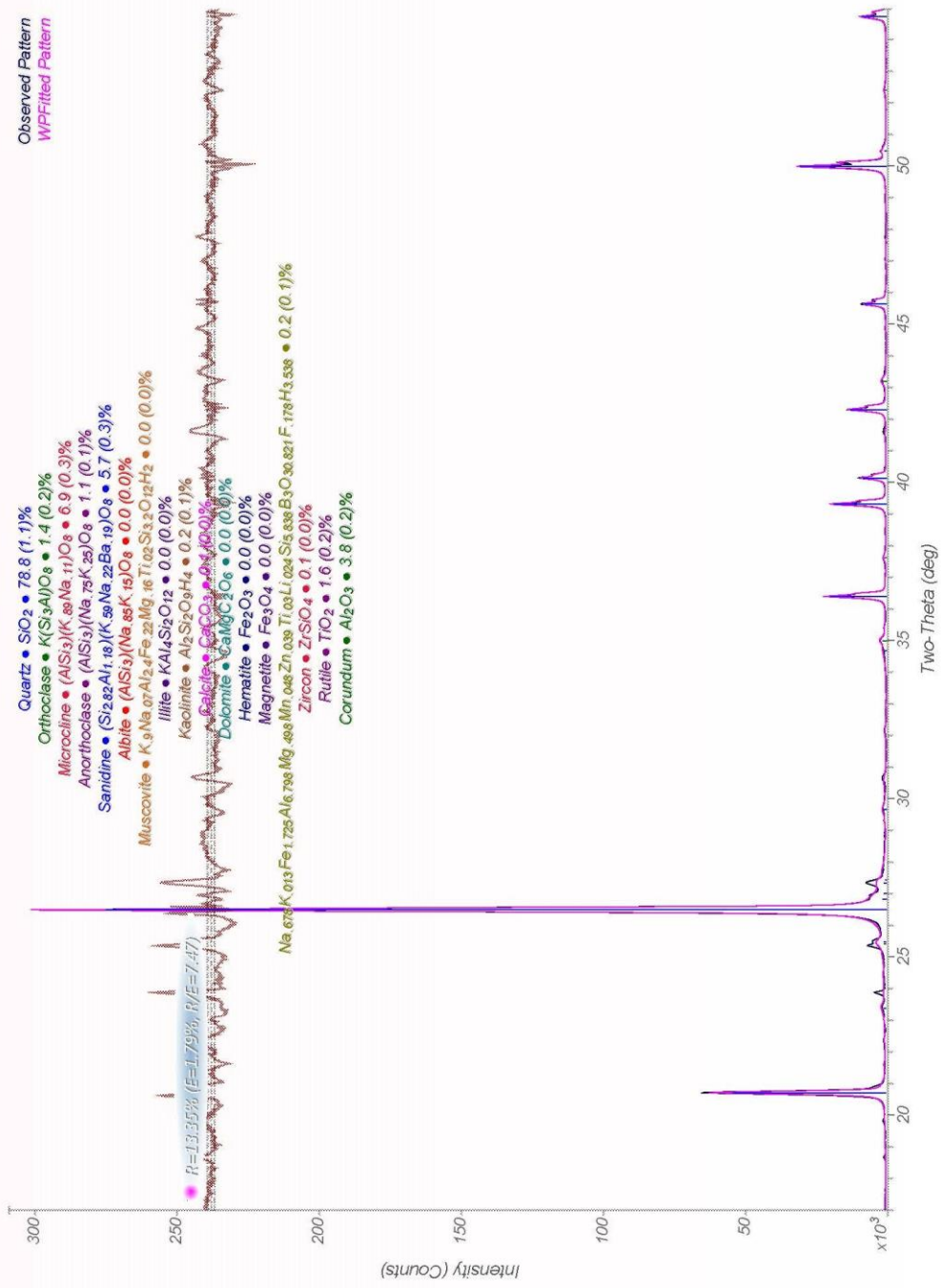


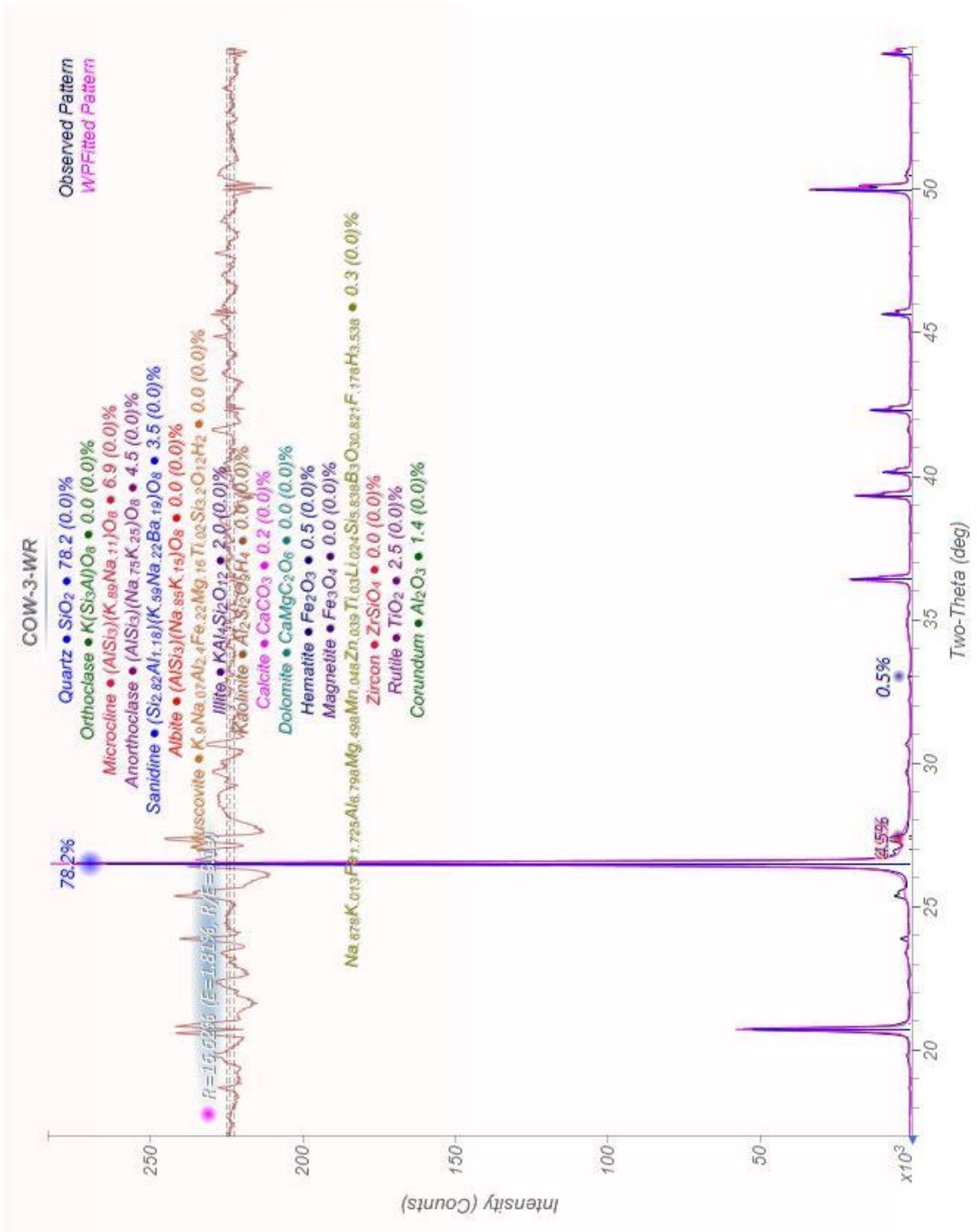
ALC-03-WR



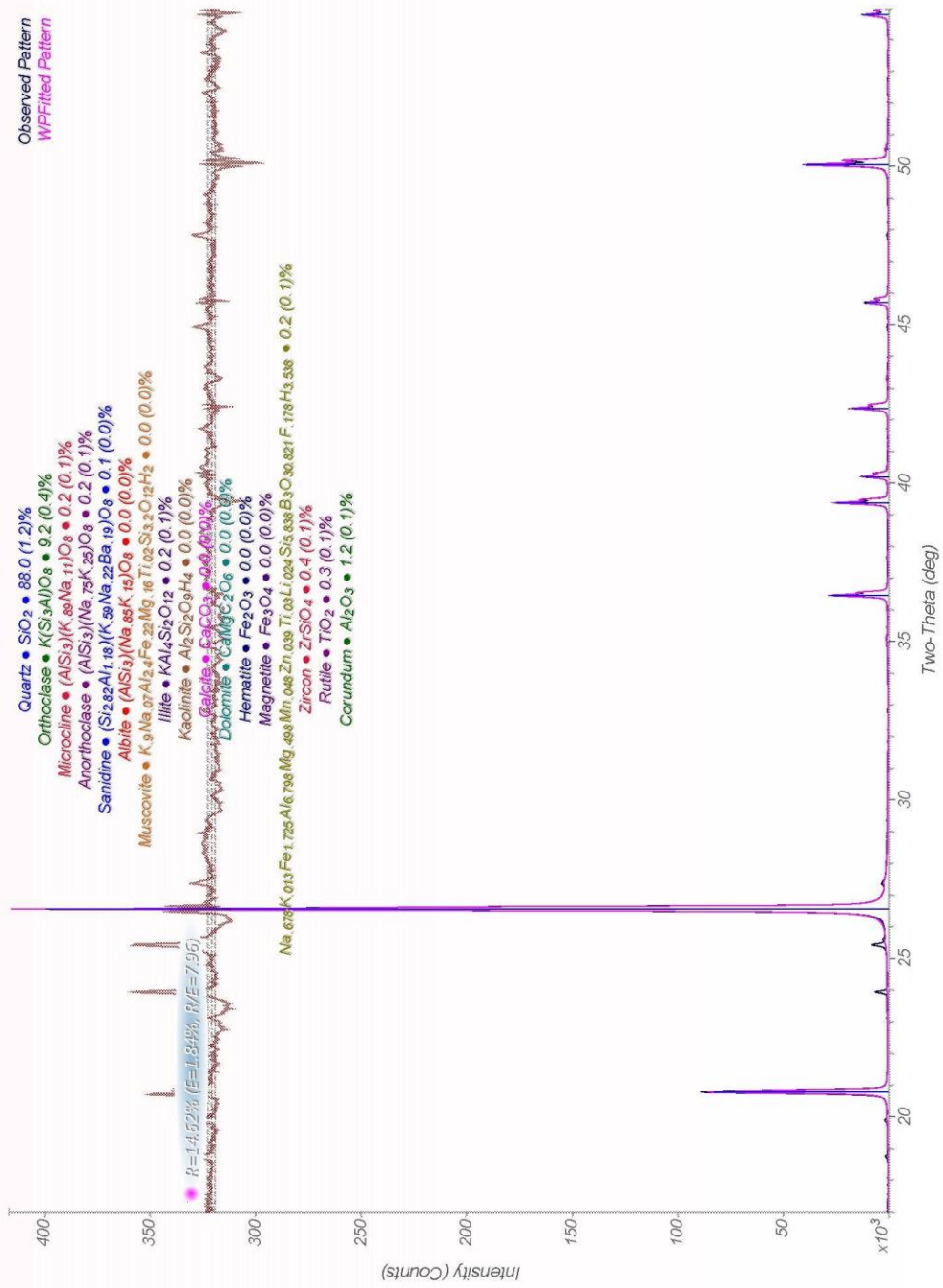
Loma Linda University

COW-3-D

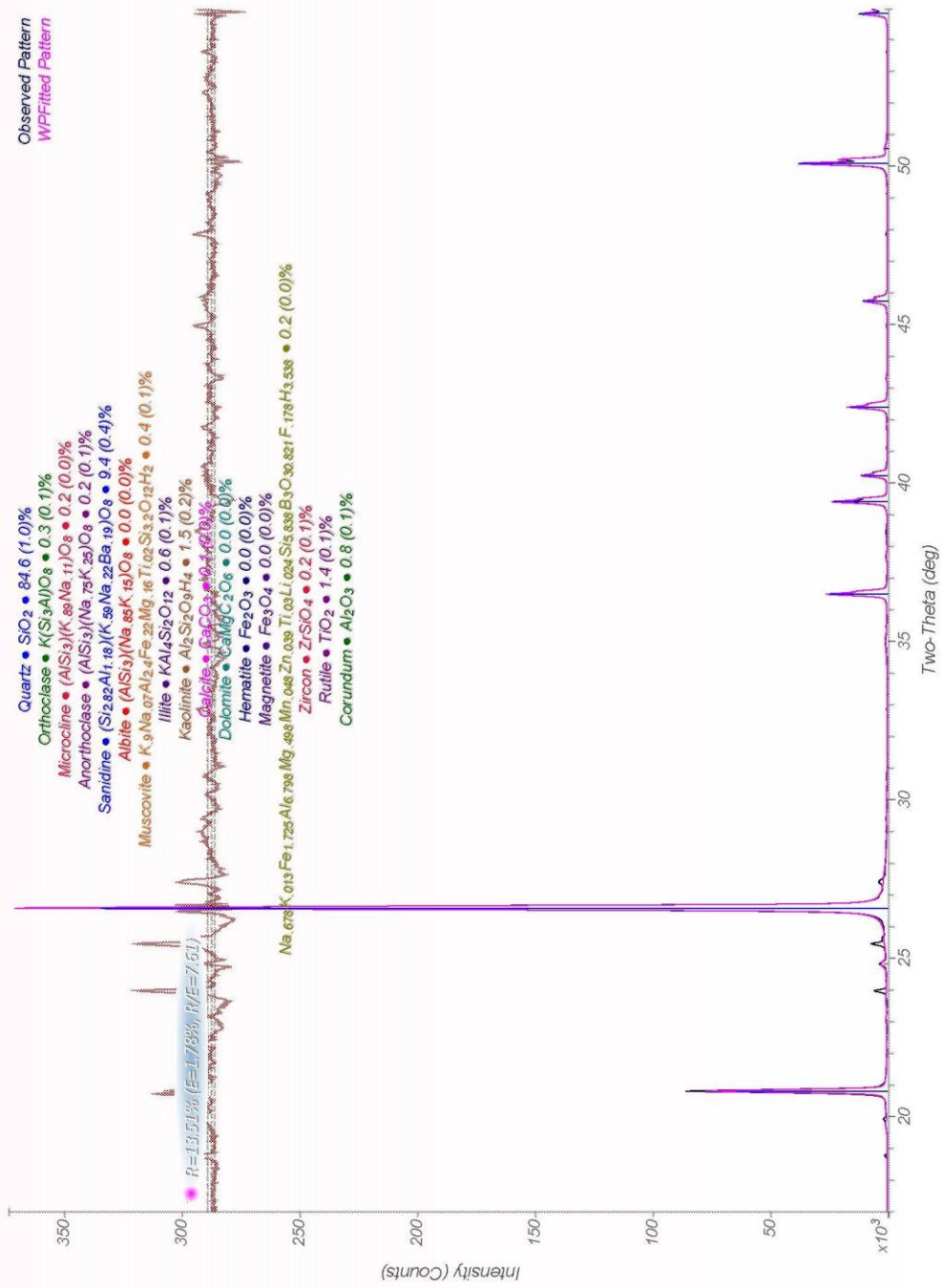




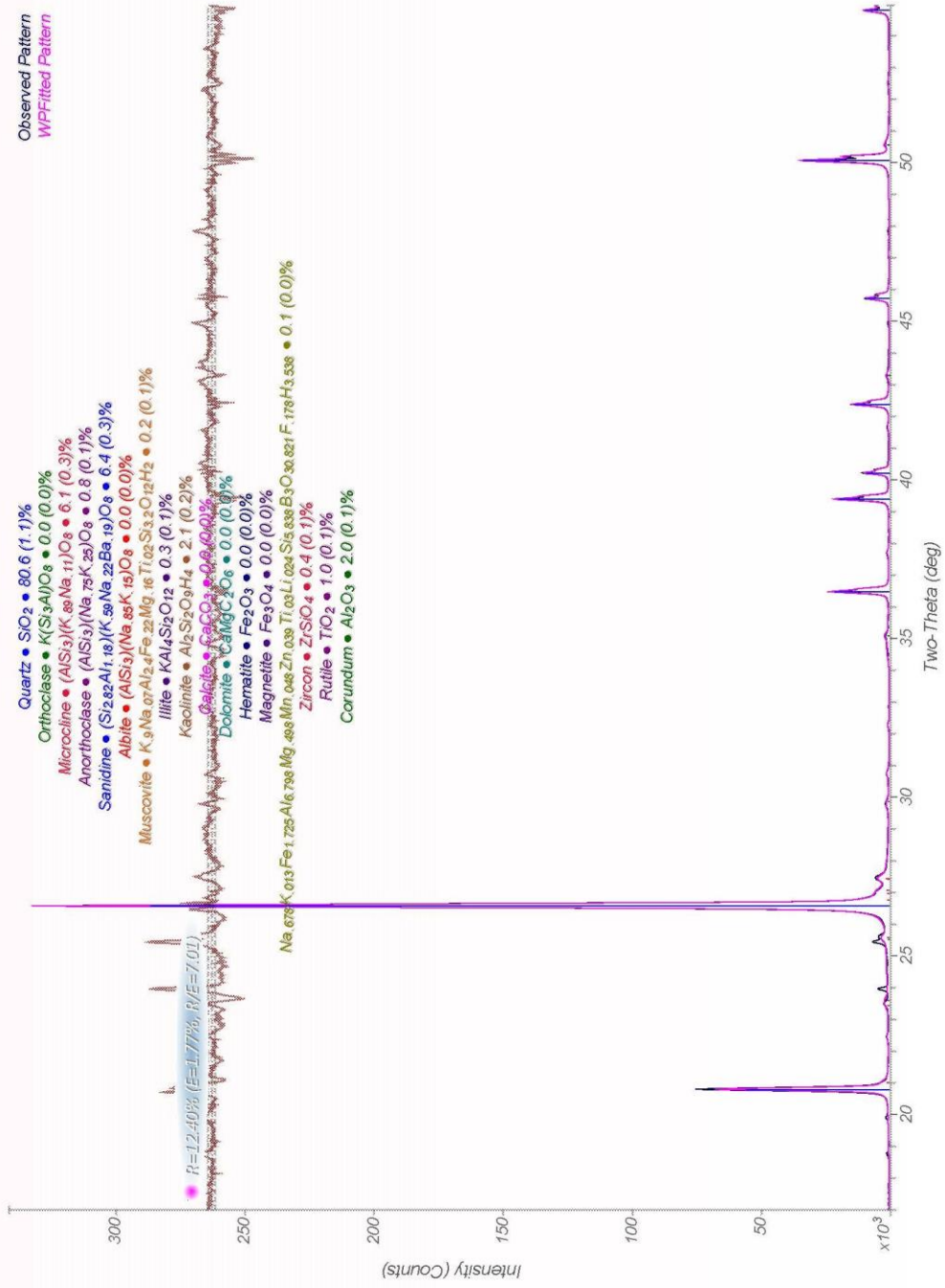
HMT-4D



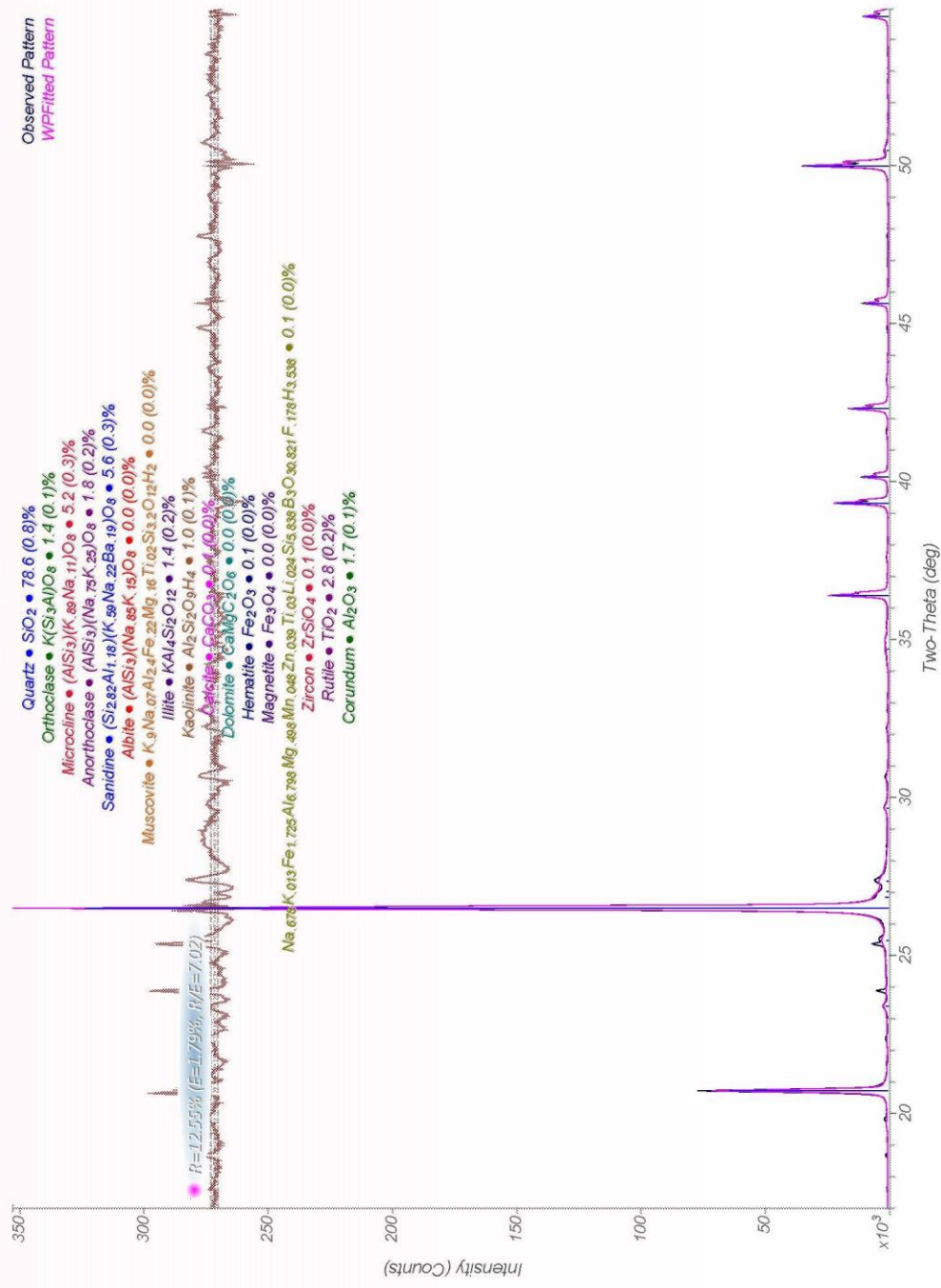
HMT-4-WR



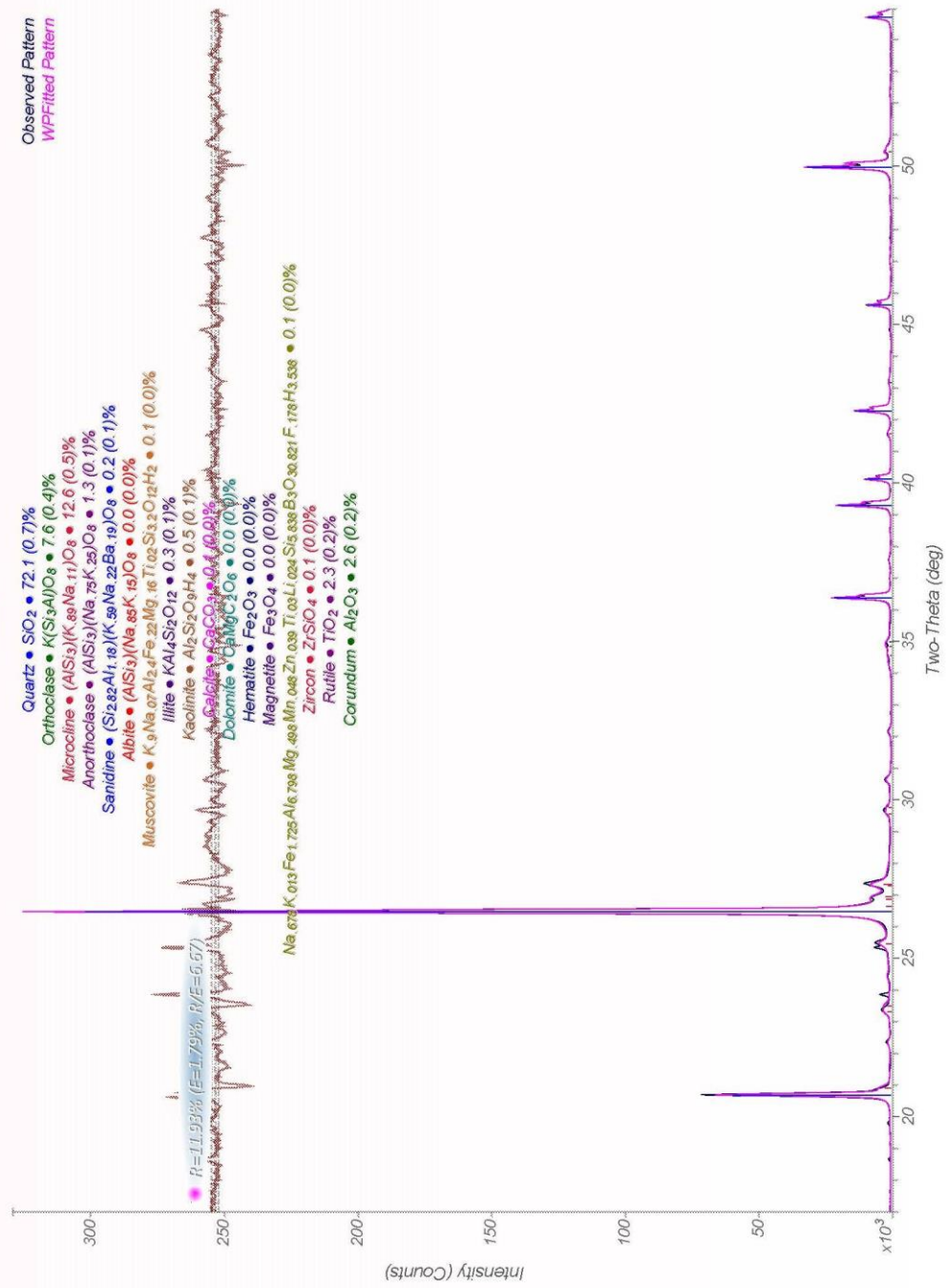
KIN-1-D



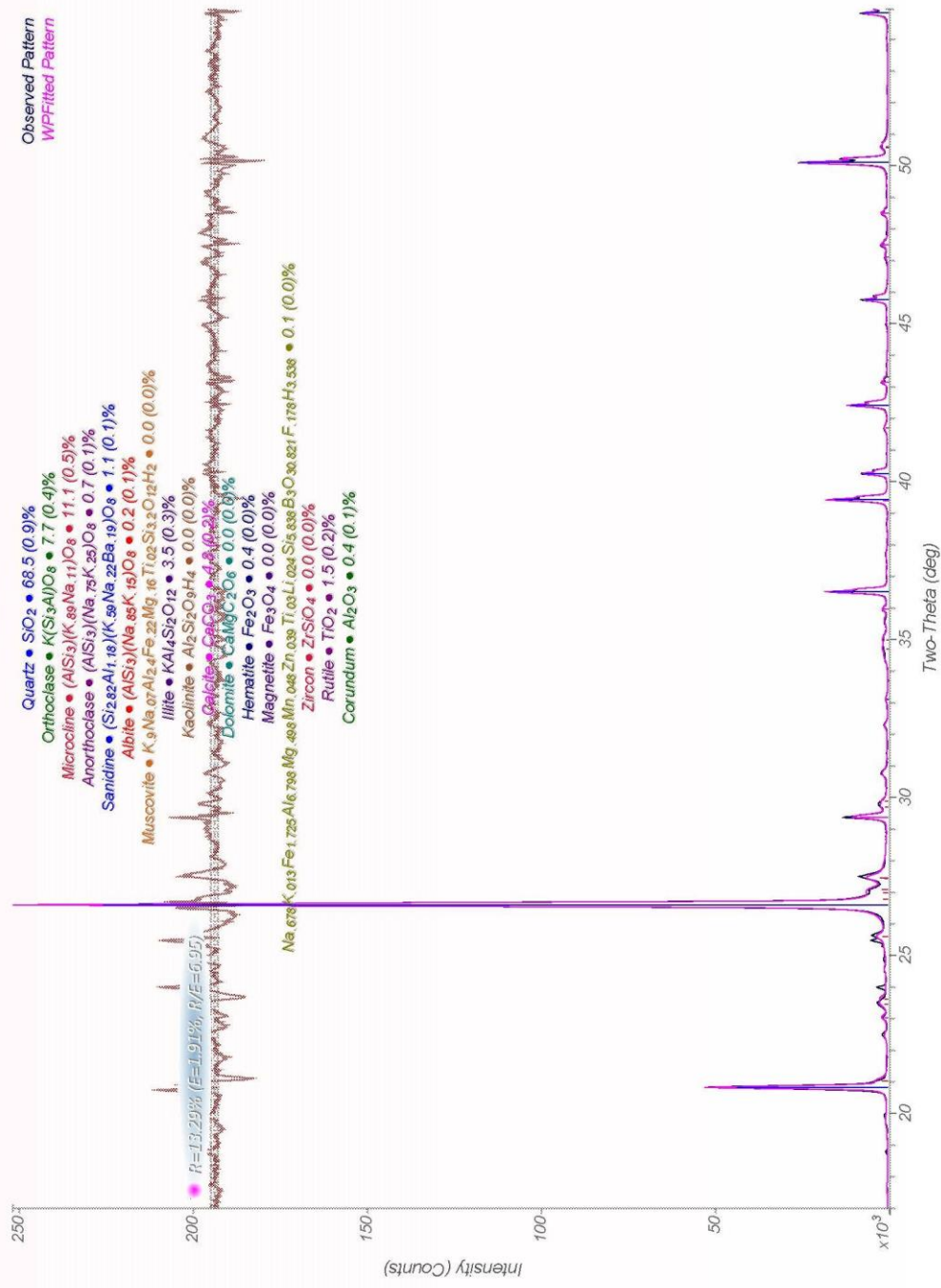
KIN-1-WR



KIN-2-D

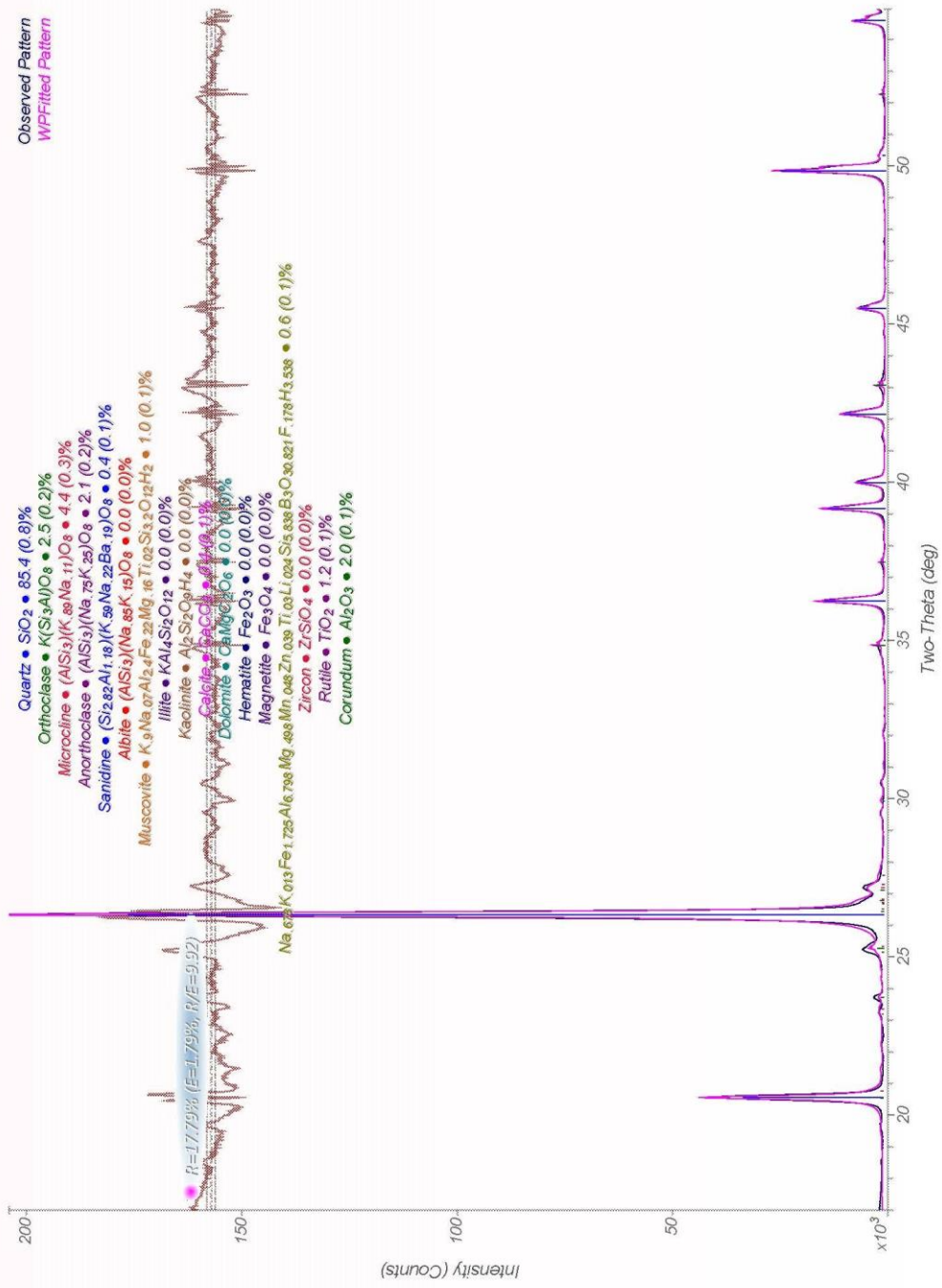


KIN-2-WR

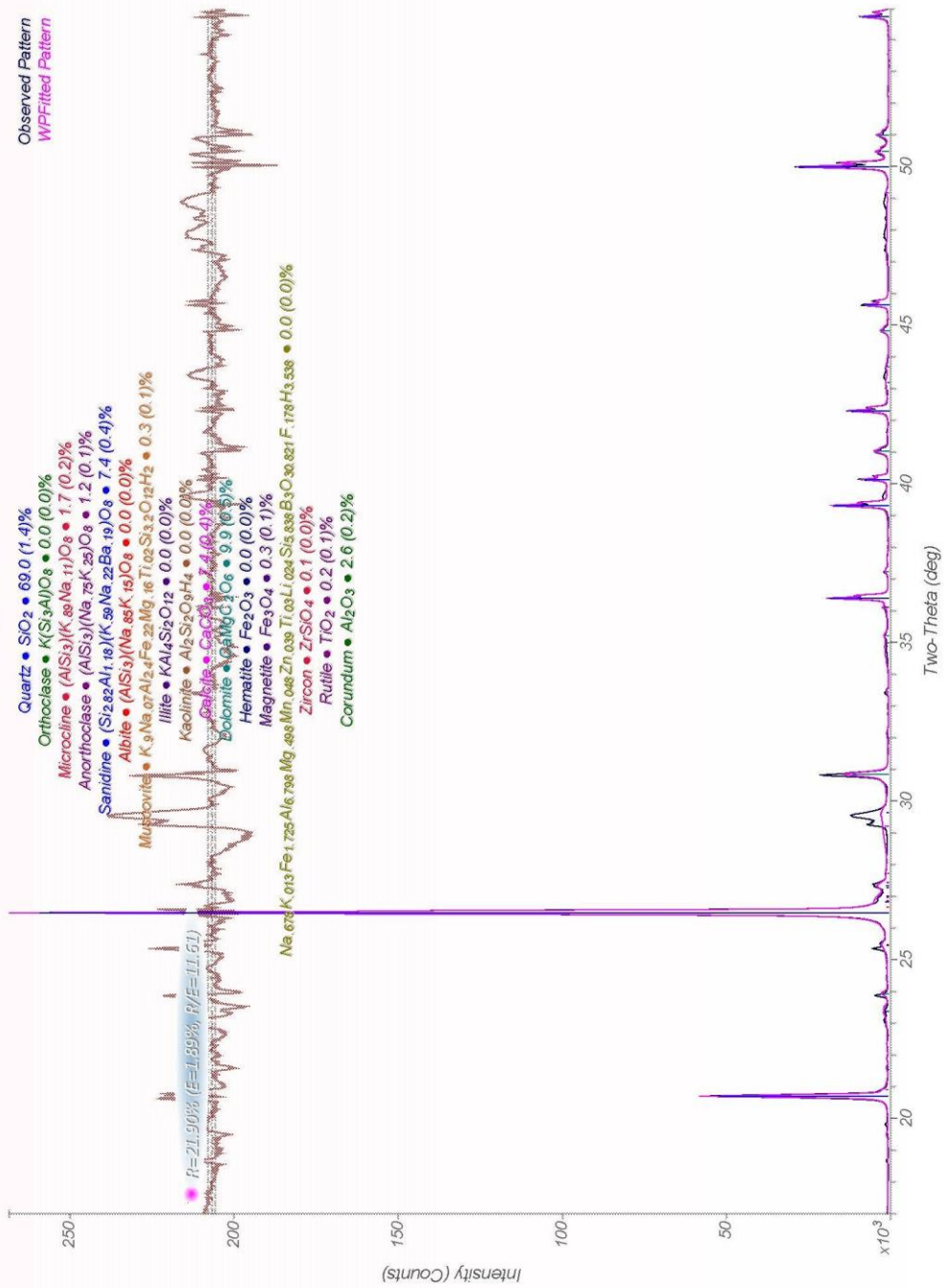


Loma Linda University

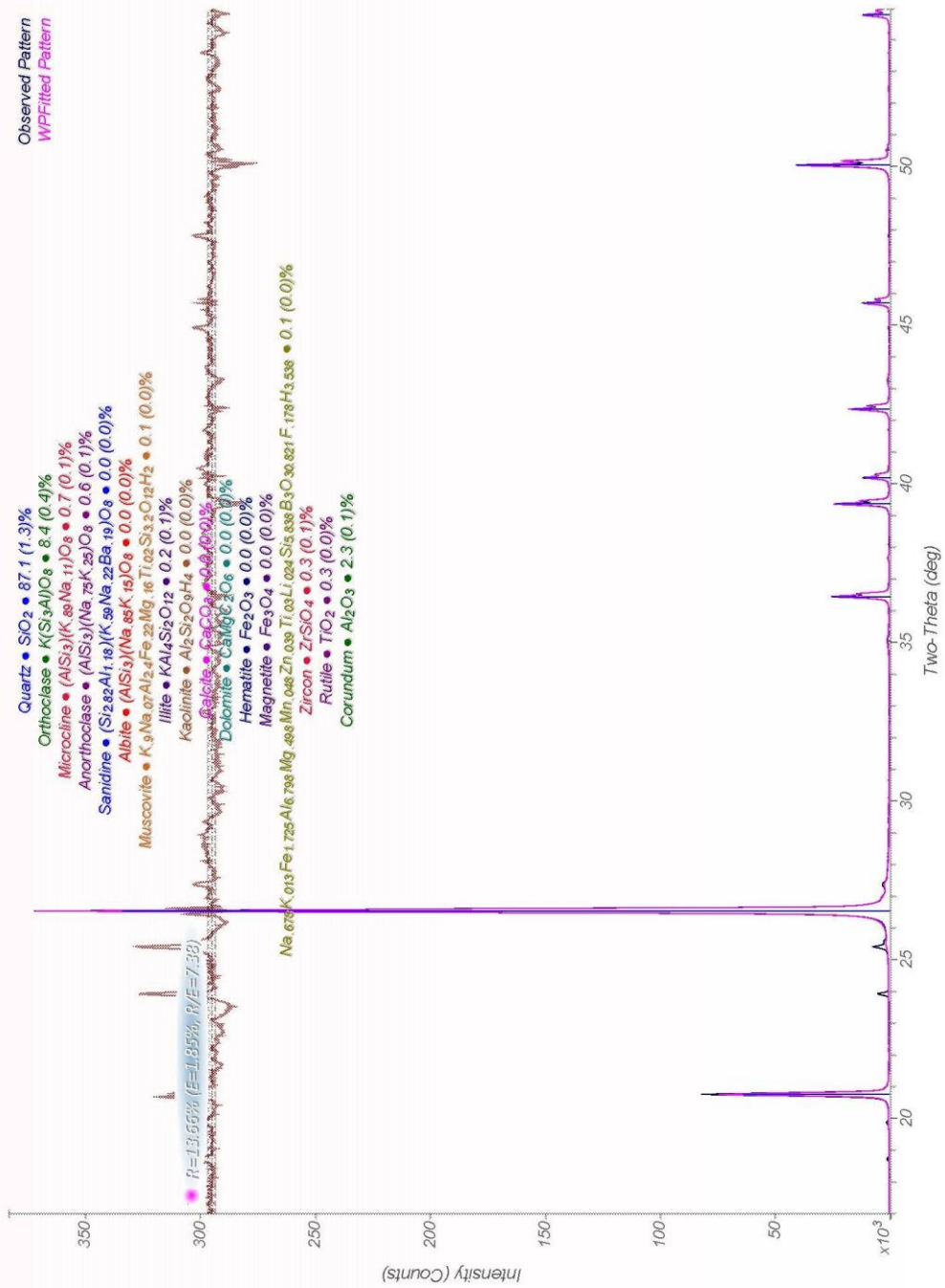
TEN-01-D

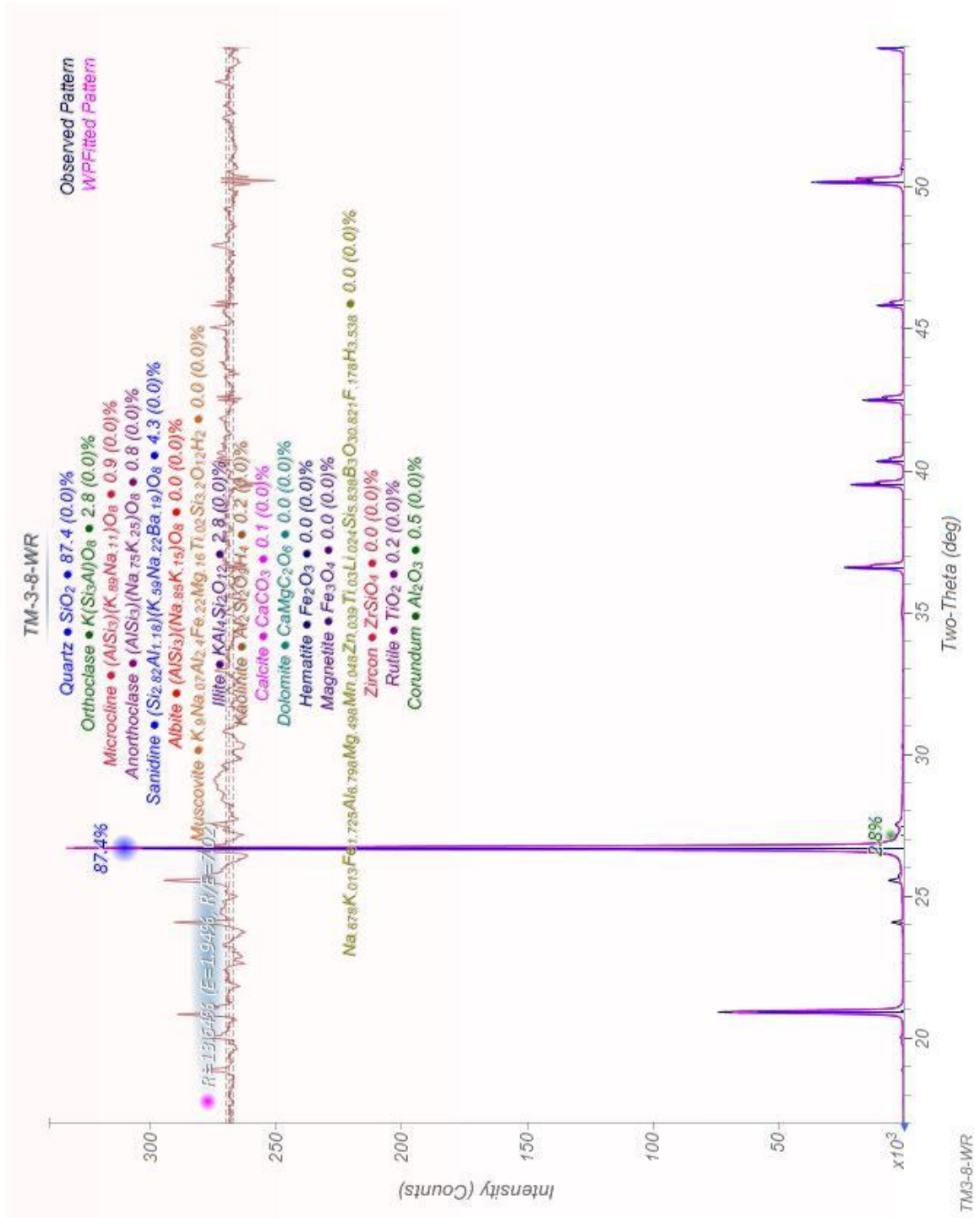


TEN-01-WR



TM-3-8-D





APPENDIX H

HIGH-RESOLUTION SCANS OF THIN SECTIONS

Thin sections were originally scanned at 4800 dpi, but the resolution has been lowered here (200 dpi) so that the images could be enlarged while maintaining reasonable file sizes.

Calcareous Rock and Materials

ASF-5-1 →

DC + FELD

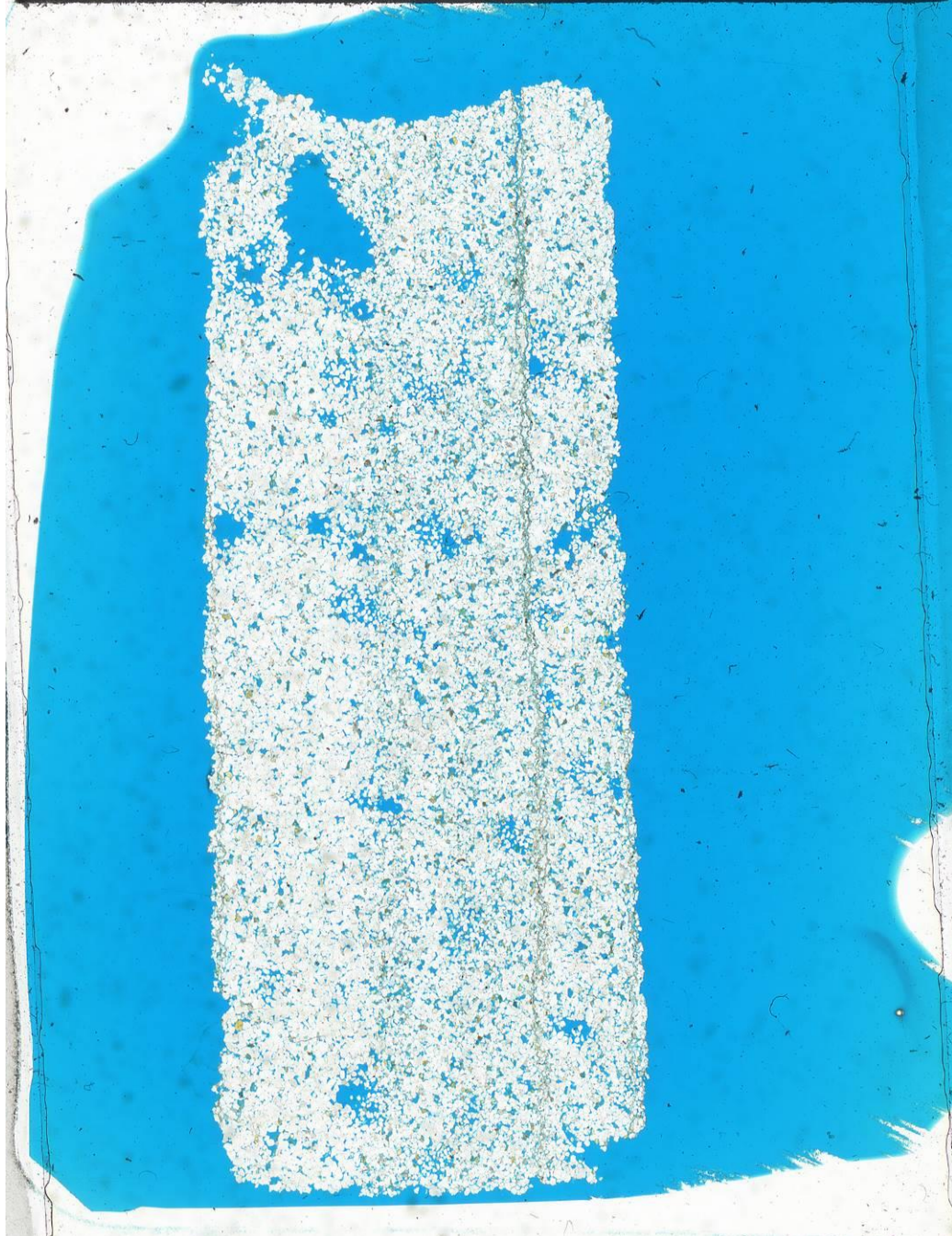


Calgary Rock and Materials

ASF-5-4



DC + FELD



Calgary Rock and Materials

ASF-5-5

DC + FELD



Calgary Rock and Materials

ASF-5-11

DC + FELD



Calgary Rock and Materials

ASF-5-12

DC + FELD



Calgary Rock and Materials

ASF-5-13

DC + FELD

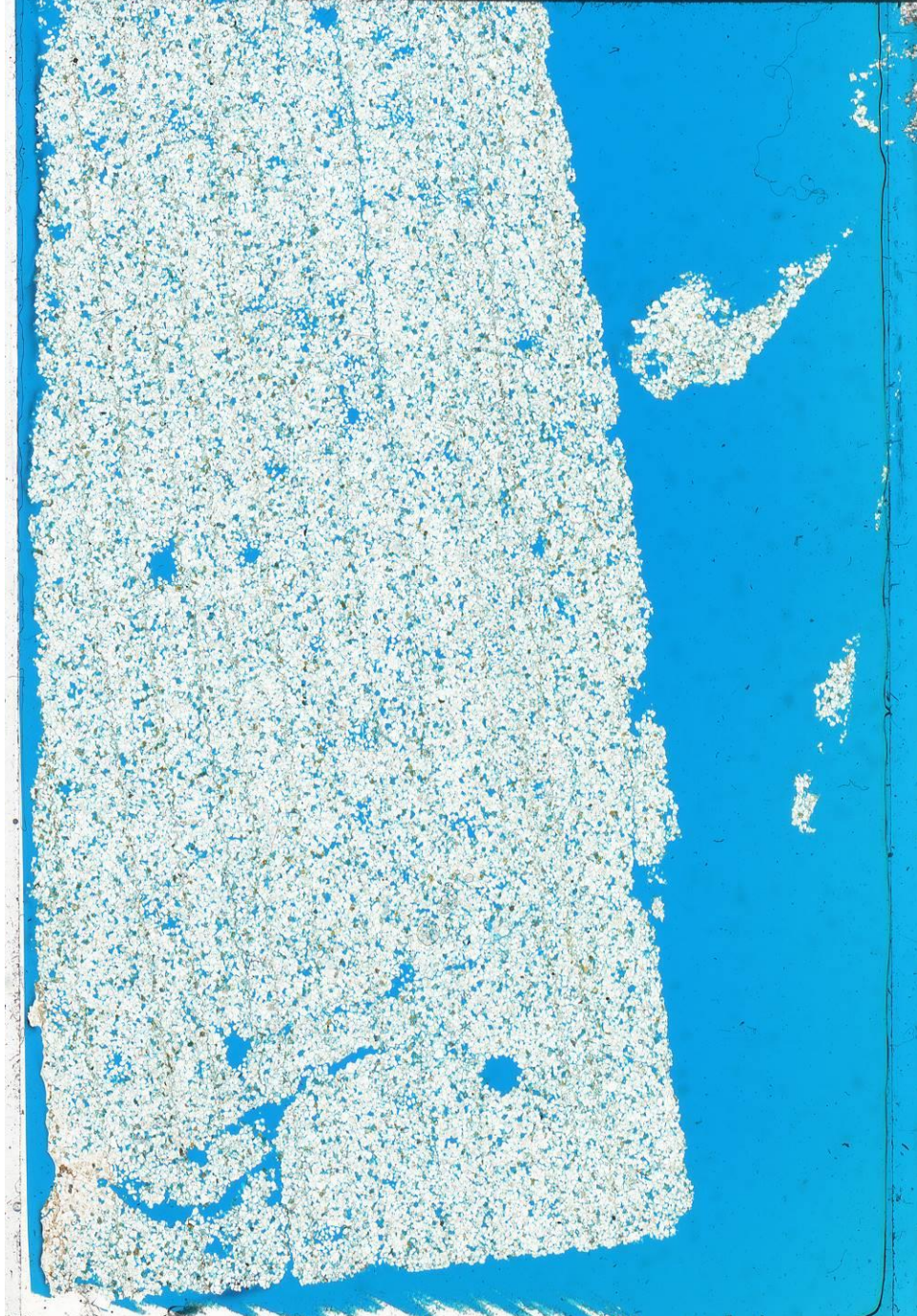


Calgary Rock and Materials

ASF-5-14



DC + FELD

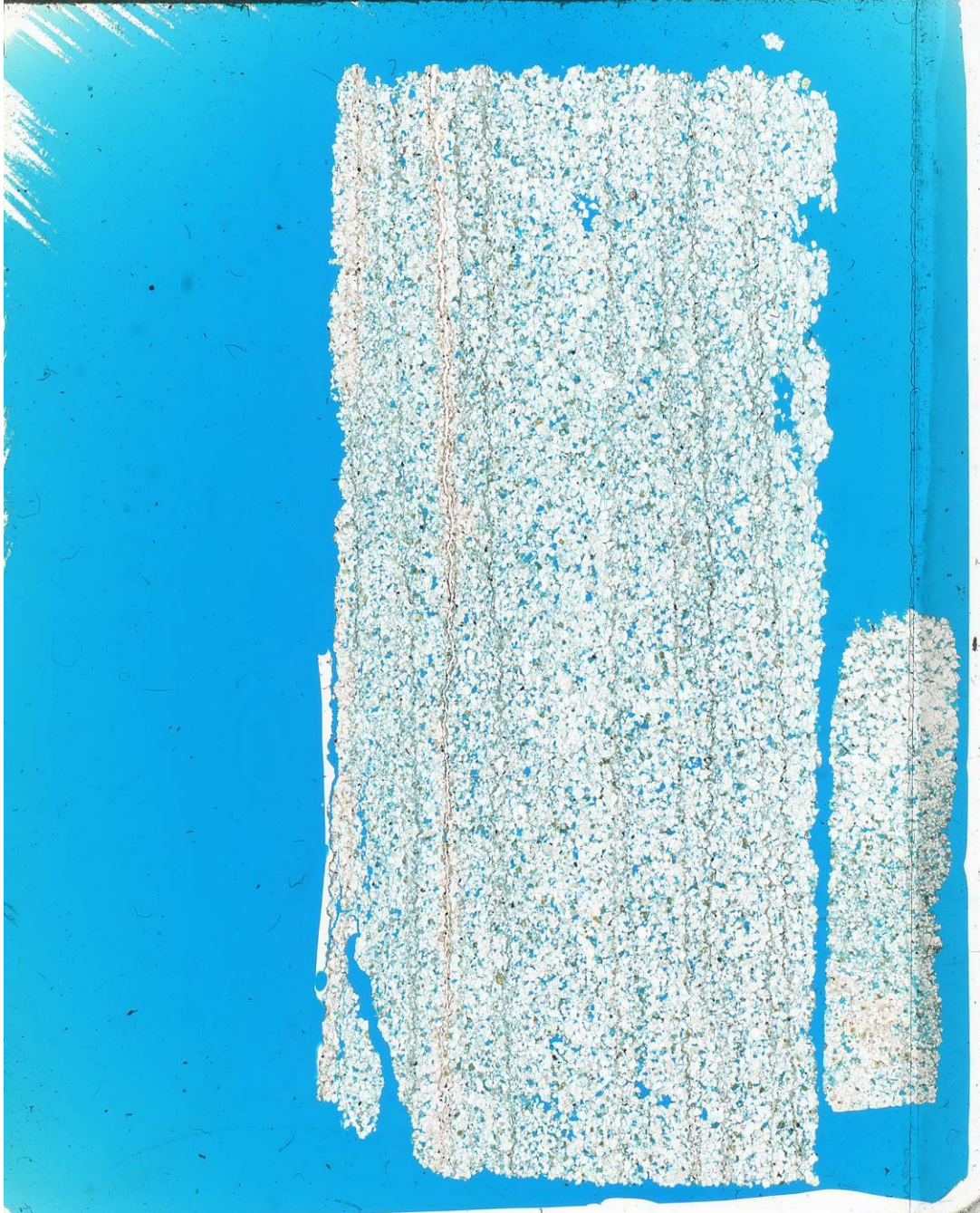


Calgary Rock and Materials

ASF-5-15



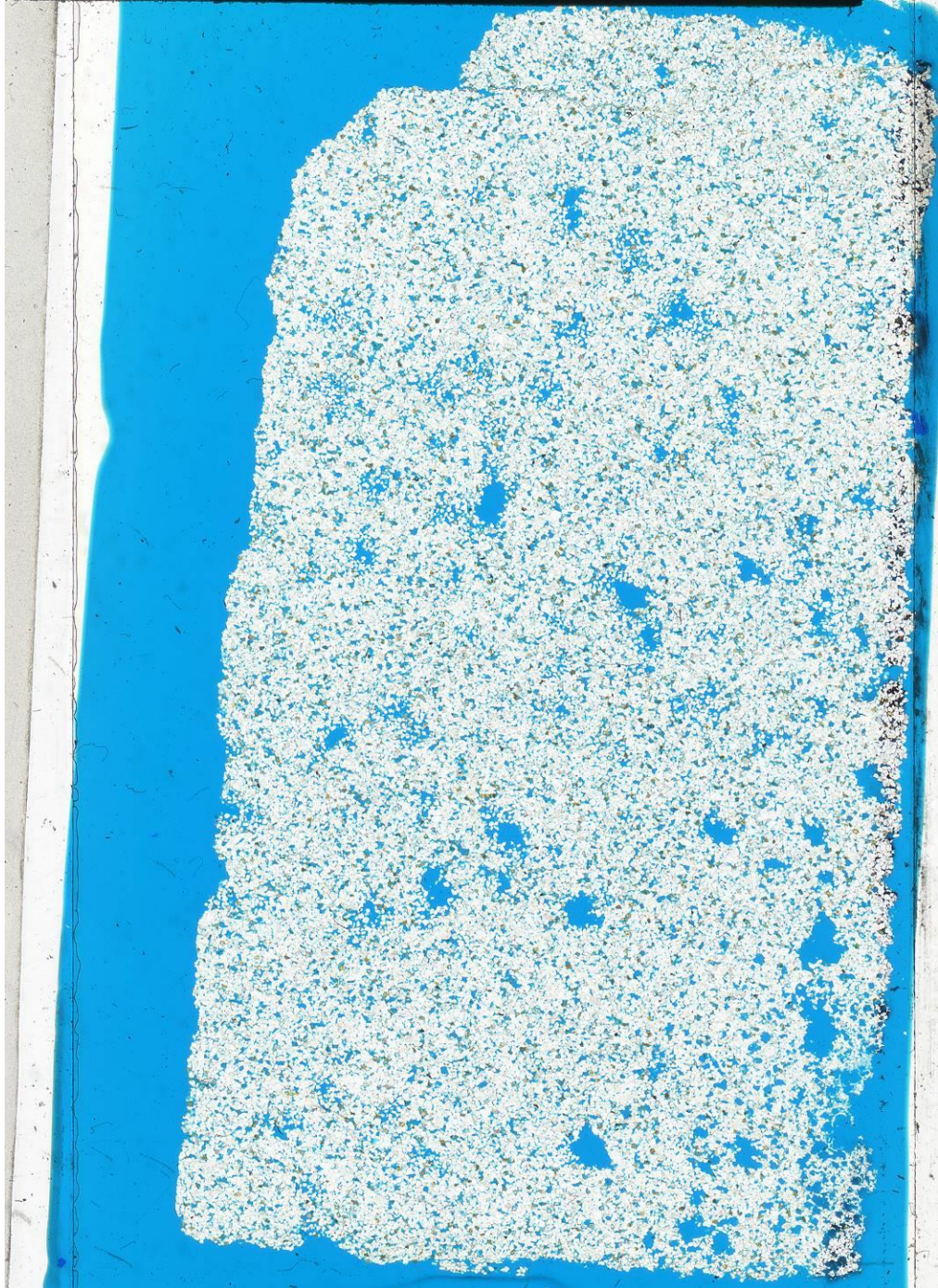
DC + FELD



Calgary Rock and Materials

ASF-5-16

DC + FELD

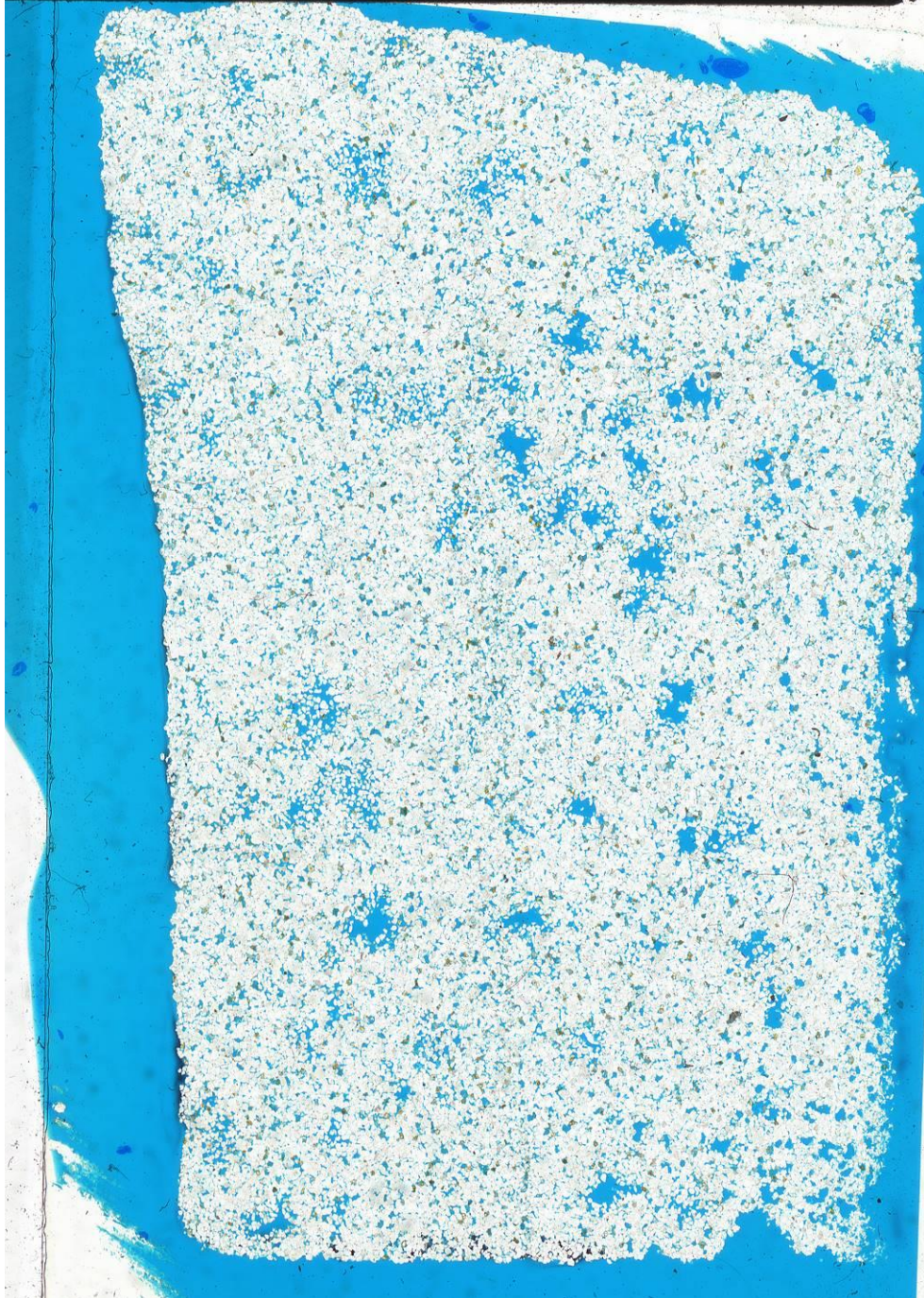


Calgary Rock and Materials

ASF-5-17



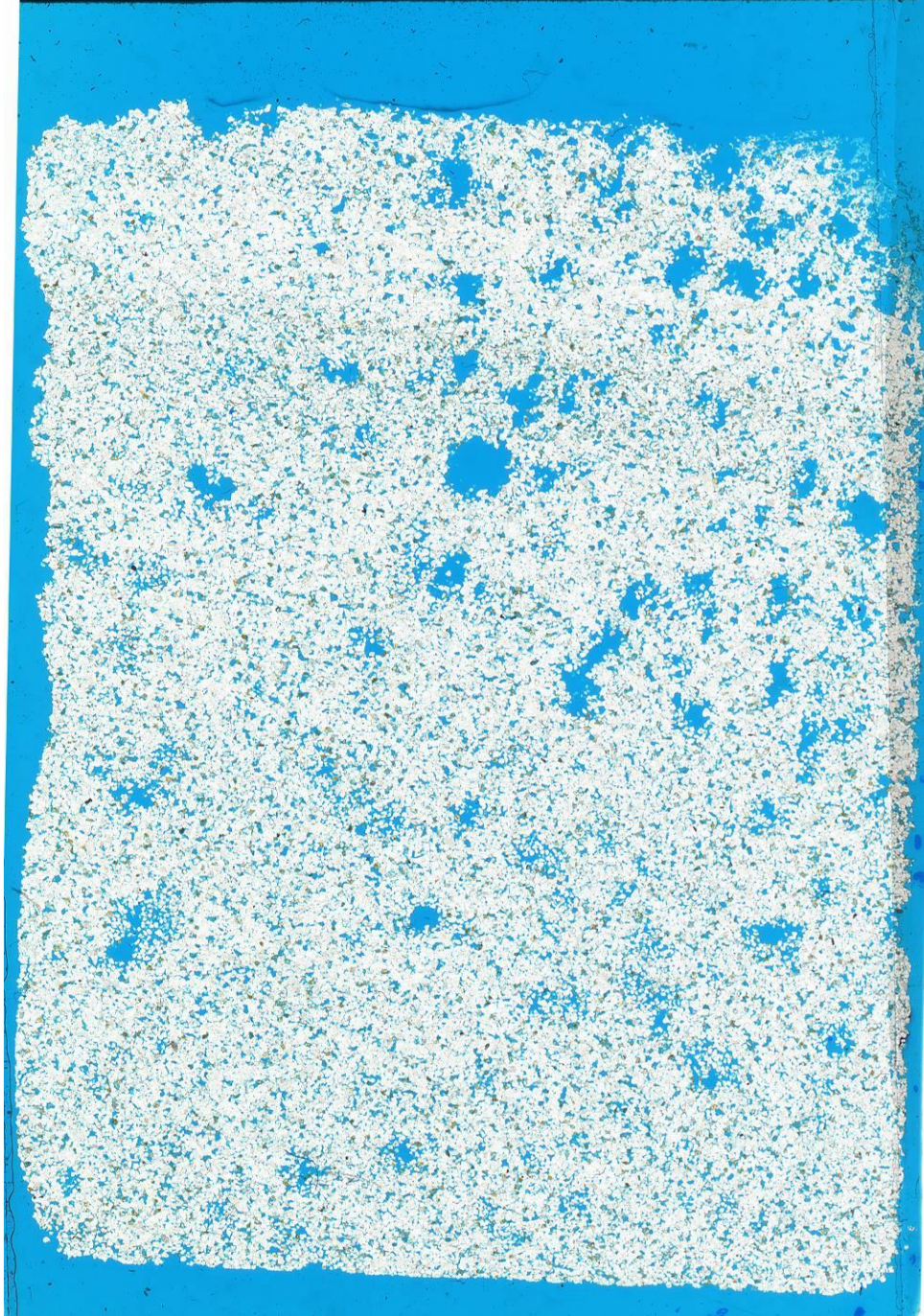
DC + FELD



Calgary Rock and Materials

ASF-5-19

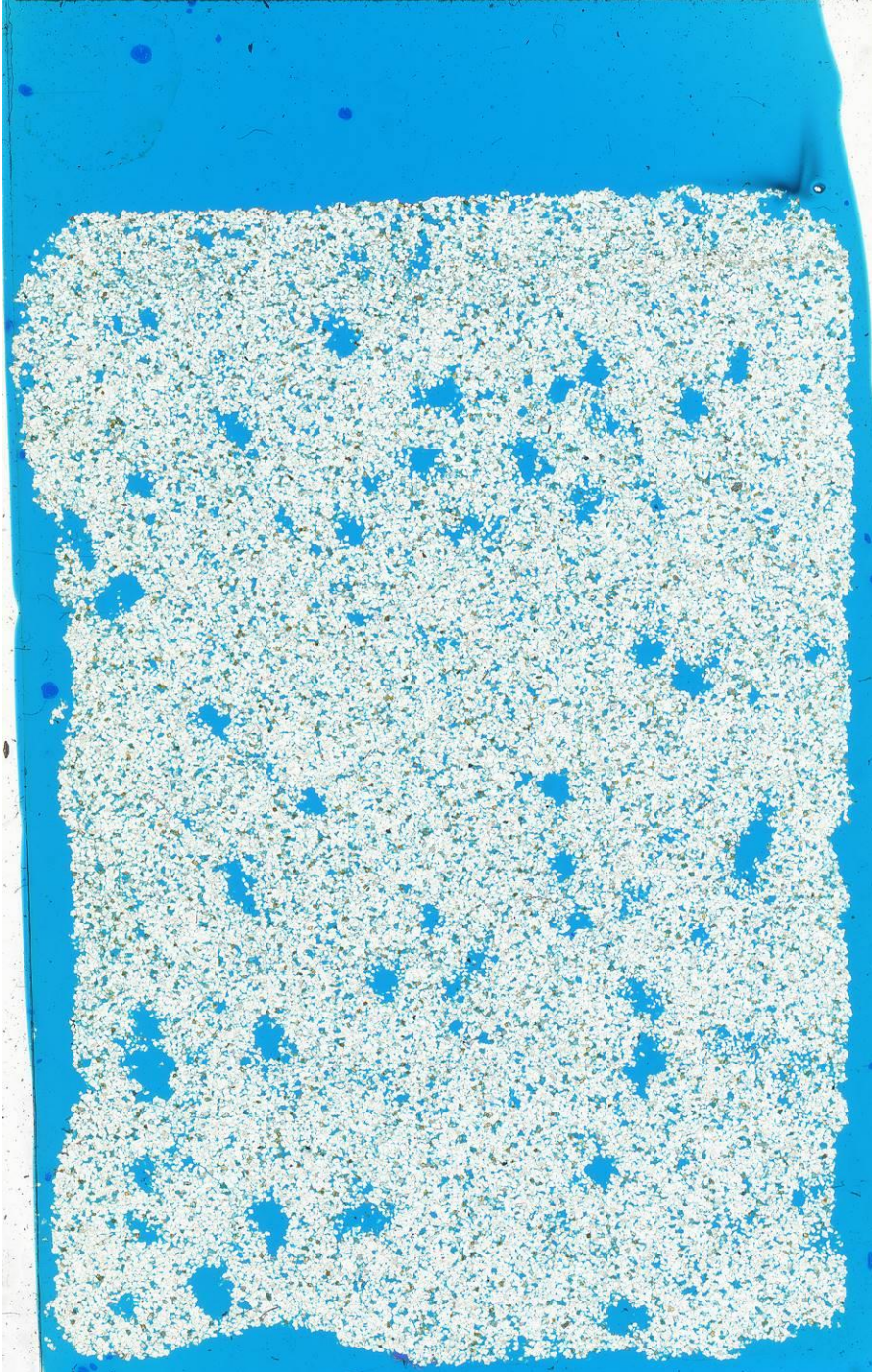
DC + FELD



Calgary Rock and Materials

ASF-5-20

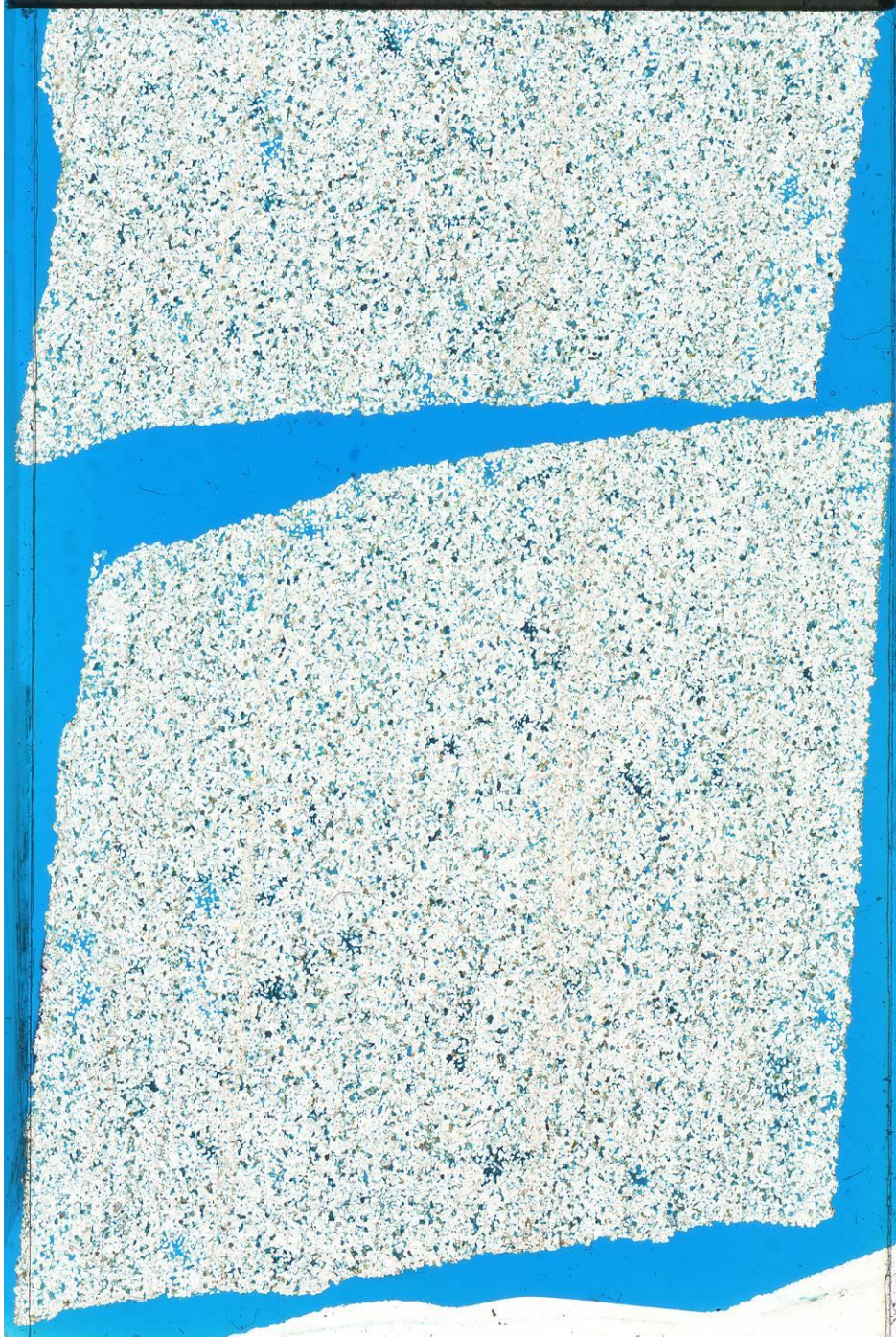
DC + FELD



Calgary Rock and Materials

ASF-5-21

DC + FELD →

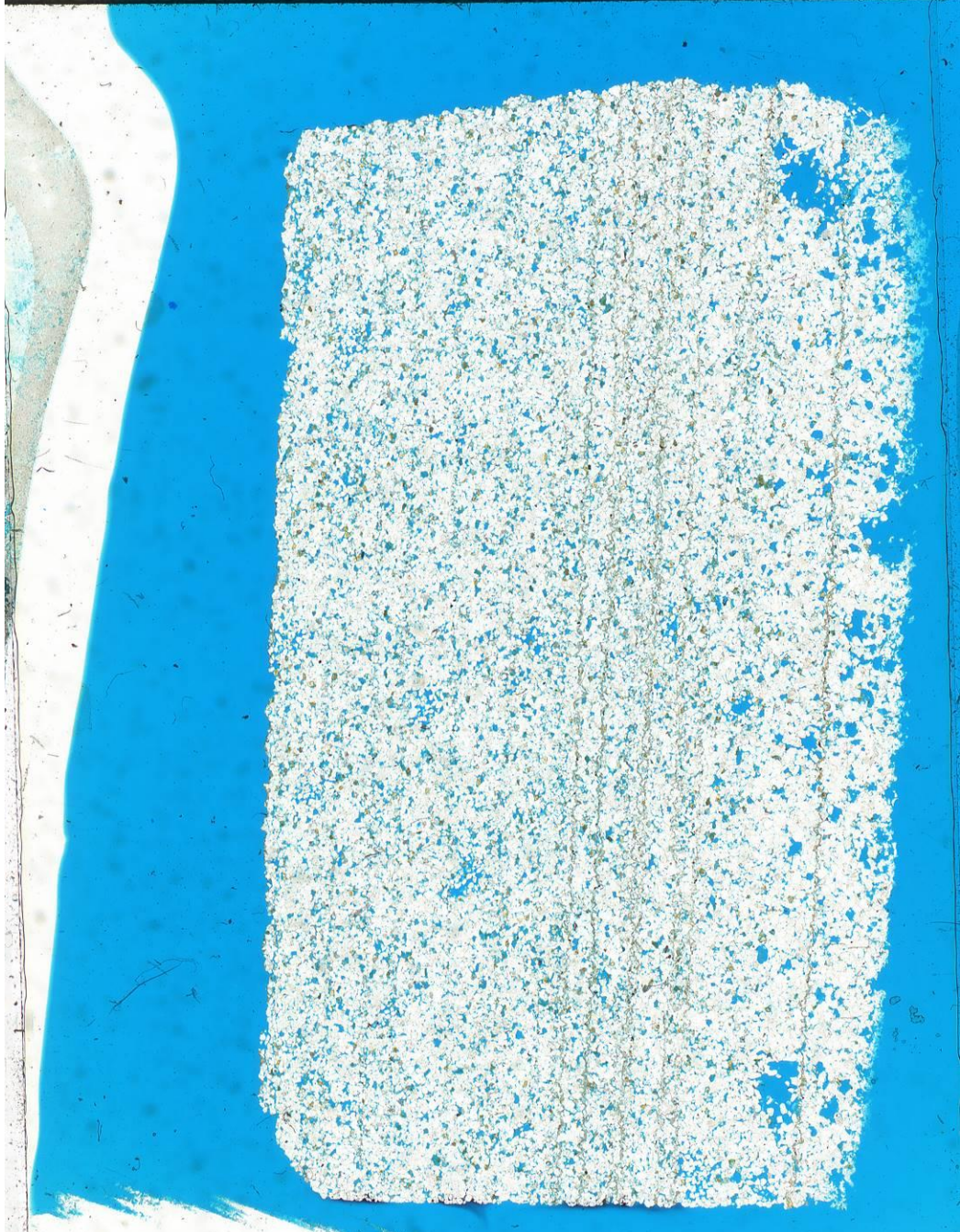


Calgary Rock and Materials

ASF-5-23



DC + FELD



Calgary Rock and Materials

ASF-5-24

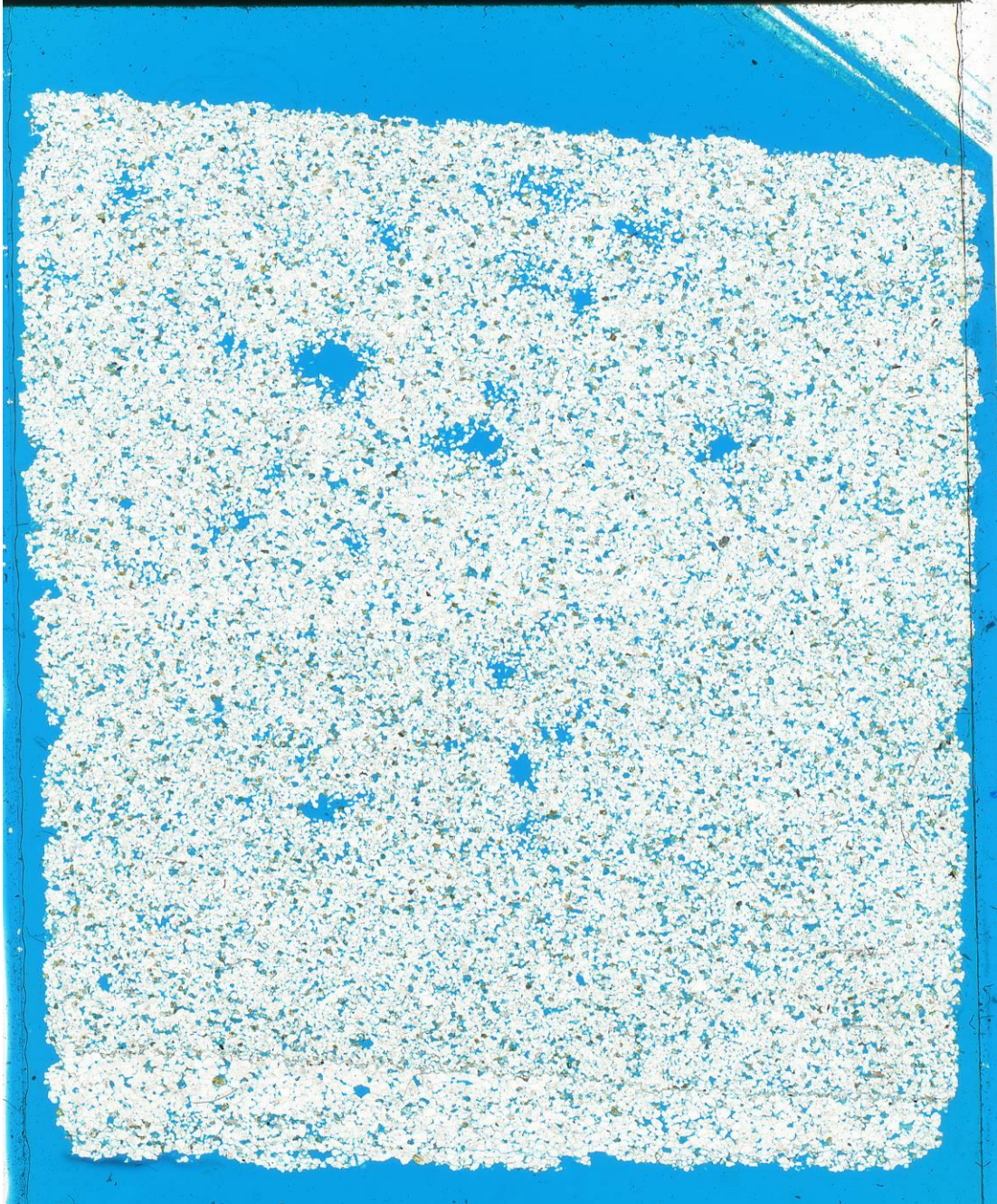
DC + FELD



Calgary Rock and Materials

ASF-5-25

DC + FELD



Calgary Rock and Materials

ASF-5-26

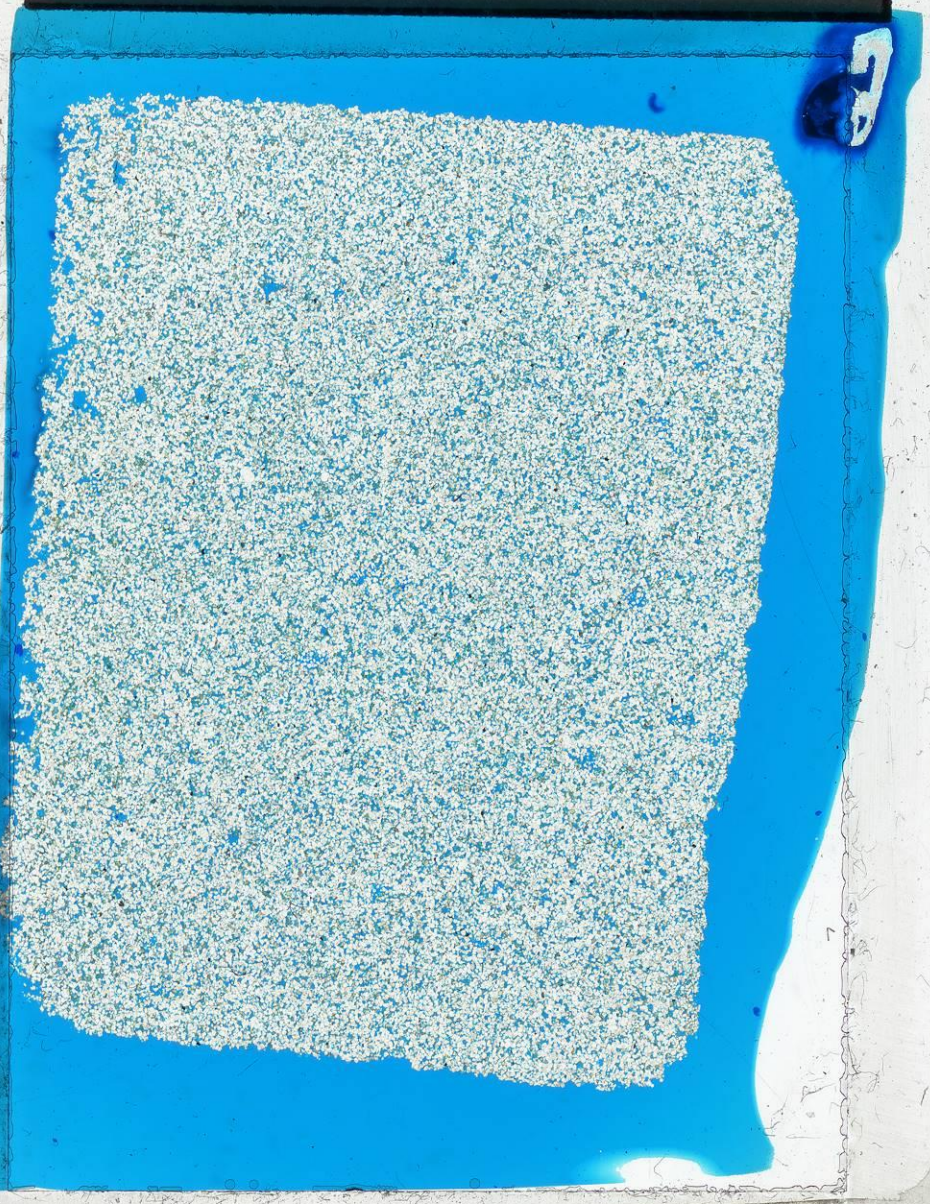
DC + FELD



Calgary Rock and Materials

ASF-22e-A

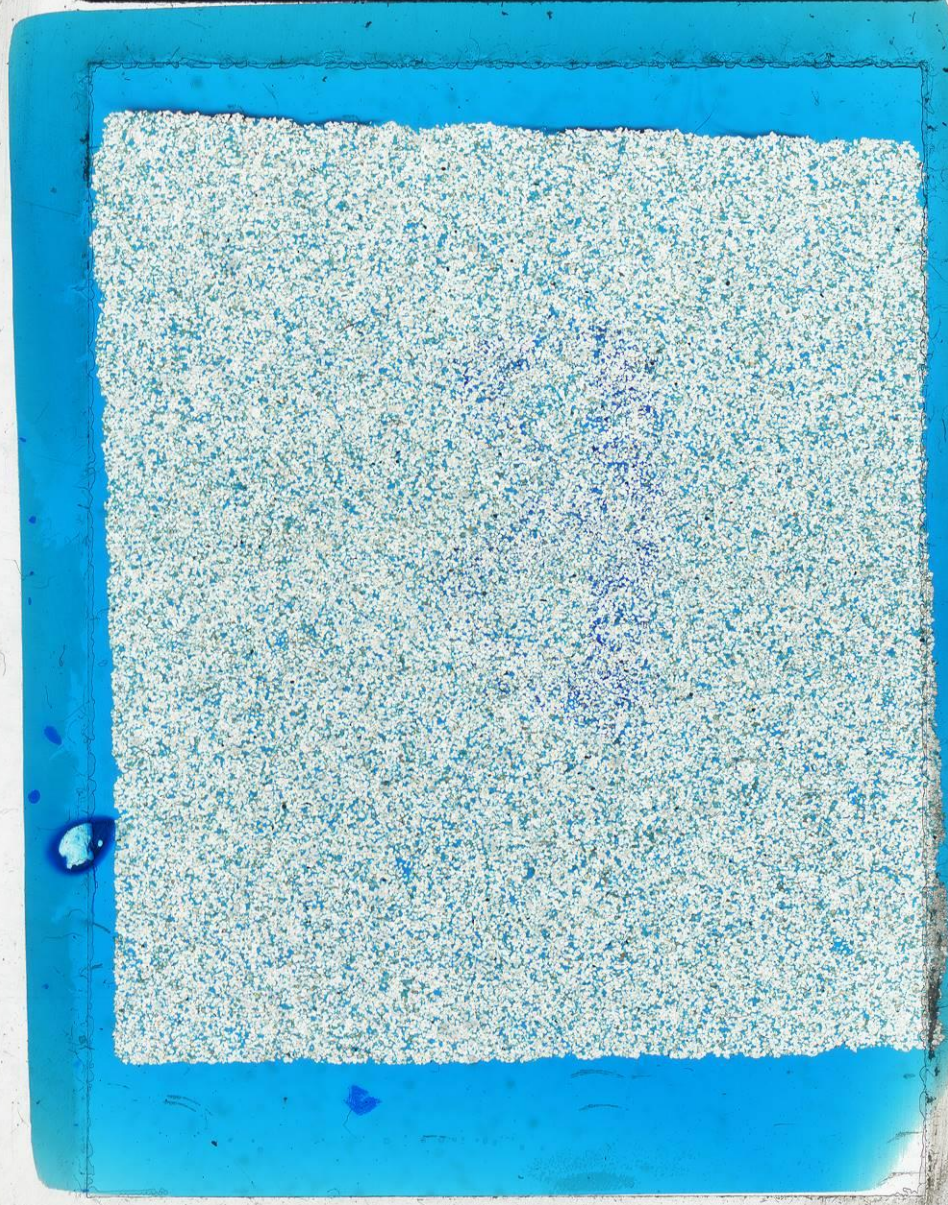
DC + FELD



Calgary Rock and Materials

ASF-22e-B

DC + FELD



Calgary Rock and Materials

ASF-22e-C

DC + FELD



Calgary Rock and Materials

ASF-22e-D

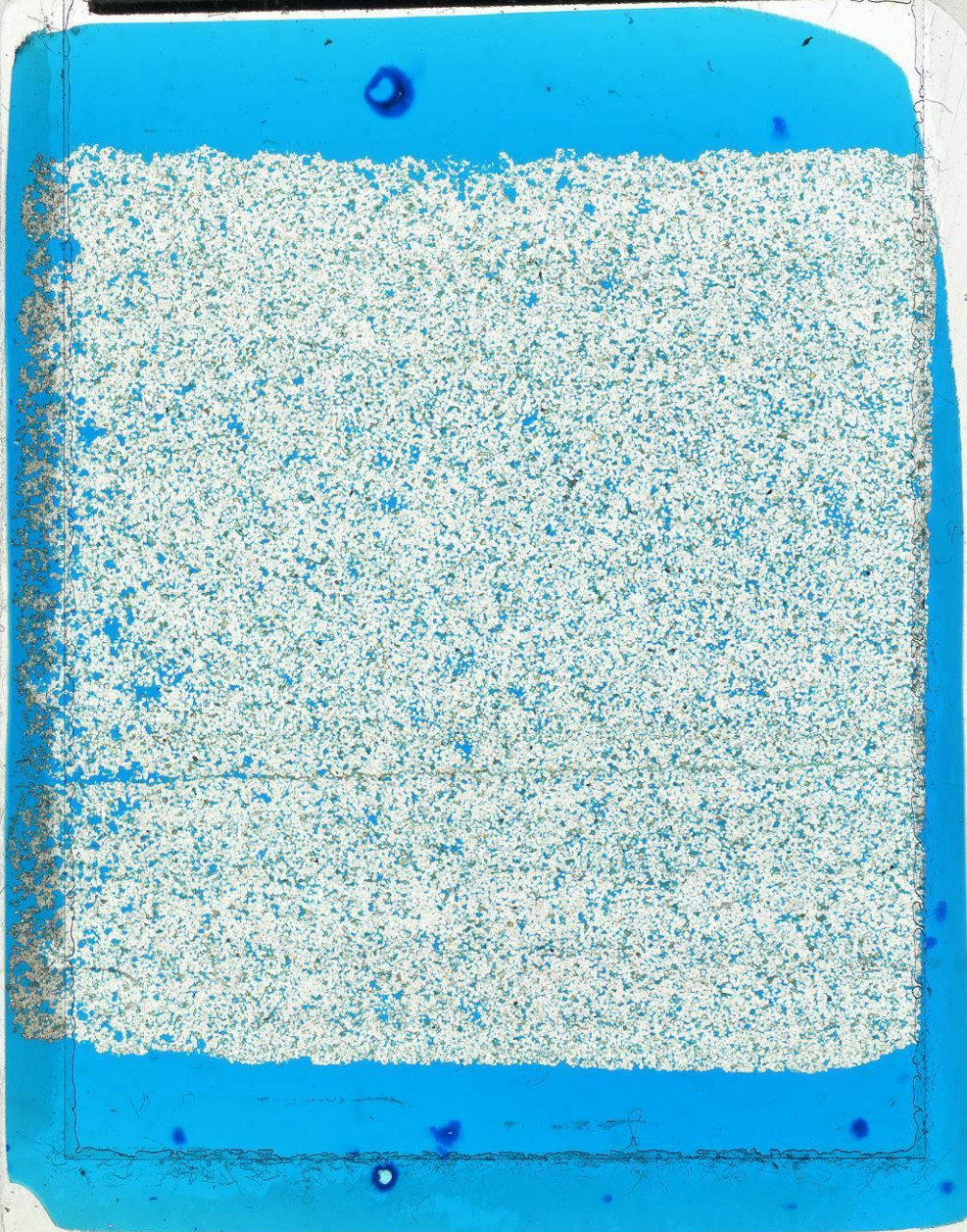
DC + FELD



Calgary Rock and Materials

ASF-22e-E

DC + FELD



Calgary Rock and Materials

ASF-22e-F

DC + FELD



Calgary Rock and Materials

ASF-22e-G



DC + FELD



Calgary Rock and Materials

ASF-22e-H
DC + FELD

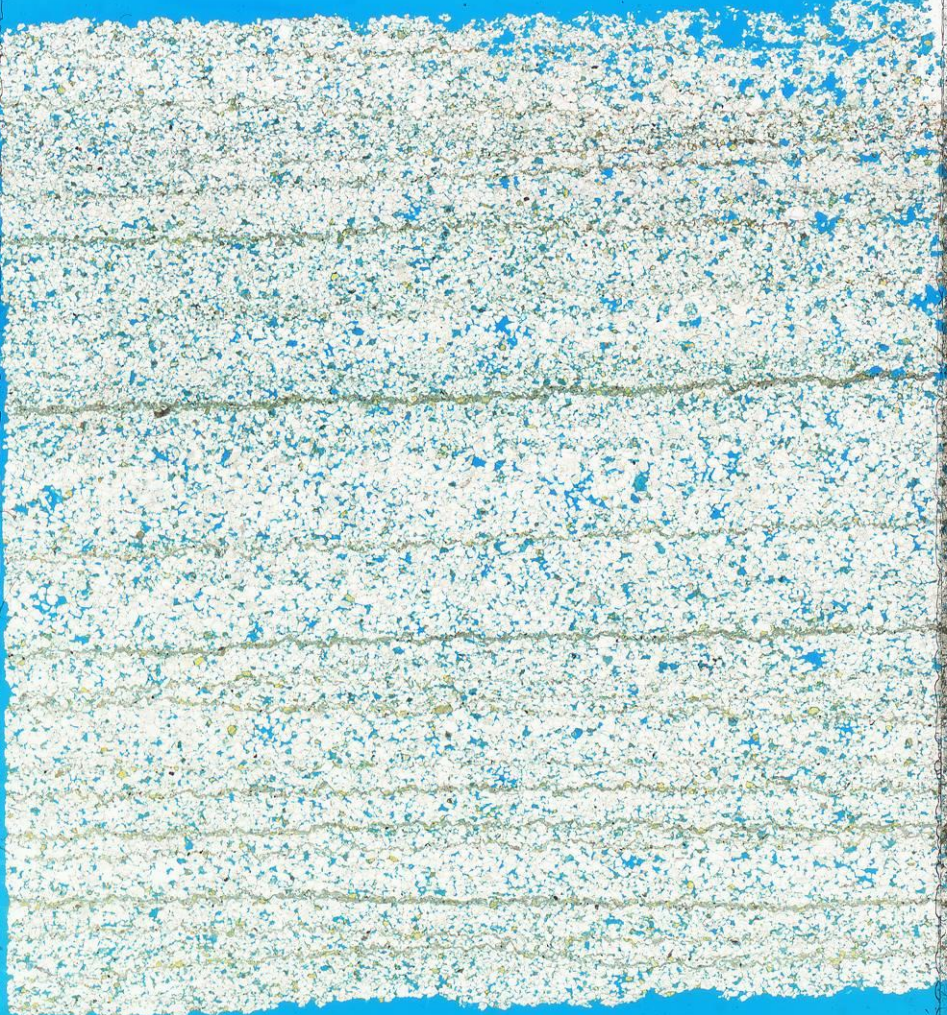


Calgary Rock and Materials

ASF-22e-I



DC + FELD

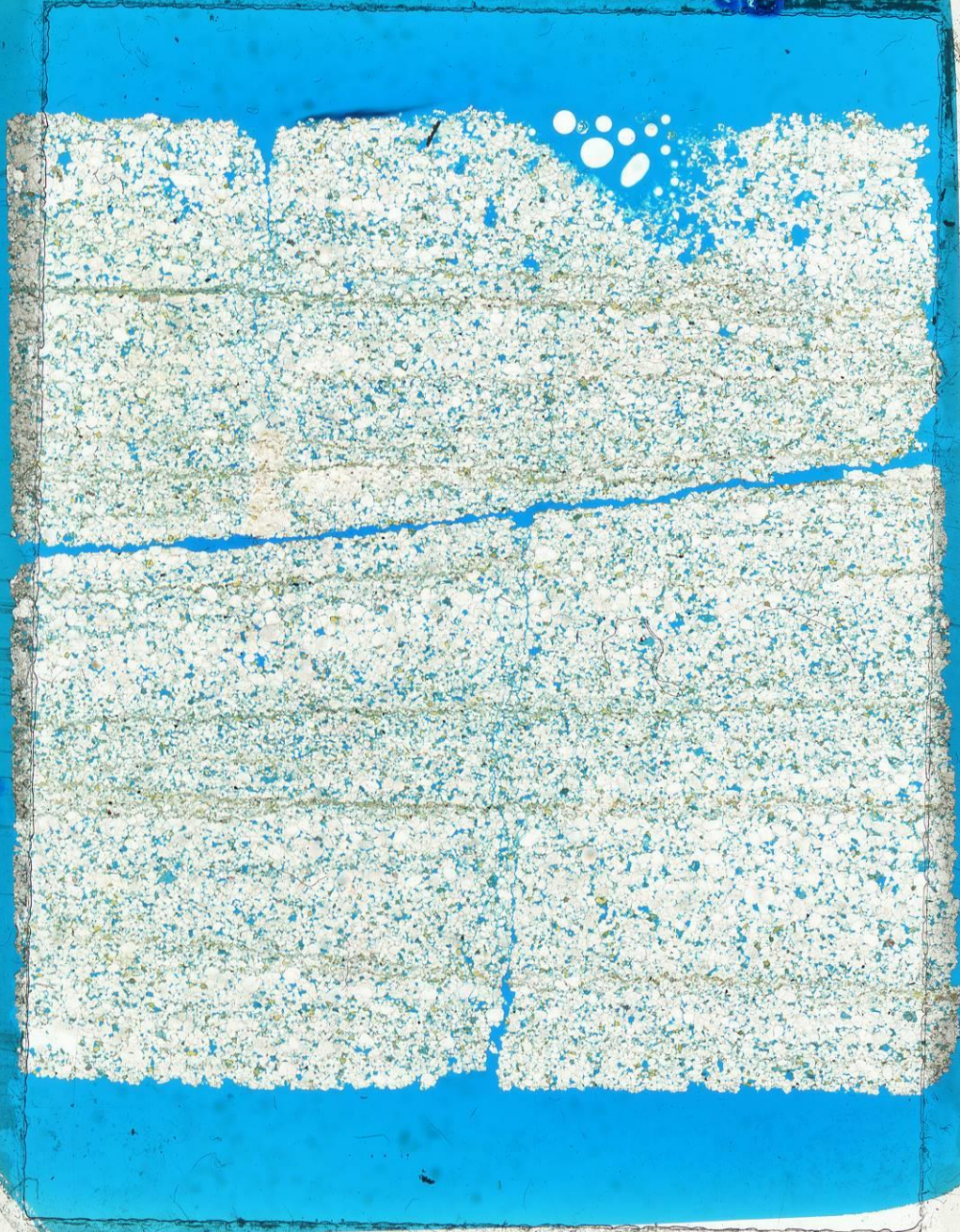


Calgary Rock and Materials

ASF-22e-J



DC + FELD

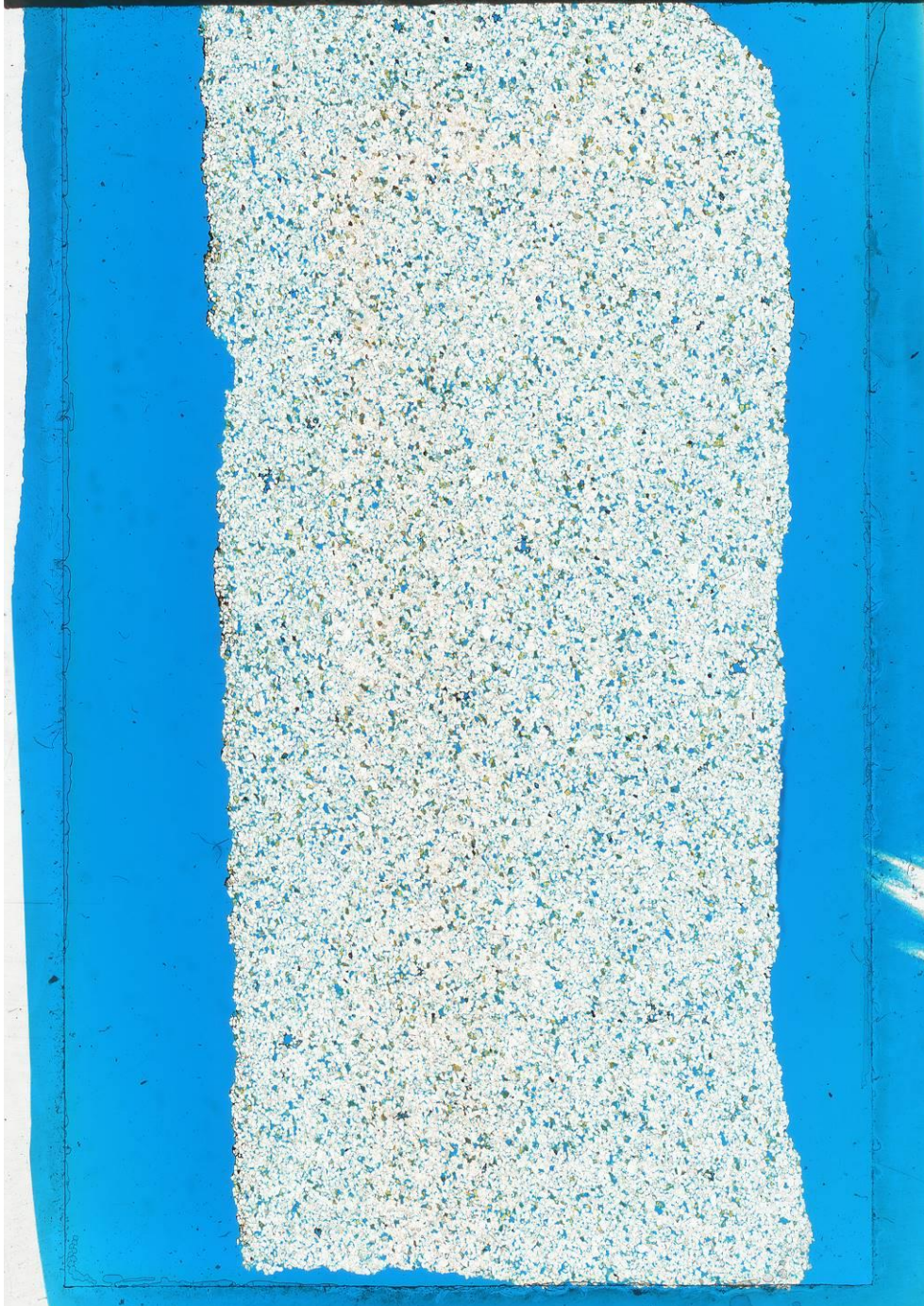


Calgary Rock and Materials

CPE 1 Strike

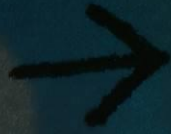


Feld + DC

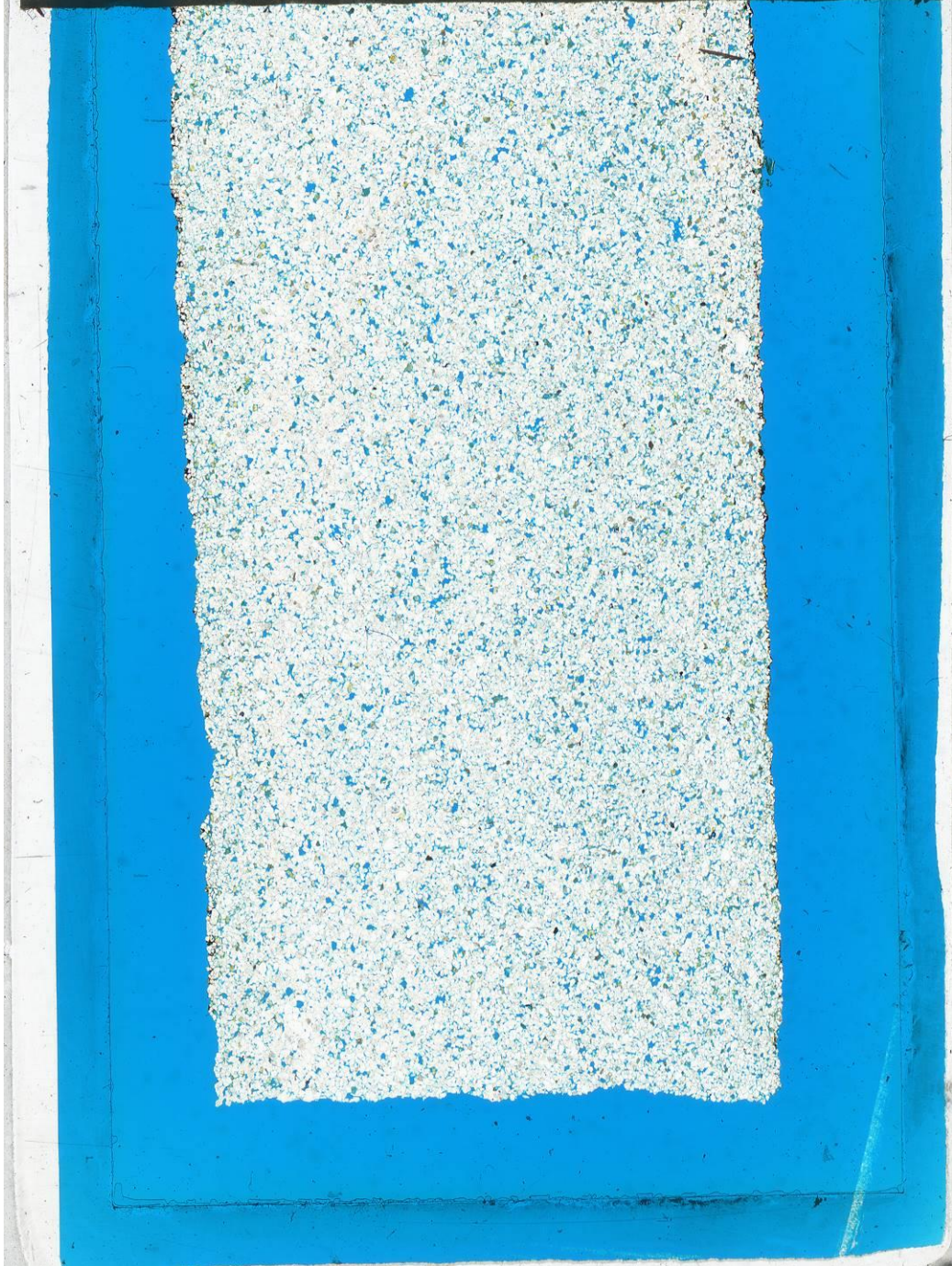


Calgary Rock and Materials

CPE 2 Strike



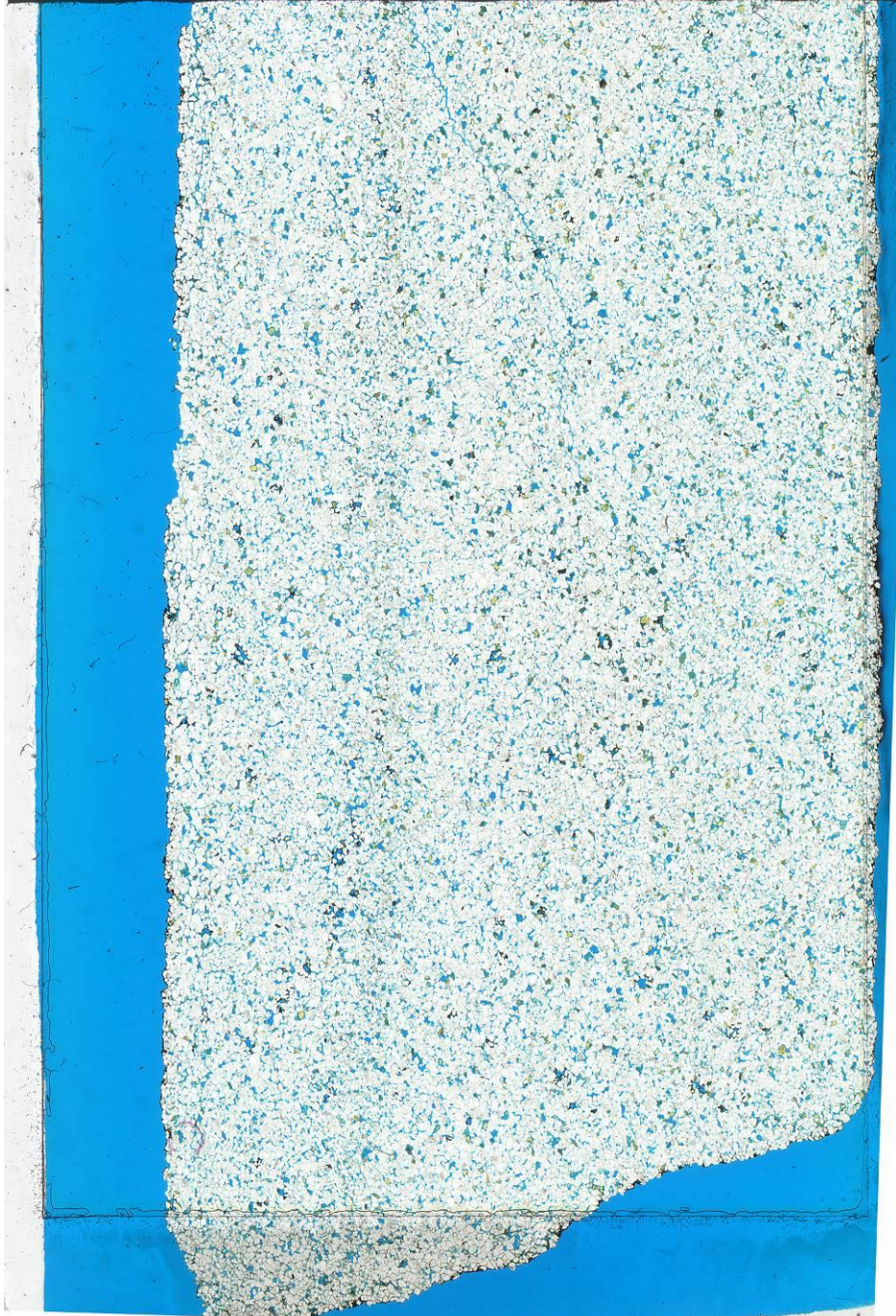
Feld + DC



Calgary Rock and Material

CPE 3 Strike

Feld + DC



Calgary Rock and Materials

CPE 4 Strike



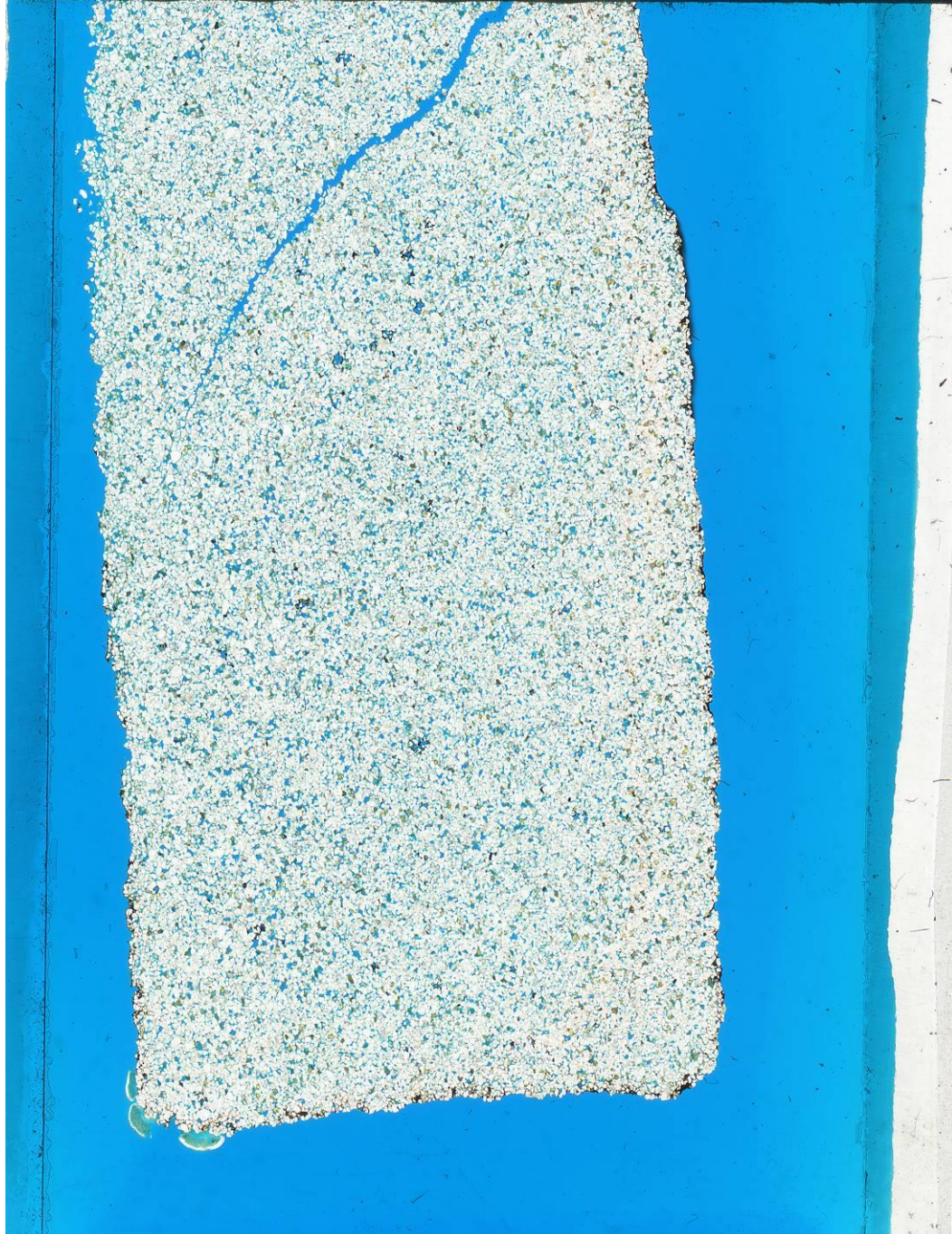
Feld + DC



Calgary Rock and Materials

CPE 5 Strike

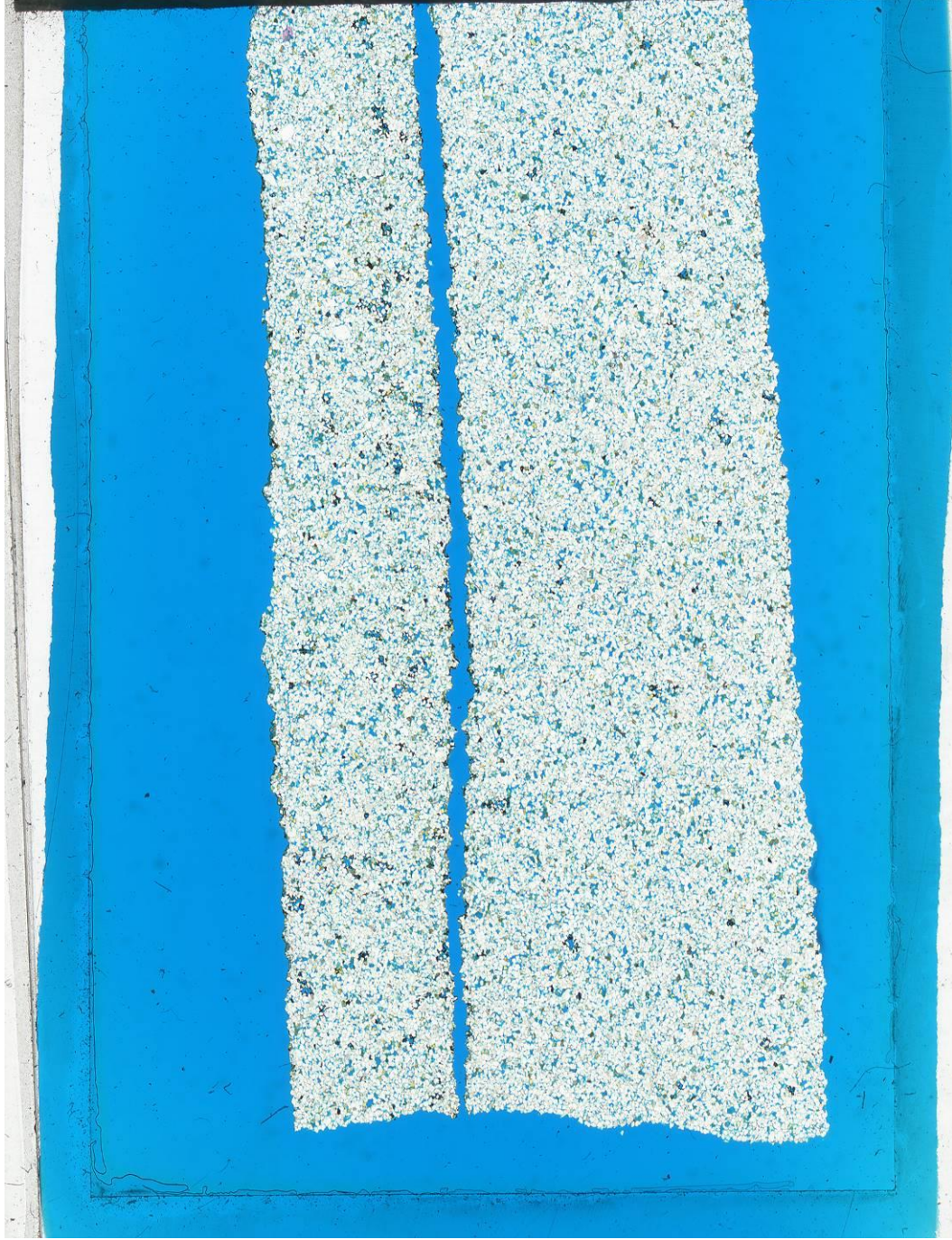
Feld + DC



Calgary Rock and Materials

CPE 6 Strike

Feld + DC



Calgary Rock and Materials

CPE 7 Strike

Feld + DC



Calgary Rock and Materials



CPE 8 Strike

Feld + DC



Calgary Rock and Materials

HMT-1

DC + FELD



Calgary Rock and Materials

HMT-2

DC + FELD



Calgary Rock and Materials

HMT-3

DC + FELD



Calgary Rock and Materials

HMT-4

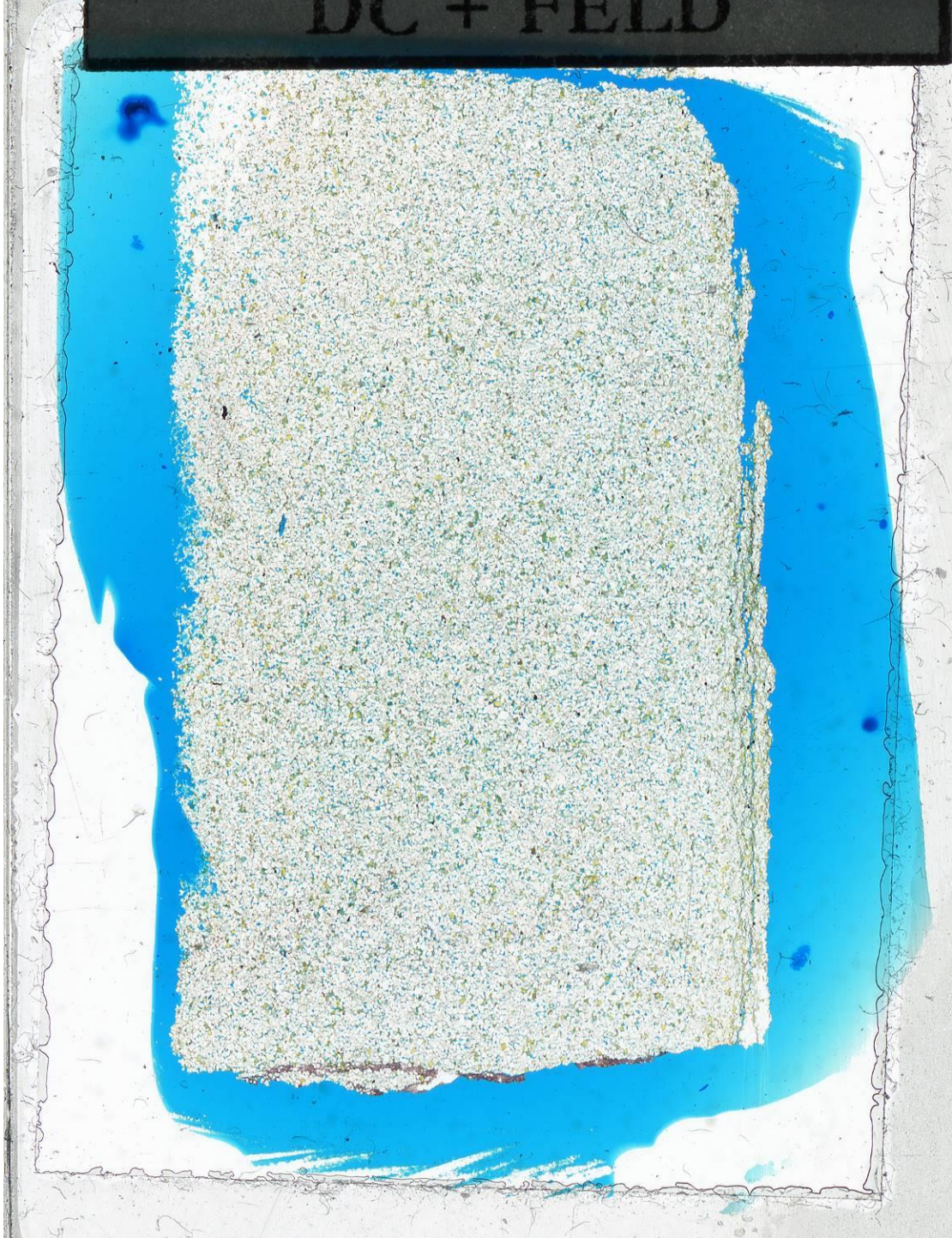
DC + FELD



Calgary Rock and Materials

HMT-5

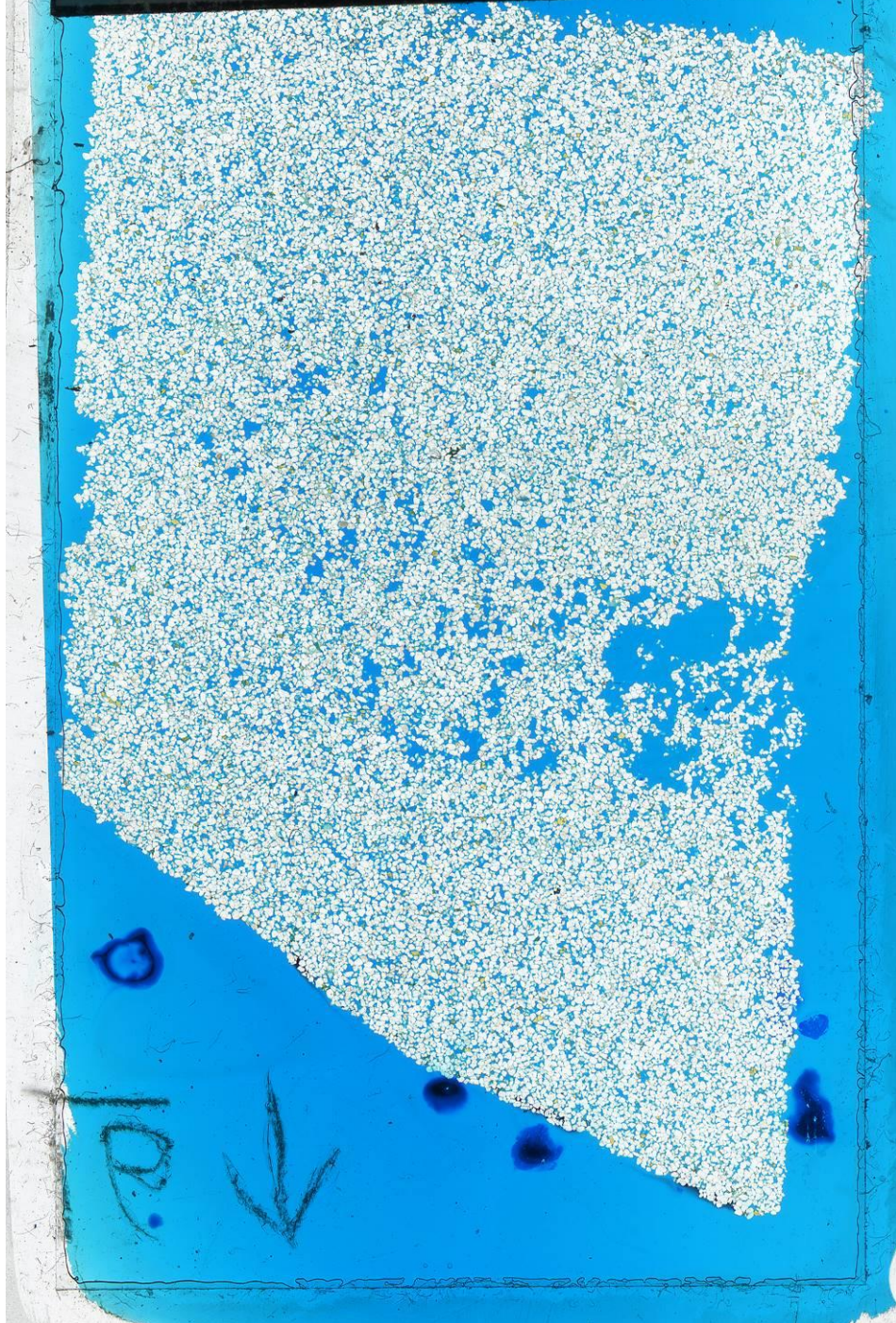
DC + FELD



Calgary Rock and Materials

HOL-E-B-3

DC + FELD



Calgary Rock and Materials

HOL-E-B-5

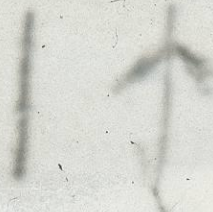
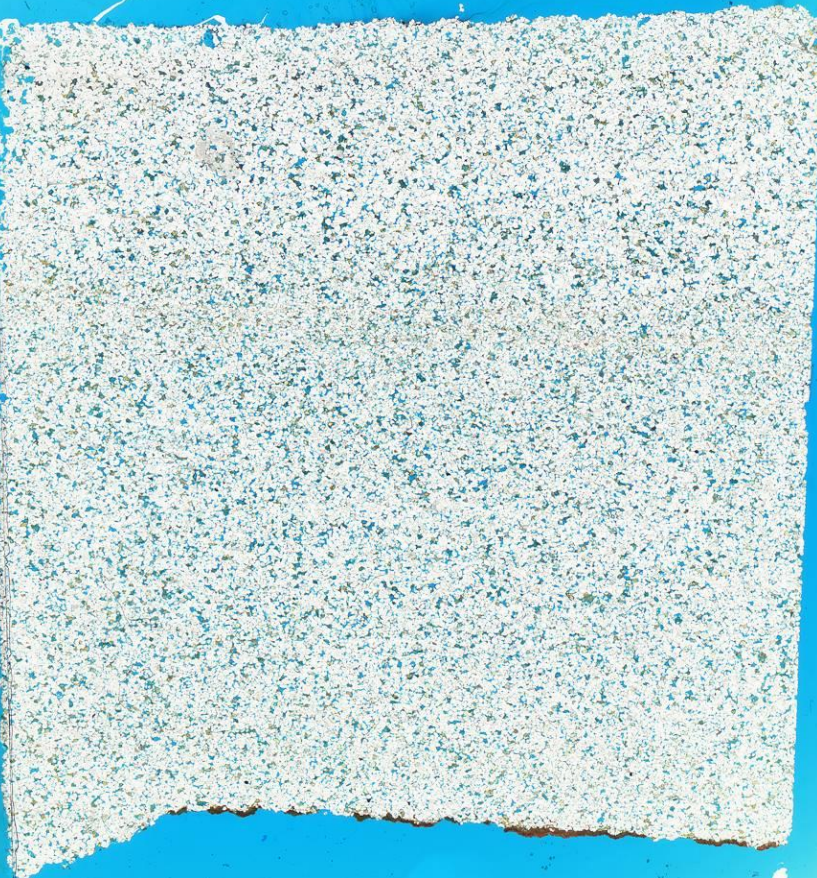
DC + FELD



Calgary Rock and Materials

TM-1-25

DC + FELD



Calgary Rock and Materials

TM-1-26

DC + FELD



Calgary Rock and Materials

TM-1-41

DC + FELD



Calgary Rock and Materials

TM-1-42

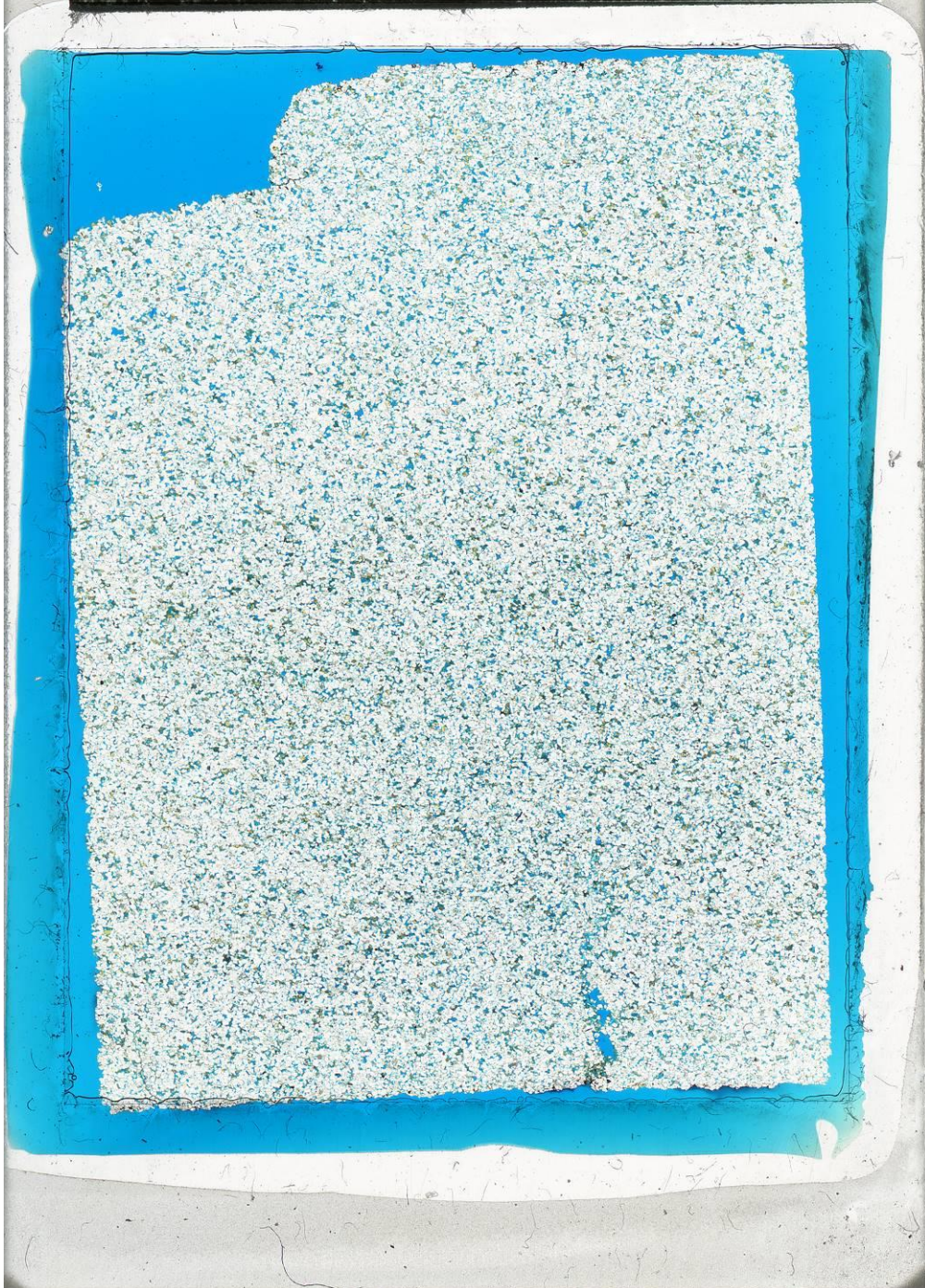
DC + FELD



Calgary Rock and Materials

TM-1-43

DC + FELD

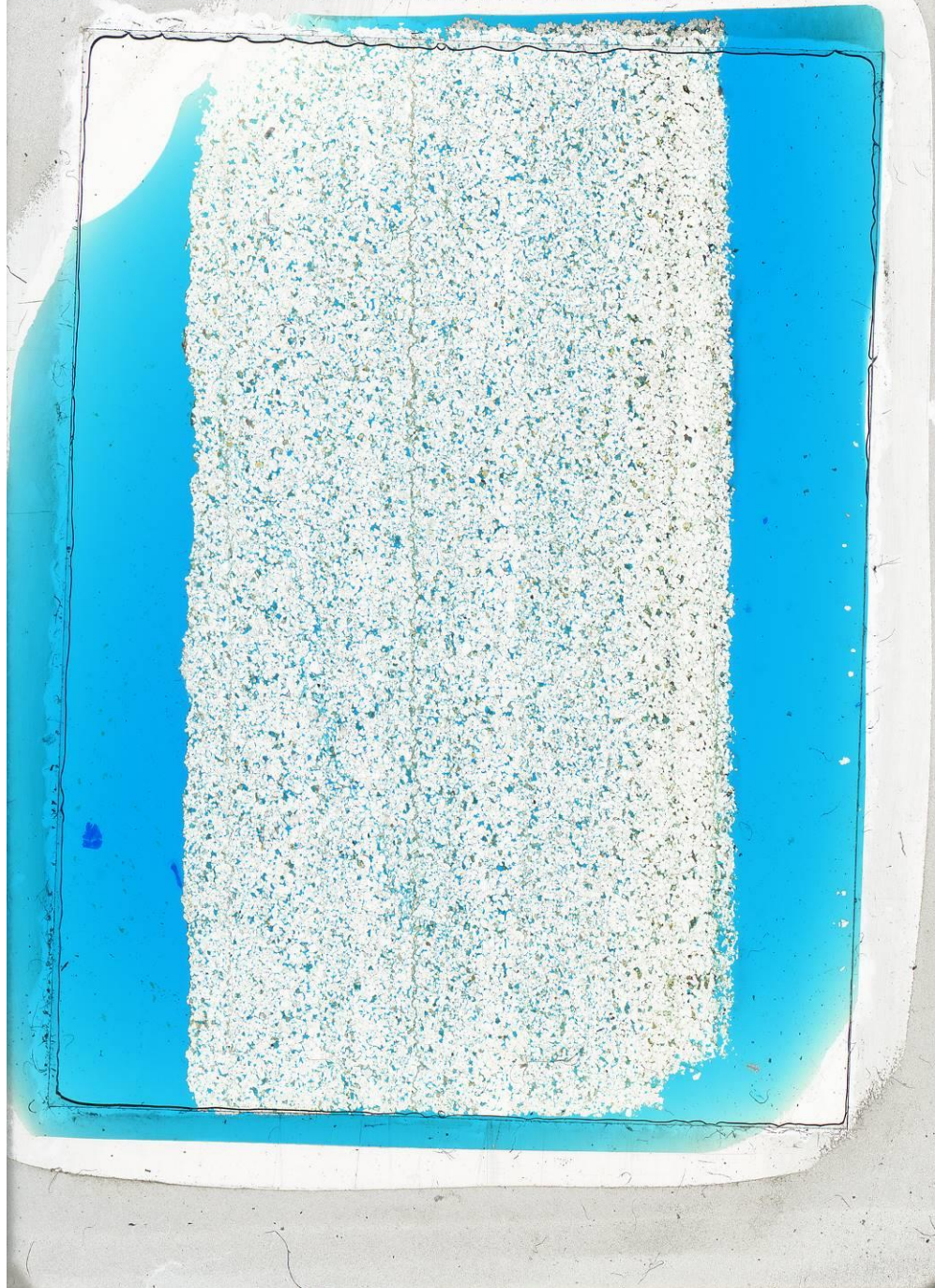


Calgary Rock and Materials

TM-1-44



DC + FELD



Calgary Rock and Materials

TM-1-45

DC + FELD



Calgary Rock and Materials

TM-1-46

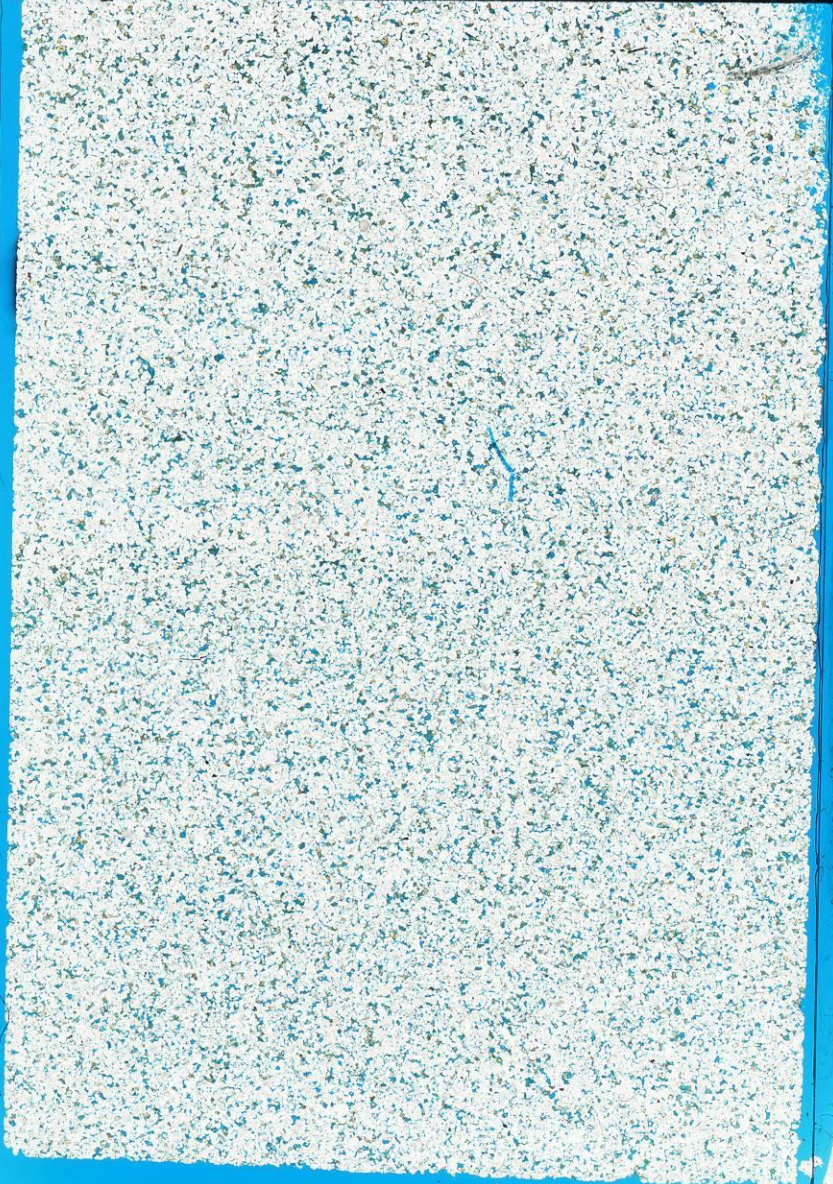
DC + FELD



Calgary Rock and Materials

TM-1-47

DC + FELD



Calgary Rock and Materials

TM-1-48

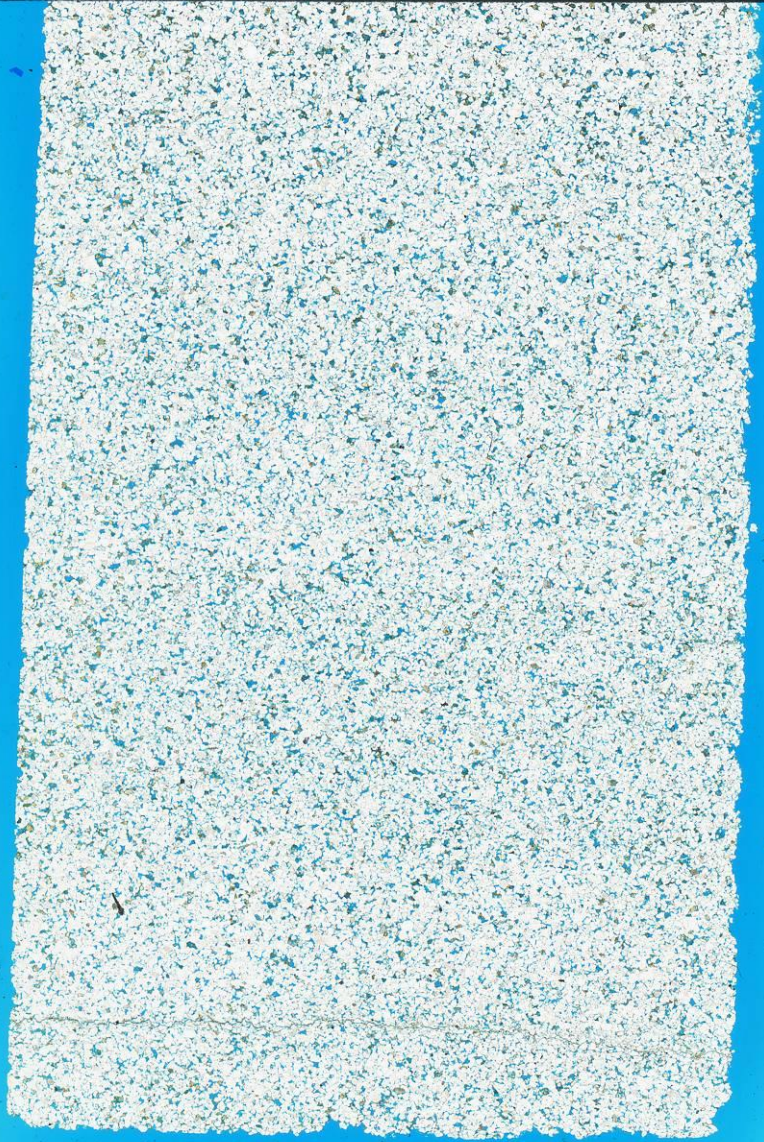
DC + FELD



Calgary Rock and Materials

TM-1-49

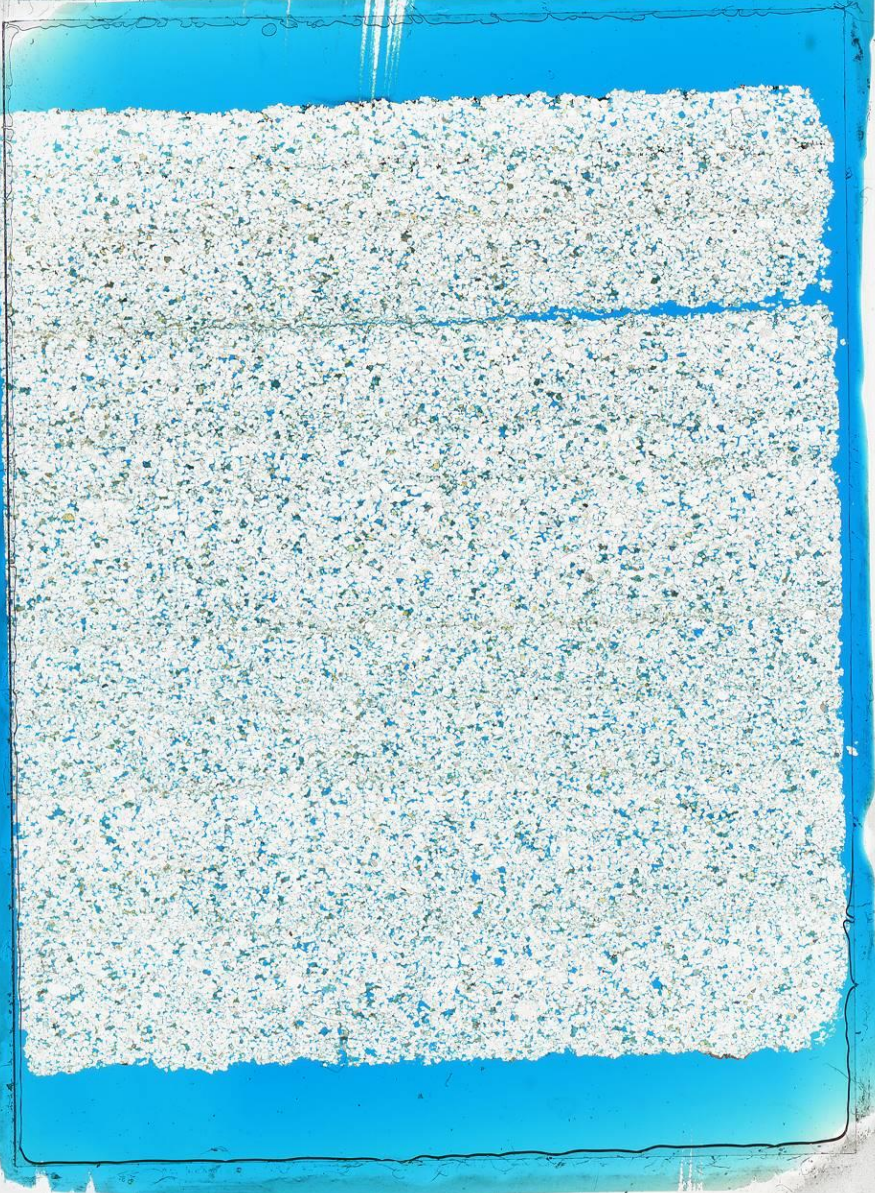
DC + FELD



Calgary Rock and Materials

TM-1-50

DC + FELD



Calgary Rock and Materials

TM-3-1



DC + FELD



Calgary Rock and Materials

TM-3-2

DC + FELD



Calgary Rock and Materials

TM-3-4

DC + FELD



Calgary Rock and Materials

TM-3-5

DC + FELD



Calgary Rock and Materials

TM-3-6



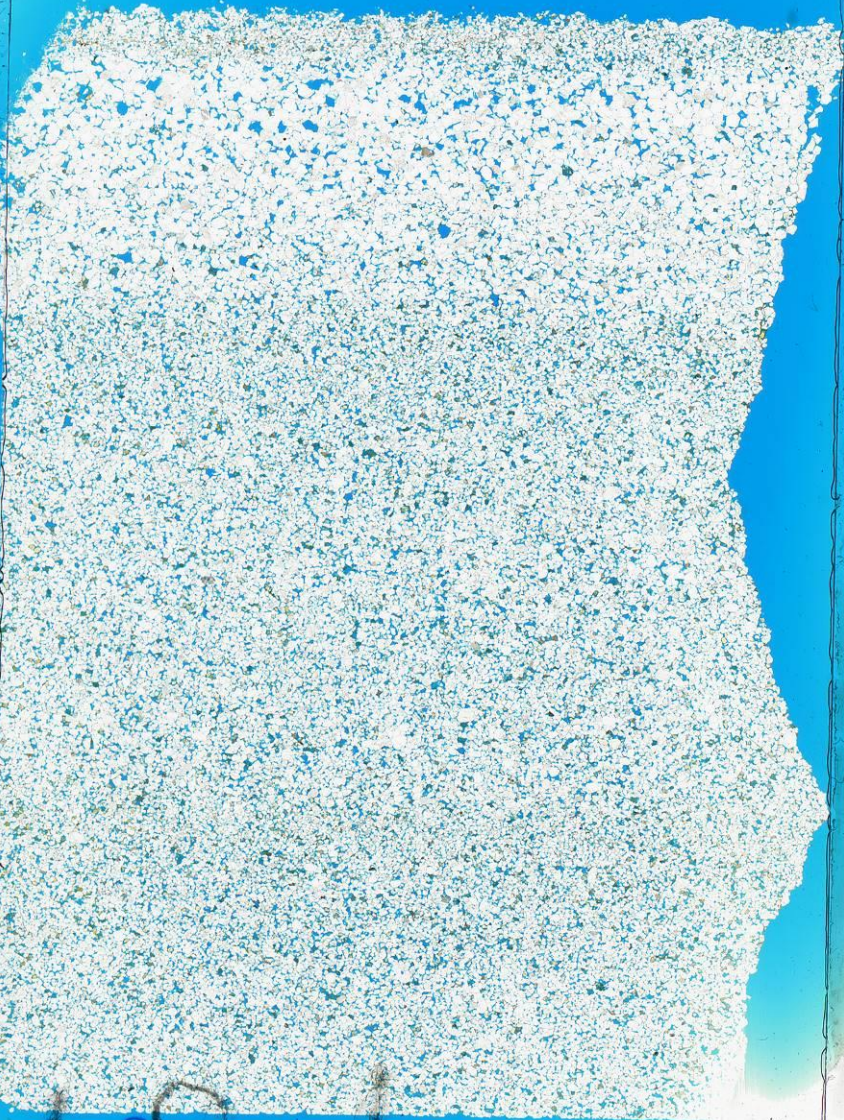
DC + FELD



Calgary Rock and Materials

TM-3-7

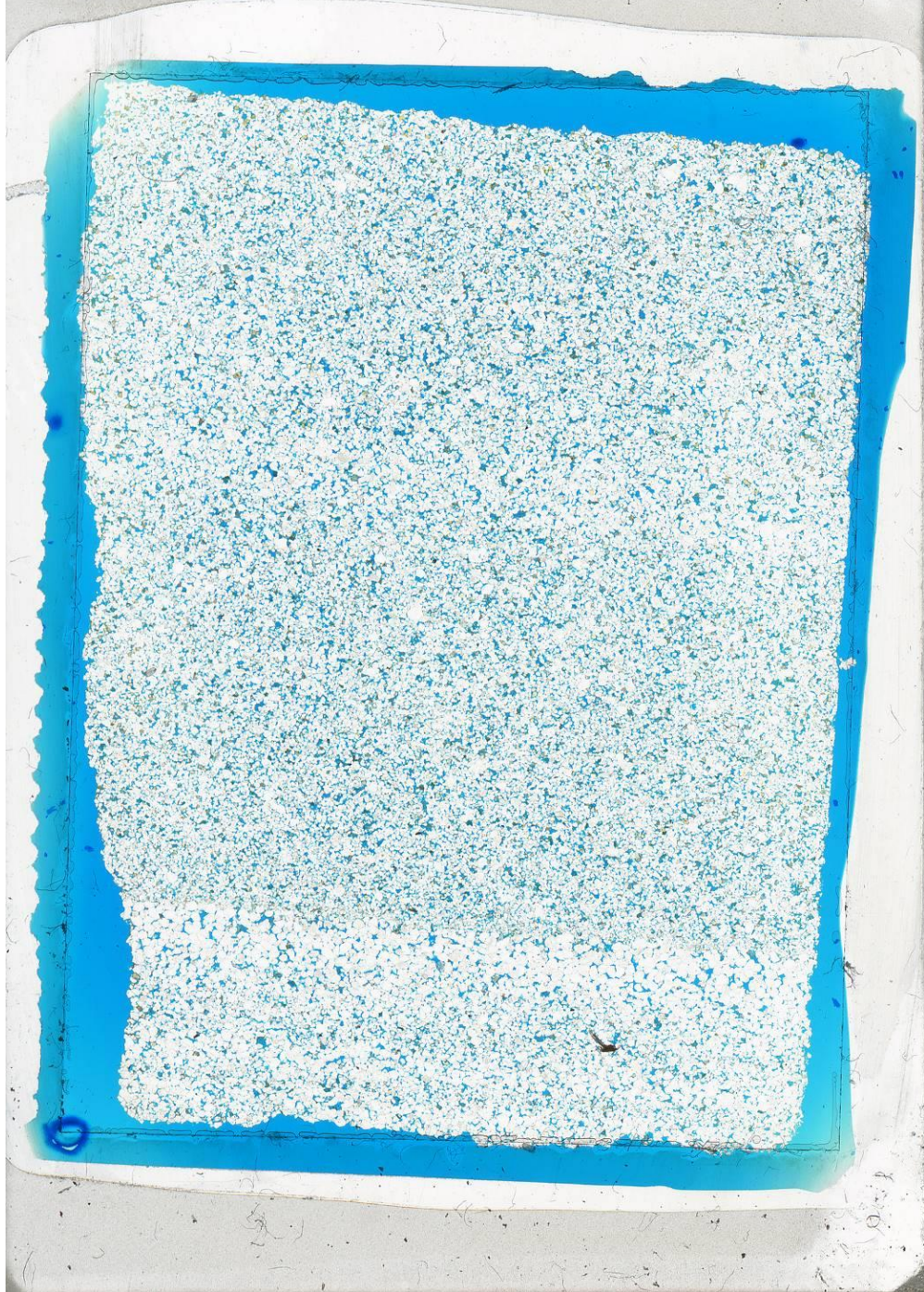
DC + FELD



Calgary Rock and Materials

TM-3-8

DC + FELD



Calgary Rock and Materials

TM-3-9

DC + FELD



50.1

Calgary Rock and Materials

TM-3-10

DC + FELD



Calgary Rock and Materials

TM-3-11

DC + FELD



Calgary Rock and Materials

TM-3-12

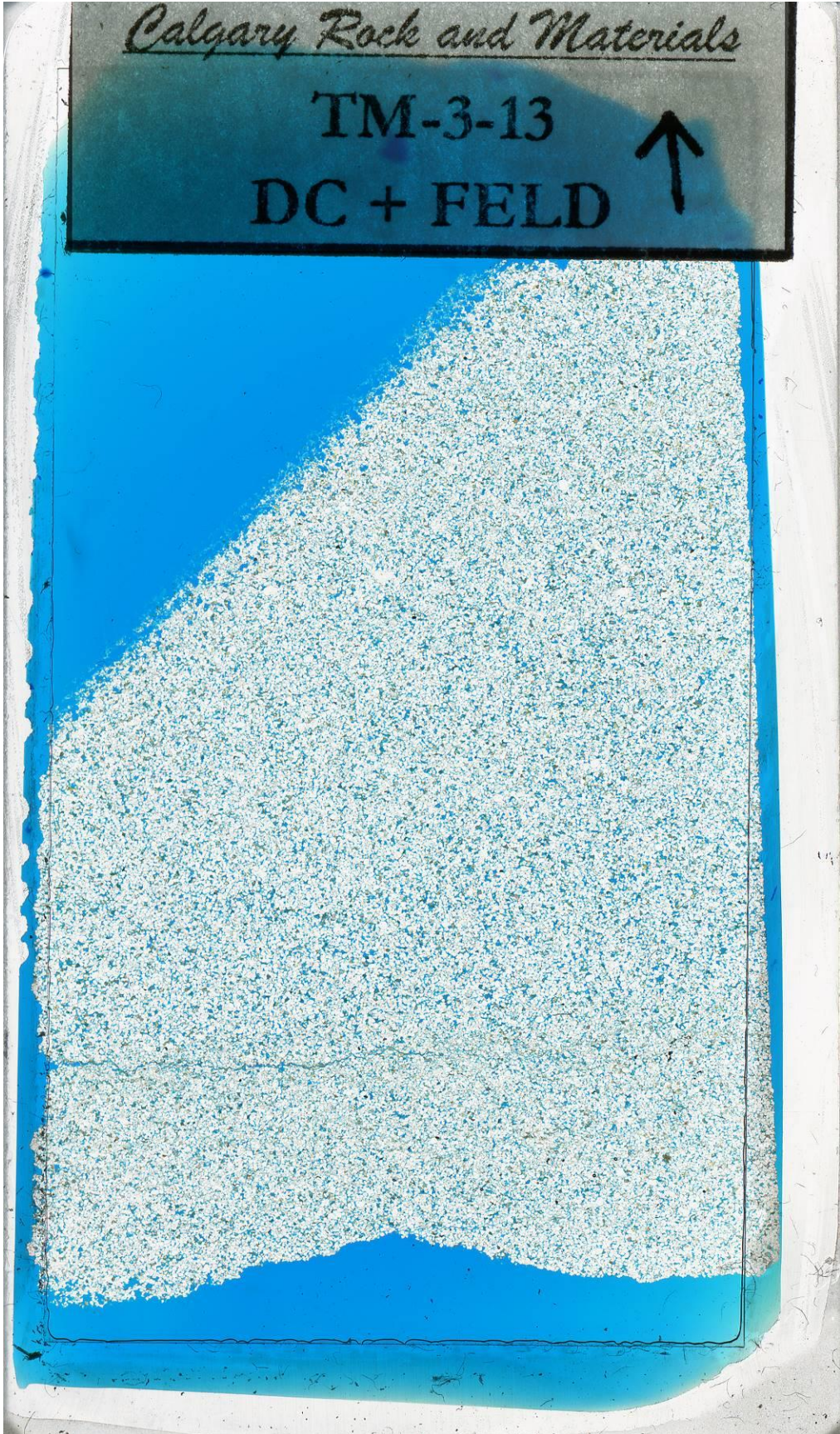
DC + FELD



Calgary Rock and Materials

TM-3-13

DC + FELD



Calgary Rock and Materials

TM-3-14

DC + FELD



Calgary Rock and Materials

TM-3-15

DC + FELD

